

Topics in Shear Flow



Version 1.0

Topics in Shear Flow

Donald Coles
Professor of Aeronautics, Emeritus
California Institute of Technology
Pasadena, California

Assembled and Edited
by Kenneth S. Coles and Betsy Coles

December 2017

©Copyright 2017 by the heirs of Donald Coles

Except for figures noted as published elsewhere, this work is
licensed under a Creative Commons
Attribution-NonCommercial-ShareAlike 4.0 International License

DOI: 10.7907/Z90P0X7D

The current maintainers of this work are Kenneth S. Coles
(kcoles@iup.edu) and Betsy Coles (betsycoles@gmail.com)

Version 1.0 December 2017

Suggested citation: Coles, Donald (2017). Topics in Shear Flow.
DOI: 10.7907/Z90P0X7D

Contents

Preface	xxv
1 INTRODUCTION	1
1.1 Generalities	1
1.2 Analytical prologue	5
1.2.1 Definitions and identities	5
1.2.2 Equations of motion	7
1.2.3 Incompressible fluids	15
1.2.4 Low-speed heat transfer	21
1.2.5 The Boussinesq approximation	25
1.2.6 Coordinate systems	29
1.3 Operational prologue	29
1.3.1 Stream functions	29
1.3.2 Boundary-layer approximations	30
1.3.3 Subcharacteristics	40
1.3.4 Reynolds averaging	44
1.3.5 Dimensions and similarity	48
2 PIPE FLOW	59

2.1	Generalities	59
2.1.1	Equations of motion	60
2.1.2	Laminar flow	64
2.1.3	An extremum principle	68
2.2	Development length	71
2.2.1	Laminar flow	71
2.2.2	Capillary-tube viscometry	76
2.2.3	Turbulent flow	98
2.3	Transition	103
2.3.1	Intermittency	103
2.3.2	Methods of measurement	109
2.3.3	The puff and the plug	114
2.3.4	Short account of flow in coiled pipes	120
2.3.5	Splitting	121
2.3.6	Celerity	124
2.4	Turbulent flow in a smooth pipe	128
2.4.1	Early work	128
2.4.2	The Nikuradse problem	144
2.4.3	A consensus on friction	150
2.5	Similarity Laws	154
2.5.1	The mixing length and the law of the wall	154
2.5.2	The Izakson-Millikan argument	162
2.5.3	The power-law profile	163
2.5.4	The dimensional argument	166
2.5.5	Interpolation formulas for the sublayer	167
2.5.6	Fully developed flow	177

2.5.7	Karman's constants κ and c	182
2.5.8	The defect law	191
2.5.9	The limit $Re \rightarrow \infty$	191
2.5.10	The formal friction law	191
2.5.11	The Reynolds stresses	192
2.6	Roughness	192
2.6.1	Friction	192
2.7	Polymers	197
2.7.1	Friction	197
2.7.2	Mean velocity	198
2.7.3	Re Stresses	198
2.8	Heat transfer	199
2.8.1	Friction	199
2.8.2	Mean temperature	199
2.8.3	Consensus on heat transfer	199
2.9	Variations on classical pipe flow	199
2.9.1	Odd shapes	199
2.9.2	Coiled pipes	199
2.9.3	Area change	199
2.9.4	Non-steady flow	199
2.9.5	Swirl	199
2.9.6	Wall suction, blowing	199
3	CHANNEL FLOW	201
3.1	Generalities	201
3.1.1	Preamble	201
3.1.2	Equations and integrals	201

3.1.3	Laminar flow	203
3.1.4	Development length	203
4	THE BOUNDARY LAYER	205
4.1	Generalities	205
4.1.1	The momentum-integral equation	208
4.2	Laminar equilibrium flow	212
4.2.1	The affine transformation	212
4.2.2	The Falkner-Skan equation	215
4.2.3	Normalization	217
4.2.4	Potential flow past a wedge	221
4.3	Morphology of the Falkner-Skan flows	223
4.3.1	The parameter β or m	223
4.3.2	Some numerical particulars	225
4.3.3	Solution maps	239
4.4	Some special cases	247
4.4.1	Blasius flow; the case $\beta = 0, m = 0$	247
4.4.2	Constant wall friction; the case $\beta = 1/2, m = 1/3$	254
4.4.3	Stagnation-point flow; the case $\beta = 1, m = 1$	254
4.4.4	Sink flow; the case $\beta = \infty, m = -1$	256
4.4.5	Separating flow; the case $\beta = -0.1988, m = -0.0904$	261
4.4.6	The singularity at $\beta = 2, m = \infty$	262
4.4.7	The Stewartson flows; $-0.1988 < \beta < 0$	269
4.5	Connections	270
4.5.1	The shear layer	270

4.5.2	The wall jet	272
4.5.3	The plane jet	276
4.6	Laminar non-equilibrium flow	282
4.6.1	The Thwaites method	282
4.6.2	The leading-edge problem	289
4.7	Transition	291
4.8	Instrumentation	291
4.8.1	Wall shearing stress	291
4.8.2	Velocity	294
4.8.3	Flow visualization	294
4.9	Similarity laws for turbulent flow	294
4.9.1	Preamble	294
4.9.2	The law of the wall and the law of the wake	294
4.9.3	The boundary-layer thickness δ	294
4.10	Hypotheses turbulent equilibrium flow	302
4.10.1	Recapitulation	302
4.10.2	Flow near a wall	303
4.10.3	External flow	306
4.10.4	Equilibrium parameters	307
4.10.5	The hypothesis D = constant	312
4.11	Morphology turbulent equilibrium flow	313
4.11.1	Pure wall flow	313
4.11.2	Pure wake flow	321
4.11.3	The momentum-integral equation	324
4.11.4	Flow at constant pressure	328
4.11.5	Entrainment	331

4.11.6	Experiments in equilibrium flow	338
4.11.7	The function $D(P)$	339
5	THE SHEAR LAYER	341
5.1	Plane laminar shear layer	341
5.1.1	Equations of motion	342
5.1.2	Similarity	344
5.1.3	Normalization	347
5.2	Plane turbulent mixing layer	352
5.2.1	The boundary-layer approximation	356
5.2.2	Structure of the shear layer	361
6	THE ROUND WAKE	369
7	THE PLANE WAKE	371
8	THE ROUND JET	373
8.1	Laminar round jet into fluid at rest	374
8.1.1	Preview	374
8.1.2	Dimensional argument	375
8.1.3	The exact solution	378
8.1.4	The boundary-layer approximation	385
8.1.5	The boundary-layer Solution	387
8.1.6	The inner limit	389
8.1.7	The outer limit	390
8.1.8	Miscellaneous remarks	394
8.2	Laminar round jet into moving fluid	395
8.3	Transition	395

8.4	Turbulent round jet into fluid at rest	397
-----	--	-----

9 THE PLANE JET 407

9.1	Laminar plane jet into fluid at rest	409
9.1.1	The equations of motion	409
9.1.2	Dimensional properties	411
9.1.3	The boundary-layer solution	419
9.1.4	Normalization	424
9.1.5	Entrainment	430
9.1.6	The composite expansion	437
9.1.7	Experimental evidence	444
9.2	Laminar plane jet into moving fluid	447
9.2.1	Similarity	447
9.3	Turbulent plane jet into fluid at rest	454
9.3.1	Dimensional preamble	454
9.3.2	The affine transformation	456
9.3.3	Normalization	462
9.3.4	Entrainment and composite flow	463
9.3.5	The boundary-layer approximation	465
9.3.6	Experimental evidence	467
9.4	Turbulent plane jet into moving fluid	475
9.5	The jet ejector	475
9.6	The Coanda effect	475
9.7	Multiple jets	475
9.8	The jet flap	475
9.8.1	Potential flow	475
9.8.2	Experiment	480

9.9	The radial jet	481
9.9.1	Dimensional preamble	481
9.9.2	Laminar similarity	483
9.9.3	The Mangler transformation	489
9.9.4	Entrainment and composite flow	495
9.9.5	Turbulent similarity	497
10	THE WALL JET	501
10.1	Laminar plane wall jet	503
10.1.1	The eigenvalue problem	503
10.1.2	Similarity	512
10.1.3	The boundary-layer solution	514
10.1.4	Normalization	517
10.1.5	Entrainment and composite flow	521
10.1.6	The laminar radial wall jet	524
10.1.7	Stability and transition	524
10.2	Laminar plane wall jet into moving fluid	524
10.2.1	Similarity	524
10.3	Turbulent plane wall jet	524
10.3.1	Similarity	524
10.3.2	The law of the jet	526
10.3.3	Entrainment and composite flow	527
10.3.4	Coanda effects	527
10.4	The turbulent radial wall jet	527
10.4.1	Similarity	527
10.5	Turbulent plane wall jet into moving fluid	532
10.5.1	Similarity	532

<i>CONTENTS</i>	ix
10.5.2 Relaxation	532
10.5.3 Effectiveness	532
10.5.4 Boundary-layer control	532
10.6 Three-dimensional wall jets	532
10.6.1 Single jets	532
10.6.2 Film cooling through holes	532
11 THE PLANE PLUME	533
11.1 Generalities	533
11.1.1 Dimensional preamble	533
11.1.2 The plane turbulent plume	544
12 FLOW CONTROL	551
Appendix A	571

List of Figures

1.1	The Bernoulli integral for an incompressible fluid and for a perfect gas with $\gamma = 1.4$	20
1.2	The laminar velocity profile for impulsive motion of an infinite flat plate in its own plane.	50
1.3	Caption for Figure with label Fig1-10 (missing). . . .	56
1.4	Topological cartoons of the vortex street and the mixing layer (caption by K. Coles).	57
1.5	Caption for Figure with label Fig1-12 (missing). . . .	58
2.1	Cylindrical polar coordinate system and notation for pipe flow.	61
2.2	The parabolic mean-velocity profile and the linear shear-stress profile for steady laminar flow in a circular pipe.	64
2.3	A schematic diagram of flow in the laminar development region of a circular pipe with uniform entrance flow.	71
2.4	Some analytical results for laminar flow development in a smooth pipe. The dependent variable u_c/\tilde{u} has an asymptotic limit of 2.	73

- 2.5 Several examples from the experimental literature showing non-axisymmetric laminar flow in circular pipes. The most likely cause is secondary flow due to thermal inhomogeneity in a gravitational field or asymmetry of the upstream channel. 77
- 2.6 A schematic representation of the pressure distribution along a tube of length L with uniform entrance flow at $x = 0$. The flow may be laminar or turbulent and the cross section need not be circular. 79
- 2.7 The raw friction data of MICKELSON (1964) for ten capillary tubes of fixed diameter and various lengths ranging from $L/D = 15$ to $L/D = 510$. The fluid is water at 30°C . The curve for turbulent flow at the right is faired through Nikuradse's data. Note that transition is slightly delayed for the two longest tubes. 85
- 2.8 The ideal friction coefficient as inferred by differentiation of Mickelson's data. The circles represent the slope of a fitted straight line in a plot of $\hat{C}_f L/D$ against L/D for constant Re . The curve for turbulent flow at the right is faired through Nikuradse's data. . 87
- 2.9 The laminar flow-development parameter m as a function of Re for a square-cut entrance according to Mickelson's data. The open circles show twice the intercept of a fitted straight line in a plot of $\hat{C}_f L/D$ against L/D for constant Re . In the laminar range, the small filled circles are from equation (2.57). 88
- 2.10 Mickelson's data from the previous FIGURE 2.7, re-plotted according to equation (2.57). The Reynolds number Re increases from right to left. The quantity m is defined by the flat laminar region at the lower right. 89

- 2.11 A modern representation of POISEUILLE's data (1846) for flow in capillary tubes. Note the displaced scales. The first series is suitable for determining the viscosity. The second series in uncorrected form is not. The lowest display shows the second series after a correction for flow development. The residual scatter here may be caused by inaccurate measurement of tube length. 94
- 2.12 Typical experimental results for turbulent flow development in a smooth pipe when transition occurs in the boundary layer well downstream, near the peak in the curve of u_c against x . The turbulent asymptotic limit for u_c/\tilde{u} depends on Reynolds number and is here approached from above. 99
- 2.13 Typical experimental results for turbulent flow development in a smooth pipe when transition occurs in the boundary layer very close to the entry. The turbulent asymptotic limit for u_c/\tilde{u} depends on Reynolds number and is approached from below. 100
- 2.14 Two photographic sequences of instantaneous exit-jet trajectories according to SACKMANN (1954) for pipe flow in the transition range. The upper and lower pictures correspond to passage of the leading and trailing edges of a puff. 105
- 2.15 The mean intermittency $\bar{\gamma}$ for pipe flow with highly disturbed entry. The data are from various sources, using the exit-jet method, streaming birefringence, hot-wire anemometry, or laser-Doppler velocimetry (figure 1 of COLES 1962) 107
- 2.16 The intermittency frequency fD/\tilde{u} for pipe flow with highly disturbed entry. The data are from various sources, using the exit-jet method, streaming birefringence, hot-wire anemometry, or laser-Doppler velocimetry (figure 3 of COLES 1962) 107

- 2.17 A least-squares fit to three successive points of a uniformly spaced time series for a variable $u(t)$ 112
- 2.18 Rotta's decomposition of a measured pipe profile in the transition regime according to the on-off model. The laminar and turbulent profiles do not have quite the correct volume flow rate. 113
- 2.19 The average duration of laminar and turbulent intervals far downstream in the transition regime of pipe flow with highly disturbed entry. (Figure of COLES (19xx)). The data are from ROTTA (1956) and VALLERANI (1964). 116
- 2.20 Some velocity signatures obtained by BREUER (1985) on the centerline of a pipe flow, showing several stages of the splitting process at $Re \sim 2400$. The traces are from different realizations of the splitting phenomenon. 117
- 2.21 Topology of the mean flow in a turbulent puff at $Re = 2230$, after WYGNANSKI *et al.* (1975). The observer is moving at the celerity of the structure, so that mean particle paths coincide with mean streamlines. The two coordinates have equal scales. 118
- 2.22 My original (top) and revised (bottom) cartoons suggesting the topology of a turbulent puff. The top cartoon is from COLES (1962). 119
- 2.23 Intermittency factor (top curve) and three components of mean velocity relative to spiral region of turbulence in circular Couette flow. Components R, T, A in radial, tangential, and axial directions are normalized. Positions a, b, c, d lie along one complete circuit at one radial position. Figure 4 of COLES and VAN ATTA 1966 (AIAA Journal), which describes the geometry of the flow measurement. (Caption provided by K. Coles) 122
- 2.24 Leading-edge and trailing-edge celerities for puffs and plugs in pipe flow as measured by several authors. . . 124

- 2.25 Diagram 2 of the paper by REYNOLDS (1883), reproduced with the aid of his tables III–V. The abscissa $i = dh/dx = (dp/dx)/\rho g$ is the dimensionless local pressure gradient. The ordinate v is the mean velocity in cm/sec. 133
- 2.26 The previous FIGURE 2.25 made dimensionless by following Reynolds' instructions. Reynolds described this figure but did not display it. 134
- 2.27 The raw capillary data of BOSE and BOSE (1911) in dimensional form. The ordinate (proportional to C_f) is the product of the pressure difference P in gm/cm² and the square of the flow time T in seconds for a fixed volume V of liquid. The abscissa (proportional to Re) is the reciprocal of the flow time. From top left, the liquids are mercury, bromoform, ethanol, water, chloroform, benzene, toluene, and acetone. 137
- 2.28 The data of the previous FIGURE 2.27 after reduction to dimensionless form following KARMAN (1911). Handbook values have been used for density and viscosity. The capillary tube was apparently quite short, with L/D perhaps about 60, and the data are therefore usable only for relative viscometry. 139
- 2.29 Reynolds' pipe data in standard dimensionless variables. The curve at the right is faired through Nikuradse's data. The low values of C_f for turbulent flow may be caused by imperfect calibration of the flowmeter. 142
- 2.30 Some measurements before 1932 of friction in smooth pipes. The solid line for turbulent flow is faired through the data of NIKURADSE (1932). A few obviously sour points have been discarded. 151

- 2.31 Three interpolation formulas for the transition region between the linear and logarithmic forms of the law of the wall. Note the displaced scales. The top display is a superposition of the other three. I recommend the formula proposed by Musker. 171
- 2.32 Placement in complex wall coordinates of the three singularities in Musker's formula (2.166) for the law of the wall. The radius of convergence of a power series for $u^+(y^+)$ is $R^+ = 9.29$ 175
- 2.33 Use of the single-parameter equations (2.176) and (2.180) to round the logarithmic mean-velocity profile near the pipe axis for the case $R^+ = Ru_\tau/\nu = 2000$ 178
- 2.34 Raw velocity-profile data from the superpipe measurements by ZAGAROLA (1996). Thirteen of the 26 measured profiles are shown. The logarithmic law of the wall and the velocity-defect law are solidly supported by these data. 186
- 2.35 Centerline data and log-region data from the superpipe measurements by ZAGAROLA (1966). The fitted lines have the same slope. The constants in the logarithmic law of the wall are $\kappa = 0.435$, $c = 6.10$ 187
- 2.36 Various measurements in wall coordinates of centerline velocity in smooth pipes. Note the displaced origins. The lower curve shows good agreement between the data of ZAGAROLA (1996; circles) and other measurements from the literature (crosses), absent Nikuradse. The middle curve shows good agreement between Zagarola's centerline data and NIKURADSE's centerline data from his table 8 (1932), except for Reynolds numbers R^+ below about 1500. The upper curve shows that the centerline points from Nikuradse's 16 profiles in his table 3 do not agree with any of the other measurements, including his own. 189

- 4.1 The displacement effect in the free stream for the Blasius boundary layer in rectangular coordinates. The hatched area extends to $y = \delta^*$ 220
- 4.2 Potential flow past a wedge of total angle $\pi\beta$ 222
- 4.3 Morphology of the Falkner-Skan boundary layers in terms of the parameters (β, m) . The various icons depict channel flows with channel heights proportional to $1/u_\infty$ 224
- 4.4 (Figures from A.M.O. Smith) 227
- 4.5 Saddle structure at $Y = \infty$ of the Falkner-Skan boundary layer for $\beta = \infty$ (sink flow, $F''(0) = 1.154701$). The integral curves are drawn for $C = 0, 2/3, 4/3$ in equation (4.83). 232
- 4.6 Pseudo-saddle structure at $Y = \infty$ of the Falkner-Skan boundary layer for $\beta = 5$. The conventional integral curves are drawn for $f''(0) = 1.11981, 1.16981, 1.19981$. Two other integral curves begin at $(f, f', f'') = (5, 1.5, -1.2)$ and $(10, 1.6, -1.1)$ 233
- 4.7 Some oscillating solutions of the Falkner-Skan boundary layer equation for $\beta = 5$. The integral curves are drawn for $F''(0) = 1.11430, 1.11447, 1.16981$. The last of these is the classical solution. 235
- 4.8 Pseudo-saddle structure at $\eta = \infty$ of the Falkner-Skan boundary layer for $\beta = 1$. The conventional integral curves are drawn for $f''(0) = 1.18259, 1.23259, 1.28259$. Two other integral curves begin at $(f, f', f'') = (5, 1.48, -1.2)$ and $(1, 1.48, -1.9)$ 236
- 4.9 Neutral structure at $\eta = \infty$, showing Töpfer mapping of the Falkner-Skan boundary layer for $\beta = 0$ (Blasius flow). The curves are drawn for $f''(0) = 0.4196, 0.4696, 0.5196$ 237

- 4.10 Pseudo-node structure at $\eta = \infty$ of the Falkner-Skan boundary layer for $\beta = -0.1$ (upper branch). The integral curves are drawn for $f''(0) = 0.21927, 0.31927, 0.41927$. Note the compressed scale at right to show the extremely slow algebraic approach of f' to the outer boundary condition when $f''(0)$ is not correct. 238
- 4.11 Pseudo-node structure at $\eta = \infty$ of the Falkner-Skan boundary layer for $\beta = -0.1$ (lower branch). The integral curves are drawn for $f''(0) = -0.180545, -0.140545, -0.100545$ 239
- 4.12 A map of some known solutions of the Falkner-Skan equation for positive β 241
- 4.13 A map of some known solutions of the Falkner-Skan equation for negative β 242
- 4.14 LEFT: some partial sums of the power-series representation of the Blasius solution $f'(\eta)$. The radius of convergence of the series is 4.03. The sum of eight terms is within 0.001 of the exact solution for $\eta < 2.8$ approximately, as marked by the right-most cross. RIGHT: the three singularities of the function $f(\eta)$ in the complex η -plane. 248
- 4.15 The Blasius velocity profile according to figure 62 of NIKURADSE (1942a). The theoretical curve is correct, but I do not accept these experimental data at face value. 253
- 4.16 The potential flow for the singular case $\beta = 2$ and $u_\infty \sim e^{cx}$ according to MANGLER (1943). The Falkner-Skan boundary conditions can be satisfied only if c is positive. There is no definite origin or scale for x 268
- 4.17 Approach of Falkner-Skan solutions to the starred shear-layer limit ($\beta = 0, f''(0) = 0$) along Stewartson's lower branch in figure 4.13 (figure 2 of CEBECI and KELLER 1971, with additions; see also figure 2 of LAINE and RINEHART 1984). 271

- 4.18 Approach of Falkner-Skan solutions to the starred wall-jet limit ($\beta = -2$, $f''(0) = \infty$) along the first Libby-Liu branch in figure 4.13 (figure 1 of STEINHEUER 1968, with additions). 273
- 4.19 Approach to Falkner-Skan solutions to the starred plane-jet limit ($\beta = -1$, $f''(0) = -1.086376$) along the second Libby-Liu branch in figure 4.13 (figure 4 of BRAUNER, LAINE, and NICOLAENKO 1982, with additions). 276
- 4.20 Failure of the momentum-integral equation for the data obtained by LUDWIEG and TILLMANN (1949) in their flow with strong pressure rise. The open circles are from the heated element (private communication). The filled circles are from the momentum-integral equation, and the crosses are from the profile fit, both according to COLES (1968) (figure missing). 281
- 4.21 Thwaites variables for the Falkner-Skan flows. 286
- 4.22 The classical Falkner-Skan family of solutions in Thwaites variables. The cusp at the left corresponds to separation ($\beta = -0.1988$). The origin corresponds to a shear layer ($\beta = 0$). The limit point at the right corresponds to sink flow ($\beta = \infty$). 287
- 4.23 Some proposals for eliminating the discontinuity in slope at $y = \delta$ in the wall law. Note the displaced scales. The illustrations are for a boundary layer with $\delta^+ = \delta u_\tau / \nu = 2000$. The upper display shows the cubic correction according to equation (4.256) and the quartic correction according to equation (4.258). The lower display shows the interpolation scheme of SANDHAM (1991) for several values of the parameter n in equation (4.266). 297
- 4.24 The sheared source-flow model corresponding to Prandtl's law of the wall. 304
- 4.25 The source-flow model for a free stream with a positive pressure gradient. 307

4.26	An attempt to fit Nikuradse's turbulent boundary-layer profile using the standard wall-wake formula.	308
4.27	A geometric interpretation of the two profile parameters D and P . The product $P\delta$ is rigorously defined, but the parameters P and δ separately are not.	310
4.28	The mean flow field for sink flow or pure wall flow (figure 5.40 of HAFEZ 1991). The variable x has the right direction but the wrong sense.	316
4.29	Analytical profiles of mean velocity and total shearing stress in pure wall flow at $\delta^+ = 10^3, 10^6, 10^9$ according to equations () and (). The data points are from SPALART ().	318
4.30	The definition of the entrainment velocity s with expanded vertical scale. Note that δ must be defined.	333
4.31	Decomposition of the wall-wake profile to show the characteristic velocity scale $\mathcal{L} = 1 - \Pi u_\tau / \kappa u_\infty$ that occurs in equation (4.388) for entrainment. [Note written corrections to add 2 to one coefficient and that k should be κ and u_i should be u_∞ . - K. Coles]	334
8.1	Caption for Figure with label Fig15-7 (missing)	375
8.2	Caption for Figure with label Fig15-6 (missing)	376
8.3	Caption for Figure with label Fig15-8 (missing)	381
9.1	A schematic representation of the laminar plane jet out of a vertical wall. J is the rate of momentum flux per unit span.	408
9.2	Visualization, using smoke filaments, of flow through a monoplane grid of cylindrical rods. The blockage is large enough to excite an entrainment instability (figure 3, plate 1, of Bradshaw 1965). Photograph courtesy of Cambridge University Press.	410

9.3 The final step of a similarity argument based on an affine transformation. For the example in the text, the curve on the right is $\hat{y} \sim \hat{x}^{2/3}$ 417

9.4 Streamlines $\Psi = \text{constant}$ of the boundary-layer approximation for the laminar plane jet according to equation (9.52). The range of Ψ is -9 (1) 9 422

9.5 Graphical definition of the maximum-slope thickness η_s for the laminar plane jet. 426

9.6 Graphical definition of the half-integral scale η_i for the laminar plane jet, on the right, and the half-width η_c for the osculating parabola, on the left. 426

9.7 The solid lines show the boundary-layer solution $f(\eta)$ and $f'(\eta)$ for the laminar plane jet according to equations (9.72) and (9.73). The dashed lines show the two-term composite solution according to equations (9.113)–(9.116) with $X = 1000$ 429

9.8 Conformal mapping of the outer flow for the upper half of a plane jet. The flow is symmetrical about the x -axis, which is a branch cut. There are upstream walls in the physical plane at an angle $\pm\sigma$ to the x -axis (see equation (9.96)). Note the preservation of angles. 433

9.9 Streamlines $\Psi_o = \text{constant}$ in the outer potential flow of a laminar plane jet out of a wall along the y axis, according to equation (9.103). The range of Ψ is -9 (1) 9 436

9.10 Composite streamlines $\Psi_c = \text{constant}$ for a laminar plane jet with a wall along the y axis, according to equation (9.107) with $\sigma = \pi/2$. The range of Ψ is -8 (1) 8 438

9.11 Composite streamlines $\Psi_c = \text{constant}$ for a laminar plane jet with a wall along the negative x axis according to equation (9.107) with $\sigma = \pi$. The range of Ψ is -9 (1) 9 439

9.12	Exploratory view of streamlines near the stagnation point that appears at $X = 0.1925$ in the composite expansion of a plane laminar jet out of a vertical wall. The streamlines are not equally spaced in Ψ . This curious result is not real; it is an artifact created by use of the boundary approximation at low Reynolds number.	441
9.13	Elements of the linearized jet flap.	475
9.14	Detail of the flow near the jet.	476
10.1	Schematic connection between the laminar plane free jet and wall jet.	502
10.2	Streamlines of the boundary-layer model for the laminar plane wall jet according to equation (10.71). The range of.....	517
10.3	Mapping of the outer entrained flow for the laminar plane wall jet.	521
10.4	Streamlines $\Psi = \text{constant}$ of the composite model for the laminar plane wall jet into a stagnant fluid according to equation (10.103).	523
11.1	Steady laminar plane plume. (Caption provided by B. Coles)	535
12.1	Flow through a screen. (Figure and caption added by K. Coles.)	552
12.2	Flow in a channel modified by a single shaped screen. (Figure and caption added by K. Coles.)	560
A.1	Caption for Figure with label 7.40 (figure on p. 54 of COLES 1962).	572
A.2	Caption for Figure with label 7.41 (figures 10 and 11 on p. 56 of COLES 1962).	573

A.3 Caption for Figure with label 7.43 (figures 12 and 13
on p. 58 of COLES 1962). 573

Preface

AUTHOR'S DRAFT PREFACE

This section was found in an early draft of this monograph. While it was not revised after the author added much of the content of this work, we include it as it conveys his motivation and approach.

– K. Coles

Even limited exposure to industrial problems involving fluid mechanics shows that there is a pervasive need for a comprehensive, critical compilation of empirical knowledge in the field of turbulent shear flow. The enormous experimental literature published during the last fifty years, literally thousands of papers, is still mostly undigested. This literature is generated in governmental and industrial research laboratories and in university departments of aeronautical, chemical, civil, environmental, and mechanical engineering at institutions all over the world. There are also important applications in ocean engineering, vehicle and building aerodynamics, dynamic meteorology and physical oceanography, and even in planetary physics and astrophysics.

With industrial problems in mind, Anatol Roshko and I have developed over the past 20 years a graduate course in aeronautics at Caltech called “Technical Fluid Mechanics.” The emphasis is strongly on turbulent shear flow. The course is normally given every year and is well attended. It draws graduate students from several engineering options other than aeronautics and is also open to se-

lected undergraduates who have had at least a first course in fluid mechanics.

For various reasons, none of the existing monographs that might be consulted by engineers or used as textbooks in advanced engineering courses on turbulent flow is a satisfactory reference for such a course. The most common defect is a lack of adequate experimental content. When I took the decision in 1986 to write this monograph, much of the lecture material for the course had already been laboriously collected from the experimental literature, although without much critical compilation or comparison of data from different sources. Nevertheless, a large part of the necessary bibliographical preparation and interpretation of data had been carried out, and a solid foundation for a monograph on technical fluid mechanics did exist. To produce this book has involved a substantial commitment for several years, once adequate support was obtained for assembling and collating experimental data.

The fundamental premise for the book is that the only reliable information about turbulent flow is experimental information. This varies greatly in quality and completeness, and needs to be carefully screened. Some additional premises will be self-evident in the text. First, it is advisable to understand thoroughly the laminar version of a particular flow, because some conceptual problems are not peculiar to turbulent flow; e.g., the third boundary condition for the mixing layer, or the integral invariant for the wall jet. Second, the most powerful organizing principle so far available for both laminar and turbulent flow is the principle of similarity. Third, the most important phenomenological concept for many turbulent flows is the concept of entrainment. The need of the user is often likely to be for hard numbers and practical insights, rather than for elegance. I have therefore made some use of mixing-length and eddy-viscosity ideas, and even power-law methods, as primitive links between fundamental and technical problems.

Each chapter of the book deals with one of the classical shear flows (mixing layers, jets, plumes, wakes, boundary layers, pipe flow, and so on) and with its ramifications, or with an important technical problem such as flow management. Wherever possible, the presen-

tation is intended to suggest how various flow problems might be connected analytically and experimentally one to another, using as far as possible a consistent notation and a consistent level of rigor and detail.

In practically all cases, I have organized and presented the data in the language of the Reynolds-averaged equations of motion, since there is general agreement that these equations, although incomplete, are at least correct. The important areas of turbulence modeling and numerical simulation are served indirectly, by extensive documentation of the experimental facts that modeling and simulation attempt to reproduce. I have made every effort to ensure that the material of the monograph will not quickly become dated. The rapidly evolving subject of coherent structure is therefore discussed only in cases where the Reynolds-averaged equations clearly do not suffice for describing the phenomenology of particular turbulent flows. An example is the sublayer of a turbulent flow near a smooth wall.

Finally, I found it essential to limit the objectives of the book. Combustion is not discussed. Neither is the very large subject of compressibility, including aerodynamic noise. Transition is viewed primarily from the turbulent side, with the elements of randomness and three-dimensionality already present. Effects of body forces associated with buoyancy or curvature are discussed, but not in the context of the classical Benard or Couette flows. Grid turbulence is mentioned mainly in connection with flow management. Instrumentation and experimental techniques are discussed mainly in connection with questions of good experimental practice.

The list of references cited in this monograph is extensive but not exhaustive. The list is most complete when my objective is to assemble and compare the experimental evidence on some special topic. In the face of a large volume of material, my task has been made easier by the evolution of the scientific literature from archival journals to abstract journals to survey and review volumes. I have made heavy use of Science Citation Index and of the surveys that are a common component of Ph.D. theses. I have also used the series of unpublished reports prepared by various groups of experts for the second (1980-1981) Stanford conference on computation of turbulent

flow. Finally, I have taken the time to study most of the original papers that have laid the foundations of fluid mechanics since the middle of the 19th century. This study changed my ideas about the way that classical contributions to mechanics have been introduced and developed. It also influenced this monograph in a way that I hope will be seen as respect for the uses of the past.

In a real sense, the part of fluid mechanics treated in this monograph is a mature subject. A histogram in time constructed for the references cited here shows that paper production is level or decreasing. A reasonable inference is that the classical turbulent shear flows are thought, rightly or wrongly, to be under good control. Activity is shifting to study of coherent structure and to exploitation of the power of large computing machines. Another area developing slowly but promising important contributions is the relationship of turbulence to dynamical systems theory. I hope that this monograph will be useful in support of these efforts as well as in solution of engineering problems.

D.C.
(July 1995)

EDITOR'S NOTE

The pages that follow represent an attempt to reconstruct the unfinished book left by Donald Coles at his death in May of 2013. Combining a large number of computer files, drafts and printouts of figures, and various scraps of manuscript and lecture notes has proven challenging. In places internal clues indicate the intent of the author the last time he reviewed or revised a section. The editing was done between late 2013 and the present by myself and Betsy Coles, who also assembled and updated the computer files.

Don Coles often said he wanted to write this work, and over twenty years ago he began writing to colleagues requesting original experimental data so he could replot them in a uniform way. The task of creating the plots for figures, with the help of assistants he

hired, occupied the great majority of time and effort in the author's later years. His intention to complete the figures before turning his attention to revising the respective chapters accounts for the fragmentary state of parts of the text.

The working title was "Topics in turbulent shear flow." We shortened this title at the suggestion of Prof. Anatol Roshko, who pointed out that the author treats laminar flow, typically at length, before considering corresponding turbulent flows. We did not track down many of the references to unspecified sections or figures elsewhere in the work; some were never created or have not been found.

The manuscript used arbitrary chapter numbers. Some references (e.g., to missing figures) use these old numbers rather than the consecutive chapter numbers of this edition. The author's typographic conventions, which we have followed where possible, include:

CAPITALS: Names of cited or referenced authors; numbered figures and tables; cited sections of this work.

Boldface: Notes to self, such as items to check or add.

Italic: Early draft or tentative material; longer notes about topics to be covered or material to be included.

Clearly the work is incomplete. Some figures and text may yet turn up in paper files, amounting to 50 to 75 cubic feet, that survive. While it is my intent to survey these, it does not make sense to delay publication of this work in the name of what will be a lengthy process that may add little. Similarly, we have not attempted to reconstruct a bibliography of the numerous literature references. We would be happy to hear from anyone who cares to compile any of these or who can suggest errors, omissions, or possible alternate readings of the text to include in a future edition. In the words of Anatol Roshko, "It pained [Don] to see anything not done absolutely as well as it could possibly be done." He would be frustrated that this work appears in less than complete and correct form. Nevertheless, we suspect it still contains much that may be useful and chose to share what we have. It is time for others to pursue the ideas that lie herein. We simply ask that those who make use of this work credit it by citation in the usual and customary manner of scholars.

We owe thanks to many. Over the years Don Coles was assisted by a number of people. We do not have all their names, but they included Dr. Paul Schatzle, Dr. Misha Pesenson, Dr. Gregory Cardell, Jim Edberg, and Evan Coles-Harris. Prof. Emeritus Anatol Roshko (Caltech) and Prof. Hassan Nagib (Illinois Tech) gave helpful input and suggestions. While no dedication survives, we do not need that evidence to know to whom Don Coles would have dedicated this book: Ellen Coles, the lifelong companion who assisted him with everything he wrote.

Ken Coles
Indiana, Pennsylvania
November 2017

Chapter 1

INTRODUCTION

1.1 Generalities

The subject of turbulent shear flow is not simply connected. Some organization is essential, and I have tried to arrange that material required in a particular discussion appears earlier in the text. Thus pipe flow is discussed first because it provides the best evidence for the existence and value of Karman's two constants in Prandtl's law of the wall. It might seem easier to begin with the simpler topic of free shear flows, such as the plane jet. However, there is then a difficulty with the natural progression to wall jets, impinging jets, and other topics that require experience with Karman's constants. The main advantage of pipe flow is that the magnitude of the wall friction in fully developed flow can be obtained unambiguously from the pressure gradient, although a preliminary study is needed to determine what conditions guarantee that a given pipe flow is axially symmetric and fully developed.

It is an accepted axiom in basic research on the classical turbulent shear flows, elegantly expressed by NARASIMHA (1984), that there exists in each case a unique equilibrium state that can be realized in different experiments and thus made the basis of a general synthesis of empirical knowledge. The equilibrium may be stationary (as in pipe or channel flow) or dynamic or developing (as in the

plane jet, the boundary layer, and most other flows). This axiom will be tested repeatedly in various parts of this monograph, usually by an emphasis on similarity laws, an emphasis that generates its own problems. There are no widely accepted similarity laws for several important turbulent flows, including boundary-layer flows with compressibility, mass transfer, heat transfer, or lateral or longitudinal curvature. Other difficult cases are the wall jet and the three-dimensional boundary layer. Because most of these problems involve walls, some attention is paid to the issue of the behavior of various mean quantities in turbulent flow near a wall. For example, there was at one time some ambiguity in the literature about the leading term in the expansion for the Reynolds shearing stress $-\rho\overline{u'v'}$. This leading term has sometimes been identified as a term in y^3 , and sometimes as a term in y^4 (see HINZE 19XX, p. 621; SPALDING 1981). In fact, a rigorous argument is analytically straightforward, and generalizations that take into account changes in coordinates and boundary conditions may eventually shed some light on the nature of the proper similarity variables for some of the flows just mentioned. Experimental evidence for the magnitude of the first few coefficients is unreliable, but these coefficients can sometimes be estimated from numerical work on solutions of the full Navier-Stokes equations for flow in channels and boundary layers. There is a clear and present need for detail here when choosing boundary conditions for large-eddy simulations.

It is remarkable that one of the ostensibly most difficult problems in fluid mechanics, the problem of surface roughness, should be in a relatively comfortable state. Missing are sound methods for characterizing roughness. It is also remarkable that an apparently unrelated problem, the flow of a dilute solution of a high-molecular-weight polymer, exhibits properties that might be more easily understood if there were such a thing as negative roughness. Although expectations are not high, the prospect of finding possible connections in the transport mechanisms for these two problems is certainly worth some effort.

A topic that involves the mechanisms of turbulence in an essential way is the problem of relaxation, especially from one classical

flow to another. One example is the strong plane jet into a moving fluid ($\delta \sim x$), with a final state describable by a linearized analysis ($\delta \sim x^{1/2}$). The round jet into a moving fluid has an equivalent behavior. Another example is the turbulent boundary layer on a finite flat plate ($\delta \sim x^{4/5}$) which relaxes downstream from the trailing edge to a plane wake ($\delta \sim x^{1/2}$). Several experimental studies exist of pipe, channel, or boundary-layer flows during a smooth-rough or rough-smooth transition of the wall boundary condition. Another instructive case is relaxation of a rectangular wake or jet to a round one. Such flows often overshoot the final state at least once. Finally, there are several flows with initially variable density that relax toward constant density as mixing proceeds. These include jets into a different medium, as well as plumes with finite initial momentum. A global view of these problems may lead to useful inferences about characteristic scales in time or space. The list of issues mentioned here is not intended to be comprehensive, but only to suggest various approaches that may or may not be productive in the future, given the fact that insight cannot be programmed.

It is also relevant that papers on models and mechanisms of turbulence tend to cite a limited standard set of experimental papers (these papers are sometimes different from one discipline to another). Endorsement by repetition often fails to present the best evidence. A positive development is that survey papers on various topics in turbulent shear flow are an increasingly important component of the contemporary literature. In a smaller setting, such surveys are also a common ingredient in Ph.D. theses although most of these latter surveys are not as critical as they could be. In any event, all of this material is a valuable resource for this monograph.

Sources of information about turbulent flow exist on several levels. In decreasing order of authority, I distinguish

1. the laws of mechanics
2. expert measurements (or numerical simulations)
3. insight
4. peripheral vision
5. brute force.

In what follows I will emphasize the first three levels of information. By “the laws of mechanics” I mean the Navier-Stokes equations and their boundary conditions. The question of “expert measurements” is more subjective. In any survey of experimental data, it is necessary somehow to assign a degree of confidence to each particular measurement. If the measurement has been made many times by different observers, like the pressure drop in a pipe, this is fairly easy to do. But if the measurement has been made only a few times, or even only once, judgment has to be backed by experience. “Insight” tends to be rare. Instances occur at intervals typically measured in years. The problem is then to pick signal out of noise in the literature, and the turbulence community is reasonably effective at doing so. An example of “peripheral vision” is the use of power laws that are not intrinsic, such as in Bradshaw’s treatment of equilibrium turbulent boundary layers. What I hope to establish in this book is a set of ideas, chosen according to criteria defined by evidence rather than by faith or tradition. I will try to avoid the last level, “brute force,” except when I am obliged to live up to the claim that part of my purpose is to deal with technical problems.¹

Two constraints dominate the whole subject of turbulent shear flow at the contemporary stage of development. One is the boundary-layer approximation and the other is the idea of Reynolds stresses. I will almost always be considering incompressible fluids in the sense that variations in density are caused by variations in temperature, not by high velocity, and are important mainly because of associated body forces in a gravitational field.

¹*The following two paragraphs appeared at this point in the 1997 draft of this work:*

The notation of this monograph tends toward usage in aeronautical engineering. I have tried to use mnemonic notation where this is possible, and I have therefore avoided arbitrary use of Greek symbols except where these are firmly established in the literature.

The literature in Russian is not well represented, primarily because the text is usually terse, the figures small, and tables nonexistent. The Russian subliteration — institute reports and theses — is not accessible at all.

1.2 Analytical prologue

1.2.1 Definitions and identities

Effects of compressibility are deliberately not emphasized in this monograph. However, effects of buoyant body forces and of heat transfer at walls are considered, so that the density of the fluid cannot always be taken as constant. In particular, I want to comment on something called the BOUSSINESQ approximation (1903), which I believe is not always well presented in the engineering literature. I will therefore outline briefly the structure of the Navier-Stokes equations for a compressible fluid and consider the limiting form of these equations, first as the Mach number approaches zero, and then as the Froude number approaches zero.

The first part of the discussion, and the notation, are taken from the classical article by LAGERSTROM (1964, 1996) in Volume IV of the Princeton handbook series. Many details are omitted here that can be found in Lagerstrom's article. The main reason for this choice of model is that the compact notation of vector calculus, with an appropriate generalization to operations on tensors, allows easy manipulations whose results are independent of any particular coordinate system.

A number of definitions and identities will be used in this and later sections of this monograph. In what follows an arrow over a symbol indicates a vector, and an underline indicates a tensor.

Some definitions from vector geometry and vector calculus, with generalizations, include the divergence of a vector,

$$\iiint \operatorname{div} \vec{a} \, dV = \iint \vec{a} \cdot \vec{n} \, dS \quad , \quad (1.1)$$

where V is a stationary control volume bounded by a surface S , and \vec{n} is the unit outward normal.

The divergence of a tensor is defined similarly,

$$\iiint \operatorname{div} \underline{A} \, dV = \iint \underline{A} \vec{n} \, dS \quad , \quad (1.2)$$

where $\underline{A}\vec{n}$ is a multiplication defined by $(\underline{A}\vec{n})_i = A_{ij}n_j$.

The gradient of a scalar is

$$\text{grad } \alpha \cdot d\vec{x} = d\alpha \quad (1.3)$$

and of a vector is

$$(\text{grad } \vec{a}) d\vec{x} = d\vec{a} \quad (1.4)$$

The dyadic product of two vectors is

$$(\vec{a} \circ \vec{b})\vec{c} = \vec{a}(\vec{b} \cdot \vec{c}) \quad \vec{c} \text{ arbitrary} \quad (1.5)$$

The deformation tensor is symmetric;

$$\text{def } \vec{a} = \underline{\text{grad } \vec{a}} + (\underline{\text{grad } \vec{a}})^* \quad (1.6)$$

where $*$ means the transpose. The corresponding antisymmetric tensor defines the curl operator;

$$(\text{curl } \vec{a}) \times \vec{b} = [\underline{\text{grad } \vec{a}} - (\underline{\text{grad } \vec{a}})^*] \vec{b}, \quad \vec{b} \text{ arbitrary} \quad (1.7)$$

The substantial derivative of a scalar is

$$\frac{D\alpha}{Dt} = \frac{\partial\alpha}{\partial t} + \text{grad } \alpha \cdot \vec{u} \quad (1.8)$$

and of a vector is

$$\frac{D\vec{a}}{Dt} = \frac{\partial\vec{a}}{\partial t} + (\underline{\text{grad } \vec{a}}) \vec{u} \quad (1.9)$$

The identity tensor \underline{I} is defined by

$$\underline{I}\vec{a} = \vec{a} \quad (1.10)$$

and the scalar product of two tensors by

$$\underline{A} \cdot \underline{B} = \sum_{i,j} A_{ij} B_{ij} \quad (1.11)$$

Various identities are also useful. These are written here in a form independent of the choice of coordinates, and are easily verified in any convenient orthogonal coordinate system, say rectangular;

$$\text{div } (\alpha\vec{a}) = \alpha \text{ div } \vec{a} + \vec{a} \cdot \text{grad } \alpha \quad (1.12)$$

$$\operatorname{div}(\alpha \underline{I}) = \operatorname{grad} \alpha ; \quad (1.13)$$

$$\operatorname{div} \operatorname{curl} \vec{a} = 0 ; \quad (1.14)$$

$$\operatorname{div}(\vec{a} \circ \vec{b}) = (\operatorname{grad} \vec{a}) \vec{b} + (\operatorname{div} \vec{b}) \vec{a} ; \quad (1.15)$$

$$\operatorname{div}(\underline{A} \vec{a}) = (\operatorname{div} \underline{A}^*) \cdot \vec{a} + \underline{A}^* \cdot \operatorname{grad} \vec{a} ; \quad (1.16)$$

$$\operatorname{div}(\vec{a} \times \vec{b}) = \vec{a} \cdot \operatorname{curl} \vec{b} - \vec{b} \cdot \operatorname{curl} \vec{a} ; \quad (1.17)$$

$$\operatorname{div}(\operatorname{grad} \vec{a})^* = \operatorname{grad}(\operatorname{div} \vec{a}) ; \quad (1.18)$$

$$\operatorname{curl}(\operatorname{grad} \alpha) = 0 ; \quad (1.19)$$

$$\operatorname{curl}(\alpha \vec{a}) = \alpha \operatorname{curl} \vec{a} + (\operatorname{grad} \alpha) \times \vec{a} ; \quad (1.20)$$

$$\operatorname{curl}(\vec{a} \times \vec{b}) = \operatorname{div} \left[(\vec{a} \circ \vec{b}) - (\vec{b} \circ \vec{a}) \right] ; \quad (1.21)$$

$$(\underline{A} \vec{a}) \cdot \vec{b} = (\underline{A} \vec{b}) \cdot \vec{a} , \quad \underline{A} \text{ symmetric} ; \quad (1.22)$$

$$\vec{a} \times (\vec{b} \times \vec{c}) = \vec{b}(\vec{a} \cdot \vec{c}) - \vec{c}(\vec{a} \cdot \vec{b}) ; \quad (1.23)$$

$$(\operatorname{grad} \vec{a}) \vec{a} = \operatorname{grad} \frac{a^2}{2} + (\operatorname{curl} \vec{a}) \times \vec{a} , \quad \alpha^2 = \vec{a} \cdot \vec{a} . \quad (1.24)$$

The three relations (1.19), (1.14), and (1.1) might be considered the basis of a *carpe diem* school of mechanics. See a gradient, take the curl. See a curl, take the divergence. See a divergence, integrate over a control volume.

1.2.2 Equations of motion

Mass. I have grown up with a derivation of the Navier-Stokes equations of motion using the device of a stationary control volume. Conservation of mass is expressed with complete clarity by the relation

$$\frac{d}{dt} \iiint \rho dV = - \iint \rho \vec{u} \cdot \vec{n} dS , \quad (1.25)$$

where ρ is density, \vec{u} is velocity, and dV and dS are elements of volume and surface, respectively. The negative sign on the right-hand side is required by the convention that \vec{n} is the unit outward normal to the surface of the control volume. No provision is ordinarily made

for sources or sinks within the control volume. If these are needed, they can be added at an appropriate later stage. With the aid of the definition (1.1) for divergence, equation (1.25) can be rewritten in terms of volume integrals only;

$$\iiint \left(\frac{\partial \rho}{\partial t} + \operatorname{div} \rho \vec{u} \right) dV = 0 . \quad (1.26)$$

Because the control volume is arbitrary, the integrand must be zero everywhere. Conservation of mass therefore requires

$$\frac{\partial \rho}{\partial t} + \operatorname{div} \rho \vec{u} = 0 . \quad (1.27)$$

A different form is obtained by use of the vector identity (1.12);

$$\frac{\partial \rho}{\partial t} + \vec{u} \cdot \operatorname{grad} \rho + \rho \operatorname{div} \vec{u} = 0 . \quad (1.28)$$

The first two terms are now a rate of change of density following an element of the fluid, already defined by equation (1.8). A final form for the continuity equation is therefore

$$\frac{D\rho}{Dt} + \rho \operatorname{div} \vec{u} = 0 . \quad (1.29)$$

Momentum. Conservation of momentum is expressed in the same simple terms by

$$\begin{aligned} \frac{d}{dt} \iiint \rho \vec{u} dV = & - \iint \rho \vec{u} (\vec{u} \cdot \vec{n}) dS + \\ & + \iiint \rho \vec{F} dV + \iint \underline{\sigma} \vec{n} dS . \end{aligned} \quad (1.30)$$

The term on the left is the time rate of change of the vector momentum within the control volume. The first term on the right is flux of momentum through the boundary, with a negative sign for the same reason given earlier. In this term the velocity \vec{u} appears twice in different roles. The first is as vector momentum per unit mass. The second is as volume flux per unit area per unit time. I consider the distinction to be important and will maintain it throughout this

monograph. The quantity \vec{F} is an internal body force per unit mass, usually due to gravity. The surface stress $\underline{\sigma}$ is a tensor, or linear vector operator, with $\underline{\sigma} \vec{n}$ the vector force per unit area on the boundary of the control volume.

Two steps are required to obtain a differential equation. The first step introduces the dyadic product of two vectors, $(\vec{a} \circ \vec{b})$, defined by equation (1.5) with $\vec{a} = \rho \vec{u}$, $\vec{b} = \vec{u}$, and $\vec{c} = \vec{n}$. The second step introduces the generalized divergence of a tensor by use of equation (1.2). With these relationships, equation (1.30) can be written in terms of volume integrals only²;

$$\iiint \left(\frac{\partial \rho \vec{u}}{\partial t} + \text{div } \rho (\underline{\tilde{u}} \circ \underline{\tilde{u}}) - \rho \vec{F} - \text{div } \underline{\sigma} \right) dV = 0 . \quad (1.31)$$

Since the control volume is arbitrary, it follows that

$$\frac{\partial \rho \vec{u}}{\partial t} + \text{div } \rho (\underline{\tilde{u}} \circ \underline{\tilde{u}}) = \rho \vec{F} + \text{div } \underline{\sigma} \quad (1.32)$$

everywhere.

This form for the transport terms is well suited for the introduction of what are called Reynolds stresses in turbulent flow. It is also the most useful form when the objective is to derive integral laws (such as Karman's momentum integral) from the differential equations, because the volume integral of a divergence usually begins life as the surface integral of a flux. It is therefore often convenient to return to the control volume for this operation.

Another form for the transport terms follows from the identity (1.15) with $\vec{a} = \vec{u}$, $\vec{b} = \rho \vec{u}$, so that

$$\text{div } \rho (\underline{\tilde{u}} \circ \underline{\tilde{u}}) = \rho (\underline{\text{grad}} \vec{u}) \vec{u} + \vec{u} \text{div } \rho \vec{u} . \quad (1.33)$$

Now the momentum equation (1.32) takes the form

$$\rho \frac{\partial \vec{u}}{\partial t} + \vec{u} \frac{\partial \rho}{\partial t} + \vec{u} \text{div } \rho \vec{u} + \rho (\underline{\text{grad}} \vec{u}) \vec{u} = \rho \vec{F} + \text{div } \underline{\sigma} . \quad (1.34)$$

²The tilde notation is not defined here but section 2.1.2 states, "[T]he tilde, here and elsewhere, is intended as a mnemonic for an integral mean value."

The second and third terms drop out, by virtue of the continuity equation (1.27), leaving

$$\rho \left[\frac{\partial \vec{u}}{\partial t} + (\underline{\text{grad}} \vec{u}) \vec{u} \right] = \rho \vec{F} + \text{div} \underline{\sigma} . \quad (1.35)$$

The quantity in brackets on the left is the substantial derivative (1.9) (the derivative following a fluid element) of the vector \vec{u} , so that finally

$$\rho \frac{D\vec{u}}{Dt} = \rho \vec{F} + \text{div} \underline{\sigma} . \quad (1.36)$$

This equation may also have explicit source or sink terms for momentum, although these are usually left in implicit form. A notation sometimes used in equation (1.36) is

$$\frac{D\vec{u}}{Dt} = \frac{\partial \vec{u}}{\partial t} + (\vec{u} \cdot \text{grad}) \vec{u} . \quad (1.37)$$

I think that this notation might be misleading in any coordinate system except a rectangular one.

The body force \vec{F} will normally be a gravity force, $\vec{F} = -g\vec{i}_y$, where \vec{i}_y is a unit vector directed vertically upward. It might also be a local force expressed as a Dirac δ -function to represent a concentrated source or sink of momentum; e.g., thrust or drag. For a Newtonian fluid, the tensor $\underline{\sigma}$ is symmetric, isotropic, and linear in the spatial first derivatives of the velocity. The most general form meeting these conditions is (cite Jeffries, Stefan)

$$\underline{\sigma} = -p \underline{I} + \lambda \text{div} \vec{u} \underline{I} + \mu \underline{\text{def}} \vec{u} = -p \underline{I} + \underline{\tau} , \quad (1.38)$$

where \underline{I} is the identity tensor, defined by $\underline{I}\vec{a} = \vec{a}$, and where

$$\underline{\tau} = \lambda \text{div} \vec{u} \underline{I} + \mu \underline{\text{def}} \vec{u} . \quad (1.39)$$

The stress tensor $\underline{\tau}$ thus involves two viscosities, λ and μ , of which the first is immaterial if $\text{div} \vec{u} = 0$. In this formulation the three state variables p , μ , λ are introduced in a single operation and are not conceptually different.

With the aid of the identity (1.13) with $\alpha = p$, the momentum equation can be written finally as

$$\rho \frac{D\vec{u}}{Dt} = -\text{grad } p + \rho\vec{F} + \text{div } \underline{\tau} . \quad (1.40)$$

Energy. A law for conservation of energy can be derived from first principles by visualizing a molecular structure for the fluid, although the result is often classified as part of continuum mechanics. Hard spherical molecules in a state of agitation have two kinds of energy: internal kinetic energy e , associated with random motion and represented as temperature, and directed or organized motion $\vec{u} \cdot \vec{u}/2$ associated with bulk velocity. Energy can be added or subtracted in the interior of a control volume by at least two processes. One is heat release Q per unit mass by chemical reactions, including phase changes such as evaporation and condensation. The other is work done by body forces $\vec{u} \cdot \vec{F}$. Energy can also be transferred at the boundary of a control volume by heat conduction \vec{q} and by work done by surface forces $\underline{\sigma}$. The latter two processes will appear as divergence terms and are neutral in the interior of the control volume. Thus write

$$\begin{aligned} \frac{d}{dt} \iiint \rho \left(e + \frac{u^2}{2} \right) dV &= - \iint \rho \left(e + \frac{u^2}{2} \right) \vec{u} \cdot \vec{n} dS + \\ &+ \iiint \rho Q dV + \iiint \vec{u} \cdot \vec{F} dV - \\ &- \iint \vec{q} \cdot \vec{n} dS + \iint (\underline{\sigma} \vec{n}) \cdot \vec{u} dS \end{aligned} \quad (1.41)$$

where $u^2 = \vec{u} \cdot \vec{u}$. The three surface integrals can be converted to volume integrals using equations (1.1) and (1.2), with the result, after use of the identity (1.22) in the last term,

$$\frac{\partial}{\partial t} \rho \left(e + \frac{u^2}{2} \right) + \text{div} \rho \left(e + \frac{u^2}{2} \right) \vec{u} = \rho Q + \vec{u} \cdot \vec{F} - \text{div } \vec{q} + \text{div}(\underline{\sigma} \vec{u}) . \quad (1.42)$$

The first two terms can be modified by differentiating the second term as a product and using the continuity equation (1.27). The last term can be modified using equation (1.38) for $\underline{\sigma}$ and the identity (1.10). Finally, with the definition (1.8) for the derivative of a scalar following a fluid element, there is obtained

$$\rho \frac{D}{Dt} \left(e + \frac{u^2}{2} \right) = \rho Q - \text{div } \vec{q} + \vec{u} \cdot \vec{F} - \text{div } p\vec{u} + \text{div } \underline{\tau} \vec{u} . \quad (1.43)$$

For a Fourierian fluid, the heat conduction vector is linear in the spatial first derivatives of the temperature,

$$\vec{q} = -k \text{ grad } T , \quad (1.44)$$

with a scalar heat conductivity k . The negative sign indicates that energy is transferred down the temperature gradient.

There is also available a mechanical energy equation, derived independently of the thermodynamic equation (1.43) by taking the scalar product of the momentum equation (1.40) with the vector velocity \vec{u} to obtain

$$\rho \frac{Du^2/2}{Dt} = -\vec{u} \cdot \text{grad } p + \vec{u} \cdot \vec{F} + \vec{u} \cdot \text{div } \underline{\tau} . \quad (1.45)$$

Equations (1.43) and (1.45) and an obvious formula for $D(p/\rho)/Dt$ lead, with the aid of the identity (1.16), to the array of energy equations displayed in TABLE 1.1. The scalar product of two tensors is defined by the identity $\underline{A} \cdot \underline{B} = A_{ij}B_{ij}$ (summed over i and j).

The middle three equations, the last three, and the first three (the equation for h is listed twice) form natural groups that describe the evolution of the quantities e and $u^2/2$ and their sum in equation (1.43), and the evolution of the terms appearing in the definitions for static and stagnation enthalpy,

$$h = e + \frac{p}{\rho} \quad (1.46)$$

and

$$h_0 = h + \frac{u^2}{2} . \quad (1.47)$$

Table 1.1
Energy equations

$$\begin{array}{rcl}
 \rho \frac{D}{Dt} h = \frac{\partial p}{\partial t} + \rho Q & & - \operatorname{div} \vec{q} + \underline{\tau} \cdot \underline{\operatorname{grad}} \vec{u} + \vec{u} \cdot \operatorname{grad} p \\
 & & \uparrow \\
 \rho \frac{D}{Dt} h_0 = \frac{\partial p}{\partial t} + \rho Q + \rho \vec{F} \cdot \vec{u} - \operatorname{div} \vec{q} + \operatorname{div} (\underline{\tau} \vec{u}) & & \\
 & & \downarrow \\
 \rho \frac{D}{Dt} \frac{u^2}{2} = & \rho \vec{F} \cdot \vec{u} & + \vec{u} \cdot \operatorname{div} \underline{\tau} - \vec{u} \cdot \operatorname{grad} p \\
 & & \uparrow \qquad \qquad \uparrow \\
 \rho \frac{D}{Dt} \left(e + \frac{u^2}{2} \right) = & \rho Q + \rho \vec{F} \cdot \vec{u} - \operatorname{div} \vec{q} + \operatorname{div} (\underline{\tau} \vec{u}) & - \operatorname{div} (p \vec{u}) \\
 & & \downarrow \qquad \qquad \downarrow \\
 \rho \frac{D}{Dt} e = & \rho Q & - \operatorname{div} \vec{q} + \underline{\tau} \cdot \underline{\operatorname{grad}} \vec{u} - p \operatorname{div} \vec{u} \\
 & & \uparrow \\
 \rho \frac{D}{Dt} h = \frac{\partial p}{\partial t} + \rho Q & & - \operatorname{div} \vec{q} + \underline{\tau} \cdot \underline{\operatorname{grad}} \vec{u} + \vec{u} \cdot \operatorname{grad} p \\
 & & \downarrow \\
 \rho \frac{D}{Dt} \frac{p}{\rho} = \frac{\partial p}{\partial t} & & + \operatorname{div} (p \vec{u})
 \end{array}$$

So far the nature of the fluid is left open. In this monograph the fluid will be either an ordinary liquid or a thermally perfect gas with an equation of state

$$p = \rho RT . \quad (1.48)$$

The gas will also be assumed to be calorically perfect; that is, the specific heats c_p and c_v will be taken as constant in the definitions

$$e = c_v T ; \quad (1.49)$$

$$h = c_p T ; \quad (1.50)$$

and in the combinations

$$R = c_p - c_v , \quad \gamma = c_p / c_v . \quad (1.51)$$

Finally, the scalar quantities k , λ , and μ are state variables that can be taken to depend on temperature only.

These full equations of motion for a compressible fluid are so complex as to be intractable. Analytical progress toward their solution therefore tends to occur in small increments, in which the equations are truncated in various ways and solved for special classes of problems. The simplest method of truncation is brute force. For example, it can be stipulated that the density of a fluid is constant, or that the viscosity and heat conductivity are zero, or that the flow depends on only one space coordinate and time. More systematic truncations can often be based on dimensional considerations. For example, suppose that the ostensible data for a class of problems, including boundary conditions and characteristic fluid properties, are sufficient to define a complete set of global scales for length, velocity, temperature, and so on. Then the equations of motion can immediately be put in non-dimensional form. The relative magnitude of various terms can be estimated, and certain terms can be discarded as negligible, along with the physical processes that they model. A limit process is often involved. If the limit is regular, suitable expansions define themselves. However, the expansion procedure is usually neither transparent nor trivial, so that it is best illustrated by a few examples.

1.2.3 Incompressible fluids

A large part of fluid mechanics deals either with liquids or with gases moving at low speeds, so that effects of compressibility are not important. The limit process that allows a gas to be treated as incompressible was first accurately described by LAGERSTROM (1964) in his handbook article on laminar flow. This limit process preserves the mechanical role of the pressure in the momentum equation (1.40) while suppressing the thermodynamic role of the pressure in the energy equation (1.43) and the state equation (1.48). The reasoning here proceeds from the general to the particular, on the premise that it is logically easier (and safer) to derive the correct equations for a compressible fluid from first principles, and then to apply the correct limit, than it is to go in the opposite direction. However, it is important to keep in mind that the reasoning is also *ad hoc*, being strictly valid in each instance only for a particular class of flows specified in advance.

Consider the class of flows of a viscous perfect gas past a finite body. Begin by converting the equations of motion to dimensionless form. Assume that there is a constant reference length \mathbf{L} in the problem, together with a constant reference velocity \mathbf{U} and a reference fluid state in which p, ρ, T have the values p_a, ρ_a, T_a (a for ambient, usually at infinity), and similarly for μ and k . The body force per unit mass, \vec{F} , is made dimensionless with g , the acceleration of gravity. Nothing essential is lost if the flow is taken to be steady, with $Q = 0$, and if λ and μ are both represented by μ . With an overbar to indicate dimensionless variables like $\bar{u} = \vec{u}/\mathbf{U}$ and $\bar{p} = p/p_a$ (and, implicitly, dimensionless operators div , grad , and D/Dt) in coordinates $\bar{x} = \vec{x}/\mathbf{L}$, the equations of motion can be written

$$\frac{D\bar{p}}{Dt} + \bar{p} \text{div } \bar{u} = 0 ; \quad (1.52)$$

$$\bar{p} \frac{D\bar{u}}{Dt} = -\frac{1}{\gamma M^2} \text{grad } \bar{p} + \frac{1}{Fr^2} \bar{p} \bar{F} + \frac{1}{Re} \text{div } \bar{\tau} ; \quad (1.53)$$

$$\bar{p} \frac{D\bar{h}}{Dt} = \left(\frac{\gamma - 1}{\gamma} \right) \bar{u} \cdot \text{grad } \bar{p} - \frac{1}{Pe} \text{div } \bar{q} + (\gamma - 1) \frac{M^2}{Re} \bar{\tau} \cdot \underline{\text{grad}} \bar{u} ; \quad (1.54)$$

$$\bar{p} = \bar{\rho} \bar{T} . \quad (1.55)$$

Several dimensionless parameters materialize as coefficients of terms on the right-hand sides. They are called, respectively, the Mach number M , the Froude number Fr , the Reynolds number Re , the Péclet number $Pé$, and the ratio of specific heats γ ;

$$M^2 = \frac{\mathbf{U}^2}{\gamma p_a / \rho_a} ; \quad (1.56)$$

$$Fr^2 = \frac{\mathbf{U}^2}{g\mathbf{L}} ; \quad (1.57)$$

$$Re = \frac{\rho_a \mathbf{U} \mathbf{L}}{\mu_a} ; \quad (1.58)$$

$$Pé = \frac{\rho_a c_p \mathbf{U} \mathbf{L}}{k_a} ; \quad (1.59)$$

$$\gamma = \frac{c_p}{c_v} . \quad (1.60)$$

The ratio $Pé/Re$, which compares the relative rates of diffusion for heat and vorticity, is a derived parameter called the Prandtl number Pr ;

$$Pr = \frac{Pé}{Re} = \frac{c_p \mu_a}{k_a} . \quad (1.61)$$

I was not aware, until some of my students pointed it out to me, that the definition of Froude number in current textbooks and monographs on fluid mechanics is not uniform. When I made an informal survey of books within easy reach in my office, I found seven authors, some of them very distinguished, who use the definition $Fr = \mathbf{U}^2/g\mathbf{L}$. Eleven other authors, equally distinguished, use the definition $Fr^2 = \mathbf{U}^2/g\mathbf{L}$. I will adopt the second definition, as in equation (1.57) above; first, because it is the form originally proposed by FROUDE (ref); second, because it is the form commonly used by writers on topics that directly involve surface waves or buoyancy forces; and third, and most important, because the symbol Fr then runs in parallel with the symbol M as the ratio of a fluid velocity to a characteristic wave velocity.

It is not necessary to use or even to know the equations of motion in order to discover these five dimensionless parameters. The Buckingham Π theorem (see SECTION X)³ is sufficient, given the presence of nine independent physical quantities in the problem, together with four independent physical units (mass, length, time, and temperature). For each of the dimensionless parameters just listed, and others to come, experience shows that much of fluid mechanics and the associated applied mathematics is concentrated near the three special values 0, 1, ∞ . Lagerstrom discusses several of these special values at length, especially the difficult cases $Re \rightarrow 0$ and $Re \rightarrow \infty$. The case at hand, the case $M \rightarrow 0$, is relatively straightforward because the perturbation is entirely regular.

For each class of problems, the global reference values used to make the variables and operators dimensionless should be chosen in such a way that the essential terms in the equations, weighted by their dimensionless coefficients, are of order unity in the limit. In the present instance of flow past a body, the transport terms on the left in the momentum equation (1.53) and in the energy equation (1.54) are essential by assumption. So is the pressure gradient term in equation (1.53). All other terms can be left to follow these leaders. This format is not universal. For example, the transport terms in the momentum equation are not important in lubrication theory, and different arguments are needed. Fortunately, in such cases the equations are usually capable of indicating the direction the argument should take as well as the nature of higher approximations.

After these preliminaries, consider the limit $M \rightarrow 0$ in equations (1.52)–(1.55). There is an obvious difficulty in the momentum equation, where the pressure term blows up. This problem can be avoided by making the pressure dimensionless with the dynamic pressure rather than the static pressure. Instead of

$$\bar{p} = \frac{p}{p_a} \quad , \quad (1.62)$$

define

$$\tilde{p} = \frac{\bar{p}}{\gamma M^2} = \frac{p}{\rho_a \mathbf{U}^2} \quad . \quad (1.63)$$

³Sections that discuss Buckingham Π include 2.4.1, 9.1.2, and 11.1.1

The difficulty in the momentum equation clears up, but a new problem appears in the state equation (1.55), which becomes

$$\bar{\rho} \bar{T} = \gamma M^2 \tilde{p} , \quad (1.64)$$

with a right-hand side that vanishes in the limit. This new problem is caused by the fact that p is defined only within an additive constant in $\text{grad } p$, but is defined in an absolute sense in the state equation. Both cases are accounted for if the dimensionless pressure is expressed in the form usually called a pressure coefficient by aeronautical and mechanical engineers. Thus define

$$\hat{p} = \tilde{p} - \frac{1}{\gamma M^2} = \frac{\bar{p} - 1}{\gamma M^2} = \frac{p - p_a}{\rho_a \mathbf{U}^2} . \quad (1.65)$$

With this change, the dimensionless equations become

$$\frac{D\bar{\rho}}{Dt} + \bar{\rho} \text{div } \bar{\mathbf{u}} = 0 ; \quad (1.66)$$

$$\bar{\rho} \frac{D\bar{\mathbf{u}}}{Dt} = -\text{grad } \hat{p} + \frac{1}{Fr^2} \bar{\rho} \bar{\mathbf{F}} + \frac{1}{Re} \text{div } \bar{\boldsymbol{\tau}} ; \quad (1.67)$$

$$\bar{\rho} \frac{D\bar{h}}{Dt} = (\gamma - 1) M^2 \bar{\mathbf{u}} \cdot \text{grad } \hat{p} - \frac{1}{P\acute{e}} \text{div } \bar{\mathbf{q}} + (\gamma - 1) \frac{M^2}{Re} \bar{\boldsymbol{\tau}} \cdot \underline{\text{grad } \bar{\mathbf{u}}} ; \quad (1.68)$$

$$\bar{\rho} \bar{T} = 1 + \gamma M^2 \hat{p} . \quad (1.69)$$

Now in the limit $M \rightarrow 0$ the flow of a viscous perfect gas about a finite body is described by the equations

$$\frac{D\bar{\rho}}{Dt} + \bar{\rho} \text{div } \bar{\mathbf{u}} = 0 ; \quad (1.70)$$

$$\bar{\rho} \frac{D\bar{\mathbf{u}}}{Dt} = -\text{grad } \hat{p} + \frac{1}{Fr^2} \bar{\rho} \bar{\mathbf{F}} + \frac{1}{Re} \text{div } \bar{\boldsymbol{\tau}} ; \quad (1.71)$$

$$\bar{\rho} \frac{D\bar{h}}{Dt} = -\frac{1}{P\acute{e}} \text{div } \bar{\mathbf{q}} ; \quad (1.72)$$

$$\bar{\rho} \bar{T} = 1 . \quad (1.73)$$

In particular, the pressure-work term and the dissipation term drop out of the energy equation (1.68), leaving only conduction to balance transport of heat. Restored to dimensional form, the equations for $M \rightarrow 0$ are

$$\frac{D\rho}{Dt} + \rho \operatorname{div} \vec{u} = 0 ; \quad (1.74)$$

$$\rho \frac{D\vec{u}}{Dt} = -\operatorname{grad} p + \rho \vec{F} + \operatorname{div} \underline{\tau} ; \quad (1.75)$$

$$\rho \frac{Dh}{Dt} = -\operatorname{div} \vec{q} ; \quad (1.76)$$

$$\rho T = \rho_a T_a . \quad (1.77)$$

The limit $M \rightarrow 0$ can also be approached more directly. For a perfect gas, the definition of stagnation enthalpy,

$$c_p T_0 = c_p T + \frac{u^2}{2} = \frac{c_p p}{R \rho} + \frac{u^2}{2} , \quad (1.78)$$

and the definition of local Mach number,

$$M^2 = \frac{\rho u^2}{\gamma p} , \quad (1.79)$$

imply

$$\frac{T_0}{T} = 1 + \frac{\gamma - 1}{2} M^2 . \quad (1.80)$$

Now suppose that the flow is steady and isentropic (inviscid, adiabatic), so that

$$\frac{T}{T_0} = \left(\frac{p}{p_0} \right)^{\frac{\gamma-1}{\gamma}} . \quad (1.81)$$

Then

$$\frac{\rho u^2}{2p_0} = \frac{\gamma}{2} \frac{p M^2}{p_0} = \left(\frac{\gamma}{\gamma - 1} \right) \frac{p}{p_0} \left[\left(\frac{p_0}{p} \right)^{\frac{\gamma-1}{\gamma}} - 1 \right] . \quad (1.82)$$

Finally, suppose that p/p_0 is nearly unity. Put $p_0/p = 1 + \epsilon$ and take the first term in an expansion in powers of ϵ of the quantity in brackets in equation (1.82);

$$\frac{\rho u^2}{2} = \left(\frac{\gamma}{\gamma - 1} \right) \left[\frac{\gamma - 1}{\gamma} \epsilon \right] p = \epsilon p , \quad (1.83)$$

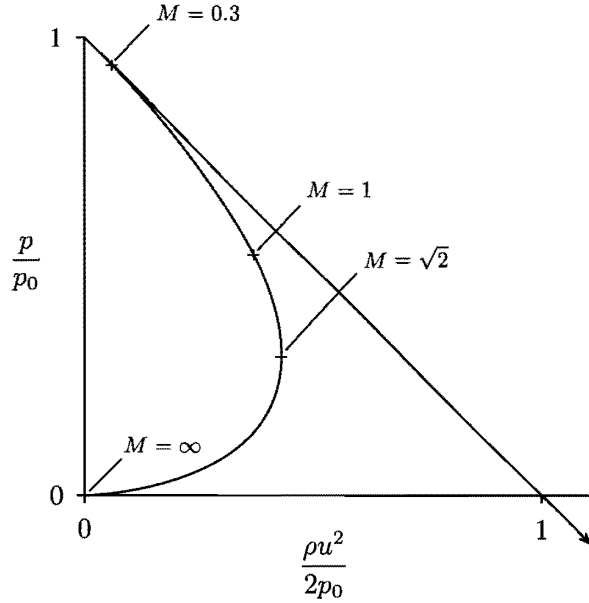


Figure 1.1: The Bernoulli integral for an incompressible fluid and for a perfect gas with $\gamma = 1.4$.

or

$$\frac{\rho u^2}{2} = p_0 - p . \quad (1.84)$$

Thus the low-speed Bernoulli integral is recovered in the limit $\epsilon \rightarrow 0$. Comparison of equations (1.79) and (1.83) shows that $\epsilon = \gamma M^2/2$, so that this is also the limit $M \rightarrow 0$. It is equation (1.82) and not equation (1.78) that should be referred to as the Bernoulli integral for a compressible perfect gas. To illustrate this limit graphically, the relationship between p/p_0 and $\rho u^2/2p_0$ from equations (1.82) and (1.84) is shown in FIGURE 1.1 for $\gamma = 7/5$. The absence of a lower bound for p in an incompressible fluid is evident, as is the basis of

an expansion for p/p_0 near unity.

Throughout this discussion of the limit $M \rightarrow 0$, the main issue is the behavior of the variable called the pressure. In its thermodynamic role, the pressure must be non-negative. In its dynamic role, there is no lower limit for the pressure. For an incompressible fluid it can go to negative infinity, according to the Bernoulli equation (1.84), when the velocity \vec{u} goes to positive infinity, as for potential flow at a sharp external corner or for flow at a source or sink. The issue is resolved formally by measuring the magnitude of the pressure in both of its roles from a local reference value, here called p_0 , and requiring changes in p to be small when compared with p_0 but of order unity when compared with $\rho_a \mathbf{U}^2$. It should not be surprising, with the pressure almost constant, that the only thermodynamic process that leaves any residue in the limit is the process at constant pressure, as represented by the enthalpy $h = c_p T$. The specific heat at constant volume c_v has dropped out, along with the internal energy $e = c_v T$ and the state constants $\gamma = c_p/c_v$ and $R = c_p - c_v$.

The argument just presented does not require the density ρ to be constant. It does require changes in density to be associated with changes in temperature, not with compressibility. If the temperature T is constant, the energy equation (1.76) with $\vec{q} = -k \text{grad } T$ is moot, and the state equation (1.77) requires the density ρ to be constant also. The continuity equation (1.74) is then reduced to $\text{div } \vec{u} = 0$, and the fluid is effectively incompressible. No distinction need be made between a gas and a liquid.

1.2.4 Low-speed heat transfer

For many low-speed flows, variations in temperature are forced by the boundary conditions. If these variations are small, both gases and liquids can be accommodated as working fluids through linearization of the state equation. Consider again the low-speed equations (1.74)–(1.77) in dimensional form. Omit the body-force term temporarily, and take $h = c_p T$. Use Newton's hypothesis $\underline{\tau} = \mu \text{ def } \vec{u}$ for the viscous terms, and Fourier's hypothesis $\vec{q} = -k \text{ grad } T$ for the heat-conduction terms. For low-speed thermal problems, replace the state

equation (1.77) by a tangent approximation,

$$\rho - \rho_a = -\beta\rho_a(T - T_a) \quad (1.85)$$

where the constant $\beta = -(\partial\rho/\partial T)_a/\rho_a$ is called the volume coefficient of expansion and depends on the reference temperature T_a . If the inventors of the linearized state equation (1.85) had chosen to include a factor T_a in the denominator of the right-hand side, then the parameter β would represent a dimensionless slope in logarithmic coordinates and would have the value unity for a perfect gas. The reference parameter T_a would still have to be specified for any other fluid, as it does now. There are also problems that may require more complex measures; for example, $\beta \rightarrow 0$ for water near 4 °C, or $\beta \rightarrow \infty$ for a liquid near its critical point.

The dimensional equations of motion become

$$\frac{D\rho}{Dt} + \rho \operatorname{div} \vec{u} = 0 ; \quad (1.86)$$

$$\rho \frac{D\vec{u}}{Dt} = -\operatorname{grad} p + \operatorname{div} (\mu \underline{\operatorname{def}} \vec{u}) ; \quad (1.87)$$

$$\rho c_p \frac{DT}{Dt} = \operatorname{div} (k \operatorname{grad} T) ; \quad (1.88)$$

together with the state equation (1.85). It will be trivial in the sequel that μ and k can be taken as constant.

An important issue involves the limiting form of the continuity equation (1.86). Because the energy equation (1.88) with constant k is linear and homogeneous in T , it can be written with the aid of equation (1.85) as an equation for ρ ;

$$\frac{D\rho}{Dt} = \frac{k}{\rho c_p} \operatorname{div} \operatorname{grad} \rho . \quad (1.89)$$

Note that the commonly accepted form of the continuity equation (1.86) for low-speed flow with heat transfer is

$$\operatorname{div} \vec{u} = 0 , \quad (1.90)$$

and that this seems to imply, according to equation (1.86),

$$\frac{D\rho}{Dt} = 0 . \quad (1.91)$$

Thus $D\rho/Dt$ is both zero and not zero. Some writers ignore the inconsistency. Others (see, for example, CHANDRASEKHAR (1961, pp. 16–17) explain it by estimates that depend on the smallness of the parameter β in equation (1.85). However, I find it more useful to think that it is the temperature difference $(T - T_a)$ in this equation that is small in some appropriate sense. The argument proceeds in the same spirit as that of the preceding section, and again contemplates flow around a body. Denote a constant reference temperature by T_w (w for wall) and an ambient temperature by T_a . Define two dimensionless parameters (the symbol P should be read as a Greek capital *rho*)

$$P = \frac{\rho_w - \rho_a}{\rho_a} , \quad \Theta = \frac{T_w - T_a}{T_a} , \quad (1.92)$$

and consider the limit $P \rightarrow 0$, $\Theta \rightarrow 0$. Suitable non-dimensional variables of order unity suggest themselves as

$$\hat{\rho} = \frac{\bar{\rho} - 1}{P} = \frac{\rho - \rho_a}{\rho_w - \rho_a} , \quad \hat{T} = \frac{\bar{T} - 1}{\Theta} = \frac{T - T_a}{T_w - T_a} . \quad (1.93)$$

Now write the dimensionless equations of motion (1.70)–(1.72) in terms of $\hat{\rho}$,

$$P \frac{D\hat{\rho}}{Dt} + (1 + P\hat{\rho}) \operatorname{div} \bar{\vec{u}} = 0 ; \quad (1.94)$$

$$(1 + P\hat{\rho}) \frac{D\bar{\vec{u}}}{Dt} = -\operatorname{grad} \hat{p} + \frac{1}{Re} \operatorname{div} \bar{\mu} \operatorname{def} \bar{\vec{u}} ; \quad (1.95)$$

$$(1 + P\hat{\rho}) \frac{D\hat{\rho}}{Dt} = \frac{1}{P\epsilon} \operatorname{div} \bar{k} \operatorname{grad} \hat{\rho} ; \quad (1.96)$$

$$P\hat{\rho} = -\beta T_a \Theta \hat{T} ; \quad (1.97)$$

and take the limit $P \rightarrow 0$, $\Theta \rightarrow 0$. The incompressible form $\operatorname{div} \bar{\vec{u}} = 0$ is evidently the correct limit of the continuity equation. The derivative $D\hat{\rho}/Dt$ is not zero in the limit; only its coefficient P is zero.

There is no effect on the momentum and energy equations. The state equation remains in the form (1.85).

In this development, the special case of a perfect gas turns out to be in no way special. In terms of the new variables (1.93), the state equation (1.73) for a perfect gas becomes

$$(1 + P\hat{\rho})(1 + \Theta\hat{T}) = 1 . \quad (1.98)$$

To first order in the small quantities P and Θ , this is

$$P\hat{\rho} + \Theta\hat{T} = 0 , \quad (1.99)$$

or, in physical variables,

$$\rho - \rho_a = -\frac{\rho_a}{T_a} (T - T_a) . \quad (1.100)$$

This equation is the same as equation (1.85) if $\beta = 1/T_a$.

The equations (1.86)–(1.88) have now become, in physical variables,

$$\text{div } \vec{u} = 0 ; \quad (1.101)$$

$$\rho \frac{D\vec{u}}{Dt} = -\text{grad } p + \mu \text{ div } \underline{\text{grad } \vec{u}} ; \quad (1.102)$$

$$\rho c_p \frac{DT}{Dt} = k \text{ div } \text{grad } T ; \quad (1.103)$$

with ρ , μ , k all constant. These equations are the stuff of low-speed heat transfer. The form of the viscous terms in the momentum equation (1.102) now takes account of vector identity (1.18) (which states that $\text{div } (\text{grad } \vec{u})^* = 0$ if $\text{div } \vec{u} = 0$). The state equation has been discarded. The momentum and energy equations are uncoupled in the sense that the momentum equation does not involve the temperature. The energy equation is linear and homogeneous in T , so that solutions can be superposed as long as the variable coefficients u and v in the transport terms remain fixed. A large literature testifies to the importance of this property.

1.2.5 The Boussinesq approximation

It remains to consider the body-force term in the momentum equation. Suppose first that the gravitational force is normal to the general direction of flow, as in a free-surface water channel. In rectangular coordinates, the body-force term is then

$$\vec{F} = -g \vec{v}_z , \quad (1.104)$$

where \vec{v}_z is a unit vector directed vertically upward (the notation is that of the literature of meteorology). This force does not necessarily play a part in the dynamics of the fluid motion. Take the velocity to be zero in the vertical component of the momentum equation (1.75) (more accurately, take $Dv/DT \ll g$). In this hydrostatic limit, denoted by the subscript zero, vertical equilibrium implies

$$0 = -\frac{dp_0}{dz} - \rho_0 g . \quad (1.105)$$

If the density is constant, the integral is

$$p_0 = p_s - \rho_0 g z , \quad (1.106)$$

where p_s is the pressure at $z = 0$ (s for sea level, say). If the fluid is a perfect gas and is compressible but isothermal, with temperature T_s , equation (1.106) is replaced by

$$p_0 = p_s e^{-gz/RT_s} . \quad (1.107)$$

(Comment on Chapman's paper.) A more accurate model of the neutral atmosphere would be isentropic (well mixed) rather than isothermal, in which case

$$p_0 = p_s \left[1 - \left(\frac{\gamma - 1}{\gamma} \right) \frac{gz}{RT_s} \right]^{\frac{\gamma}{\gamma - 1}} . \quad (1.108)$$

Equations (1.107) and (1.108) both reduce to equation (1.106) if z is small enough. For an isothermal atmosphere, the pressure and density decrease exponentially with increasing height, with an e -folding distance z_e given by $g z_e / RT_s = \gamma g z_e / a^2 = 1$, where a is the speed

of sound. For the earth's atmosphere, z_e is several thousand meters. For any motion that occupies a sufficiently small fraction of this distance, the atmosphere can be treated as homogeneous.

Next, subtract equation (1.105) from equation (1.75) to obtain

$$\rho \frac{D\vec{u}}{Dt} = -\text{grad}(p - p_0) - (\rho - \rho_0) g \vec{z} + \text{div} \underline{\tau} . \quad (1.109)$$

In particular, if the density is constant the hydrostatic pressure is irrelevant, because pressure changes associated with fluid motion are measured from a variable hydrostatic datum p_0 . An exception may occur if the vertical acceleration $w\partial w/\partial z$ is not negligibly small compared with the acceleration of gravity. This will certainly be the case if a liquid has a free surface that is not sensibly flat, so that the hydrostatic datum p_s is itself disturbed.

Now to the main point in connection with buoyancy effects, and the reason that an argument for the Boussinesq approximation is needed. The energy equation (11.3) can be written,⁴ with the aid of equation (11.4), in the form

$$\frac{1}{\rho} \frac{D\rho}{Dt} = \frac{1}{\rho h} \text{div} \vec{q} - \frac{Q}{h} \quad (1.110)$$

whereas the continuity equation (11.1) reads

$$\frac{1}{\rho} \frac{D\rho}{Dt} = -\text{div} \vec{u} . \quad (1.111)$$

The Boussinesq approximation sets the two sides of (1.111) separately to zero, but leaves (1.110) intact, in order to retain heat conduction as an essential process.

This apparent inconsistency can be resolved with the aid of another limiting process, this time involving the Froude number. Suppose that the motion is driven entirely by buoyancy forces, and that density changes are small enough to permit linearization of the relationship $\rho(T)$. The linearized state equation is usually taken in the form

$$\rho - \rho_0 = -\beta\rho_0(T - T_0) \quad (1.112)$$

⁴The equations cited in this paragraph are discussed in Section 11.1.1.

where β is the relative change in density, or with a sign change the relative change in specific volume, per degree change in temperature. The parameter β depends on temperature and is ordinarily positive, since for most fluids the density decreases as the temperature increases at constant pressure. There are occasional exceptions in nature. A familiar example is water between 0 °C and 4 °C. For a perfect gas, $\beta = 1/T$. For water at 20 °C, $\beta = xxxx$ (**check**).

If heat addition Q is negligible, the energy equation (11.3) is linear in T and therefore in ρ , given the linearized state equation (1.112). The equations of motion for buoyancy-driven flows become

$$\frac{D\rho}{Dt} = -\rho \operatorname{div} \vec{u} , \quad (1.113)$$

$$\rho \frac{D\vec{u}}{Dt} = -\operatorname{grad} (p - p_0) - (\rho - \rho_0) q\vec{v}_z + \operatorname{div} \mu \operatorname{grad} \vec{u} , \quad (1.114)$$

$$\rho \frac{D\rho}{Dt} = \operatorname{div} k \operatorname{grad} \rho , \quad (1.115)$$

$$\rho - \rho_0 = -\beta\rho_0(T - T_0) . \quad (1.116)$$

Define dimensionless variables according to the schedule

$$\begin{aligned} \vec{u} &= U\bar{\vec{u}} \\ \vec{x} &= L\bar{\vec{x}} \\ p - p_0 &= \rho_0 U^2 p^* \\ \rho &= \rho_0 \bar{\rho} \\ T &= T_0 \bar{T} \\ \mu &= \mu_0 \bar{\mu} \\ k &= k_0 \bar{k} \end{aligned} \quad (1.117)$$

where U and L are global scales. The relation for p already incorporates the conclusion reached in this introduction about the proper form in the limit $M \rightarrow 0$. There is no loss of force in taking the flow to be steady and in omitting the heat-addition term Q in the energy equation. In dimensionless form, equations (1.113)–(1.116) are

$$\frac{D\bar{\rho}}{D\bar{t}} = -\operatorname{div} \bar{\vec{u}} , \quad (1.118)$$

$$\frac{D\bar{u}}{D\bar{t}} = -\text{grad } p^* - \frac{(\bar{\rho} - 1)}{Fr^2} \vec{i}_z + \frac{1}{Re} \text{div } \bar{\mu} \underline{\text{grad } \bar{u}} , \quad (1.119)$$

$$\frac{D\bar{\rho}}{D\bar{t}} = \frac{1}{PrRe} \text{div } \bar{k} \text{grad } \bar{\rho} , \quad (1.120)$$

$$(\bar{\rho} - 1) = -\beta T_0(\bar{T} - 1) , \quad (1.121)$$

where

$$Fr^2 = \frac{U^2}{gL} . \quad (1.122)$$

The objective of the exercise here is to reduce all of the essential terms to order unity, free of dimensionless parameters that may be either large or small. In the viscous and heat-conduction terms, this is the business of the boundary-layer approximation, where μ_0 and κ_0 are incorporated into the independent variables. The issue here is the buoyancy term. The form of this term suggests a change in the dependent variable, namely putting

$$\rho^* = \frac{\bar{\rho} - 1}{Fr^2} \quad (1.123)$$

or

$$\bar{\rho} = 1 + Fr^2 \rho^* . \quad (1.124)$$

When this change is made, the equations become

$$Fr^2 \frac{D\rho^*}{D\bar{t}} = -\text{div } \bar{u} , \quad (1.125)$$

$$\frac{D\bar{u}}{D\bar{t}} = -\text{grad } p^* - \rho^* \vec{i}_z + \frac{1}{Re} \text{div } \bar{\mu} \underline{\text{grad } \bar{u}} , \quad (1.126)$$

$$\frac{D\rho^*}{D\bar{t}} = \frac{1}{PrRe} \text{div } \bar{k} \text{grad } \rho^* , \quad (1.127)$$

$$\rho^* = -\beta T_0 T^* , \quad (1.128)$$

where $T^* = (\bar{T} - 1)/Fr^2$. The Boussinesq approximation appears as the limit $Fr \rightarrow 0$, for which the left side of equation (1.125) vanishes, leaving

$$\text{div } \bar{u} = 0 , \quad (1.129)$$

together with equations (1.126)–(1.128). The parameters $\bar{\mu}$ and \bar{k} can be expressed in parallel with (1.124) for ρ , and therefore can be replaced by μ_0 and κ_0 .

In short, the limit $Fr = 0$ means that density differences are required to be small, of order U^2/gL , for ρ^* to be of order unity. Put another way, velocities in such a flow should be small compared with the velocity associated with free fall under gravity through a distance L . If $L = 1$ meter, for example, U should be small compared with 3 meters per second. If not, it is necessary to revert to the full equations. (Read White, viscous flow, on Boussinesq approximation.)

1.2.6 Coordinate systems

1.3 Operational prologue

1.3.1 Stream functions

The stream function is a device used to simplify the form of the equations of motion by satisfying the continuity equation identically. Assume that the fluid is incompressible. The equation

$$\operatorname{div} \vec{u} = 0 \quad (1.130)$$

can be satisfied by at least two methods. One invokes a vector identity (1.14) from SECTION 1.2.1; $\operatorname{div} \operatorname{curl} \vec{a} = 0$, and puts

$$\vec{u} = \operatorname{curl} \vec{a} , \quad (1.131)$$

where \vec{a} is sometimes called the acceleration potential. The dependent variables of the problem are now the three components of the vector \vec{a} , and there is no obvious simplification in substituting these for the three components of the velocity itself.

The second device invokes two vector identities (1.17) and (1.19) from SECTION 1.2.1, $\operatorname{div} (\vec{a} \times \vec{b}) = \vec{b} \cdot \operatorname{curl} \vec{a} - \vec{a} \cdot \operatorname{curl} \vec{b}$ and $\operatorname{curl} (\operatorname{grad} \alpha) = 0$, and puts

$$\vec{u} = \operatorname{grad} \psi \times \operatorname{grad} \Psi . \quad (1.132)$$

There are now two scalar stream functions, ψ and Ψ , for a general three-dimensional problem. Because \vec{u} in equation (1.132) is normal to $\text{grad } \psi$ and to $\text{grad } \Psi$, the velocity vector lies in the intersection of the surfaces $\psi = \text{constant}$ and $\Psi = \text{constant}$. The most effective use of equation (1.132) therefore occurs for plane or axisymmetric flows in which the velocity vectors always lie in one family of coordinate surfaces, say $\beta = \text{constant}$ for coordinates (α, β, γ) . It is then sufficient to take $\Psi = \beta$.

All of the flows taken up in this monograph are two-dimensional in the sense just defined and also have a preferred direction. The velocity in this direction will be uniformly taken as the component u of the velocity vector (u, v, w) . The other two components should follow a right-hand convention. In rectangular coordinates (x, y, z) , for example, suppose the flow lies in the planes $z = \text{constant}$. Then the velocities are related to the stream function by

$$\vec{u} = \text{grad } \psi \times \text{grad } z = \left(\frac{\partial \psi}{\partial y}, -\frac{\partial \psi}{\partial x}, 0 \right) = (u, v, w) . \quad (1.133)$$

Other coordinate systems require other results. In cylindrical polar coordinates (r, θ, z) , suppose the flow is axial and radial and thus lies in planes $\theta = \text{constant}$. Then

$$\vec{u} = \text{grad } \psi \times \text{grad } \theta = \left(-\frac{1}{r} \frac{\partial \psi}{\partial z}, 0, \frac{1}{r} \frac{\partial \psi}{\partial r} \right) = (u, v, w) . \quad (1.134)$$

1.3.2 Boundary-layer approximations

The reason for the plural will become apparent shortly. For an incompressible fluid, the Navier-Stokes equations of motion for steady laminar two-dimensional flow (u, v) in rectangular coordinates are the continuity equation,

$$\frac{\partial u}{\partial x} + \frac{\partial v}{\partial y} = 0 , \quad (1.135)$$

and two momentum equations,

$$u \frac{\partial u}{\partial x} + v \frac{\partial u}{\partial y} = -\frac{1}{\rho} \frac{\partial p}{\partial x} + \nu \left(\frac{\partial^2 u}{\partial x^2} + \frac{\partial^2 u}{\partial y^2} \right) ; \quad (1.136)$$

$$u \frac{\partial v}{\partial x} + v \frac{\partial v}{\partial y} = -\frac{1}{\rho} \frac{\partial p}{\partial y} + \nu \left(\frac{\partial^2 v}{\partial x^2} + \frac{\partial^2 v}{\partial y^2} \right) . \quad (1.137)$$

There are three dependent variables, u , v , p , whether the viscous terms are present (Navier-Stokes equations) or not (Euler equations). In the latter case, the order of the equations is lowered, and a boundary condition has to be omitted. Normally this is the no-slip condition at any walls that bound the flow. If the viscosity is not zero, the viscous terms are present and the no-slip condition has to be enforced or the walls must move with a velocity and direction that accommodates the flow.

To fix the ideas, consider flow along a wall placed along the positive x -axis, at $y = 0$, $x > 0$. In the absence of separation, what is expected for small viscosity is the appearance of a thin layer near the wall in which the velocity changes rapidly from zero to some finite value characteristic of the inviscid flow. The viscous terms in this layer present themselves as large derivatives multiplied by a small coefficient, with the product having a magnitude comparable with that of other terms in the equations. The structure of this thin layer is the business of the boundary-layer approximation, which was first formulated analytically by PRANDTL (1905) and was first applied by Prandtl's student BLASIUS (1908) to the case of flow over a semi-infinite flat plate at constant pressure.

Prandtl's original description of his concept was so terse that it was probably almost unintelligible to his audience of mathematicians at Heidelberg. GOLDSTEIN (1969) writes that in 1928 he asked Prandtl why this was so, "and he replied that he had been given ten minutes for his lecture at the congress and that, being still quite young [he was 29], he had thought that he could publish only what he had had time to say." Neither was Prandtl's paper well placed to reach the applied mathematicians and aerodynamicists (in today's terminology) for whom it was intended. Historical accounts by SCHLICHTING (1960) and TANI (1977) make a point of the fact that the power of boundary-layer theory was not appreciated outside Germany for nearly twenty years. LAMB, in the 1916 and 1924 editions of his monumental treatise *Hydrodynamics*, disposed of the work by Prandtl and Blasius in a dozen lines, with the remark

“the results obtained, and presented graphically, are interesting.” Lamb did not himself present the results, graphically or otherwise, until the 1932 edition. The NACA translation of Prandtl’s 1905 paper was published only in 1928 and refers only to the 1927 reprint, without mentioning the original publication. The NACA translation of the paper by Blasius did not appear until 1950.

The essence of Prandtl’s idea, as described by Blasius, is to represent the thickness of the viscous layer by a parameter ϵ , where ϵ , like ν , is a small quantity. In general, the level of rigor in what follows is not high, insofar as no attention is being paid to dimensions or to the formal machinery of singular-perturbation theory. In particular, the parameter ϵ is never defined precisely. It is not a boundary-layer thickness because it is not necessarily a length, and in any case it does not depend on x .

The boundary-layer approximation first expands the thickness of the viscous layer so as to make structural details easily visible. Define a new variable

$$\bar{y} = \frac{y}{\epsilon} \quad (1.138)$$

that is of order unity inside the boundary layer, and rewrite the equations, except the pressure terms, as

$$\frac{\partial u}{\partial x} + \frac{1}{\epsilon} \frac{\partial v}{\partial \bar{y}} = 0 ; \quad (1.139)$$

$$u \frac{\partial u}{\partial x} + \frac{v}{\epsilon} \frac{\partial u}{\partial \bar{y}} = -\frac{1}{\rho} \frac{\partial p}{\partial x} + \frac{\nu}{\epsilon^2} \left(\epsilon^2 \frac{\partial^2 u}{\partial x^2} + \frac{\partial^2 u}{\partial \bar{y}^2} \right) ; \quad (1.140)$$

$$u \frac{\partial v}{\partial x} + \frac{v}{\epsilon} \frac{\partial v}{\partial \bar{y}} = -\frac{1}{\rho} \frac{\partial p}{\partial y} + \frac{\nu}{\epsilon^2} \left(\epsilon^2 \frac{\partial^2 v}{\partial x^2} + \frac{\partial^2 v}{\partial \bar{y}^2} \right) . \quad (1.141)$$

In the pending limit $\epsilon \rightarrow 0$, the continuity equation and the transport operator will be pathological unless the v -component of velocity is also modified by putting

$$\bar{v} = \frac{v}{\epsilon} . \quad (1.142)$$

When this is done, the equations become

$$\frac{\partial u}{\partial x} + \frac{\partial \bar{v}}{\partial \bar{y}} = 0 ; \quad (1.143)$$

$$u \frac{\partial u}{\partial x} + \bar{v} \frac{\partial u}{\partial \bar{y}} = -\frac{1}{\rho} \frac{\partial p}{\partial x} + \frac{\nu}{\epsilon^2} \left(\epsilon^2 \frac{\partial^2 u}{\partial x^2} + \frac{\partial^2 u}{\partial \bar{y}^2} \right) ; \quad (1.144)$$

$$\epsilon \left(u \frac{\partial \bar{v}}{\partial x} + \bar{v} \frac{\partial \bar{v}}{\partial \bar{y}} \right) = -\frac{1}{\rho} \frac{\partial p}{\partial y} + \epsilon \frac{\nu}{\epsilon^2} \left(\epsilon^2 \frac{\partial^2 \bar{v}}{\partial x^2} + \frac{\partial^2 \bar{v}}{\partial \bar{y}^2} \right) . \quad (1.145)$$

If the continuity equation is satisfied by the introduction of a stream function, with

$$u = \frac{\partial \psi}{\partial \bar{y}} , \quad v = -\frac{\partial \psi}{\partial x} , \quad (1.146)$$

use of boundary-layer variables leads to

$$u = \frac{1}{\epsilon} \frac{\partial \psi}{\partial \bar{y}} , \quad \bar{v} = -\frac{1}{\epsilon} \frac{\partial \psi}{\partial x} . \quad (1.147)$$

Thus it is also necessary to modify the stream function by putting

$$\bar{\psi} = \frac{\psi}{\epsilon} . \quad (1.148)$$

The variables x and u are deliberately left undisturbed by these manipulations, on the premise that the external flow is not much affected by the presence of a thin boundary layer (in the absence of flow separation, as emphasized by Prandtl in his original paper).

The final step is to take the formal inner or boundary-layer limit $\epsilon \rightarrow 0$, with the boundary-layer independent variables x and \bar{y} held constant. During the limit process the viscous layer and its structure are preserved, along with the no-slip condition, when viewed in boundary-layer coordinates (x, \bar{y}) . At the same time, the viscous layer shrinks to zero thickness when viewed in outer coordinates (x, y) .

This final step has three important consequences. One is that the first viscous term vanishes in each of the momentum equations (1.144) and (1.145). The physical effect is to suppress diffusion of vorticity in the x -direction, so that the boundary conditions have no upstream influence. The mathematical effect is to change the type of the boundary-layer equations from elliptic to parabolic and to introduce real double characteristics $x = \text{constant}$.

The second consequence of the boundary-layer approximation is that it imposes the condition

$$\epsilon \sim \nu^{1/2} \quad (1.149)$$

when the surviving viscous term $(\nu/\epsilon^2) \partial^2 u / \partial \bar{y}^2 = \nu \partial^2 u / \partial y^2$ in equation (1.144) is required to be of the same order as the transport terms in the limit. At this point the definition of ϵ becomes irrelevant, because the argument can be repeated with ϵ replaced everywhere by $\nu^{1/2}$. Although few constraints have so far been put on the nature of solutions to the boundary-layer equations, the condition (1.149) already controls the form of dimensionless similarity variables. For the Blasius problem, for example, the mandatory combinations y^2/ν and ψ^2/ν have the dimensions of time and length²/time, respectively. The only combinations of x and u_∞ having these same dimensions are x/u_∞ and $u_\infty x$. The dimensionless variables $y(u_\infty/\nu x)^{1/2}$ and $\psi/(u_\infty \nu x)^{1/2}$ thus follow automatically.

The third consequence is that the pressure is moved from the list of dependent variables to the list of boundary conditions. The order of the system of equations is thereby reduced from fourth order to third order in ψ . In the y -momentum equation (1.145), $\partial p / \partial y$ is at most of order ϵ and thus is negligible in the limit, as are the other terms in this equation, which can therefore be discarded. In any application of the x -momentum equation (1.144), $\partial p / \partial x = dp/dx$ is typically specified at the outset and is sometimes tailored to generate certain special classes of solutions (see, for example, SECTION 4.2.2).

When the original variables are restored after taking the limit, the boundary-layer approximation in rectangular coordinates is

$$\frac{\partial u}{\partial x} + \frac{\partial v}{\partial y} = 0 ; \quad (1.150)$$

$$u \frac{\partial u}{\partial x} + v \frac{\partial u}{\partial y} = -\frac{1}{\rho} \frac{dp}{dx} + \nu \frac{\partial^2 u}{\partial y^2} ; \quad (1.151)$$

$$p = p(x) . \quad (1.152)$$

These equations correspond to the limit $\nu \rightarrow 0$ or $Re \rightarrow \infty$. However, they are normally applied for Reynolds numbers that are large compared to unity but by no means infinite. Once a solution has been obtained, it is a tangible advantage of the formal boundary-layer method that the magnitude of terms discarded or retained, and thus the degree of approximation, can be estimated *a posteriori*.

The argument just given is not universal. Several plane laminar flows with the property of similarity are treated within the boundary-layer approximation (1.150)–(1.152) in various parts of this monograph. These flows include the boundary layer in SECTION 4.2.2, the shear layer in SECTION 5.1.2, the plane plume in CHAPTER 11, the plane jet in SECTION 9.1.2, the plane wall jet in SECTION 10.1.2, and the asymptotic suction later in this section. The first two of these flows fit the pattern just described, but the last four do not, as demonstrated in TABLE 1.3.⁵

The obvious difference is the presence or absence of an external stream. For the boundary layer and the shear layer, there is an external stream, and the boundary-layer approximation includes a matching condition $u \rightarrow u_\infty$ applied at the outer edge of the boundary-layer flow. For the plume, the jet, and the wall jet, all in a stagnant fluid, there is no external stream, and thus no matching condition. The condition involving u_∞ is replaced by an integral constraint on thermal or momentum flux, and the form of this constraint is different in each case. The flows listed in the table are ordered according to the exponents attached to the viscosity ν , but I have not discovered any deep significance in this order.

As an example of one such flow, consider the laminar plane jet into fluid at rest. Suppose that the boundary-layer equations (1.150)–(1.152) are valid, and in particular that the pressure is everywhere constant. The momentum equation (1.151) can then be integrated across the jet (see SECTION 9.1.1 *et seq.* for details) to

⁵No Table numbered 1.2 appears in the manuscript.

Table 1.3

Boundary-layer variables
for laminar plane flows with similarity

Flow	\bar{x}	\bar{y}	$\bar{\psi}$	\bar{u}	\bar{v}
Boundary layer	x	$\frac{y}{\nu^{1/2}}$	$\frac{\psi}{\nu^{1/2}}$	u	$\frac{v}{\nu^{1/2}}$
Shear layer	x	$\frac{y}{\nu^{1/2}}$	$\frac{\psi}{\nu^{1/2}}$	u	$\frac{v}{\nu^{1/2}}$
Plane plume	x	$\frac{y}{\nu^{3/5}}$	$\frac{\psi}{\nu^{2/5}}$	$u\nu^{1/5}$	$\frac{v}{\nu^{2/5}}$
Plane jet	x	$\frac{y}{\nu^{2/3}}$	$\frac{\psi}{\nu^{1/3}}$	$u\nu^{1/3}$	$\frac{v}{\nu^{1/3}}$
Plane wall jet	x	$\frac{y}{\nu^{3/4}}$	$\frac{\psi}{\nu^{1/4}}$	$u\nu^{1/2}$	$\frac{v}{\nu^{1/4}}$
Suction layer	x	$\frac{y}{\nu}$	ψ	$u\nu$	v

obtain an integral invariant,

$$J = \int_{-\infty}^{\infty} \rho u u \, dy = \text{constant} \quad , \quad (1.153)$$

that dominates the further analysis. The global constant J is the momentum flux per unit span in the jet, or equivalently the reaction force per unit span at the jet source. Require this quantity J to be conserved as $\epsilon \rightarrow 0$ in the boundary-layer limit. Then equation (1.153) should be written in boundary-layer variables as

$$J = \int_{-\infty}^{\infty} \rho \bar{u} \bar{u} \, d\bar{y} = \text{constant} \quad , \quad (1.154)$$

where $\bar{y} = y/\epsilon$ as before, but now

$$\bar{u} = u\epsilon^{1/2} \quad , \quad (1.155)$$

rather than $\bar{u} = u$. With this information in hand, rewrite the full Navier-Stokes equations (1.135)–(1.137) as

$$\frac{\partial \bar{u}}{\partial x} + \frac{1}{\epsilon^{1/2}} \frac{\partial v}{\partial \bar{y}} = 0 \quad ; \quad (1.156)$$

$$\bar{u} \frac{\partial \bar{u}}{\partial x} + \frac{v}{\epsilon^{1/2}} \frac{\partial \bar{u}}{\partial \bar{y}} = -\frac{\epsilon}{\rho} \frac{\partial p}{\partial x} + \frac{\nu}{\epsilon^{3/2}} \left(\epsilon^2 \frac{\partial^2 \bar{u}}{\partial x^2} + \frac{\partial^2 \bar{u}}{\partial \bar{y}^2} \right) \quad ; \quad (1.157)$$

$$\frac{\bar{u}}{\epsilon^{1/2}} \frac{\partial v}{\partial x} + \frac{v}{\epsilon} \frac{\partial v}{\partial \bar{y}} = -\frac{1}{\rho} \frac{\partial p}{\partial y} + \frac{\nu}{\epsilon^{3/2}} \left(\frac{\epsilon^2}{\epsilon^{1/2}} \frac{\partial^2 v}{\partial x^2} + \frac{1}{\epsilon^{1/2}} \frac{\partial^2 v}{\partial \bar{y}^2} \right) \quad . \quad (1.158)$$

Evidently it is now necessary to take

$$\bar{v} = \frac{v}{\epsilon^{1/2}} \quad , \quad (1.159)$$

rather than $\bar{v} = v/\epsilon$. The equations of motion become

$$\frac{\partial \bar{u}}{\partial x} + \frac{\partial \bar{v}}{\partial \bar{y}} = 0 \quad ; \quad (1.160)$$

$$\bar{u} \frac{\partial \bar{u}}{\partial x} + \bar{v} \frac{\partial \bar{u}}{\partial \bar{y}} = -\frac{\epsilon}{\rho} \frac{\partial p}{\partial x} + \frac{\nu}{\epsilon^{3/2}} \left(\epsilon^2 \frac{\partial^2 \bar{u}}{\partial x^2} + \frac{\partial^2 \bar{u}}{\partial \bar{y}^2} \right) \quad ; \quad (1.161)$$

$$\epsilon \bar{u} \frac{\partial \bar{v}}{\partial x} + \bar{v} \frac{\partial \bar{v}}{\partial \bar{y}} = -\frac{\epsilon}{\rho} \frac{\partial p}{\partial y} + \epsilon \frac{\nu}{\epsilon^{3/2}} \left(\epsilon^2 \frac{\partial^2 \bar{v}}{\partial x^2} + \frac{\partial^2 \bar{v}}{\partial \bar{y}^2} \right), \quad (1.162)$$

instead of equations (1.143)–(1.145). The stream function should be taken in its turn as

$$\bar{\psi} = \frac{\psi}{\epsilon^{1/2}}, \quad (1.163)$$

rather than ψ/ϵ .

Two of the consequences of taking the limit $\epsilon \rightarrow 0$ have changed. First, equation (1.149) is replaced for the plane jet by

$$\epsilon \sim \nu^{2/3}, \quad (1.164)$$

so that the boundary-layer variables take the form displayed in the fourth line of TABLE 1.3. Second, all that can be said about the pressure gradient $\partial p/\partial y$ within the viscous layer is that it is at most of order unity rather than of order ϵ , which is to say that $\partial p/\partial \bar{y}$ is of order ϵ . The difference here is connected with the phenomenon of entrainment and with the associated fact that the streamlines in the outer part of the jet are strongly curved (see, for example, FIGURE 9.4), unlike the streamlines in a boundary layer. During the limit process $\epsilon \rightarrow 0$, the viscous layer and its structure are again preserved in boundary-layer coordinates (x, \bar{y}) . In outer coordinates (x, y) , the jet thickness shrinks to zero while the jet velocity u becomes infinite in such a way that the momentum flux J is conserved. Finally, the question of the proper dimensionless form for y and ψ is again settled. The mandatory combinations y^3/ν^2 and ψ^3/ν have the dimensions $\text{time}^2/\text{length}$ and $\text{length}^4/\text{time}^2$, respectively. The only combinations of the remaining variables J/ρ and x with these same dimensions are $\rho x^2/J$ and Jx/ρ . The appropriate similarity variables are therefore $y(J/\rho \nu^2 x^2)^{1/3}$ and $\psi(\rho/J \nu x)^{1/3}$.

It is important that the limit $\epsilon \rightarrow 0$ in equations (1.160)–(1.162) leads back to the original boundary-layer approximation (1.150)–(1.152), except for the minor reservation already stated for the pressure. The argument just given for the laminar plane jet is therefore circular, consistent, and closed. However, this argument is not the one usually found in textbooks and monographs on viscous flow. Of

eight such volumes in my personal library, only those by LOITSYAN-SKII (1966, pp. 559–565) and TRITTON (1977) are faithful to the fourth line of TABLE 1.3. The others begin either with $\psi/\nu^{1/2}$, $y/\nu^{1/2}$, following GOLDSTEIN (1938, Vol. 1, pp. 145–146) or with ψ/ν , y , following ROSENHEAD (1963, pp. 254–256). The correct variables $\psi/\nu^{1/3}$, $y/\nu^{2/3}$ do eventually emerge, but only after the argument is adjusted to satisfy the integral invariant (1.153). The point of this discussion is that the thickness of a diffusing layer does not necessarily vary as the square root of the diffusivity. This property can be shown more directly by using the Lagrangian device of a moving observer, in the style of H.W. Liepmann. This device often allows the exponents to be established correctly without recourse to the governing equations except through integral constraints such as equation (1.153). Return to the case of the Blasius boundary layer or the mixing layer in a uniform half-flow. Suppose that an observer travels with constant free-stream velocity along the streamline (of the inviscid flow) that represents the site of the thin viscous layer. A clock carried by the observer shows a time $t \sim x/u_\infty$. Diffusion of vorticity requires a stationary clock at any station to show a time $t \sim \delta^2/\nu$, where $\delta(x)$ is the local thickness of the diffusing viscous layer. Consequently, a plausible estimate of δ can be obtained by equating times;

$$\delta(x) \sim \left(\frac{\nu x}{u_\infty} \right)^{1/2}. \quad (1.165)$$

Now consider the plane jet into a stagnant fluid. An observer moving with the local fluid velocity along a streamline (of the viscous flow) in the plane of symmetry reads a time $t \sim x/u_c$ (c for center line). The thickness δ is governed by the same equation (1.165), with u_∞ replaced by $u_c(x)$;

$$\delta(x) \sim \left(\frac{\nu x}{u_c} \right)^{1/2}. \quad (1.166)$$

But the integral invariant (1.153) requires $\delta u_c^2 \sim J/\rho = \text{constant}$. Elimination of u_c then yields for δ , instead of equation (1.165), the power law

$$\delta(x) \sim \left(\frac{\rho \nu^2 x^2}{J} \right)^{1/3}, \quad (1.167)$$

and the proper similarity variables are reached in another way.

1.3.3 Subcharacteristics

These qualitative differences for various boundary-layer flows are connected with the role of subcharacteristics in the boundary-layer approximation, as pointed out by KEVORKIAN and COLE (1981, pp. 370–373) for slightly different model equations. The important consideration is that the steady Euler equations; i.e., the inviscid approximation to the Navier-Stokes equations (1.135)–(1.137), have real characteristics. These are the streamlines, on which the stagnation pressure is constant and across which discontinuities in streamwise velocity are permitted. The text of boundary-layer theory is a palimpsest. The real characteristics of the Euler equations are imperfectly erased by addition of the viscous terms and by passage to the boundary-layer limit. They become subcharacteristics of the viscous problem and have subtle but important effects on the form of boundary-layer solutions.

Of various methods for finding characteristic curves for systems of partial differential equations, the one used here has the property that it automatically finds not only the characteristic curves, but also any invariants that may exist on these curves. When applied to isentropic supersonic flow, for example, it produces the Mach lines and the Riemann invariants. As an illustration of this method, consider the Euler equations of motion for steady, inviscid, two-dimensional, laminar flow of an incompressible fluid in rectangular coordinates. When the derivatives of highest order are written in terms of a stream function, with $u = \partial\psi/\partial y$ and $v = -\partial\psi/\partial x$, these equations are

$$u \frac{\partial^2 \psi}{\partial x \partial y} + v \frac{\partial^2 \psi}{\partial y^2} + \frac{1}{\rho} \frac{\partial p}{\partial x} = 0 ; \quad (1.168)$$

$$-u \frac{\partial^2 \psi}{\partial x^2} - v \frac{\partial^2 \psi}{\partial x \partial y} + \frac{1}{\rho} \frac{\partial p}{\partial y} = 0 . \quad (1.169)$$

To these, add three definitions for appropriate total differentials;

$$dx \frac{\partial^2 \psi}{\partial x \partial y} + dy \frac{\partial^2 \psi}{\partial y^2} = du ; \quad (1.170)$$

$$-dx \frac{\partial^2 \psi}{\partial x^2} - dy \frac{\partial^2 \psi}{\partial x \partial y} = dv ; \quad (1.171)$$

$$dx \frac{\partial p}{\partial x} + dy \frac{\partial p}{\partial y} = dp . \quad (1.172)$$

Let these five equations be viewed as a system of linear algebraic equations for the three second derivatives of ψ and the two first derivatives of p . The solution is readily worked out by the method of determinants and verified by substitution. It is

$$\frac{\partial^2 \psi}{\partial x^2} = \frac{(dy)^2 dp_0 - \rho d\psi(dvdx + dudy)}{\rho(ds)^2 d\psi} ; \quad (1.173)$$

$$\frac{\partial^2 \psi}{\partial x \partial y} = \frac{-dx dy dp_0 + \rho d\psi(du dx - dv dy)}{\rho(ds)^2 d\psi} ; \quad (1.174)$$

$$\frac{\partial^2 \psi}{\partial y^2} = \frac{(dx)^2 dp_0 + \rho d\psi(dvdx + dudy)}{\rho(ds)^2 d\psi} ; \quad (1.175)$$

$$\frac{\partial p}{\partial x} = \frac{dp dx + \rho dy(udv - vdu)}{(ds)^2} ; \quad (1.176)$$

$$\frac{\partial p}{\partial y} = \frac{dp dy - \rho dx(udv - vdu)}{(ds)^2} , \quad (1.177)$$

where $(ds)^2 = (dx)^2 + (dy)^2$ and $p_0 = p + \rho(u^2 + v^2)/2$. The given data on the right-hand sides include the velocity, $\vec{u} = (u, v)$; the direction of the derivative, $d\vec{x} = (dx, dy)$; and the associated differentials, dp and $d\vec{u} = (du, dv)$.

Characteristic curves are determined by the condition that the right-hand sides of the system (1.173)–(1.177) take on the form

0/0, so that the highest derivatives are not defined. In the last two equations, (1.176) and (1.177), the denominator never vanishes, and the static pressure is therefore continuous. In the first three equations, (1.173)–(1.175), the denominators vanish on streamlines, where $d\psi = -vdx + udy = 0$, or $v/u = dy/dx$. The numerators then vanish when $dp_0 = 0$. It follows that the streamlines are characteristics of the Euler equations, and that the stagnation pressure p_0 is constant on streamlines (there are, of course, easier ways to prove this particular result). On a streamline, the five equations (1.168)–(1.172) are no longer linearly independent. The quantities u , v , du , dv , dp cannot be chosen independently/ but must satisfy the condition $dp + \rho u du + \rho v dv = 0$.

At the next level of detail, it is necessary to consider whether the inviscid flow is rotational or irrotational. To distinguish the two cases, add equations (1.173) and (1.175) to construct the Laplacian,

$$\frac{\partial^2 \psi}{\partial x^2} + \frac{\partial^2 \psi}{\partial y^2} = \frac{1}{\rho} \frac{dp_0}{d\psi} , \quad (1.178)$$

and recall from SECTION X⁶, for flow of an incompressible fluid in two dimensions, that

$$\frac{\partial^2 \psi}{\partial x^2} + \frac{\partial^2 \psi}{\partial y^2} = -\frac{\partial v}{\partial x} + \frac{\partial u}{\partial y} = -\zeta , \quad (1.179)$$

where ζ is the z -component of vorticity. Hence

$$\frac{1}{\rho} \frac{dp_0}{d\psi} = -\zeta , \quad (1.180)$$

and the numerators in equations (1.173)–(1.175), like the denominators, have $d\psi$ as a factor, whether the flow is rotational or not. This factor can be cancelled unless $d\psi = 0$.

To recapitulate: in the viscous problem, with ν small but not zero, a viscous layer may develop along a subcharacteristic; i.e., a characteristic of the inviscid equations (1.168)–(1.169). If it does, then the original boundary-layer approximation (1.150)–(1.152) is

⁶Unclear what section is intended.

appropriate, because there is an external stream, and the thickness of the viscous layer is proportional to $\nu^{1/2}$. If the viscous layer does not develop along a subcharacteristic, each case has to be treated separately. Three flows in TABLE 1.3 fall into the second class, because there is no external stream, and thus no subcharacteristics.

Because the same boundary-layer equations are ultimately obtained in the limit $\epsilon \rightarrow 0$, this discussion of subcharacteristics may seem to be irrelevant, or at least academic. The discussion is not academic, however, if higher-order solutions are wanted and basis functions are required for a systematic expansion. Moreover, at least two of the three flows in question can also appear as flows into a moving fluid, shifting the problem from the second class to the first one and altering the dimensionless similarity variables.

Two further examples reinforce these comments and demonstrate that the presence of a free stream is neither a necessary nor a sufficient condition for the thickness of a laminar viscous layer to vary like $\nu^{1/2}$. The first example is boundary-layer flow with suction or blowing at the wall. Although the flow has a free stream, streamlines of the inviscid flow pass through the wall. A special case mentioned in many texts on viscous flow is the laminar asymptotic suction layer. The asymptotic flow has no x -dependence, and the continuity equation therefore requires $v = v_w = \text{constant} < 0$. The velocity profile in the boundary layer is easily worked out as

$$\frac{u}{u_\infty} = 1 - \exp(yv_w/\nu) . \quad (1.181)$$

The wall friction for this flow can be obtained either from the truncated momentum-integral equation or by calculating $\mu(\partial u/\partial y)_w$ directly for the profile (4.51).⁷ In either case,

$$\tau_w = -\rho v_w u_\infty . \quad (1.182)$$

The flow is pathological in the sense that the wall friction does not depend on the viscosity of the fluid. It depends only on the product $(\rho u_\infty)(v_w)$, where ρu_∞ is the initial x -momentum per unit volume

⁷See Section 4.2.3.

of the fluid that is eventually removed at the wall, and $-v_w$ is the volume flow of this fluid per unit wall area per unit time. The proper entry for this flow in TABLE 1.3 is $x, y/\nu, \psi, u\nu, v$.

The second example is the free-convection boundary layer on a vertical wall, or the wall plume, discussed in SECTION X. By inspection of the results (**check**), the proper entry for this flow in TABLE 1.3 is $x, y/\nu^{1/2}, \psi/\nu^{1/2}, u, v/\nu^{1/2}$, exactly as for the Blasius boundary layer, despite the fact that the wall plume has no free stream.

1.3.4 Reynolds averaging

This monograph deals with motions that are turbulent, by which I mean motions that are locally three-dimensional, non-steady, rotational, and, for practical purposes, random, at least in the components of intermediate and small scales. Define any physical variable ϕ , such as a component of the velocity vector \vec{u} , as the sum of a mean value and a fluctuation. The mean value is traditionally denoted by an overbar, representing a time or a statistical average. For example,

$$\bar{\phi} = \lim_{T \rightarrow \infty} \frac{1}{T} \int_0^T \phi(t) dt \quad \text{or} \quad \bar{\phi} = \int_{-\infty}^{\infty} \phi p(\phi) d\phi, \quad (1.183)$$

where T is some suitable time interval. In the second definition, the probability density $p(\phi)$ refers to relative frequency of a particular value of ϕ in a large number of repeated observations. In this monograph I will seldom consider problems that are not steady in the mean.

Reynolds stresses, first defined in a seminal paper by REYNOLDS (1895), are generated by replacing each variable in the equations of motion by a mean value plus a fluctuation and then averaging. The method of averaging insures that fluctuations have zero mean, because

$$\phi = \bar{\phi} + \phi' \quad (1.184)$$

becomes

$$\bar{\phi} = \overline{\bar{\phi} + \phi'}, \quad (1.185)$$

from which

$$\overline{\phi'} = 0 . \quad (1.186)$$

The averaging operation for a steady mean flow of an incompressible fluid yields

$$\text{div } \overline{\vec{u}} = 0 ; \quad (1.187)$$

$$\rho \text{ div } (\overline{\vec{u} \circ \vec{u}}) = -\text{grad } \overline{p} + \text{div } \overline{\tau} , \quad (1.188)$$

where $\overline{\vec{u} \circ \vec{u}'} = 0$ and

$$\overline{\tau} = \mu \text{ div } \underline{\text{grad } \vec{u}} - \rho (\overline{\vec{u}' \circ \vec{u}'}) . \quad (1.189)$$

The last term is the Reynolds stress tensor. (*Discuss kinetic theory, $\tau \sim -\rho \overline{c_i c_j}$. Check Reynolds; did he mention this? See Kennard, p 178.*)

Averaging of the dyadic product $\vec{u} \circ \vec{u}$ generates the Reynolds stresses together with the product of the means, $\overline{\vec{u}} \circ \overline{\vec{u}}$. Thus the continuity equation can be used if desired to recover the form of equation (1.32) for mean quantities. However, the general result of the averaging operation is best described as dry water. There are six new unknowns; only six because $\overline{\vec{u}' \circ \vec{u}'}$ is a symmetric tensor. Unfortunately, there are no new equations. In simplistic terms, what is normally done about the six new variables is to reduce their number, by plausible arguments, or by brute force, until there is only one left, usually the shearing stress $\overline{u'v'}$. Then one additional equation is invented. The new equation has no physics in it, although it may (must, to be successful) have some insight. For example, Prandtl's mixing-length model shows profound insight, and I am quite willing to use it if there is nothing better. Not much is contributed to understanding of turbulence by analysis of what has been written down for the missing equation or equations, although the record of the two Stanford contests () may be worth study.

To see what can be done, consider a turbulent shear flow that is two-dimensional and steady in the mean. The mean velocity is $(\overline{u}, \overline{v})$; the velocity fluctuations are (u', v', w') ; and the Reynolds

stress tensor in rectangular coordinates is

$$\underline{\tau} = -\rho \begin{pmatrix} \overline{u'u'} & \overline{u'v'} & \overline{u'w'} \\ \overline{v'u'} & \overline{v'v'} & \overline{v'w'} \\ \overline{w'u'} & \overline{w'v'} & \overline{w'w'} \end{pmatrix} . \quad (1.190)$$

Two of the six Reynolds stresses can be assumed to have zero mean, namely $\overline{u'w'}$ and $\overline{v'w'}$, on the ground of reflection symmetry. There is no correlation, as there is for $\overline{u'v'}$. The equations to be considered are

$$\frac{\partial u}{\partial x} + \frac{\partial v}{\partial y} = 0 , \quad (1.191)$$

$$\begin{aligned} \rho u \frac{\partial u}{\partial x} + \rho v \frac{\partial u}{\partial y} = -\frac{\partial p}{\partial x} + \\ + \mu \left(\frac{\partial^2 u}{\partial x^2} + \frac{\partial^2 u}{\partial y^2} \right) + \frac{\partial}{\partial x} (-\rho \overline{u'u'}) + \frac{\partial}{\partial y} (-\rho \overline{u'v'}) , \end{aligned} \quad (1.192)$$

$$\begin{aligned} \rho u \frac{\partial v}{\partial x} + \rho v \frac{\partial v}{\partial y} = -\frac{\partial p}{\partial y} + \\ + \mu \left(\frac{\partial^2 v}{\partial x^2} + \frac{\partial^2 v}{\partial y^2} \right) + \frac{\partial}{\partial x} (-\rho \overline{v'u'}) + \frac{\partial}{\partial y} (-\rho \overline{v'v'}) , \end{aligned} \quad (1.193)$$

$$0 = \frac{\partial}{\partial z} (-\rho \overline{w'w'}) , \quad (1.194)$$

where mean values for u , v , p are now understood rather than expressed by an overbar, to simplify the notation.

Equation (1.194) is empty but is displayed as a reminder that $\overline{w'w'}$ is not zero. All the muscle is gone from Prandtl's order-of-magnitude argument for a boundary-layer approximation, because the order of magnitude of the turbulent terms is not known with any precision in the absence of experimental data. It is not possible to say that equations (1.191)–(1.193) are an elliptic or parabolic system. There may be no time-like or x -like characteristics of the system. Nevertheless, upstream influence in time or in x is not expected except for separation. There is little guidance about what to do in the turbulent case except by analogy.

Now consider channel flow, which like pipe flow is a special case because of the geometry. All x -derivatives are zero except for the pressure. In particular, $v = 0$. The equations of motion are reduced to

$$0 = -\frac{\partial p}{\partial x} - \frac{\partial}{\partial y} (\rho \overline{u'v'}) + \mu \frac{\partial^2 u}{\partial y^2} , \quad (1.195)$$

$$0 = -\frac{\partial p}{\partial y} - \frac{\partial}{\partial y} (\rho \overline{v'v'}) . \quad (1.196)$$

The first equation can also be written

$$0 = -\frac{\partial p}{\partial x} + \frac{\partial \tau}{\partial y} , \quad (1.197)$$

where

$$\tau = \mu \frac{\partial u}{\partial y} - (\rho \overline{u'v'}) . \quad (1.198)$$

The second equation can be integrated rigorously to obtain

$$p + \rho \overline{v'v'} = p_w , \quad (1.199)$$

where w indicates a wall value. In channel flow this equation may be useful in estimating the mean pressure p away from the wall, this being more difficult to measure than the velocity fluctuation v' . Note that p_w is a function only of x and that $\overline{v'v'}$ is a function only of y , but that p is a function of both. Occasionally, an author will cite equation (1.199) for turbulent boundary-layer flow. The argument is that $v \ll u$ and $\partial/\partial x \ll \partial/\partial y$, so that the laminar boundary-layer approximation holds. Then equation (1.199) can be differentiated with respect to x and the result substituted in equation (1.192) to obtain

$$\begin{aligned} \rho u \frac{\partial u}{\partial x} + \rho v \frac{\partial u}{\partial y} &= -\frac{\partial p_w}{\partial x} + \\ + \frac{\partial}{\partial x} (\rho \overline{v'v'} - \rho \overline{u'u'}) - \frac{\partial}{\partial y} (\rho \overline{u'v'}) + \mu \frac{\partial}{\partial y} \frac{\partial u}{\partial y} . \end{aligned} \quad (1.200)$$

Then if $\overline{u'u'}$ and $\overline{v'v'}$ are very nearly equal (they are not) the only surviving Reynolds stress is the shearing stress $-\rho \overline{u'v'}$. I don't recommend this argument, since the boundary-layer version is not on

solid ground. I prefer to be guided by the aphorism that the only truth about turbulence is experimental truth, including the results of careful computer simulations. Liepmann, who was no respecter of archaic traditions, once said that the invention of Reynolds stresses impeded research in turbulence in the same way that the invention of the vacuum tube impeded the development of the transistor. In fact, eighty years passed while the turbulence research community struggled with the absence of phase information in Reynolds' model, until the rise of computer-assisted instrumentation finally provided access to the revolutionary concept of coherent structure.

1.3.5 Dimensions and similarity

Fluid mechanics is characterized by an almost religious dedication to the concept of dimensionless variables. The rules of this discipline are sometimes applied at a primitive level, the objective being to discover dimensionless variables without necessarily discovering any bond between them except through experiment. Turbulent pipe flow is a good example. The spirit of this subject is the same one that prompts the use of semi-log or log-log coordinates to display exponential or power-law behavior and occasionally to show that different laws are operating in different ranges of the variables. A case in point is the plane jet from a long unshielded rectangular orifice into an unconfined fluid. Near the orifice, the flow behaves like a plane jet. Far downstream, the flow must behave like a round jet, with different similarity laws. For each of the flows discussed in this monograph it is assumed that the flow is determined by a finite number of global parameters, physical or geometrical, some important and some not. These parameters are the ostensible data of the problem. They are numbers that would have to be communicated from one observer to another in order for a particular experiment to be duplicated precisely.

The subject of dimensional analysis is so important in fluid mechanics that it has generated its own literature (SEDOV, more). Applications can be divided roughly into two categories; those that apply when the problem is defined by differential equations, and

those that apply when it is not. Both categories will be illustrated in what follows.

Stokes. My first example is a dimensional argument that uses group theory to solve a linear problem, the unsteady laminar motion produced in an incompressible fluid by the impulsive motion of an infinite flat plate in its own plane. The differential equation in question is

$$\frac{\partial u}{\partial t} = \nu \frac{\partial^2 u}{\partial y^2} , \quad (1.201)$$

with the boundary conditions

$$\begin{aligned} u(y, t) &= 0 & t < 0 , \\ u(0, t) &= U & t > 0 , \end{aligned} \quad (1.202)$$

$$u(\infty, t) = 0 \quad \text{all } t ,$$

where U is a constant velocity. The resulting motion is shown in FIGURE 1.2. The fluid problem was first solved by STOKES (19XX), who had at the time reservations about the validity of the no-slip condition. One method of solution that is both physical and general is group theory, because it can serve for problems that are linear or non-linear. Consider an affine transformation of all of the variables and parameters of problem (1.201)–(1.202). Let unmarked quantities refer to one flow, and let quantities marked by a circumflex refer to another flow obtained by the transformation

$$\begin{aligned} y &= a\hat{y} , \\ t &= b\hat{t} , \\ u &= c\hat{u} , \\ U &= d\hat{U} , \\ \nu &= e\hat{\nu} , \end{aligned} \quad (1.203)$$

where the scaling parameters a, b, \dots are finite dimensionless numbers. No distinction is made in this formulation between independent variables, dependent variables, and parameters, whether entering through the equation or the boundary conditions. Everything

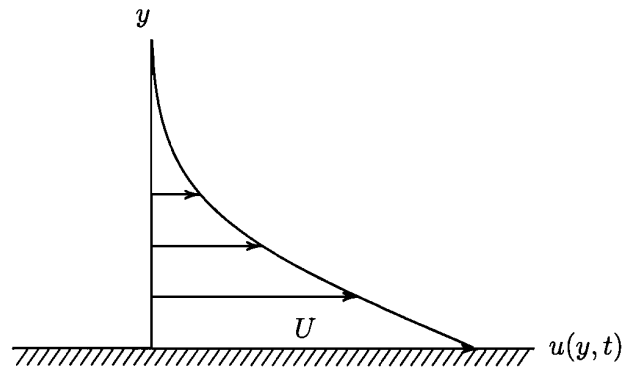


Figure 1.2: The laminar velocity profile for impulsive motion of an infinite flat plate in its own plane.

is included. Equations (1.203) form a group. Application of the transformation to the differential equation (1.201) and the boundary conditions (1.202) gives

$$\frac{c}{b} \frac{\partial \hat{u}}{\partial \hat{t}} = \frac{ce}{a^2} \hat{\nu} \frac{\partial^2 \hat{u}}{\partial \hat{y}^2} , \quad (1.204)$$

together with

$$\begin{aligned} c\hat{u}(a\hat{y}, b\hat{t}) &= 0 , & b\hat{t} < 0 , \\ c\hat{u}(0, b\hat{t}) &= d\hat{U} , & b\hat{t} > 0 , \\ c\hat{u}(\infty, b\hat{t}) &= 0 , & \text{all } b\hat{t} . \end{aligned} \quad (1.205)$$

The conditions that make the differential equation (1.204) and the middle boundary condition (1.205) invariant to the transformation are evidently

$$\frac{a^2}{be} = 1, \quad \frac{c}{d} = 1 . \quad (1.206)$$

These are the key relationships. Substitution in equations (1.206) for a, b, c, \dots from equations (1.203) yields

$$\frac{y^2}{\hat{y}^2} \frac{\hat{t}}{t} \frac{\hat{\nu}}{\nu} = 1 , \quad \frac{u}{\hat{u}} \frac{\hat{U}}{U} = 1 , \quad (1.207)$$

or better

$$\eta = \frac{y}{(\nu t)^{1/2}} = \frac{\hat{y}}{(\hat{\nu} \hat{t})^{1/2}} = \hat{\eta} , \quad (1.208)$$

$$f = \frac{u}{U} = \frac{\hat{u}}{\hat{U}} = \hat{f} . \quad (1.209)$$

At this point the material of the problem has been reduced to two dimensionless combinations, η and f . It is natural to assume that one combination must be a function of the other;

$$\frac{u}{U} = f \left(\frac{y}{\sqrt{\nu t}} \right) . \quad (1.210)$$

A rigorous argument that this assumption is correct can be found in SECTION 9.1.2 of Chapter 9. The function in question satisfies the ordinary differential equation

$$f'' + \frac{1}{2} \eta f' = 0 . \quad (1.211)$$

With the boundary conditions (1.202) and use of a table of integrals, the solution emerges as the complementary error function,

$$f(\eta) = 1 - \frac{1}{\sqrt{\pi}} \int_0^{\eta} e^{-x^2} dx . \quad (1.212)$$

This group method will be applied throughout this monograph to a variety of flows, laminar and turbulent. Similarity solutions are important. Nature tends to them carefully, and they may play a role in non-similar problems as well.

Kolmogorov. My second example of dimensional analysis is a celebrated prediction by KOLMOGOROV (1941) of a property of homogeneous isotropic turbulence called the $-5/3$ power law. Note that a periodic function calls for a Fourier series. A function that vanishes at infinity calls for a Fourier integral. Turbulence is neither of these. It requires a new kind of mathematics called generalized harmonic analysis. This subject was introduced to the fluid mechanics community in three papers by G. I. TAYLOR () and later in a monograph by BATCHELOR (). The primary elements are the two-point covariance and the spectral density as Fourier transforms of each other. (**Check**)

Consider an energy density $E(\kappa)$, defined by

$$\int_0^{\infty} E(\kappa) d\kappa = \frac{1}{2} (\overline{u'u'} + \overline{v'v'} + \overline{w'w'}) , \quad (1.213)$$

where κ is wave number or waves per unit length. The dimensional units of E are energy per unit mass and per unit wave number. The function $E(\kappa)$ may depend on numerous parameters, including various properties of the mechanism that is stirring the fluid.

Kolmogorov's first assumption is that only two parameters are important. These are ϵ , the rate of energy dissipation per unit mass and unit time, and ν , the kinematic viscosity of the fluid. Assume, therefore, that there exists for some range of κ a relationship

$$E = E(\kappa; \epsilon, \nu) . \quad (1.214)$$

The dimensions of the independent variable κ and the dependent variable E are, respectively,

$$[\kappa] = \frac{1}{\text{length}} = \frac{1}{L} , \quad (1.215)$$

$$[E] = \frac{\text{energy} \cdot \text{length}}{\text{mass}} = U^2 L . \quad (1.216)$$

These relationships are not equations in the normal sense. The notation $[\dots] =$ is read "the dimensions of $[\dots]$ are." The two parameters ϵ and ν have dimensions

$$[\epsilon] = \frac{\text{energy}}{\text{mass} \cdot \text{time}} = \frac{U^2}{T} = \frac{U^3}{L} , \quad (1.217)$$

$$[\nu] = \text{velocity} \cdot \text{length} = UL . \quad (1.218)$$

Suppose that E and κ are to be made dimensionless with ϵ and ν . It is almost self-evident that in the present problem there are just enough dimensional relationships to make this possible. Schematically, look for dimensionless combinations

$$[\kappa \epsilon^a \nu^b] = 0 = \frac{1}{L} \left(\frac{U^3}{L} \right)^a (UL)^b , \quad (1.219)$$

$$[E \epsilon^c \nu^d] = 0 = U^2 L \left(\frac{U^3}{L} \right)^c (UL)^d . \quad (1.220)$$

These statements can be satisfied only if $a = -1/4$, $b = 3/4$ and $c = -1/4$, $d = -5/4$. The desired dimensionless form of the relationship (1.214) is therefore

$$\frac{E}{\epsilon^{1/4} \nu^{5/4}} = F \left(\frac{\kappa \nu^{3/4}}{\epsilon^{1/4}} \right) = F(\eta) , \quad \text{say} . \quad (1.221)$$

Kolmogorov introduced the notion of what is now called the inertial subrange. His first hypothesis that the spectral density $E(\kappa)$ is uniquely determined by the quantities ν and ϵ is securely formulated in the dimensional argument. The largest eddies in a flow are the scale at which it is stirred. The smallest eddies are at a scale where dissipation dominates. If the two scales are well separated, the important quantity becomes the rate that energy is supplied to the system at large scales and removed at small scales. The problem is assumed to be stationary. The energy flows through a series of scales through a mechanism that is called a cascade but is difficult to describe.

Kolmogorov's second hypothesis is that in the inertial subrange $E(\kappa)$ is uniquely determined by the quantity ϵ and does not depend on ν . That is, there are intermediate scales, not small enough for viscosity to be important, but not large enough to have significant memory of the process that supplies energy to the flow. In the inertial subrange, the hypothesis is that $\partial E/\partial \nu = 0$. Equation (1.221) then implies

$$\frac{5}{3} F + \eta \frac{dF}{d\eta} = 0 \quad , \quad (1.222)$$

and thus immediately

$$F = c \eta^{-5/3} \quad , \quad (1.223)$$

where c is a constant of integration. In dimensional form,

$$E(\eta) = c \epsilon^{2/3} \kappa^{-5/3} \quad . \quad (1.224)$$

A formally equivalent but physically more transparent argument illustrates a different approach to the same problem. In this argument, quantities like M , L , U , T are no longer the dimensions of a quantity, but physical scales that are characteristic of the process. The distinction will be made by using bold-face symbols for such quantities. In the present instance, equations (1.217) and (1.218) are replaced by

$$\epsilon = \frac{\mathbf{U}^3}{\mathbf{L}} \quad , \quad (1.225)$$

$$\nu = \mathbf{U} \mathbf{L} \quad , \quad (1.226)$$

where the absence of the notation [...] means that these equations now *define* physical scales \mathbf{U} and \mathbf{L} . When the last two equations are solved for \mathbf{U} and \mathbf{L} , the result is

$$\mathbf{U} = (\nu \epsilon)^{1/4} , \quad (1.227)$$

$$\mathbf{L} = \left(\frac{\nu^3}{\epsilon} \right)^{1/4} . \quad (1.228)$$

Normalization of E and κ in the form

$$\frac{E}{\mathbf{U}^2 \mathbf{L}} = F(\kappa \mathbf{L}) \quad (1.229)$$

leads again to equation (1.221). The advantage of the second approach is that it creates an image of fluid elements of size \mathbf{L} moving at velocity \mathbf{U} . These characteristic scales are related to each other and to the global parameters by

$$\frac{\mathbf{U} \mathbf{L}}{\nu} = 1 , \quad (1.230)$$

$$\frac{\epsilon \mathbf{L}}{\mathbf{U}^3} = 1 , \quad (1.231)$$

so that the characteristic Reynolds number is unity.

The argument just given is in one sense unique. If my understanding is correct, equation (1.224) is the only prediction about turbulent flow that was made before there were any reliable measurements. The ideas of Kolmogorov are not of themselves central to this monograph. However, there is a close connection, developed in SECTION X below, with an idea that *is* central, namely, the existence of a logarithmic law for the mean-velocity profile in flow near a wall.

Readers who consult Kolmogorov's paper may be surprised to discover that he did not use the variables E and κ , but rather the double correlation of velocity fluctuations measured at different points in the fluid. Consequently, Kolmogorov's assumptions are tailored to the argument. If there were another scale, say the mesh size of a grid in a wind tunnel, the argument might break down. There would also be the solidity of the grid, which is already a dimensionless number.

PLACEHOLDER

Figure 1.3: Caption for Figure with label Fig1-10 (missing).

FIGURE 1.3 is a collection of spectral measurements from a variety of sources found in nature or manufactured in a laboratory. These include boundary layer, channel, pipe, jet, wake, tidal channel, and grid turbulence. In general, these flows are neither homogeneous nor isotropic. I have not vetted this figure, but the display may not be as simple as it seems. What is measured is usually frequency, which is not directly convertible to wave number without a knowledge of phase velocity. The critical quantity fueling equation (1.224), the dissipation ϵ , is difficult to measure except perhaps in grid turbulence.

Two flows that are not represented in figure 1.3 are the mixing layer and the vortex street. These two flows have several features in common, and their mechanisms can be tested by descriptions that are at present more than conjecture but less than conviction. They appear in laminar and turbulent versions and tend to a two-dimensional form. The topology is also similar. There is a fundamental instability leading to periodic vorticity concentrations. When the motion is viewed in coordinates moving at the celerity of the large eddies, the pattern is as sketched in the two cartoons in FIGURE 1.4, which is reproduced from COLES (1985). In each case the pattern consists of alternating centers and saddles. An unexpected common property of the two flows is the location of the region of maximum turbu-

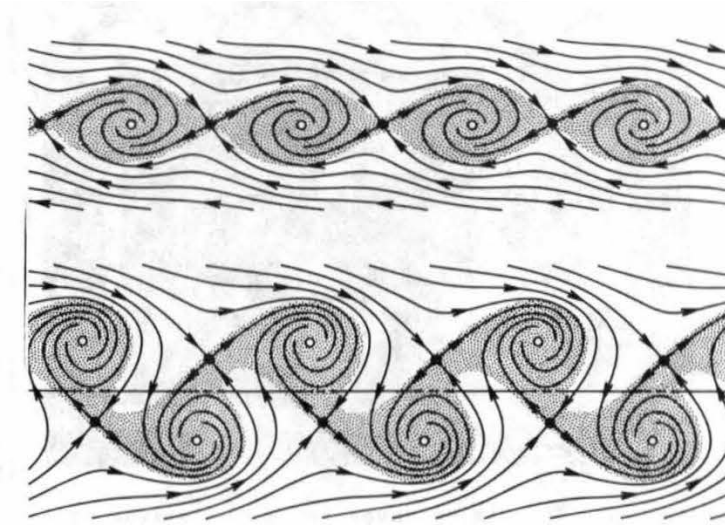


Figure 1.4: Topological cartoons of the vortex street and the mixing layer (caption by K. Coles).

lence production, defined as $\overline{\tau \cdot \text{grad } \vec{u}}$. It was shown experimentally for the mixing layer by HUSSAIN () and for the vortex street by CANTWELL and COLES () that this maximum is closer to the saddle points than it is to the large turbulent centers. Each saddle lies in a novel structure, called a braid, that is the locus of contact between irrotational fluids arriving from the two sides of the mixing layer or vortex street. The braid contains the two outgoing separatrices of the saddle. These carry entrained fluid in both directions to the two nearest centers. In this process, vortex tubes, called ribs, are formed in the braid by another instability that is not yet completely understood, although the potential flow very near a two-dimensional saddle point may be eligible to undergo Taylor-Görtler instability. Vortex tubes of alternate sign are shown in the elegant view of a mixing layer in FIGURE 1.5 from a paper by METCALF *et al.* (1987). This paper records elaborate numerical solutions of the Navier-Stokes equations for the laminar mixing layer. The emphasis is on vorticity rather than velocity, so the figure does not display the

PLACEHOLDER

Figure 1.5: Caption for Figure with label Fig1-12 (missing).

alleged saddle points directly.

Chapter 2

PIPE FLOW

2.1 Generalities

On both historical and pedagogical grounds, fully developed flow in a smooth pipe of circular cross section is an ideal point of entry for technical fluid mechanics. The reason is that a crucial quantity, the friction at the wall, is proportional to the axial pressure gradient, which is usually easily measured. More than a century ago, experiments by Hagen, Poiseuille, Couette and others used this property to confirm the hypothesis of Newton that the viscosity of ordinary fluids, particularly water and air, is a real physical quantity that depends on the state of the fluid but not on the particular motion. These early experimenters encountered turbulence in larger facilities at higher speeds, and the issue quickly became the need for a better qualitative and quantitative appreciation of turbulence. In fact, it was an investigation of transition in pipe flow by Reynolds that led to the discovery of the fundamental dimensionless number that bears his name.

Study of turbulent flow in smooth round pipes led about 1930 to development of the mixing-length model, which in some situations still represents the best available approach to the problem of turbulent flow near a wall. An important mechanism, just beginning to be understood, involves the effect of the no-slip condition at the

wall on turbulent fluctuations. Pipe flow is the vehicle of choice for exploring the effect of wall roughness and the effect of drag-reducing polymers on turbulent flow. Pipe flow is also a useful vehicle for investigating heat transfer, with numerous practical applications. Secondary flow in non-circular pipes exposes the non-Newtonian nature of the Reynolds stresses, unfortunately without exposing any plausible constitutive relations. Other variations on pipe flow, such as flow with curvature or flow with an abrupt change in cross section, reveal strong effects on mixing processes. Similarity laws originally developed for pipe flow provide a point of contact with the boundary layer and the wall jet.

The main experimental disadvantage of pipe flow is difficulty of access for instrumentation, particularly optical instrumentation. A major source of experimental scatter in fundamental work is failure to provide sufficient length for the flow to become fully developed.

2.1.1 Equations of motion

The Reynolds equations of mean motion were derived in SECTION 1.3.4 for the cylindrical polar coordinates sketched in FIGURE 2.1. These equations are easily specialized for the case of steady flow in a round pipe of radius R . To make the notation consistent with that for plane flow, take the axial, radial, and azimuthal coordinates as (x, r, θ) and the corresponding velocity components as (u, v, w) . Take the mean flow to be fully developed, which is to say rectilinear. Thus $\bar{v} = \bar{w} = 0$, and $\bar{u} \neq 0$. All derivatives of mean quantities with respect to θ are zero, as are all derivatives with respect to x except $\partial\bar{p}/\partial x$, this term being the engine that drives the flow. The continuity equation is moot. For simplicity, the overbar indicating a mean value will be suppressed hereafter except in the Reynolds stresses. The three momentum equations are reduced to

$$0 = -\frac{\partial p}{\partial x} + \frac{1}{r} \frac{d}{dr} r \left(\mu \frac{du}{dr} - \rho \overline{u'v'} \right) ; \quad (2.1)$$

$$0 = -\frac{\partial p}{\partial r} + \frac{1}{r} \left(\rho \overline{w'w'} - \frac{d}{dr} r \rho \overline{v'v'} \right) ; \quad (2.2)$$

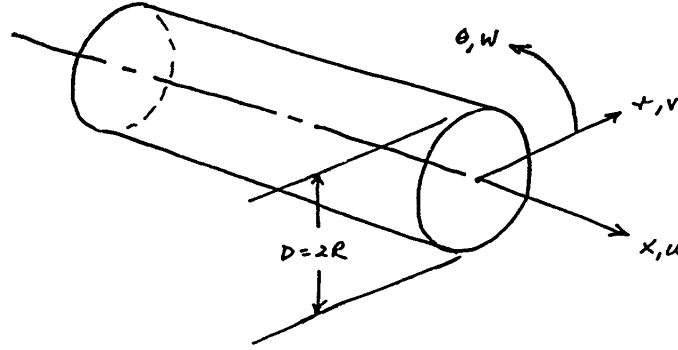


Figure 2.1: Cylindrical polar coordinate system and notation for pipe flow.

$$0 = -\frac{1}{r^2} \frac{d}{dr} r^2 \overline{\rho v' w'} . \quad (2.3)$$

The fluctuations u', v', w' vanish at the wall. The three equations (2.1)–(2.3) are rigorously correct, and must be satisfied by the mean flow under the specified conditions. The equations are obviously not complete, since there are three equations for six unknown quantities. Two of the Reynolds stresses, $-\overline{\rho u' u'}$ and $-\overline{\rho u' w'}$, fail to appear. Of these, the absence of the mean product $\overline{u' w'}$ is expected if the turbulent motion is random. Given a sampled value for the axial fluctuation u' , it is reasonable to suppose, in view of the axial symmetry of the problem, that positive and negative values for the azimuthal fluctuation w' are equally probable. That this argument can be dangerous will be demonstrated in SECTION 2.5.5, where it leads to a wrong conclusion for the viscous sublayer near a wall. In the case of $-\overline{\rho u' u'}$, the failure of the Reynolds equations even to contain this streamwise normal stress is embarrassing. It appears that nothing can be learned about this stress from the laws of mechanics in Reynolds-averaged form. At the same time, it is this Reynolds stress $-\overline{\rho u' u'}$ that is most easily and most commonly measured.

Consider the three equations of motion (2.1)–(2.3). The third equation (2.3) has the integral $r^2 \rho \overline{v'w'}$ = constant, and the constant is zero whether evaluated on the axis or at the wall. The second equation (2.2) is more instructive. Formal integration from r to R , with the boundary condition $p = p_w$ at the wall, gives

$$p + \rho \overline{v'v'} = p_w - \rho \int_r^R \frac{(\overline{w'w'} - \overline{v'v'})}{r} dr . \quad (2.4)$$

When the lower limit is taken at the pipe axis, $r = 0$, the integral diverges unless $\overline{v'v'} = \overline{w'w'}$ on the axis. The equality is intuitively obvious. If two traverses are made along a diameter of the pipe to measure in one case the radial velocity fluctuation v' along the traverse direction and in the other case the azimuthal velocity fluctuation w' normal to it, the two measurements must be statistically equivalent on the axis.

As the lower limit r in equation (2.4) approaches the upper limit R , the definite integral is eventually small compared with the term $\rho \overline{v'v'}$ on the left. In some vicinity of the wall, therefore, a useful approximation suggests itself;

$$p + \rho \overline{v'v'} = p_w = \text{constant} . \quad (2.5)$$

This approximation will be examined more closely in SECTION X¹.

Finally, the quantity in parentheses in the first momentum equation (2.1) is evidently the total shearing stress τ , here defined with a change in sign in the derivative and in v' because $y = R - r$ is a more natural independent variable for an observer viewing the flow from the wall;

$$\tau = - \left(\mu \frac{du}{dr} - \rho \overline{u'v'} \right) . \quad (2.6)$$

At the wall of the pipe, where all velocity fluctuations vanish, the corresponding value is

$$\tau_w = -\mu \left(\frac{du}{dr} \right)_w . \quad (2.7)$$

¹Unclear reference, possibly 5.2.1

By assumption, the terms in parentheses in equations (2.1) and (2.2) do not depend on x , so that

$$\frac{\partial^2 p}{\partial x^2} = \frac{\partial^2 p}{\partial r \partial x} = 0 . \quad (2.8)$$

It follows that $\partial p / \partial x$ is a constant, independent of x and r , although p itself depends on x and also on r if the flow is turbulent, according to equation (2.4). Equation (2.1) in the form

$$0 = -\frac{\partial p}{\partial x} - \frac{1}{r} \frac{dr\tau}{dr} \quad (2.9)$$

can therefore be integrated from r to R , with the boundary condition $\tau = \tau_w$ when $r = R$, to obtain

$$R\tau_w - r\tau = -\frac{(R^2 - r^2)}{2} \frac{\partial p}{\partial x} . \quad (2.10)$$

On putting $r = 0$, this becomes

$$\tau_w = -\frac{D}{4} \frac{\partial p}{\partial x} , \quad (2.11)$$

where $D = 2R$ is the diameter. The last expression is also easily obtained from a global momentum balance on a length of the pipe, given that $\partial p / \partial x$ is constant. Elimination of $\partial p / \partial x$ between equations (2.10) and (2.11) yields finally the linear stress profile shown in FIGURE 2.2,

$$\frac{\tau}{\tau_w} = \frac{r}{R} . \quad (2.12)$$

So far, the flow has usually not been specified to be either laminar or turbulent. In either case, equation (2.11) provides an accurate and unambiguous method for determining τ_w for fully developed flow, and this property is the main reason that pipe flow is discussed here before all other flows involving walls. In a real pipe, there will be problems with entrance flow and development length, to be discussed in SECTION 2.2.1. The fact that the stress τ defined by equation (2.6) is linear in r also provides an opportunity for proof and calibration of instruments, such as hot-wire anemometers,

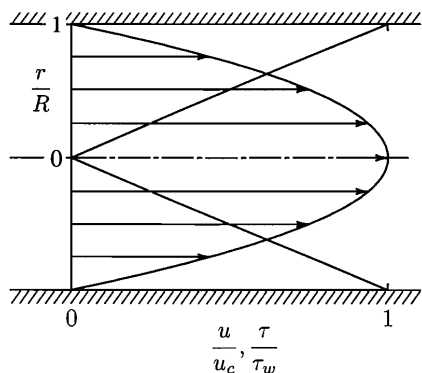


Figure 2.2: The parabolic mean-velocity profile and the linear shearing-stress profile for steady laminar flow in a circular pipe.

commonly used for measurement of the Reynolds shearing stress. See, for example, NEWMAN and LEARY (1950), KJELLSTRÖM and HEDBERG (1970), and PATEL (1974). A more cogent use of equation (2.12), as one criterion for equilibrium at second order of a developing turbulent flow, will be taken up in SECTION 2.5.1.

2.1.2 Laminar flow

If the flow is laminar, p is independent of r , according to equation (2.2), so that $\partial p/\partial x$ becomes dp/dx . The velocity profile is the integral of equation (2.12), given $\tau = -\mu du/dr$, that takes the value $u = u_c$ (c for centerline) at $r = 0$ and satisfies the boundary condition $u = 0$ at $r = R$. In dimensionless form, this profile is the parabola shown in FIGURE 2.2,

$$\frac{u}{u_c} = 1 - \frac{r^2}{R^2}, \quad (2.13)$$

where the centerline velocity u_c is related to the other parameters of the problem by

$$\tau_w = 2\mu \frac{u_c}{R} . \quad (2.14)$$

This solution (2.13) of the Navier-Stokes equations for laminar pipe flow, like solutions of the Stokes approximation for low Reynolds numbers, represents a balance between pressure forces and viscous forces. However, the transport terms vanish here because of the special geometry, not because the Reynolds number is necessarily small.

Finally, the volume flow Q in the pipe can be calculated, and a mean velocity \tilde{u} defined, from

$$Q = \int_0^R 2\pi r u dr = \pi R^2 \tilde{u} \quad (2.15)$$

(the tilde, here and elsewhere, is intended as a mnemonic for an integral mean value). Given equation (2.13) for u , it follows on integration that

$$\tilde{u} = \frac{u_c}{2} . \quad (2.16)$$

Several of the earliest experiments with pipe flow and with flow between concentric rotating cylinders in the 19th century were undertaken primarily for a reason that may now seem almost unnatural. The equations of NAVIER (1823) and STOKES (1849) independently incorporate a hypothesis first proposed by NEWTON in his *Principia Mathematica*, published in 1687. According to STANTON and PANNELL (1914), the proper attribution to Newton was first pointed out by Sir George Greenhill, who would presumably have been at home in both the subject and the Latin language. The relevant passage introduces Section IX, “The circular motion of fluids,” in Book II, “The motion of bodies.” In the elegant prose of the revised translation by Cajori (1934):

Hypothesis: The resistance arising from the want of lubricity in the parts of a fluid is, other things being equal,

proportional to the velocity with which the parts of the fluid are separated from one another.

This hypothesis is explicit in the tensor relation $\underline{\tau} = \mu \text{def } \underline{u}$ in the introduction. The scalar constant of proportionality, the viscosity, is assumed to be an intrinsic or state property of the fluid (it may, for example, vary significantly with temperature), independent of the motion. In the case of pipe flow, the technique was and is used to show the existence of such a fluid property by showing that the quantity μ , expressed theoretically for the case of fully developed laminar pipe flow by a combination of equations (2.11), (2.14), and (2.16),

$$\mu = -\frac{D^2}{32\tilde{u}} \frac{dp}{dx}, \quad (2.17)$$

is experimentally independent of particular choices for D and \tilde{u} , since these must be precisely compensated for by variations in dp/dx . As a practical matter, it is usually not the mean velocity \tilde{u} that is measured, but the volume flux Q defined by equation (2.15). Equation (2.17) is therefore better expressed as

$$\mu = -\frac{\pi D^4}{128Q} \frac{dp}{dx} \quad (2.18)$$

to emphasize that in capillary-tube viscometry the diameter D needs to be very accurately known. Many common fluids, including air and water, possess the property of viscosity in the sense just defined and are therefore referred to as Newtonian fluids. A second important issue, the validity of the no-slip boundary condition at the wall, has for practical purposes been resolved experimentally in favor of no slip. Residual doubts about this condition for the case of non-wetting combinations, such as mercury on glass, or water on tetrafluoroethylene (teflon), have been mostly quieted by BINGHAM and THOMPSON (1928) and by BROCKMAN (1956), respectively. Exceptions to Newtonian behavior are known, and these present formidable difficulties in formulating a constitutive relationship between the stress and rate-of-strain tensors. The relatively unstructured literature of rheology and of turbulence modeling testifies, in a familiar idiom, that Newton is a hard act to follow.

The Reynolds number for both laminar and turbulent pipe flow is commonly defined in terms of the mean velocity \tilde{u} and the pipe diameter D ;

$$Re = \frac{\tilde{u}D}{\nu} . \quad (2.19)$$

Usage varies in defining a dimensionless friction coefficient (see SECTION X).² In mechanical and aeronautical engineering, where the boundary layer and its global momentum balance are in the foreground, the usual form for the dimensionless friction, and the one that I will adopt here, is

$$C_f = \frac{\tau_w}{\rho\tilde{u}^2/2} . \quad (2.20)$$

This quantity is also denoted by f and called the Fanning factor by mechanical engineers. For laminar flow, equations (2.14), (2.16), (2.19), and (2.20) imply

$$C_f = \frac{16}{Re} . \quad (2.21)$$

To the extent that pipe flow can be viewed as a boundary layer on the inside of a cylindrical body, it might be more consistent to use u_c and R instead of \tilde{u} and D in the definition (2.19) for the Reynolds number, and u_c^2 instead of \tilde{u}^2 in the definition (2.20) for the friction coefficient. Probably the usage described here has survived because no value for u_c is available for most of the existing pipe data. In practice, the definition of dimensionless coefficients to characterize pipe flow over a large range of Reynolds numbers has been preempted by the turbulent case, for which the wall friction is only weakly dependent on the viscosity, and the dynamic pressure is the important reference quantity.

In principle, both τ_w and \tilde{u} are easily measured for fully developed pipe flow, the former in terms of $\partial p/\partial x$ and the latter by a variety of methods. These include direct evaluation from the integral definition (2.15), if a velocity profile is available; or measurement of volume flow rate, by weighing or by use of a calibrated volume if

²Possibly section 2.4.1

the fluid is a liquid; or by blowdown techniques if the fluid is a gas. Other methods include use of a calibrated venturi, orifice plate, or other type of flow meter; or, for best regulation, use of a constant-displacement pump or even a piston-cylinder displacement mechanism.

2.1.3 An extremum principle

It was pointed out by LIN (1952), in a short paper whose roots lie in work by HELMHOLTZ (1868) and KORTEWEG (1883) on arbitrarily slow steady viscous motions, that the parabolic laminar profile in a round pipe can be obtained from an extremum principle. Consider all possible axisymmetric rectilinear motions $u(r)$ satisfying the no-slip condition at the wall, and minimize the total rate of energy dissipation,

$$\tilde{\Phi} = \mu \int_0^R 2\pi r \left(\frac{du}{dr} \right)^2 dr , \quad (2.22)$$

subject to the constraint of a constant volume flux,

$$Q = \int_0^R 2\pi r u dr = \pi R^2 \tilde{u} = \text{constant} . \quad (2.23)$$

The notation $\tilde{\Phi}$ means a volume integral of the local rate of dissipation over the pipe cross section and over unit length in the flow direction.

The problem just formulated is an example of what COURANT and HILBERT (1953, Vol. 1, Chapter IV) call the simplest problem in the variational calculus. This is to find the function $u(r)$ that minimizes the integral

$$\tilde{\Phi} = \int_0^R F(r, u, u') dr , \quad (2.24)$$

subject to the constraint

$$Q = \int_0^R G(r, u, u') dr = \text{constant} . \quad (2.25)$$

The prime here indicates differentiation with respect to r . The Euler equation for the problem is

$$\left(u'' \frac{\partial^2}{\partial u' \partial u'} + u' \frac{\partial^2}{\partial u \partial u'} + \frac{\partial^2}{\partial r \partial u'} - \frac{\partial}{\partial u} \right) (F + \lambda G) = 0 , \quad (2.26)$$

where λ is a Lagrange multiplier. In the present case, with

$$F = 2\pi\mu r(u')^2, \quad G = 2\pi r u , \quad (2.27)$$

equation (2.26) becomes

$$2\mu \frac{d}{dr} \left(r \frac{du}{dr} \right) - \lambda r = 0 . \quad (2.28)$$

The indefinite integral of this equation is

$$u = \frac{1}{2\mu} \left(\frac{\lambda r^2}{4} + A \ln r + B \right) , \quad (2.29)$$

where A and B are constants of integration. A logarithmic term appears in equation (2.29), but not in equation (2.13), because the earlier derivation already required τ (i.e., du/dr) to be linear in r . The logarithmic term is needed if the no-slip boundary condition is to be satisfied for the more general case of axial flow in an annulus. For flow in a pipe, the boundary conditions $u = u_c$ at $r = 0$ and $u = 0$ at $r = R$ require $A = 0$ and $B = 2\mu u_c = -\lambda R^2/4$. Equation (2.14) is recovered,

$$\frac{u}{u_c} = 1 - \frac{r^2}{R^2} , \quad (2.30)$$

with now

$$\lambda = -\frac{8\mu u_c}{R^2} . \quad (2.31)$$

Use of the three equations (2.31), (2.14), and (2.11) implies

$$\lambda = 2 \frac{dp}{dx} , \quad (2.32)$$

as does a direct comparison of equation (2.28) with the laminar version of the momentum equation (2.1).

For the parabolic profile in a pipe, therefore, the rate of dissipation is an extremum. That the extremum is a minimum is easily shown by adding to the parabolic profile an arbitrary axisymmetric perturbation that vanishes at the wall and does not contribute to the volume flux. The result (2.32), derived here for a very special motion of an incompressible viscous fluid, should be read in the same sitting as SOMMERFELD's argument (1950, pp. 89–92) that for an incompressible inviscid fluid the pressure p can be interpreted as a Lagrange multiplier representing the constraint of incompressibility.

Finally, the pressure gradient and the rate of dissipation can be related directly for fully developed pipe flow, whether laminar or turbulent. The general form for energy loss from the mean flow per unit time and per unit volume is **(cite introduction)** $\underline{\tau} \cdot \underline{\text{grad}} \vec{u}$, so that equation (2.22) can be written

$$\tilde{\Phi} = \int_0^R 2\pi r \tau \frac{du}{dr} dr . \quad (2.33)$$

Integration by parts, with $\tau = 0$ at $r = 0$ and $u = 0$ at $r = R$, gives

$$\tilde{\Phi} = -2\pi \int_0^R u \frac{dr\tau}{dr} dr . \quad (2.34)$$

Use of equation (2.12) for τ , (2.15) for the volume flow Q , and (2.11) for τ_w then gives

$$\tilde{\Phi} = -Q \frac{\partial p}{\partial x} . \quad (2.35)$$

The point of this exercise in the calculus of variations for laminar pipe flow is that a similar principle may hold for turbulent flow. If so, it would not be surprising if the resulting mean velocity profile turned out to be logarithmic.

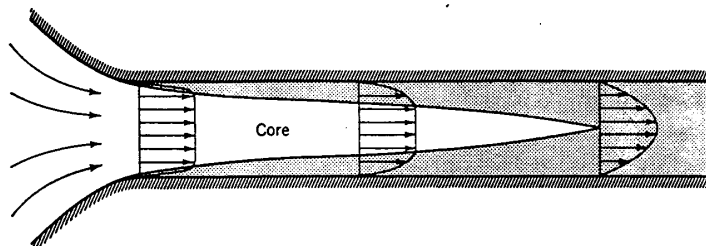


Figure 2.3: A schematic diagram of flow in the laminar development region of a circular pipe with uniform entrance flow.

2.2 Development length

In any attempt to define the properties of a hypothetical fully developed or equilibrium flow experimentally, a useful first step is to observe the rate of approach to equilibrium from a disturbed initial condition. In the case of pipe flow, the process most commonly observed is the evolution of the flow downstream from the pipe entrance. The response to other disturbances, such as a step change in diameter, can also provide estimates of a characteristic time scale or spatial scale for approach to equilibrium.

2.2.1 Laminar flow

The parabolic profile requires some distance to develop in the entrance region of a real pipe, especially at large Reynolds numbers, and the need for adequate development length is not always recognized by experimenters. Let this development length be estimated approximately in terms of the inward growth of internal laminar boundary layers that start at the pipe entrance at $x = 0$, as shown in FIGURE 2.3. Note that the artist was apparently not told of the doubling of the velocity on the pipe axis during laminar develop-

ment. Global parameters available for making the estimate dimensionless are the kinematic viscosity ν , the pipe diameter D , and the mean velocity \tilde{u} . That the latter quantity is independent of x in the development region can be shown by reinstating the axisymmetric continuity equation in the form

$$\frac{\partial u}{\partial x} + \frac{1}{r} \frac{\partial rv}{\partial r} = 0 \quad (2.36)$$

and calculating the derivative of \tilde{u} from the definition (2.15); thus

$$\pi R^2 \frac{d\tilde{u}}{dx} = \int_0^R 2\pi r \frac{\partial u}{\partial x} dr = - \int_0^R 2\pi \frac{\partial rv}{\partial r} dr = 0 \quad , \quad (2.37)$$

since v vanishes at both limits.

A qualitative estimate of development length in terms of diffusion time and transport time can be obtained by using the device of a moving observer applied to a growing internal boundary layer. Assume that the entrance is cut square with the axis so that the origin for x is well defined. Take the flow to be uniform at the pipe entrance; i.e., $u = \tilde{u}$ at $x = 0$. Vorticity generated at the wall by the axial pressure gradient diffuses inward through a distance δ in a time $t \sim \delta^2/\nu$ (**see the Rayleigh problem in the introduction**). An observer following the mean flow travels a distance x in a time $t = x/\tilde{u}$. At equal times, $x/\delta \sim \tilde{u}\delta/\nu$. If the development length X is defined as the value of x when $\delta = D/2$, then X is proportional to DRe and x/X is proportional to x/DRe .

Since the first papers by BOUSSINESQ (1890a,b,c; 1891a,b), work on the problem of laminar flow development in a round pipe has become almost a cottage industry. Of more than forty experimental, analytical, or numerical papers on this topic, about half aim at estimates of a particular constant m belonging to the art of capillary-tube viscometry (see the next SECTION 2.2.2). The remainder view the problem as an exercise in classical fluid mechanics. The first analysis using boundary-layer theory was carried out by SCHILLER (1922). This paper was a natural application of the integral method of Karman and Pohlhausen, published a year earlier. The model combined parabolic profiles near the wall with a

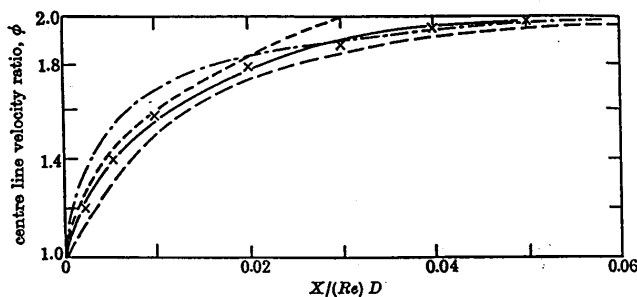


Figure 2.4: Some analytical results for laminar flow development in a smooth pipe. The dependent variable u_c/\tilde{u} has an asymptotic limit of 2.

flat profile near the centerline. The predicted evolution of the axial velocity on the pipe axis is one of the curves shown in FIGURE 2.4. The analysis ignores the fact that a boundary-layer approach is complicated by effects of lateral curvature and by interaction between the axial pressure gradient in the inviscid core flow and the growing displacement thickness of the boundary layer, each affecting the other. Moreover, the boundary-layer approximation fails before the flow development is complete, and an asymptotic analysis is eventually required. The growing power of computers now allows the laminar problem to be treated by numerical integration of the full Navier-Stokes equations for quite large Reynolds numbers.

The other data in FIGURE 2.4 are chosen from the work of

DORSEY (1926)
 MÜLLER (1936) figure 4
 ATKINSON and GOLDSTEIN (1938)
 LANGHAAR (1942) figure 1
 ASTHANA (1951)
 TATSUMI (1952)
 SIEGEL (1953)

RIVAS and SHAPIRO (1956)
 BOGUE (1959)
 TOMITA (1961)
 CAMPBELL and SLATTERY (1963)
 COLLINS and SCHOWALTER (1963)
 LUNDGREN et al. (1964)
 SPARROW et al. (1964) figure 3
 CHRISTIANSEN and LEMMON (1965) figures 2, 3
 HORNBECK (1965) figures 3, 6
 McCOMAS and ECKERT (1965)
 VRENTAS et al. (1966) figures 3–8
 McCOMAS (1967)
 FRIEDMANN et al. (1968) figures 1–4
 LEW and FUNG (1968) tables
 SCHMIDT and ZELDIN (1969)
 FARGIE and MARTIN (1971) figure 4
 CHEN (1973) figure 1
 KESTIN et al. (1973) figure 8
 KANDA and OSHIMA (1986) figures 5–8

The main imperfection of these contributions lies in the frequent assumption of a flat velocity profile at the station $x = 0$, with an unphysical upstream flow that is often left undefined. However, there is general agreement that the independent variable x/DRe is a natural and appropriate one in the laminar development region, whether a boundary-layer model is used or not.

A few experiments include the work of

BOND (1921)
 RIEMAN (1928)
 ZUCROW (1929)
 KLINE and SHAPIRO (1953)
 SHAPIRO et al. (1954)
 KREITH and EISENSTADT (1957)
 WELTMANN and KELLER (1957)
 RESHOTKO (1958) figure 9
 PFENNINGER (1961) figure 12

McCOMAS and ECKERT (1965) figure 3
 ATKINSON et al. (1967) figure 4
 DAVIS and FOX (1967) figure 11
 EMORY and CHEN (1968)
 BERMAN and SANTOS (1969) figures 3–7
 BURKE and BERMAN (1969) figures 3–6, 8
 FARGIE and MARTIN (1971) figure 4
 WYGNANSKI and CHAMPAGNE (1973)
 MESETH (1974)
 MOHANTY and ASTHANA (1979)

(Why does nobody plot $\tilde{\tau}_w$? Mention honeycombs. No calculations for square-cut entrance with bubble.)

From all of this work, the evidence is persuasive that development is complete for practical purposes when

$$\frac{1}{Re} \frac{x}{D} \approx 0.07 \approx \frac{1}{14} , \quad (2.38)$$

provided that the Reynolds number Re is not less than about 100. For a pipe of given diameter and length, the largest Reynolds number for which a parabolic profile can be established is about $14 L/D$. For a given Reynolds number, the smallest L/D is about $Re/14$. Consequently, to identify the record holder for highest Reynolds number with fully developed laminar flow, it is necessary only to look for large values of L/D and to test the state of the exit flow. By this criterion, the record is about $\tilde{u}D/\nu = 13,000$ and is held by LEITE (1958).

With sufficient care, it is possible to maintain laminar flow in relatively short pipes up to very large Reynolds numbers, 50,000 or more. However, the parabolic profile is never fully developed in such cases, and the decisive element for transition becomes the disturbance level outside the boundary layer in the early development region. In any contest to establish the highest achievable laminar Reynolds number in short pipes, the results are a measure of the degree of care taken to avoid such disturbances, rather than of any directly useful physical quantity. For example, blowdown methods can reduce disturbance levels far below the best obtainable in flows driven

by an upstream pump or compressor, and a gas flow can be quieted by use of a sonic orifice to isolate the test section from a downstream pump. As far as I know, the record here is held by PFENNINGER and MEYER (1953), who used a long conical contraction fitted with 13 screens, as well as elaborate vibration isolation, to obtain a flow free of turbulence at a Reynolds number $\tilde{u}D/\nu = 88,000$. The corresponding number $\tilde{u}x/\nu$ was about 50×10^6 , an order of magnitude higher than the number that can be obtained on flat plates in conventional wind tunnels. The boundary layer in Pfenninger's pipe occupied about 60 percent of the area at the pipe exit. To obtain a fully developed parabolic profile in air under these conditions would need a length of about 140 meters, together with heroic measures to minimize disturbances in the flow and to account for changes in density. Even if this could be done, I see no particular profit from an attempt.

Finally, several experimenters have found that it is not safe to assume that a laminar pipe flow in the laboratory will automatically be axisymmetric. LEITE (1958), RESHOTKO (1958), HOULIHAN (1969), WYGNANSKI and CHAMPAGNE (1973), and BREUER (1985), all working on difficult questions of stability and transition, and all working with air in pipes having a diameter of a few centimeters, describe problems in obtaining axisymmetric fully-developed flow. Some of their results are illustrated in FIGURE 2.5. They comment in particular on the need for close control of thermal inhomogeneities, pipe alignment, and axial symmetry of conditions far upstream. Most other experimenters have had a better experience or have not tested their flows for symmetry.

2.2.2 Capillary-tube viscometry

Numerous devices are commercially available for measuring the viscosity of fluids used in laboratory experiments or manufacturing processes. They include cone-plate, rotating-cylinder, falling-ball, and capillary-tube viscometers. The choice is usually governed by the range of viscosity involved, by the volume of the sample committed to the measurement, and occasionally by special conditions such as

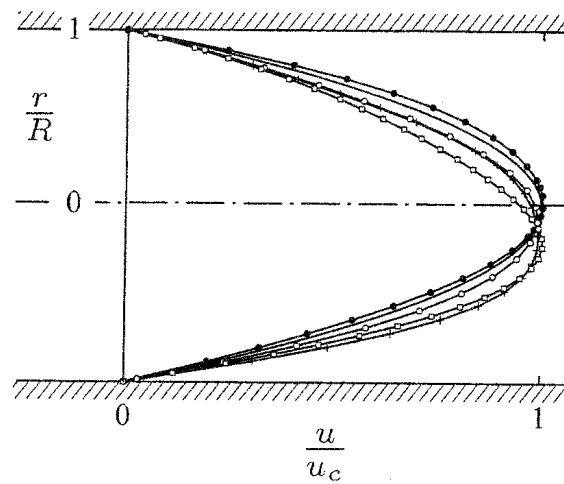


Figure 2.5: Several examples from the experimental literature showing non-axisymmetric laminar flow in circular pipes. The most likely cause is secondary flow due to thermal inhomogeneity in a gravitational field or asymmetry of the upstream channel.

a need in process work to immerse the device in the bulk fluid. Typically, such viscometers are calibrated by the manufacturer or the user, using fluids of known viscosity, to take into account various effects of finite geometry.

The question of how a known viscosity comes to be known is far from trivial. This question is the business of standards laboratories. For example, SWINDELLS, COE, and GODFREY (1952) describe a painstaking program in capillary-tube viscometry, carried on from 1931 to 1941 and from 1947 to 1952 at the U.S. National Bureau of Standards (now the U.S. National Institute of Standards and Technology), whose singular result was to establish the value $\mu = 0.010019 \pm 0.000003$ poise for pure water at 20°C . This value is still the cornerstone of viscosity tables for water that are constructed from more extensive but less accurate measurements. The geometry in capillary viscometry at the standards level is apparently standardized, requiring a square-cut entrance and exit, although other geometric details, such as the tube outer diameter, are usually left open. The need for close control of several variables is self-evident. In order to obtain four significant figures in the viscosity, according to equation (2.18), the absolute temperature, the volume flow rate, the tube length, the pressure difference, and especially the tube diameter must all be known to better accuracy, with a further allowance for errors introduced by differentiation of experimental data. It may be necessary, for example, to represent the cross section of a real tube by an ellipse rather than by a circle, with a corresponding adjustment in the theory. A long tube of small diameter provides an easily measurable pressure difference, although this pressure difference is necessarily global rather than local if pressure taps cannot be provided along the length of the tube. At the same time, the diameter must not be so small that it cannot be measured with the necessary accuracy. The length is also limited in practice by the need to maintain the flow system at constant temperature in a bath of practical size without having to coil the tube and accept a much more complex theory.

The expected pressure distribution in a finite tube is shown schematically in FIGURE 2.6. Certain general relationships that

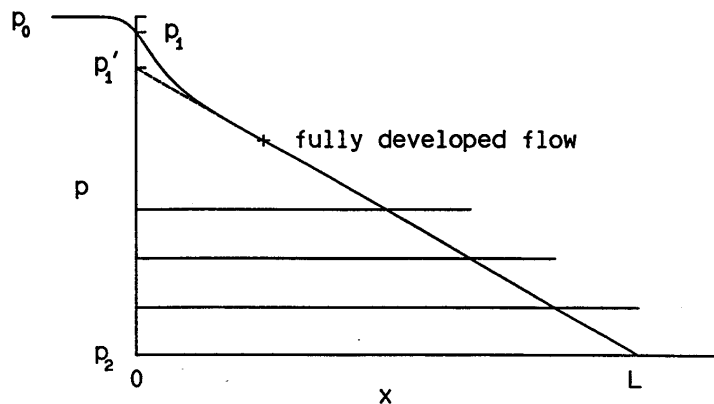


Figure 2.6: A schematic representation of the pressure distribution along a tube of length L with uniform entrance flow at $x = 0$. The flow may be laminar or turbulent and the cross section need not be circular.

emerge from the figure do not depend on the shape of the tube cross section or the shape of the tube entrance, as long as these are fixed. Suppose for convenience that entrance and exit are cut square, so that L is well defined. The quantities p_0 and p_2 are the static pressures in the entrance and exit reservoirs. The quantity p_1' is the static entrance pressure associated with a fictitious fully developed flow over the full length of the tube. Anomalous pressure effects at both entrance and exit are included in principle, although exit effects are not treated explicitly. It is not necessary to distinguish between laminar and turbulent flow, or even mixed flow at Reynolds numbers in the transition regime.

The strategy associated with FIGURE 2.6 is one of experimental differentiation. Suppose that the Reynolds number is held constant as the length of the tube is varied, and suppose that the shortest tube is long enough to achieve fully developed flow. Then a unit increment in the length of the tube will give rise to a unit

increment in total pressure drop. Begin with the identity

$$p_0 - p_2 = (p_0 - p'_1) + (p'_1 - p_2) . \quad (2.39)$$

For the general case, define an ideal friction coefficient for fully developed flow,

$$C_f = \frac{D(p'_1 - p_2)}{2L\rho\tilde{u}^2} , \quad (2.40)$$

where $\tilde{u} = Q/A$ is again a mean velocity over the cross section A . For the special case of a circular tube, the definition (2.40) reduces through equation (2.11) to equation (2.20). Define also a global friction coefficient,

$$\widehat{C}_f = \frac{D(p_0 - p_2)}{2L\rho\tilde{u}^2} , \quad (2.41)$$

where the circumflex over C_f denotes a mean value over the entire length of the tube, reservoir to reservoir. Equation (2.39) then takes the form

$$\widehat{C}_f \frac{L}{D} = \frac{(p_0 - p'_1)}{2\rho\tilde{u}^2} + C_f \frac{L}{D} . \quad (2.42)$$

For fully developed flow at the exit, the first term on the right is a constant that is characteristic of the complete development process for particular entrance conditions and Reynolds number. Without the factor of 2 in the denominator, this constant is usually denoted by m in the literature of capillary-tube viscometry;

$$m = \frac{(p_0 - p'_1)}{\rho\tilde{u}^2} , \quad (2.43)$$

so that

$$\widehat{C}_f \frac{L}{D} = \frac{m}{2} + C_f \frac{L}{D} . \quad (2.44)$$

Except possibly for a square-cut entrance, the development parameter \underline{m} , defined graphically in figure 2.6, will depend on the entrance geometry and flow conditions for a particular tube. A plot of $\widehat{C}_f L/D$ against L/D is a straight line whose slope C_f and intercept $m/2$ are characteristic for the Reynolds number in question. In particular,

$$C_f = \frac{\partial(\widehat{C}_f L/D)}{\partial(L/D)} . \quad (2.45)$$

A simple implementation of this differentiation scheme was proposed and used by COUETTE (1890), but has since been used only rarely, and then mostly by professionals such as Swindells *et al.* The technique is to construct two capillary viscometers by connecting two tubes in series with a third reservoir inserted between them. The two tubes are assumed to be identical in diameter and all other geometrical details except length. When in equilibrium, they have the same flow rate. The two parameters C_f and m are then readily evaluated from a single experiment.

Discuss m from $p(x)$. Cite bibliography.

Equation (2.44) is usually cast in a more direct and more literal form for use in viscometry with a round tube. From equation (2.39), with $p'_1 - p_2 = -Ldp/dx = 4L\tau_w/D = 8\mu\tilde{u}L/R^2$, and with $\tilde{u} = Q/\pi R^2$, this form is

$$\frac{\pi^2 R^4 (p_0 - p_2)}{\rho Q^2} = m + \frac{8\pi\mu L}{\rho Q} . \quad (2.46)$$

For constant Q and R and variable L , a dimensional plot of $(p_0 - p_2)$ against L yields a straight line whose slope is proportional to μ and whose intercept is proportional to m . Such a plot is a practical realization of FIGURE 2.6.

A different form, appropriate for a single tube with changing flow rate, is obtained on multiplying by Q and making the important assumption that m is independent of Reynolds number;

$$\frac{\pi^2 R^4 (p_0 - p_2)}{\rho Q} = mQ + \frac{8\pi\mu L}{\rho} . \quad (2.47)$$

Now, for constant L and R and variable Q , a plot of $(p_0 - p_2)/Q$ against Q yields a straight line whose slope is proportional to m and whose intercept is proportional to μ . This formulation is the one used by Swindells *et al.* Such a plot is sometimes called a Knibbs plot, after KNIBBS (1895). The assumption that the entrance parameter m defined by equation (2.44) is independent of Reynolds number in some range of Re needs verification for both smooth and square-cut entrances, since the parameters \tilde{u} , D , and ν define two lengths, D and ν/\tilde{u} , together with their ratio Re .

Finally, still for a single tube, multiplication of equation (2.47) by ρQ yields

$$\pi^2 R^4 (p_0 - p_2) = \rho m Q^2 + 8\pi\mu L Q . \quad (2.48)$$

The conclusion that the overall pressure drop should be the sum of a term in Q (or \tilde{u}) and a term in Q^2 (or \tilde{u}^2) was noted by HAGEN (but not by Poiseuille) and is probably the reason that the term containing m is often referred to, not quite correctly, as a kinetic-energy correction.

For the case of a circular tube, it is also possible to calculate $p_0 - p'_1$ in FIGURE 2.6 from first principles, given a suitable model of the flow in the development region. By definition,

$$m = \frac{(p_0 - p'_1)}{\rho \tilde{u}^2} = \frac{(p_0 - p_1) + (p_1 - p_2) - (p'_1 - p_2)}{\rho \tilde{u}^2} . \quad (2.49)$$

Visualize an ideal entrance, for which the velocity profile at an initial station $x = 0$ is uniform, with velocity \tilde{u} and pressure p_1 that do not depend on r . Assume frictionless acceleration from rest upstream of this station. The Bernoulli equation then determines the first term on the right in equation (2.49);

$$p_0 - p_1 = \frac{1}{2} \rho \tilde{u}^2 . \quad (2.50)$$

The middle term can be partially evaluated for laminar flow. For steady axisymmetric laminar flow in the development region, the equations of motion (**see introduction**) can be written, with no boundary-layer approximation, as

$$\frac{\partial r u}{\partial x} + \frac{\partial r v}{\partial r} = 0 ; \quad (2.51)$$

$$\rho \left(\frac{\partial r u u}{\partial x} + \frac{\partial r u v}{\partial r} \right) = -r \frac{\partial p}{\partial x} + \mu r \left(\frac{\partial^2 u}{\partial x^2} + \frac{1}{r} \frac{\partial}{\partial r} r \frac{\partial u}{\partial r} \right) . \quad (2.52)$$

When both equations are integrated over a cross section of a tube of constant diameter, the result can be reduced to a simple momentum

integral,

$$\frac{d}{dx} \int_0^R (\rho uu + p) r dr + R\tau_d = 0 \quad , \quad (2.53)$$

where τ_d , the local viscous stress at the wall, is a function of x in the development region (d for development).

Now integrate equation (2.53) from $x = 0$ to $x = L$. At $x = 0$ the flow is uniform, with velocity \tilde{u} and pressure p_1 . At $x = L$, the flow is fully developed. The static pressure p_2 is then independent of r , according to the laminar version of equation (2.2). The velocity profile $u(r)$ at $x = L$ is the parabolic distribution (2.13), with u_c replaced by $2\tilde{u}$. Integration of equation (2.53) gives

$$p_1 - p_2 = \frac{1}{3} \rho \tilde{u}^2 + \frac{2}{R} \int_0^L \tau_d dx \quad . \quad (2.54)$$

Finally, consider a fictitious fully developed flow over the length L , for which

$$p'_1 - p_2 = -L \frac{dp}{dx} = 2 \frac{L}{R} \tau_w = \frac{2}{R} \int_0^L \tau_w dx \quad . \quad (2.55)$$

Substitution of equations (2.50), (2.54), and (2.55) in (2.49) yields

$$m = \frac{1}{2} + \frac{1}{3} + \frac{2}{R} \int_0^L \frac{(\tau_d - \tau_w)}{\rho \tilde{u}^2} dx \quad . \quad (2.56)$$

This formula is not commonly quoted. I have encountered it only in the textbook by WHITE (1974, p. 336).

The numerous calculations mentioned in the previous SECTION 2.2.1 almost invariably assume that the flow is uniform at the entrance station $x = 0$, so that equation (2.56) qualifies as a proper definition for m . All that is then required from the calculation is the quantity τ_d in the development region, although most authors have chosen to report instead the pressure at the wall or the velocity on

the axis. In equation (2.56), flow adjustment near the tube exit has been ignored. There is evidence (**where; cite refs**) that this approximation is valid for Reynolds numbers greater than about 100, on the empirical ground that a jet from a sharp-edged orifice into a large reservoir of the same fluid comes to rest without significant pressure recovery (**ref**). Some commercial capillary-tube viscometers have a flared or rounded exit, and the exit pressure recovery may be finite and sensitive to Reynolds number.

An experimenter might not concede that direct calculation of m from equation (2.56) or some equivalent equation is either necessary or desirable. For a given entrance geometry, fluid, and flow rate, m is a well-defined number. However, it is not necessarily the same number for a tube with a square-cut entrance, common in viscometry at the standards level, as for a tube with a rounded entrance, common in some commercial capillary-tube viscometers. The model leading to equation (2.56) makes no distinction. It assumes that the wall friction τ_d begins abruptly at $x = 0$ with an integrable singularity. For a smooth entrance it is likely, and for a sharp entrance it is certain, that the boundary layer is not being described correctly. In effect, the pressure p_1 and the length L are legislated rather than defined unambiguously by the geometry. **Mention Hagenbach, Wilberforce, Boussinesq, Swindells, Schiller on m .**

Mickelson. There remains the empirical differentiation scheme of equation (2.45), which does not involve p_1 . Some nice measurements reported in the thesis by MICKELSON (1964) were designed to exploit the simple empirical approach represented by this equation. Mickelson worked at a more than ordinary level of accuracy, although not at the level of a standards laboratory. He measured the total pressure drop between reservoirs for water flowing in ten glass tubes having the same nominal diameter of 0.1 cm but different values of L/D ranging from 15 to 510. The tubes had a square-cut entrance and exit, so that L is well defined. The volume flow was regulated by a positive-displacement gear pump whose noise level and speed regulation are not described in detail. Most of the measurements described here were made at 30 °C, and I have taken the viscosity of water at this temperature to be 0.007975 poise (ref)

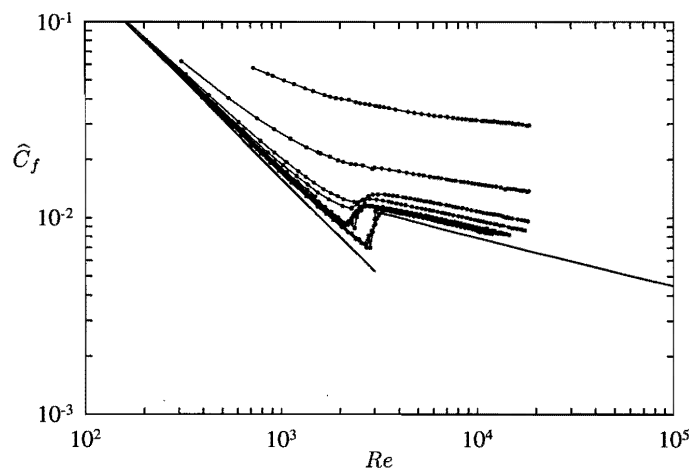


Figure 2.7: The raw friction data of MICKELSON (1964) for ten capillary tubes of fixed diameter and various lengths ranging from $L/D = 15$ to $L/D = 510$. The fluid is water at 30°C . The curve for turbulent flow at the right is faired through Nikuradse's data. Note that transition is slightly delayed for the two longest tubes.

rather than the value 0.008007 used by Mickelson. The calculations that follow mostly reproduce Mickelson's work, and my results are in very good agreement with his.

Mickelson tabulated the global pressure difference $\hat{C}_f L/D$, which he called f_m . His raw data for \hat{C}_f as a function of Re , with L/D as parameter, are shown in FIGURE 2.7. Because Mickelson was interested in turbulent flow as a prototype problem for viscometric studies of complex rheological fluids, he included measurements for turbulent flow of water. These measurements will be discussed in the next SECTION 2.2.3.

The differentiation of experimental data according to equation

(2.45) is straightforward. The governing relationship is a combination of equation (2.44) with the ideal friction law (2.21);

$$m = 2 \left(\widehat{C}_f - \frac{16}{Re} \right) \frac{L}{D} . \quad (2.57)$$

For each value of L/D , a value of \widehat{C}_f at a specified Re can be determined by interpolation in FIGURE 2.7. For this purpose, I have fitted parabolas to quartets of adjacent data points, two on each side of the specified Re , with both \widehat{C}_f and Re represented by their logarithms. The range of Re for which this operation can be carried out for nine of the ten tubes is from 330 to 2020. A straight line is then fitted to a plot of $\widehat{C}_f L/D$ against L/D at constant Re , omitting any points for which L/DRe is less than $1/14$. The resulting values of the slope C_f and the intercept m inferred from equation (2.44) are plotted for uniform increments in Re in FIGURES 2.8 and 2.9, respectively. The range of L/D at any Re is required to be at least 2 to 1. This condition is met for Re from 400 to 1400. The laminar friction coefficients differ from $16/Re$ by less than 0.3 percent, and the values of m are sensibly independent of Reynolds number, with a mean value of about

$$m = 1.22 . \quad (2.58)$$

The presumption that m is experimentally constant makes it possible to take a global view of Mickelson's laminar data. Suppose that the parameter m in equation (2.44) is in fact independent of both L/D and Re . Natural coordinates for determining m are then defined by equation (2.57). The data are shown in FIGURE 2.10, where the region of interest is the laminar plateau at the lower right. Note that the independent variable L/DRe in equation (2.57) is the same one appearing in equation (2.38), so that laminar flows that are not fully developed (say flows with $14L/DRe$ less than unity) can readily be excised from the plot at the left. Note also that, for long tubes at low Reynolds numbers, m is a small difference between two large quantities. The expanding envelope on the right represents the effect on m of an uncertainty of 2 parts in 10^3 in $\widehat{C}_f L/D$. On the ground that it is better to look for something where it is large rather than where it is small, I have also excised values of $14L/DRe$ greater than 10. The

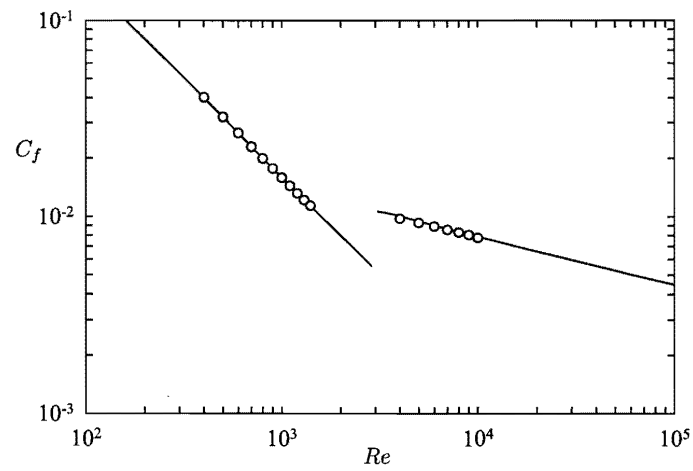


Figure 2.8: The ideal friction coefficient as inferred by differentiation of Mickelson's data. The circles represent the slope of a fitted straight line in a plot of $\hat{C}_f L/D$ against L/D for constant Re . The curve for turbulent flow at the right is faired through Nikuradse's data.

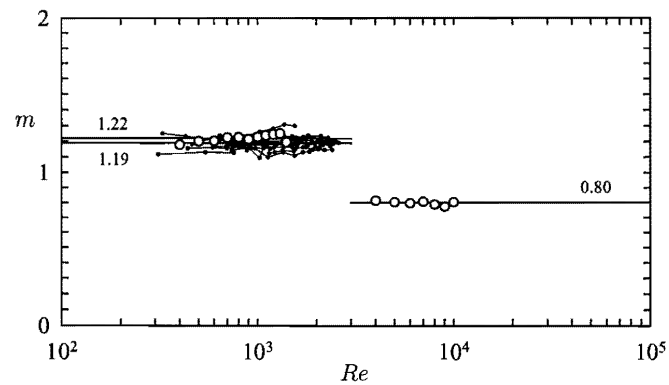


Figure 2.9: The laminar flow-development parameter m as a function of Re for a square-cut entrance according to Mickelson's data. The open circles show twice the intercept of a fitted straight line in a plot of $\widehat{C}_f L/D$ against L/D for constant Re . In the laminar range, the small filled circles are from equation (2.57).

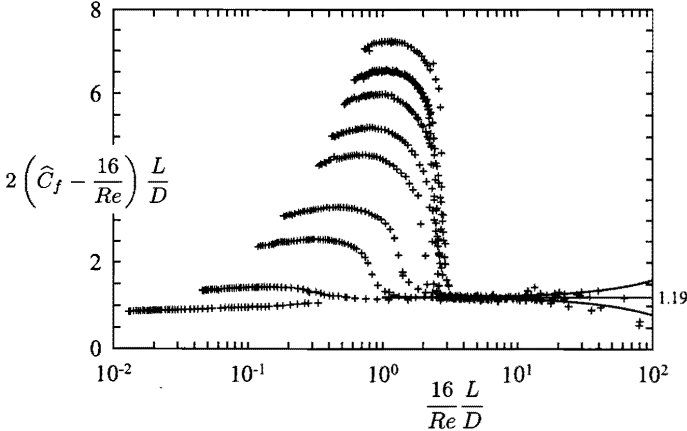


Figure 2.10: Mickelson's data from the previous FIGURE 2.7, replotted according to equation (2.57). The Reynolds number Re increases from right to left. The quantity m is defined by the flat laminar region at the lower right.

surviving data are plotted as small solid circles in FIGURE 2.9. In principle, a single observation would suffice to determine m by this method. In practice, the mean of 110 values is

$$m = 1.19 \quad , \quad (2.59)$$

with a dispersion of a few percent. There is no clear indication of any dependence of \bar{m} on Reynolds number.

One anomaly in these experiments was pointed out by Mickelson and is visible in FIGURE 2.7. The tubes of intermediate length show essentially normal behavior in the transition regime, which lies as expected in the range $2000 < Re < 2800$ (see SECTION 2.3.1). The two longest tubes do not. The reason is unknown.

The data in FIGURE 2.10 are consistent with the previous estimate for the minimum length required to achieve a fully developed laminar flow in a pipe with a square-cut entrance; namely, $L/D = Re/14$. At this condition the penalty paid for entry losses amounts to about a third of the overall pressure drop. This topic is developed further in SECTION X³, where the subject is the use of honeycombs for flow control and for measurement of flow rate.

This discussion of Mickelson's work is out of chronological order, but is presented first because I consider this work to be the best available evidence for the value of the laminar (or turbulent) parameter m . Theory must yield to experiment, at least for the case of a square-cut entrance. In this context, two important papers from the 19th century are more typical in showing the early evolution of the concept of viscosity and capillary viscometry.

Poiseuille. A paper on pipe flow of water by POISEUILLE (1846) belongs on any short list of fundamental contributions to the art of experimental fluid mechanics. This work was first reported in three short notes in *Comptes Rendus* (1840a, 1840b, 1841). The novelty and importance of the research caused the French academy to appoint a committee to verify the methods and results and judge their suitability for publication in full. The favorable report of this committee was published twice in French and once in German (see

³Reference unclear, possibly a section that was not completed.

ARAGO et al. 1842, 1843a, 1843b), and Poiseuille's full paper followed in due course in *Mémoires Présentés par Divers Savants*. After a lapse of almost a century, the latter paper was translated into English at the instance of a distinguished rheologist, E.C. Bingham, who added some critical notes. The tabulated data had earlier been reprinted by BINGHAM as Appendix D of his monograph *Fluidity and Plasticity* (1922), and some typographical errors in this appendix were later corrected by BINGHAM (1930).

A short account of Poiseuille's life and work, with emphasis on the paper of 1846, can be found in a recent appreciation by SUTERA and SKALAK (1993). Poiseuille was a physician interested in the flow of blood, especially in vessels of capillary dimension. He attempted some measurements *in vivo*, but concluded that controlled experiments would be required to formulate the laws governing blood flow, and turned to experiments with water in glass tubing of very small inside diameter, as small as 14 μm .

Poiseuille attacked the problem with an admirable combination of skill and luck. Knowing nothing of the concept of streamline flow, he was comfortable with a square-cut entrance. Consequently, the length of his tubes, except for the shortest ones, was well defined. Moreover, the method of construction of his glass apparatus required him to decrease the length of his tubes by removing successive downstream portions, leaving the entrance geometry unchanged. An experimenter today might well adopt the same strategy by design.

Poiseuille determined systematically that the flow rate in many of his tubes was directly proportional to the pressure drop and to the fourth power of the diameter, and inversely proportional to the length; thus

$$Q = K'' \frac{h D^4}{L} . \quad (2.60)$$

The units of Q in equation (2.60) are mm^3/sec . The overall pressure drop h (called P by Poiseuille) is in mm Hg, and L and D are in mm. The units of K'' are then $(\text{sec} \cdot \text{mm Hg})^{-1}$. For a fixed temperature of 10 $^\circ\text{C}$, Poiseuille reported the average value of the dimensional

constant K'' for a variety of experiments as

$$K'' = 2495.224 \quad , \quad (2.61)$$

in which the first four digits may be significant. When the lengths in Q , h , L , and D are all expressed in cm, and the pressure drop is written as $\Delta p = \rho_m g h$, where ρ_m is the density of the manometer fluid and g is the acceleration of gravity, Poiseuille's empirical equation (2.60) becomes (**clear up signs**)

$$Q = 10K'' \frac{D^4}{\rho_m g} \frac{\Delta p}{L} \quad . \quad (2.62)$$

Comparison with the theoretical equation (2.18) derived in SECTION 2.1.2,

$$Q = \frac{\pi D^4}{128\mu} \frac{dp}{dx} \quad , \quad (2.63)$$

shows that Poiseuille was dealing with the combination

$$K'' = \frac{\pi \rho_m g}{1280\mu} \quad , \quad (2.64)$$

under the implicit assumption that entrance effects were negligible; i.e., that $\Delta p/L$ could be identified with dp/dx . The values quoted by Poiseuille for g and ρ_m are $g = 980.8 \text{ cm/sec}^2$ at the latitude of Paris and $\rho_m = 13.57 \text{ gm/cm}^3$ for mercury at a manometer temperature of 11.5°C . Consequently, his numerical result (2.61) is equivalent to

$$\mu = 0.01309 \frac{\text{gm}}{\text{cm sec}} \quad . \quad (2.65)$$

The unit used for this quantity in the CGS system has come to be called the poise, following a suggestion by DEELEY and PARR (1913). The accepted value today for water at 10°C is 0.01307 poise. Poiseuille also obtained data for viscosity at other temperatures between 0°C and 45°C , with errors never larger than one percent.

Poiseuille was intuitively aware of the entrance effect, although he had no way to define it quantitatively. The main sequence of his experiments consists of 34 tables for six tubes of different diameters, each of which was progressively shortened as the work proceeded. He

separated these results into a first series, for which the pressure drop was found to be very nearly inversely proportional to flow time for a fixed flow volume, as in equation (2.60), and a second series that showed a more complex behavior. The two series are plotted separately in the two upper curves in FIGURE 2.11. Poiseuille did not attempt to explain the difference in behavior, although he did note that most of the data of the second series were associated with short tubes at high flow rates. A brief inspection of the tables confirms that development of the parabolic profile in these tubes probably did in fact occupy a large fraction, up to and exceeding the whole, of the tube length.

Recall the entrance parameter m defined by equation (2.57) above, for which a numerical value $m = 1.19$ (assumed to be independent of Reynolds number) was extracted from Mickelson's data in FIGURE 2.9 of SECTION 2.2.2. For a square-cut entrance,

$$m = 2 \left(\widehat{C}_f - \frac{16}{Re} \right) \frac{L}{D} , \quad (2.66)$$

where \widehat{C}_f is an empirical friction coefficient that distributes the total pressure drop uniformly over the length of the pipe. The ideal friction coefficient C_f has been replaced by $16/Re$. Rearrangement of this equation gives

$$\widehat{C}_f Re = 16 + 8m \left(\frac{Re}{16} \frac{D}{L} \right) . \quad (2.67)$$

This form applies as long as the quantity in parenthesis is less than unity; i.e., as long as the parabolic profile is established somewhere within the pipe.⁴ One is use of the precise theoretical laminar friction law, $C_f Re = 16$. The other is use of the approximate empirical condition $L/Re D \geq 0.06$, which I take as $L/Re D \geq 1/14$, for the parabolic profile to be fully developed. With this proviso, the cor-

⁴A sentence at this point in the 1997 draft read, "Note that the number 16 appears in these formulas, by deliberate coincidence, in two different ways." Author evidently removed the sentence after recalculating equation 2.38 in Section 2.2.1 and revising the approximate value from 1/16 (0.06) to 1/14 (0.07). He revised the result where he employed it in the discussion after equation (2.57), but not here. We leave it to the reader to revise what follows.

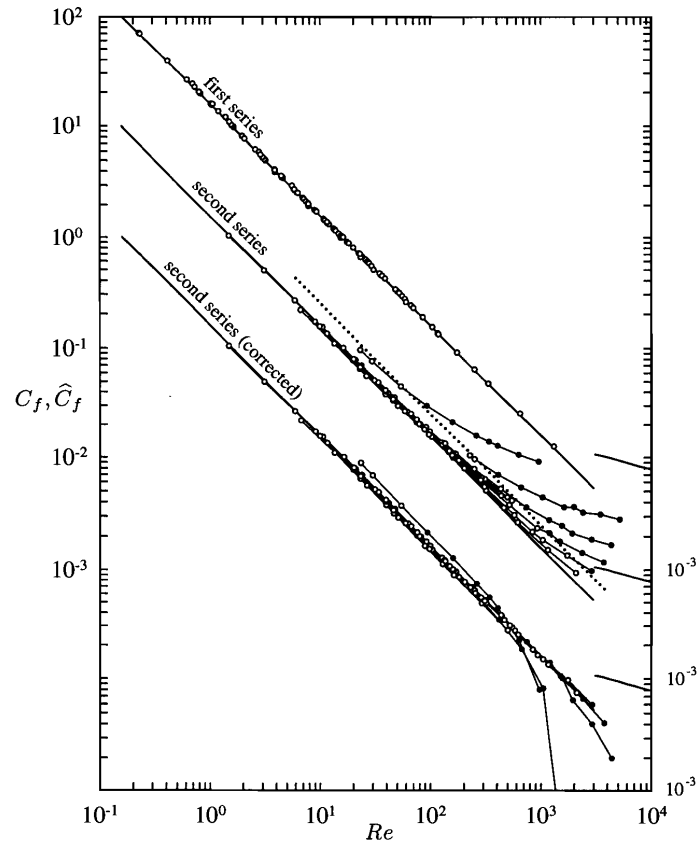


Figure 2.11: A modern representation of POISEUILLE's data (1846) for flow in capillary tubes. Note the displaced scales. The first series is suitable for determining the viscosity. The second series in uncorrected form is not. The lowest display shows the second series after a correction for flow development. The residual scatter here may be caused by inaccurate measurement of tube length.

rection (2.44) for entrance effect is accurate as long as

$$\widehat{C}_f Re \leq 16 + 8m . \quad (2.68)$$

For $m = 1.19$, this is

$$\widehat{C}_f Re \leq 25.5 . \quad (2.69)$$

The equality in this equation defines the dotted line near the middle curve in FIGURE 2.11. Below this line, the original data of the second series are shown by open circles; above the line, by filled circles. The ideal or corrected value of the friction coefficient for fixed L/D is obtained by subtracting a constant from \widehat{C}_f ;

$$C_f = \widehat{C}_f - \frac{m}{2} \frac{D}{L} . \quad (2.70)$$

When this correction with $m = 1.19$ is applied to all of the data of the middle curve in FIGURE 2.11, the result is as shown in the bottom curve. The symbols are the same.

Poiseuille's data show no obvious effect of transition, and leave open the question of the possible dependence of m on Re . Each of his tables for the first series and the (corrected) second series generates a line with the proper slope of -1 in logarithmic coordinates, but with a constant that varies more or less randomly from the ideal value of 16 for the product $C_f Re$, sometimes by several percent or more. This observation implies that one of the two fixed parameters for such a line (L, D) must have been incorrectly measured. My candidate is L , mostly because the problem worsens in the second series, where L is small. The extreme case is a run with very small and uncertain length and moderate Reynolds numbers, a run that another author might have discarded. My comments are consistent with the conclusion by several authors that Poiseuille's data are not sharp enough to determine m accurately, although they are sharp enough to benefit from a correction. At the other extreme of accuracy, the evidence shows that Poiseuille succeeded in measuring the diameter of his tubes to an accuracy comparable to the wave length of visible light. He refers to the instrument he used as a *camera lucida*. After finding a description of this device in an old encyclopedia, I understand why the French committee was impressed.

I have a mild reservation about the lack of scatter in the table in Poiseuille's section 130. The seven numbers listed for K'' are each traceable to a single measurement, whose flow volume was recalculated to correspond to standard values for pressure drop (775 mm Hg), tube length (25 mm), and flow duration (500 sec). The adjustment was carried out in terms of proportionalities, which Poiseuille referred to as laws. Constants of proportionality did not appear, and no statistical measures were used except in the final average for K'' . A different choice for the selected single measurements out of the dozens available would almost certainly increase the scatter in K'' .

This criticism aside, I think that the skill and insight demonstrated by Poiseuille transcend his exaggerations as to accuracy. The execution and interpretation of the measurements are remarkable, considering the state of the fluid-mechanical art at the time. In 1840 there was no precedent for expecting or requiring integer exponents in what amounts to a dimensional statement. In fact, there was no precedent for dimensional statements. Even a name for the hypothetical fluid property at issue, the viscosity, was lacking. Moreover, Poiseuille worked completely outside the small establishment dedicated to the activity that we now call basic research.

Finally, one remark is needed about priority for the empirical equation (2.62) and the theoretical equation (2.63). In the literature, the theoretical equation is sometimes erroneously attributed to Poiseuille. In fact, this integral of the equations of motion was published some years later by at least six authors, (**check Hagen**),

WIEDEMANN (1856)	JACOBSON (1860)
HAGENBACH (1860)	STEFAN (1862)
HELMHOLTZ (1860)	MATHIEU (1863)

among whom Jacobson attributes the result to unpublished notes by Neumann. Together, these writers probably hold the record for number of authors arriving independently and almost simultaneously at a single theoretical result.

Both NAVIER (1823) and STOKES (1849) in their original papers considered pipe flow as a problem suitable for application of the new equations of motion for a viscous fluid. Navier's result

contained a wrong exponent, with Q varying like D^3 rather than like D^4 . This discrepancy was noted by Poiseuille, who did not attempt to revise Navier's analysis. Stokes derived the parabolic profile, but did not calculate the flow rate because at the time he had reservations about the no-slip condition. If he had known of Poiseuille's work, published in final form three years earlier, these reservations surely would never have arisen.

(DISCUSS HAGEN 1839, 1854)

Need paragraphs on pipe flow of air with something about Millikan oil-drop experiment, Maxwell's result.

As $L/D \rightarrow 0$, a tube with square-cut entrance and exit becomes an orifice, and it can be expected that the flow will become independent of L/D provided that the reservoirs are very large, with flat walls and thin boundary layers near the orifice (not pipe flow). Data in the transition region for L/D were published by Kreith and Eisenstadt. These data are very ragged, and I think that the orifice diameters were not under good control. The data for their test rigs 1, 2, 3, nominally identical, differ by 30 percent. The quantity called $\tilde{C}_f L/D$ becomes a pressure coefficient C_p .

For other data see

BOND (1921)
 ZUCROW (1929)
 LINDEN and OTHMER (1949)
 KLINE and SHAPIRO (1953)
 SHAPIRO et al. (1954)
 IVERSON (1956)
 CAMPBELL and SLATTERY (1963)
 MICKELSON (1964)
 EMORY and CHEN (1968)
 LEW and FUNG (1968)
 BENDER (1969)
 FARGIE and MARTIN (1971)
 MOHANTY and ASTHANA (1979)

As the tube becomes shorter, the first observable effect is that

the parabolic profile is not achieved, and the pressure gradient is everywhere larger than the fully developed value. For short enough tubes, the reattachment region becomes involved with the exit flow. (This is not a practical problem, except that it prevents getting the bubble length from the pressure drop.) Finally, reattachment does not occur at all, and the flow shows a vena contracta, unless Re is of order unity or less. (Include drag of perforated plate?)

2.2.3 Turbulent flow

Mickelson also observed turbulent flow in his tubes, as already shown in FIGURE 2.7. The empirical differentiation scheme leading to equation (2.45) is equally useful for the case of developed turbulent flow, although the ideal friction law is not known *a priori*. Mickelson's data for turbulent flow are included in FIGURE 2.9 and FIGURE 2.8 for $4000 < Re < 10000$. The value of m appears to be close to 0.80 for a square-cut entrance. **(Check other sources; see Bingham p 18.)** The accuracy imputed to Mickelson's data for laminar flow is a fraction of one percent. If the same accuracy can be imputed to the data for turbulent flow, and I believe that it can, in spite of the small diameters involved, these measurements can be taken as definitive for fully developed turbulent pipe flow in the specified Reynolds-number range.

Estimates of required development length for turbulent pipe flow play an important part in the design of test facilities in which the flow is intended to achieve classical turbulent equilibrium. If intermittent turbulence is to be avoided (see SECTION 2.3.1), the Reynolds numbers of interest are larger than about 3000. FIGURES 2.12 and 2.13 show, in terms of evolution of centerline velocity, two modes of development. On the one hand, in FIGURE 2.12 the entrance flow is moderately quiet, and laminar boundary layers develop in the normal way. However, disturbances, although small, are large enough to cause transition in the boundary layer, which then grows rapidly because of enhanced mixing. The centerline velocity can decrease locally near transition because the displacement thickness decreases while the momentum thickness continues to in-

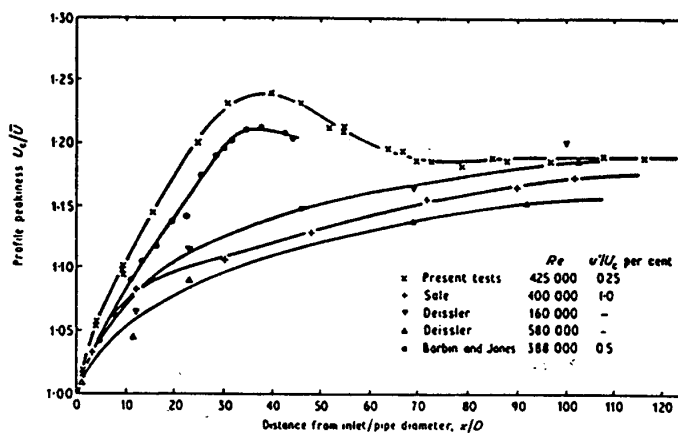


Figure 2.12: Typical experimental results for turbulent flow development in a smooth pipe when transition occurs in the boundary layer well downstream, near the peak in the curve of u_c against x . The turbulent asymptotic limit for u_c/\tilde{u} depends on Reynolds number and is here approached from above.

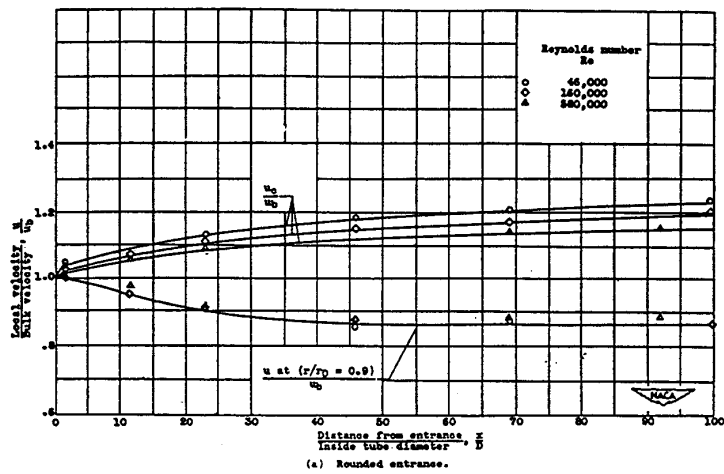


Figure 2.13: Typical experimental results for turbulent flow development in a smooth pipe when transition occurs in the boundary layer very close to the entry. The turbulent asymptotic limit for u_c/\tilde{u} depends on Reynolds number and is approached from below.

crease. On the other hand, in FIGURE 2.13 the entrance flow is deliberately made noisy, by one means or another. The boundary layer becomes turbulent quickly, and the centerline velocity then approaches an equilibrium value from below, as in laminar flow. At $Re = 100,000$, for example, the boundary layer can be turbulent one diameter from the entrance. In either figure, the equilibrium value of u_c/\tilde{u} depends on Reynolds number, according to experience reviewed in SECTION X.⁵

Studies of turbulent flow development include

BROOKS et al. (1943)
 DEISSLER (1950)
 BARNES (1952)
 BRENKERT (1954)
 BARBIN and JONES (1963)
 WILLIAMS (1969)
 RICHMAN and AZAD (1973)
 SHARAN (1974)
 WANG and TULLIS (1974)
 WEIR et al. (1974)
 REICHERT and AZAD (1976)
 UEMURA and IMAICHI (1977, 3G)
 LAWS et al. (1979)
 KLEIN (1981)

Variables on the axis include u_c and $\overline{u'u'}$. Variables at the wall include C_f and p .

Finally, there is the obvious advantage of a square-cut entrance as a standard tripping device. The flow near a square-cut entrance will be marked by a separation bubble and by Kelvin-Helmholz instability of the associated inflected profile. (Cite Schiller.) Radial pressure gradients near the reattachment point may mean for very short pipes that flow adjustment near the exit should not be neglected.

For data, see

⁵Unclear reference, possibly a section not completed.

SCHILLER (1922)
KIRSTEN (1927)
DEISSLER (1950)
BARBIN and JONES (1963)
BRIGHTON (1965)
SHARAN (1972)
WANG and TULLIS (1974)
POZZORINI (1976)
REICHERT and AZAD (1976)
HANKS et al. (1979)
LAWS et al. (1979)
KLEIN (1981)

Protocol for estimating required development length for turbulent pipe flow. Produce two log-log plots of x/D against Re , one each for quiet and noisy entrance flow. Use different symbols for flows that pass or fail.

(1) If τ is linear in r , flow passes. See Kjellstrom and Hedberg, Brighton, Bourke et al, Barbin and Jones, Patel, Sharan, Wagnanski and Champagne, Wichner, Gessner, Bremhorst and Walker, Chen and Robertson, Brookshire, Powe and Townes, Schildknecht et al.

(2) If u_c/\tilde{u} is normal, flow passes. See Weir et al, Reichert and Azad, Deissler, Wang and Tullis, Laws et al, Brenkert. For normal values, see Rotta, Senecal and Rothfus, Patel and Head, Morrow, Clark, Nikuradse, and all profile data.

(3) If u'/\tilde{u} on centerline is normal, flow passes. See Pennell et al and all data on Reynolds stresses.

(4) If u_c/u_τ is normal, flow passes. Similar to (2), but requires C_f to be normal also. See discussion in section on friction coefficient and value of Karman's κ .

2.3 Transition

2.3.1 Intermittency

All classical flows pass through a transition from laminar to turbulent flow as the Reynolds number increases. However, transition processes, like similarity rules, are very different from one classical flow to another. In most cases, nature does not provide a continuum of flow states that evolve gradually from a recognizably laminar flow at one transition boundary to a recognizably turbulent flow at the other. It is more common to find autonomous regions of laminar and turbulent flow that are separated by irregular but well defined interfaces. The local state of such flows at any point in space and time is usually described by a binary number $\gamma(t)$, called the intermittency, that takes the values $\gamma = 0$ if the flow is laminar and $\gamma = 1$ if the flow is turbulent. Methods for classifying the state as laminar or turbulent will be taken up in the next section. The mean value $\bar{\gamma}$, usually averaged over time or ensemble, will be called the intermittency factor. For the purposes of this monograph, the intermittency factor can be interpreted as the fraction of time that the flow at a fixed point spends in the turbulent state.

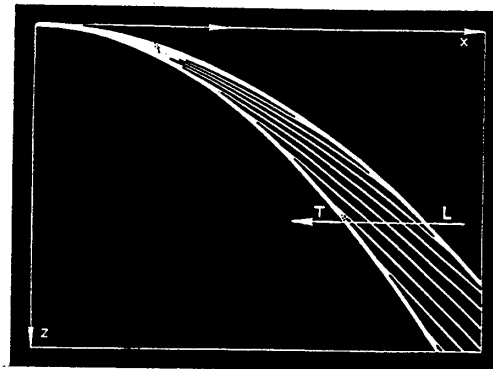
There is ample experimental, analytical, and numerical evidence that fully developed laminar pipe flow is unconditionally stable for Reynolds numbers $Re = \tilde{u}D/\nu$ below about 2000. No matter how disturbed the initial state of the flow may be, the state far downstream relaxes to the laminar parabolic profile. For Reynolds numbers above about 2800, an initial disturbed state leads eventually to continuous turbulence that is usually assumed to be homogeneous in the flow direction, although this assumption may not have been sufficiently tested. In an intermediate range of Reynolds numbers, $2000 < Re < 2800$, transition far downstream from a noisy entrance takes the form of alternating regions of laminar and turbulent fluid moving down the pipe.

Experimental observations of intermittency in pipe flow began very early. REYNOLDS (1883), using a dye filament for flow visualization, described intermittent dispersion of the dye filament by rapid

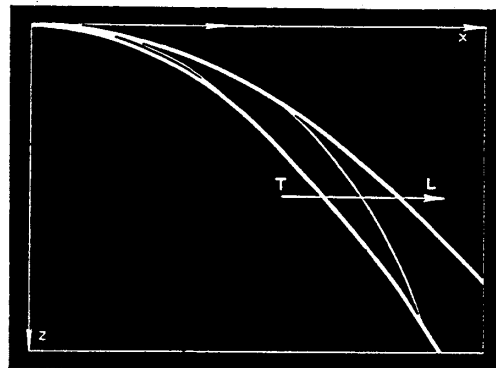
local mixing. HAGEN (1854) and COUETTE (1890) independently noted large fluctuations in the trajectory of a water jet emerging horizontally from a square-cut pipe exit into air. These fluctuations occurred only for a small range of flow rates and were accompanied by changes in the appearance of the jet surface (“glassy,” “frosty”). The explanation is easier today than it was a century ago. Under the action of gravity, the trajectory of the exit jet in free fall from a horizontal pipe is very nearly a parabola. For a fixed volume flux, the momentum flux is greater by a factor $4/3$ when the exit velocity profile is parabolic than when the exit velocity profile is uniform (as an approximation to a turbulent exit profile). The experiment is best carried out with a long pipe of small enough diameter so that surface tension forces are relatively large, although not large enough to cause early breakup of the jet. Otherwise, slow fluid near the outside of the initial free jet may fall away before it can be accelerated by internal viscous forces. This latter phenomenon is visible in some scenes in the educational motion picture by STEWART (1969).

After an interval during which the range of Reynolds numbers for transition was well established by measurements of mean flow rate and mean pressure drop, the behavior of the exit jet in transition was revisited by SACKMANN (1947–1954) in a series of short papers in *Comptes Rendus*. These papers have little structure or content beyond the content of FIGURE 2.14, which is taken from the paper of 1954. I believe that the images are analytical versions of jet trajectories derived from motion-picture frames for the transitions laminar \rightarrow turbulent and turbulent \rightarrow laminar. There is a dramatic difference between the slow transition at the leading or downstream edge of a turbulent region and the rapid transition at the trailing or upstream edge.

Two major contributions to the subject of transition in pipe flow were published almost simultaneously by ROTTA (1956) and LINDGREN (1957). Lindgren worked in water; Rotta worked in both water and air. Both investigators used a highly disturbed entry. Both analyzed recorded analog signals manually to observe the relaxation of the flow to an intermittent state. Two quantities that are relatively easily measured by ignoring details of shape are the global



Passage
du régime
laminaire
au régime
turbulent
(Établissement
de la
turbulence)



Passage
du régime
turbulent
au régime
laminaire
(Amortissement
de la
turbulence)

Figure 2.14: Two photographic sequences of instantaneous exit-jet trajectories according to SACKMANN (1954) for pipe flow in the transition range. The upper and lower pictures correspond to passage of the leading and trailing edges of a puff.

intermittency factor $\bar{\gamma}$ (now averaged over pipe cross section as well as time) and the dimensionless intermittency frequency fD/\tilde{u} , where f is the rate of alternation between laminar and turbulent flow.

Lindgren used a transparent pipe and an optical probe based on the phenomenon of streaming birefringence, which rotates the plane of polarization of an incident polarized light beam according to the local rate of strain in the fluid. His chemical solutions were corrosive and were not Newtonian except at small concentrations. Lindgren's paper shows that relaxation can involve the emergence of laminar regions from an initially fully turbulent flow. It is this laminar flow, rather than the turbulent flow, that demands to be explained in terms of pressure drop or flow rate. FIGURE X⁶ shows passage of a turbulent region, now called a puff, in Lindgren's tube.

Rotta measured the global intermittency for flow of water by the exit-jet technique. He collected the water in the jet in two calibrated containers, using a double funnel. One container captured the fluid having a long or laminar trajectory, and the other captured the fluid having a short or turbulent trajectory. The two together captured the total volume flow rate Q . The intermittency frequency was determined visually. One possible source of scatter in such measurements is apparent on considering the exit-jet traces in FIGURE 2.14. As these traces cross the line $L-T$, which can be visualized as the top of a double-funnel receiver, it is sensible to have the septum always close to the laminar position. That is, the best discriminant in intermittency measurements by this method is not the transition laminar/turbulent, which is not always well defined, but the transition laminar/non-laminar.

The intermittency data of Rotta and Lindgren are shown in FIGURES 2.15 and 2.16, together with other measurements of $\bar{\gamma}$ and/or fD/\tilde{u} by

MORROW (1905)
BINNIE and FOWLER (1947)
MATTIOLI and ZITO (1960)

⁶Apparently this was to be a figure number from Lindgren's paper.

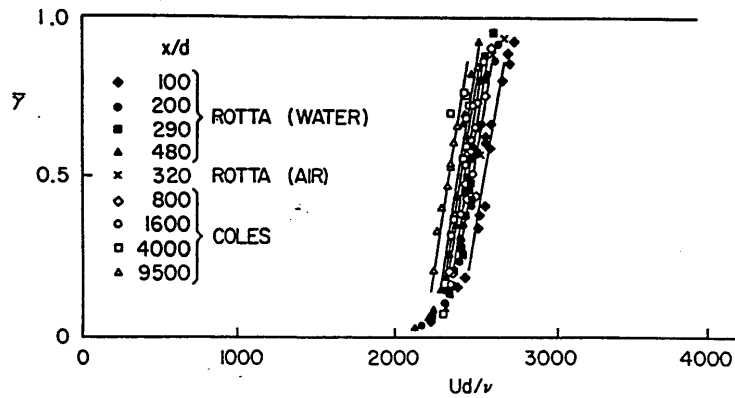


Figure 2.15: The mean intermittency $\bar{\gamma}$ for pipe flow with highly disturbed entry. The data are from various sources, using the exit-jet method, streaming birefringence, hot-wire anemometry, or laser-Doppler velocimetry (figure 1 of COLES 1962)

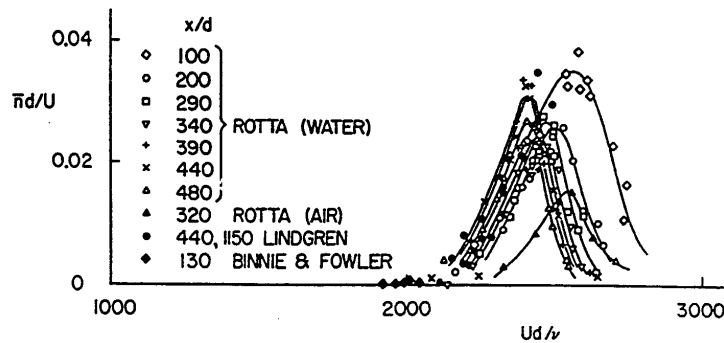


Figure 2.16: The intermittency frequency fD/\tilde{u} for pipe flow with highly disturbed entry. The data are from various sources, using the exit-jet method, streaming birefringence, hot-wire anemometry, or laser-Doppler velocimetry (figure 3 of COLES 1962)

COLES (1962)
VALLERANI (1964)
GILBRECH and HALE (1965)
YELLIN (1966)
CASTRO and SQUIRE (1967)
OHARA (1968)
PATEL and HEAD (1969)
STERN (1970)
WYGNANSKI and CHAMPAGNE (1973)
CLAMEN and MINTON (1977)
RAMAPRIAN and TU (1979)
STETTLER and HUSSAIN (1986)

The transition range $2000 < Re < 2800$ can be picked out clearly. Some of the scatter in these figures may be traceable to insufficient pipe length or to poor control of temperature. With better control, it is conceivable that such measurements could provide an acceptable means for measuring viscosity.

The terms “noisy entrance flow” and “far downstream” may need clarification. The work of several investigators (**refer to Schiller, Prandtl**) suggests that flow separation at a square-cut entrance is a sufficient but not excessive disturbance, capable of causing transition in the range of Re just defined. If stronger initial turbulence is desired, various axisymmetric geometries can be used as variations on the square-cut entry. These include an orifice plate, a step increase in diameter, and a bluff central body. All of these geometries involve separated flow and free shear layers that rapidly undergo transition, filling the pipe with turbulence near the entrance if it is not already full. The first measurements of the distance required for such a noisy flow to relax to an equilibrium intermittent state were made by Rotta. This distance can be 500 diameters or more, depending on the Reynolds number. It is important, for the sake of statistical security, to have a large number of alternations within the pipe. If the flow rate is independently regulated, then a given pipe is longest at about $Re = 2400$. Rotta was not certain about the final state of his flows far downstream, and may have supposed that this state would always be either fully laminar or fully turbulent.

To test this point, I once caused some double-funnel measurements to be made for water in a pipe 9500 diameters long ($D = 0.2$ cm, $L = 1900$ cm). The data were obtained by students as a laboratory project, and the students were a little careless about temperature and thus Reynolds number. The original data have been lent and lost. However, the results were reported in a survey paper (COLES 1962) and showed $\bar{\gamma}$ increasing from 0 to 1 in the standard range of Re from 2000 to 2800. The data are included in FIGURE 2.15. For practical purposes, I consider 9500 diameters to be infinity, and I am quite satisfied that the final equilibrium state in the transition regime is a statistically steady state of intermittent turbulence.

2.3.2 Methods of measurement

The exit-jet phenomenon is peculiar to pipe flow and perhaps to channel flow. Other experimental techniques for measuring intermittency have been developed for other shear flows, and a short digression to describe these techniques is in order. (**Cite Hedley and Keffer 1974 and Narasimha 1985.**) The classification of a flow as locally laminar or turbulent is always somewhat subjective, but different observers using different signals and different methods tend to obtain similar results. In my experience, the most useful and reliable criterion for classifying a flow as turbulent is the presence of fluctuations at high frequencies, since such fluctuations will decay and disappear if they are not being continuously supplied with fresh energy through a hypothetical cascade mechanism. This observation explains why intermittency measurements did not become routine until after the development of instruments capable of detecting and recording turbulent fluctuations.

The property of intermittency near free edges of turbulent shear flows was first noted explicitly by CORRSIN (1943) for the case of a round jet, although it has always been an obvious feature of clouds and of smoke plumes from chimneys and open fires, and also appears in photographs of projectile wakes going back to the work of MACH (18xx) (**check**). I have consulted several colleagues in an effort to determine why the phenomenon of intermittency was

not followed up at Caltech. The reason seems to be that Karman at the time considered it to be of secondary importance compared to the rapid emergence of transonic flow as a demanding new field of aerodynamics. Corrsin did return to the problem later at Johns Hopkins (CORRSIN and KISTLER 1954), although in the meantime the topic was preempted when the first quantitative measurements of intermittency were made in a plane far wake by TOWNSEND (1956).

Townsend's method was indirect and almost intuitive. Consider a fluctuating signal $e_o(t)$ having zero mean in a homogeneous turbulent flow. Townsend, for example, took $e_o = \partial u / \partial t$, as measured by a hot-wire probe and processed by analog vacuum-tube circuitry. Let $e_i(t)$ be the same signal in an intermittently turbulent flow (i for intermittent). The flatness factors for e_o and e_i are defined formally by

$$F(e_o) = \frac{\overline{e_o^4}}{(\overline{e_o^2})^2}, \quad F(e_i) = \frac{\overline{e_i^4}}{(\overline{e_i^2})^2}, \quad (2.71)$$

where the overbar indicates a mean value. The crucial assumption of the technique is that $e_i(t)$ is related to $e_o(t)$ by an on-off operator $\gamma(t)$, with $\gamma = 0$ or 1 and

$$\overline{e_i^2} = \overline{(\gamma e_o)^2} = \overline{\gamma} \overline{e_o^2}, \quad \overline{e_i^4} = \overline{(\gamma e_o)^4} = \overline{\gamma} \overline{e_o^4}. \quad (2.72)$$

Consequently,

$$F(e_i) = \frac{\overline{\gamma} \overline{e_o^4}}{\overline{\gamma}^2 (\overline{e_o^2})^2} = \frac{1}{\overline{\gamma}} F(e_o), \quad (2.73)$$

and

$$\overline{\gamma} = \frac{F(e_o)}{F(e_i)}. \quad (2.74)$$

The required reference flatness factor $F(e_o)$ can be measured in a fully turbulent region of the same flow, or simply approximated by the value $F = 3$ appropriate to a Gaussian variable.

Many experimenters, beginning with TOWNSEND in a later paper (1949), have developed methods for classification of an inhomogeneous flow as laminar or turbulent by using various kinds of analog

(later digital) signal processing. By now there are almost as many methods for determining intermittency as there are experimenters. Typically, a continuous analog signal from a hot wire, say, is differentiated at least once with respect to time. The resulting signal is bandpass filtered to further emphasize high frequencies, rectified, and fed into a trigger circuit with an adjustable threshold level. The irregular output pulse train can be fed to an averaging or smoothing circuit (later a retriggerable one-shot whose output remains high whenever the time interval between input pulses is less than the pulse width of the one-shot). (The output of the intermittency circuit is a binary bit that was often recorded in my work as the least significant bit of digital data samples of the same analog signal.) The circuit parameters (pass band, threshold level, decay time or one-shot pulse width) can be adjusted until the intermittency output consistently confirms a subjective judgment that turbulence is intermittently present or absent in a variety of hot-wire signals typical of the actual experiment. This scheme, applied to each wire of a 24-wire rake, was used by SAVAS and COLES (1985) to map the development of turbulent regions in the outer part of a turbulent boundary layer. (Also Laufer and Kaplan?)

A different kind of discrimination can be carried out numerically for a uniformly spaced time series, say $u(t)$. This scheme has the advantage that it can readily be applied after the fact to any data stream for which a suitable time series exists, including data from computer simulations. Consider a least-squares fit of a straight line to three successive data points in such a series, as displayed in FIGURE 2.17. The fitted line turns out to be parallel to a line through the first and third points. The rms deviation of the three points from the fitted line is

$$\epsilon = \frac{|u_1 - 2u_2 + u_3|}{\sqrt{6}} \quad (2.75)$$

The intermittency is set to unity or zero for the center point according to whether ϵ is above or below a chosen threshold. This threshold should be well above the noise level and well below the typical sample-to-sample excursion of the signal in regions that are believed to be turbulent. The time interval between points can also be varied by taking every second, third . . . point, as long as the signal

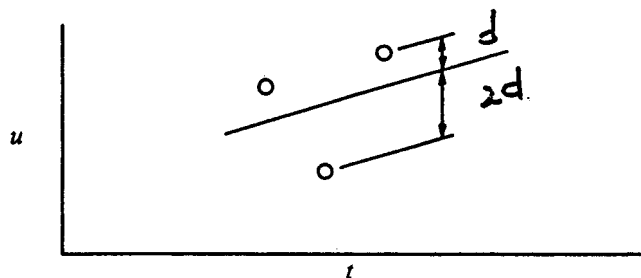


Figure 2.17: A least-squares fit to three successive points of a uniformly spaced time series for a variable $u(t)$.

contains appreciable turbulent energy. In my experience it has usually been possible to choose the two parameters of the method, the sampling frequency and the threshold level, so that γ is not sensitive to either. The resulting time series of ones and zeros can be edited as many times as desired by assigning to each point the value belonging to a majority of points in a group of 3, 5, ... symmetrically placed points.

Several writers since Townsend have proposed as a first approximation an on-off transition model. That is, intermittent pipe flow should be viewed as a quite literal alternation between fully developed laminar and turbulent regimes. By observing the DC and low-frequency components of a hot-wire signal in a flow of air at $R = 2550$, ROTTA (1956) found that the axial velocity at a fixed point fluctuated between two values characteristic of laminar and turbulent flow respectively. These values are shown in FIGURE 2.18 together with the mean profile indicated in the same flow by a heavily damped pitot tube. Although neither of the momentary profiles yields the correct mass flow, which was independently measured by means of a downstream sonic orifice, the momentary state of the flow seems always to be close to one limiting profile or the other. Support-

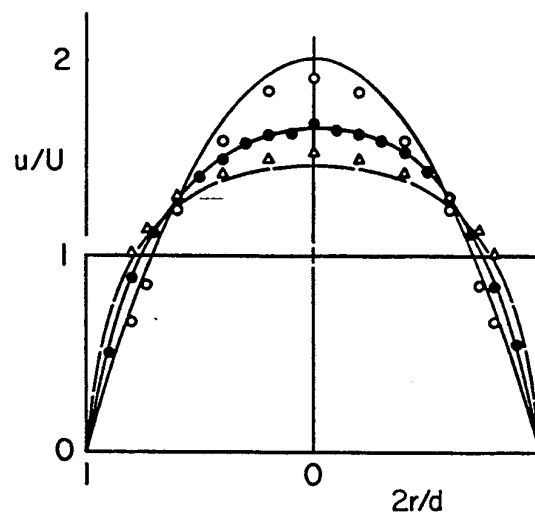


Figure 2.18: Rotta's decomposition of a measured pipe profile in the transition regime according to the on-off model. The laminar and turbulent profiles do not have quite the correct volume flow rate.

ing evidence for this conclusion can also be drawn from Lindgren's work. The pressure records in figures 5.9 and 5.10 of his 1957 paper allow an estimate of the local axial pressure gradient inside a relatively long turbulent plug. At both Reynolds numbers studied (3180 and 3480), this pressure gradient is about 1.9 times that in the intervening laminar intervals, while the ratio of commonly accepted friction coefficients for fully developed turbulent and laminar flow at these Reynolds numbers is about 2.0. However, a strong objection to the on-off model can be made on the ground that the model requires the properties of a fully turbulent flow to be defined under conditions where a fully turbulent flow cannot be observed experimentally, and so I do not recommend it.

The concept of intermittency need not be limited to flows with visible interfaces. It can also be invoked in flows that are approximately homogeneous, since these flows may consist internally of regions where the energy at high frequencies is widely variable. Such regions were first detected experimentally in the turbulent boundary layer, using analog pass-band methods, in a neglected study by SANDBORN (19xx). A related generalization by KOLMOGOROV (1962) of his 1941 inertial theory of turbulence took into account intermittent internal dissipation. These developments may also be connected to the experimental distinction made by BRADSHAW (19xx) (and others) between active and passive regions in turbulent flow. The connection, if any, with coherent structure has so far not been established. Internal intermittency, like many other topics in turbulence, is an answer for which the question is not known.

2.3.3 The puff and the plug

The consensus of the frequency measurements in FIGURE 2.16 is that the frequency fD/\tilde{u} in pipe flow has a maximum value of about 0.025 at about $Re = 2400$, where the celerity is about $0.9\tilde{u}$ (see FIGURE 2.24 below). The average interval between turbulent regions is thus about 35 diameters. Given an intermittency factor of 0.45, this interval can be divided into lengths of about $20D$ and $15D$, respectively, for laminar and turbulent regions. According to

measurements by ROTTA (1956) and VALLERANI (1964), shown in FIGURE 2.19, the flow at the exit of a very long pipe for Re between 2000 and 2400 tends to consist of standard regions of turbulent flow about 15 diameters long, separated by non-standard regions of laminar flow ranging upward in length from about 20 diameters. For Re between 2400 and 2800, the flow tends to consist of standard regions of laminar flow about 10 diameters long, separated by non-standard regions of turbulent flow ranging upward in length from about 15 diameters.

A colorful collection of names has been proposed for the two kinds of turbulence; flash, plug, spot, puff, slug (I do not know the usage in other languages than English). WYGNANSKI and CHAMPAGNE (1973) call the turbulent structure within the transition range a puff, and the structure above the transition range a slug. They make the distinction strictly in terms of origin; disturbed entry for the puff, boundary-layer instability for the slug. A distinction is certainly desirable, but I do not think it ought to involve the conditions of origin. I prefer a distinction in terms of the operational properties of the two kinds of structures, taking into account the well-documented change in behaviour near $Re = 2400$. I propose to call the structures puff and plug, respectively, partly for the sake of (a) alliteration and (b) ease of translation. The term puff always means the structure that is at home in the range of Reynolds numbers from 2000 to 2400. The term plug refers to higher Reynolds numbers. The term slug includes both. The only new feature in equilibrium flow at higher Reynolds numbers is the disappearance of laminar regions by about $Re = 2800$, a disappearance that probably occurs gradually and may mean only that relatively quiet regions are being classified as turbulent rather than laminar. To resolve this question, it would be useful to have flatness factors for turbulent fluctuations on the pipe axis through the transition range and beyond. In all of these estimates, the most uncertain quantity is the intermittency factor itself, because the leading interface is not well defined in the lower transition region, and in any event the interfaces are not plane. The term "length" is therefore used very loosely.

The puff has a characteristic velocity signature, apparently first

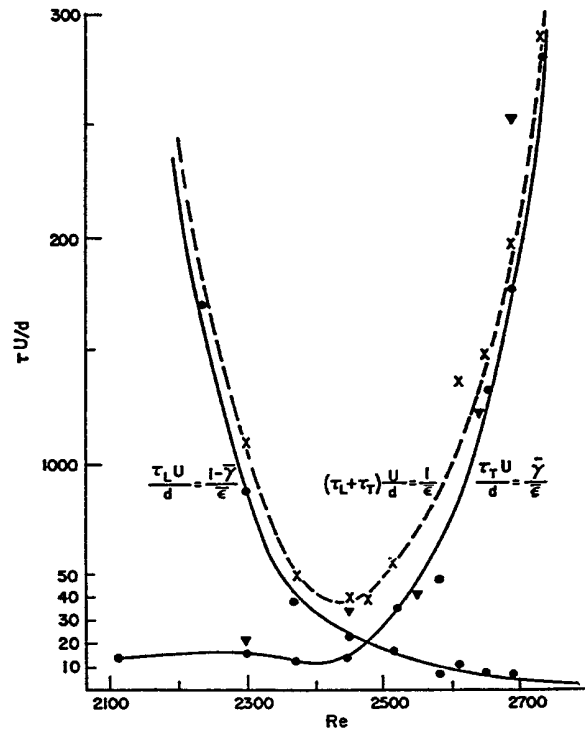


Figure 2.19: The average duration of laminar and turbulent intervals far downstream in the transition regime of pipe flow with highly disturbed entry. (Figure of COLES (19xx)). The data are from ROTTA (1956) and VALLERANI (1964).

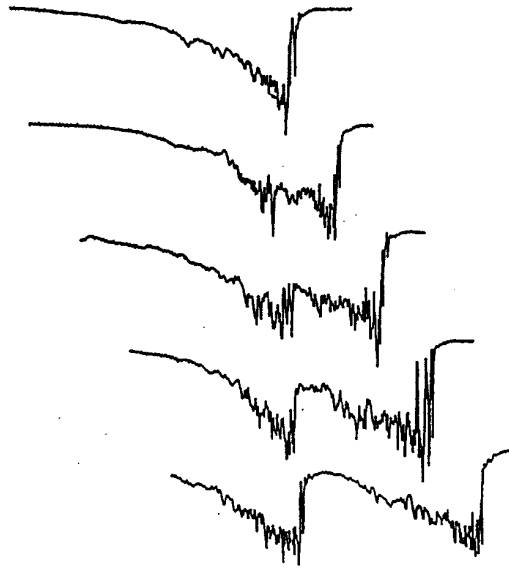


Figure 2.20: Some velocity signatures obtained by BREUER (1985) on the centerline of a pipe flow, showing several stages of the splitting process at $Re \sim 2400$. The traces are from different realizations of the splitting phenomenon.

recorded by BOND (1931) in water with the aid of a sensitive mechanical galvanometer whose mirror was mounted on a flake of mica deflected by the exit jet. A more recent hot-wire signature is shown as the top trace in FIGURE 2.20. A fixed probe shows the velocity on the centerline decreasing rather slowly as a function of time as the puff approaches, and then increasing abruptly. The length of pipe involved is about 15 diameters. (**Discuss Meseth, figure 3.**) Mean streamlines have been mapped in a nice experiment by WYGNANSKI, SOKOLOV, and FRIEDMAN (1975) for an ensemble of artificially generated puffs at $Re = 2230$ (a value chosen to

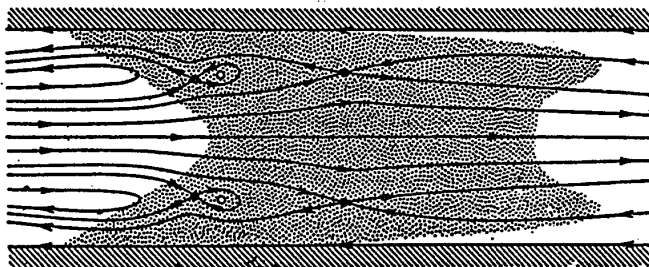


Figure 2.21: Topology of the mean flow in a turbulent puff at $Re = 2230$, after WYGNANSKI *et al.* (1975). The observer is moving at the celerity of the structure, so that mean particle paths coincide with mean streamlines. The two coordinates have equal scales.

minimize effects of splitting), as shown in FIGURE 2.21. The mean flow is steady in a coordinate system moving downstream with a velocity of about $0.90 \tilde{u}$ to $0.95 \tilde{u}$. The value used to construct the figure is not stated, but may be \tilde{u} itself. The puff has a long, rather vaguely defined nose of decaying low-frequency turbulence at the right that is visible in photographs (LINDGREN 1959; MATTIOLI and ZITO 1960; YELLIN 1966; WYGNANSKI and CHAMPAGNE 1973; BANDYOPADHYAY 1986) (*but is missing in the present figure because the interface is represented by the locus of a relatively high fluctuation level ($u'/\tilde{u} = 0.10$ in figure 12d of Wygnanski *et al.* 1975)*).

It is a common practice in presenting structural models such as the one in FIGURE 2.21 to stretch the coordinate normal to the general flow. I have come to deplore this practice, although I have used it more than once, and I will try to avoid it in this monograph. Because of its stability and reproducibility, the puff is a plausible candidate for standard coherent structure in pipe flow. FIGURE 2.21 suggests that the puff as structure is a vortex ring, a property that I missed completely in my contribution to the 1961 colloquium in

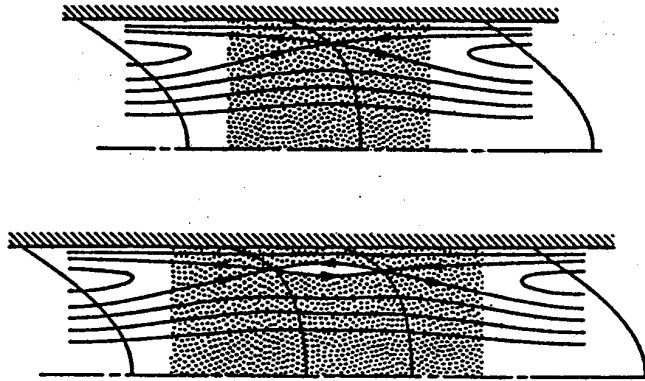


Figure 2.22: My original (top) and revised (bottom) cartoons suggesting the topology of a turbulent puff. The top cartoon is from COLES (1962).

Marseille (COLES 1962). That contribution included the cartoon shown in the upper half of FIGURE 2.22. The basis for this figure was a strictly kinematic use of Rotta's laminar and turbulent profiles. In a coordinate system moving with the puff velocity c (c for celerity), the mean flow far downstream can be taken as steady, and an axially-symmetric stream function can be computed for the two limiting profiles in FIGURE 2.18; i.e. for the solid and dashed lines. The resulting mean streamlines, which are the same as the mean particle paths, must have the topology shown schematically in the lower part of FIGURE 2.22. Near the wall, which is now moving to the left at the velocity c , fluid enters the puff at the nose and leaves at the tail. Near the centerline the situation is reversed; fluid enters at the tail and leaves at the nose (with a relative velocity in both cases of about $1.2c$), meanwhile slowing down inside (to about $0.6c$). There is a small net flow to the right corresponding to the excess of \tilde{u} over c . The important point, however, is that a substantial fraction of the fluid entering the slug from the rear reverses direction inside and emerges again at the rear, with a similar situation obtaining at

the front. After the publication of the paper by Wygnanski *et al.*, it became obvious that the cartoon should be dynamic, and should look like the lower half of FIGURE 2.22, this being topologically equivalent to FIGURE 2.21. The term vortex implies here (as it does in the case of the inviscid Hill spherical vortex, say) only the existence of closed mean streamlines in a suitable moving coordinate system, and not necessarily the existence of a local peak in mean vorticity.

Given the present view, an explanation also presents itself for the strong stabilizing effect of curvature noted by TAYLOR (1929). Puffs survive in a straight pipe for Re greater than about 2000, but puffs survive in a pipe coiled to a diameter of $100 D$, say, only for Re greater than about 5000. I believe that in a puff the vortex ring is the engine that makes the structure run. The secondary flow in the curved pipe presumably disables this engine by interfering with the geometric and dynamic equilibrium between the puff and its environment. Note that I am answering G.I.'s question (**give ref**) nearly 50 years later.

2.3.4 Short account of flow in coiled pipes

Bits and pieces of circumstantial evidence can be found to suggest that the vortex ring is (or is not) the prototype large eddy in fully developed turbulent pipe flow. LINDGREN (1969) thought he recognized puffs in flow at Reynolds numbers near 6000. Champagne (private communication) has verified the emergence of puffs when an initially turbulent flow was reduced in Reynolds number from 11300 to 2260 in a long diffuser, but no hard numbers are available. RUBIN, WYGNANSKI, and HARITONIDIS (1980) suggested that the length of plugs might be quantized in multiples of $25 D$, but I do not find their evidence to be completely persuasive.

Both flow-visualization studies and data on fluctuations indicate that the turbulence level is relatively high at the rear of a puff, and that the transition from a laminar to a turbulent state for fluid entering the puff from the rear occurs abruptly. The fluid leaving the puff at the front, on the other hand, undergoes a slow acceleration

requiring at least several pipe diameters for completion, while at the same time the turbulence becomes progressively coarser and weaker until it is no longer detectable. The most mysterious and challenging aspect of these observations is the fact that fluid is flowing through the turbulent region, entering and leaving. Another confirmed instance of this behavior is spiral turbulence in circular Couette flow (COLES 1965). The possibility arises of an unnatural phenomenon that might be called anti-transition, perhaps with negative turbulence production, in which fluid crosses a laminar/turbulent interface from the turbulent to the laminar side. After some ambitious measurements in spiral turbulence by C. VAN ATTA (1964) were analyzed to a point where the three-dimensional mean flow was adequately defined, as in FIGURE 2.23, it became apparent that the mean flow near an anti-transition interface was in fact nearly parallel to the interface, and thus that the dynamical process in this flow was a dissipative process of the conventional kind. It is therefore not constructive to say that fluid leaves the turbulence. It is more accurate to say that turbulence leaves the fluid, through viscous decay, until the state can only be described as laminar. The flow in the long downstream nose of a puff meets this condition.

2.3.5 Splitting

Another striking phenomenon discovered by Lindgren is splitting of individual turbulent puffs at Reynolds numbers in the lower transition region (see the records in LINDGREN 1957, figures 4.7, 4.19, 5.4). For x/D greater than about 200, the dimensionless frequency fD/\tilde{u} has a maximum value at a Reynolds number of about 2400, as already shown in FIGURE 2.16. On either side of the maximum the plug frequency decreases sharply, because the plug population near the entrance is reduced at lower Reynolds numbers by the demise, and at higher Reynolds numbers by the consolidation, of individual plugs. Rotta apparently doubted the accuracy of his data for intermittency frequency at the lower Reynolds numbers and the more downstream stations, because the data showed the frequency increasing with increasing x/D at fixed Re . He speculated that vibration

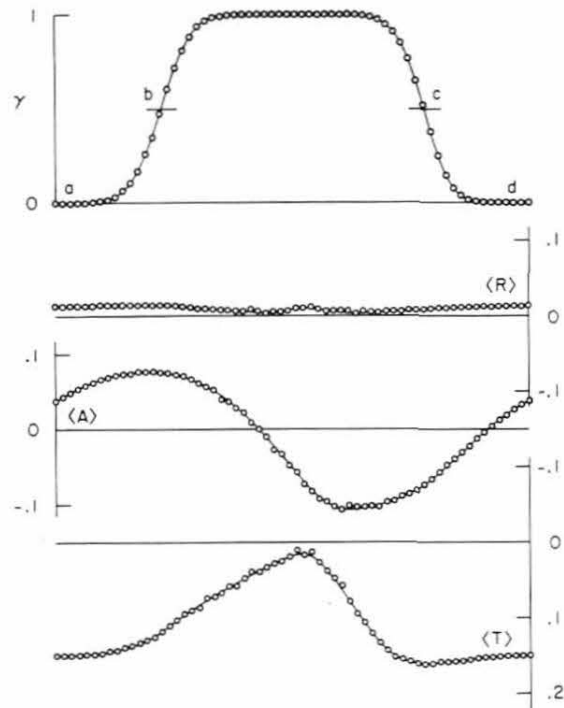


Figure 2.23: Intermittency factor (top curve) and three components of mean velocity relative to spiral region of turbulence in circular Couette flow. Components R, T, A in radial, tangential, and axial directions are normalized. Positions a, b, c, d lie along one complete circuit at one radial position. Figure 4 of COLES and VAN ATTA 1966 (AIAA Journal), which describes the geometry of the flow measurement. (Caption provided by K. Coles)

and capillary forces may have caused the exit jet to break up for the longer tubes. Rotta smoothed his original data in an effort to remove the observed increase in f . He thus missed the most remarkable transition phenomenon of all, the phenomenon of splitting of turbulent regions of flow.

Some puff signatures observed in a flow subject to splitting are included in FIGURE 2.20. The data are from the master's thesis by BREUER (1985) and were obtained in air using a hot wire on the pipe axis. The five traces are from five different events that have been selected from a larger population to represent various stages of the splitting process. There is a strong impression that splitting occurs near the trailing edge of the puff, in the region where turbulent fluctuations are large and may extend to include momentarily laminar behavior.

Splitting introduces complications in any study of celerity in the lower transition regime. One turbulent region can become two, three, four . . . regions as puffs move downstream, provided that space is available in the pressure field. Different observers do not agree about the site of this splitting. LINDGREN (1957) seems to place the site at the front, while WYGNANSKI, SOKOLOV, and FRIEDMAN (1975) seem to place it at the rear. Quantitative information about splitting is rare and inconsistent. Wagnanski *et al.* report up to four turbulent regions in train at a station $450 D$ downstream from a single disturbance. VALLERANI (1964) reports the same number at a station almost an order of magnitude farther downstream in an apparatus having a better-developed laminar profile but poor flow regulation. The difference may be partly a matter of Reynolds number and partly a matter of flow regulation. Vallerani also noted some variations in the length of laminar regions created by splitting, depending on Reynolds number and on the number of turbulent regions in train. There are evidently several important unresolved issues involving the mechanisms that promote splitting and prevent coalescence of turbulent regions in pipe transition. The experiments are technically simple, and more study will probably be fruitful if the right questions are asked.

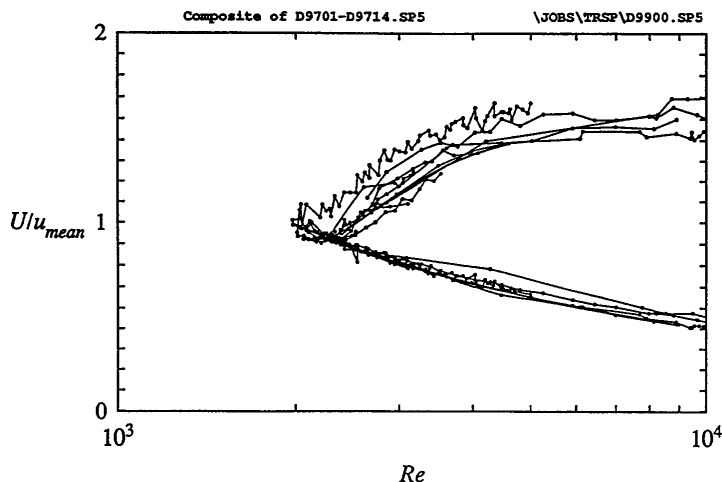


Figure 2.24: Leading-edge and trailing-edge celerities for puffs and plugs in pipe flow as measured by several authors.

2.3.6 Celerity

Much of Lindgren's work is concerned with the evolution of individual turbulent regions relatively near the pipe entrance, rather than with asymptotic conditions far downstream. One quantity that seems to be quite insensitive to the details of the flow is the trailing-edge velocity. Lindgren obtained data in various tubes with various fluids and entry conditions, using both optical and pressure instrumentation. The measurements by various authors, shown in FIGURE 2.24, extend beyond the real transition range in both directions, so that the flows in questions cannot be statistically stationary in x . On the one hand, Lindgren's observations at low values of Re confirm that turbulence originating near the entrance tends to decay far downstream. Consequently, his measurements of interface velocity in this range refer to puffs that have survived long enough to be detected at two successive stations along the pipe (see the oscillographic records in Lindgren's figures 4.6, 4.7, 4.19, 4.20, as well as his table 2.5; also

LINDGREN 1960, figure 5). For the measurements at values of Re above the transition range, on the other hand, a low level of inlet turbulence was necessary in order to observe intermittency at all. Plugs first appeared somewhere downstream of the entrance, probably in the manner described by REYNOLDS (1883), and grew rapidly (see the oscillographic records in Lindgren's figures 4.14, 5.9, 5.10; also LINDGREN 1960, figures 6, 7). Provided that these plugs had not yet merged, Lindgren was also able to measure the leading-edge velocity shown in FIGURE 2.24. He does not comment on these data in terms of the implied rate of approach to a fully turbulent state, nor does he provide any information about flow at quite low Reynolds numbers, where the relative magnitude of the two velocities should in principle be reversed as evidence of decay.

Leading-edge and trailing-edge velocities for puffs and plugs have been measured as a function of Reynolds number by several investigators;

LINDGREN (1957)
 VALLERANI (1964)
 SARPKEYA (1966)
 STERN (1970)
 PATERSON and ABERNATHY (1972)
 WYGNANSKI and CHAMPAGNE (1973)
 MESETH (1974)
 TEITGEN (1980)
 ZALZAL et al. (1994)

with the results recorded in FIGURE 2.24. The quantities plotted in the figure are essentially phase velocities, or more accurately velocities at constant phase. Early experimenters, particularly Favre (ref) and Kovaszny (ref), tried to give such velocities a special meaning by choosing the French word *célérité*, rather than the more conventional word *vitesse*. In this monograph, I will consistently use the word *celerity* to refer to velocities associated with structure and phase. The figure leaves no doubt that different processes are occurring in the upper and lower parts of the transition regime, with a divide at about $Re = 2400$. Below this divide, turbulent regions

have approximately constant length and therefore essentially a single celerity, which is most easily measured at the trailing interface. The measurement may be hampered by splitting. Above the divide, the leading interface moves faster than the trailing one if space is available, as first noted by Lindgren. Hence celerity at these higher Reynolds numbers is usually measured in a different mode. Laminar flow is set up in a pipe with smooth entry, and the time interval is measured between a local artificial disturbance and the associated response at one or more downstream stations.

The measurements in FIGURE 2.24 suffer from deficiencies that raise the question of reproducibility among the various experiments. In part this is because of different detection schemes for the interfaces. More generally, however, the data may be subject to ambiguity coming from at least four sources.

First, the entry flow should be smooth and quiet, and the laminar flow in the test region should have a fully developed parabolic profile, with x/D at least equal to $Re/16$ at the site of any programmed disturbance. When this condition is not met, the shape of the laminar-turbulent interfaces will imitate the shape of the laminar profile and will depend on x/D (WYGNANSKI 1970; WYGNANSKI and CHAMPAGNE 1973; TEITGEN 1975). Moreover, the proper reference velocity for celerity is no longer the theoretical maximum velocity $2\tilde{u}$ for the parabolic profile, but rather the actual maximum velocity at a given station (WYGNANSKI and CHAMPAGNE 1973). In a short pipe, this velocity may be closer to \tilde{u} than to $2\tilde{u}$, and may vary over the observation distance. Measurements of celerity at high Reynolds numbers have a particularly *ad hoc* quality in short pipes when transition occurs spontaneously or is triggered artificially in the developing laminar boundary layer (LINDGREN 1957; WYGNANSKI 1970; WYGNANSKI and CHAMPAGNE 1973). In such cases it is relevant that the boundary layer in the pipe has thickness $\delta \sim (\nu x/u_\infty)^{1/2}$. In any event, far downstream the concept of celerity eventually has no meaning outside the transition range of Reynolds numbers. I therefore have serious doubts about the usefulness of the measurements in FIGURE 2.24.

Second, the formation time should be excluded from measure-

ments of celerity by making observations at two stations, each of which is sufficiently far downstream for the structure of the turbulent region to become independent of details of the formation process. In some cases (VALLERANI 1964, MESETH 1974), the response was observed at only one downstream station so that the formation process for the turbulent region was not excluded from the measured time intervals.

Third, the disturbance should be of short duration, especially in the lower transition regime, where a puff passes a fixed station in a time $15 D/\tilde{u}$. In some cases (Gilbrech & Hale 1965, Sarpkaya 1966), the duration of the disturbance was probably too long, at least at low Reynolds numbers, where an almost impulsive disturbance is called for.

Finally, close attention must be paid to flow regulation. If the mean velocity is not regulated by the experimenter, say by use of a sonic orifice, a positive-displacement pump, or a massive flow restriction, it will be regulated by the experiment, and will vary with the relative fractions of laminar and turbulent flow at each instant. This transient effect is probably less important for intermittent flow with disturbed entry at low Reynolds numbers than for intermittent flow with smooth entry at higher Reynolds numbers. In cases where enough information is available to judge the matter, poor flow regulation is more the rule than the exception. Lindgren, for example, recognized that his flow circuit was unstable and that a limit cycle could occur in his apparatus.

PRANDTL and TIETJENS (19xx, pp. x) give a glimpse of some data for such an oscillation from experiments at Göttingen. They cite Couette's experience as a precedent, although I believe that Couette was describing intermittency of the normal kind. Other evidence in the literature (**Brockmann, Mickelson**) suggests that the oscillation is not unusual. I am surprised that there are no hard numbers, although the conditions must be quite special and may include restricted ranges for Re and L/D as well as a delicate control of disturbances at the pipe entry. (**Pantulu, Jenkinson.**) There is even a standard for this relaxation process. Suppose that the flow state in a pipe is fully turbulent, and let the flow be subjected to

a gradual or abrupt increase in pipe diameter from D_1 to D_2 . The Reynolds number will decrease from Re_1 to $Re_2 = (D_1/D_2)Re_1$. Laufer (ref) and Sibulkin (ref) studied such flows for the case of a gradual area change, with $Re_1 > 3000$ and $Re_2 < 2000$.

Transition in pipe flow is intermittent. Pipe or channel flow, like the round wake (**check**), is special in that the Reynolds number is constant in the flow direction. A higher Reynolds number does not refer to a more downstream location in a given flow, but to a physically different flow in parameter space. This fact in turn makes the length-to-diameter ratio L/D an important dimensionless parameter.

2.4 Turbulent flow in a smooth pipe

2.4.1 Early work

Fundamental research on turbulent pipe flow goes back to the period 1840–1860 and the work of Hagen, Hagenbach, and Darcy. The contributions by early civil engineers are well summarized in the short history by ROUSE and INCE (1957). This work often involved the effect of roughness in commercial pipes, especially after long use, and the problem of roughness was very slow in coming under control. Fundamental research on pipe flow also requires an understanding of the effects of entrance conditions, especially for short pipes. Some of these effects are known, and others can be inferred by examining discrepancies among available measurements of friction and other quantities in turbulent flow. The issue once again is whether or not turbulent pipe flow tends far downstream to a unique state, as it must if pipe flow is to be a fit subject for fundamental research on the mechanisms of turbulence.

For flow in a smooth pipe far downstream from a noisy entrance, the empirical evidence, even in the transition regime, appears to be that the wall friction (i.e., the pressure gradient) is determined uniquely by the fluid properties, the pipe diameter, and the flow rate (i.e., the mean velocity). Engineers today understand that the ex-

istence of five dimensional physical quantities ρ , μ , D , Q , and τ_w , and the existence of three fundamental dimensional scales for mass, length, and time, together imply the existence of two dimensionless combinations and a functional relationship between them. The formal argument, first formulated by BUCKINGHAM (1914), serves well in situations like turbulent pipe flow in which the important variables are known but the governing equations are not.

According to equation (2.11) of SECTION 2.1.1, the variable τ_w is equivalent to $D dp/dx$ or approximately to $D \Delta p/L$, so that τ_w can be replaced by Δp and L in the list of variables just given. A third dimensionless number appears and can be taken immediately as L/D . Suppose that the first two dimensionless numbers, F and G , say, each depend on only one of Δp and Q . That is, take

$$F = F(\rho, \mu, D, \Delta p) , \quad (2.76)$$

$$G = G(\rho, \mu, D, Q) . \quad (2.77)$$

The associated table of dimensions is (**define notation**)

$$[\rho] = M/L^3 ,$$

$$[\mu] = M/LT ,$$

$$[D] = L , \quad (2.78)$$

$$[\Delta p] = M/LT^2 ,$$

$$[Q] = L^3/T .$$

Require F to be dimensionless, and assume

$$[F] = [\rho^a \mu^b D^c \Delta p^d] = 0 . \quad (2.79)$$

An equivalent assumption is

$$[F] = \left[\left(\frac{M}{L^3} \right)^a \left(\frac{M}{LT} \right)^b (L)^c \left(\frac{M}{LT^2} \right)^d \right] = 0 , \quad (2.80)$$

or

$$\left[M^{a+b+d} L^{-3a-b+c-d} T^{-b-2d} \right] = 0 . \quad (2.81)$$

Three simultaneous algebraic equations are obtained for the four exponents;

$$\begin{aligned} a + b + d &= 0 , \\ -3a - b + c - d &= 0 , \\ b + 2d &= 0 . \end{aligned} \quad (2.82)$$

Let one exponent, say d , be treated as given. These equations then have the one-parameter solution

$$\begin{aligned} a &= d , \\ b &= -2d , \\ c &= 2d . \end{aligned} \quad (2.83)$$

(Comment that the Π theorem involves the matrix properties of systems like equations (2.82).) Consequently, equation (2.79) must have the form

$$[F] = \left[\left(\frac{\rho D^2 \Delta p}{\mu^2} \right)^d \right] = 0 , \quad (2.84)$$

in which the value of d is immaterial, since any ratio or product of dimensionless combinations or their powers is also dimensionless. A similar treatment of equation (2.77) for G leads to

$$[G] = \left[\left(\frac{\rho Q}{\mu D} \right)^b \right] = 0 . \quad (2.85)$$

The exponents d and b , since they are associated with dimensionless scales and not with physical variables, can play no physical role. The three dimensionless parameters for pipe flow therefore emerge from Buckingham's analysis as

$$\frac{L}{D} , \quad \frac{\rho Q}{\mu D} , \quad \frac{\rho D^2 \Delta p}{\mu^2} . \quad (2.86)$$

The second of these is equivalent to the Reynolds number Re , according to equations (2.15) and (2.19), and the third is equivalent to the product $Re^2 C_f$. It is possible, and may even be useful, to think of pipe flow as a nonlinear fluid operator whose primary input variable is a flow rate Q or \tilde{u} and whose primary output variable is a pressure difference Δp or τ_w , or conversely. It is no accident that these input and output variables were deliberately isolated by Reynolds in the original definitions (2.76) and (2.77). This choice also amounts to defining three characteristic velocities \tilde{u} , $(\tau_w/\rho)^{1/2}$, and ν/D , whose ratios can be taken as $\tilde{u}D/\nu$ and $\tau_w D^2/\rho\nu^2$.

By common consent, the standard combinations have by now become C_f and Re , where

$$C_f = \frac{\tau_w}{\rho\tilde{u}^2/2} \quad (2.87)$$

and

$$Re = \frac{\tilde{u}D}{\nu} . \quad (2.88)$$

The implied functional relationship $C_f = C_f(Re)$ is capable of collapsing information from numerous sources into a clear and widely accepted system of description. For laminar flow, this system is the equation $C_f = 16/Re$ already derived in SECTION 2.1.2. The next several sections describe one possible system for turbulent flow. For both laminar and turbulent regimes of flow, however, the existence of any system was recognized only after the major conceptual advance that underlies the previous discussion of this section; namely, development of the art of dimensional analysis.

Reynolds. A classical paper by REYNOLDS (1883) is frequently cited in this context but, I suspect, not frequently read. In one part of his paper, Reynolds used some imaginative flow visualization in water to observe and describe intermittent transition in a circular pipe in terms of the properties of the internal flow, rather than the properties of a liquid jet at the exit (see SECTION 2.3.1). By observing the behavior of filaments of dye, he found that the onset of transition within the pipe was local and sudden and occurred at essentially the same value of $\tilde{u}D/\nu$ for three glass pipes of different

diameters. The pipes had a faired inlet and a quiet entrance flow. When inlet disturbances were reduced to a practical limit, the constant value of $\tilde{u}D/\nu$ in question was about 12,800. Because the pipes were far too short to provide a fully developed parabolic profile, it is clear that Reynolds was observing the effects of boundary-layer instability in the development region, and that no special meaning ought to be attached to the value quoted for $\tilde{u}D/\nu$. In fact, EKMAN (1911) repeated some of Reynolds' work, using Reynolds' original apparatus, and verified a strong sensitivity of transition to upstream disturbance level. What is of permanent value in this part of Reynolds' paper is his observation that both of the primary experimental variables, the flow rate and the pressure gradient, could be expressed in dimensionless form, at least for the limited purpose of describing the onset of transition. It is not at all clear that Reynolds intended this observation to apply for more general purposes.

In the remainder of his paper, Reynolds reported new data on friction for water flowing in two drawn lead pipes. He avoided the development problem by carefully tapping his pipes for local pressure measurements well downstream. The entrance flow was deliberately made noisy, because his objective in this part of his study was to establish conditions for which all disturbances would decay and laminar pipe flow could be described as unconditionally stable. FIGURE 2.25 reproduces Reynolds' results, as displayed in his diagram 2. The abscissa $i = (dp/dx)/\rho g$ is the quantity tabulated by Reynolds and is inadvertently dimensionless. If the local static pressure p is measured by observing the height h reached by the working liquid in a manometer tube connected to a hole in the pipe wall, then $p = \rho gh$ and $dp/dx = \rho g dh/dx = \rho gi$. The quantity i is commonly called the hydraulic grade, hydraulic slope, or hydraulic gradient by civil engineers.

In presenting his data, Reynolds twice displayed a generic formula relating pressure drop to flow rate. This formula is essentially the form $Re^2 C_f = g(Re)$ already mentioned. However, Reynolds' version of the formula is not strictly dimensionless and as written is valid only for water. Where I have Re , Reynolds has $\nu_0 Re$, and where I have $Re^2 C_f$, Reynolds has $(2\nu_0^2/g)Re^2 C_f$, with ν_0 the kine-

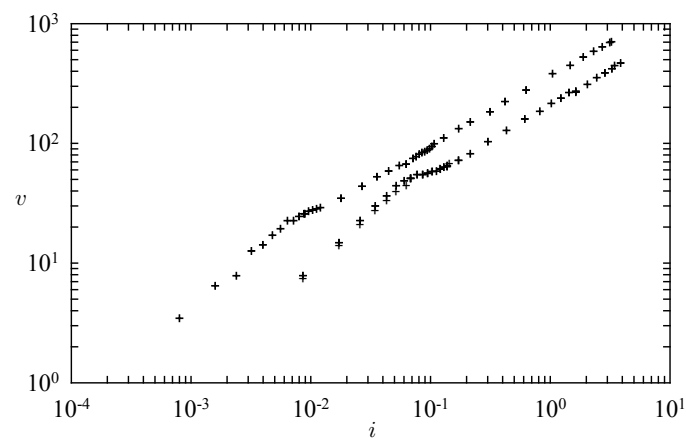


Figure 2.25: Diagram 2 of the paper by REYNOLDS (1883), reproduced with the aid of his tables III--V. The abscissa $i = dh/dx = (dp/dx)/\rho g$ is the dimensionless local pressure gradient. The ordinate v is the mean velocity in cm/sec.

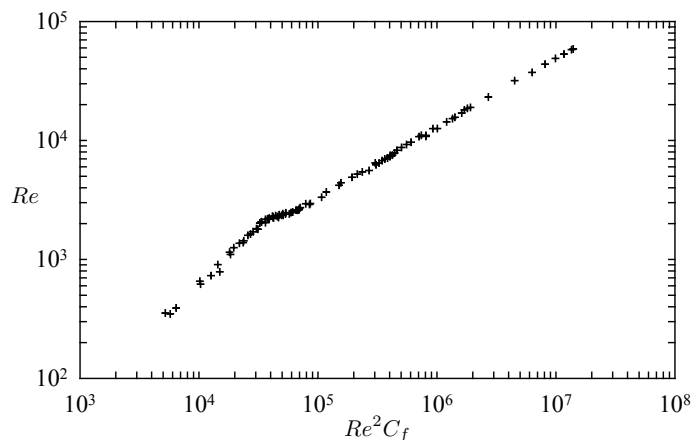


Figure 2.26: The previous FIGURE 2.25 made dimensionless by following Reynolds' instructions. Reynolds described this figure but did not display it.

matic viscosity of water at 0°C and g the acceleration of gravity. Reynolds commented more than once that the dimensional data for his two pipes, as well as data obtained by other investigators, could be superposed by a suitable displacement in logarithmic coordinates, and he gave explicit rules for calculating the necessary displacements. For example, $\log \tilde{u}$ should be replaced by $\log \tilde{u} + \log D - \log \nu + \log \nu_0$. I have applied these rules to the data in FIGURE 2.25, omitting the constant dimensional factors ν_0 and g , to obtain FIGURE 2.26. I consider it truly remarkable that Reynolds did not himself carry out the calculations, and thus did not arrive at FIGURE 2.26, which would have revealed at one stroke the power of dimensional analysis and the importance of what is now called the Reynolds number.

The consequences of this omission were profound. Reynolds' paper had no real impact on his contemporaries. Thirty years passed, and more than fifty papers on turbulent pipe flow, before the last step

was taken independently by BLASIUS (1913) and by STANTON and PANNELL (1914), and the modern point of view was established. These two papers did have an immediate impact, amounting almost to epiphany. In particular, they demonstrated by example that data from different experiments, not only in water but in a variety of fluids, could be made to fall on a single curve.

A common feature of the intervening literature is an awkward struggle to understand the separate effects of pipe diameter and surface roughness in dimensional logarithmic plots like FIGURE 2.25. A list of authors who cited the 1883 paper by Reynolds, without recognizing the real issue, includes **(REMOVE THE DETAILED CITATIONS LATER)** at least

MAIR (1886) PICE **84**, 424 3A
 SMITH (1886) Book 3A
 COUETTE (1890) ACP **21**, 433 3G
 WHETHAM (1890) PT **181**, 559 3A
 WILBERFORCE (1891) Phil Mag **31**, 407 3A
 RUDSKI (1893) PM **35**, 439 3A
 KNIBBS (1897) PRSNSW **31**, 314 3A
 BOVEY and STRICKLAND (1898) TRSC **4**, 45 3A
 COKER and CLEMENT (1903) PTRS **A201**, 45 3A
 SAPH and SCHODER (1903) TASCE **51**, 253 3A
 BARNES and COKER (1905) PRSA **74**, 341 3A
 MORROW (1905) PRSA **76**, 205 3A
 REIGER (1906) AP **19**, 985 3A
 BIEL (1907) Foheft 44 3A
 BRILLOUIN (1907) Visc **1**, 209 3A
 GLASER (1907) AP **22**, 694 3A
 LADENBURG (1907) AP **22**, 287 3A
 FRITZSCHE (1908) VDI Heft 60 3A
 GRINDLEY and GIBSON (1908) PRSA **80**, 114 3A
 HOSKING (1908) RSNSW **42**, 34 3A (Knibbs only)
 RUCKES (1908) AP **25**, 983 3A
 GIBSON (1909) Phil Mag **17**, 389 3A
 NUSSELT (1910) VDI Heft 89 3F

UNWIN (1910) Enc Brit 3
 BOSE and BOSE (1911) PZ **12**, 126 3A
 EKMAN (1911) AMAF **6**, 1 3G
 RONCERAY (1911) Ann CP **22**, 107 3A
 SOENNECKEN (1911) Foheft 108, 109 3F
 CAROTHERS (1912) PRSA **87**, 154 3A
 LECHNER (1913) AP **42**, 614 3A
 GIBSON (1914) PIME **201**, 201 3A
 KOHLRAUSCH (1914) AP **44**, 297 3A
 RAPP (1914) Phys Rev **2**, 363 3A

A similar list can be constructed of authors who wrote about pipe flow in this period 1883–1913 but did not cite the 1883 paper by Reynolds. It is probably not a coincidence that this second list contains almost all of the papers that report measurements with air or some other gas as a working fluid (**check**). Apparently the perception of Reynolds' ideas by his contemporaries, and perhaps by Reynolds himself, notwithstanding the remarks in his sections 36 and 37, was the one already stated; namely, that these ideas apply only for water, and that the combination $\tilde{u}D/\nu$ plays a role only in connection with the onset of transition, and not as a generic dimensionless variable.

Several of these early papers will be mentioned again in SECTION 2.4.3, where the available measurements of friction will be reviewed for the classical case of fully developed turbulent flow in a smooth circular pipe. The Encyclopaedia Britannica article by Unwin, in particular, is a good account of the shapeless empiricism practiced by civil and mechanical engineers of the time. References to other early work can be found in the papers by Biels, Fritzsche, and Blasius, and in surveys by OMBECK (1914), DAVIES and WHITE (1929), DREW, KOO and McADAMS (1932), and KEMLER (1933). (Check GUMBEL 1913, SCHILLER 1925). The paper by NUSSELT (1910) approaches, but does not quite achieve, dimensional completion.

Karman. The paper by BOSE and BOSE (1911; for complete data, see BOSE and RAVERT 1909) deserves particular attention for another reason. These authors determined the time T required for

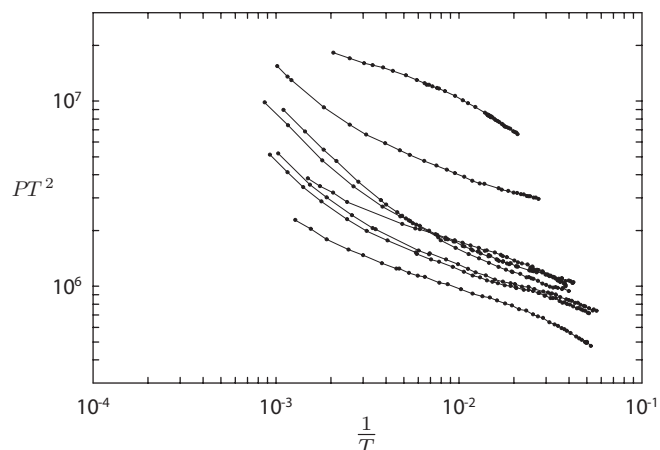


Figure 2.27: The raw capillary data of BOSE and BOSE (1911) in dimensional form. The ordinate (proportional to C_f) is the product of the pressure difference P in gm/cm^2 and the square of the flow time T in seconds for a fixed volume V of liquid. The abscissa (proportional to Re) is the reciprocal of the flow time. From top left, the liquids are mercury, bromoform, ethanol, water, chloroform, benzene, toluene, and acetone.

a specified volume $V = 8.81 \text{ cm}^3$ of various liquids to flow through a capillary viscometer, together with the associated pressure difference P . The length L and the diameter D of the capillary are not mentioned. The dimensional raw data are shown in FIGURE 2.27. The solid circles refer to water, the seven other curves, from lowest to highest at the left side of the figure, refer respectively to acetone, toluene, benzene, chloroform, ethanol, bromoform, and mercury. Data for ethyl acetate have been omitted. The formal objective of the work was not to determine the viscosity, but to determine the exponent in the relation for P as a function of $1/T$ at velocities above Reynolds' upper critical value (**check**). It might seem under

the given conditions that there is no presentation that will collapse the Buse data to a single curve. However, KARMAN, while still at Göttingen, pointed out such a presentation (1911). His original short paper lacks figures and is otherwise opaque, and apparently attracted no attention. The matter is more clearly presented in a passage in his tutorial volume *Aerodynamics* (1954), where both the problem and its solution are illustrated by figures.

Recall the friction coefficient C_f and Reynolds number Re defined by equations (2.20) and (2.19) respectively. Three auxiliary equations, (2.15) for \tilde{u} , (2.11) for τ_w , and the definition of the flow rate Q ,

$$Q = \frac{V}{T} , \quad (2.89)$$

are needed. From these, it is easy to verify the identities (define \hat{C}_f)

$$\frac{\rho V^{2/3}}{\mu T} = \frac{\pi}{4} \left(\frac{D}{V^{1/3}} \right) Re \quad (2.90)$$

and

$$\frac{gPT^2}{\rho V^{2/3}} = \frac{32}{\pi^2} \left(\frac{LV^{4/3}}{D^5} \right) \hat{C}_f , \quad (2.91)$$

together with their product

$$\frac{gPT}{\mu} = \frac{8}{\pi} \left(\frac{LV}{D^4} \right) \hat{C}_f Re . \quad (2.92)$$

In each of these equations, the quantities on the left are known experimentally. The dimensionless combinations in parentheses on the right are not known, but are not needed to make Karman's point. Note that the last equation makes the product PT constant for ideal laminar flow, as stated by Poiseuille in the first of his laws.

Karman worked out the variables on the left in these dimensionless relationships by an argument based on proportional scaling of various terms in the momentum equation. A length scale was needed for this argument. There are three obvious candidates, L , D , and $V^{1/3}$, all of which are constant for the whole course of the experiments. Karman used $V^{1/3}$, since this is the only length that

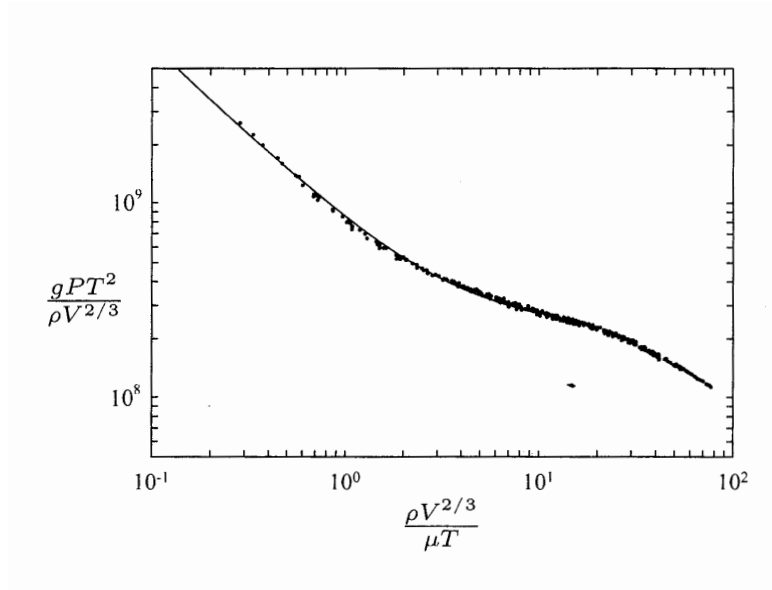


Figure 2.28: The data of the previous FIGURE 2.27 after reduction to dimensionless form following KARMAN (1911). Handbook values have been used for density and viscosity. The capillary tube was apparently quite short, with L/D perhaps about 60, and the data are therefore usable only for relative viscometry.

is specified numerically. He showed that the data for different fluids then defined a single curve, as displayed in FIGURE 2.28. Such a display is not quite viscometry, because it cannot be reduced to standard dimensionless variables C_f and Re as long as L and D are unknown. However, if μ is known for any one liquid, such as water, the tabulated data can be used to infer μ for each of the other liquids.

This contribution by Karman required little in the way of equations or models except for overall mass and momentum balance. It does not involve empirical constants and makes no distinction between laminar and turbulent flow. It is therefore an impressive early illustration of the power and beauty of the dimensional art. Moreover, later developments in modeling applied to capillary-tube vis-

cometry allow some further deductions from the Bose data. The curve in FIGURE 2.28 resembles some of the curves for short tubes obtained by MICKELSON (1964) and shown earlier in FIGURE 2.7. In FIGURE 2.28, the putative laminar region at the left, say for $0.3 < \rho V^{2/3}/\mu T < 3$, can be fitted to equation (2.57), rewritten as

$$\widehat{C}_f = \frac{16}{Re} + \frac{D}{L} \frac{m}{2} . \quad (2.93)$$

Substitution for Re and \widehat{C}_f from equations (2.90) and (2.91) leads to

$$\frac{gPT^2}{\rho V^{2/3}} = A \frac{\mu T}{\rho V^{2/3}} + B \quad (2.94)$$

where

$$A = \frac{128}{\pi} \frac{LV}{D^4} \quad (2.95)$$

$$B = \frac{16}{\pi^2} m \frac{V^{4/3}}{D^4} . \quad (2.96)$$

With $V = 8.81 \text{ cm}^3$ and $m = 1.20$, a least-squares fit yields the curve shown in the figure⁷, with

$$A = \quad , \quad B = \quad (2.97)$$

and therefore

$$L = \quad \text{cm} , \quad D = \quad \text{cm} . \quad (2.98)$$

The Reynolds-number range for the fitted region, according to equation (2.90), is $\quad < Re < \quad$, and is entirely plausible. These estimates are otherwise rough, because the value $m = 1.20$ refers to a square-cut entry and exit, whereas the glass tube used by Bose was fully faired at both ends. At any rate, the small value inferred for L/D means that the objective of finding the desired exponent for turbulent flow was not realistic.

I have not found any indication that Reynolds ever thought that his paper of 1883 needed clarification. In another important

⁷The values missing in these equations have not been found in any copy of the manuscript.

paper on turbulent flow (REYNOLDS 1895), he did no more than remove the dimensional factor ν_0 in Re and propose a value of 1900–2000 as an upper limit for unconditional stability of laminar pipe flow. Reynolds also let pass opportunities to influence the presentation of data in the papers by Coker and Clements and by Barnes and Coker, both of which deal only with dimensional data, and both of which bear a note “communicated by O. Reynolds.” I am told by Philip Saffman that communication of a paper to a journal of the Royal Society through a fellow (a requirement now abolished) meant only that the paper was believed by the fellow to be written in English, and did not imply any judgment about the scientific merit of the work.

This evidence presented so far does not mean that the engineering community in 1883, and for three decades thereafter, was unready for the concept of dimension. The published record on the reception of Reynolds’ ideas has been explored by ROUSE and INCE (1934) and by ROTT (1990, 1992). These authors point out that RAYLEIGH, in several short publications between 1892 and 1915, showed with professional facility that dimensional analysis, which he called dynamical similarity, could be applied to a great variety of physical problems. The first of these papers dealt specifically with Reynolds’ formula for pipe flow. Reynolds himself made skillful use of modeling laws in his paper of 18xx on lifeboats, where he cited Froude as a pioneer, and in his paper of 18xx on flow in estuaries. He may not have thought of models in connection with pipe flow, although one such flow can certainly be taken as a model for another. The contribution by Karman has already been described at length. PRANDTL (1905) used dimensional reasoning as a tool in his boundary-layer theory, and a later paper by PRANDTL (1910) certainly influenced the work of Blasius, just as the papers by Rayleigh certainly influenced the work of Stanton. **(Mention Froude?)** It was SOMMERFELD (1908) who proposed using the term Reynolds number (Reynolds’sche Zahl) for the quantity $\tilde{u}D/\nu$, thus establishing a practice of naming dimensionless numbers that has since evolved in unpredictable directions. The method of dimensions was eventually provided with an axiomatic foundation, in Rott’s phrase,

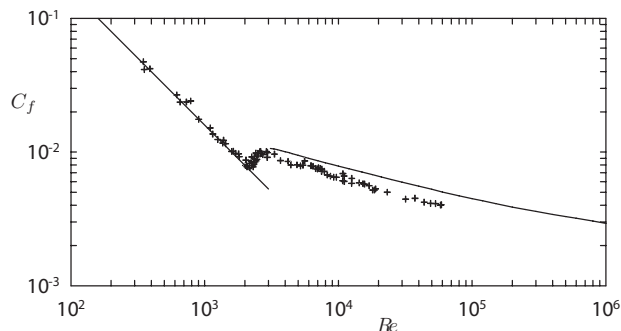


Figure 2.29: Reynolds' pipe data in standard dimensionless variables. The curve at the right is faired through Nikuradse's data. The low values of C_f for turbulent flow may be caused by imperfect calibration of the flowmeter.

in the definitive paper by BUCKINGHAM (1914). I think that these matters are important enough to deserve the attention of analytical historians of science who have the resources to reach the unpublished record. The evolution of the Reynolds number is also worth study as part of a larger development of the time, which was the slow and difficult emergence of applied mathematics from pure mathematics as a separate and eventually homologous discipline.

Finally, to close this discussion, the friction measurements by Reynolds are plotted in standard form as $C_f(Re)$ in FIGURE 2.29. The scatter is probably caused mainly by difficulties in manual regulation of supply pressure in a flow system connected directly to the building water supply some of the values of C_f for turbulent flow are low by 15 to 25 percent, perhaps because of imperfect calibration of

the flowmeter.

By contrast with the case of the Reynolds number, dimensionless combinations equivalent to the definition (2.87) for the friction coefficient in pipe flow were introduced very early (*look up Chezy*). The rationale was and is mainly philosophical. Experience shows that the pressure drop for turbulent flow in large pipes is roughly proportional to the square of the velocity, so that the ratio $(dp/dx)/\rho\tilde{u}^2$ is nearly a constant. The reduction of empirical knowledge to a constant is of itself valuable evidence of order. However, notation has varied widely, and still does. Several authors have used $-Ddp/dx$ or $-Rdp/dx$ as numerator in equation (2.87) rather than $-(D/4)dp/dx = \tau_w$, denoting the resulting dimensionless combination by λ or ψ . The factor $1/2$ in the denominator was also sometimes omitted. In defining the Reynolds number, some authors used R rather than D , and at least one author substituted u_c for \tilde{u} . UNWIN (1910), in his Encyclopaedia Britannica article, used the definition (2.87) but the symbol ζ . It is common to see in the literature of mechanical and civil engineering the symbol f , known as the Fanning friction factor, for what is here called C_f (Fanning himself used the symbol m). It is worth noting that the quantity $D/4$ in equation (2.11) coincides, by accident or otherwise, with the hydraulic radius, if this is defined as the ratio of wetted cross-sectional area to wetted circumference for non-circular channels, closed or open. I have not been able to discover why this definition was originally formulated so that the hydraulic radius for a circular pipe is not the same as the geometric radius. **(See Prandtl and Tietjens.)**

Turbulent flow in pipes has been studied from two points of view, beginning about 1850. Civil engineers of the time were often concerned with hydraulic aspects of the problem and with design of efficient conduits for water distribution, sewage or storm-water collection, and chemical process engineering? Their field installations tend to be large, with rough surfaces and with numerous joints, bends, elbows, and tees. Such conduits may not always run full. Direct field measurements of friction in such conduits are a better guide to performance than estimates derived by extrapolation from a remote classical base. Technical data of this kind have been col-

lected by (refs.). In general, however, civil engineers tend not to be producers of basic information. One exception was DARCY (1858), who was a half century or more ahead of his time. He made careful measurements of the mean-velocity profile in large conduits having various degrees of roughness and invented the defect law. This law was also proposed independently by (refs.). It was finally established firmly by systematic profile measurements by NIKURADSE (1933) in rough pipes.

2.4.2 The Nikuradse problem

The measurements that for 60 years have been taken to be definitive for turbulent flow in smooth and rough pipes were published in 1932 and 1933 in a remarkable pair of papers by J. Nikuradse. The work was done at Göttingen under the direction of Prandtl, as was an earlier thesis (1926) that is seldom cited. The issue in the thesis was secondary flow in uniform ducts having various cross sections; rectangular, trapezoidal, triangular; circular shaft with keyway. The data consisted mostly of contours of constant axial velocity. Nikuradse apparently also worked on smaller problems, such as laminar flow development in the entrance region of a circular tube (see figure x of PRANDTL and TIETJENS 19xx), but none of this work was published in usable form. **(What about Tollmien-Schlichting instability?)**

The important contribution by Nikuradse in the 1932 paper was a systematic study of the mean-velocity profile in smooth pipes over a large range of Reynolds number. These measurements are a refreshing counter-example to a description of the scientific method sometimes given to beginning students: form a hypothesis; test the hypothesis; accept, revise or reject the hypothesis. Prandtl had no hypothesis; or, if he did, it was overtaken by the events described in SECTION X.⁸ I think that Prandtl simply believed that properly constructed experiments could not fail to lead to new and important conclusions about turbulent flow. This belief was certainly correct, because it led directly to the logarithmic profile. An im-

⁸Unclear reference, possibly to a section not completed.

portant question about the measurements, first raised publicly by MILLER (1949), concerns an unexplained discrepancy between the mean-velocity profiles as plotted in figure 15 of Nikuradse's preliminary paper of 1930 and in figure 24 of his final paper of 1932. The discrepancy is also apparent from an examination of tables 2 and 3 of the latter paper. Miller was concerned with the need to describe the profile accurately in and near the sublayer in studies of heat and mass transfer (see SECTIONS X and Y).⁹

Miller in 1946 unsuccessfully sought an explanation of the discrepancy from Nikuradse, Prandtl, and von Karman. A second effort, which travelled the route Miller-Rouse-Prandtl-Wieghardt-Nikuradse and back, established that Nikuradse had in fact altered his data for the mean velocity profile by adding 7 units to the dimensionless abscissa y^+ . The effect was to portray the viscous sublayer more realistically by ensuring that the measured velocity never fell above the linear line inferred from the wall friction. Prandtl remarked later that the correction was justified, but the failure to describe it was not. Nevertheless, Miller maintained in his 1949 paper that there was in fact no evidence for the existence of a sublayer, although ample evidence was provided a little later by several other sources.

The discrepancy is sometimes described as a crude correction for probe-wall interference. It amounted to deletion of the two points nearest the wall in each profile, which scatter badly, and an increase of seven units in the coordinate yu_τ/ν for the remaining data. This shift is in fact obvious from a comparison of the tabulated dimensional and dimensionless data, as is a dislocation in the first three entries for φ in Nikuradse's table 3 for the case $Re = 1.11 \times 10^6$. The profiles were measured in a plane 0.01 to 0.02 cm downstream from the square-cut pipe exit, where a cylindrical water jet emerged into a confined water-filled chamber. This technique may be a relict of the thesis research. Nikuradse's 1932 paper describes some data obtained near the pipe wall with probes of different diameters, but does not justify or apply the implied correction, and I have not been able to make any sense of his description.

⁹Sections evidently not completed.

The reason for Miller's initial difficulty was that Prandtl in 1946 no longer recognized Nikuradse, for a reason not related to the pipe measurements. In 1934, Nikuradse, perhaps driven to an uncommon level of hubris by compliments about his research on pipe flow, and inspired by Hitler's assumption of power in Germany, attempted through a *putsch* to replace Prandtl as director of the Kaiser-Wilhelm-Institute at Göttingen. There was a brief confrontation, which rapidly became a test of strength between other parties in the German political structure. At the end of a "mad and dangerous brawl," as Wieghardt puts it, Prandtl was confirmed in his position and Nikuradse was exiled to a post as dozent at the Technische Hochschule at Breslau. These events are described very briefly in the historical article by OSWATITSCH and WIEGHARDT (1988). This history is not complete, and further information is obtained only with great difficulty. Witnesses are few and becoming fewer, and the career of Nikuradse at the Kaiser-Wilhelm Institute is still a source of embarrassment there.

In 1942, Nikuradse published two monographs for the German air force, neither of which can be taken at face value. The first, on laminar boundary layers, claims to be a publication of data obtained by Nikuradse at Prandtl's institute at Göttingen in 1933. Five velocity profiles are tabulated in his table 6 and plotted in my FIGURE X.¹⁰ This figure has appeared without comment in all seven editions of the text *Boundary Layer Theory* by Schlichting. I am supported in my skepticism by H.W. Liepmann, whose first assignment at GALCIT by Karman was to measure once more the Blasius profile. The paper by Nikuradse gives no information about the tunnel, the instrumentation, or other experimental circumstances that led to the remarkably low scatter. In particular, there was apparently no need to shift the data to a displaced origin in x . If the measurements were actually made (and they left no trace at Göttingen) they were made by a believer in Miller's inference from his study of the smooth-pipe data, which I paraphrase slightly; "Having more faith in the theory than in his experimental results, Nikuradse adjusted

¹⁰This and later references to Figure X in this section are to a figure that has not been found.

the results to make them seem to be in accord with the theory.” I would undertake to produce such a figure by measurement of many data points, most of which I would discard on the ground that they did not agree with the theory and were therefore in error. (**Millikan oil-drop?**) There still remains at Göttingen a sour joke based on a phrase attributed to Nikuradse, “das passt sich nicht,” which becomes roughly in English “that does not conform.” The meaning is different from “das passt nicht,” meaning “that does not pass.”

The second 1942 paper dealt with the turbulent boundary layer at constant pressure. The experiments were carried out in two wind tunnels on two flat plates. The work in a small KWI tunnel at Göttingen is dated 1932–1933, and the work in a small DVL tunnel at Berlin-Adlershof is dated 1939. There is no useful description of the experimental facilities, models, or instrumentation in either case. Altogether, 50 mean-velocity profiles were measured. Eight of these, four from each tunnel, are plotted in Nikuradse’s figures 22 and 39 and in my FIGURE X. The text claims that the profiles are accurately described by the formula

$$\frac{u}{u_\infty} = f\left(\frac{y}{\delta^*}\right), \quad (2.99)$$

and the plots confirm this statement precisely. Moreover, the profile formula is eventually restated as a power law,

$$\frac{u}{u_\infty} = 0.723\left(\frac{y}{\delta^*}\right)^{0.130}. \quad (2.100)$$

This formula is also shown in FIGURE X, but is never reconciled with the data or with any competent analysis. The Reynolds numbers based on x have a range of about one decade. I have included in the figure the two profiles calculated from the model in SECTION X for the highest and lowest Reynolds numbers. The differences are too large to ignore. I do not know how I would ever obtain such profiles.

The formula (2.100) implies

$$1 = \int_0^\infty (1 - f) d\eta \quad (2.101)$$

and

$$\frac{\theta}{\delta^*} = \int_0^{\infty} f(1-f) d\eta \quad (2.102)$$

where $\eta = y/\delta^*$. It follows that the shape factor δ^*/θ is a number, which Nikuradse evaluates for the experimental profile f ;

$$\frac{\delta^*}{\theta} = 1.304 . \quad (2.103)$$

The values of δ^*/θ implied by Nikuradse's table 2 are plotted in FIGURE X, along with some data obtained by the rest of the world. I cannot imagine how I would obtain such data, and therefore I do not accept these measurements.

Finally, there is the episode of the slippery paint, which occurred about 1956 (SKFK was a student). I am indebted to F. Clauser and S.K.F. Karlsson for the information that follows. About 1956, Johann Nikuradse and his younger brother Alexander attempted to interest various naval and industrial representatives in a coating that was claimed to produce substantial decreases in skin friction in both air and water. The chemistry of the coating was a secret. An executive of a major American chemical company spent a large amount of money in attempting to confirm the claims of the inventors, without any conclusive result. Finally, recognizing that his company had no expertise in fluid mechanics, particularly in boundary-layer flow, the executive retained Clauser as a consultant.

The proof of drag reduction was based on measurements of momentum thickness near the trailing edge of one or another flat-plate model. Clauser and Karlsson at Johns Hopkins first carried out a series of measurements in air on their own plates, coated by the Nikuradse brothers or uncoated, and found no effect whatever of the coating on drag. The Nikuradses disparaged these results as irrelevant and inapplicable.

Further tests were therefore carried out in a small, primitive closed water channel maintained by the Nikuradse brothers near Munich. Clauser and Karlsson observed these tests, which duplicated earlier favorable results in the same channel. The antic aspects of

these events are illustrated by the fact that Clauser, knowing something of J. Nikuradse's reputation at Göttingen, took his own pitot-static tube along on his trip to Germany. Clauser was allowed to make his own tests on one plate. The plate was not coated, but the measured drag was lower than the drag of any coated plate. Clauser, however, deliberately installed his plate at a slight angle, so as to place the stagnation line firmly on the working surface and provide a negative pressure gradient. Both conditions are known to delay transition. J. Nikuradse was incensed by Clauser's result, which he claimed was impossible. The situation deteriorated to one of senseless confrontation, and this particular contest came rapidly to an inconclusive end. Clauser believes that other agencies, perhaps military, may have pursued the same elusive goal and fared no better.

Clauser came away from this experience with two strong impressions. One was that the Nikuradse brothers believed in the power of their coating. Since Johann knew no chemistry and Alexander knew no fluid mechanics, they may have been misleading each other out of the best intentions. Clauser's second impression was that Johann had no understanding of the effect of pressure gradient and leading-edge shape on transition and boundary-layer development, and did not even grasp the purpose and usefulness of the momentum-integral equation, despite his 10-year tenure at Prandtl's institute. I find this conclusion to be quite consistent with the text of the two 1942 papers.

This part of the history of Göttingen has very little to do with science, but it has a great deal to do with the degree of insight and credibility that should be attributed to Johann Nikuradse. It is part of the reason that I think Nikuradse and his published work should be examined at much higher magnification than are usual for contributions to the subject.

Nikuradse's data for friction coefficient in smooth pipes are included in figure *x* and repeated as reference for the other measurements. In the meantime, I will try in the next sections to establish the main properties of pipe flow without using Nikuradse's data as a standard. More on this subject, including a critique, is in section *x*.

This issue, and rumors of other anomalies in Nikuradse's work, have been part of the unwritten record of the subject for years. I feel that I have to inform myself as far as I can at this remove in time and to record what I have learned about the Nikuradse problem.

There is also a discrepancy for $Re < 10^5$ between the values of u_c/\bar{u} measured as part of the profile study and as measured in more detail in separate tests (*show plot?*). Some of the measurements published in 1930 may have been replaced by new data, since the Reynolds numbers listed in the two figures are different for about half of the data.

The need for these comments arises because Nikuradse's data are widely accepted as definitive. My own opinion, after careful study, is that the measurements of 1926-1932 in smooth and rough pipes can be accepted at face value. I have not found any evidence that Nikuradse possessed the imagination required to manipulate data so expertly that sixty years of close examination have not revealed any serious inconsistencies.

2.4.3 A consensus on friction

Accurate experimental definition of the classical smooth-pipe flow had to wait for the appearance of pipe or tubing of uniform diameter, particularly tubing made of drawn brass, and for appreciation of the need for adequate development length. The classical pipe flow is by assumption unique and reproducible to an accuracy determined primarily by quality of instrumentation. Some early pre-1932 data are collected in FIGURE 2.30. The solid line is faired through the data of Nikuradse without benefit of any formula. Nikuradse's measurements evidently added little to knowledge of surface friction, except for a modest extension of the Reynolds-number range. *Reynolds (1883) was the first (Darcy?) to measure pressure drop between orifices drilled in the pipe rather than between reservoirs. Hagen (18xx) used the latter scheme in some very careful measurements included in FIGURE 2.30. Hagen's pipes had a square-cut entrance, and I have used Mickelson's data to correct for flow development. I am also grateful for a section in Prandtl and Tietjens (19xx) that explains*

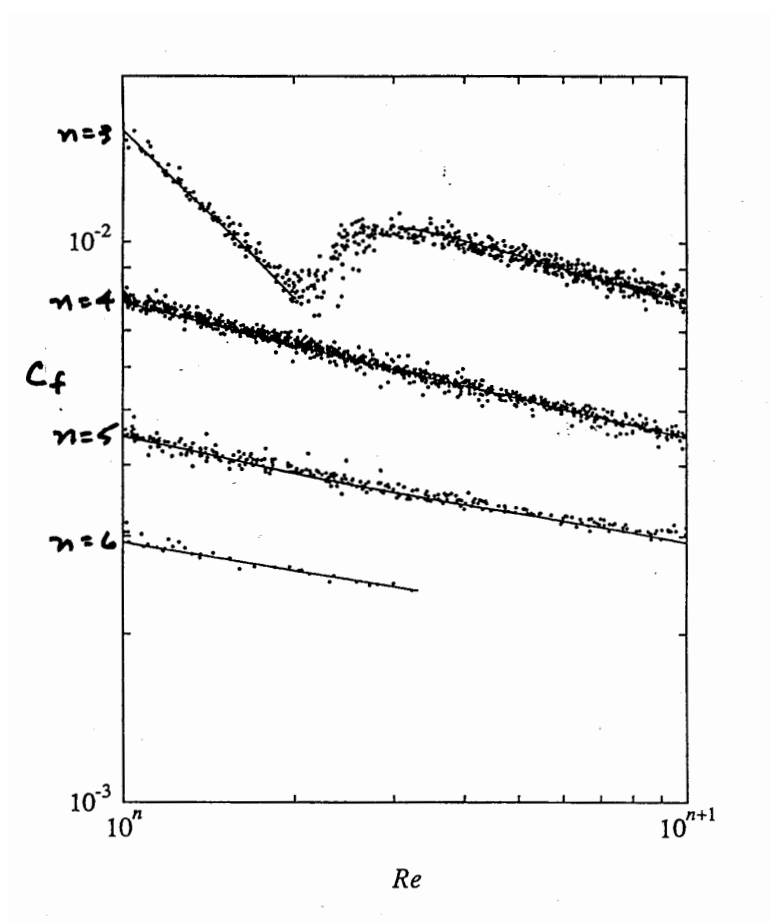


Figure 2.30: Some measurements before 1932 of friction in smooth pipes. The solid line for turbulent flow is faired through the data of NIKURADSE (1932). A few obviously sour points have been discarded.

the system of units used by Hagen. Some valuable measurements by Freeman (1892) were published only after a lapse of fifty years and even now are not well known. This neglected monograph also contains useful data on pressure loss due to pipe elbows and area discontinuities. Most of the investigators represented in figure x were not aware of the bulk of previous work, and the same can be said of many investigators today. Need a figure for post-1932 data.

Some more recent friction results for turbulent pipe flow are collected in FIGURE X.¹¹ (Why are Ombeck's data skewed; air versus water.) Post-Nikuradse data for C_f are often concerned mainly with polymers, roughness, and non-steadiness. Discussion should include question of fully developed flow and try to account for any remaining discrepancies.

Pre-Nikuradse friction data

FREEMAN (1892) 3A
 COKER and CLEMENT (1903) 3A
 SAPH and SCHODER (1903) 3A
 BLASIUS (1913) 3A
 KOHLRAUSCH (1914) 3A
 OMBECK (1914) 3A
 STANTON and PANNELL (1914) 3A
 STANTON et al. (1920) 3A
 HERSCHEL (1921) 3A
 FROMM (1923) 3D
 JAKOB and ERK (1924) 3A
 RICHTER (1932) 3A
 NIKURADSE (1932) 3A

Post-Nikuradse friction data

NIKURADSE (1932) 3A
 FAGE (1936) 3A
 LING (1937) 3A
 ROHONCZI (1939) 3F

¹¹This figure appears never to have been created.

HUMBLE et al. (1951) 3F
SAMS (1952) 3D
SENECAL and ROTHFUS (1953) 3G
BROCKMAN (1956) 3A
NUNNER (1956) 3D
SLATER et al. (1957) 3A
SACKS (1958) 3D
BOGUE (1963) 3E
HUANG and LAURSEN (1963) 3D
SAVINS (1964) 3E
ELATA and TIROSH (1965) 3E
WELLS (1965) 3E
GOREN and NORBURY (1967) 3E
GUPTA et al. (1967) 3E
HERSHEY and ZAKIN (1967) 3E
MIH and PARKER (1967) 3E
SEYER and METZNER (1967) 3E
VIRK et al. (1967) 3E
HAHNEMANN (1968) 3E
OHARA (1968) 3G
WELLS et al. (1968) 3E
FORESTER et al. (1969) 3E
PATEL and HEAD (1969) 3G
SIRKAR (1969) 3A
SPANGLER (1969) 3E
WHITE (1969) 3E
PATERSON and ABERNATHY (1970) 3E
TOMITA (1970) 3E
VAN DRIEST (1970) 3E
VIRK and BAHER (1970) 3E
WHITE and McELIGOT (1970) 3E
LAWN (1971) 3A
VIRK (1971) 3E
CHUNG and GRAEBEL (1972) 3E
ROLLIN and SEYER (1972) 3E
WANG (1972) 3E
SYLVESTER and KUMOR (1973) 3E

THOMAS and GREENE (1973) 3E
 MIZUSHINA et al. (1974) 3E
 GUSTAVSSON (1977) 3E
 DE LOOF et al. (1977) 3E
 MIZUSHINA and USUI (1977) 3E
 PERRY and ABELL (1977) 3D
 VIRK and SURAIYA (1977) 3E
 KUBO (1979) 3E
 SEDOV et al. (1979) 3E
 GEE and WEBB (1980) 3D
 WALSTROM et al. (1988) 3A

Some contributions to the technical literature have missed the mark for reasons worth recording. A brave effort was made by Burke (19xx) to extend the range of Reynolds number by an order of magnitude by profile measurements in a penstock pipe of 160-cm diameter. The pipe was tar-coated and was arguably smooth, although the difficulty of obtaining a smooth surface increases with the Reynolds number (see SECTION X). In Burke's experiments, the dynamic loads were large and were carried by a substantial cruciform probe-support structure, which probably subjected the local flow to the displacement called drift by Lighthill (ref.). (Continue.)

2.5 Similarity Laws

2.5.1 The mixing length and the law of the wall

The mixing-length model was developed in the years from 1925 to 1932 by Prandtl and Karman, who were assisted by some seminal profile measurements in smooth pipes by Nikuradse. (**Look up Taylor 1915.**) PRANDTL (1925, 1926) began an exchange by invoking an analogy with the kinetic theory of gases (**explain**) and by supposing that the shearing stress and the mean-velocity field for a general turbulent flow are related by

$$\tau = \rho \ell^2 \frac{\partial u}{\partial y} \left| \frac{\partial u}{\partial y} \right|. \quad (2.104)$$

In effect, ignorance about the mechanisms of turbulent flow was shifted from the shearing stress τ to the mixing length ℓ , with the hope that ℓ might have a more regular and perhaps a more universal behavior. Numerous rationalizations of equation (2.104) have been published; the most detailed one by Prandtl is in (ref **Durand, Betz**). For free shear flows like the jet or wake, Prandtl proposed to take ℓ as constant in the direction normal to the plane of the flow, and proportional to the layer thickness; thus $\ell \sim \delta$. Calculations for several such flows were made according to this model by TOLLMIEN (1926). PRANDTL (1926) also noted in passing that the linear stress profile (2.12) for pipe flow, with the assumption $\ell = \text{constant}$, leads from equation (2.104) to a formula for mean velocity away from the pipe wall that can be written

$$\frac{u_c - u}{(\tau_w/\rho)^{1/2}} = \frac{2}{3} \frac{R}{\ell} \left(\frac{r}{R} \right)^{3/2} . \quad (2.105)$$

Apparently Prandtl was not aware that this same velocity-defect formula, with an empirical constant of proportionality on the right-hand side, had been proposed more than 60 years earlier by DARCY (1858). (**Who else in the meantime?**) Darcy's experiments, later memorialized by BAZIN (1902), were carried out with sound methods in pipes that had various degrees of commercial roughness, but were probably in no case smooth. His prescient use of a defect law anticipated today's practice (see SECTION 2.6.1), which explicitly assumes that the velocity profile in defect form is independent of Reynolds number and roughness. (**Stanton?**)

After a pause of a few years to await more rigorous measurements, events moved rapidly. Karman in early 1930 had the advantage of access to Nikuradse's then unpublished smooth-pipe data, which were innocently supplied to him by Prandtl. (**How about 1926 data?**) The account in KARMAN's biography (1967, pp. 134–140) about the course of subsequent events is illuminating, although the description of the streetcar episode should perhaps be taken with a little salt. In any case, Karman discovered, by one means or another, that the data showed u behaving like $\log y$. The issue then became the development of a hypothesis for ℓ that would be consistent with this behavior.

KARMAN (1930) proposed a local similarity argument, in effect taking ℓ to be defined by the first terms of a local Taylor-series expansion about an arbitrary value y_a of y (a for arbitrary), where y is the distance from some suitable reference surface;

$$u = u_a + \left(\frac{\partial u}{\partial y}\right)_a (y - y_a) + \left(\frac{\partial^2 u}{\partial y^2}\right)_a \frac{(y - y_a)^2}{2!} + \left(\frac{\partial^3 u}{\partial y^3}\right)_a \frac{(y - y_a)^3}{3!} + \dots \quad (2.106)$$

The term in u_a should not play a role, because the length being sought, like the mixing mechanism, should be Galilean invariant. The coefficients of the next two terms (or of any two adjacent terms) define a length, which Karman took to be

$$\ell = -\kappa \frac{\partial u / \partial y}{\partial^2 u / \partial y^2} \quad , \quad (2.107)$$

with the comment that the dimensionless constant κ should be universal; i.e., it should depend only on the fact of turbulence, but not on its form. The definition (2.107) includes a minus sign because $\partial u / \partial y$ and $\partial^2 u / \partial y^2$ have opposite signs for a logarithmic profile. Karman applied his similarity hypothesis for ℓ to channel flow, for which the shearing-stress profile is also linear (see SECTION X), but the argument serves without modification for pipe flow. Given the accurate stress profile

$$\tau = \tau_w \frac{r}{R} \quad , \quad (2.108)$$

equations (2.104) and (2.107) lead to the defect form

$$\frac{u_c - u}{(\tau_w / \rho)^{1/2}} = -\frac{1}{\kappa} \left\{ \left(\frac{r}{R}\right)^{1/2} + \ln \left[1 - \left(\frac{r}{R}\right)^{1/2} \right] \right\} \quad . \quad (2.109)$$

Of the two constants of integration, one is eliminated by requiring $\partial u / \partial y$ to be unbounded at $y = 0$ or $r = R$, and the other is suppressed by writing the profile in defect form. The fact that u_c rather than \tilde{u} appears in equation (2.109) prevents any direct application to the majority of pipe data, for which \tilde{u} was measured but u_c was not. (?) **(Can calculate?)**

Defect laws were well established in the literature, and Karman noted the immediate extension to the case of a rough wall. He also

noted (**where?**) that in the limit $y/R \rightarrow 0$, with $\tau = \tau_w$ and $y = R - r$, his profile formula is reduced to

$$\frac{u}{u_\tau} = \frac{1}{\kappa} \ln \frac{y}{y_0} , \quad (2.110)$$

where y_0 is a constant of integration. The definition for ℓ is reduced to (**who?**)

$$\ell = \kappa y , \quad (2.111)$$

although $\ell = \kappa y$ cannot then be distinguished from $\ell = -\kappa(\partial u/\partial y) / (\partial^2 u/\partial y^2)$. The notion that ℓ is proportional to y allows an attractive interpretation of ℓ as the range of a moving fluid element, a range limited in one direction by the presence of a wall, and thus varying in a sensible way with the position or perhaps the size of the turbulent eddies.

If in Prandtl's formula (2.104) the shearing stress is taken as constant,

$$\tau = \tau_w , \quad (2.112)$$

then equation (2.110) becomes an exact integral of equation (2.104), with either form for ℓ , when $\partial u/\partial y$ is taken to be unbounded for $y \rightarrow 0$. (Need sublayer.) The defect form is

$$\frac{u_c - u}{(\tau_w/\rho)^{1/2}} = \frac{1}{\kappa} \ln \left(1 - \frac{r}{R} \right) . \quad (2.113)$$

It remains to consider the combination of equation (2.111) for ℓ with equation (2.108) for τ . The corresponding defect form is

$$\frac{u_c - u}{(\tau_w/\rho)^{1/2}} = -\frac{1}{\kappa} \left\{ 2 \left(\frac{r}{R} \right)^{1/2} + \ln \left[\frac{1 - (r/R)^{1/2}}{1 + (r/R)^{1/2}} \right] \right\} . \quad (2.114)$$

To recapitulate, two hypotheses (2.107) and (2.111) were proposed for $\ell(u, y)$ and two relationships (2.108) and (2.112) for $\tau(r)$. The four combinations are listed in the adjacent TABLE 2.1, together with the associated profile formulas. (**Mention values for κ .**) The formula proposed by Darcy is included mainly for completeness. The first profile equation was displayed by KARMAN (1930); the third

TABLE 2.1

Mixing-length profiles

mixing length	shearing stress	equation	defect profile
ℓ	τ		$\frac{u_c - u}{u_\tau}$
constant	$\tau_w \frac{r}{R}$	(2.105)	$\frac{2}{3} \frac{R}{\ell} \left(\frac{r}{R}\right)^{3/2}$
$-\kappa \frac{du/dy}{d^2u/dy^2}$	$\tau_w \frac{r}{R}$	(2.109)	$-\frac{1}{\kappa} \left\{ \left(\frac{r}{R}\right)^{1/2} + \ln \left[1 - \left(\frac{r}{R}\right)^{1/2} \right] \right\}$
$-\kappa \frac{du/dy}{d^2u/dy^2}$	τ_w	(2.113)	$-\frac{1}{\kappa} \ln \left(1 - \frac{r}{R} \right)$
κy	$\tau_w \frac{r}{R}$	(2.114)	$-\frac{1}{\kappa} \left\{ 2 \left(\frac{r}{R}\right)^{1/2} + \ln \left[\frac{1 - (r/R)^{1/2}}{1 + (r/R)^{1/2}} \right] \right\}$
κy	τ_w	(2.113)	$-\frac{1}{\kappa} \ln \left(1 - \frac{r}{R} \right)$

by NIKURADSE (1930); and the second and fourth by KARMAN (1930, 1932), NIKURADSE (1932), and PRANDTL (1932). Apparently by 1932 all parties to these developments had accepted the formulas (2.110) and (2.113), together with their primitive antecedents, (2.111) and (2.112), as fundamental.

The important parameter $(\tau_w/\rho)^{1/2}$ was eventually given the name friction velocity (Reibungsgeschwindigkeit) by KARMAN (1932) and denoted by u_τ ;

$$u_\tau^2 = \frac{\tau_w}{\rho} . \quad (2.115)$$

PRANDTL (1927) originally included a factor 1/2 on the left in the definition (2.115), in parallel with the definition of dynamic pressure, but later (1932) endorsed the form (2.115) as it stands. One consequence is that a factor of 2 survives in the formula $C_f = 2\tau_w/\rho\tilde{u}^2 = 2(u_\tau/\tilde{u})^2$, but a factor of 2 is avoided in several other places, particularly in the definition of Newtonian friction at a smooth wall, which in the limit requires $\partial u/\partial y = \tau_w/\mu = u_\tau^2/\nu \approx u/y$, and therefore

$$\frac{u}{u_\tau} = \frac{yu_\tau}{\nu} . \quad (2.116)$$

The dimensionless variables u/u_τ and especially yu_τ/ν both take on values much larger than unity in the turbulent part of the flow. However, the reference velocity u_τ serves another purpose as the proper quantity for making the Reynolds stresses dimensionless, at least near a wall. Given that these stresses are of comparable magnitude and that $-\overline{\rho u'v'} \approx \tau \approx \tau_w = \rho u_\tau^2$, the dimensionless Reynolds stresses near a wall are necessarily of order unity. Boundary-layer flows that are jet-like or wake-like require different treatment (see SECTION Y).

At least two serious flaws are contained in equation (2.110). The first is that the formula is a fragment. Within the mixing-length model, there is no communication with the wall, and no boundary condition to define the constant y_0 . (*This property is, however, useful in dealing with roughness, although a dimensional argument is better. Log law implies $y_0 = 0.49\nu/u_\tau$ in (2.110)?*) For a smooth wall, there is the independent linear limit (2.116). If the complete

profile equation is to apply everywhere from the wall to the vicinity of the pipe axis, the independent variable must be yu_τ/ν , and equation (2.110) should be written

$$\frac{u}{u_\tau} = \frac{1}{\kappa} \ln \frac{yu_\tau}{\nu} + c \quad (2.117)$$

outside a transition region first miscalled the laminar sublayer and now commonly called the viscous sublayer. It is then necessary to explain why the viscosity is needed to describe the flow in a region where essentially all of the transport is by a turbulent mechanism. In a dimensional argument first used by KARMAN (1921) in connection with the power-law profile (2.131) (see SECTION 2.5.3), the mean velocity profile is assumed not to depend explicitly on R . It follows that

$$\frac{u}{u_\tau} = f\left(\frac{yu_\tau}{\nu}\right) . \quad (2.118)$$

This dimensional argument was repeated in this new context by NIKURADSE (1930) in what must have been a hastily prepared paper on his experiments, and can probably be attributed to Prandtl. The relationship (2.118), with its linear and logarithmic limits, is now viewed as fundamental and is commonly referred to as Prandtl's law of the wall. The constant κ is known as Karman's constant. I consider these assignments to be fair. Perhaps the best evidence for equation (2.117), if not equation (2.118), is that it fits the experimental data. How well it fits, and the best values for the constants κ and c , will be taken up in SECTION 2.5.7. **(How did \tilde{u} make its way into Nikuradse's friction law?)**

The second and more serious flaw in equation (2.110) is that it honors the momentum equation in the breach. The shearing stress τ in a pipe is assumed to be constant in a region where it is known to vary substantially. Nevertheless, the logarithmic formula is found to fit the data. More extreme cases having the same property, particularly the sink-flow boundary layer and the wall jet, are cited in SECTIONS X and Y below. In any case, the logarithmic profile has no certain connection with the laws of mechanics as these laws are presently understood for turbulent flow.

To make this same point in another way for the case of pipe flow, the three distinct formulas in the table are plotted in defect form in FIGURE X,¹² together with an experimental profile from the work of LAUFER (1953) that uses an approximate value $Ru_\tau/\nu = xxx$. The best agreement is seen for the logarithmic profile based on the condition $\tau = \tau_w$. This fact may or may not justify the concept of a constant-stress layer (**amplify**). The discrepancy between formula and data is larger when the momentum equation and the exact formula $\tau = \tau_w r/R$ are used, rather than the approximation $\tau = \tau_w$. The discrepancy near the center of the pipe is real (see SECTION X), so that this observation may not be central. However, it illustrates a problem common to many mixing-length methods for modeling turbulent flow, in that attempts to increase the level of rigor or the range of application often lead to a worse result.

Thus the provenance of the logarithmic law of the wall. The mixing length is an exasperating concept. It survives because it points easily to a logarithmic dependence of the mean velocity on the distance from a wall. There is no doubt that this observation was a huge step forward at the time. A cynic might say that it rescued engineers from the tyranny of log-log paper and delivered them to the greater tyranny of semi-log paper. A romantic would say that it led to important real advances, because the whole episode of the mixing-length analogy raised the consciousness of engineers and scientists by revealing an intrinsic order in the subject and by suggesting that there might be other equally simple phenomenological relationships waiting to be discovered. There is still no better formalism for organizing the effects of mass transfer at a wall, of lateral curvature, or of compressibility. Nevertheless, the ideas that could be classified as insight in 1930 must by now be reclassified as peripheral vision, in the terminology of the introduction.

My position is that the mixing-length model does not explain the logarithmic profile. Neither does either of two alternative arguments (section x , Millikan, and section y , singular perturbation), or any other argument known to me. (Work on extremum principle.) For the present, I accept the logarithmic profile as an empirical fact,

¹²This figure appears never to have been created.

and will turn in SECTION 2.5.7 to the practical question of determining values for the constants κ and c in equation (2.117). Some valuable inferences from the law of the wall in the more general form (2.118) will be presented in section x of the chapter on boundary layers.

2.5.2 The Izakson-Millikan argument

An important contribution to the subject was made by IZAKSON (1937) and repeated by MILLIKAN (1938). The logarithmic formula (2.117) was originally proposed to describe nearly the whole flow in a pipe, for which departures from the formula outside the sublayer are experimentally small and were not emphasized at the time. These departures are more conspicuous in a boundary layer, and are discussed at length in SECTION X. For the moment, it is enough to note that equation (2.117) becomes at the center of the pipe

$$\frac{u_c}{u_\tau} = \frac{1}{\kappa} \ln \frac{Ru_\tau}{\nu} + c , \quad (2.119)$$

where u_c is the mean velocity on the axis and R is the pipe radius. The viscosity can be eliminated by subtraction to obtain a formula first proposed by Karman (ref),

$$\frac{u_c - u}{u_\tau} = -\frac{1}{\kappa} \ln \frac{y}{R} . \quad (2.120)$$

This formula is experimentally incomplete, and needs another term, now commonly called the wake component, that also depends only on y/R . Thus, more generally, equation (2.117) can be written, in Millikan's notation,

$$\frac{u}{u_\tau} = \frac{1}{\kappa} \ln \frac{yu_\tau}{\nu} + c + h\left(\frac{y}{R}\right) , \quad (2.121)$$

from which

$$\frac{u_c - u}{u_\tau} = -\frac{1}{\kappa} \ln \frac{y}{R} + h(1) - h\left(\frac{y}{R}\right) = F\left(\frac{y}{R}\right) . \quad (2.122)$$

This expression is usually called Karman's velocity-defect law. It is at least plausible that the mean-velocity defect should depend only on the stress level τ_w and not on μ .

The Izakson-Millikan argument assumes that there is a finite region where both equation (2.118) and equation (2.122) are valid. In this region,

$$\frac{\partial u}{\partial y} = \frac{u_\tau^2}{\nu} f' = -\frac{u_\tau}{R} F' \quad , \quad (2.123)$$

or, in an obvious notation,

$$zf'(z) = -\zeta F'(\zeta) \quad . \quad (2.124)$$

Since the Reynolds number Ru_τ/ν , which is the ratio z/ζ of the two arguments, is arbitrary, the two sides of equation (2.124) must be separately constant. Call this constant $1/\kappa$. Integrate to obtain

$$f(z) = \frac{1}{\kappa} \ln z + \text{constant} \quad , \quad (2.125)$$

or, in physical variables,

$$\frac{u}{u_\tau} = \frac{1}{\kappa} \ln \frac{yu_\tau}{\nu} + c \quad . \quad (2.126)$$

Thus the mean-velocity profile in the common region is logarithmic. The terms of the derivation just given imply that the constant κ is independent of Reynolds number. (**Note fashions, timing, and many examples of papers being ignored.**) This argument was published in 1937-1938, when the major activity in the subject was development of the mixing-length model. It languished for more than 15 years until Hans Liepmann called it to my attention about 1950 when I was searching for an alternative argument for the logarithmic behavior of the profile in terms of similarity laws rather than mixing-length ideas.

2.5.3 The power-law profile

A proper chronology requires a short summary here of the power-law velocity profile, which was first proposed publicly by KARMAN

(1921) in a powerful paper that is notable for other reasons; namely that it contains the boundary-layer approximation as a formal inner limit of the Navier-Stokes equations for small ν , as well as the essence of the singular-perturbation method, including inner and outer expansions, the matching condition, and the composite expansion. It also introduces the momentum-integral equation for the boundary layer, an equation that is exploited for the case of laminar flow in the following paper by POHLHAUSEN (1921). These practical developments finally forced the acceptance of the boundary-layer concept, with all of its associated advances, by the rest of the world fluid-mechanics community. In fact, Karman discussed pipe flow and the power-law profile primarily as a device to model the boundary layer. He derived a formula for flat-plate friction that agreed reasonably well with early towing-tank measurements of total drag. Note that there were, for practical purposes, no profile measurements in boundary layers in 1921, and precious few profile measurements in classical pipe flow (**check work on roughness**).

Part of the reason for this was lack of proper instrumentation as well as the poor quality of existing wind tunnels, as made evident by a paper by Prandtl (1924; check). (Did the British have good tunnels? See Prandtl and Tietjens.) This lack probably inspired work in 1924 by van der Hegge Zijnen under Burgers, taken up in section x. It probably also inspired in part the profile measurements in smooth pipes by Nikuradse (1930, 1932), following Nikuradse's thesis on secondary flow in non-circular pipes.

Karman based the relevant section of his 1921 paper on the observation by BLASIUS (1913) that the friction coefficient for turbulent pipe flow at Reynolds numbers from 5,000 to 100,000 could be well fitted by a power law,

$$C_f = \text{constant } Re^{-1/4} . \quad (2.127)$$

In dimensional form this is

$$\tau_w = \rho u_\tau^2 = \text{constant } \rho \tilde{u}^{7/4} (\nu/D)^{1/4} . \quad (2.128)$$

This relationship emerges from a pursuit of straight lines on log-log paper. Karman noted that the systematic dependence of C_f

on Re implied a systematic variation of the mean-velocity profile. He assumed that the profile in some region, eventually taken to be the whole of a pipe flow except for a thin layer very near the wall, depended on a restricted set of variables,

$$u = u(\rho, \mu, \tau_w, y) \quad (2.129)$$

where the radius R is omitted and $y = R - r$ is measured from the wall toward the axis. The pressure gradient dp/dx need not be considered because it is interchangeable with τ_w according to equation (2.11). **(What about D ?)** The mean velocity \tilde{u} need not be considered because it is an integral of the profile u according to equation (2.15). Equation (2.129) in dimensionless form implies the relationship known as the law of the wall (see SECTION 2.5.4),

$$\frac{u}{u_\tau} = g\left(\frac{yu_\tau}{\nu}\right) . \quad (2.130)$$

In the present context, this relationship is taken to be a power law,

$$\frac{u}{u_\tau} = B\left(\frac{yu_\tau}{\nu}\right)^n \quad (2.131)$$

Then

$$u = Bu_\tau^{n+1}(y/\nu)^n \quad (2.132)$$

and, if the formula extends to the axis,

$$u_c = Bu_\tau^{n+1}(R/\nu)^n \quad (2.133)$$

so that u/u_c depends only on y/R , independent of Reynolds number.

Finally, the mean velocity \tilde{u} is obtained by putting the profile (2.132) in the definition (2.15),

$$\tilde{u} = \frac{2B}{(n+1)(n+2)} u_\tau^{n+1} (R/\nu)^n \quad (2.134)$$

from which **(need constants)**

$$\rho u_\tau^2 = \text{constant } \rho \tilde{u}^{2/(n+1)} (\nu/D)^{2n/(n+1)} . \quad (2.135)$$

Comparison with equation (2.128) yields immediately $n = 1/7$ from either exponent. This is a local and empirical result that applies at best only in a restricted range of Reynolds numbers. It has since been overtaken by events, as will be explained in the next section. Nevertheless, it may occasionally be useful for making rapid estimates.

KARMAN (1921, 1930) noted that Prandtl had already obtained these results in 1920 by a somewhat different argument, and PRANDTL eventually published his own version some years later (1927, III Lieferung). The main difference is the means used to pass from the mean velocity \tilde{u} , used in the friction equation, to the centerline velocity u_c , used in the profile equation. **(check)**.

2.5.4 The dimensional argument

The preceding section moves the empirical content of the mean-velocity profile in turbulent pipe flow from the mixing length to the similarity laws (2.118) and (2.122). These laws can be rationalized, although not explained, by a dimensional argument. First, suppose that the velocity as observed from the wall depends on the parameters according to **(this needs work)**

$$u = f(y, \rho, \nu, \tau_w, R, u_c) , \quad (2.136)$$

where the mean velocity \tilde{u} is not displayed because it is implicit when f is known, and dp/dx is not displayed because it is determined for a pipe by τ_w and R **(redundant)**. Suppose that u is found not to depend on R or u_c . **(Mention atmosphere; no δ or u_c .)** The only dimensionally correct form for $u(y)$ is then equation (2.118). Suppose further that the velocity observed from the pipe center,

$$u_c - u = F(y, \rho, \nu, \tau_w, R) , \quad (2.137)$$

is found not to depend on ν . The only dimensionally correct form for $[u_c - u(y)]$ is then equation (2.122), and the Izakson-Millikan argument follows. The weakness of this argument becomes clear only when there is another parameter with the dimensions of a velocity or

a length, such as a suction or blowing velocity v_w , or a roughness scale k at the wall, or a body diameter D in the case of boundary-layer flow on the outside of a cylindrical body. The nature and role of the new dimensionless parameter have to be determined in each case by a fresh empirical assault on the problem. Effects of compressibility and effects of suction or blowing at the wall, in particular, are still best described in terms of the mixing-length model (van Driest), and are therefore not under control.

*(Straighten out the question of an analogy with Kolmogorov's argument for the spectrum; see the introduction. See Narasimha. Mention separation of variables and singular perturbations.) (Introduce u^+ , y^+ notation.)*¹³

2.5.5 Interpolation formulas for the sublayer

The linear and logarithmic versions of the law of the wall, equations (2.116) and (2.117), intersect at a point near $u^+ = y^+ = 11$, depending on the values chosen for the constants κ and c . (Another intersection, at a free outer boundary of flow near a wall, is discussed in SECTION X of Chapter 4 on boundary layers.) For some purposes, the idea of a sharp intersection can be valuable, because it serves as a primitive definition of sublayer scale. For example, DONALDSON (1952) used a model with a linear sublayer and a power-law outer profile to argue that the main effect of compressibility in boundary-layer flow is to increase the relative thickness of the sublayer. For the present purpose, what matters is that the discontinuity in $\partial u/\partial y$ at the linear-logarithmic intersection implies a corresponding discontinuity in both components of the total shearing stress. Let this total stress be taken as constant; thus

$$\tau = \mu \frac{\partial u}{\partial y} - \overline{\rho u'v'} = \tau_w \quad , \quad (2.138)$$

or, in dimensionless wall units,

$$\frac{\tau}{\tau_w} = \frac{du^+}{dy^+} - \frac{\overline{u'v'}}{u_\tau^2} = 1 \quad . \quad (2.139)$$

¹³This notation is explained in section 2.5.6

Equation (2.139) is exact for plane Couette flow (SECTION X) and is otherwise an approximation in and near the sublayer for large Reynolds numbers. This equation is the point of departure for the modeling that follows. The discussion will neglect any effects of lateral curvature, pressure gradient, or low Reynolds number on the law of the wall, since it is not certain that these effects are experimentally detectable (see SECTION X).

When the law of the wall is expressed in Prandtl's form, $u^+ = f(y^+)$, the implication is that the sublayer intersection has been rounded off by recourse to some formula based on experimental data. A corresponding rounding is needed for the laminar and turbulent shearing stresses in equation (2.138). These stresses have a constant sum, with the laminar stress $\mu\partial u/\partial y$ rapidly decreasing and the turbulent stress $-\rho\overline{u'v'}$ rapidly increasing in a close neighborhood of the wall. In fact, it is the region in which the exchange of mechanisms takes place that is properly called the sublayer. Because the laminar shearing stress is known if the function $u^+ = f(y^+)$ is known, the key to the problem lies in the turbulent shearing stress, and specifically in the fact that the quantity $\overline{u'v'}$ behaves like y^3 very near the wall. I will argue this property in detail, I hope persuasively, in SECTION X. For the present, it is sufficient to stipulate that $(\overline{u'u'})^{1/2}$ behaves like y and that $(\overline{v'v'})^{1/2}$ behaves like y^2 , according to the continuity equation. The result $\overline{u'v'} \sim y^3$ then follows, as was first argued, somewhat tentatively, by REICHARDT (1951).

The need for an interpolation formula is most apparent in problems of heat transfer, especially at high Prandtl numbers (see SECTION X). MURPHREE (1932) and KARMAN (1939) introduced a primitive buffer layer for such problems (look up Murphree, others; Reynolds' analogy). Since then, more than 50 papers have been published on the interpolation problem. The literature up to about 1965 is thoroughly surveyed in the thesis by COANTIC (1966), and the more recent literature can be traced through papers by LEWKOWICZ (1982) and by NARAYANA and RAMANA (1988). Many of these papers patch various sublayer profiles to the logarithmic profile. A few papers provide a single continuous analytic formula for the entire region; i.e., an explicit formula $u^+ = f(y^+)$, or its inverse.

I will discuss three such formulas and recommend one of them.

Van Driest. A formula based on the mixing-length model and the approximation $\tau = \tau_w$ was proposed by VAN DRIEST (1956). Van Driest explains his approach by writing

$$-\overline{u'v'} = r(\overline{u'u'})^{1/2}(\overline{v'v'})^{1/2}, \quad (2.140)$$

where r is a dimensionless correlation coefficient that is known experimentally to be the most nearly universal number in all of turbulence, having a value near 0.4 or 0.5 in large regions of many different shear flows. (**Give phase argument?**) The universality of r can be interpreted as evidence that various active Reynolds stresses tend to be proportional to each other in fully developed turbulent flow, or more constructively as a statement about a common phase relationship between the fluctuations u' and v' . Van Driest writes $(\overline{u'u'})^{1/2}$ and $(\overline{v'v'})^{1/2}$ as $\ell' \partial u / \partial y$ and $\ell'' \partial u / \partial y$. The two mixing lengths ℓ' and ℓ'' and the coefficient r are then combined as ℓ^2 to obtain Prandtl's equation,

$$-\rho \overline{u'v'} = \rho \ell^2 \left(\frac{\partial u}{\partial y} \right)^2. \quad (2.141)$$

To model the effect of damping by the wall, Van Driest invokes the STOKES solution (1851) for a wall oscillating harmonically in its own plane in a stationary viscous fluid. For this flow, the fluctuations away from the wall are exponentially damped, like $e^{-y/L}$, where the damping scale $L = (2\nu/\omega)^{1/2}$ depends on frequency. Van Driest assumes that for a fixed wall and an oscillating fluid the corresponding damping factor is $(1 - e^{-y/\lambda})$, although the solution derived by LAMB (1932, p. 622) behaves differently. This assumed damping factor is applied twice, together with $\ell = \kappa y$, to obtain

$$-\rho \overline{u'v'} = \rho \kappa^2 y^2 (1 - e^{-y/\lambda})^2 \left(\frac{\partial u}{\partial y} \right)^2. \quad (2.142)$$

Unfortunately, this equation has $\overline{u'v'}$ behaving like y^4 near the wall. CHAPMAN and KUHN (1986) argue that the correct behavior can be obtained if the damping factor is associated with $\overline{u'u'}$, as suggested

by the Stokes solution, but not with $\overline{v'v'}$. They therefore propose, instead of equation (2.142),

$$-\rho\overline{u'v'} = \rho\kappa^2 y^2 (1 - e^{-y/\lambda}) \left(\frac{\partial u}{\partial y} \right)^2 . \quad (2.143)$$

To the extent that this revision amounts to putting

$$(\overline{u'u'})^{1/2} \sim y (1 - e^{-y/\lambda}) \frac{\partial u}{\partial y} , \quad (2.144)$$

$$(\overline{v'v'})^{1/2} \sim y \frac{\partial u}{\partial y} , \quad (2.145)$$

there is a hopeless dimensional contradiction, both for $\overline{u'u'}$, which must behave like y^2 near the wall, and for $\overline{v'v'}$, which must behave like y^4 . Perhaps it is better not to attempt to explain the unexplainable about the concept of mixing length.

Substitution of equation (2.143) for $\overline{u'v'}$ in equation (2.139) and use of wall variables lead to a complete mean-velocity profile $u^+ = f(y^+)$ as the integral of

$$\frac{du^+}{dy^+} = \frac{2}{1 + [1 + 4\kappa^2 y^{+2} (1 - e^{-y^+/\lambda^+})]^{1/2}} . \quad (2.146)$$

This equation has to be integrated numerically. The value obtained for the intercept c in the logarithmic region depends on the value of λ^+ . For $\kappa = 0.41$ and $c = 5.0$,¹⁴ the fit requires $\lambda^+ = 61.485$, and the interpolated profile appears as shown by the curve labeled Van Driest in FIGURE 2.31. The leading term in a power series for the turbulent shearing stress is

$$-\frac{\overline{u'v'}}{u_\tau^2} = \frac{\kappa^2}{\lambda^+} y^{+3} + O(y^{+4}) . \quad (2.147)$$

The numerical value of the coefficient κ^2/λ^+ is 0.002734.

¹⁴These values are revised in SECTION 2.5.7

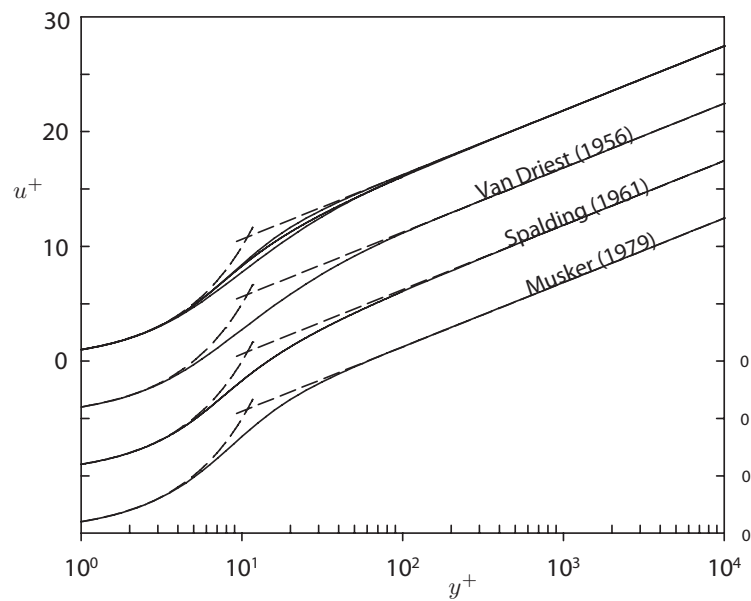


Figure 2.31: Three interpolation formulas for the transition region between the linear and logarithmic forms of the law of the wall. Note the displaced scales. The top display is a superposition of the other three. I recommend the formula proposed by Musker.

Equation (2.147) defines a family of profiles, with λ^+ or c as parameter. Check these for suitability for showing effects of roughness or polymers. Van Driest has a more general scheme that does not inspire confidence. What value of ω goes with the specified λ ?

Spalding. A quite different proposal was put forward by SPALDING (1961) and independently by KLEINSTEIN (1967). The difficulty that $u(y)$ does not have a power-series expansion valid into the log region can be avoided if $y(u)$ is examined instead. The logarithmic law,

$$u^+ = \frac{1}{\kappa} \ln y^+ + c , \quad (2.148)$$

has the inverse

$$y^+ = e^{-\kappa c} e^{\kappa u^+} . \quad (2.149)$$

This expression does have a power-series expansion about $u^+ = 0$, namely

$$y^+ = e^{-\kappa c} \left[1 + (\kappa u^+) + \frac{(\kappa u^+)^2}{2} + \frac{(\kappa u^+)^3}{6} + \frac{(\kappa u^+)^4}{24} + \frac{(\kappa u^+)^5}{120} + \dots \right] , \quad (2.150)$$

with an infinite radius of convergence. If a valid expansion is to begin with a term in u^+ and continue with a term in $(u^+)^4$, on the premise that u^+ begins with a term in y^+ and continues with a term in $(y^+)^4$ (see SECTION X), it is sufficient to cancel the first four terms of the series and append a term in u^+ ; thus

$$y^+ = u^+ + e^{-\kappa c} \left[e^{\kappa u^+} - 1 - (\kappa u^+) - \frac{(\kappa u^+)^2}{2} - \frac{(\kappa u^+)^3}{6} \right] . \quad (2.151)$$

This manufactured interpolation formula incorporates the two limiting forms (2.116) and (2.117) of the wall law, as shown by the curve labeled Spalding in FIGURE 2.31. However, convergence to the logarithm is relatively slow, and there are no disposable parameters. The leading term in an expansion of $\overline{u'v'}$ is found to be

$$-\frac{\overline{u'v'}}{u_\tau^2} = \frac{e^{-\kappa c} \kappa^4}{6} y^{+3} + O(y^{+4}) . \quad (2.152)$$

For $\kappa = 0.41$ and $c = 5.0$, the coefficient of y^{+3} has the numerical value 0.000606.

Musker. It remains to put in evidence MUSKER's proposal (1979), which emerges from the concept of eddy viscosity. With equation (2.138) in mind, define an eddy viscosity μ_t by

$$-\rho \overline{u'v'} = \mu_t \frac{\partial u}{\partial y} \quad (2.153)$$

and a kinematic eddy viscosity $\nu_t = \mu_t/\rho$ by (cite **Boussinesq**)

$$-\frac{\overline{u'v'}}{u_\tau^2} = \frac{\nu_t}{\nu} \frac{du^+}{dy^+} . \quad (2.154)$$

Equation (2.139) can now be written

$$\frac{\tau}{\tau_w} = \left(1 + \frac{\nu_t}{\nu}\right) \frac{du^+}{dy^+} = 1 . \quad (2.155)$$

Very close to the wall, where $\overline{u'v'}$ behaves like y^3 , the left side of equation (2.154) is $O(y^{+3})$, and du^+/dy^+ is $O(1)$. Consequently, put

$$\frac{\nu_t}{\nu} = sy^{+3} \quad \text{for} \quad \frac{\nu_t}{\nu} \ll 1 , \quad (2.156)$$

where s (for shearing stress) is an empirical constant.

(Note that equation (??) in section x is an exact consequence of the law of the wall in the form $u^+ = f(y^+)$. By coincidence, the leading term in an expansion of the integral in this equation is also a term in y^3 . However, this term is normally orders of magnitude smaller than the estimate (2.156) because of the factor λ^+ in the denominator.) (λ twice).

In the logarithmic region, where $du^+/dy^+ = 1/\kappa y^+$, take the shearing stress to be constant and put

$$\frac{\nu_t}{\nu} = \kappa y^+ \quad \text{for} \quad \frac{\nu_t}{\nu} \gg 1 . \quad (2.157)$$

Musker's proposal is to satisfy the two limiting conditions (2.156) and (2.157) on ν_t/ν simultaneously by using what I call the lens formula,

$$\frac{1}{\nu_t/\nu} = \frac{1}{sy^{+3}} + \frac{1}{\kappa y^+} = \frac{\kappa y^+ + sy^{+3}}{s\kappa y^{+4}} . \quad (2.158)$$

Consequently, from equation (2.155),

$$\frac{du^+}{dy^+} = \frac{\frac{y^{+2}}{\kappa} + \frac{1}{s}}{y^{+3} + \frac{y^{+2}}{\kappa} + \frac{1}{s}} . \quad (2.159)$$

This equation can be expanded in a power series about $y^+ = 0$ to obtain

$$-\frac{\overline{u'v'}}{u_\tau^2} = 1 - \frac{du^+}{dy^+} = sy^{+3} - \frac{s^2}{\kappa}y^{+5} + O(y^{+6}) . \quad (2.160)$$

Term-by-term integration gives

$$u^+ = y^+ - \frac{s}{4}y^{+4} + \frac{s^2}{6\kappa}y^{+6} + O(y^{+7}) . \quad (2.161)$$

To lowest order, the turbulent shearing stress is half of the total when y^+ is about 7.7, in keeping with traditional ideas about the scale of the sublayer. (*Cite Spalart's calculations for the boundary layer at constant pressure, which indicate that the first two terms for $\overline{u'v'}$ are terms in y^3 and y^5 . Coincidence? Mention consequences for full expansion in chapter 7.*)

Musker's analytical integration of equation (2.159) is worth study. Let the denominator be expressed as $(y^+ - a)(y^+ - b)(y^+ - c)$. One of the three roots is real and negative, and the other two are complex conjugates, as shown in FIGURE 2.32. Write

$$a < 0, \quad b = \alpha + i\beta, \quad c = \alpha - i\beta . \quad (2.162)$$

The three roots satisfy the identities

$$a + b + c = a + 2\alpha = -\frac{1}{\kappa} , \quad (2.163)$$

$$ab + ac + bc = 2a\alpha + R^2 = 0 , \quad (2.164)$$

$$abc = aR^2 = -\frac{1}{s} , \quad (2.165)$$

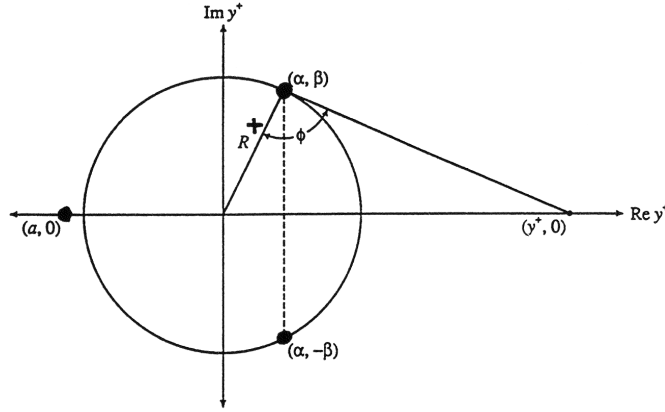


Figure 2.32: Placement in complex wall coordinates of the three singularities in Musker's formula (2.166) for the law of the wall. The radius of convergence of a power series for $u^+(y^+)$ is $R^+ = 9.29$.

where $R^2 = \alpha^2 + \beta^2$ (the constants c and R have special meanings for this development). There is only one free parameter, since α , β , R , s are all expressible in terms of a and κ , say.

A surfeit of algebra leads to the mean-velocity profile

$$u^+ = \frac{1}{\kappa} \ln \left(\frac{y^+ - a}{-a} \right) + \frac{R^2}{a(4\alpha - a)} \left[(4\alpha + a) \ln \Phi + \frac{\alpha}{\beta} (4\alpha + 5a) \phi \right], \quad (2.166)$$

where

$$\Phi = -\frac{a}{R} \frac{[(y^+ - \alpha)^2 + \beta^2]^{1/2}}{(y^+ - a)} \quad (2.167)$$

is a mix of distances measured from the origin or from the point y^+ in FIGURE 2.32 to the singularities of equation (2.159), and where

$$\phi = \tan^{-1} \left(\frac{y^+ - \alpha}{\beta} \right) + \tan^{-1} \left(\frac{\alpha}{\beta} \right) \quad (2.168)$$

is the angle marked in the figure.

The boundary condition $u^+ = 0$ at $y^+ = 0$ is evidently satisfied by equation (2.166). Passage in either direction to verify that this equation is the integral of equation (2.159) is aided by the identities (2.163)–(2.165). Because equations (2.163) and (2.164) imply $R^2/a^2 < 1$, the complex roots determine the radius of convergence R of the power series expansions (2.160) and (2.161).

For sufficiently large values of y^+ , the profile equation takes the form

$$u^+ = \frac{1}{\kappa} \ln y^+ + c , \quad (2.169)$$

where c is now the constant of integration first defined in equation (2.117);

$$c = -\frac{1}{\kappa} \ln(-a) + \frac{R^2}{a(4\alpha - a)} \left\{ (4\alpha + a) \ln\left(-\frac{a}{R}\right) + \frac{\alpha}{\beta}(4\alpha + 5a) \left[\frac{\pi}{2} + \tan^{-1}\left(\frac{\alpha}{\beta}\right) \right] \right\} . \quad (2.170)$$

Since c and s can both be expressed parametrically in terms of a , they are uniquely related to each other. Given $\kappa = 0.41$, the values that correspond to $c = 5.0^{15}$ are $a = -10.593$, $\alpha = 4.077$, $\beta = 8.352$, $R = 9.294$, and $s = 0.001093$. These constants in equation (2.166) produce the lowest labeled curve in FIGURE 2.31.

Musker's profile slightly overshoots the log profile, by a maximum of about 0.02 in u^+ near $y^+ = 150$. This minor defect could probably be removed by slightly increasing the coefficient of the middle term in the denominator of (2.159), to decrease the derivative du^+/dy^+ locally without disturbing the two limiting conditions, but I prefer to rest my case.

Although the profile equation (2.166) is untidy, Musker's interpolation scheme works so well that its use amounts to making a necessity out of virtue. First, the leading terms in the power series for $\overline{u'v'}$ agree with the leading terms extracted from SPALART'S numerical results (1988) for the turbulent boundary layer at constant pressure, as shown in FIGURE X.¹⁶ **(Check this. Get channel numbers**

¹⁵Values of κ and c are revised in SECTION 2.5.7

¹⁶This figure has not been found.

from Moin.) Second, there is an encouraging resemblance between the pattern of singularities in FIGURE 2.32 and the corresponding pattern for the Blasius boundary layer (see SECTION X), thus providing another point of contact in the power-series approach to both laminar and turbulent regimes of flow near a wall. Finally, Musker's scheme, although it has only one disposable constant, is capable of generating a plausible family of profiles for fixed κ and arbitrary c , and I will use it for this purpose when I take up some effects of surface roughness and long-chain polymers in SECTIONS 2.6 and 2.7.

2.5.6 Fully developed flow

One test for fully developed pipe flow can be based on the properties of the mean velocity profile, provided that an accurate analytical description of the profile is available. Such a description is given in part by the empirical formula

$$\frac{u}{u_\tau} = f\left(\frac{yu_\tau}{\nu}\right) + \frac{\Pi}{\kappa} w\left(\frac{y}{R}\right), \quad (2.171)$$

where u_τ and Π are parameters. The function f outside the sublayer is a logarithm, and w is an antisymmetric function that is adequately represented by $\sin^2(\pi y/2R)$. The distance y is measured from the wall toward the axis and beyond.

One defect in the formula (2.171) is the presence of a corner, or discontinuity in slope, on the pipe axis. The equivalent defect at the edge of a boundary layer is discussed at length in SECTION 4.9.3 below. In the present section, the need is to develop a quantitative measure of the degree of rounding of the experimental velocity profile near the pipe axis, thus creating a new and sensitive criterion for judging the approach to full developments. The notation refers to pipe flow, but the physical meaning may be clearer if the calculations are associated with channel flow.

The discontinuity in slope appears when the wall law outside the sublayer is written as

$$\frac{u}{u_\tau} = \frac{1}{\kappa} \ln \frac{yu_\tau}{\nu} + c \quad (2.172)$$

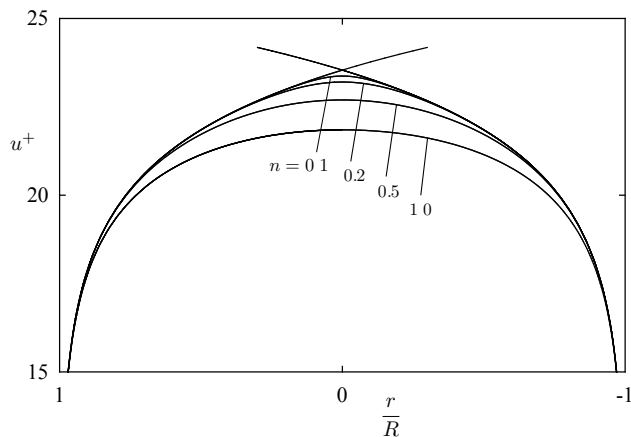


Figure 2.33: Use of the single-parameter equations (2.176) and (2.180) to round the logarithmic mean-velocity profile near the pipe axis for the case $R^+ = Ru_\tau/\nu = 2000$.

and this law is assumed to hold to the pipe axis at $y = R$. Recall the analytical device that I called the lens formula in the previous section. (**check**) The objective there was to interpolate between the linear and logarithmic parts of the mean-velocity profile in the sublayer. The same device will be used here. The notation is shown in FIGURE 2.33. For the left half of the figure, the law of the wall has the form (2.172). For the right half of the figure, write

$$\frac{u}{u_\tau} = \frac{1}{\kappa} \ln \frac{(2R - y)u_\tau}{\nu} + c, \quad (2.173)$$

where y in both formulas is measured from the left wall. For brevity, introduce the $+$ notation, with $u^+ = u/u_\tau$, $y^+ = yu_\tau/\nu$, and $R^+ = Ru_\tau/\nu$. Close to the left wall in FIGURE 2.33, define a new variable

Y^+ by the identity

$$Y^+ = y^+ . \quad (2.174)$$

Close to the right wall, define the same variable by

$$Y^+ = 2R^+ - y^+ , \quad (2.175)$$

so that the single formula

$$u^+ = \frac{1}{\kappa} \ln Y^+ + c \quad (2.176)$$

applies close to both walls. Near the axis, the two definitions for Y^+ can be joined smoothly with the aid of the lens formula,

$$\frac{1}{(Y^+)^{1/n}} = \frac{1}{(y^+)^{1/n}} + \frac{1}{(2R^+ - y^+)^{1/n}} ; \quad (2.177)$$

or

$$Y^+ = \left[\frac{(2R^+ - y^+)^{1/n} (y^+)^{1/n}}{(2R^+ - y^+)^{1/n} + (y^+)^{1/n}} \right]^n , \quad (2.178)$$

where the parameter n determines the amount of rounding near the axis. Finally, replace the distance y , measured from the left wall, by the distance r , measured from the axis of the pipe;

$$y^+ = R^+ - r^+ . \quad (2.179)$$

Given that y^+ is always positive, the radius r^+ must be interpreted as positive (negative) in the left (right) half of FIGURE 2.33. Equation (2.178) becomes

$$Y^+ = \left[\frac{(R^{+2} - r^{+2})^{1/n}}{(R^+ + r^+)^{1/n} + (R^+ - r^+)^{1/n}} \right]^n . \quad (2.180)$$

This form shows explicitly the desired symmetry about the pipe axis, with $Y^+(r^+) = Y^+(-r^+)$ everywhere. Some typical rounded profiles defined by equations (2.176) and (2.180) are shown in the figure for several values of n . On the axis, where $r^+ = 0$, $Y^+ = R^+/2^n$. If a more physical interpretation of the parameter n is wanted, it can be

had by calculating the radius of curvature of the function $u^+(r^+)$ at $r^+ = 0$, most simply by way of power-series expansions. (**Do this.**)

(Two paragraphs out of order.) A few remarks are in order about the conceptual nature of the variables just considered. The quantities called the Reynolds stresses are part of the Reynolds-averaged momentum equations, and so must answer to the laws of mechanics. My view is that at least the Reynolds shearing stress can be interpreted as a real physical variable. Within the boundary-layer approximation, a numerical value can be assigned to $-\overline{\rho u'v'}$ in at least two ways. The first defines this quantity as an apparent force required to balance other forces and accelerations that can be evaluated independently. The second measures the fluctuations u' and v' and the mean value of their product. The two quantities so determined will be compared for a variety of flows in different sections of this monograph. If the two values do not agree, the difference is ordinarily blamed on failure of the boundary-layer approximation or on experimental error. This view may survive the assumption $\tau = \tau_w$, although the laws of mechanics are then abandoned, as already pointed out in SECTION X.

The mixing length and the eddy viscosity are conceptually different from the Reynolds stresses and from each other. A numerical value can be assigned to ℓ or to μ_t in only one way, through the definition (2.141), in the case of ℓ , or the definition (2.153), in the case of μ_t . These definitions lie outside the laws of mechanics, being part of turbulence modeling. They are inventions that are intended to supply an additional equation to be used with momentum equations like (2.1), but in practice are often used alone. The eddy viscosity is the kinder concept, being a direct surrogate for the velocity field.

My plan is to fit turbulent profiles and determine Π and n . Plot Π and n vs R^+ . Plot Π vs n . Look for evidence of lack of development or lack of symmetry.

Suitable profiles are in papers by

COSTRELL process
FOWLES

ELENA
STANTON (1911) 3D process
NIKURADSE (1932) 3A process
FAGE (1936) 3A
LING (1937) 3A process
NEWMAN and LEARY (1950) 3A
LAUFER (1953) 3A
SANDBORN (1955) 3A process
WEISSBERG and BERMAN (1955) 3J
BROWN et al. (1957) 3K
SLEICHER (1958) 3F process
BROOKSHIRE (1961) 3A
WELLS (1965) 3E
WICHNER (1965) 3A process
COANTIC (1966) 3A process
ELATA et al. (1966) 3E
OLSON and ECKERT (1966) 3J
PATTERSON (1966) 3E
VIRK et al. (1967) 3E
BAKEWELL and LUMLEY (1967) 3A process
ERNST (1967) 3E
MIH and PARKER (1967) 3E
SHERWOOD et al. (1968) 3A
WELLS et al. (1968) 3E
LINDGREN and CHAO (1969) 3A
MORRISON (1969) 3A
SEYER and METZNER (1969) 3E process
SIRKAR (1969) 3A
SPANGLER (1969) 3E
CLARK (1970) 3A
KJELLSTROM and HEDBERG (1970) 3A
LAWN (1970) 3A
TOMITA (1970) 3E
VAN DRIEST (1970) 3E
POWE and TOWNES (1971) 3D
ARUNACHALEM et al. (1972) 3E
ROLLIN and SEYER (1972) 3E

TOWNES et al. (1972) 3D
 CARPENTER (1973) 3D
 LU et al. (1973) 3H
 BERTELHUD (1974) 3A process
 CHEN and ROBERTSON (1974) 3D
 DURST and KELLER (1974) 3E
 PATEL (1974) 3A process
 SCRIVENER (1974) 3E
 AQUINO and LAMONTAGNE (1975) 3E
 PERRY and ABELL (1975) 3A process
 SABOT and COMTE-BELLOT (1976) 3A
 MIZUSHINA and USUI (1977) 3E
 HISHIDA and NAGANO (1979) 3A
 KUBO (1979) 3E
 SCHILDKNECHT et al. (1979) 3J
 RAMAPRIAN and TU (1980) 3H
 HASSAN (1980) 3A
 DURST et al. (1981) 3E
 LANGEHEINEKEN (1981) 3A
 TU and RAMAPRIAN (1983) 3H
 BEWERSDORFF (1985) 3E
 BULLOCK et al. (1990) 3D

2.5.7 Karman's constants κ and c

NOTE: The first four paragraphs in this section were included in the draft of this chapter. A separate file dated 1 April 1999 with new conclusions of the author on the same topic has been added at the label 'Revision of values.' -K. Coles

The values of Karman's constants κ and c in the logarithmic profile are usually thought to be determined from Nikuradse's smooth pipe data, whether or not the wake component is clearly recognized. The universal parameter κ originates in the heuristic definition $du/dy = u_\tau/\kappa y$ in Prandtl's equation (2.104) with $\ell = \kappa y$ and $\tau = \tau_w$, although sometimes κ is inferred after one or more stages of manipulation. Numerous other measurements of pipe profiles have

been made, and should also be considered as evidence. A preliminary step is to ensure from other evidence that the flow is fully developed. A suitable test is to obtain the strength of the wake component and look for a universal behavior. I take figure x as the best evidence for the value of these constants.

A second major source of systematic data on the mean-velocity profile in a smooth pipe at large Reynolds numbers is the thesis by LING (1939), who studied under Schoder at Cornell University. This thesis has some anomalous properties. The experimental apparatus is not described in convincing detail. There is no attempt to compare the results with the results of other experimenters. Finally, there is little evidence in some sections of the thesis that the work was properly supervised. It is not possible sixty years later to account for these anomalies, or even to determine why the research was done at all. Nevertheless, I am willing to accept Ling's results, and they are shown in figure x.

(Select possible experiments from DATA3A. Evaluate two constants by plotting the wall law in the range $y^+ > 50$ (or 100) and $y/R < 0.25$, to isolate the logarithmic region. Look at u_c/\bar{u} to find poor data. Look at u_c/u_τ or friction coefficient for the same purpose. Can anything be done with Burke's data? Emphasize that κ and c are defined in terms of the mean-velocity profile, equation (2.117). Collect data; there are at least 50 sources. (Data are available for Nikuradse, Stanton, Bertelrud, Ramaprian and Tu, Deissler, Wichner, Brookshire, Coantic, Ling, Patel, Hettler, Fowles, Sirkar, Shaver and Merrill, Bogue and Metzner, Hershey, Virk et al, Seyer and Metzner, Wang. Data are needed for Chen and Robertson, Laufer, Langeheineken, Hishida and Nagano, Hassan, Morrison, Fage, Clark, Bakewell and Lumley, Sherwood et al, Durst et al, Durst and Keller, Patterson et al, Wells, Perry and Abell, Sleicher, Olson and Eckert, Lu et al, Lawn, Lindgren and Chao.) Segregate fully developed flows. Use x/D , u_c/u_τ as criteria. Accept authors' values for C_f . Look hard at lower Reynolds numbers. Come up with slope and intercept. Say something about errors in sublayer, wake component.

(Move somewhere) Despite these objections, the mixing-length formulation for turbulence near a wall defined the state of the art

for a generation, until the first Stanford contest in 1968 (ref). My own preference is for strict adherence to the principles of similarity. I consider the log law to be an empirical result, an answer for which the question is unknown. Perhaps a substantial prize should be awarded for a new and persuasive question. (endmove).

Revision of values of κ and c . Various values can be found in the literature for the constants κ and c . From the beginning, I have taken these constants to be the [reciprocal of the] slope and the intercept of a straight line fitted in semi-log coordinates to a fragment of the mean-velocity profile near a smooth wall;

$$\frac{u}{u_\tau} = \frac{1}{\kappa} \ln \frac{yu_\tau}{\nu} + c . \quad (2.181)$$

The fragment begins at the edge of the sublayer and ends before the wake component becomes appreciable. Some authors have chosen to take a defining agency for these constants other than the profile fragment (2.181), or alternatively its derivative,

$$\frac{\partial u}{\partial y} = \frac{u_\tau}{\kappa y} . \quad (2.182)$$

Instead, they choose some derived quantity that modifies the definition (2.181) by introducing further approximations and assumptions that vary from author to author. An example is use of a friction coefficient formula derived by Karman in his 19xx paper. In my 1956 survey I assigned to κ and c the values 0.40 and 5.1. In 1962, on the uncertain ground of a hypothetical mapping of floating-element friction data in supersonic boundary layers onto like data at Mach number zero, I revised these values to 0.41 and 5.0. I retained the latter values in my 1968 survey for the first Stanford contest.

The measurements in smooth pipes by NIKURADSE (1930, 1932) have always had a central place in this part of the turbulence picture, primarily because of their relatively large range of Reynolds number. However, there has been for decades a growing mistrust of Niduradse's data. In fact, I have felt obliged to include here and elsewhere in this monograph a critique of the man and his methods based on whatever evidence I have been able to find. From time to

time, there have been attempts to obtain new data in pipes at large Reynolds numbers, in part because of the mistrust just mentioned, but also in part because of suggestions from work in boundary layers at high Reynolds numbers that the concept of a defect law is not firmly supported by the available evidence. (**Mention Burke, van Sciver**).

Efforts to increase the Reynolds number by increasing the velocity eventually encounter compressibility for a gas and cavitation for a liquid. Modest decreases in viscosity can be realized in gases by cooling, and in liquids by heating, as was demonstrated by Nikuradse. Large physical scales usually mean a large test facility and exposure to field conditions, which anyone with previous field experience would try to avoid if the context is fundamental research.

There remains the possibility of an increase in density for a gas as working fluid. (**Look for examples**) In 1996, in time to have a profound effect on this monograph, ZAGAROLA at Princeton completed a thesis reporting new profile measurements in pipe flow at pressures to about 200 atmospheres. FIGURE 2.34 is essentially raw data, presented as a replica of a figure in Zagarola's thesis. (**Check**) To avoid crowding, only half of his 26 profiles are included. The remarkable regularity of these data leaves no doubt whatever about the validity for pipe flow of the logarithmic law of the wall and the wake-like (here jet-like) momentum-defect law. In my opinion, the paradigm represented by these and other similarity laws is completely safe. Except that I might wish to see the measurements in the lower range of Reynolds number repeated with a tripping device, and also to see some rigorous quantitative evidence on surface roughness, I accept Zagarola's data as definitive, and I therefore accept the conclusion that the two constants in the law of the wall have to be revised once more.

Let new values of κ and c be defined by FIGURE 2.35 which shows by 26 open circles Zagarola's experimental values for the dimensionless velocity on the pipe centerline. Also shown by small filled circles are uncorrected velocity measurements (as tabulated in the thesis) in the region near the wall (i.e., for $y^+ > 200$, $y/R < 0.1$), where the profile is expected to be logarithmic. The latter data are

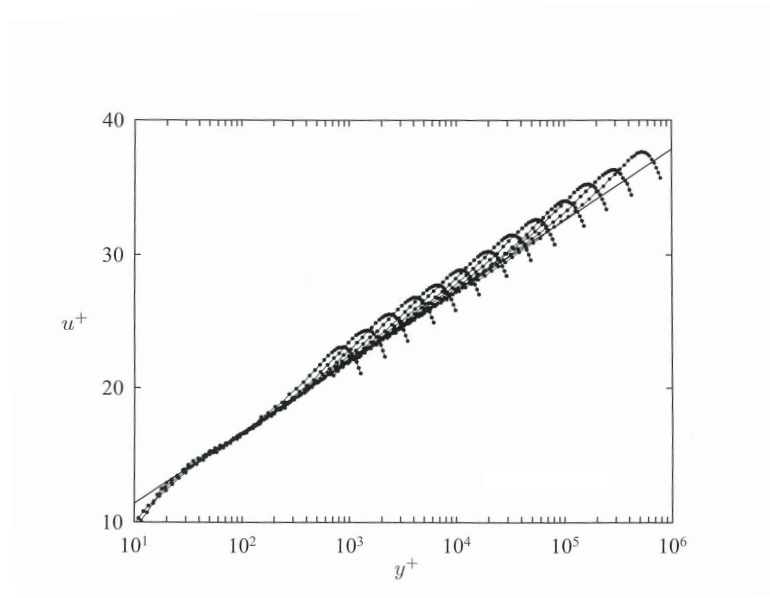


Figure 2.34: Raw velocity-profile data from the superpipe measurements by ZAGAROLA (1996). Thirteen of the 26 measured profiles are shown. The logarithmic law of the wall and the velocity-defect law are solidly supported by these data.

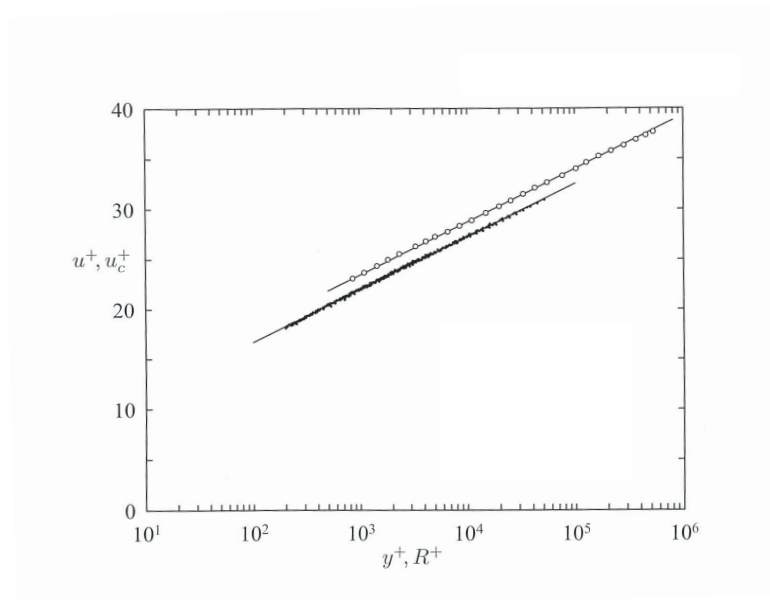


Figure 2.35: Centerline data and log-region data from the superpipe measurements by ZAGAROLA (1966). The fitted lines have the same slope. The constants in the logarithmic law of the wall are $\kappa = 0.435$, $c = 6.10$.

what I take to define κ and c . Note that the centerline data are of a different quality, because they do not encounter corrections for probe displacement or for effects of high turbulence level near the wall. On the basis of FIGURE 2.34, I am satisfied that the defect law is valid and that two straight lines having the same slope can be fitted to the two sets of data in FIGURE 2.35. Such lines define themselves easily within the small experimental uncertainty of the data. The revised constants for the lower line, with is the logarithmic law of the wall according to equation 2.181, are then

$$\kappa = 0.435, \quad c = 6.10 \quad . \quad (2.183)$$

For the upper line, which represents the local friction coefficient in the form

$$u^+ = \frac{1}{\kappa} \ln R^+ + C \quad , \quad (2.184)$$

the constants are

$$\kappa = 0.435, \quad C = 7.56 \quad . \quad (2.185)$$

(Say that these are used willy-nilly in every part of this monograph.)

In their journal paper, as in the thesis, ZAGAROLA and SMITS (1999) do not relate their new data explicitly to the body of earlier measurements, particularly the measurements by Nikuradse. I have therefore constructed FIGURE 2.36 for this purpose. Note that no mechanism or model is assumed in this presentation of experimental centerline velocities, unless the choice of semilog coordinates can be called a model.

Begin with the lowest part of FIGURE 2.36. The crosses represent an experimental data base collected from the work of about 15 authors not including Nikuradse (see the appendix)¹⁷. The open circles are Zagarola's 26 points, and the line is my best fit, both being transferred verbatim from FIGURE 2.35. I first constructed FIGURE 2.36¹⁸ using a larger data base, but found more scatter than I thought reasonable. This scatter became reasonable when I

¹⁷It is unclear if this appendix was not completed or is incorporated elsewhere.

¹⁸Probable reading of manuscript - K. C.

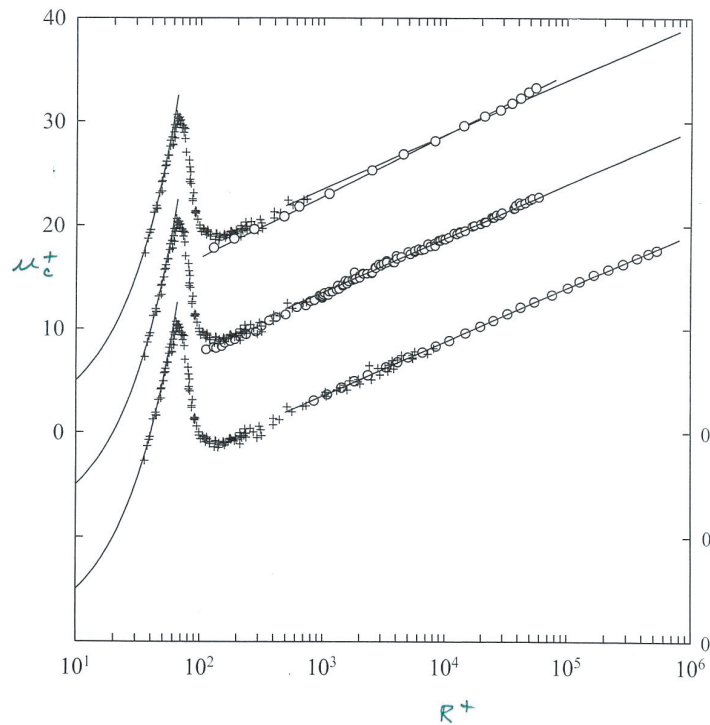


Figure 2.36: Various measurements in wall coordinates of centerline velocity in smooth pipes. Note the displaced origins. The lower curve shows good agreement between the data of ZAGAROLA (1996; circles) and other measurements from the literature (crosses), absent Nikuradse. The middle curve shows good agreement between Zagarola's centerline data and NIKURADSE's centerline data from his table 8 (1932), except for Reynolds numbers R^+ below about 1500. The upper curve shows that the centerline points from Nikuradse's 16 profiles in his table 3 do not agree with any of the other measurements, including his own.

discarded all data for which the necessary measurements of pressure or velocity were made closer to the pipe entrance than 100 diameters.

In passing, observe that the transition range is well defined by the work of SENEAL (1953) and PATEL and HEAD (1969). A square-cut entrance appears to be an adequate tripping device at all Reynolds numbers. (**check**) The beginning of transition is abrupt, at about $R^+ = 60$, or $Re = 2100$, but the end of transition is not so well defined, probably because of a slow approach to equilibrium. As a test for final equilibrium, it would be useful to have flatness-factor data for velocity fluctuations on the pipe axis far downstream over a range of Re from 2000 to perhaps 10,000, to verify the disappearance of the bimodal laminar/turbulent probability-density function associated with intermittency. (See SECTION X on transition).

In the lowest part of FIGURE 2.36, where the old and new data overlap, there is good agreement, although the straight line in the figure may not be the best overall representation in the early part of the turbulent regime, below $R^+ = 10^3$.

The central part of FIGURE 2.36 repeats part of the data base and repeats the fitted line, but replaces Zagarola's centerline data by Nikuradse's centerline data from table 8 of his 1932 paper. At least for R^+ greater than about 2000, there is no appreciable difference between the two sets of measurements, despite the lower length/diameter ratio for Nikuradse's pipes. However, for the lowest Reynolds numbers Nikuradse's values seem low, indicating that transition may have been over-tripped in this region.

Finally, the upper part of FIGURE 2.36 shows Nikuradse's centerline points from the profiles in his table 3, together with the base data and Zagarola's straight line. There is a discrepancy in slope that (**give value**) is evidently internal to Nikuradse's work and cannot be ignored. I have found nothing in his 1932 paper to explain his difficulty with the rule that an experimenter must be able to repeat his own measurements, and I suspect that the values of u_τ for the profiles have been adjusted. There is more on this question in SECTION X. (**Check profiles of 1930 against 1932.**)

2.5.8 The defect law

(Discuss as outer component in a singular-perturbation argument. Combine with next section? Validity depends on smoothness of u_c/u_τ against $\ln Ru_\tau/\nu$.)

2.5.9 The limit $Re \rightarrow \infty$

A philosophical question about turbulent pipe flow concerns the limit of infinite Reynolds number. The defect law in the limit represents a square profile with a boundary layer at the wall (what about the wake component?). The turbulence is mixing so effectively that there is no gradient in mean velocity. The problem looks like a classical singular perturbation problem, except that the equations are not known. Several people have tried this problem. A reasonable test is to ask how the logarithm gets into the analysis, and the answer so far is that the authors put it in, by one device or another. I think this is an important exercise, and should be done correctly from the beginning. Plot u_τ/u_c against $1/\ln(Ru_c/\nu)$ and argue $C_f \rightarrow 0$ as $Re \rightarrow \infty$?

The atmosphere is a boundary layer at very large Reynolds number. There is only a wall component, since there is no way to define a thickness or a free-stream velocity. One problem is that the flow should be neutrally stable. Another is that the effect of the earth's rotation on the flow near the surface should be negligible. Another is that the surface should be smooth, and in practice this means smoother than smooth concrete. A last problem is that the approaching flow should have a long fetch. (*Look at meteorological literature.*)

2.5.10 The formal friction law

Karman (ref) noted the local friction law obtained by evaluating the profile formula (2.117) on the pipe axis, with a slightly different

constant,

$$\frac{u_c}{u_\tau} = \frac{1}{\kappa} \ln \frac{Ru_\tau}{\nu} + A . \quad (2.186)$$

He applied this formula to estimate $\kappa = 0.38$ from Nikuradse's data for u_c , u_τ , and R in a smooth pipe. The fact that u_c rather than \tilde{u} appears here prevents any direct connection with the bulk of pipe data. (*Use profile formula for u_c/u_τ . Document behavior at low Re . Try Burke again. How to replace u_c by \tilde{u} ?*)

2.5.11 The Reynolds stresses

(*Plot fluctuations in sublayer for $y^+ = 15, 50$; also centerline values. See Lehigh paper.*) Perry and Abell are looking for evidence that the turbulent fluctuations obey a wall/wake decomposition like the mean velocity.

(*Two topics so far are sudden area change; see Krall, Boger and Halmos, and Khezzer et al, and effect of coiling, especially on transition; see Taylor, White, Sreenivasan. Another is non-steady pipe-flow. Mention that roughness and polymers are treated separately.*)

2.6 Roughness

2.6.1 Friction

Most of the early data on flow in pipes, from about 1860 to about 1900, were obtained by civil engineers in pipes characteristic of water distribution systems, long vehicular tunnels and even sewers. These pipes were typically made of wood, riveted iron (sometimes corrugated), cast iron or cast concrete, or excavated rock, and they often deteriorated over time because of accumulating corrosion or other deposits. Thus engineers lived with rough surfaces, and they tended to carry out their experiments in the same circumstances where the information was to be applied. In the absence of any formalism for

organizing their knowledge, they were simply good engineers. Collections of some of these early measurements can be found in papers by Blasius, Ombeck, and others. (**Mention others.**)

The Reynolds numbers in the early work were often large, and the evidence showed that the pressure drop in a given pipe tended to vary as the square of the flow velocity, although exponents closer to 7/4 were sometimes reported for especially smooth and clean pipes. Work on pipe flow as a classical problem in turbulent shear flow began near the end of the 19th century, and some of this work is cited in SECTION X. Work on the effects of roughness lagged, there being no systematic studies taking into account geometric similarity and other questions of good experimental definition until the appearance of a remarkable contribution by Nikuradse in 1933. This paper by Nikuradse is still considered to be the seminal work on the problem of surface roughness, although there are several open questions to be taken later.

The discussion here begins where the subject ends, with the subject of the fully rough regime. The main effect of large wall roughness is to replace the condition $\tau_w = \mu(\partial u/\partial y)_w$ by a drag condition that treats three-dimensional roughness elements as bluff bodies, with a local pressure drag that is quadratic in some characteristic velocity \hat{u} and independent of viscosity. If N is the number of such elements and F is the total drag force, both per unit area, write approximately

$$F = C_D \frac{\rho \hat{u}^2}{2} N k^2 = \rho u_\tau^2, \quad (2.187)$$

where C_D is a drag coefficient and k is a roughness scale, to be defined later.

For packed roughness, Nk^2 is of order unity. If C_D is also of order unity, as it is for a sphere, say, at a Reynolds number $\hat{u}k/\nu$ greater than about 1000, then \hat{u} should be of order u_τ (**check this with real data**). Moreover, if C_D is independent of Reynolds number, so is

$$C_f = \frac{F}{\frac{1}{2}\rho \tilde{u}^2} \approx C_D \left(\frac{\hat{u}}{\tilde{u}} \right)^2, \quad (2.188)$$

where \tilde{u} is a suitable external or reference velocity. This property defines the fully rough regime.

(If roughness is not packed, try a linear combination of the two forms for F ? 2D vs 3D? Who first understood roughness?)

A more elegant approach is in terms of similarity laws for the mean-velocity profile, as these laws developed in connection with flow in smooth pipes. A useful point of attack is the defect law outside the sublayer,

$$\frac{u_c - u}{u_\tau} = g\left(\frac{y}{R}\right), \quad (2.189)$$

which does not involve the viscosity and was in fact proposed independently by several authors, beginning with DARCY (1858). This empirical law does not depend on the mechanism by which the retarding force F acts at the wall.

Now consider the law of the wall as a product of the mixing-length argument. This law emerged first in the form

$$\frac{u}{u_\tau} = \frac{1}{\kappa} \ln \frac{y}{y_0}, \quad (2.190)$$

without giving any information about the nature of the constant of integration y_0 . If this constant depends only on conditions at the wall, then for a smooth wall the only possible form is

$$y_0 = \frac{1}{A} \frac{\nu}{u_\tau}, \quad (2.191)$$

where A is a constant. Equation (2.190) becomes

$$\frac{u}{u_\tau} = \frac{1}{\kappa} \ln \frac{yu_\tau}{\nu} + \frac{1}{\kappa} \ln A. \quad (2.192)$$

For a fully rough wall, on the premise that the viscosity is irrelevant, the most obvious choice is

$$y_0 = \frac{1}{B} k, \quad (2.193)$$

where B is another constant. Instead of equation (2.192), there is obtained

$$\frac{u}{u_\tau} = \frac{1}{\kappa} \ln \frac{y}{k} + \frac{1}{\kappa} \ln B. \quad (2.194)$$

Let the last expression be rewritten in the customary wall variables as

$$\frac{u}{u_\tau} = \frac{1}{\kappa} \ln \frac{yu_\tau}{\nu} - \frac{1}{\kappa} \ln \frac{ku_\tau}{\nu} + \frac{1}{\kappa} \ln B . \quad (2.195)$$

Each of the four relationships so far given for u/u_τ , if it is valid to the pipe center, is consistent with the defect law (2.189).

Finally, consider the difference between equations (2.192) and (2.195). The vertical displacement of the logarithmic profile at a fixed value of yu_τ/ν , on subtraction of equation (2.192) from equation (2.195), is

$$\Delta \left(\frac{u}{u_\tau} \right) = -\frac{1}{\kappa} \ln \frac{ku_\tau}{\nu} + \frac{1}{\kappa} \ln B - \frac{1}{\kappa} \ln A . \quad (2.196)$$

Nikuradse's data are central to all of these relationships. One figure corresponds to equation (2.194) and gives a value $(1/\kappa) \ln B = 8.5$, where data in smooth pipes according to equation (2.192) gave $(1/\kappa) \ln A = 5.0$ (see SECTION X). The expectation is therefore that the profile shift in the fully rough regime should be described by

$$\Delta \left(\frac{u}{u_\tau} \right) = -\frac{1}{\kappa} \ln \frac{ku_\tau}{\nu} + 3.5 . \quad (2.197)$$

Nikuradse gives this result in a different and less universal form. The representation (2.197) has become standard since it was first plotted by (**who?**).

FIGURE X¹⁹ shows C_f as a function of Re for Nikuradse's experiments. What is obvious and impressive is that the roughnesses used by Nikuradse have no effect on laminar flow or on transition, or even on turbulent flow, until a critical roughness (which depends on Reynolds number) is exceeded. Then there is a departure from the smooth curve and an eventual quadratic drag behavior above another critical Reynolds number (note that C_f and \hat{u}/\tilde{u} or u_τ/\tilde{u} are independent of Re here). In terms of the vertical displacement of the velocity profile, the same behavior is shown in FIGURE X. The effects of roughness are first felt at roughly $ku_\tau/\nu = 5$, where the roughness

¹⁹Figures cited in this paragraph are missing.

elements begin to project beyond the linear part of the smooth-wall profile, and the fully rough behavior occurs for $ku_\tau/\nu > 70$, which is, by coincidence or otherwise, approximately the thickness of the sublayer for a smooth wall. The slope is $1/\kappa$ as it should be.

All of this is conventional wisdom and appears in numerous books. A number of questions need discussion in the light of the whole literature of the subject.

(1) What is meant by “mean velocity”? How is it to be defined below the top of the roughness? By a mean over a plane $y = \text{constant}$? There are no data in what used to be the sublayer.

(2) What happens to maintain the velocity at the center of the pipe, u_c/u_τ , when the profile displacement becomes very large? Is there a limiting behavior?

(3) How should k be defined, and also R , for the roughness? How does B in equation (27.13) depend on k ? Where should the origin be taken for y ? Is a volume criterion generally useful, as proposed by Nikuradse? See Clauser. What about rib and slot roughness?

These issues are attached to the mixing-length argument, which is implausible. However, it is an occasional success like this one that keeps the mixing length alive. It is astonishing that roughness is under such good control. The defect law is a clue.

(Comment on Nikuradse problem and cite paper on boundary layers. The man who wrote that paper was not bright enough to invent the roughness data, which have been tested and accepted as real by dozens of investigators, including me.)

(Pipeline people are consumers of information, not producers. The cost of making and maintaining smooth pipe is probably greater than the cost of pumping through a commercially rough pipe.)

2.7 Polymers

2.7.1 Friction

Two problems that seem at least superficially to be related are the effects of surface roughness and the effects of high-molecular-weight polymers on flow of liquids past a smooth wall. Most of the work with polymers has been carried out in pipe flow, because the surface friction can be unambiguously determined from the pressure gradient.

It was discovered independently by two groups about 1945 that a very dilute solution of a long-chain polymer in a suitable solvent has remarkable properties in reducing the pressure loss in pipe flow. Important names include Metzner and Virk for the period 1965-1975 when most of the work was done.

Difficulties include degradation by pumps, so that the most systematic data have been obtained in one-pass systems. Temperature matters; so does pH. There are problems with probes, either hot-film or pitot-static probes. Mixing of solutions requires care. The LDV is hard to use in a circular pipe.

Taylor's four-roller apparatus is sometimes used to generate a strain field for studying the question of a critical velocity or a critical strain rate.

A characteristic dimensionless number is the Deborah number,

$$De = \epsilon\tau \quad (2.198)$$

where ϵ is strain rate and τ is some characteristic physical or chemical time for the polymer. A packed bed of particles can be used for the same purpose.

The effect of a polymer is to raise the logarithmic part of the mean velocity profile, as if there exists a concept of negative roughness. The effect on the friction coefficient is to cause a decrease, toward but never to the curve for laminar flow. Virk has a special limit curve.

It is very difficult to make this association plausible, except that roughness and polymer both affect primarily the flow in the sublayer.

Remarks on handout.

Most experiments use gravity-fed pipe flow.

Tomita. This is the same pipe and same polymer. Figure 5 shows critical shear rate constant but R changing? Figure 6 shows limit independent of polymer (see Virk).

Huang. Used cone-plate viscometer to measure ν independently. Tubes tend to be very small, to fit in a bath, and involve very large pressure drops. Solutions remain Newtonian at concentrations used. Figure 9: note $\Delta u/u_\tau$ is proportional to square root of concentration.

Janberg. Nice velocity profiles; also temperature.

Van Driest. Neglected paper. Note high concentrations. Guar gum is not Newtonian for concentrations above one percent. Note that transition is independent of concentration. Note Fig. 21 for asbestos fibers.

White. Used smooth and rough pipes. Figures 5 and 6 show reversal of effect. Soap also reverses (Fig. 7).

Mizushima and Usui. LDV data do not check asymptotic sublayer.

Rollin and Seyer. Used particle tracing to get profiles. See particularly sublayer profile.

Spangler. Profiles look strange. Derive coordinates in Fig. 6. In Fig. 7b, slope is wrong for polymer.

Virk. Friction asymptote is purely empirical. It has an effect on the profile also. There is some kind of saturation.

2.7.2 Mean velocity

2.7.3 Re Stresses

2.8 Heat transfer

2.8.1 Friction

2.8.2 Mean temperature

2.8.3 Consensus on heat transfer

2.9 Variations on classical pipe flow

2.9.1 Odd shapes

2.9.2 Coiled pipes

2.9.3 Area change

2.9.4 Non-steady flow

2.9.5 Swirl

2.9.6 Wall suction, blowing

Chapter 3

CHANNEL FLOW

3.1 Generalities

3.1.1 Preamble

Channel flow will be taken here to include plane Couette flow, and thus some aspects of lubrication theory. An important application is in ducting for ventilation. There is a strong parallel between pipe flow and channel flow, extending to the techniques used, the laboratories involved, and even the investigators. This parallel does not extend to applications.

3.1.2 Equations and integrals

Channel flow is described by the equations of motion in rectangular coordinates (x, y, z) , with velocity components (u, v, w) . The mean flow is two-dimensional and rectilinear. Thus $v = w = 0$ and $\partial/\partial x = \partial/\partial z = 0$, except for the driving term $\partial p/\partial x$. The continuity equation is automatically satisfied. The momentum equations in the

appendix¹ become

$$0 = -\frac{\partial p}{\partial x} + \frac{\partial}{\partial y} \left(\mu \frac{\partial u}{\partial y} - \overline{\rho u'v'} \right) ; \quad (3.1)$$

$$0 = -\frac{\partial p}{\partial y} - \frac{\partial}{\partial y} (\overline{\rho v'v'}) ; \quad (3.2)$$

$$0 = -\frac{\partial}{\partial z} (\overline{\rho w'w'}) . \quad (3.3)$$

As in pipe flow, the quantities in parentheses do not depend on x , so that

$$\frac{\partial^2 p}{\partial x^2} = \frac{\partial^2 p}{\partial x \partial y} = 0 . \quad (3.4)$$

It follows that

$$\frac{\partial p}{\partial x} = \text{constant} = \frac{dp}{dx} . \quad (3.5)$$

The second equation has the integral

$$p + \overline{\rho v'v'} = p_w = x \frac{dp}{dx} + \text{constant} . \quad (3.6)$$

The shearing stress is conveniently defined as

$$\tau = \mu \frac{\partial u}{\partial y} - \overline{\rho u'v'} \quad (3.7)$$

and equation (3.1) has the integral

$$\tau - \tau_w = y \frac{dp}{dx} \quad (3.8)$$

where the origin for y is taken (say) as the lower channel wall. If the channel height is h , then with $\tau = 0$ at $y = h/2$ and $\tau = -\tau_w$ at $y = h$,

$$\tau_w = -\frac{h}{2} \frac{dp}{dx} . \quad (3.9)$$

This expression can also be obtained by an overall force balance over a length of the channel.

The third equation (3.3) needs a comment about sublayer vortices; see section x. Note that no information is obtained about two of the Reynolds normal stresses, $\overline{u'u'}$ and $\overline{w'w'}$.

¹This appendix was not found.

3.1.3 Laminar flow

If the flow is laminar, the velocity profile is determined by a combination of equations (3.7) and (3.8),

$$\mu \frac{\partial u}{\partial y} - \tau_w = y \frac{dp}{dx} \quad (3.10)$$

with the integral

$$u = \frac{\tau_w}{\mu} \left(y - \frac{y^2}{h} \right) + \text{constant} . \quad (3.11)$$

With $u = 0$ at $y = 0$, the constant of integration is zero. With $u = u_c$ at $y = h/2$,

$$u_c = \frac{\tau_w h}{4} \mu . \quad (3.12)$$

The velocity profile is the parabola

$$\frac{u}{u_c} = 1 - \left(1 - \frac{y}{h/2} \right)^2 . \quad (3.13)$$

The mean velocity is defined by

$$h\tilde{u} = \int_0^h u \, dy . \quad (3.14)$$

Equation (3.13) then implies

$$\tilde{u} = \frac{2}{3} u_c . \quad (3.15)$$

3.1.4 Development length

The same argument and the same numbers apply as for pipe flow.

Chapter 4

THE BOUNDARY LAYER

4.1 Generalities

Since its beginning in an inspired paper by PRANDTL (1905) the literature of boundary-layer theory and practice has become probably the largest single component of the literature of fluid mechanics. The most important and practical cases are often the least understood, because there are few organizing principles for turbulent flow. In fact, a list of these principles almost constitutes a history of the subject. They all are based on experimental results or on particular insight into the meaning of experimental results, sometimes with a strong element of serendipity. They have often also required development of new instrumentation. For example, the first competent measurements in turbulent boundary layers at constant pressure were made in Prandtl's institute at Göttingen by SCHULTZ-GRUNOW (1940). These data extended the validity of the wall law and defect law from pipe flow to boundary-layer flow. The means to this end was the first use of a floating element on a laboratory scale to measure directly the local wall friction. An associated major advance at Göttingen was the development and use of a wind tunnel designed with sound understanding of the relevant fluid mechanics.

Perhaps the most important early use of the boundary-layer concept was the application of KARMAN's momentum-integral equation (1921) to turbulent flows approaching separation, say on airfoils or in diffusers. However, the available data seemed to show the wall friction in a positive pressure gradient increasing rapidly in the downstream direction as separation was approached, rather than decreasing toward zero. This result was not credible, but it could only be displaced by a direct attack based on some reliable method for measuring the wall friction in a pressure gradient. The instrument devised for this purpose at Göttingen by LUDWIEG (1949) was the heated element, which depends for its operation on a link between the equations describing transfer of heat and momentum in low-speed flow near a wall, as described in SECTION 1.2.6 of the introduction. The measured results (LUDWIEG and TILLMANN 1949) showed the friction decreasing in a positive pressure gradient as expected, and the anomalous increase was traced in the thesis by TILLMANN (1947) to three-dimensional mean flow. What was not expected from this research was the observation that the similarity law called the law of the wall proved to be insensitive to pressure gradient, either positive or negative, and also to free-stream turbulence level. This observation made it possible to infer the wall friction very cheaply, by fitting part of the mean-velocity profile to the standard logarithmic formula near the wall.

A few years later, CLAUSER (1954) used this result to support a corresponding generalization of the defect law to certain special boundary-layer flows with pressure gradient. Since the friction velocity is a required element of the defect law, say through demonstration of a constant value for the combination $\delta^* u_\infty / \delta u_\tau$, Clauser's method depended on a cut and try adjustment of the pressure variation. Clauser chose the term "equilibrium" to define the class of flows involved. It is important to appreciate that Clauser's contribution was not a discovery, but an invention.

The next step fell to me when I used Clauser's work to generalize the profile formula to flows not in equilibrium; *i.e.*, not having a defect law, by introducing a second universal component that I called the law of the wake (COLES 1956). I provided a rough phys-

ical interpretation for the formula as a description of a wake-like flow modified by the no-slip condition at the wall. A new profile parameter, which I called Π , measures the relative magnitude of the wake and wall components and is constant for any one of Clauser's equilibrium flows, including the flow at constant pressure.

These concepts involving similarity for turbulent flow will be developed in more detail in this chapter. They are in place and are accepted by most but not all of the fluid-mechanics community. It may or may not be significant that they were almost all contributed by relatively young professionals working at academic or near-academic institutions. Except for the concept of coherent structure, little has been added in the last fifty years, which have seen a steady accumulation of experiments and a gradual and valuable proliferation of turbulence models and direct solutions based on the increasing power of digital computers. In particular, plausible similarity laws for flows with mass transfer, compressibility, and other features are still not available.

In 1957 I proposed a model for equilibrium turbulent boundary-layer flow that was based on an analogy between the laminar equilibrium flows of Falkner and Skan and the turbulent equilibrium flows of Clauser. This model has not been accepted. However, I still see value in it, and I therefore have described it in SECTION 4.10.1 of this chapter. If it is ever to be useful, the model will eventually have to be developed like the Thwaites method for laminar flow, using similarity laws that are compound rather than simple.

My strategy here is first to discuss thoroughly the laminar problem, in the hope that some qualitative analogy with turbulent flow will emerge and will suggest questions whose answers, if found, may lead to better understanding. The first part of this chapter will therefore be concerned with two-dimensional laminar boundary layers. They will be treated within the boundary-layer approximation of PRANDTL (1905), which was derived in CHAPTER 1.

4.1.1 The momentum-integral equation

Karman. An important tool in the boundary-layer trade is an integral relationship first derived by KARMAN (1921) and applied to laminar flow in a companion paper by K. POHLHAUSEN (1921). It may have been this example of practical application that finally brought about the acceptance of the boundary-layer concept by the fluid-mechanics community outside Germany. Incidentally, Karman's powerful paper deserves a high place in the literature of the subject for another and quite different reason, which is that it derived the boundary-layer approximation as a formal limit of the Navier-Stokes equations for small viscosity and it anticipated quite accurately the essence of the method of matched asymptotic expansions, including inner and outer expansions, the matching condition, and the composite expansion.

The raw material needed here consists of the continuity and momentum equations in boundary-layer form, as set out in SECTION 1.3.2. These are written for steady two-dimensional flow of a compressible fluid, since there is no extra cost at this stage for including compressibility and mass transfer. For the present there is also no need to distinguish between laminar and turbulent flow, and both are included in the equations

$$\frac{\partial \rho u}{\partial x} + \frac{\partial \rho v}{\partial y} = 0 \quad , \quad (4.1)$$

$$\frac{\partial \rho u^2}{\partial x} + \frac{\partial \rho uv}{\partial y} = -\frac{dp}{dx} + \frac{\partial \tau}{\partial y} \quad , \quad (4.2)$$

where τ is the shearing stress, laminar or turbulent. The second of these equations can also be written, with the aid of the first, as

$$\rho u \frac{\partial u}{\partial x} + \rho v \frac{\partial u}{\partial y} = -\frac{dp}{dx} + \frac{\partial \tau}{\partial y} \quad . \quad (4.3)$$

It is part of the boundary-layer approximation that the pressure p is no longer treated as a dependent variable, but enters through the boundary conditions imposed by the external flow. A relationship between p and u_∞ follows on evaluating equation (4.3) outside

the boundary layer, where $\partial u/\partial y = \tau = 0$, $u = u_\infty$, and $\rho = \rho_\infty$. Thus

$$\rho_\infty u_\infty \frac{du_\infty}{dx} = -\frac{dp}{dx} . \quad (4.4)$$

There remain two equations for two dependent variables, u and v (and τ , if the flow is turbulent). Begin by integrating both equations from the wall to some value of y within the local boundary layer. Use of the boundary conditions $u = 0$, $v = v_w$, $\tau = \tau_w$ at $y = 0$ yields

$$\rho v - \rho_w v_w = -\int_0^y \frac{\partial \rho u}{\partial x} dy ; \quad (4.5)$$

$$\int_0^y \frac{\partial \rho u u}{\partial x} dy + \rho u v = \int_0^y \rho_\infty u_\infty \frac{du_\infty}{dx} dy + \tau - \tau_w . \quad (4.6)$$

These can be combined in the single equation

$$\int_0^y \frac{\partial \rho u u}{\partial x} dy + u \left(\rho_w v_w - \int_0^y \frac{\partial \rho u}{\partial x} dy \right) = \int_0^y \rho_\infty u_\infty \frac{du_\infty}{dx} dy + \tau - \tau_w . \quad (4.7)$$

The integrals in this expression diverge as $y \rightarrow \infty$, unless the range of y is artificially limited by introducing a boundary-layer thickness. The integrals were left in this condition by Karman, who was concerned with larger issues. Pohlhausen disposed of the divergence by adding to equation (4.7) the identity

$$-\int_0^y \frac{\partial \rho u u_\infty}{\partial x} dy + \int_0^y u_\infty \frac{\partial \rho u}{\partial x} dy = -\int_0^y \rho u \frac{du_\infty}{dx} dy \quad (4.8)$$

to obtain

$$\begin{aligned} \frac{\partial}{\partial x} \int_0^y \rho u (u - u_\infty) dy + \rho_w v_w u + (u_\infty - u) \frac{\partial}{\partial x} \int_0^y \rho u dy + \\ + \frac{du_\infty}{dx} \int_0^y (\rho u - \rho_\infty u_\infty) dy = \tau - \tau_w . \end{aligned} \quad (4.9)$$

Now let $y \rightarrow \infty$. Provided that $(u_\infty - u)$ and $(\rho_\infty u_\infty - \rho u)$ approach zero sufficiently rapidly, there is now convergence;

$$\begin{aligned} \tau_w = \frac{d}{dx} \int_0^\infty \rho u (u_\infty - u) dy - \rho_w v_w u_\infty + \\ + \frac{du_\infty}{dx} \int_0^\infty (\rho_\infty u_\infty - \rho u) dy . \end{aligned} \quad (4.10)$$

Equation (4.10) is the momentum-integral equation in rectangular coordinates for a compressible fluid for laminar or turbulent flow. Other coordinate systems can be treated in the same way.

Gruschwitz. The notation in equation (4.10) can be simplified by defining an integral displacement thickness δ^* as

$$\rho_\infty u_\infty \delta^* = \int_0^\infty (\rho_\infty u_\infty - \rho u) dy \quad (4.11)$$

and an integral momentum thickness θ as

$$\rho_\infty u_\infty^2 \theta = \int_0^\infty \rho u (u_\infty - u) dy . \quad (4.12)$$

These definitions, together with the notation δ^* , θ , were introduced by GRUSCHWITZ (1931). Equation (4.10) becomes

$$\tau_w = \frac{d}{dx} \rho_\infty u_\infty^2 \theta + \rho_\infty u_\infty \delta^* \frac{du_\infty}{dx} - \rho_w v_w u_\infty . \quad (4.13)$$

A different form of this equation is sometimes preferable. Expand the first term on the right into three derivatives, and replace $d\rho_\infty$ by the isentropic equivalent dp/a_∞^2 , a being the speed of sound. When terms are collected, equation (4.13) is replaced by

$$\tau_w = \rho_\infty u_\infty^2 \frac{d\theta}{dx} - \theta \left(2 + \frac{\delta^*}{\theta} - M_\infty^2 \right) \frac{dp}{dx} - \rho_w v_w u_\infty , \quad (4.14)$$

where $M_\infty = u_\infty/a_\infty$. Experiments in adiabatic turbulent flow at nominally constant pressure have been collected by FERNHOLZ and FINLEY (1977). They show that the ratio δ^*/θ increases with increasing Mach number, but less rapidly than M_∞^2 , and that the quantity in parentheses in equation (4.14) changes sign at a Mach number near 2.5 at laboratory Reynolds numbers. Consequently, flow irregularities might be expected to have the least influence on flow description at this Mach number.

The thicknesses δ^* and θ are sometimes denoted by δ^* and δ^{**} or by δ_1 and δ_2 in the European literature. The latter forms are most useful if higher moments are needed. They have simple physical meanings. In the sketch¹, let $y = Y$ be a value of Y well outside the boundary layer. Then the mass flux past the station in the sketch is defined by the stream function

$$\psi(Y) = \int_0^Y \rho u \, dy = \rho_\infty u_\infty Y - \int_0^Y (\rho_\infty u_\infty - \rho u) \, dy = \rho_\infty u_\infty (Y - \delta^*) . \quad (4.15)$$

Thus δ^* is the position of a wall bounding a hypothetical flow that coincides with the given flow at infinity but has the density ρ_∞ and velocity u_∞ throughout. Appropriately, δ^* is called the displacement thickness. It can also be viewed as an integral scale for the profile (need equation). (**Need corresponding argument for θ . See Bradshaw.**)

One potentially valuable property of the momentum-integral equation (4.13) is that it provides a means for determining the wall stress τ_w experimentally, provided that all other factors that control the momentum flux near a wall can be measured. This property is less valuable if du_∞/dx is large and negative, because τ_w is then obtained as a small difference between two large terms, and the calculation is degraded by even slight three-dimensionality.

The momentum-integral equation is at the center of several calculation schemes that represent a boundary-layer flow in terms of a specified family of mean-velocity profiles. The first such scheme

¹This sketch has not been found.

was proposed in K. Pohlhausen's original paper on laminar flow. A variation is discussed in SECTION X. Possible applications to turbulent flow are discussed in SECTION X.²

4.2 Laminar equilibrium flow

4.2.1 The affine transformation

For the rest of this chapter, the fluid will be assumed to be incompressible. The two-dimensional laminar boundary-layer equations for steady flow are

$$\frac{\partial u}{\partial x} + \frac{\partial v}{\partial y} = 0 ; \quad (4.16)$$

$$\rho \left(u \frac{\partial u}{\partial x} + v \frac{\partial u}{\partial y} \right) = -\frac{dp}{dx} + \mu \frac{\partial^2 u}{\partial y^2} . \quad (4.17)$$

If there is no mass transfer, the boundary conditions are the no-slip and streamline conditions at the wall,

$$u(x, 0) = 0 , \quad v(x, 0) = 0 \text{ or } \psi(x, 0) = 0 , \quad (4.18)$$

together with the specification of a free-stream pressure or velocity,

$$p = p(x) \quad \text{or} \quad u(x, \infty) = u_\infty(x) . \quad (4.19)$$

Similarity. The topic to be developed in the next few sections is the topic of laminar similarity. When the equations and boundary conditions that govern a problem are known, as they are here, the purpose of a similarity argument is to decrease the number of independent variables through what usually amounts to an application of group theory. A more physical statement in the present context is that flows with similarity are understood to be in equilibrium, in the sense that all of the processes represented by the terms in the momentum equation (4.17) have the same relative importance everywhere and always. Acceleration, pressure force, and viscous force

²It is not clear what section(s), if any, cover these topics.

are all acting in concert and in continuous equilibrium. In laminar flows with pressure gradient, in particular, vorticity is continuously being generated at the wall and diffusing outward as it is transported downstream. In an equilibrium flow, diffusion cooperates with production and transport to keep the vorticity and velocity profiles in a state of similarity. Finally, there is persuasive evidence that equilibrium flows represent limits to which flows tend provided that the boundary conditions are propitious. **(See “Remarks” paper; cite Libby and Narasimha; mention eigenvalues).**

Another important property of similarity arguments is that they provide a unifying principle for associating different solutions of the two-dimensional Navier-Stokes equations or their boundary-layer approximation. In this chapter, these solutions include the boundary layer at constant pressure (SECTION 4.4.1), which first demonstrated the power of Prandtl’s boundary-layer approximation; the stagnation-point flow (SECTION 4.4.3), which showed that the boundary-layer approximation can sometimes be exact; the sink flow (SECTION 4.4.4), for which the Navier-Stokes equations can be solved exactly for any Reynolds number, allowing the nature of the boundary-layer approximation to be analyzed in arbitrary detail; and the continuously separating boundary layer (SECTION 4.4.5), which raises new and complex issues in boundary-layer theory. These flows are all special solutions of an equation called the Falkner-Skan equation, and they will be discussed separately after this equation has been derived.

The immediate objective is to seek solutions of equations (4.16) and (4.17) in similarity form. To simplify the boundary conditions and avoid some awkward algebra, the dependent variables u and v are first fused in a stream function, ψ , defined in rectangular coordinates by the equation

$$\vec{u}(x, y) = \text{grad } \psi \times \text{grad } z . \quad (4.20)$$

Two vector identities from the introduction,

$$\text{div}(\vec{a} \times \vec{b}) \equiv \vec{b} \cdot \text{curl } \vec{a} - \vec{a} \cdot \text{curl } \vec{b} \quad (4.21)$$

and

$$\text{curl grad } c \equiv 0, \quad (4.22)$$

then imply

$$\operatorname{div} \vec{u} = 0 , \quad (4.23)$$

so that the continuity equation (4.16) is automatically satisfied. The velocity vector lies in the intersection of the surfaces $\psi = \text{constant}$ and $z = \text{constant}$, and the velocity components calculated from equation (4.20) are

$$(u, v, w) = \left(\frac{\partial \psi}{\partial y}, -\frac{\partial \psi}{\partial x}, 0 \right) . \quad (4.24)$$

The use of a stream function reduces equation (4.17) to a third-order equation for a single dependent variable ψ ;

$$\rho \left(\frac{\partial \psi}{\partial y} \frac{\partial^2 \psi}{\partial x \partial y} - \frac{\partial \psi}{\partial x} \frac{\partial^2 \psi}{\partial y^2} \right) = \rho u_\infty \frac{du_\infty}{dx} + \mu \frac{\partial^3 \psi}{\partial y^3} , \quad (4.25)$$

where $u_\infty(x)$ is a given function that has to be specified in each case. Conventional boundary conditions at a solid wall are

$$\psi = 0 , \quad \frac{\partial \psi}{\partial x} = 0 \quad \text{at} \quad y = 0 . \quad (4.26)$$

Equation (4.25) is of parabolic type, with real characteristics $x = \text{constant}$. Integration proceeds in the direction of increasing x , and there is no upstream effect of downstream boundary conditions (see SECTION 4.4.1 and FIGURE 4.1).

Throughout fluid mechanics, sufficient conditions for the property of similarity can often be established by dimensional arguments, provided that the number of global parameters in the problem is not too large or too small. For example, assume the existence of local scales $U(x)$ and $L(x)$, usually representing local free-stream velocity and local layer thickness, respectively, for equation (4.25). When solutions are sought in the form $\psi/UL = f(y/L)$, and no separate dependence on x is allowed, sufficient conditions usually emerge to determine the functions $U(x)$ and $L(x)$ in adequate detail. The method is powerful, and its results are not limited to power laws. Examples can be found in SECTIONS 4.4.6 and 10.1.1.

In this monograph I will usually prefer another more formal and more efficient means to the same end. This method is to determine the affine transformation group for the equations and boundary conditions of a problem. In fact, the theory of Lie groups was originally developed and applied as a method for the solution of partial differential equations, (**Lie, Ovsinnikov, Barenblatt, Bluman and Cole, others**).

4.2.2 The Falkner-Skan equation

What is wanted is an affine transformation that transforms equation (4.25) and its boundary conditions (4.19) and (4.26) into themselves. To discover this transformation, every variable or parameter is mindlessly scaled, or transformed, or mapped, according to a standard program;

$$\begin{aligned} x &= a\hat{x} ; \\ y &= b\hat{y} ; \\ \psi &= c\hat{\psi} ; \\ \rho &= d\hat{\rho} ; \\ \mu &= e\hat{\mu} ; \\ u_\infty &= f\hat{u}_\infty ; \end{aligned} \tag{4.27}$$

where a, b, c, \dots are dimensionless scaling constants that are finite and positive. Some authors (**cite Birkhoof, Sedov**) seek to express all of these constants in terms of one of them through some tedious algebra, but I find this variation to be neither as simple nor as instructive as the one used here.

The result of the mapping (4.27) in the case of equation (4.25) is

$$\frac{dc^2}{ab^2} \hat{\rho} \left(\frac{\partial \hat{\psi}}{\partial \hat{y}} \frac{\partial^2 \hat{\psi}}{\partial \hat{x} \partial \hat{y}} - \frac{\partial \hat{\psi}}{\partial \hat{x}} \frac{\partial^2 \hat{\psi}}{\partial \hat{y}^2} \right) = \frac{df^2}{a} \hat{\rho} \hat{u}_\infty \frac{d\hat{u}_\infty}{d\hat{x}} + \frac{ec}{b^3} \hat{\mu} \frac{\partial^3 \hat{\psi}}{\partial \hat{y}^3} . \tag{4.28}$$

Given that u transforms like $\partial\psi/\partial y$, the corresponding statement for the boundary condition (4.19) is

$$\frac{c}{b} \hat{u}(a\hat{x}, \infty) = f\hat{u}_\infty(a\hat{x}, \infty) . \tag{4.29}$$

The other two boundary conditions (4.18) yield no information. Invariance of the equation and boundary conditions evidently requires

$$\frac{bcd}{ae} = 1, \quad \frac{b^3df^2}{ace} = 1, \quad \frac{c}{bf} = 1 . \quad (4.30)$$

Division of the first of these equations by the second yields the third, which is therefore redundant; u_∞ and u transform according to the same rule.

Although the dependent variable is $\psi(x, y)$, the essence of most descriptive processes is the functional relationship between $u = \partial\psi/\partial y$ and y at constant x . This observation suggests that the first two of equations (4.30) should be revised to isolate c and b , which are the scaling factors for ψ and y , respectively. Other strategies will work, but may be awkward. The result can be stated as

$$\frac{c^2d}{aef} = 1, \quad \frac{b^2df}{ae} = 1 . \quad (4.31)$$

Now let the affine-transformation table (4.27) be interpreted as a group of definitions for a, b, c, \dots , and let these definitions be substituted into equations (4.31). Two invariants of the transformation appear;

$$\frac{\psi}{(\nu u_\infty x)^{1/2}} = \frac{\hat{\psi}}{(\hat{\nu} \hat{u}_\infty \hat{x})^{1/2}}, \quad \left(\frac{u_\infty}{\nu x}\right)^{1/2} y = \left(\frac{\hat{u}_\infty}{\hat{\nu} \hat{x}}\right)^{1/2} \hat{y} . \quad (4.32)$$

These combinations are dimensionless by construction, since each term in equation (4.25) must have the same physical dimensions.

A non-trivial reasoning process described in SECTION 1.3.2 of the introduction implies finally that similarity solutions are to be found by adopting the ansatz

$$A \frac{\psi}{(\nu u_\infty x)^{1/2}} = f \left[B \left(\frac{u_\infty}{\nu x}\right)^{1/2} y \right] = f(\eta) , \quad (4.33)$$

in which two dimensionless scaling constants A and B are included for later use in normalizing the final differential equation and its boundary conditions. No harm is done if the step from equations

(4.32) to equation (4.33) is treated as intuitive rather than exact. The ansatz (4.33) shows explicitly that the variables ψ , x , and y should be combined as $\psi/x^{1/2}$ and $y/x^{1/2}$. The appearance of $\nu^{1/2}$ is a more subtle question already discussed in SECTION 1.3.2.

When the stream function from equation (4.33) is inserted in the momentum equation (4.25), four transport terms are generated, but two of these cancel. This property is typical of similarity analyses in the boundary-layer theory of viscous shear flows. The result can be written

$$2AB f''' + \left(1 + \frac{x}{u_\infty} \frac{du_\infty}{dx}\right) f f'' + 2 \frac{x}{u_\infty} \frac{du_\infty}{dx} \left(\frac{A^2}{B^2} - f' f'\right) = 0 \quad , \quad (4.34)$$

where primes indicate differentiation with respect to η , the argument of f in equation (4.33). From left to right, the original source of the four terms in f is viscous (highest derivative), transport (nonlinear), pressure force (lacking f), and again transport. If η is to be the only independent variable, the coefficients cannot depend on x , and it is necessary to require

$$\frac{x}{u_\infty} \frac{du_\infty}{dx} = \text{constant} = m \text{ (say)} \quad . \quad (4.35)$$

The external flow condition is therefore specified by the power law

$$u_\infty \sim x^m \quad . \quad (4.36)$$

This conclusion ignores the question of algebraic signs for quantities inside the square roots in equation (4.33), a question that will be taken up in SECTION 4.3.1. With this reservation, equation (4.34) becomes

$$2AB f''' + (1+m) f f'' + 2m \left(\frac{A^2}{B^2} - f' f'\right) = 0 \quad . \quad (4.37)$$

4.2.3 Normalization

It remains to choose the constants A and B , mainly on the basis of esthetic considerations. On the way from equation (4.25) to equation

(4.37), use was made of the derivative relationship

$$u = \frac{\partial \psi}{\partial y} = \frac{B}{A} u_{\infty} f' . \quad (4.38)$$

A convenient condition on A and B is therefore

$$7A = B , \quad (4.39)$$

because it yields the simple result

$$\frac{u}{u_{\infty}} = f'(\eta) . \quad (4.40)$$

This same condition (4.39) is also suggested by the form of the third term in the differential equation (4.37). The boundary conditions (4.18) and (4.19) become

$$f(0) = f'(0) = 0, \quad f'(\infty) = 1 . \quad (4.41)$$

An operator. It is typical of similarity arguments for laminar flow in rectangular coordinates that they lead to an operator $f''' + f f''$, sometimes with numerical coefficients that differ from one problem or one author to another. I propose to give this operator $f''' + f f''$ a uniform aspect, free of coefficients, throughout this monograph. I therefore take in equation (4.37)

$$\frac{1+m}{2AB} = \frac{1+m}{2A^2} = 1 , \quad (4.42)$$

so that, still without regard to signs,

$$A = B = \left(\frac{1+m}{2} \right)^{1/2} . \quad (4.43)$$

Equation (4.37) is reduced to a one-parameter equation,

$$f''' + f f'' + \frac{2m}{1+m} (1 - f' f') = 0 , \quad (4.44)$$

and the perfected form of the ansatz (4.33) is

$$\left(\frac{1+m}{2\nu u_{\infty} x} \right)^{1/2} \psi = f \left[\left(\frac{(1+m)u_{\infty}}{2\nu x} \right)^{1/2} y \right] = f(\eta) . \quad (4.45)$$

The equation (4.44) with the boundary conditions (4.41) is called the Falkner-Skan equation, after the authors of the fundamental paper on the subject (FALKNER and SKAN 1931). When related equations appear in other parts of this book, the term Falkner-Skan will sometimes be used to emphasize the community of similarity formulations for various laminar shear flows.

Hartree. HARTREE (1937) introduced another notation β for the single parameter of the problem,

$$\beta = \frac{2m}{1+m} \quad \text{or} \quad m = \frac{\beta}{2-\beta} , \quad (4.46)$$

so that equation (4.45) can also be written

$$\left(\frac{1}{(2-\beta)\nu u_\infty x} \right)^{1/2} \psi = f \left[\left(\frac{u_\infty}{(2-\beta)\nu x} \right)^{1/2} y \right] = f(\eta) . \quad (4.47)$$

Neither notation, β or m , has any particular mnemonic value, but both are established by long usage. The change from m to β in equation (4.44) yields the commonly accepted form of the Falkner-Skan equation,

$$f''' + ff'' + \beta(1 - f'f') = 0 , \quad (4.48)$$

with a single parameter β (or m). Both notations can be useful for identifying a particular member of the family of Falkner-Skan flows, depending on the circumstances. These circumstances will be developed in SECTION 4.4.6 below. For the present, note from equations (4.46) that there are two exceptional cases. The first is the case $m = -1$, $\beta = \pm\infty$, and the second is the case $\beta = 2$, $m = \pm\infty$. These cases are discussed in detail in SECTION 4.4.4 and SECTION 4.4.6, respectively.

Displacement. The notation and normalization adopted here are the ones often found in the literature. For later use (see SECTION 4.6.1), expressions for the surface friction and the two important thickness scales of the boundary layer are

$$\delta^* = \int_0^\infty \left(1 - \frac{u}{u_\infty} \right) dy = \left(\frac{2\nu x}{(1+m)u_\infty} \right)^{1/2} \int_0^\infty (1 - f') d\eta ; \quad (4.49)$$

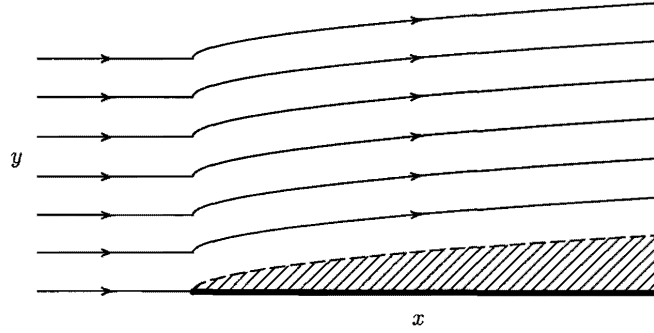


Figure 4.1: The displacement effect in the free stream for the Blasius boundary layer in rectangular coordinates. The hatched area extends to $y = \delta^*$

$$\theta = \int_0^{\infty} \frac{u}{u_{\infty}} \left(1 - \frac{u}{u_{\infty}}\right) dy = \left(\frac{2\nu x}{(1+m)u_{\infty}}\right)^{1/2} \int_0^{\infty} f'(1-f') d\eta ; \quad (4.50)$$

$$\tau_w = u \left(\frac{\partial u}{\partial y}\right)_w = \left(\frac{(1+m)\rho^2 \nu u_{\infty}^3}{2x}\right)^{1/2} f''(0) . \quad (4.51)$$

With $u_{\infty} \sim x^m$, these imply

$$\delta^* \sim x^{(1-m)/2} ; \quad (4.52)$$

$$\theta \sim x^{(1-m)/2} ; \quad (4.53)$$

$$\tau_w \sim x^{(3m-1)/2} . \quad (4.54)$$

The displacement thickness δ^* is an effective thickness for the boundary layer profile, as shown earlier in FIGURE 4.1. This thickness defines the apparent shape of a body plus boundary layer. Rewrite equation (4.49) as (see SECTION 4.4.1)

$$C = \int_0^{\infty} (1-f') d\eta = \delta^* \left(\frac{(1+m)u_{\infty}}{2\nu x}\right)^{1/2} , \quad (4.55)$$

and note also that

$$\lim_{\eta \rightarrow \infty} \int_0^{\eta} (1 - f') d\eta = \lim_{\eta \rightarrow \infty} (\eta - f) = \text{constant} = C \quad (4.56)$$

outside the boundary layer, where η is large enough so that the integrand is effectively zero. The constant C is defined by equation (4.55), and the dimensionless relation $f = \eta - C$ becomes in physical coordinates

$$\psi = u_{\infty}(y - \delta^*) . \quad (4.57)$$

This expression does not describe an irrotational flow, except in one special case $m = 1$, $\beta = 1$, for which δ^* does not depend on x . This special case is taken up in SECTION 4.4.3.

4.2.4 Potential flow past a wedge

The physical significance of m is clear enough in equation (4.36). The physical significance of β was pointed out by Falkner and Skan, who recognized that their flows corresponded to plane potential flow past a wedge of included angle $\pi\beta$, as shown at the right in FIGURE 4.2. The flow in the upper half plane is most easily found by a conformal mapping, with the flow in the lower half plane obtained by reflection in the x -axis. For uniform flow in the ζ -plane at the left, the complex potential is

$$F(\zeta) = \phi + i\psi = U_0\zeta \quad (\text{say}). \quad (4.58)$$

Assume a mapping of the form

$$\zeta = L_0^{1-p} z^p e^{i\sigma} , \quad (4.59)$$

where L_0 has the dimension of length, and the parameter σ allows a possible rotation. Put $\zeta = R e^{i\Theta}$ and $z = r e^{i\theta}$ to obtain

$$\Theta = p\theta + \sigma . \quad (4.60)$$

The mapping in the upper half plane in the sketch requires $\theta = \pi\beta/2$ when $\Theta = 0$, and $\theta = \pi$ when $\Theta = \pi$. These two conditions imply for p and σ

$$p = \frac{2}{2 - \beta}, \quad \sigma = -\frac{\pi\beta}{2 - \beta} . \quad (4.61)$$

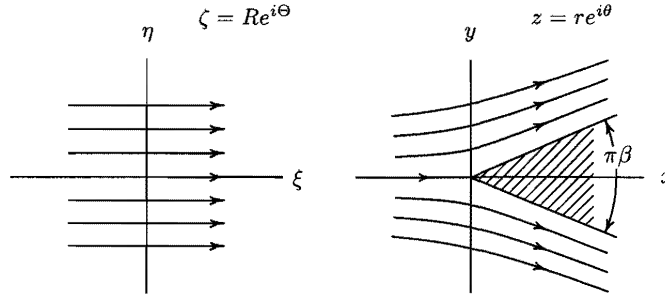


Figure 4.2: Potential flow past a wedge of total angle $\pi\beta$.

The complex potential in the z -plane is

$$F(z) = U_0\zeta(z) = U_0L_0^{-\frac{\beta}{(2-\beta)}} r^{\frac{2}{2-\beta}} e^{i\left(\frac{2\theta-\pi\beta}{2-\beta}\right)} = \phi + i\psi . \quad (4.62)$$

The stream function,

$$\psi = U_0L_0^{-\frac{\beta}{(2-\beta)}} r^{\frac{2}{2-\beta}} \sin\left(\frac{2\theta-\pi\beta}{2-\beta}\right) , \quad (4.63)$$

vanishes when $\theta = \pi$ and when $\theta = \pi\beta/2$, as desired. The radial velocity is

$$u_r = \frac{1}{r} \frac{\partial\psi}{\partial\theta} = \frac{2U_0L_0^{-\frac{\beta}{(2-\beta)}}}{2-\beta} r^{\frac{\beta}{2-\beta}} \cos\left(\frac{2\theta-\pi\beta}{2-\beta}\right) . \quad (4.64)$$

On the wall, where $\theta = \pi\beta/2$, this is

$$u_r = \frac{2U_0L_0^{-\frac{\beta}{2-\beta}}}{2-\beta} r^{\frac{\beta}{2-\beta}} . \quad (4.65)$$

With u_r replaced by u_∞ , r by $x > 0$, and $\beta/(2 - \beta)$ by m , equation (4.65) is equivalent to $u_\infty \sim x^m$. The Falkner-Skan flows therefore represent the boundary layer on a wedge with total included angle $\pi\beta$, at least in the range $-2 < \beta < 2$.

4.3 Morphology of the Falkner-Skan flows

4.3.1 The parameter β or m

There is an important and sometimes overlooked question concerning algebraic signs in equations (4.45) and (4.47). If the variables f and η are to be real, the product $u_\infty x$ (or the ratio u_∞/x) must have the same sign as the parameter $(1 + m)$ or $(2 - \beta)$. The point is made graphically in FIGURE 4.3, where m is plotted against β to establish the morphology of the Falkner-Skan flows. Either of equations (4.46) can be written

$$(m + 1)(\beta - 2) = -2 . \quad (4.66)$$

In these variables, the relationship between $m + 1$ and $\beta - 2$ is described by two hyperbolas in the second and fourth quadrants. The dashed lines in the figure are the asymptotes $m = -1$ and $\beta = 2$. These asymptotes mark the occurrence of a change in sign of x or u_∞ . GOLDSTEIN (1939, 1965) chose to require x to be always positive and therefore referred to flows with $\beta > 2$ as backward boundary layers, with u_∞ negative. For the sake of a consistent physical interpretation, I prefer to require u_∞ to be always positive. That is, the flow is always directed from left to right in (x, y) coordinates. Consequently, it is x that must be negative if $\beta > 2$.

For purposes of graphical description, the Falkner-Skan boundary layers can be associated not only with flow past a symmetrical wedge, at least for a certain range of β , but also in an equally qualitative way with flow in an equivalent channel of height $h(x)$. Given a variation of u_∞ with x as $u_\infty \sim |x|^m$, the one-dimensional mass-conservation law $\rho u_\infty h = \text{constant}$ then implies a definite variation of channel height h with x as $h \sim |x|^{-m}$. This variation is displayed in a number of small inserts, or icons, in FIGURE 4.3. Several equiv-

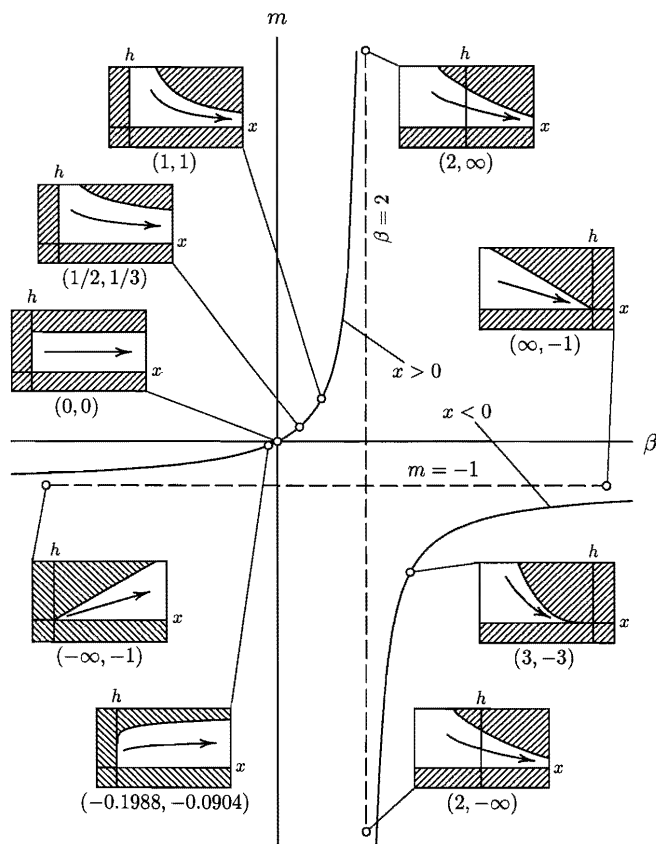


Figure 4.3: Morphology of the Falkner-Skan boundary layers in terms of the parameters (β, m) . The various icons depict channel flows with channel heights proportional to $1/u_\infty$.

alent channels are sketched, including various flows discussed in detail in the following sections. In particular, it is important whether the asymptote $m = -1$ is approached from above (source flow) or from below (sink flow), but not whether the asymptote $\beta = 2$ is approached from the left or from the right.

Consider first the upper branch in FIGURE 4.3, where $(m+1)$ is positive and therefore u_∞ and x have the same sign. It follows that x is positive, and the flow is to the right, away from the origin. If also m is positive, as for the cases $m = 1/3$ and $m = 1$, for example, the origin is a stagnation point, and the equivalent channel is convergent, with infinite velocity at $x = \infty$. If $m+1$ is positive, but m is negative, as for the case $m = -0.1988$, the velocity u_∞ is infinite at the origin, and the stagnation point is at plus infinity.

Now consider the lower branch in FIGURE 4.3, where u_∞ and x have opposite signs. It follows that x is negative, as shown for the sink flow, and the flow is always toward the origin from $x = -\infty$. Since m on this branch is always negative, the stagnation point is at minus infinity and the velocity is infinite at the origin.

4.3.2 Some numerical particulars

Integration. From the point of view of apparent speed and simplicity, the method of first resort for integrating the Falkner-Skan equation,

$$f''' + f f'' + \beta(1 - f' f') = 0 \quad , \quad (4.67)$$

is probably the one that is usually associated with the name of WEYL (1942), although the method was used earlier by PIERCY and PRESTON (1936) for the Blasius equation, by HARTREE (1937) for the Falkner-Skan equation, and perhaps by others. This method determines $f(\eta)$ through successive approximations $f_n(\eta)$ that each satisfy a linear equation for f_n'' ,

$$f_n''' + f_{n-1} f_n'' + \beta(1 - f_{n-1}' f_{n-1}') = 0 \quad (4.68)$$

Equation (4.68) is in a standard form,

$$\frac{dy}{dx} + P(x)y = Q(x) \quad , \quad (4.69)$$

with $y = f''$, $P = f$, and $Q = -\beta(1 - f'f')$. This standard form is soluble by quadratures as

$$y = e^{-\int P dx} \left\{ \int Q e^{\int P dx} dx + K \right\}, \quad (4.70)$$

where K is a constant of integration. Almost any reasonable first approximation will do for the classical boundary-layer regime. For $\beta = 0$, for example, Piercy and Preston used $f_0 = \eta$, meaning uniform flow. The next approximation f_1 is then the solution of the boundary-layer form of the Oseen equations; namely, $f_1''' + \eta f_1'' = 0$. This linear equation also governs the unsteady laminar boundary layer associated with the impulsive motion of a flat plate in its own plane, as discussed in SECTION 1.3.5 of the introduction. Higher approximations must proceed numerically. By a process amounting to numerical continuation, an efficient first choice is a solution for a closely adjacent value of β , if one is available. Practical details of the Weyl method can be found in two fine papers by KATAGIRI (1969, 1986), where an averaging scheme first proposed by Hartree is further developed for assuring and improving the convergence of successive approximations, since experience shows that convergence is not automatic.

A more frequently used method is the shooting method described by CEBECI and KELLER (1971) and already mentioned in SECTION 4.4.1.³ The procedure integrates the two-point boundary value problem from the wall to the free stream by aiming at the outer boundary condition $f'(\infty) = 1$ from an iterated inner boundary condition $f''(0)$. SMITH (1954) pointed out that there is a strong qualitative difference in the behavior of the shooting trajectories for positive and for negative values of β . Smith's figure 1 is reproduced here as my FIGURE 4.4. (**Locate and scan this figure.**) In the language of autonomous linear equations, the figure suggests that the integration is toward a node if β is negative and toward a saddle point if β is positive. This difference is the subject of the present section. A quantitative explanation is difficult, because these topological concepts are strictly defined only for a first-order autonomous

³Several places in ms indicate this section and Section 4.4.1, Blasius flow, were originally in the opposite sequence. These cross references have been left as found.

PLACEHOLDER

Figure 4.4: (Figures from A.M.O. Smith)

system. The brief account that follows is based on presentations by STOKER (1950), by FRIEDRICHS (1965) and by PERRY and FAIRLIE (1974) of material that dates back to POINCARÉ (1892). The notation is essentially that of Perry and Fairlie, with vector components ordered as $(u, v) \sim (U, V) \sim (\text{abscissa}, \text{ordinate})$.

Critical points. Consider an ordinary first-order differential equation of the form

$$\frac{dv}{du} = \frac{G(u, v)}{F(u, v)} = \frac{\dot{v}}{\dot{u}} , \quad (4.71)$$

where the notation \dot{u}, \dot{v} implies an option of expressing both variables as functions of a single variable, say t . If this latter variable t does not appear explicitly in equation (4.71), the system is said to be autonomous, and its behavior is fully described by integral curves in the (u, v) plane (usually called the phase plane) and by appropriate initial and boundary conditions.

For an autonomous system, integral curves in the phase plane have a local direction whose slope is dv/du . This direction is well defined except when

$$\frac{dv}{du} = \frac{0}{0} . \quad (4.72)$$

A point where this condition is satisfied is called an isolated singular point or critical point. It is usually convenient to displace the vari-

ables so that each singular point in turn lies at the origin in (u, v) space and to linearize in terms of the displaced variables. Provided that this can be done, a standard form is

$$\begin{pmatrix} \dot{u} \\ \dot{v} \end{pmatrix} = \begin{pmatrix} a & b \\ c & d \end{pmatrix} \begin{pmatrix} u \\ v \end{pmatrix}, \quad (4.73)$$

or

$$\dot{u} = au + bv, \quad \dot{v} = cu + dv. \quad (4.74)$$

The behavior of the system near the singular point depends on the matrix of coefficients in equation (4.73). The problem can be restated in terms of the eigenvalues of this matrix, which are the numbers λ satisfying **(more on eigenvalue)**

$$\begin{vmatrix} a - \lambda & c \\ b & d - \lambda \end{vmatrix} = 0 \quad (4.75)$$

or

$$\lambda^2 + p\lambda + q = 0, \quad (4.76)$$

where

$$p = -(a + d), \quad q = ad - bc. \quad (4.77)$$

Thus

$$\lambda = \frac{-p \pm (p^2 - 4q)^{1/2}}{2}. \quad (4.78)$$

Stoker gives a table, and Perry and Fairlie give a figure, that are each

equivalent to the array (**check again**)

Parameters			Singularity
$p^2 - 4q$	q	p	
positive	positive	positive	stable node
positive	positive	negative	unstable node
positive	negative		saddle
0		positive	stable node
0		negative	unstable node
negative		positive	stable focus
negative		0	center
negative		negative	unstable focus

For the last three cases, the eigenvalues are complex conjugates. The term stable (unstable) means here that an integral curve drawn for increasing values of t ends (begins) at the critical point.

Sink flow. There is only one Falkner-Skan flow for which the material just given is directly applicable. This is the sink flow discussed in SECTION 4.4.4, where variables that are appropriate for large β are shown to be

$$\begin{aligned}
 F &= (\beta - 2)^{1/2} f = \left(-\frac{1}{\nu u_\infty x} \right)^{1/2} \psi , \\
 Y &= (\beta - 2)^{1/2} \eta = \left(-\frac{u_\infty}{\nu x} \right)^{1/2} y .
 \end{aligned}
 \tag{4.79}$$

In these variables the Falkner-Skan equation becomes

$$F''' + \frac{FF''}{(\beta - 2)} + \frac{\beta}{(\beta - 2)}(1 - F'F') = 0 , \quad (4.80)$$

where the prime now denotes differentiation with respect to Y . In the limit $\beta \rightarrow \infty$,

$$F''' + 1 - F'F' = 0 . \quad (4.81)$$

The boundary conditions are the usual ones,

$$F(0) = F'(0) = 0 , \quad F'(\infty) = 1 . \quad (4.82)$$

Equations (4.67) and (4.80) are identical when $\beta = 3$. The terms small (large) β might conveniently be used to refer to values of β that are smaller (larger) than three.

Sink flow is a special case within the Falkner-Skan family because the transformation from $f(\eta)$ to $F(Y)$ and the limiting process $\beta \rightarrow \infty$ in equation (4.80) together remove the term FF'' that would otherwise defeat the requirement of autonomy for the linearized equation, because F is formally replaced by $Y + \text{constant}$. The first integral of equation (4.81) is equation (4.142),

$$(F'')^2 + 2F' - \frac{2}{3}(F')^3 = \text{constant} = 2C , \quad (4.83)$$

which connects two variables F' and F'' that present themselves for use as a phase space. The boundary condition at infinity is satisfied if $C = 2/3$, and the associated value of $F''(0)$ is $2/\sqrt{3} = 1.154701$. The isolated critical point of interest is at infinity in physical space, which is to say at the point $(0, 1)$ in phase space (F'', F') . To study this point, prepare for linearization by changing the variables to

$$U = F'' , \quad V = F' - 1 . \quad (4.84)$$

Then, by construction from equation (4.81),

$$\frac{dV}{dU} = \frac{F''}{F'''} = \frac{U}{(1 + V)^2 - 1} . \quad (4.85)$$

For small values of U and V , this is approximately

$$\frac{dV}{dU} = \frac{U}{2V} , \quad (4.86)$$

which has the required form $0/0$ at the new origin. In terms of the model (4.74),

$$a = 0, \quad b = 2, \quad c = 1, \quad d = 0 , \quad (4.87)$$

so that

$$p = 0, \quad q = -2, \quad p^2 - 4q = 8 . \quad (4.88)$$

The singularity is a saddle, and the eigenvalues are $\lambda = \pm\sqrt{2}$. Recall that an integral curve satisfies the Falkner-Skan equation, while a solution satisfies the boundary conditions as well. The integral curve defined by equation (4.83) with $C = 2/3$ is plotted in FIGURE 4.5. The desired solution, which is the portion of this integral curve that joins the two boundary points, is accented. Two other integral curves for $C = 0$ and $C = 4/3$ are also plotted to clarify the topology. The slope of the integral curves at the saddle is given by equation (4.86), whose integral $U^2 = 2V^2$ implies to first order

$$\frac{dF'}{dF''} = \frac{dV}{dU} = \frac{U}{2V} = \pm \frac{1}{\sqrt{2}} . \quad (4.89)$$

It is not hard to visualize (or calculate) the integral curves in FIGURE 4.5 that would be obtained by shooting from initial values of $F''(0)$ slightly larger or smaller than the known exact value $2/\sqrt{3}$. Without an appreciation of the topology of the integral curves, their behavior might indeed seem to be mysterious. The benefit derived from an appreciation of topology is the primary reason that I prefer to use the shooting method rather than the Weyl method to integrate the Falkner-Skan equation.

Further examples. For other values of β the term ff'' or FF'' appears in the Falkner-Skan equation, and linearization with, say, $f'(\eta) \rightarrow 1$ or $f(\eta) \rightarrow \eta + \text{constant}$ leads to a term $\eta f''$ or YF'' that cannot be avoided. The linearized equation is no longer autonomous, and the discussion of classical singular points loses all

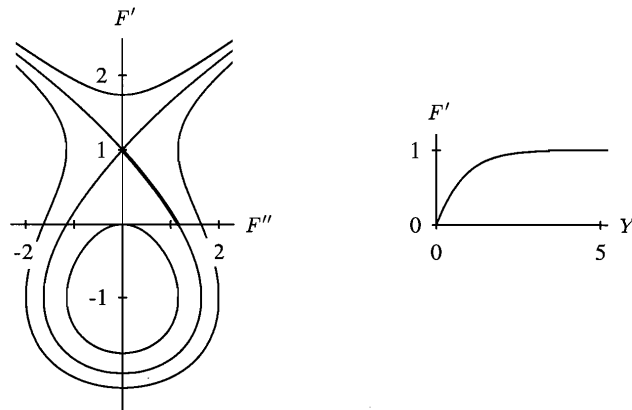


Figure 4.5: Saddle structure at $Y = \infty$ of the Falkner-Skan boundary layer for $\beta = \infty$ (sink flow, $F''(0) = 1.154701$). The integral curves are drawn for $C = 0, 2/3, 4/3$ in equation (4.83).

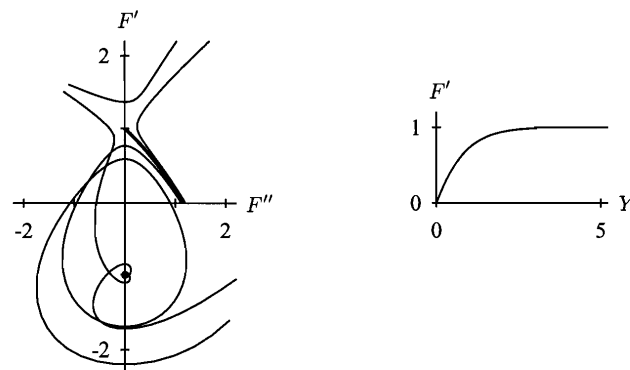


Figure 4.6: Pseudo-saddle structure at $Y = \infty$ of the Falkner-Skan boundary layer for $\beta = 5$. The conventional integral curves are drawn for $f''(0) = 1.11981, 1.16981, 1.19981$. Two other integral curves begin at $(f, f', f'') = (5, 1.5, -1.2)$ and $(10, 1.6, -1.1)$.

rigor but not all relevance. For the case $\beta = 5$, FIGURE 4.6 shows several integral curves, again in variables suitable for large β . The regularity of FIGURE 4.5 has been lost, but there remains near the point $(0, 1)$ a feature having some resemblance to a saddle. Three of the curves in the figure are generated by the shooting method, with initial values $F''(0) = 1.11981, 1.16981, \text{ and } 1.19981$. The second of these includes the solution. Portions of two other integral curves are also displayed in order to better define a full neighborhood of the singularity. Because FIGURE 4.6 shows only projections of integral curves on the (F'', F') plane, these curves do not necessarily intersect in (F'', F', η) -space, and the hypothetical isolated singular point in question is not a saddle in the usual sense. It is, however, a distinguished point in the sense that it repels all projected integral curves in its neighborhood except one, which is the desired solution. Note in FIGURES 4.5 and 4.6 and elsewhere that the point $(0, -1)$ also occupies a special place in the structure of integral curves.

For the same value $\beta = 5$ as in FIGURE 4.6, another set of integral curves is shown in FIGURE 4.7 to illustrate a conclusion first drawn by IGLISH (1954) that solutions of the Falkner-Skan equation for positive β are unique only if backflow is prohibited. The curves in FIGURE 4.7 are for the initial values $F''(0) = 1.11430, 1.11447, 1.16981$, and they are all solutions because they all satisfy the boundary condition $F' = 1$ at infinity. However, the profiles show $0, 1, 2 \dots$ excursions into negative F' -space before eventually satisfying this boundary condition. Uniqueness is restored if the restriction $0 \leq F' < 1$ is imposed, or, in a very loose sense, if a condition of earliest approach to the boundary condition $F'(\infty) = 1$ is enforced. For $\beta \geq 1$, families of solutions of this kind were first reported by CRAVEN and PELETIER (1972b) and were studied in more detail by BOTTA, HUT, and VELDMAN (1986). The latter authors also noted the existence of periodic integral curves for $\beta > 1$ under certain conditions and listed the calculated period in η for a number of cases. In FIGURE 4.5 and equation (4.83), for example, such a condition is $-2/3 < C < 2/3$.

FIGURE 4.8 shows some integral curves for $\beta = 1$ and $f''(0) = 1.18259, 1.23259, 1.28259$, as well as two additional integral curves

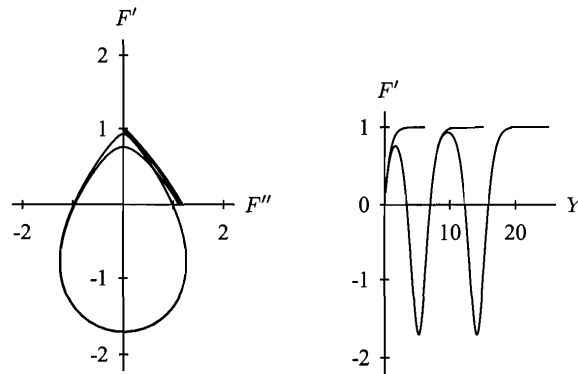


Figure 4.7: Some oscillating solutions of the Falkner-Skan boundary layer equation for $\beta = 5$. The integral curves are drawn for $F''(0) = 1.11430, 1.11447, 1.16981$. The last of these is the classical solution.

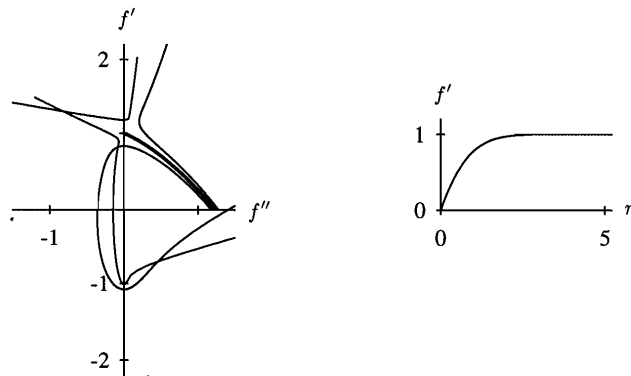


Figure 4.8: Pseudo-saddle structure at $\eta = \infty$ of the Falkner-Skan boundary layer for $\beta = 1$. The conventional integral curves are drawn for $f''(0) = 1.18259, 1.23259, 1.28259$. Two other integral curves begin at $(f, f', f'') = (5, 1.48, -1.2)$ and $(1, 1.48, -1.9)$.

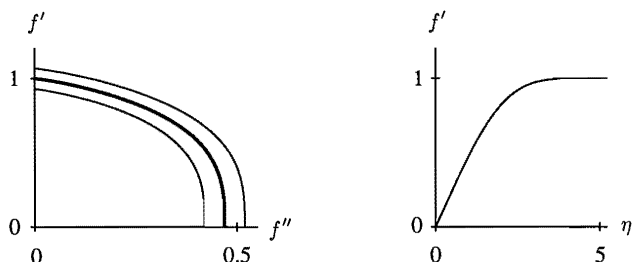


Figure 4.9: Neutral structure at $\eta = \infty$, showing Töpfer mapping of the Falkner-Skan boundary layer for $\beta = 0$ (Blasius flow). The curves are drawn for $f''(0) = 0.4196, 0.4696, 0.5196$.

that pass close to the point $(0, 1)$. The display is topologically similar to that in FIGURE 4.6.

The Blasius flow for $\beta = 0$, shown in FIGURE 4.9 is a special case intermediate between node and saddle in the sense that it does not show either pattern. Any integral curve in the first quadrant of the phase plane can be transformed into the desired solution by the Töpfer mapping $\varphi(\eta) = cf(c\eta)$, where c is a suitable positive constant. This mapping is discussed in SECTION 4.4.1, and implies, according to equation (4.116),

$$\frac{[f'(\infty)]^{3/2}}{f''(0)} = \text{constant} = \frac{1}{0.4696\dots} \quad (4.90)$$

COPPEL (1960) pointed out that if f' becomes constant in the Falkner-Skan equation (4.67) as η goes to infinity, so that f'' (more accurately, ff'') and f''' go to zero, then necessarily $f'(\infty) = \pm 1$, except when $\beta = 0$. Part of this remark has its origin in a particular normalization of boundary-layer variables, but not all. The exception for $\beta = 0$ is what informs the Töpfer mapping and the node/saddle

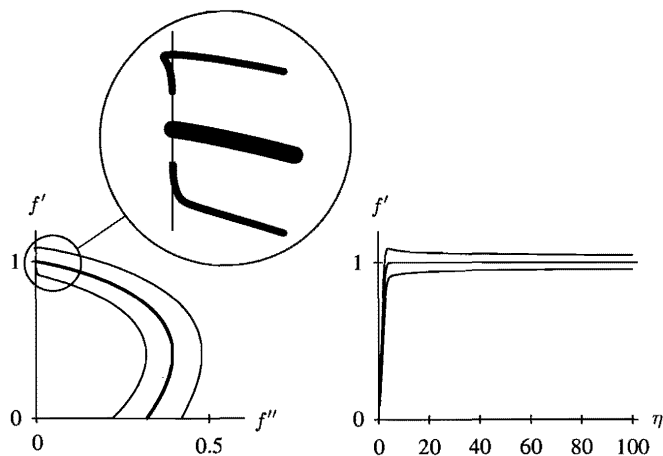


Figure 4.10: Pseudo-node structure at $\eta = \infty$ of the Falkner-Skan boundary layer for $\beta = -0.1$ (upper branch). The integral curves are drawn for $f''(0) = 0.21927, 0.31927, 0.41927$. Note the compressed scale at right to show the extremely slow algebraic approach of f' to the outer boundary condition when $f''(0)$ is not correct.

dichotomy discussed here.

Finally, consider values of β that are negative, but not more negative than -0.1988 . It has long been known that there are two branches of solutions, depending on whether or not the condition $0 \leq f' < 1$ is enforced. In the first instance, the solutions lie on the upper branch first explored by FALKNER and SKAN (1931) and HARTREE (1937). In the second instance, the solutions lie on the lower branch first explored by STEWARTSON (1954). Phase planes for these two branches are depicted in FIGURES 4.10 and 4.11 for the case $\beta = -0.1$. In both figures, it seems that all integral curves eventually satisfy the outer boundary condition, as would be the case if a singularity behaving like a stable node were present at $\eta = \infty$.

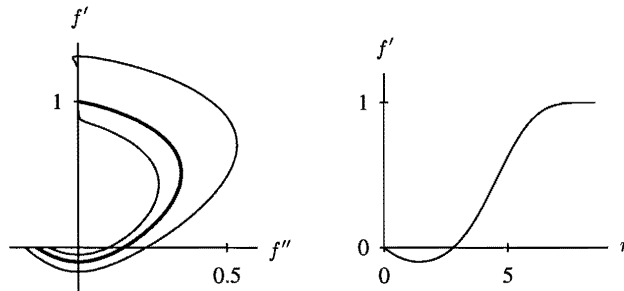


Figure 4.11: Pseudo-node structure at $\eta = \infty$ of the Falkner-Skan boundary layer for $\beta = -0.1$ (lower branch). The integral curves are drawn for $f''(0) = -0.180545, -0.140545, -0.100545$.

The integral curves in the phase plane for negative β form a bundle, all with the same steep slope at the singularity in the left figure, together with a single stem that comes in from the side at nearly a right angle. This stem is the desired solution and the one that approaches $f' = 1$ exponentially. The approach to the boundary point $(0, 1)$ in the phase plane is otherwise algebraic and can be extremely slow, as demonstrated in FIGURE 4.10. Such properties were inferred for $\beta < 0$, without the topological interpretation, by Hartree, by HASTINGS (1972) and others.

4.3.3 Solution maps

The Falkner-Skan problem is a subject large enough to support a small monograph of its own. My reason for reviewing this subject in an essay about turbulent flow is my perception, right or wrong, that these laminar flows with similarity may eventually provide not a model but at least a metaphor for description of turbulent flows, albeit with similarity of a different and more difficult kind. In this

section I will summarize a part of present knowledge about integrals and solutions of this similarity system for the laminar boundary layer. By an integral I mean any function $f(\eta)$ that satisfies the Falkner-Skan equation,

$$f''' + ff'' + \beta(1 - f'f') = 0 , \quad (4.91)$$

without regard to boundary conditions. By a solution I mean an integral having a place in boundary-layer theory because the velocity profile $f'(\eta)$ satisfies no-slip boundary conditions at a wall and approaches a suitable constant value at large distances from the wall;

$$f(0) = 0 , \quad f'(0) = 0 , \quad f'(\infty) = 1 , \quad (4.92)$$

with $f''(0)$ the primary dependent parameter when β is given. For wake and jet flows, there are closely related solutions that satisfy a symmetry condition rather than a no-slip condition; i.e.,

$$f(0) = 0 , \quad f''(0) = 0 , \quad f'(\pm\infty) = 1 , \quad (4.93)$$

with $f'(0)$ the primary dependent parameter. These flows are taken up in SECTION X.⁴

In general, I will not discuss mass transfer at walls or the flow of compressible fluids, although these were the first important extensions of the classical similarity problem. Neither will I discuss laminar flows with similarity in three dimensions or flows that are non-steady. Finally, I will only mention in passing the role of eigenfunctions in solving non-similar problems, particularly relaxation problems.

Some lesser issues sometimes deserve attention. In SECTION 4.3.2 I described some topological properties of solutions that may influence the numerical methods used to obtain them. Other topics that are mostly of mathematical rather than fluid-mechanical interest include oscillating and periodic integrals; slip at the wall; the unphysical boundary condition $f'(\infty) = -1$; generalization of the quantities f or η or both to be complex variables; and conjectures about the dreaded chaos.

⁴May refer to section 9.3.2 or 4.5.2.

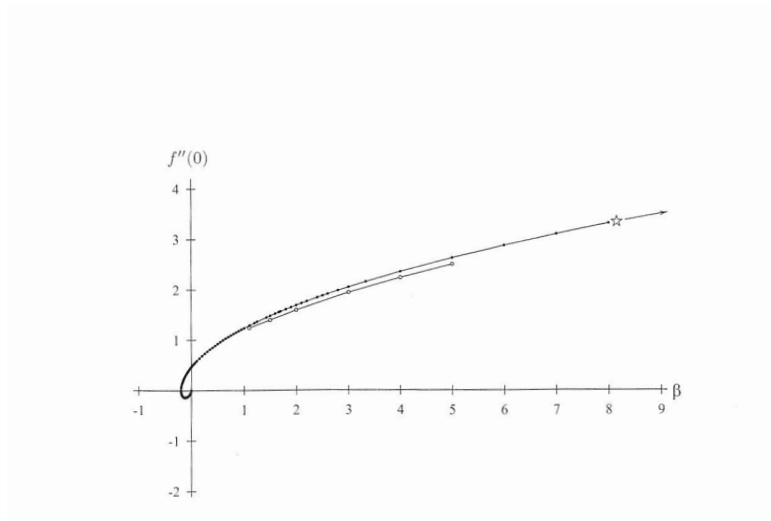


Figure 4.12: A map of some known solutions of the Falkner-Skan equation for positive β .

The primary sequence. The reader may be surprised, as I was, by the range and complexity of the Falkner-Skan equation and its solutions. FIGURES 4.12 and 4.13 show solutions in the plane $(\beta, f''(0))$. Among the values of the pressure-gradient parameter β that turn out to be distinguished for one reason or another are the values $-\infty, -2, -1, -0.1988\dots, 0, 1, 2, 3, \infty$. In FIGURE 4.12, the curve that spirals outward from the origin into the first quadrant is the primary sequence of solutions. This curve is plotted in part using fresh calculations carried out by my associates G. Cardell and M. Pesenson. Numerical values are listed in TABLE X and are believed to be accurate to one or two units in the last decimal place. Extensive tables include those by SMITH (1954), FORBRICH (1973), and KATAGIRI (1986). Less useful are the tables by EVANS (1968), because not enough attention is paid by this author to the matter of algebraic signs.

FALKNER and SKAN (1931) considered the range $-0.1978 < \beta < 4/3$ for the primary independent parameter of the boundary-layer application. They pointed to the model of potential flow of a

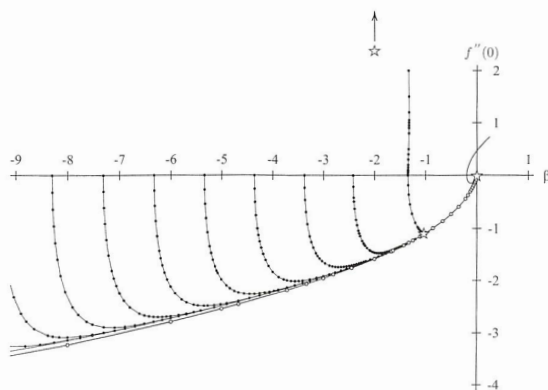


Figure 4.13: A map of some known solutions of the Falkner-Skan equation for negative β .

viscous fluid past a wedge at high Reynolds numbers, as described in SECTION 4.2.4, and kept their calculations within a range of β for which this model might be physically achievable. HARTREE (1937) introduced the modern notation, enlarged the range of β slightly in both directions for positive wall friction, and identified the turning point corresponding to continuously separating flow at $\beta = \beta_0$ say $= -0.1988\dots$. The latter estimate has since been refined by CHEN and LIBBY (1968), BANKS and DRAZIN (1973), and Forbrich, who all agree on a value

$$\beta_0 = -0.1988377 \quad . \quad (4.94)$$

Hartree argued that the curve very near the turning point in FIGURE 4.12 should be a symmetric parabola, and this conjecture was confirmed numerically by Banks and Drazin, who obtained to first order the result

$$f''(0) = \pm 0.8446(\beta - \beta_0)^{1/2} \quad . \quad (4.95)$$

Hartree also found that the mathematical problem is indifferent to the physical anomaly at $\beta = 2$, and he included the value $\beta = 2.4$ as

an aid in interpolation. The reason that numerical solutions progress smoothly through $\beta = 2$, while the physical model does not, is explained in SECTION 4.4.6.

One difficulty that arises for large positive β is more apparent than real. In the limit $\beta \rightarrow \infty$, indicated by the star at the right in FIGURE 4.12, the Falkner-Skan equation (4.91) becomes formally

$$1 - f'f' = 0 \quad , \quad (4.96)$$

and the velocity u approaches u_∞ everywhere except at the wall. The boundary-layer thickness goes to zero in terms of the original variable η . The reduction in the order of the differential equation and the non-uniformity at $\eta = 0$ are the classical signals of a singular-perturbation problem. However, it is not necessary here to invoke the idea of matched asymptotic expansions, at least as long as the fluid is incompressible. A change of variables discussed in SECTION 4.4.4 on sink flow is sufficient, and the solution in closed form given there for the case $\beta = \infty$ was in fact published very early by K. POHLHAUSEN (1921). A few numerical values for $\beta > 2$ can be found in papers by MILLS (1968), CHRISTIAN, HANKEY, and PETTY (1970), CRAVEN and PELETIER (1972b), and BOTTA, HUT, and VELDMAN (1986). BRODIE and BANKS (1986) go as high as $\beta = 100$, changing to a large- β formulation at $\beta = 20$ because of the rapidly decreasing boundary-layer thickness in terms of the variable η . The latter authors also discuss eigenvalues for large β together with the associated spatial stability problem. Finally, COPPEL (1960) provides some close bounds on the friction $f''(0)$ for large positive β . His relation is

$$\left(\frac{4\beta}{3}\right)^{1/2} < f''(0) < \left(\frac{4\beta + 1}{3}\right)^{1/2} \quad . \quad (4.97)$$

Some additional solutions near the origin in FIGURE 4.12, with β and $f''(0)$ both negative, were added to the map by STEWARTSON (1954) in a trenchant analysis that introduced the concept of similarity with reverse flow. Stewartson rejected solutions for $\beta > 2$, and also solutions having $f' > 1$, as physically unrealizable. Except for this lapse, his paper clarified Hartree's treatment

and laid a solid foundation for studies of the Falkner-Skan equation as an exercise in applied mathematics. The two regimes in FIGURE 4.12, with positive and negative values for the wall stress $f''(0)$ at the same value of β , are commonly referred to as upper branch and lower branch, respectively. Later developments led BRAUNER, LAINE, and NICOLAENKO (1982) to propose that boundary-layer solutions of the Falkner-Skan equation should be divided into three classes. In all cases the function $f(\eta)$ is defined for $0 \leq \eta < \infty$ and satisfies the no-slip condition and the external boundary condition $f'(\infty) = 1$. Hence $f'(\eta)$ in these cases is at least formally a possible velocity profile.

- (1) A *classical solution* is one for which $0 \leq f'(\eta) < 1$ for all η . (These solutions are found only on the upper branch in FIGURE 4.12.)
- (2) A *reverse-flow solution* is one for which $f'(\eta) < 0$ in some region. (It is sufficient but not necessary that $f''(0) < 0$. See, for example, FIGURE 4.7)
- (3) An *overshoot solution* is one for which $f'(\eta) > 1$ in some region. (This classification and the previous one are not mutually exclusive.)

Hartree. For positive β , WEYL (1942), IGLISH (1954), and Coppel have settled the issues of existence and uniqueness for the classical solutions. After looking at the asymptotic form of the classical solutions for large η , Hartree concluded that uniqueness for negative β , and thus placement of the upper branch, requires a closer boundary condition; namely, that $f'(\eta)$ should approach unity from below as rapidly as possible when the initial value $f''(0)$ is varied for fixed β . The issue is the behavior for large η of a linearized difference variable g , defined as

$$g(\zeta) = 1 - f'(\eta) . \quad (4.98)$$

The new independent variable ζ is formed like η in equation (4.47),

but with $y - \delta^*$ as length scale rather than y ;

$$\zeta = \left[\frac{u_\infty}{(2 - \beta)\nu x} \right]^{1/2} (y - \delta^*) . \quad (4.99)$$

In the Falkner-Skan equation (4.91), f' becomes g , the factor f is replaced by its limit, ζ , and the term in g^2 is dropped. The result is a second-order linear equation,

$$g'' + \zeta g' - 2\beta g = 0 , \quad (4.100)$$

with one boundary condition,

$$g(\infty) = 0 . \quad (4.101)$$

A final substitution,

$$D(\zeta) = e^{\zeta^2/4} g(\zeta) , \quad (4.102)$$

leads to an equation for one of the special functions of mathematical physics, the parabolic cylinder function,

$$D'' + \left(\nu + \frac{1}{2} - \frac{\zeta^2}{4} \right) D = 0 , \quad (4.103)$$

where (**look up** D_0)

$$\nu = -1 - 2\beta . \quad (4.104)$$

Equation (4.103) has two linearly independent solutions $D_\nu(\zeta)$. These functions are described, for example, in ERDELYI *et al.* (1953), where asymptotic expansions are given for large ζ . The expansions in turn can be combined in the form offered by Hartree,

$$1 - f' \approx A\zeta^{-1-2\beta} e^{-\zeta^2/2} + B\zeta^{2\beta} . \quad (4.105)$$

If β is positive, the solution $g = 1 - f'$ diverges for large ζ unless $B = 0$, in which case the solution approaches zero exponentially. If β is negative, the term $B\zeta^{2\beta}$ dominates the solution for large ζ , and $1 - f'$ approaches zero algebraically, unless again $B = 0$. Then $1 - f'$ approaches zero exponentially; i.e., “as rapidly as possible.”

Algebraic behavior is illustrated graphically in FIGURE 4.10 of SECTION 4.3.2. Shooting methods are normally designed to minimize the coefficient B in equation (4.105).

This analysis by Hartree has been developed by COPPEL (1960), ROSENHEAD (1963), and HARTMANN (1964). The issue of uniqueness aside, there seems to be no particular need to restrict the range of f' or to require f' to approach unity from below. The argument for $B = 0$ in equation (4.105) is transparent, and was employed by BLASIUS (1908) in the course of obtaining an outer expansion suitable for matching to a power series from the wall (**Check. See Coppel p 110**).

(Unfinished business. D is entire function. Nonlinear problem may have singularity for negative z . Also D has zeros if β is negative, but in the wrong places. See Bateman, p 123, for case $\beta \rightarrow \infty$, z bounded.)

There is more to the Falkner-Skan story for positive β . For given $\beta > 1$, families of oscillating reverse-flow solutions have been discovered near the upper branch in FIGURE 4.12 that all satisfy the boundary condition $f' = 1$ at infinity, but show $0, 1, 2, 3, \dots$ excursions into negative f' -space before reaching this condition. The open circles in FIGURE 4.12 define a tentative limit line as the number of oscillations increases indefinitely. Uniqueness is restored only if the restriction $0 \leq f' < 1$ is imposed, or, in a very loose sense, if a condition of earliest approach to the condition $f'(\infty) = 1$ is enforced. For various values of β beyond $\beta = 1$, families of such solutions were first reported by CRAVEN and PELETIER (1972b) and later in a powerful paper by BOTTA, HUT, and VELDMAN (1986). According to CRAVEN and PELETIER (1972a) and HASTINGS and TROY (1988), this oscillating behavior cannot occur for $0 < \beta < 1$. One example for $\beta = 5$ is shown in FIGURE 4.7 of SECTION 4.3.2 below⁵. More complex oscillating flows as well as periodic flows can occur for $\beta > 2$; and have been partially classified by Botta *et al.*, with a particular one sometimes being selected by exquisitely small differences in $f''(0)$, in the tenth decimal place or beyond. (A recent

⁵As noted in that section, it was originally placed after this one.

survey paper by SWINNERTON-DYER and SPARROW (1995) is a valuable reference?) (Omit this?)

4.4 Some special cases

4.4.1 Blasius flow; the case $\beta = 0$, $m = 0$

The Blasius equation and its boundary conditions at the wall are

$$f''' + f f'' = 0 , \quad (4.106)$$

$$f(0) = 0, \quad f'(0) = 0, \quad f''(0) \neq 0 . \quad (4.107)$$

The procedure used by BLASIUS (1908) to solve equation (4.106) was to match a power-series expansion from the wall to an asymptotic expansion near the free stream. This procedure is inherently insecure, not because the power series converges slowly, which it does, but because the power series has a finite radius of convergence. Repeated differentiation of equation (4.106) gives

$$f'''' + f' f'' + f f''' = 0 ; \quad (4.108)$$

$$f''''' + f'' f'' + 2 f' f''' + f f'''' = 0 ; \quad (4.109)$$

$$f'''''' + 4 f'' f''' + 3 f' f'''' + f f''''' = 0 ; \quad (4.110)$$

and so on. Evidently,

$$f'''(0) = 0, \quad f''''(0) = 0, \quad f'''''(0) = -[f''(0)]^2 , \quad (4.111)$$

and so on. Blasius gave a recursion formula and listed the first eight terms of the series for f as

$$\begin{aligned} f(\eta) = & f''(0) \frac{\eta^2}{2!} - [f''(0)]^2 \frac{\eta^5}{5!} + 11[f''(0)]^3 \frac{\eta^8}{8!} - 375[f''(0)]^4 \frac{\eta^{11}}{11!} + \\ & + 27,897[f''(0)]^5 \frac{\eta^{14}}{14!} - 3,817,137[f''(0)]^6 \frac{\eta^{17}}{17!} + \quad (4.112) \\ & + 865,874,115[f''(0)]^7 \frac{\eta^{20}}{20!} - 303,083,960,103[f''(0)]^8 \frac{\eta^{23}}{23!} + \dots \end{aligned}$$

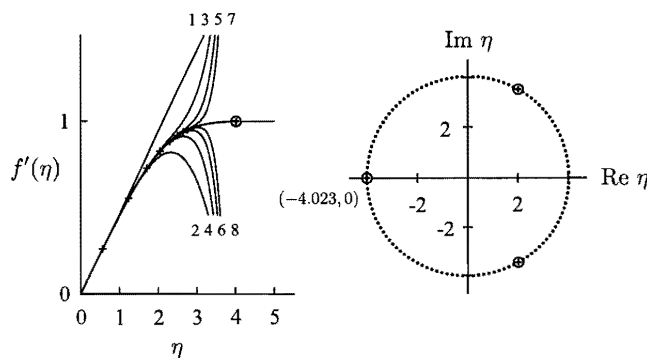


Figure 4.14: LEFT: some partial sums of the power-series representation of the Blasius solution $f'(\eta)$. The radius of convergence of the series is 4.03. The sum of eight terms is within 0.001 of the exact solution for $\eta < 2.8$ approximately, as marked by the right-most cross. RIGHT: the three singularities of the function $f(\eta)$ in the complex η -plane.

Having in mind a footnote by Blasius, I have caused the numerical coefficient of the last term in this series to be recalculated independently by three observers, and I believe that it is now correct. I will argue in SECTION X that the first two terms in the series for the stream function for turbulent flow near a wall at constant pressure may again be terms in y^2 and y^5 . The implication is that a laminar transport mechanism is important to this order in the turbulent case, but probably not beyond.

The left half of FIGURE 4.14 shows some successive partial sums for the (derivative of the) series (4.112), assuming $f''(0) = 0.4696$, together with the complete profile obtained numerically. The crosses mark the points where the various sums differ from the exact profile by 0.001. For eight terms, the range of agreement does not extend beyond $\eta = 2.8$. A connection made in SECTION X between

laminar and turbulent flows near a smooth wall involves the nature of the singularities that limit the radius of convergence of series expansions like equation (4.112). For the Blasius layer, it was first pointed out by WEYL (1941, 1942) that this radius of convergence R is less than the sensible thickness of the layer. Weyl gave bounds that imply, given the present normalization, $3.37 < R < 5.04$. Later authors have sharpened these bounds. PUNNIS (1956) obtained the values $4.00 < R < 4.03$. He demonstrated, by numerical integration for real $\eta < 0$ of a transformed equation, that one singularity of f is a simple pole with residue 3 on the negative η -axis. This property can be anticipated because of the alternation of signs in the series (4.112). MEKSYN (1959) pointed out that there must be three such poles, equally spaced on a circle of radius R , because the first integral of equation (4.112) is a power series in η^3 and thus a power series in the complex argument $z = -(\omega\eta)^3$, where ω is a cube root of -1 . In essentially unpublished work, SHANKS (1953) derived the estimate

$$R^+ = 4.02347 . \quad (4.113)$$

This value was obtained using a proprietary method for accelerating the convergence of slowly convergent sequences (SHANKS 1954, 1955). The method has been described to me by Julian Cole as an art form, but I would not dare to doubt its validity, particularly since Shanks also specified the bounds $0.469599 < f''(0) < 0.469600$ in 1953, without benefit of a modern computer. I should mention one other provocative piece of evidence on this point. During the construction of the phase diagrams presented in SECTION 4.3.2 below,⁶ it was a trivial matter to integrate the Blasius equation from $\eta = 0$ toward negative η , following the example of Punnis. The initial condition was $f''(0) = 0.4696$. The integration was carried out using a subroutine `NDsolve` [`... t, -5, 5 ...`] in the commercial program Mathematica. The calculation halted with the error message, “At $t = -4.02343$, step size is effectively zero; singularity suspected.”

These conclusions about the radius of convergence of the Blasius series are summarized graphically at the right in FIGURE 4.14. Little is known about the question of convergence for other val-

⁶As noted in that section, it and this one were originally reversed.

ues of β , except for some remarks by Meksyn for the case $\beta = -0.1988$ ($f''(0) = 0$), with the series proceeding in powers of η^4 rather than η^3 . The question of convergence is easier for the case of sink flow discussed in SECTION 4.4.4, and also for certain free shear flows such as the laminar plane jet in SECTION 9.1.3, the laminar wall jet in SECTION 10.1.3, and the laminar round jet in SECTION 8.1.5, because the boundary-layer solution in each of these cases is known in closed form.

Especially since the introduction of electronic computers, many methods have been used to integrate the Falkner-Skan equation. One method suitable in principle for two-point boundary conditions is an iterative shooting method aimed at the outer condition $f'(\infty) = 1$ (see, for example, CEBECI and KELLER 1971 and the discussion in SECTION 4.3.2 below). For the special case of Blasius flow, iteration can be avoided by substituting an initial-value problem, as first noted by TÖPFER (1912). The argument depends on the mapping properties of the Blasius equation (4.106). If $f(\eta)$ is a solution of this equation, so is $g(\eta) = cf(c\eta)$, where c is any positive constant. Consideration of the boundary conditions gives

$$g'(\infty) = c^2 f'(\infty) , \quad (4.114)$$

$$g''(0) = c^3 f''(0) , \quad (4.115)$$

where primes indicate differentiation with respect to η . If c is eliminated between the last two equations, the result is

$$\frac{f''(0)}{g''(0)} = \left[\frac{f'(\infty)}{g'(\infty)} \right]^{3/2} . \quad (4.116)$$

Let the equation $g''' + gg'' = 0$ be solved as an initial-value problem, with initial conditions $g(0) = g'(0) = 0$, $g''(0) = 1$, say. The essence of this solution is the value for $g'(\infty)$. If the original problem is to be solved with a boundary condition $f'(\infty) = 1$, say, the required value of $f''(0)$ follows immediately from equation (4.116). Unfortunately, Töpfer's argument cannot be applied to the general Falkner-Skan equation, because the presence of a pressure-gradient term defeats the mapping just described.

There has been a steady evolution over the last century in the accuracy of numerical values for the wall friction $f''(0)$ for the Blasius problem. Some of these values are

BLASIUS (1908)	0.4690
TÖPFER (1912)	0.46960
HOWARTH (1938)	0.469604
SHANKS (1953)	0.4695998
SMITH (1954)	0.4696000
HATTA et al (1985)	0.46959999
KATAGIRI (1986)	0.469599988361
LIEPMANN (1994)	0.46959998836101330

Liepmann (private communication) offered his contribution not as serious science, but rather as the outcome of a pleasant recreation played with Töpfer, Weyl, and Wolfram.

The Blasius solution as a member of the Falkner-Skan family serves to illustrate an important topic, which is the role of coordinate systems in boundary-layer theory. It was shown in SECTION 4.2.3 that the boundary condition of uniform flow far outside the boundary layer requires $f' = 1$ and therefore $f = \eta - C$, where C is a positive constant related to the displacement thickness. If the pressure is constant, it follows from equations (4.55)–(4.57) that streamlines of the boundary-layer approximation outside the Blasius boundary layer are defined by

$$y = \frac{\psi}{u_\infty}, \quad x < 0 ; \quad (4.117)$$

$$y = \frac{\psi}{u_\infty} + \delta^* = \frac{\psi}{u_\infty} + C \left(\frac{2\nu x}{u_\infty} \right)^{1/2}, \quad x > 0 ; \quad (4.118)$$

where C is the integral in equation (4.55). These formulas generate the streamlines shown schematically in FIGURE 4.1. The effect of the boundary layer on the outer flow is accurately described as a displacement effect, since the flow near the wall looks to the external flow like a distributed source. However, in rectangular coordinates the parabolic boundary-layer equations have real characteristics $x = \text{constant}$, and the singularity at the leading edge propagates outward along the characteristic $x = 0$, where it is manifested as

a discontinuity in the v -component of velocity. The second equation (4.118) redefines the free stream as a rotational flow whose streamlines are a family of displaced parabolas. This behavior is strictly a consequence of the choice of a rectangular coordinate system. Another coordinate system would lead to another behavior. The point here is that the boundary-layer solution has no meaning outside the boundary layer unless the coordinate system is artfully chosen. This point has been developed in a beautiful paper by KAPLUN (19XX), whose work was later extended by (**who?**). A related issue is the role of the boundary-layer approximation as the first term in a sequence that is probably neither convergent nor uniformly valid at any approximation (see **Van Dyke, plane jet**). (**Discuss higher approximations, pressure. Blasius in 1908 used an affine transformation to obtain the similarity form of the boundary-layer equations (check). Discuss $f''(0)$, factor of root two. Formula for $C_f(R_x)$. Mean friction is twice local friction**).

There are several reasons for studying the Blasius boundary layer experimentally. In practice, this flow serves as a useful initial condition for certain more complex flows, such as flow approaching an obstacle; as a site for calibration of instrumentation; and as a resource for studies of mechanisms involved in instability and transition. It will be established in SECTION X that the experimenter has one adjustable constant, which is the origin for the streamwise coordinate x . Given this single degree of freedom, any remaining discrepancies are likely to be associated with recovery from non-similar initial conditions or with experimental error. Excellent fidelity has been reported by (**refs**) and others. What appear to be very precise data published by NIKURADSE (1942a) are shown in FIGURE 4.15. These data are displayed in successive editions of the book by SCHLICHTING (date), but in my opinion should not be taken at face value, for reasons set forth in SECTION 2.4.2.

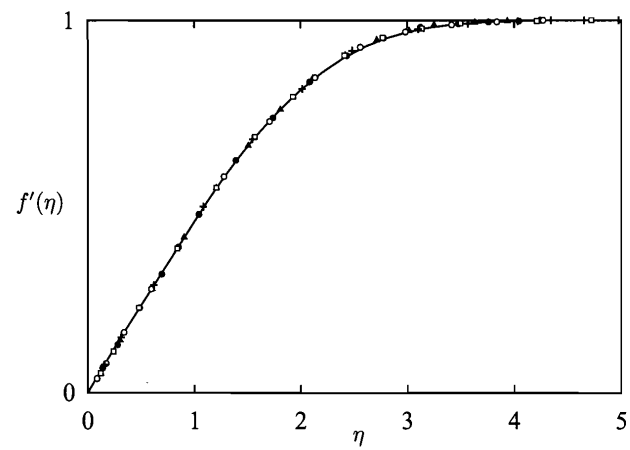


Figure 4.15: The Blasius velocity profile according to figure 62 of NIKURADSE (1942a). The theoretical curve is correct, but I do not accept these experimental data at face value.

4.4.2 Constant wall friction; the case $\beta = 1/2$, $m = 1/3$

(finish or omit)

(Axially symmetric stagnation point. Note $\tau_w = \text{constant}$ in plane case). (Use Mangler transformation?)

4.4.3 Stagnation-point flow; the case $\beta = 1$, $m = 1$

This case $m = 1$ has a special property. In SECTION 4.4.1 on the Blasius flow, the streamlines outside the boundary layer were shown to be described in rectangular coordinates by

$$\psi = u_\infty(y - \delta^*) , \quad (4.119)$$

where $\delta^*(x)$ is defined for the Falkner-Skan flows by equation (4.49) of SECTION 4.2.3. (**Check for generality.**) It is instructive to ask whether or not equation (4.119) can represent an irrotational flow. Note that $\partial^2\psi/\partial y^2 = 0$, so that the Laplacian of ψ (*i.e.*, the vorticity) is zero when

$$\frac{\partial^2\psi}{\partial x^2} = \frac{\partial^2}{\partial x^2}u_\infty(y - \delta^*) = 0 , \quad (4.120)$$

or when ψ has the form

$$\psi = xp(y) + q(y) . \quad (4.121)$$

But from equation (4.49), with $u_\infty \sim x^m$ for the Falkner-Skan flows,

$$u_\infty(y - \delta^*) = ax^m y - bx^{(1+m)/2} . \quad (4.122)$$

The last two equations are consistent if $m = 1$, in which case $p(y) = ay - b$ and $q(y) = 0$. The displacement thickness is constant, from equation (4.52), and the velocity $u_\infty(x)$ increases linearly with x . The flow is the flow about a wedge with a total angle $\pi\beta = \pi$, or the plane stagnation-point flow. This flow was first discussed by HIEMENZ (1911) and HOWARTH (1935).

For this particular case, the ansatz (4.45) becomes

$$\left(\frac{1}{\nu\alpha}\right)^{1/2} \frac{\psi}{x} = f \left[\left(\frac{\alpha}{\nu}\right)^{1/2} y \right], \quad (4.123)$$

where

$$\alpha = \frac{u_\infty}{x} = \text{constant}. \quad (4.124)$$

Note that η and f are independent of x . Substitute this ansatz in the full Navier-Stokes equations in rectangular coordinates (equations (xxx) of the introduction). The x -momentum equation becomes

$$\frac{\partial p}{\partial x} = -\rho\alpha^2 x, \quad (4.125)$$

and the y -momentum equation becomes

$$\frac{\partial p}{\partial y} = -\rho\alpha(\alpha\nu)^{1/2}(ff' + f''). \quad (4.126)$$

The last equation can be integrated to

$$p = -\rho\nu\alpha \left(\frac{f^2}{2} + f' \right) + g(x) \quad (4.127)$$

and equation (4.125) used to produce

$$p = -\rho\nu\alpha \left(\frac{f^2}{2} + f' \right) - \rho\alpha^2 \frac{x^2}{2} + C. \quad (4.128)$$

With $f = -v/(\alpha\nu)^{1/2}$, $f' = u/\alpha x$, $\alpha x = u_\infty$, and $C = p_0$, this is equivalent to

$$p + \frac{\rho}{2}(u_\infty^2 + v^2) + \rho \frac{\nu u}{x} = p_0. \quad (4.129)$$

Outside the boundary layer, this equation reduces to the Bernoulli integral (1.xx) except for the viscous term, which is of order $\nu/u_\infty x$ compared to terms of order unity. (Blows up at $x = 0$.) At the stagnation point $x = y = 0$ and $u/x = 0$ (**check**), the full stagnation pressure is recovered. The conclusion is that the solution of the Falkner-Skan equation is not an exact solution of the Navier-Stokes equation, but differs by a term of order $1/Re$. However, the

boundary-layer approximation contains the outer flow to this order, and rectangular coordinates are therefore optimal in the sense of Kaplun for the stagnation-point flow.

This relationship defines a family of hyperbolas representing the irrotational (inviscid) plane stagnation-point flow. An irrotational flow satisfies the Navier-Stokes equations, although it is almost always incompatible with the no-slip boundary conditions (plane or circular Couette flow). Thus the boundary-layer solution is exact; it is a solution of the full Navier-Stokes equations. An important but less powerful statement is that rectangular coordinates are optimal for the plane stagnation-point flow. (Cite Kaplun. Do the exact solution and the inner limit; comment on order of $\partial p/\partial y$.)

4.4.4 Sink flow; the case $\beta = \infty$, $m = -1$

The Falkner-Skan similarity variables f and η are defined in general by equation (4.45) of SECTION 4.2.3 as

$$f = \left(\frac{1+m}{2\nu u_\infty x} \right)^{1/2} \psi ; \quad \eta = \left(\frac{(1+m)u_\infty}{2\nu x} \right)^{1/2} y . \quad (4.130)$$

If the parameter m is more negative than -1 , then f and η are real only when u_∞ and x have opposite signs. Such flows were called backward boundary layers by GOLDSTEIN (1939, 1965), who chose to take x as always positive. I prefer the sign convention that u_∞ is always positive, so that x must be negative for $m < -1$, and the flow is from left to right toward the origin. These are the conditions that apply on the lower curve in FIGURE 4.3. An important special case is the limit $m = -1$ approached from below, so that β approaches $+\infty$. The programmed free-stream velocity then corresponds to sink flow;

$$u_\infty = \frac{c}{x} , \quad (4.131)$$

with x and c both negative. The much more difficult limit with $m = -1$ approached from above, so that β approaches $-\infty$, corresponds to source flow and is discussed briefly in SECTION X.

The term “sink flow” for $\beta = \infty$ is meant to be taken literally. Choose cylindrical polar coordinates and consider flow toward the origin in a sector bounded by radial walls, as shown in FIGURE X. The volume flow per unit time, Q , flowing inward across any arc $r = \text{constant}$ between $\theta = \Theta$ and $\theta = \pi$ is

$$Q = \int_{\Theta}^{\pi} ur d\theta = \text{constant} , \quad (4.132)$$

where $u(r, \theta)$ is the radial velocity, here taken as positive inward. The ostensible data of the problem are the volume rate of flow Q into the sink, the total angle $(\pi - \Theta)$, and the viscosity ν . The angle Θ is dimensionless. Both Q and ν have dimensions $\text{length}^2/\text{time}$, and their dimensionless ratio $Re = Q/\nu$, or perhaps $Re = Q/(\pi - \Theta)\nu$, exhausts the supply of dimensional information. There is no characteristic scale for the radial coordinate, and the dimensionless stream function ψ/ν must therefore depend only on θ . These comments do not require the explicit equations of motion. They apply whether the (mean) flow is laminar or turbulent, with or without a boundary-layer approximation. The turbulent case will be taken up in SECTION X.⁷

The prescription of sink flow implies that the physical flow is the one shown by the lower icon in the first quadrant in FIGURE 4.3. A similar icon for source flow in the third quadrant is unrealistic, since similar solutions of the boundary-layer equations do not exist for large negative β if Θ is too large (some are known for $\beta < -0.1988$). For sink flow, the full Navier-Stokes equation can be solved exactly in cylindrical polar coordinates for any Reynolds number (see —, —). The solution appears in terms of elliptic functions, and an inner limit process applied to this solution recovers the Falkner-Skan boundary-layer solution presented here. The outer limit of the exact solution for $Re \rightarrow \infty$ is uniform radial inflow except at the walls. However, the usefulness of this problem as a prototype problem for illustrating the method of matched asymptotic expansions is depreciated by the absence of entrainment, and it will be argued in Chapter 8 that the case of a laminar round jet

⁷Possibly Section 4.11.1

is mathematically simpler and physically more instructive for this purpose.

In the Falkner-Skan similarity equation (4.48), the coefficient of the last term becomes infinite when $m = -1$ or $\beta = \infty$, and the equation reduces in the limit to

$$1 - f'f' = 0 . \quad (4.133)$$

The derivatives of higher order have been lost, and the boundary layer in terms of the original independent variable η has shrunk to zero thickness. This behavior is a classical signal that a singular-perturbation analysis is required. However, the apparent singularity is not real. It is easily removed by a different scaling of the variables. With the limit $\beta \rightarrow +\infty$ in mind, first rewrite the ansatz (4.47) to read

$$\left(-\frac{1}{(\beta-2)\nu u_\infty x}\right)^{1/2} \psi = f \left[\left(-\frac{u_\infty}{(\beta-2)\nu x}\right)^{1/2} y \right] = f(\eta) . \quad (4.134)$$

Note that $f(\eta)$ satisfies the equation

$$f''' + ff'' + \beta(1 - f'f') = 0 , \quad (4.135)$$

with the boundary conditions

$$f(0) = f'(0) = 0 , \quad f'(\infty) = 1 . \quad (4.136)$$

Now introduce new variables

$$F = (\beta-2)^{1/2} f, \quad Y = (\beta-2)^{1/2} \eta , \quad (4.137)$$

to obtain in the limit;

$$\left(-\frac{1}{\nu u_\infty x}\right)^{1/2} \psi = F \left[\left(-\frac{u_\infty}{\nu x}\right)^{1/2} y \right] = F(Y) . \quad (4.138)$$

This modified ansatz, like the original one, can be substituted in the x -momentum equation (4.17) to derive a revised form of equation (4.135). Simpler is direct substitution of F , Y from equations

(4.137) for f , η in the Falkner-Skan equation (4.135). Both of these methods lead to the ordinary differential equation

$$F''' + \frac{FF''}{(\beta - 2)} + \frac{\beta}{(\beta - 2)}(1 - F'F') = 0 \quad (4.139)$$

with the boundary conditions

$$F(0) = F'(0) = 0, \quad F'(\infty) = 1 . \quad (4.140)$$

Primes now indicate differentiation with respect to Y . Note in passing that the two formulations (4.135)–(4.136) and (4.139)–(4.140) become identical in every respect for $\beta = 3$ or $m = -3$, a value that provides a sensible divide for calculations in the range between $\beta = 0$ and $\beta = \infty$. The limit $\beta \rightarrow \infty$ is no longer singular, inasmuch as equation (4.139) becomes in the limit

$$F''' + 1 - F'F' = 0 . \quad (4.141)$$

Equation (4.141) was first derived and solved in closed form by K. POHLHAUSEN (1921) in a paper aimed at another problem. To recover his solution, note first that F'' is an integrating factor. One integration gives

$$(F'')^2 = \frac{2}{3}[(F')^3 - 3F' + 3C] , \quad (4.142)$$

where C is a constant of integration. The boundary conditions $F'(\infty) = 1$, $F''(\infty) = 0$ require $C = 2/3$. The cubic polynomial can be factored to obtain

$$F'' = -\sqrt{2/3}(F' - 1)(F' + 2)^{1/2} , \quad (4.143)$$

where the minus sign is required because $F'' > 0$, $F' < 1$ inside the boundary layer. Put temporarily $F' = H$. Then, with $H = 0$ when $Y = 0$,

$$Y = -\sqrt{3/2} \int_0^H \frac{dh}{(h - 1)(h + 2)^{1/2}} . \quad (4.144)$$

Integration by the method of partial fractions gives

$$Y = \sqrt{2} \left[\tanh^{-1} \left(\frac{2+H}{3} \right)^{1/2} - \tanh^{-1} \sqrt{2/3} \right]. \quad (4.145)$$

This expression can be solved for $H = F'$ to obtain the velocity profile

$$F' = 3 \tanh^2 \left[\frac{Y}{\sqrt{2}} + \tanh^{-1} \sqrt{2/3} \right] - 2. \quad (4.146)$$

One more integration gives the stream function;

$$F(Y) = Y + 2\sqrt{3} - 3\sqrt{2} \tanh \left[\frac{Y}{\sqrt{2}} + \tanh^{-1} \sqrt{2/3} \right]. \quad (4.147)$$

Equation (4.147) represents sink flow in both the boundary layer and the free stream. With the aid of equation (4.131), the general ansatz (4.138) for $\beta = \infty$ can be written as

$$\left(-\frac{1}{c\nu} \right)^{1/2} \psi = F \left[-\left(-\frac{c}{\nu} \right)^{1/2} \frac{y}{x} \right], \quad (4.148)$$

where $y/x = \tan(\pi - \Theta)$. Thus the streamlines are everywhere straight lines through the origin. This property can also be shown by noting that $u = \partial\psi/\partial y = cF'/x$ and $v = -\partial\psi/\partial x = cyF'/x^2$, from which

$$\frac{v}{u} = \frac{y}{x} \quad (4.149)$$

in the boundary layer, with F' , u , and y positive and c , v , and x negative.

(Need displacement thickness, momentum thickness, and Thwaites parameters. Is there a F - S flow with R_θ decreasing? Argue zero, negative entrainment. Discuss re-laminarization, parameter K .)

This solution can also be obtained as the inner limit of the exact conical solution (ref) for large Reynolds numbers (see equilibrium paper). It is unique among the Falkner-Skan flows in that there is

a closely equivalent turbulent equilibrium flow (see SECTION X). (What about source flow? What about separating flow? Discuss source flow, rapid oscillations, precursor in Libby and Liu. Do the exact solution and inner limit; discuss order of pressure term qua boundary layer approximation.)

4.4.5 Separating flow; the case $\beta = -0.1988$, $m = -0.0904$

If the static pressure in a boundary layer increases in the direction of flow, the fluid near the wall is retarded relatively more than the fluid in the free stream because of its longer exposure to the pressure gradient, and separation may occur. One of the Falkner-Skan solutions represents flow continuously on the verge of separation, with du/dy always zero at the wall. Similarity is maintained by continuous relaxation of the gradient. The corresponding value of β can be estimated rather easily. If $\tau_w = 0$, the momentum-integral equation (4.14) can be rewritten in the form

$$\frac{1}{\theta} \frac{d\theta}{dx} + \left(2 + \frac{\delta^*}{\theta}\right) \frac{1}{u_\infty} \frac{du_\infty}{dx} = 0 \quad (4.150)$$

and integrated, given that the profile shape factor δ^*/θ is constant, to obtain (**cite Townsend**)

$$\theta u_\infty^{2+\delta^*/\theta} = \text{constant} . \quad (4.151)$$

A second general relationship for the Falkner-Skan flows is implicit in the definition (4.50) of the momentum thickness;

$$\frac{\theta^2 u_\infty}{x} = \text{constant} . \quad (4.152)$$

When the second equation is divided by the square of the first, the result can be written

$$u_\infty x^{1/(3+2\delta^*/\theta)} = \text{constant} . \quad (4.153)$$

Some typical Falkner-Skan velocity profiles have been displayed in FIGURE X (**do this**). For the continuously separating flow, what

is important is that the profile u/u_∞ is S-shaped and nearly anti-symmetric, like $\sin^2(\pi y/2\delta)$. As a model profile, the latter function implies $\delta^*/\theta = 4$, from equations (4.11) and (4.12), and equation (4.153) becomes

$$u_\infty \sim x^{-1/11} \sim x^{-0.0909} . \quad (4.154)$$

With $m = -1/11$, it follows from equation (4.46) that

$$\beta = \frac{2m}{1+m} = -1/5 = -0.2000 . \quad (4.155)$$

Numerical solutions (see TABLE X) yield the more accurate values $\delta^*/\theta = 4.02923$, $m = -0.090429$, $\beta = -0.198838$ (**check**).

The half-angle of the corresponding wedge flow, $\pi\beta/2$, is about -18° . For what it is worth, this value might be interpreted as a very coarse upper limit for the half-angle of a laminar plane diffuser without separation at the entrance. A real laminar diffuser, of course, will have other walls, a finite entrance velocity, a finite initial boundary-layer thickness, three-dimensional flow, and great sensitivity to instability, loss of symmetry, and transition.

4.4.6 The singularity at $\beta = 2$, $m = \infty$

Another and more complex singularity in the Falkner-Skan problem occurs when $\beta = 2$ or $m = \pm\infty$, so that both of the variables f and η in the original ansatz,

$$f = \left(\frac{1}{(2-\beta)\nu u_\infty x} \right)^{1/2} \psi ; \quad \eta = \left(\frac{u_\infty}{(2-\beta)\nu x} \right)^{1/2} y , \quad (4.156)$$

become infinite, along with the physical pressure gradient. Some authors, led by Stewartson, were apparently so distracted by the presence of this singularity as to discount the physical value of Falkner-Skan solutions for $\beta > 2$. However, computed solutions pass smoothly through this value of the parameter. The real challenge is in the physical interpretation of the variables, since the value $\beta = 2$ is the site of a mandatory change in sign for the x -coordinate (or the free-stream

velocity) and has other special properties, including the need for an additional parameter.

GOLDSTEIN (1939) was the first to point out that the laminar boundary-layer equations admit similarity solutions not only for the free-stream velocity program $u_\infty \sim x^m$ but also for the program $u_\infty \sim e^{cx}$, and that the latter solutions correspond to the special value $\beta = 2$ or $m = \infty$. The affine transformation of SECTION 4.2.2 in its original form does not discover these special solutions, because the additional dimensional parameter c is not present in the transformation group (4.27). The obvious strategy of re-scaling the Falkner-Skan variables as $F = f/(1+m)^{1/2}$, $Y = \eta/(1+m)^{1/2}$ is not successful because the term of highest order is lost. Two other strategies are more successful, and will be outlined briefly.

First, return to the original boundary-layer equation (4.25) of SECTION 4.2.1,

$$\rho \left(\frac{\partial \psi}{\partial y} \frac{\partial^2 \psi}{\partial x \partial y} - \frac{\partial \psi}{\partial x} \frac{\partial^2 \psi}{\partial y^2} \right) = \rho u_\infty \frac{du_\infty}{dx} + \mu \frac{\partial^3 \psi}{\partial y^3}, \quad (4.157)$$

for the stream function $\psi(x, y)$. Assume that characteristic local scales $U(x)$ and $L(x)$ can be defined, and put

$$\frac{\psi}{UL} = f\left(\frac{y}{L}\right). \quad (4.158)$$

Substitution yields a third-order ordinary differential equation for f , and similarity requires the three coefficients in this equation, namely

$$\frac{UL}{\nu} \frac{dL}{dx}, \quad \frac{L^2 u_\infty}{\nu U} \frac{du_\infty}{dx}, \quad \frac{L^2}{\nu} \frac{dU}{dx}, \quad (4.159)$$

to be constant. Division of the third combination by the second shows that $U \sim u_\infty$, and there is no reason not to choose $U \equiv u_\infty$. The first two combinations then imply

$$u_\infty \sim L^{\text{const}} = L^b, \quad \text{say}, \quad (4.160)$$

where b is a constant to be determined. It follows that

$$\frac{L^{1+b}}{\nu} \frac{dL}{dx} = \text{constant}, \quad \frac{u_\infty^{2/b}}{\nu} \frac{du_\infty}{dx} = \text{constant}. \quad (4.161)$$

There are two possibilities. If $b \neq -2$, integration leads to power-law behavior;

$$u_\infty \sim x^{b/(2+b)} \sim x^m . \quad (4.162)$$

and similarly for L . But if $b = -2$, integration leads to exponential behavior;

$$u_\infty \sim e^{cx} , \quad (4.163)$$

where c is a constant, and similarity for L . This singular case, although it is one point in a continuum for β , is itself a single-parameter family of flows with c as parameter.

The second strategy is more elegant. Recall the integrated momentum equation in the form (4.14) of SECTION 4.1.1, with $M_\infty = 0$ and $v_w = 0$, and make this equation dimensionless by dividing by a characteristic viscous stress $\mu u_\infty/\theta$. The result,

$$\frac{\tau_w \theta}{\mu u_\infty} = \frac{1}{2} \frac{u_\infty}{\nu} \frac{d\theta^2}{dx} + \left(2 + \frac{\delta^*}{\theta}\right) \frac{\theta^2}{\nu} \frac{du_\infty}{dx} , \quad (4.164)$$

will be discussed at length in SECTION 4.6.1. In the meantime, the relations of SECTION 4.2.3 require that the two dimensionless combinations

$$\frac{u_\infty}{\nu} \frac{d\theta^2}{dx} , \quad \frac{\theta^2}{\nu} \frac{du_\infty}{dx} \quad (4.165)$$

are separately constant for any one of the Falkner-Skan flows. But if $(u_\infty/\nu)d\theta^2/dx$ and $(\theta^2/\nu)du_\infty/dx$ are constant, so is their sum;

$$\frac{d}{dx} \frac{\theta^2 u_\infty}{\nu} = \text{constant} = c , \text{ say.} \quad (4.166)$$

Again there are two possibilities. If $c \neq 0$, then

$$\frac{\theta^2 u_\infty}{\nu} = cx . \quad (4.167)$$

Thus

$$\frac{\theta^2}{\nu} \frac{du_\infty}{dx} = c \left(\frac{x}{u_\infty} \frac{du_\infty}{dx} \right) = \text{constant} \quad (4.168)$$

and

$$\frac{u_\infty}{\nu} \frac{d\theta^2}{dx} = u_\infty \frac{d}{dx} \left(\frac{cx}{u_\infty} \right) = c \left(1 - \frac{x}{u_\infty} \frac{du_\infty}{dx} \right) = \text{constant} . \quad (4.169)$$

Both relationships imply $u_\infty \sim x^m$, where m is a constant, and nothing new emerges. However, if $c = 0$, then

$$\frac{\theta^2 u_\infty}{\nu} = \text{constant} = \lambda, \quad \text{say,} \quad (4.170)$$

where λ is a positive constant with units of length. Moreover,

$$\frac{\theta^2}{\nu} \frac{du_\infty}{dx} = -\frac{u_\infty}{\nu} \frac{d\theta^2}{dx} = \frac{\lambda}{u_\infty} \frac{du_\infty}{dx} = \text{constant} = C, \quad \text{say,} \quad (4.171)$$

so that $u_\infty \sim e^{Cx/\lambda}$. Note that the quantity $(\theta^2/\nu)du_\infty/dx$ is assigned different constant values (cm and C) in equations (4.168) and (4.171), respectively. The special case is uniform with the general one if $c = 0$ and $m = \infty$, so that the product $cm = 0 \times \infty$ has the finite value C . The special case again corresponds to $\beta = 2$.

The ansatz (4.158) can now be perfected for the singular case. It follows from equation (4.160) with $b = 2$ that $u_\infty L^2 = \text{constant}$. The two local scales U and L can therefore be taken in the form

$$U = u_\infty \sim k\nu e^{2kx}, \quad L \sim \frac{e^{-kx}}{k}, \quad UL^2 \sim \frac{\nu}{k}, \quad (4.172)$$

where two global constants k (with units 1/length) and ν have been introduced to make the equations dimensionally correct. These equations can also be written in a more attractive form by first eliminating the exponential, whereupon

$$L = \frac{1}{B} \left(\frac{\nu}{ku_\infty} \right)^{1/2}, \quad UL = u_\infty L = \frac{1}{A} \left(\frac{\nu u_\infty}{k} \right)^{1/2}, \quad (4.173)$$

say. The ansatz (4.158) for the case $\beta = 2$ now becomes

$$A \left(\frac{k}{\nu u_\infty} \right)^{1/2} \psi = f \left[B \left(\frac{ku_\infty}{\nu} \right)^{1/2} y \right] = f(\eta). \quad (4.174)$$

Substitution into the x -momentum equation (4.157) gives

$$\left(\frac{2ABku_\infty}{du_\infty/dx} \right) f''' + f f'' + 2 \left(\frac{A^2}{B^2} - f' f' \right) = 0. \quad (4.175)$$

The normalization that gives $u = u_\infty f'$ again requires $A = B$. The condition that reduces the coefficient of f''' to unity is once again a differential equation,

$$\frac{du_\infty}{dx} = 2A^2 k u_\infty . \quad (4.176)$$

My sign convention for the Falkner-Skan flows is that u_∞ is always positive, with flow always from left to right. Consequently, if the function f and its argument in equation (4.174) are real, the quantities k and du/dx must both be positive. The ansatz and its enabling condition become

$$\left(\frac{k}{\nu u_\infty}\right)^{1/2} \psi = f \left[\left(\frac{k u_\infty}{\nu}\right)^{1/2} y \right] , \quad (4.177)$$

$$u_\infty = k\nu e^{2kx} , \quad (4.178)$$

Note that the free-stream velocity u_∞ is equal to $k\nu$ when $x = 0$, according to equation (4.178), and thus $u_\infty \theta / \nu = k\theta$. Both numbers must be large compared with unity if boundary-layer theory is to be a valid approximation. Consider the quantity denoted earlier by m and defined by $u_\infty \sim x^m$. For $\beta = 2$ the equivalent quantity m^* , say, is

$$m^* = \frac{x}{u_\infty} \frac{du_\infty}{dx} = 2kx = 2(k\theta) \frac{x}{\theta} . \quad (4.179)$$

When x/θ is positive (negative) and of order unity, m^* is very large and positive (negative). This behavior is consistent with the behavior in FIGURE 4.3 of the quantity m slightly to the left and slightly to the right, respectively, of the singularity at $\beta = 2$. The icon that shows the equivalent channel flow is duplicated for $m = +\infty$ and $m = -\infty$ to suggest the fact that the conditions $x > 0$ for $\beta < 2$ and $x < 0$ for $\beta > 2$ are connected.

The ansatz (4.177) in the singular case can also be obtained formally by generalizing the affine transformation (4.27) of SECTION 4.2.2, taking into account the new parameter k . Thus add

$k = \widehat{gk}$ to the list of transformed quantities and transform the additional boundary condition (4.176) to obtain the scaling law

$$ag = 1 . \quad (4.180)$$

Evidently $1/g$ can be substituted for a in the alphabetical combinations (4.31), and therefore $1/k$ can be substituted for x in the original ansatz (4.33) to arrive immediately at equation (4.174).

Note that the local scale L for the singular Falkner-Skan flow is the geometric mean of ν/u_∞ and $1/k$ and that x does not appear.

In SECTION 4.2.4, the Falkner-Skan flows were associated with potential flow past a wedge of included angle $\pi\beta$. The velocity u_∞ at the wedge vertex is zero (infinite) when the exponent m in $u_\infty \sim x^m$ is positive (negative). In FIGURE 4.3, the parameters m and β are related by

$$m = \frac{\beta}{2 - \beta} , \quad \beta = \frac{2m}{m + 1} . \quad (4.181)$$

In general, the wedge vertex is a natural origin for the coordinate x . The flow is away from (toward) this origin when the parameter β is less than (more than) 2. These are the properties intended to be expressed by the channel-flow icons in the figure.

However, the wedge model is only physical when the included angle $\pi\beta$ lies in the range $-2\pi < \pi\beta < 2\pi$. An attempt was made by MANGLER (1943) to devise other geometric models for other values of β . One of these models, for the case $\beta = 2$, is particularly relevant here. Consider the potential flow

$$w(z) = \varphi + i\psi = e^z , \quad (4.182)$$

where

$$z = x + iy . \quad (4.183)$$

A mathematician might not have an engineer's care for dimensions in these expressions. The engineer would write

$$\varphi + i\psi = \mathbf{UL}e^{\pi z/\mathbf{L}} , \quad (4.184)$$

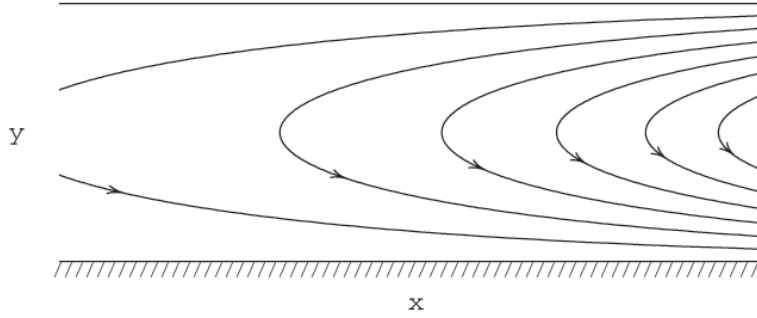


Figure 4.16: The potential flow for the singular case $\beta = 2$ and $u_\infty \sim e^{cx}$ according to MANDLER (1943). The Falkner-Skan boundary conditions can be satisfied only if c is positive. There is no definite origin or scale for x .

or where \mathbf{U} , \mathbf{L} are intrinsic constants, independent of X .

$$\psi = \mathbf{U}\mathbf{L}e^{\pi x/\mathbf{L}} \sin \pi \frac{y}{\mathbf{L}}, \quad (4.185)$$

$$u = \pi \mathbf{U}e^{\pi x/\mathbf{L}} \cos \pi \frac{y}{\mathbf{L}}, \quad (4.186)$$

$$v = -\pi \mathbf{U}e^{\pi x/\mathbf{L}} \sin \pi \frac{y}{\mathbf{L}}. \quad (4.187)$$

FIGURE 4.16 shows the streamlines in the first half cycle, $0 < y < \mathbf{L}$, of the periodic flow defined by equation (4.185). If the streamlines at $y = 0$ and $y = \mathbf{L}$ are taken as walls, the potential flow occurs in a uniform channel. The velocity at the lower wall,

$$u_\infty = \pi \mathbf{U}e^{\pi x/\mathbf{L}}, \quad (4.188)$$

has the required exponential form (4.178) for the case $\beta = 2$.

This reasoning accounts for the design of the icon for $\beta = 2$ or $m = \pm\infty$ in FIGURE 4.3. There is no length \mathbf{L} available. The height of the channel will not serve, since this dimension is associated with the free stream, not the boundary layer. Hence x/\mathbf{L} , y/\mathbf{L} are virtual variables (see also SECTION 8.1 on the laminar round jet).

In particular, if a constant is added to x in equation (4.185) for ψ , the effect is the same as multiplying the stream function by a constant. All streamlines are obtained by displacement in x of any one, without change in shape. Thus the fact that there is no natural origin for x is self-evident, and the paradox of an infinite exponent in the condition $u_\infty \sim x^m$ is rendered harmless.

There is a strong analogy between the Falkner-Skan boundary layers and Clauser's equilibrium turbulent boundary layers. For typical profiles, see the class notes.⁸ The input is β , and the output is $f''(0)$. In terms of the wedge flow, u_∞ is zero at the origin if β is positive, finite if β is zero, and infinite at the origin if β is negative. (Check Stewartson for most rapid algebraic approach to free stream. Transform variables for sink flow. Discuss signs; x is negative and u_∞ is positive if β is greater than two. Why do calculations go smoothly through $\beta = 2$?) A number for the shape factor H tells a lot; 2.5 for Blasius flow, 1.3 for turbulent flow; 4 for a separating boundary layer.

4.4.7 The Stewartson flows; $-0.1988 < \beta < 0$

Large negative β . It was supposed for some time that no useful Falkner-Skan solutions would be found for β more negative than $\beta^* = -0.1988\dots$. This belief is justified only if the condition $-1 \leq f' \leq 1$ is imposed, so that the last term of the equation (4.91) does not change sign. Otherwise, there exist jet-like boundary-layer solutions, specifically for $\beta \leq -1$, that overshoot the outer boundary condition $f' = 1$ one or more times. The surface friction $f''(0)$ can be positive or negative. These solutions were discovered by LIBBY and LIU (1967) and have since been studied by TROY (1979), BRAUNER, LAINE, and NICOLAENKO (1982), OSKAM and VELDMAN (1982), LAINE and RINEHART (1984), and HASTINGS and TROY (1985). A series of curves obtained by Oskam and Veldman for $\beta < -1$ is shown in the solution map of FIGURE 4.13. Each curve is identified by an integer index N (**is this done?**) whose

⁸This is a reference to a course taught by the author and source of some material in this monograph.

significance is that the function $f' - 1$ has N zeros within the viscous layer. Given that β is negative, this property is at least qualitatively linked (**think**) with the fact that the parabolic cylinder function D_ν governed by equation (4.103) has $[-2\beta]$ real zeros, where $[\sigma]$ is the largest positive integer less than σ . There is apparently no upper bound on N . I associate this property also with the fact that the equation for $\beta = -\infty$, representing source flow in a wedge-shaped channel, generates functions at large Reynolds number that oscillate indefinitely often between forward and reverse flow (**check; see ROSENHEAD 1940**). (**Need a figure.**)

The overshoot solutions in FIGURE 4.13 have an envelope below that seems again to be close to a parabola in $(\beta, f''(0))$ -space. (**Cite references.**) The envelope and the solutions end in midair at the point $\beta = -1$, $f''(0) = -1.0863757$, according to Brauner et al. This singularity is described by Oskam and Veldman (also Botta?) as a giant branch point, and the limiting solution there will be associated shortly with the flow in a plane jet. (Special attention to this branch point has been paid by Chen, Mills, Moulden, Oskam, Yang.) In all of this, an important mathematical role is played by a possible boundary condition $f'(\infty) = -1$ which seems not to have an explicit fluid-mechanical meaning. (**Discuss open circles.**)

4.5 Connections

4.5.1 The shear layer

In addition to the case of sink flow for $\beta = \infty$ already discussed in SECTION 4.4.4, there are at least three other points of contact between the Falkner-Skan solutions in FIGURES 4.12 and 4.13 and other standard topics in laminar viscous flow within the rubric of similarity. They are marked by stars and labels in FIGURE 4.13. The first of these, at the origin, is the connection with the laminar shear layer. STEWARTSON (1954) made two conjectures in his original paper about solutions of the Falkner-Skan problem,

$$f''' + f f'' + \beta(1 - f' f') = 0 \quad , \quad (4.189)$$

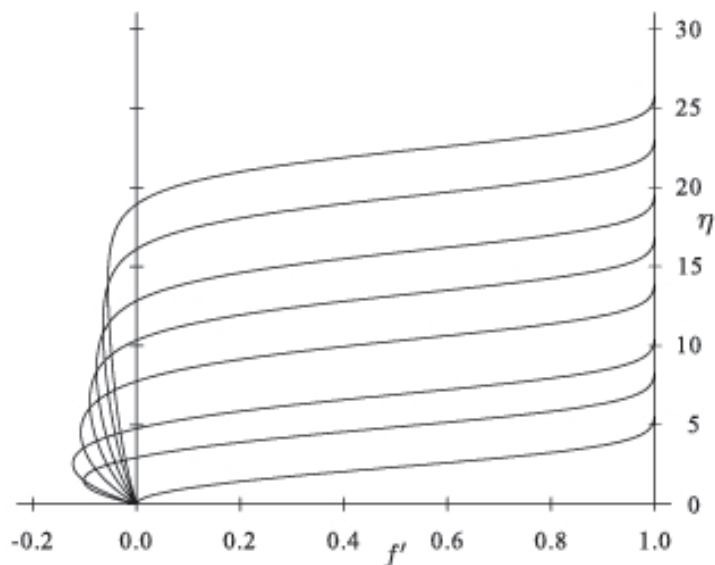


Figure 4.17: Approach of Falkner-Skan solutions to the starred shear-layer limit ($\beta = 0$, $f''(0) = 0$) along Stewartson's lower branch in figure 4.13 (figure 2 of CEBECI and KELLER 1971, with additions; see also figure 2 of LAINE and RINEHART 1984).

$$f(0) = 0, \quad f'(0) = 0, \quad f'(\infty) = 1, \quad (4.190)$$

very near the origin in $(\beta, f''(0))$ space. For $\beta \rightarrow 0$ from below, the region of reverse flow, $0 < \eta < \eta^*$, say, should become indefinitely thick and almost stagnant, and the wall friction $f''(0)$ should approach zero from below as indicated in FIGURE 4.17 He proposed two rules to describe this limiting behavior;

$$-f''(0) = c(-\beta)^{3/4}, \quad (4.191)$$

$$\eta^* = k(-\beta)^{-1/4}, \quad (4.192)$$

where c and k are positive constants. He gave an upper bound of 2.1 for the coefficient c in equation (4.191) and BROWN and STEWARTSON (1966) later derived a value $c = 1.544$, and OSKAM and

VELDMAN (1982) improved this estimate to

$$-f''(0) = 1.54400(-\beta)^{3/4} . \quad (4.193)$$

The length η^* in equation (4.192) is conveniently measured from the origin to the zero of f' , where the velocity f' becomes positive and begins to increase rapidly toward $f' = 1$. Numerical solutions by CEBECI and KELLER (1971) and LAINE and RINEHART (1984), as well as results obtained by Stewartson (1964) and KENNEDY (1964) for the wake/jet version of the Falkner-Skan problem, confirm graphically that η^* increases to very large values as β approaches zero from below. Oskam and Veldman proposed the mapping

$$\varphi(\xi) = f(\eta) , \quad (4.194)$$

$$\xi = \eta - \eta^* , \quad (4.195)$$

which transforms equation (4.189) for $\beta = 0$, $\eta^* = \infty$, into the Blasius equation for the classical shear layer separating a uniform flow from the same fluid at rest;

$$\varphi''' + \varphi\varphi'' = 0 , \quad (4.196)$$

$$\varphi'(-\infty) = 0 , \quad \varphi'(\infty) = 1 . \quad (4.197)$$

A third boundary condition for the shear layer, which presumably specifies the location of the dividing streamline, is not firmly established but in any case is not central to the present argument.

4.5.2 The wall jet

Another point of contact in FIGURE 4.13 was pointed out by STEINHEUER (1968) in a perceptive comment on the asymptotic behavior of the first Libby-Liu branch in the limit $f''(0) \rightarrow \infty$. The associated value of β is -2 , as indicated by the star at the top of the figure, and the asymptotic flow is the Tetervin-Glauert wall jet, as indicated in FIGURE 4.18. The analysis by Steinheuer was inspired by the observed evolution of the calculated profiles in his figure 1 toward a thinner viscous layer and a larger peak velocity as the solution point

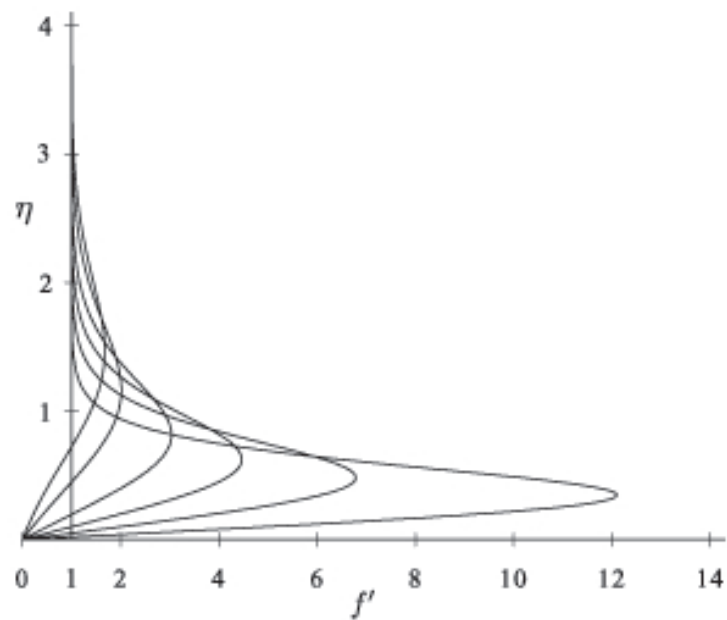


Figure 4.18: Approach of Falkner-Skan solutions to the starred wall-jet limit ($\beta = -2$, $f''(0) = \infty$) along the first Libby-Liu branch in figure 4.13 (figure 1 of STEINHEUER 1968, with additions).

moved upward in FIGURE 4.13. As the peak velocity becomes large compared to unity, the value u_∞ ceases to be a useful velocity scale, and a replacement must be sought.

Steinheuer's analysis rests on a transformation of the Falkner-Skan problem of SECTION 4.2.3 for $f(\eta)$,

$$f''' + ff'' + \beta(1 - f'f') = 0 , \quad (4.198)$$

$$f = \left[\frac{1}{(2 - \beta)\nu u_\infty x} \right]^{1/2} \psi , \quad \eta = \left[\frac{u_\infty}{(2 - \beta)\nu x} \right]^{1/2} y , \quad (4.199)$$

$$f(0) = 0 , \quad f'(0) = 0 , \quad f'(\infty) = 1 , \quad f''(0) = c , \quad (4.200)$$

into the wall-jet problem of SECTION 10.1.2 below for $\varphi(\xi)$,

$$\varphi''' + \varphi\varphi'' + 2\varphi'\varphi' = 0 , \quad (4.201)$$

$$\varphi = A \left(\frac{\rho}{F\nu x} \right)^{1/4} \psi , \quad \xi = B \left(\frac{F}{\rho\nu^3 x^3} \right)^{1/4} y , \quad (4.202)$$

$$\varphi(0) = 0 , \quad \varphi'(0) = 0 , \quad \varphi'(\infty) = 0 , \quad \varphi''(0) = k , \quad (4.203)$$

by means of a suitable limit process. The primes in the two cases indicate differentiation with respect to η and ξ , respectively. The fourth boundary condition on $\varphi''(0)$ and the invariant F are both needed for scaling and for incorporation of the eigenvalue property discussed in SECTION 10.1.1. A normalizing condition $4AB = 1$ has already been applied to the first term of equation (4.201).

Recall the mapping first proposed by Töpfer and discussed in SECTION 4.4.1;

$$\varphi(\xi) = \alpha f(\alpha\xi) = \alpha f(\eta) , \quad \xi = \frac{\eta}{\alpha} , \quad (4.204)$$

from which

$$\varphi' = \alpha^2 f' , \quad \varphi'' = \alpha^3 f'' , \quad \varphi''' = \alpha^4 f''' . \quad (4.205)$$

This transformation began life as a device for integrating the Blasius equation. In more modern and more general terms, the transformation has the useful property that it preserves the core operator

$f''' + ff''$ while allowing manipulation of the pressure-gradient term in the Falkner-Skan equation. Equations (4.198) and (4.200) become

$$\varphi''' + \varphi\varphi'' - \beta\varphi'\varphi' + \alpha^4\beta = 0 , \quad (4.206)$$

$$\varphi(0) = 0 , \quad \varphi'(0) = 0 , \quad \varphi'(\infty) = \alpha^2 , \quad \varphi''(0) = \alpha^3 c . \quad (4.207)$$

Comparison of equations (4.206) and (4.201) shows that the transformation requires $\beta = -2$ and $\alpha = 0$, whereupon

$$\varphi(0) = 0 , \quad \varphi'(0) = 0 , \quad \varphi'(\infty) = 0 \quad (4.208)$$

and

$$\varphi''(0) = \alpha^3 c = k . \quad (4.209)$$

Thus $c = f''(0)$ must become infinite in the limit $\alpha = 0$ if $k = \varphi''(0)$ does not vanish. Steinheuer showed by numerical integration along the first Libby-Liu branch that the conditions on β and α are eventually met. His last point, at $\beta = -1.99963$, $f''(0) = 1,000,000$, is slightly off scale in FIGURE 4.13. The transformed boundary condition $\varphi'(\infty) = 0$ means that the wall-jet flow is at constant pressure, so that the parameter β has lost its usual physical meaning as a measure of pressure gradient. The scaling parameter α , evaluated as φ/f or as η/ξ for $\beta = -2$, can take two forms;

$$\alpha = \left(\frac{16A^4 \rho \nu u_\infty^2 x}{F} \right)^{1/4} , \quad \alpha = \left(\frac{\rho \nu u_\infty^2 x}{16B^4 F} \right)^{1/4} , \quad (4.210)$$

which are the same if $4AB = 1$. The limit $\alpha = 0$ is evidently a dimensionless version of the limit $u_\infty = 0$. Note that α is automatically independent of x if $\beta = -2$, since similarity requires

$$u_\infty^2 x \sim x^{2m+1} \sim x^{(2+\beta)/(2-\beta)} . \quad (4.211)$$

It appears graphically from FIGURE 4.13 and numerically from Steinheuer's table 1 that the Falkner-Skan solution on the first branch is not uniquely determined by β in a narrow range $-1.347 < \beta = -1.325$, approximately. Solutions for other values of N may show a like behavior.

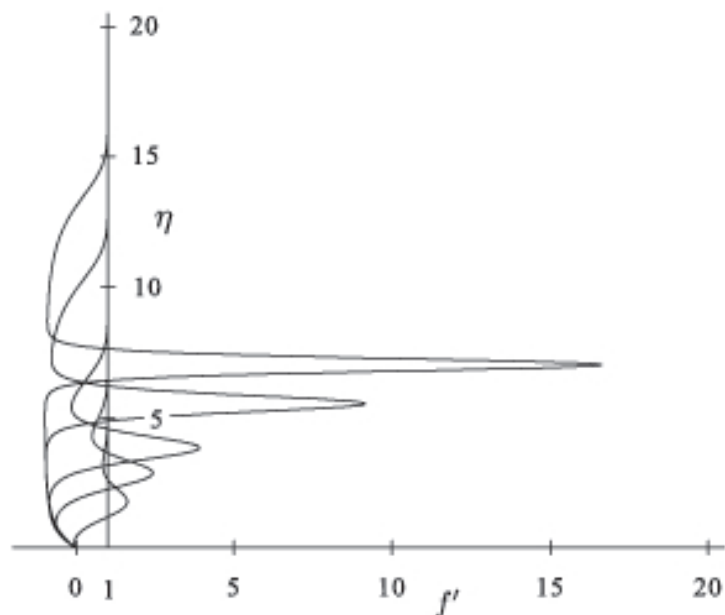


Figure 4.19: Approach to Falkner-Skan solutions to the starred plane-jet limit ($\beta = -1$, $f''(0) = -1.086376$) along the second Libby-Liu branch in figure 4.13 (figure 4 of BRAUNER, LAINE, and NICOLAENKO 1982, with additions).

4.5.3 The plane jet

The final point of contact, at $\beta = -1$, $f''(0) = -1.0864\dots$, in FIGURE 4.13, also indicated by a star, is an alleged connection with the plane jet into a fluid at rest. Start with the conjecture that a single velocity peak at $\eta = \eta^*$, say, as seen in profiles calculated for the boundary-layer problem by OSKAM and VELDMAN (1982, figure 2) and by LAINE and RINEHART (1984, figure 4), moves an infinite distance away from the wall and rises to an infinite height in the limit $\beta = -1$. The beginning of this process is shown in FIGURE 4.19. The location of the velocity peak is specified here by $f''(\eta^*) = 0$. The

magnitude of the peak is denoted by $f'(\eta^*) = p$ in the Falkner-Skan problem and by $\varphi'(0) = k$ in the jet problem. The streamline condition $f(0) = 0$ at the wall is dropped. The boundary-layer equations for $f(\eta)$ are

$$f''' + ff'' + \beta(1 - f'f') = 0 , \quad (4.212)$$

$$f = \left[\frac{1}{(2 - \beta)\nu u_\infty x} \right]^{1/2} \psi , \quad \eta = \left[\frac{u_\infty}{(2 - \beta)\nu x} \right]^{1/2} y , \quad (4.213)$$

$$f'(0) = 0 , \quad f'(\eta^*) = p , \quad f'(\infty) = 1 , \quad f''(\eta^*) = 0 . \quad (4.214)$$

This Falkner-Skan problem is to be transformed into the laminar plane-jet problem of SECTION 9.1.3, where the variable is denoted by $\varphi(\xi)$;

$$\varphi''' + \varphi\varphi'' + \varphi'\varphi' = 0 , \quad (4.215)$$

$$\varphi = A \left(\frac{\rho}{J\nu x} \right)^{1/3} \psi , \quad \xi = B \left(\frac{J}{\rho\nu^2 x^2} \right)^{1/3} y , \quad (4.216)$$

$$\varphi'(-\infty) = 0 , \quad \varphi'(0) = k , \quad \varphi'(\infty) = 0 , \quad \varphi''(0) = 0 . \quad (4.217)$$

The coefficient $3AB$ of φ''' has been normalized to unity in equation (4.215).

My tentative analysis contains elements of two of the transformations described earlier. The outward movement of the peak is first accounted for by a displacement,

$$F(Y) = f(\eta) , \quad Y = \eta - \eta^* , \quad (4.218)$$

leading to the system

$$F''' + FF'' + \beta(1 - F'F') = 0 , \quad (4.219)$$

$$F'(-\eta^*) = 0 , \quad F'(0) = p , \quad F'(\infty) = 1 , \quad F''(0) = 0 . \quad (4.220)$$

The increase in peak amplitude is then compensated for by the Töpfer mapping,

$$\varphi(\xi) = \alpha F(\alpha\xi) = \alpha F(Y) , \quad \xi = \frac{Y}{\alpha} , \quad (4.221)$$

from which

$$\varphi' = \alpha^2 F' , \quad \varphi'' = \alpha^3 F'' , \quad \varphi''' = \alpha^4 F''' , \quad (4.222)$$

and

$$\varphi''' + \varphi\varphi'' - \beta\varphi'\varphi' + \alpha^4\beta = 0, \quad (4.223)$$

$$\varphi'\left(-\frac{\eta^*}{\alpha}\right) = 0, \quad \varphi'(0) = \alpha^2 p, \quad \varphi'(\infty) = \alpha^2, \quad \varphi''(0) = 0. \quad (4.224)$$

The desired transformation into equations (4.215)-(4.217) is obtained if $\beta = -1$, $\alpha = 0$. The boundary conditions become

$$\varphi'(-\infty) = 0, \quad \varphi'(\infty) = 0, \quad \varphi''(0) = 0 \quad (4.225)$$

and

$$\varphi'(0) = \alpha^2 p = k. \quad (4.226)$$

Hence $p = f'(\eta^*)$ must be infinite in the limit $\alpha = 0$ if $k = \varphi'(0)$ does not vanish. The constant α is again given in two forms,

$$\alpha = \frac{\varphi}{F} = \left(\frac{27A^6 \rho^2 \nu u_\infty^3 x}{J^2}\right)^{1/6}, \quad \alpha = \frac{Y}{\xi} = \left(\frac{\rho^2 \nu u_\infty^3 x}{27B^6 J^2}\right)^{1/6}, \quad (4.227)$$

which are the same if $3AB = 1$. The limit $\alpha = 0$ is again a dimensionless version of the limit $u_\infty = 0$, and the combination

$$u_\infty^3 x \sim x^{3m+1} = x^{(2\beta+2)/(2-\beta)} \quad (4.228)$$

is constant when $\beta = -1$.

The conjecture about peak velocity that forms a basis for this last exercise would be more convincing with numerical support like that provided by Steinheuer in the case of the wall jet. ASTIA and CHEN (1969) and WILKS (1996) treat not the boundary-layer flow but the related problem of symmetric wake/jet flow. A major difficulty is that the boundary condition $f''(0) \equiv 0$ makes the limit process (more accurately, its projection on the plane of FIGURE 4.13) proceed along the horizontal axis, so that no contact is made with the branch point at $(\beta, f''(0)) = (-1, -1.086\dots)$. Hence the crucial point is missed. This difficulty did not occur for the mixing layer, which lies at $(0, 0)$.

A more cogent argument has been given by OSKAM and VELDMAN (1982). Their functions exist on the axis $f''(0) = 0$ and are

(a) periodic, (b) of the symmetric wake/jet type, and (c) subject to the initial condition $f'(0) = -1$. The velocity peaks appear symmetrically on the two sides of $\eta = 0$, with interval and amplitude that increase without limit as β approaches -1 . A Töpfer mapping and a limit process are applied but not interpreted. These authors carry their analysis to second order and draw the quantitative conclusion that the peaks are described, in the limit $\beta \rightarrow -1$ from below, by

$$\eta^* = \left(-\frac{12}{1+\beta} \right)^{1/2}, \quad p = f'(\eta^*) = -\frac{3/2}{1+\beta}. \quad (4.229)$$

These estimates are reinforced by numerical integration, which yields for $\beta = -1.0003$ the values $\eta^* = 200$, $f'(\eta^*) = 5000$. Obviously it does not matter that $f'(0)$ has the value -1 rather than zero. However, it does matter that the other conditions applied are $f(0) = 0$, $f''(0) = 0$, $f(\eta^*) = 0$, $f''(\eta^*) = 0$. These imply that the limit is taken along the negative β axis in FIGURE 4.13, and also that the flows in question all have zero net volume flux. The question of a connection with the plane jet is still open. (**Consult Veldman?**)

Finally, several authors (**cite them**) have attacked the case $\beta = -1$ directly by noting that equation (4.210) with $\beta = -1$ and with the boundary conditions (4.92) can be integrated twice in closed form. The result is a Riccati equation

$$f' + \frac{f^2}{2} = \eta f''(0) + \frac{\eta^2}{2} \quad (4.230)$$

which seems not to have a unique solution satisfying the standard boundary conditions. (**Needs more.**)

There is another point to be made about these multiple solutions for negative β . If a track is laid out for a trackless regime of flow, there should be a plausible explanation when the track ends in mid air. This is the case at the point $(-1, -1.086376)$ or $(-1, -1.086381)$, where the values are owed to BRAUNER et al. (1982) or OSKAM and VELDMAN (1982). This point is a singular limit point for the family of branches and its envelope. It also has a strong connection with the mathematical problem posed by the unphysical boundary condition $f'(\infty) = -1$ rather than $+1$, a condition that is

significant for understanding the complete structure of the Falkner-Skan equation. But not for the purposes of this monograph.

(Mention Evans)

Non-uniqueness of solutions of the Falkner-Skan equation in the range $-0.1988 < \beta < 0$ is by now accepted as natural. HASTINGS (1972) proved that solutions on both upper and lower solutions on the main branch have the property of exponential approach of the velocity profile to the free-stream value, while all other integrals approach the value $f'(\eta) = 1$ algebraically (check). A graphical interpretation of this property in terms of nodal behavior can be found in SECTION X.XX.

These boundary conditions have specific physical meanings. The condition $f(0) = 0$ means that the wall $y = 0$ is a streamline. The condition $f'(0) = 0$ means that the no-slip condition applies at a stationary wall. The condition $f'(\infty) = 1$ means that there is a well defined free stream.

In other chapters I will be interested in other boundary conditions; e.g., $f(0) \neq 0$, corresponding to mass transfer at a wall, or $f'(0) \neq 0$ with $f''(0) = 0$, as for flow in a symmetrical plane jet or wake. The latter flows are discussed in SECTION X. Finally, I will ignore a class of solutions satisfying the external boundary condition $f'(\infty) = -1$, because I do not recognize these solutions as real flows.

The essence of numerical calculations for boundary-layer flows is the variation of wall friction as a function of pressure gradient, or $f''(0)$ as a function of β . Some published results are collected in FIGURE 4.20. Either β may be specified and $f''(0)$ calculated, or vice versa. In the earliest papers, which dealt strictly with boundary-layer flow, $f'(\eta)$ was not allowed to exceed unity. It was found that for negative β , $f'(\eta)$ should be required to approach unity as fast as possible (exponentially) for large η (Hartree, Stewarston).

PLACEHOLDER

Figure 4.20: Failure of the momentum-integral equation for the data obtained by LUDWIEG and TILLMANN (1949) in their flow with strong pressure rise. The open circles are from the heated element (private communication). The filled circles are from the momentum-integral equation, and the crosses are from the profile fit, both according to COLES (1968) (figure missing).

4.6 Laminar non-equilibrium flow

4.6.1 The Thwaites method

Numerous methods have been proposed for integrating the laminar boundary-layer equations for a general pressure distribution. These include both field methods and integral methods (**see books by Thwaites, Rosenhead, Curle, others**). Integral methods have by now been mostly overtaken by field methods based on use of computers. However, the emphasis in this monograph is supposed to be on turbulent flow, for which the state of the art is much more primitive. Laminar flows are discussed mostly as a vehicle for practicing technique. Integral methods have the advantage that they circumvent the need to adduce some relationship between shearing stress and velocity field. As a possible qualitative model for turbulent flow, the method proposed by Thwaites for laminar flow will be outlined in detail. This method is a good example of what was called “peripheral vision” in the introduction. It allows use of similar profiles because the connection with pressure gradient is cleverly made. The discussion will be based initially on properties of the Falkner-Skan flows, and this is the main reason that these flows have already been presented at length.

In a typical problem, such as flow over a two-dimensional body, $u_\infty(x)$ is specified together with an appropriate initial condition at some station $x = 0$. The objective is to integrate the momentum-integral equation (4.13), which retains the parabolic nature of the original boundary-layer equations, so that integration proceeds in the downstream direction. Equation (4.13) involves four dependent variables, τ_w , u_∞ , δ^* , and θ , as functions of one independent variable, x . A common strategy is to take the dependent variables (more accurately, dimensionless combinations of these variables with each other) as functions of a single parameter whose nature may be specified *a priori* or may emerge from the analysis. A single-parameter family of equilibrium profiles is chosen for this purpose, ranging from algebraic approximations (Pohlhausen) to the equilibrium family of Falkner-Skan solutions (**see book by Thwaites**). Note that there

is an implied assumption of quasi-equilibrium, in the sense that equilibrium relationships are retained locally regardless of the local rate of change of the equilibrium parameter β . (*Discuss diffusion time, transport time; see Smith and Clutter for relaxation problems. There is no choice about how to make the equation dimensionless. Note $C_f R_\theta = \text{constant}$ for Falkner-Skan flow. What about $C_f R_x$?*)

The central equation of the analysis is the momentum-integral equation (4.14) with $M_\infty = 0$. In the absence of mass transfer, this equation can be rewritten in the form

$$\frac{\tau_w \theta}{\mu u_\infty} = \frac{1}{2} \frac{u_\infty}{\nu} \frac{d\theta^2}{dx} + \left(2 + \frac{\delta^*}{\theta}\right) \frac{\theta^2}{\nu} \frac{du_\infty}{dx} . \quad (4.231)$$

The appearance of θ^2 rather than θ will be important in what follows. Each of the four combinations

$$\frac{\tau_w \theta}{\mu u_\infty} , \quad \frac{u_\infty}{\nu} \frac{d\theta^2}{dx} , \quad \frac{\delta^*}{\theta} , \quad \frac{\theta^2}{\nu} \frac{du_\infty}{dx} \quad (4.232)$$

in this equation is constant and nominally of order unity for any one of the Falkner-Skan flows. Given the general form of the stream-function ansatz (4.45) for the Falkner-Skan family, the two definitions (4.49) and (4.50) for displacement thickness and momentum thickness imply, respectively,

$$\left(\frac{(1+m)u_\infty}{2\nu x}\right)^{1/2} \delta^* = \int_0^\infty (1-f') d\eta = I(\beta) ; \quad (4.233)$$

$$\left(\frac{(1+m)u_\infty}{2\nu x}\right)^{1/2} \theta = \int_0^\infty f'(1-f') d\eta = J(\beta) . \quad (4.234)$$

From the derivative relationship $\tau_w = \mu(\partial u/\partial y)_w = \mu(\partial^2 \psi/\partial y^2)_w$, it follows that

$$\left(\frac{2\nu x}{(1+m)u_\infty}\right)^{1/2} \frac{\tau_w}{\mu u_\infty} = f''(0) . \quad (4.235)$$

One more derivative, with $(\partial \tau/\partial y)_w = dp/dx = -\rho u_\infty du_\infty/dx$, yields

$$\left(\frac{2\nu x}{(1+m)u_\infty}\right) \frac{1}{\nu} \frac{du_\infty}{dx} = -f'''(0) . \quad (4.236)$$

I propose to express each of the four dimensionless combinations 4.232 in terms of β , $I(\beta)$, $J(\beta)$. A preliminary step is to express $f''(0)$ and $f'''(0)$ in this way. First, the Falkner-Skan equation,

$$f''' + ff'' + \beta(1 - f'f') = 0 \quad , \quad (4.237)$$

with the boundary conditions $f(0) = f'(0) = 0$, implies

$$f'''(0) = -\beta \quad . \quad (4.238)$$

The same result is implicit in equation (4.236). The other main parameter $f''(0)$ can be evaluated formally by first writing equation (4.237) in the equivalent form

$$f''' - [f(1 - f')] + \beta(1 - f') + (1 + \beta)f'(1 - f') = 0 \quad . \quad (4.239)$$

Integration through the boundary layer, with use of the boundary conditions $f'(\infty) = 1$ and $f''(\infty) = 0$, then yields

$$f''(0) = \beta \int_0^{\infty} (1 - f')d\eta + (1 + \beta) \int_0^{\infty} f'(1 - f')d\eta = \beta I + (1 + \beta)J \quad . \quad (4.240)$$

In view of equations (4.233) and (4.234) above, it follows that the surface friction $f''(0)$ vanishes if

$$\beta = -\frac{J}{I + J} = -\frac{1}{1 + \delta^*/\theta} \quad . \quad (4.241)$$

This result, which was derived by a different method in SECTION 4.4.5, provides a convenient check on the numerical solution for the continuously separating flow.

To recapitulate, the right side in each of the four equations (4.233)–(4.236) depends only on the Falkner-Skan parameter β or m . The combination $[(1 + m)u_{\infty}/2\nu x]^{1/2} = \partial\eta/\partial y = \eta/y$ occurs on the left. To prevent the variable x from appearing explicitly, it is convenient to eliminate this combination in favor of J/θ using equation (4.234); thus

$$\frac{\delta^*}{\theta} = \frac{I}{J} \quad ; \quad (4.242)$$

$$\frac{\tau_w \theta}{\mu u_\infty} = J^2 \left(1 + \beta + \beta \frac{I}{J} \right) ; \quad (4.243)$$

$$\frac{\theta^2}{\nu} \frac{du_\infty}{dx} = J^2 \beta . \quad (4.244)$$

The remaining combination is most easily obtained directly from the momentum-integral equation (4.231), to ensure that this equation will be automatically satisfied;

$$\frac{u_\infty}{\nu} \frac{d\theta^2}{dx} = 2J^2(1 - \beta) . \quad (4.245)$$

(Continue? Expand in $(\beta - \beta_c)$ to show square-root singularity?)

The adjacent FIGURE 4.21 has the Falkner-Skan parameter β as (temporary) leading entry, followed by the four quantities defined by equation (4.242)–(4.245). **(Such a table is no longer needed; solutions can be generated as needed.)** These quantities can all be expressed in terms of β , $I(\beta)$, $J(\beta)$. Each of these quantities is a constant for a particular Falkner-Skan flow and a candidate to serve in place of β as the single parameter of the problem. So is any algebraic combination of the four quantities; for example, θ could be replaced by δ^* in the last three columns. The leading entry $\beta(m)$, where $m = (x/u_\infty)du_\infty/dx$, is not itself a suitable single parameter, because it requires a knowledge of x for numerical evaluation. The leading column is therefore best suppressed.

According to the table headings, the four entries are not equivalent (**which columns dominate in what range?**). The last two, in particular, involve only $u_\infty(x)$ and $\theta^2(x)$ and their first derivatives. THWAITES (1949) chose to assume quasi-equilibrium, which is to say that the table continues to apply for a general flow. He also tested this assumption by plotting the particular relationship defined by the last two columns of the table (input, output),

$$\frac{u_\infty}{\nu} \frac{d\theta^2}{dx} = F \left(\frac{\theta^2}{\nu} \frac{du_\infty}{dx} \right) , \quad (4.246)$$

for the equilibrium Falkner-Skan flows (weighted lightly) and for a number of numerical solutions available at the time for other flows

$$\frac{\Gamma}{J} J^2 (1 + \beta + \beta \frac{\Gamma}{J}) \quad J^2 \beta \quad 2J^2 (1 - \beta)$$

β (or η)	$\frac{\delta^*}{\theta}$	$\frac{\tau_w \theta}{\mu u_\infty}$	$\frac{\theta^2}{\nu} \frac{d\tau_w}{dx}$	$\frac{u_\infty}{\nu} \frac{d\theta^2}{dx}$
			INPUT	OUTPUT
			λ	$F(\lambda)$

Figure 4.21: Thwaites variables for the Falkner-Skan flows.

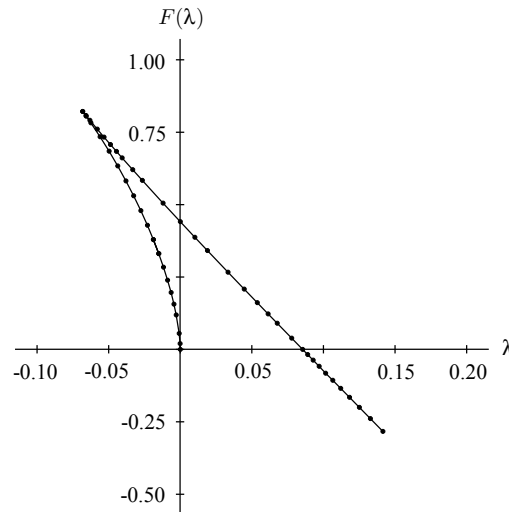


Figure 4.22: The classical Falkner-Skan family of solutions in Thwaites variables. The cusp at the left corresponds to separation ($\beta = -0.1988$). The origin corresponds to a shear layer ($\beta = 0$). The limit point at the right corresponds to sink flow ($\beta = \infty$).

(weighted heavily). His figure is equivalent to a plot of experimental data. In Thwaites' notation, the argument of F on the right is λ and the variable on the left is $F(\lambda)$. These two quantities can be thought of as input and output for the boundary-layer mechanism. In principle, with $u_\infty(x)$ given, this relationship could be integrated numerically to obtain $\theta[x, u_\infty(x)]$. The remaining two dependent variables, τ_w and δ^* , then follow from the table and from local values for $(\theta^2/\nu)du_\infty/dx$.

The function $F(\lambda)$ in equation (4.246) is tabulated in the FIGURE 4.21 and plotted against λ in FIGURE 4.22 for numerical solutions of the Falkner-Skan equation newly generated for this purpose, especially in the range $2 < \beta < \infty$. (Engineers like Smith anticipate

the need for dimensionless values of δ^* and θ , but applied mathematicians like Stewartson do not.) An unplanned result is that both variables F and λ are bounded throughout the normal range of the Falkner-Skan equation. The cusp is associated with the value $\beta = -0.1988$. (**Need Libby and Liu.**) The data terminate at the right at the point corresponding to $\beta = \infty$, for which the solution is given in closed form in SECTION 4.4.4. Beyond this point, entrainment is negative (see SECTION X).

Note that it is not the momentum-integral equation (4.231) that is to be integrated, but the surrogate equation (4.246). The method of Thwaites reduces the problem to quadratures. Thwaites noticed that the relationship (4.246) for attached flow is very nearly linear over a considerable range of the variables, as shown in FIGURE 4.22. That is,

$$\frac{u_\infty}{\nu} \frac{d\theta^2}{dx} = a - b \frac{\theta^2}{\nu} \frac{du_\infty}{dx} . \quad (4.247)$$

This result also could not be expected. In Thwaites' notation, $(\theta^2/\nu) du_\infty/dx = \lambda$, $(u_\infty/\nu)d\theta^2/dx = F(\lambda)$. The constants a and b (as revised by Curle, **ref**) are said to have the values $a = 0.45$, $b = 6.0$. These constants need comment. An important issue in FIGURE 4.22 is the issue of quasi-equilibrium; i.e., the validity of the single-parameter representation. Thwaites plotted the two dimensionless variables in equation (4.246) for several exact solutions of the boundary-layer equations, and I have added several more (**do this**). At least for these cases (but see Smith and Clutter), the evidence supports the assumption that equilibrium relationships hold locally regardless of the local rate of change of u_∞ , say. (Fit at $\beta = 0, 1$?)

Equation (4.247) is in a standard form $dy/dx + P(x)y = Q(x)$, with $y = \theta^2$. The desired integral is

$$\theta^2 - \theta_0^2 = \frac{\nu a}{u_\infty^b} \int_{x_0}^x u_\infty^{b-1} dx , \quad (4.248)$$

where x_0, θ_0 refer to some reference station.

Easy access to computers has by now made the Thwaites method somewhat academic. It is a relatively easy matter to integrate the boundary-layer equations directly, except for problems with separation. The main reason for discussing the method here is the prospect that a similar method might be developed for turbulent flow, especially since the quasi-equilibrium hypothesis is demonstrably correct for most turbulent flows, as pointed out by COLES (1956). For turbulent flow it is not possible to integrate the field equations uniquely, since the equations are not complete without recourse to turbulence modeling. There is a strong incentive for seeing what can be done without postulating a transport mechanism. **(But try $\tau_w \theta / \mu u_\infty$ instead of $\tau_w / \rho u_\infty^2$ for turbulent flow?)**

The point of view is now essentially the same as it would be if the points in the figure were experimental data being fitted by a straight line. Thus the analysis from this point on is essentially empirical. (Plot some exact solutions; see Roshko's notes.)

Depending on the problem in hand, certain of the Falkner-Skan flows may play a prominent part in the fitting operation. These include the stagnation-point flow, the Blasius flow, and the continuously separating flow. All are marked in the figure.

4.6.2 The leading-edge problem

(This section will start from A.M.O. Smith's potential-flow pressure distribution for a flat plate of finite thickness with a hemi-elliptical nose of various degrees of slenderness. The issue is use of a blunt leading edge as a tripping device. Also needed are calculations for T-S instability as a function of β . Some method for assigning a local value for β is required.)

Describe Smith calculation. How to reenter table to get τ_2 , δ^ , when straight line is not exact?*

(Argue about passing through three special points; work out stagnation-point flow; effect of initial thickness will eventually be depreciated by growth of layer. Distinguish between airfoils (β decreasing) and nozzles (β increasing). Find point in figure for $\beta = \infty$

using closed-form solution. Note that linear fit is accidental and local and could not be expected. Fit by series expansion or go numerical?)

This parameter λ combines input and output measures. The important result is that $F(\lambda)$ is linear in λ . Why does table not include $F(\lambda)$?

More on Thwaites. The input is given as $u_\infty(x)$. The output is $\theta(x)$, considered first as $\theta(u_\infty)$, and last as the more complicated combination selected by Thwaites, in which θ is the dominant variable. See class notes for various combinations for Falkner-Skan flows. These turn out to be $f''(0, \lambda)$, $f'''(0, \lambda) = -\beta$, and some integrals.

Try writing Thwaites's $F(\lambda)$ in terms of these variables, $f'''(0)$ etc.

Comment on passage through separation and reattachment, which do not affect pressure distribution.

Try integrating Thwaites's final formula for Falkner-Skan exponent n ; choose a and b to match stagnation-point flow and flat-plate flow, with an eye on blunt leading edges as a common problem.

The scatter would be considered small if the plot were for experimental data.

Problem: near the leading edge, there is a velocity maximum, and then a region of positive pressure gradient. This makes the boundary layer tender to instability or possibly to separation, if the local β is more negative than -0.1988 .

It is unlikely that a rapid scheme like the Thwaites' method can be developed for turbulent flow. First, the velocity derivative at the wall is not a suitable variable. Second, the normalization of τ_w requires ρu_∞^2 rather than $\mu u_\infty/\theta$. Third, the turbulent profiles are a two-parameter family rather than a one-parameter family.

Show how to use stagnation-point flow as an initial condition.

What if τ_w is specified and p is wanted? Check literature. Comment on x as dependent variable.

Check relative size and importance of four terms in momentum integral; see table.

Discuss generation of vorticity by pressure gradient at wall and subsequent diffusion in terms of characteristic times. When are terms in momentum equation negligible or out of balance? Why does Thwaites method go smoothly through a separation bubble, as in leading-edge problem? Transport time dx/du_∞ ; diffusion time θ^2/ν ; ratio is λ , which is less than unity by an order of magnitude.

Clue for the leading edge problem. Given s along body and β recovered from table, find m , $(x/u_\infty)du_\infty/dx$, and x . Plot $x - s$ to get displacement of origin.

4.7 Transition

4.8 Instrumentation

4.8.1 Wall shearing stress

Transfer of similarity technology from pipe flow to boundary-layer flow preceded acceptable measurements in boundary layers (see Schlichting). The reason was that research in boundary-layer flow had to wait for the development of usable wind tunnels, and this did not occur until a decade after pipe flow was under good control (see earlier section on Nikuradse).

Another impediment to work in boundary layers was the lack of acceptable methods for measuring local surface friction. Two such methods present themselves in the normal course of observing the mean-velocity profile. The first is

(1) velocity gradient at the wall, $\mu(\partial u/\partial y)_w$. (Mention Reynolds.)

This method is unreliable. It requires a probe capable of operating in the part of the sublayer where the turbulent contribution to τ is small. It is also subject to problems with interference of the probe with the flow, and with effects of turbulence, finite probe volume, and velocity gradient on the probe signal. These problems are most serious with impact or total-pressure probes, less serious with hot-wire probes, and least serious with the laser-Doppler interferometer (cite literature?). There is usually also some non-trivial uncertainty about the actual probe position relative to the wall. Finally, the determination of the terminal slope of the profile at the wall is not easy, and it would be useful to have at least one more term in a series expansion (see section below on power series). On the other hand, the difficulty of the method is not increased by the presence of pressure gradients or three dimensionality. (What else? No good with roughness or separation; marginal with mass transfer.) (Cite van der Hegge Zijnen.) (Discuss Stanton tube.)

The second primitive method is

(2) momentum-integral equation.

This equation is recorded above as equation (x.xx); it was first derived in 1921. The main defect in this equation is that it assumes two-dimensional mean flow. In positive pressure gradients the surface stress τ_w is obtained as a small difference between two large numbers, one of which (say more) is very sensitive to three-dimensionality. There are regions of slow, sluggish fluid in boundary layers close to separation, and this fluid is easily moved in the spanwise direction by small spanwise pressure gradients caused (say) by the presence of side walls and corners in the flow channel (see Tillman). Discrepancies were also sometimes blamed on neglect of other Reynolds stresses than $\overline{u'v'}$, and thus on a failure of the simplest boundary-layer approximation, but the evidence is against this claim (cite somebody). The indication from the momentum-integral equation is often that the surface stress rises as separation is approached.

A direct means for measurement of τ_w , at least in the boundary layer at constant pressure, is the

(3) *floating element. (need a list of references)*

The technique measures the force on a part of the surface that is able to move a small distance in the stream direction, or is maintained in a null position by application of a suitable restoring force. This technique was first used in water (ref), but the application that made the technique respectable was carried out by Schultz-Grunow (1940). The technique is useful in flows at constant pressure in the absence of heat transfer or mass transfer, although it has been tried in both these cases (refs.). One problem is the gap around the element, and flow through this gap caused by pressure difference. The associated force (sometimes called the buoyancy force) can be calculated or measured, but a more serious interference is caused by associated changes in the surface friction near the gap by jet flow. In air, the stress τ_w is small (perhaps 0.3 percent of the dynamic pressure, which is itself small) except at supersonic speeds, since $\rho u_\infty^2 = \gamma M_\infty^2 / 2$. (Make a table of floating elements; mention commercial device by Kistler.) (Mention towing tank data.)

With the advent of hot-wire anemometers, and particularly the X-wire probe, another means for measuring τ_w became available;

(4) *extrapolation of τ to the wall.*

The quantity being extrapolated is $\mu \partial u / \partial y - \overline{\rho u'v'}$, presumably dominated by the turbulent term or correctable using the associated data for $u(y)$. This method is most effective in positive pressure gradients (Schubauer and Klebanoff), although it was also used in some definitive measurements in flow at constant pressure by Klebanoff. It goes without saying that errors in measuring $\overline{u'v'}$ must be avoided.

A substantial advance was made by development of the

(5) *heated element*

by Ludwig (1949) and the application by Ludwig and Tillmann (1949). (Derive formula, cite literature, make a table?). Fabrication is not simple, but complex geometries are possible to allow measurement of fluctuating magnitude and direction of τ_w . The technique is very similar to hot-wire technology. The main difficulty is calibration, because much of the heat goes into the substrate. In suitable

liquids, this problem can be avoided by use of an equivalent chemical element, most widely applied for other purposes in pipe flow. Commercial heated-element gauges are available. The governing equation is linear, simplifying analysis. A flat surface is no longer necessary.

A less reliable method is

(6) heat transfer or mass transfer analogy.

Development of the floating element and the heated element was instrumental in showing the near-universality of the law of the wall, except for effects of roughness or mass transfer, and provided another method for determining τ_w ; namely,

(7) fit to the law of the wall outside the sublayer.

Related methods include the

(8) Preston tube.

(Add oil surface interferometer.)

4.8.2 Velocity

4.8.3 Flow visualization

4.9 Similarity laws for turbulent flow

4.9.1 Preamble

4.9.2 The law of the wall and the law of the wake

4.9.3 The boundary-layer thickness δ

In work with turbulent shear flows having free boundaries, including the turbulent boundary layer, it is a chronic difficulty that there is no generally accepted definition of the layer thickness δ . In fact, it is

exasperating that a quantity of such basic importance has no standard form. At the most primitive level, δ is sometimes taken as the value of y for which $u/u_\infty = 0.99$, or some other arbitrary number. I deplore this practice, which requires unreasonably accurate measurements of velocity near the edge of the layer as well as a knowledge of probe response to intermittent turbulence. At a somewhat higher level, profile formulas such as the power law $u/u_\infty = (y/\delta)^{1/n}$ or the wall-wake formula $u/u_\tau = f(yu_\tau/\nu) + g(y/\delta)$ for wall-bounded flows usually carry an inherent definition. With a little care, such definitions can serve equally for pipe, channel, and boundary layer. Finally, in certain situations connected with the concept of turbulent similarity, the definition of δ can sometimes be finessed. For the special case of equilibrium boundary-layer flow, for example, CLAUSER (1954) pointed out that the momentum-defect law and the definition of displacement thickness imply a relation

$$\frac{\delta^* u_\infty}{\delta u_\tau} = \text{constant} \quad (4.249)$$

that allows a direct test for the existence of the equilibrium property.

The difficulty with δ has another aspect for the turbulent boundary layer. It is implicit in figure 2 of my original paper on the law of the wake (COLES 1956) that my profile formula involves a corner at $y = \delta$. Outside the sublayer, this profile formula is

$$\frac{u}{u_\tau} = \left[\frac{1}{\kappa} \ln \frac{yu_\tau}{\nu} + c \right]_{\text{wall}} + \left[\frac{\Pi}{\kappa} w \left(\frac{y}{\delta} \right) \right]_{\text{wake}}, \quad y/\delta < 1, \quad (4.250)$$

where the function $w(\eta)$ satisfies three conditions; namely, $w(0) = 0$, $w(1) = 2$, and $\int_0^1 w d\eta = 1$, that express a rudimentary antisymmetry. The wake component is well represented by an analytical form first suggested by HINZE (1959),

$$w \left(\frac{y}{\delta} \right) = 2 \sin^2 \left(\frac{\pi}{2} \frac{y}{\delta} \right). \quad (4.251)$$

Far enough from the wall, the variable terms “wall” and “wake” in the profile formula (4.250) take on appropriate constant values,

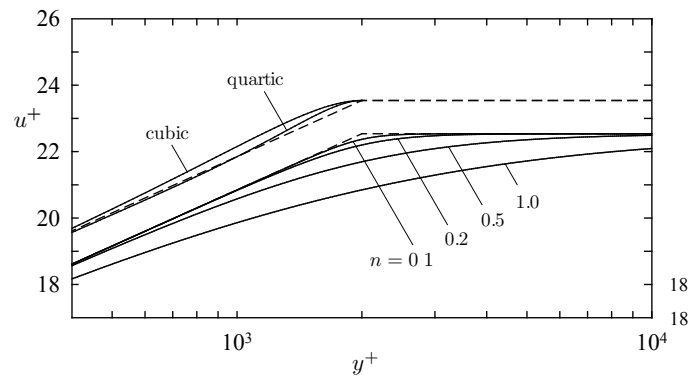


Figure 4.23: Some proposals for eliminating the discontinuity in slope at $y = \delta$ in the wall law. Note the displaced scales. The illustrations are for a boundary layer with $\delta^+ = \delta u_\tau / \nu = 2000$. The upper display shows the cubic correction according to equation (4.256) and the quartic correction according to equation (4.258). The lower display shows the interpolation scheme of SANDHAM (1991) for several values of the parameter n in equation (4.266).

and the complete profile formula (4.250) becomes

$$\frac{u}{u_\tau} = \left[\frac{1}{\kappa} \ln \frac{yu_\tau}{\nu} + c + \frac{1}{\kappa} \left(\frac{y}{\delta}\right)^2 \left(1 - \frac{y}{\delta}\right) \right]_{\text{wall}} + \left[\frac{2\Pi}{\kappa} \left(\frac{y}{\delta}\right)^2 \left(3 - 2\frac{y}{\delta}\right) \right]_{\text{wake}} \quad (4.256)$$

for $y/\delta < 1$.

Some authors refer to the polynomial (4.255) as a modified wake function. However, the polynomial is in fact a hybrid, consisting of two parts. The part that is multiplied by $1/\Pi$ and is therefore included in “wake” in equation (4.256) has nothing to do with the wake component $w(y/\delta)$ in equation (4.250). This part removes the discontinuity in slope, at the cost of introducing a second independent variable y/δ in the law of the wall in addition to yu_τ/ν . Higher derivatives are discontinuous at $y/\delta = 1$, since continuation by a constant is as before. The other part, which appears as “wake” in equation (4.256), has nothing to do with the corner problem. It is functionally equivalent to the original trigonometric form (4.251), and has the same antisymmetric property. Either representation can serve as the wake component $w(y/\delta)$ in equation (4.250) if it gives a satisfactory fit to the data. In fact, the polynomial wake component in equation (4.256) was first proposed for this purpose by MOSES (1964).

The behavior of the wall component given by equation (4.256) is displayed in FIGURE 4.23 for a typical value of 2000 for $\delta u_\tau/\nu$. The local friction law, obtained by putting $y/\delta = 1$, is unchanged. However, the classical values for the slope and intercept of the logarithmic representation are slightly compromised.

A variation on this theme by LEWKOWICZ (1982) takes w as a quartic rather than a cubic polynomial, with the additional antisymmetry condition

$$w\left(\frac{1}{2}\right) = 1 \quad (4.257)$$

The corresponding profile formula is

$$\frac{u}{u_\tau} = \left[\frac{1}{\kappa} \ln \frac{yu_\tau}{\nu} + c + \frac{1}{\kappa} \left(\frac{y}{\delta} \right)^2 \left(1 - \frac{y}{\delta} \right) \left(2 \frac{y}{\delta} - 1 \right) \right]_{\text{wall}} + \left[\frac{2\Pi}{\kappa} \left(\frac{y}{\delta} \right)^2 \left(3 - 2 \frac{y}{\delta} \right) \right]_{\text{wake}} \quad (4.258)$$

for $y/\delta < 1$. The wall component is different from that in equation (4.256), as demonstrated in FIGURE 4.23, but the wake component is not. This version is preferred, for example, by TANI and MOTOHASHI (1985) and by PERRY, MARUSIC, and LI (1994).

Sandham. A quite different interpolation scheme, first proposed by SANDHAM (1991), leads to a genuine rounding of the wall function in the vicinity of the corner at $y/\delta = 1$. This is the scheme that I prefer. It does not matter that there is no physics in it, because there is little physics worthy of the name in any of the other empirical functions used here to describe the mean profile. Sandham's scheme is initially a modification only to the logarithmic law of the wall, and the material that follows is probably best read in the context of sink flow or pure wall flow as described in SECTION 4.11.1 below.

The system to be interpolated is

$$u^+ = \frac{1}{\kappa} \ln y^+ + c, \quad y^+ < \delta^+, \quad (4.259)$$

$$u^+ = u_\infty^+ = \frac{1}{\kappa} \ln \delta^+ + c, \quad y^+ > \delta^+, \quad (4.260)$$

with a corner at $y = \delta$. Sandham writes the law of the wall outside the sublayer in terms of an artificial variable Y^+ as

$$u^+ = \frac{1}{\kappa} \ln Y^+ + c, \quad (4.261)$$

where Y^+ is defined by an ansatz that I call the lens formula,

$$\frac{1}{Y^+} = \frac{1}{y^+} + \frac{1}{\delta^+}. \quad (4.262)$$

This interpolation device accommodates at one stroke the two limiting behaviors

$$\begin{aligned} Y^+ &\rightarrow y^+ , & \frac{y}{\delta} &\ll 1 , \\ Y^+ &\rightarrow \delta^+ , & \frac{y}{\delta} &\gg 1 . \end{aligned} \quad (4.263)$$

The wall component in physical variables becomes

$$u^+ = \frac{1}{\kappa} \ln \frac{y^+}{(1 + y/\delta)} + c \quad (4.264)$$

and again depends on the two arguments yu_τ/ν and y/δ . The local friction law (4.252) is unchanged, although it now emerges as an asymptotic limit. However, a brief trial (see the curve for $n = 1$ in FIGURE 4.23) shows that an adjustable constant is needed. Sandham suggests, although he does not develop, the more general ansatz

$$\frac{1}{(Y^+)^{1/n}} = \frac{1}{(y^+)^{1/n}} + \frac{1}{(\delta^+)^{1/n}} , \quad (4.265)$$

where n is a disposable constant. This ansatz leads to the formula

$$u^+ = \frac{1}{\kappa} \ln \frac{y^+}{\left[1 + (y/\delta)^{1/n}\right]^n} + c . \quad (4.266)$$

Equation (4.266), like equation (4.264), reduces to equation (4.259) for $y/\delta \ll 1$ and to equation (4.260) for $y/\delta \gg 1$. The residuals; i.e., the differences between equation (4.266) and the original equations (4.259) and (4.260), are

$$u^+ - \frac{1}{\kappa} \ln y^+ - c = -\frac{n}{\kappa} \ln \left[1 + \left(\frac{y^+}{\delta^+}\right)^{1/n}\right] , \quad y^+ < \delta^+ , \quad (4.267)$$

$$u^+ - \frac{1}{\kappa} \ln \delta^+ - c = -\frac{n}{\kappa} \ln \left[1 + \left(\frac{\delta^+}{y^+}\right)^{1/n}\right] , \quad y^+ > \delta^+ . \quad (4.268)$$

The maximum residual is $-n(\ln 2)/\kappa$ at the point $y/\delta = 1$, and is independent of δ^+ . Since the maximum residual for flow at

constant pressure with a quiet free stream is experimentally about 0.2 in units of u^+ , the parameter n should be expected to be roughly 0.1. The lower curves in FIGURE 4.23 show the interpolated profile for several values of n . The residuals are symmetrical about $y/\delta = 1$ in the semi-logarithmic coordinates of the figure and for given n are a function of y/δ only, so that the defect law holds, and the pattern in FIGURE 4.23 can be translated arbitrarily along the logarithmic base line.

After testing this profile scheme against various profile measurements, I eventually noticed the advantage of using the artificial variable Y in the argument of the definition (4.251) for the wake component as well. Thus put

$$\frac{u}{u_\tau} = \frac{1}{\kappa} \ln \frac{Y u_\tau}{\nu} + c + \frac{2\Pi}{\kappa} \sin^2 \left(\frac{\pi}{2} \frac{Y}{\delta} \right). \quad (4.269)$$

The result is a small improvement in the goodness of fit and a large improvement in the esthetic content of the model. Let the ansatz (4.265) be rewritten in the form

$$\frac{1}{(Y/\delta)^{1/n}} = 1 + \frac{1}{(y/\delta)^{1/n}} \quad (4.270)$$

to isolate the relationship between the physical variable y/δ and the artificial variable Y/δ for a given value of n . The layer thickness δ is now defined by the condition

$$Y/\delta = (1/2)^n, \quad (4.271)$$

and the structure of the profile extends well beyond the point $y = \delta$. However, the variable Y/δ never exceeds unity as the physical variable y/δ goes to infinity. Thus the question of a corner never comes up. The physical profile outside the sublayer has continuous derivatives of all orders.

The development just given provides a possible connection between the shape of the mean-velocity profile near the free stream and the intensity and/or scale of the free-stream turbulence. This connection is discussed in SECTION X below, along with the relationship between n and the penetration of the intermittency property toward the wall as a function of pressure gradient. **(Check this later.)**

4.10 Hypotheses for turbulent equilibrium flow

4.10.1 Recapitulation

I now want to describe a close analogy between the laminar equilibrium flows defined by Falkner and Skan and the turbulent equilibrium flows defined by Clauser. I first proposed this analogy (COLES 1957) in a paper that has been cordially ignored by the turbulence community. The analysis belongs at this point in the development, and I welcome the opportunity to present my own views.

The material that underlies the analysis includes: the recognition of the defect law by Darcy, Stanton, and others (SECTION X); the recognition of a logarithmic profile near the wall by Karman and Nikuradse (SECTION X); the generalization called the law of the wall by Prandtl (SECTION X); the demonstration of universality by Ludwig and Tillmann (SECTION X); the generalization of the defect law by Clauser (SECTION X); and the recognition of the law of the wake by Coles (SECTION X). None of this material prejudices the question of turbulent mixing mechanisms. After these developments, the empirical evidence for similarity laws in the turbulent boundary layer was essentially complete, and there have been no major developments since 1956. What was lacking and still is lacking is some connection between input and output, the external boundary conditions and the behavior of the flow. This statement is true even for equilibrium flow, since Clauser had to establish his pressure distributions by cut-and-try methods. The analysis here attempts to clarify this problem for equilibrium flow, although it does not touch on the problem for an arbitrary specified pressure distribution. My original motivation for looking at the continuity equation was to test the usefulness of the entrainment velocity as a flow variable for calculations (**ref Head?**). (See SECTION X below on entrainment.) The specific question that emerges is the extent to which divergence or convergence of external streamlines, as a result of pressure gradient, penetrates into the boundary layer. Moreover, when the wall-wake profile is used to calculate the shearing stress τ , the velocity component v is encountered on the way. The level of rigor is uniform

with the one established historically. There is an esthetic value in an argument that proceeds naturally, without complications. What is simple is likely also to be correct.

4.10.2 Flow near a wall

Consider again the universal law of the wall for two-dimensional mean flow in the general form

$$u^+ = f(y^+) . \quad (4.272)$$

The wall is assumed to be smooth, with $\psi = u = v = 0$ at $y = 0$. Three important and useful consequences of this formula should be recorded here (COLES 1955). The first is that u^+ and y^+ are constant on mean streamlines. Integration of equation (4.272) at constant x yields

$$\psi^+ = \frac{\psi}{\nu} = \frac{1}{\nu} \int_0^y u dy = \int_0^{y^+} f(y^+) dy^+ = g(y^+) . \quad (4.273)$$

An equivalent statement is

$$\frac{Du^+}{Dt} = \frac{Dy^+}{Dt} = 0 , \quad (4.274)$$

so that the edge of the sublayer, by any sensible definition, is a mean streamline. Despite a very energetic local transfer of fluid into or out of such a sublayer by turbulent fluctuations, there is no net transfer. This conclusion, moreover, is independent of pressure gradient to the same extent as equation (4.272).

The second consequence of the universal law of the wall, like the first one, uses only the continuity equation. When v is calculated from ψ , the result is

$$v = -\frac{\partial\psi}{\partial x} = -\frac{yu}{u_\tau} \frac{du_\tau}{dx} . \quad (4.275)$$

Define a length $\lambda(x)$ as

$$\frac{1}{\lambda} = -\frac{1}{u_\tau} \frac{du_\tau}{dx} . \quad (4.276)$$

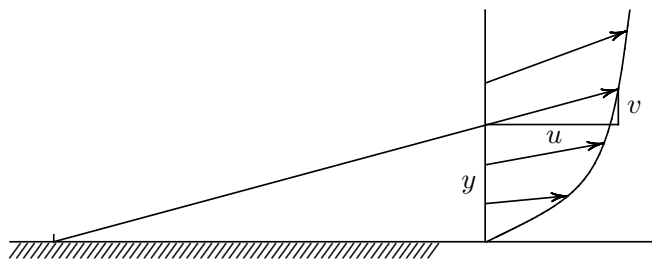


Figure 4.24: The sheared source-flow model corresponding to Prandtl's law of the wall.

Then

$$\frac{v}{u} = \frac{y}{\lambda} . \quad (4.277)$$

This relation describes a sheared source flow, as illustrated by the similar triangles in FIGURE 4.24. All of the mean-velocity vectors, whether in the sublayer or in the logarithmic region, intersect at a common origin on the wall. My sign convention is that this origin lies upstream when λ is positive. The divergence or convergence of the mean streamlines near the wall is entirely determined by $\tau_w(x)$, without reference to dp/dx (although dp/dx will indirectly determine τ_w). This property will be recalled at least twice in later sections; once in connection with a turbulent boundary layer called the pure sink flow, and once in connection with a general similarity scheme for describing what are called equilibrium turbulent boundary layers. A non-trivial property of equation (4.277) is that it provides an easy method for calculating $v(y)$ when $u(y)$ and $\tau_w(x)$ are known.

Finally, the third consequence of the universal law of the wall

follows from the mean momentum equation in boundary-layer form;

$$\frac{\partial \tau}{\partial y} = \frac{dp}{dx} + \rho \left(u \frac{\partial u}{\partial x} + v \frac{\partial u}{\partial y} \right) . \quad (4.278)$$

The continuity equation allows $\partial u / \partial x$ to be replaced by $-\partial v / \partial y$, and the quantity in parentheses can then be written as $-u^2 \partial(v/u) / \partial y$. Substitution for v/u from equation (4.277) leads immediately to

$$\frac{\partial \tau}{\partial y} = \frac{dp}{dx} - \frac{\rho u^2}{\lambda} . \quad (4.279)$$

This result implies, in the + notation,

$$\tau^+ = \frac{\tau}{\tau_w} = 1 + \frac{y}{\tau_w} \frac{dp}{dx} - \frac{1}{\lambda^+} \int_0^{y^+} (u^+)^2 dy^+ . \quad (4.280)$$

For fully developed channel flow ($u_\tau = \text{constant}$ or $\lambda = \infty$), equation (4.280) is trivially exact. More generally, within the boundary-layer approximation, equations (4.279) and (4.280) are an exact consequence of equation (4.272). As long as the equations of motion are incomplete, this is as far as a similarity argument based on the empirical law of the wall can go, or can be expected to go. For flow at constant pressure, the relation (4.280) both preempts and contradicts the condition $\tau = \tau_w = \text{constant}$ that leads, in the mixing-length model of section x, to a logarithmic behavior for the mean-velocity profile (see section x). **(The integral behaves like y^3 for small y and like $y(\ln y)^2$ farther from the wall. See pure wall flow.)**

I leave as an exercise the demonstration that any one of the four relations (4.272), (4.274), (4.277), and (4.279) implies the other three. All are independent of the analytical form of the law of the wall (4.272), and they mark this law as a powerful agency for order in the empirical description of turbulent flow, not to be abandoned without good cause. Moreover, each is a possible source of inspiration for generalizations of the law of the wall to more complex flows, although I must say that my own efforts in this direction have not been inspired. **(For example, the relation (4.277) might suggest the conjecture $(v - v_w)/u = y/\lambda$ for flow with mass**

transfer at the wall. Comment on Clauser's equilibrium parameter. What about wall jet, roughness, mass transfer? Does not apply for laminar flow. Note that $\partial\tau/\partial y = dp/dx$ is accurate only at the wall.)

4.10.3 External flow

Equation (4.277) suggests a parallel development for the external flow. In the absence of a boundary layer, the continuity equation with a boundary-layer approximation is

$$\frac{\partial v}{\partial y} = -\frac{du_\infty}{dx} . \quad (4.281)$$

Integration gives a velocity field that is not quite irrotational,

$$v = -y\frac{du_\infty}{dx} . \quad (4.282)$$

Thus

$$\frac{v}{u_\infty} = \frac{y}{\Lambda} , \quad (4.283)$$

where

$$\frac{1}{\Lambda} = -\frac{1}{u_\infty} \frac{du_\infty}{dx} . \quad (4.284)$$

Within the boundary-layer approximation, the inviscid flow is also a source flow whose velocity vectors have a common origin at the wall at a distance Λ upstream, as shown in FIGURE 4.25.

When the presence of a boundary layer is taken into account, this argument is modified. Outside the boundary layer, the continuity equation $\partial u/\partial x + \partial v/\partial y = 0$ implies

$$\begin{aligned} v &= -\int_0^{y>\delta} \frac{\partial u}{\partial x} dy = \frac{d}{dx} \int_0^{y>\delta} (u_\infty - u - u_\infty) dy = \frac{d\delta^* u_\infty}{dx} - y \frac{du_\infty}{dx} \\ &= u_\infty \frac{d\delta^*}{dx} - (y - \delta^*) \frac{du_\infty}{dx} . \end{aligned} \quad (4.285)$$

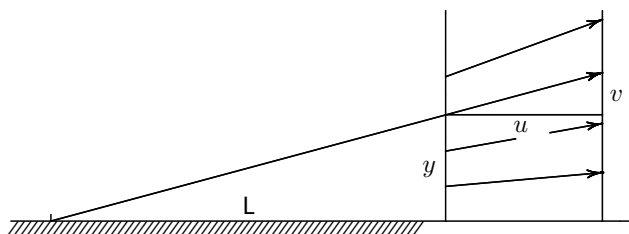


Figure 4.25: The source-flow model for a free stream with a positive pressure gradient.

Equation (4.285) reduces to equation (4.282) when δ^* is zero. The implied presence of the variable y/δ suggests that equation (4.277), originally derived from the law of the wall, should be put in the form

$$\frac{\lambda v}{\delta u} = \frac{y}{\delta} \quad (4.286)$$

The corresponding form for equation (4.285) is

$$\frac{\lambda v}{\delta u} = \frac{\lambda}{\delta u_\infty} \frac{d\delta^* u_\infty}{dx} + \frac{y}{\delta} D \quad (4.287)$$

where

$$D(x) = \frac{d \ln u_\infty}{d \ln u_\tau} = \frac{\lambda}{\Lambda} \quad (4.288)$$

is the first of two primary kinematic parameters of the problem.

4.10.4 Equilibrium parameters

The two equations (4.286) and (4.287) are plotted in FIGURE 4.26. They intersect at the point (P, P) , where P is defined by putting

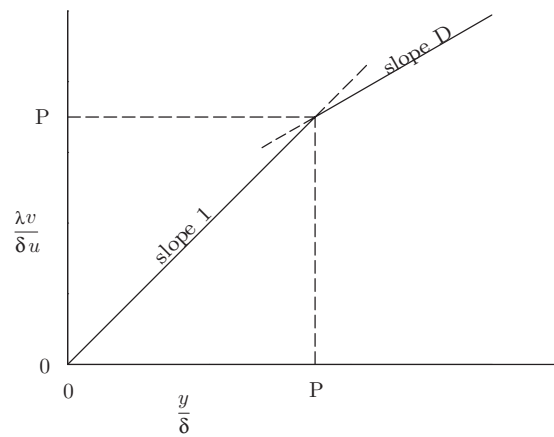


Figure 4.26: An attempt to fit Nikuradse's turbulent boundary-layer profile using the standard wall-wake formula.

$\lambda v/\delta u = y/\delta = P$ in equation (4.287);

$$P(x) = \frac{\lambda}{\delta u_\infty} \frac{d\delta^* u_\infty}{dx} \cdot \quad (4.289)$$

After use of equations (4.277) and (4.288), the second kinematic parameter of the problem is obtained as

$$P(x) = \frac{\delta^*}{\delta} \frac{d \ln(\delta^* u_\infty/\nu)}{d \ln(u_\infty/u_\tau)} \cdot \quad (4.290)$$

Note that x does not appear explicitly in equations (4.288) and (4.290). Note also that P is not well defined, because δ is not. Nevertheless, the product $P\delta$ is well defined. A more practical presentation of the results so far is therefore the one in FIGURE 4.27, where both abscissa and ordinate are scaled with $1/P$. (**Complete by calculating and plotting full curves for several equilibrium flows; data also? Note lack of precise similarity.**) Finally, note that the flow has not been stipulated to be laminar or turbulent or even steady. I consider it to be remarkable that so much mileage can be got out of the continuity equation.

The two parameters that appear in the analysis just concluded are called D (for divergence) and P (for pressure gradient). It is easily shown that D and P are separately constant for any one of the Falkner-Skan laminar boundary layers. Recall (from SECTION 4.6.1) that the quantities $\theta \tau_w/\mu u_\infty$ and δ^*/θ are constant for a Falkner-Skan flow (**compare the column headings in table x**). When θ is replaced by δ^* and τ_w is replaced by ρu_τ^2 , these statements imply

$$\frac{\delta^* u_\infty}{\nu} \frac{u_\tau^2}{u_\infty^2} = \text{constant} \cdot \quad (4.291)$$

From this expression and the definition (4.290) for P , it follows for Falkner-Skan flow that

$$P = 2 \frac{\delta^*}{\delta} \cdot \quad (4.292)$$

To evaluate D , note from equation (4.51) of SECTION 4.2.3 that if $u_\infty \sim x^n$, then $\tau_w \sim u_\infty^{3/2}/x^{1/2} \sim x^{(3n-1)/2}$ and $u_\tau \sim x^{(3n-1)/4}$.

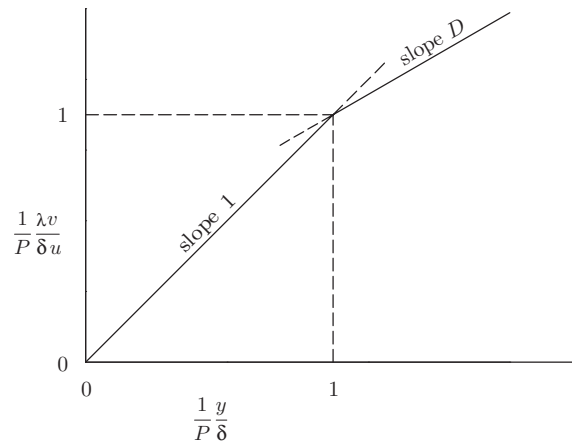


Figure 4.27: A geometric interpretation of the two profile parameters D and P . The product $P\delta$ is rigorously defined, but the parameters P and δ separately are not.

It follows for Falkner-Skan flow that

$$D = \frac{4n}{3n-1} = \frac{2\beta}{2\beta-1} . \quad (4.293)$$

Thus P and D can be added to the collective of parameters that can be used to identify and order various members of the Falkner-Skan family of equilibrium flows. A disadvantage in the case of P is that the numerical value assigned to P depends on the definition of the thickness δ .

(Move). *(There is a profound difference between laminar and turbulent flow. The development of computers has made slide-rule methods like the Thwaites method almost obsolete. The laminar problem is well defined, and it is simpler to solve the full boundary layer equations directly for a non-equilibrium flow. The turbulent problem is not well defined, since the equations are incomplete. The equivalent operation involves what is called turbulence modeling, a subject deliberately excluded from this monograph. The development of a turbulent equivalent to the Thwaites method is therefore a useful objective. What follows is along this line, in an effort to use phenomenological evidence to bypass the specification of turbulent transport mechanisms, which lie in the eye of the beholder.)* **(Endmove)**

By definition, Clauser's equilibrium flows are described by a defect law,

$$\frac{u_\infty - u}{u_\tau} = F\left(\frac{y}{\delta}\right) . \quad (4.294)$$

When this profile is inserted in the definition (4.11) for δ^* and the discrepancy in the sublayer is ignored, there is obtained

$$\frac{\delta^* u_\infty}{\delta u_\tau} = \text{constant} . \quad (4.295)$$

It appears that the typical slow increase of u_∞/u_τ with increasing x in an equilibrium flow is compensated for by a slow decrease of δ^*/δ . The local friction law is equation (x),

$$\frac{u_\infty}{u_\tau} = \frac{1}{\kappa} \ln \frac{\delta u_\tau}{v} + \text{constant} , \quad (4.296)$$

or, in view of (4.295),

$$\frac{u_\infty}{u_\tau} = \frac{1}{\kappa} \ln \frac{\delta^* u_\infty}{v} + \text{constant} . \quad (4.297)$$

Equation (4.290) for P then implies

$$P = \kappa \frac{\delta^* u_\infty}{\delta u_\tau} = \text{constant} \quad (4.298)$$

for equilibrium turbulent flow. If the specific wall-wake formula

$$\frac{u_\infty - u}{u_\tau} = -\frac{1}{\kappa} \ln \frac{y}{\delta} + \frac{\Pi}{\kappa} \left[2 - w\left(\frac{y}{\delta}\right) \right] \quad (4.299)$$

is used instead, with $w(y/\delta) = 2 \sin^2(\pi y/2\delta)$, there is obtained

$$\kappa \frac{\delta^* u_\infty}{\delta u_\tau} = 1 + \Pi , \quad (4.300)$$

from which

$$P = 1 + \Pi = \text{constant} . \quad (4.301)$$

Note that laminar equilibrium flows do not have the property (4.294); they have the property

$$\frac{u_\infty - u}{u_\infty} = G\left(\frac{y}{\delta}\right) . \quad (4.302)$$

4.10.5 The hypothesis $D = \text{constant}$

Given that P and D were originally defined with impressive generality, that P and D are separately constant for a laminar equilibrium flow, and that P is constant for a turbulent equilibrium flow, it is natural to take as a plausible hypothesis that

$$D = \text{constant} \quad (4.303)$$

for a turbulent equilibrium flow as well (COLES 1957). Certainly this hypothesis is attractive in the sense that it is necessary and perhaps also sufficient for similarity in coordinates $(\lambda v/\delta u, y/\delta)$. The

hypothesis can also be tested directly, by plotting $\ln u_\infty$ against $\ln u_\tau$ for turbulent boundary layers that obey the defect law, accidentally or by design. (*Do this. Add Launder and Jones, Stratford, Bradshaw, East and Sawyer. Comment on sign convention for separated flow. Mention parameters of Clauser, Bradshaw. Review Perry's work showing non-similar τ . If u were hard to measure and τ were easy, our similarity "laws" would be different. Show this for laminar flow?*) I recall that I once presented this material in a seminar, and I used a metaphor to suggest the sense of the parameters P and D . "Hansel goes into the woods alone. Presently he returns with a little girl named Gretel. Hansel's parents have never seen Gretel before, but Hansel insists that she is his sister." John Laufer, who was in the audience, recommended changing the notation to H and G .

4.11 Morphology of turbulent equilibrium flow

4.11.1 Pure wall flow

Two limiting cases of equilibrium turbulent flow, the cases $\Pi = 0$ and $\Pi = \infty$, can be developed analytically with relatively little effort. The first of these is pure wall flow, which is defined in the context of the general profile equation (4.250) by the conditions

$$\Pi = 0, \quad \frac{u}{u_\tau} = f\left(\frac{yu_\tau}{\nu}\right) = f(\eta) . \quad (4.304)$$

I submit that this limit corresponds to sink flow in a wedge-shaped channel. This submission amounts at best to a plausible conjecture, supported by experimental and numerical evidence and by a powerful set of inferences, including the absence of a characteristic scale. For the present, it is not necessary to specify the function $f(\eta)$ except for the boundary conditions $f(0) = 0$, $f(\infty) = u_\infty/u_\tau$. The discussion begins with a reprise of a derivation given earlier in SECTION 4.10.2. The stream function obtained by integrating the profile (4.304) with respect to y is

$$\frac{\psi}{\nu} = \frac{1}{\nu} \int u \, dy = \int f(\eta) d\eta = g(\eta) = g\left(\frac{yu_\tau}{\nu}\right) . \quad (4.305)$$

Differentiation gives

$$u = u_\tau g', \quad v = -y \frac{du_\tau}{dx} g' . \quad (4.306)$$

Elimination of g' gives

$$\frac{v}{u} = \frac{y}{\lambda} , \quad (4.307)$$

where

$$\frac{1}{\lambda} = -\frac{1}{u_\tau} \frac{du_\tau}{dx} \quad (4.308)$$

as before. Further differentiation gives

$$\frac{\partial u}{\partial x} = \frac{du_\tau}{dx} \left(g' + \frac{yu_\tau}{\nu} g'' \right), \quad \frac{\partial u}{\partial y} = \frac{u_\tau^2}{\nu} g'' . \quad (4.309)$$

These expressions allow the momentum equation (x.xx) to be written

$$\rho \left(u \frac{\partial u}{\partial x} + v \frac{\partial u}{\partial y} \right) = \rho u_\tau \frac{du_\tau}{dx} g' g' = \rho u_\infty \frac{du_\infty}{dx} + \frac{\partial \tau}{\partial y} \quad (4.310)$$

or

$$\rho \frac{u_\infty^2}{u_\tau} \frac{du_\tau}{dx} \left(\frac{u^2}{u_\infty^2} - D \right) = \frac{\partial \tau}{\partial y} , \quad (4.311)$$

where, by definition,

$$D = \frac{u_\tau}{u_\infty} \frac{du_\infty}{du_\tau} . \quad (4.312)$$

The tentative outer boundary condition $\partial \tau / \partial y = 0$ at the edge of the layer (see below) then requires

$$D = 1 \quad (4.313)$$

for pure wall flow, and conversely. But if $D = 1$, then $u_\infty / u_\tau =$ constant from the integral of equation (4.312), and $\delta u_\tau / \nu =$ constant from equation (4.304). The condition on $\partial \tau / \partial y$ is a little tender, because $\partial u / \partial y$ according to equation (4.304) is discontinuous at $y = \delta$, changing from $u_\tau / \kappa y$ to zero. Further inferences can be drawn by reformulating equation (4.310) for $D = 1$ and integrating, with the boundary condition $\tau = 0$ at $y = \delta$, to obtain

$$\tau_w = \mu \frac{du_\tau}{dx} C = -\mu \frac{u_\tau}{\lambda} C , \quad (4.314)$$

where

$$C = \int_0^{\infty} \left(\frac{u_{\infty}^2}{u_{\tau}^2} - g'g' \right) d\eta = \frac{1}{\nu u_{\tau}} \int_0^{\infty} (u_{\infty}^2 - u^2) dy . \quad (4.315)$$

The definite integral C is evidently a positive constant, independent of x , whose value depends on the constant value of u_{∞}/u_{τ} . At least for this special case of pure wall flow, the characteristic scale for τ_w , which was $\mu u_{\infty}/\theta$ for laminar flow (see the Thwaites variables in SECTION 4.6.1), is now $-\mu u_{\tau}/\lambda$.

The essence of equation (4.314) is the equality

$$\frac{1}{u_{\tau}^2} \frac{du_{\tau}}{dx} = \frac{1}{C\nu} . \quad (4.316)$$

Let the origin for x be defined by the condition $x = 0$ when $u_{\tau} = \infty$. Then equation (4.316) and its integral imply

$$C = -\frac{u_{\tau}x}{\nu} = -\frac{u_{\tau}\lambda}{\nu} > 0 , \quad (4.317)$$

from which

$$\lambda = x . \quad (4.318)$$

It follows from equation (4.307) that $v/u = y/x$ everywhere. Thus the pure wall flow is a sink flow, like the Falkner-Skan flow for $\beta = \infty$. In fact, the argument just outlined applies for either laminar or turbulent flow. If my sign convention is adopted, that u_{∞} and u_{τ} are positive, then x and λ are required by equation (4.317) to be negative. The local length scales δ and λ vary like x , and the local velocity scales u_{∞} and u_{τ} vary like $1/x$. The mean streamlines are rays through the origin, both inside and outside the boundary layer, as shown in FIGURE 4.28. It follows that there is no entrainment of external fluid, a property that is crucial in any discussion of structure for the turbulent case. These properties of a hypothetical turbulent sink flow, or pure wall flow, were first described in useful detail by COLES (1957) before the flow had been observed experimentally.

This formal identification of pure wall flow with sink flow, laminar or turbulent, is almost obvious, because there is no global length

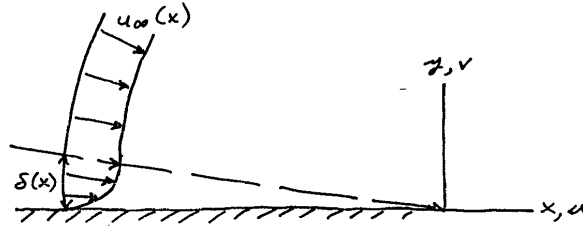


Figure 4.28: The mean flow field for sink flow or pure wall flow (figure 5.40 of HAFEZ 1991). The variable x has the right direction but the wrong sense.

scale for flow toward the origin in a wedge-shaped channel (**show this**). In the laminar case (section x), the flow depends on y/x , or y/δ , or yu_τ/ν ; all are equivalent. In the turbulent case, it can also be shown that any one of the four conditions $D = 1$, $\Pi = 0$, $C_f = \text{constant}$, or zero entrainment implies the others (**show this**).

Now consider again the primitive profile representation

$$\frac{u}{u_\tau} = \frac{1}{\kappa} \ln \frac{yu_\tau}{\nu} + c, \quad (4.319)$$

which ignores any refinements in the sublayer or at the edge of the boundary layer. The corresponding local friction law is

$$\frac{u_\infty}{u_\tau} = \frac{1}{\kappa} \ln \frac{\delta u_\tau}{\nu} + c. \quad (4.320)$$

Together, these formulas imply the logarithmic defect law,

$$\frac{u_\infty - u}{u_\tau} = -\frac{1}{\kappa} \ln \frac{y}{\delta}. \quad (4.321)$$

The conditions $D = 1$ and $\lambda = x$ allow the momentum equation (4.311)

4.11. MORPHOLOGY TURBULENT EQUILIBRIUM FLOW 317

to be written

$$\frac{\partial \tau}{\partial y} = \frac{\rho}{x} (u_\infty^2 - u^2) . \quad (4.322)$$

This can be integrated in closed form as

$$\tau - \tau_w = \frac{\rho u_\tau^2}{\kappa^2} \frac{\delta}{x} \frac{y}{\delta} \left[2 \left(\kappa \frac{u_\infty}{u_\tau} - 1 \right) \left(1 - \ln \frac{y}{\delta} \right) - \ln^2 \frac{y}{\delta} \right] . \quad (4.323)$$

When $y = \delta$ and $\tau = 0$, this becomes

$$\frac{\delta}{x} = - \frac{\kappa^2/2}{\kappa \frac{u_\infty}{u_\tau} - 1} , \quad (4.324)$$

and equation (4.323) can therefore be written

$$\frac{\tau}{\tau_w} = 1 - \frac{y}{\delta} \left(1 - \ln \frac{y}{\delta} \right) + \frac{1}{2} \frac{\frac{y}{\delta} \ln^2 \frac{y}{\delta}}{\left(\kappa \frac{u_\infty}{u_\tau} - 1 \right)} . \quad (4.325)$$

This relationship is plotted in FIGURE 4.29. for several values of u_∞/u_τ . Because $\partial\tau/\partial y \rightarrow 0$ as $y/\delta \rightarrow 1$ from below, the argument closes with respect to the assumption $D = 1$. The last term in equation (4.325) makes no contribution when $y/\delta = 0$ or $y/\delta = 1$ and vanishes identically at infinite Reynolds number ($u_\infty/u_\tau \rightarrow \infty$). At $y/\delta = 1/2$, this term contributes less than 0.02 to τ/τ_w at the lowest practical Reynolds number ($u_\infty/u_\tau = 20$). Thus the shearing stress profile τ/τ_w is nearly the same function of y/δ for all Reynolds numbers (give a figure for $Re_\theta = 10^3, 10^6, 10^9$? Plot u and τ for three Re. Use the proper profile in the sublayer; better or worse?). The same lower limit $u_\infty/u_\tau = 20$ in equation (4.324), with $\kappa = 0.41$, suggests that $-\delta/x$ cannot be larger than about 0.012 for pure wall flow. According to equation (4.320), $\delta u_\tau/\nu$ cannot then be smaller than about 470. These estimates help to explain some difficulties encountered in attempts to produce such a flow in a wind tunnel, as discussed below (see *Laundry, four papers; Sreenivasan; Simpson; Kline. A simple experimental test for the pure wall flow is the condition $Re_\theta = \text{constant}$. Look at slope of (4.325) at wall?*

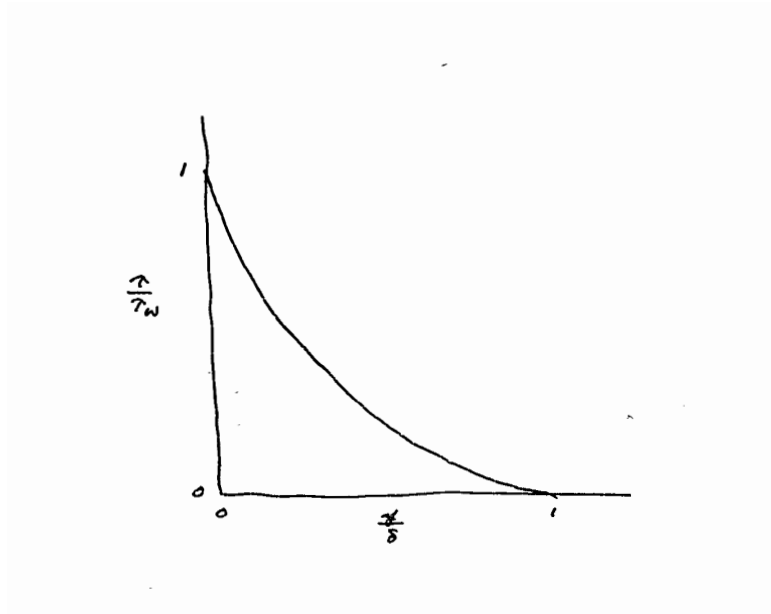


Figure 4.29: Analytical profiles of mean velocity and total shearing stress in pure wall flow at $\delta^+ = 10^3, 10^6, 10^9$ according to equations () and (). The data points are from SPALART ().

4.11. MORPHOLOGY TURBULENT EQUILIBRIUM FLOW 319

Comment on inconsistency with mixing-length theory, constant-stress layer, log profile. The shape of the stress profile makes it difficult to believe that the stress must be constant to obtain a logarithmic velocity; cf. the mixing-length model in SECTION X.)

The displacement thickness and momentum thickness for the primitive profile (4.319) are

$$\delta^* = \int_0^\infty \left(1 - \frac{u}{u_\infty}\right) dy = \frac{u_\tau}{\kappa u_\infty} \delta \quad (4.326)$$

and

$$\theta = \int_0^\infty \frac{u}{u_\infty} \left(1 - \frac{u}{u_\infty}\right) dy = \frac{u_\tau}{\kappa u_\infty} \left(1 - 2 \frac{u_\tau}{\kappa u_\infty}\right) \delta, \quad (4.327)$$

so that

$$\frac{\delta^*}{\theta} = \frac{\kappa \frac{u_\infty}{u_\tau}}{\kappa \frac{u_\infty}{u_\tau} - 2}. \quad (4.328)$$

The profile shape factor δ^*/θ varies from about 4/3 for $u_\infty/u_\tau = 20$ to unity for $u_\infty/u_\tau \rightarrow \infty$ (see Fiedler and Head). The largest value of the friction coefficient $C_f = 2(u_\tau/u_\infty)^2$ and the smallest value of the momentum-thickness Reynolds number $Re_\theta = u_\infty\theta/\nu$ for fully developed flow are 0.0050 and 880, respectively. Clauser's parameter, which is unfortunately also denoted in the literature by β , is defined as

$$\beta = \frac{\delta^*}{\tau_w} \frac{dp}{dx} = \frac{\delta}{x} \frac{u_\infty}{\kappa u_\tau}, \quad (4.329)$$

and is not constant. According to equations (4.324) and (4.329), it varies slowly from about -0.59 for $u_\infty/u_\tau = 20$ to $-1/2$ for $u_\infty/u_\tau \rightarrow \infty$. Bradshaw's parameter a is equal to -1 .

At this writing, digital computers are able to solve the full Navier-Stokes equations for turbulent flow at low but still useful values of Reynolds number. The limit on Reynolds number is imposed by the size of currently available fast memory, and this size can be expected to increase rapidly. The sink flow has recently been computed

by SPALART (1986), using an ingenious formulation that allows the use of periodic streamwise boundary conditions while allowing the layer thickness to vary. Spalart's paper emphasizes relaminarization of sink flow in sufficiently strong negative pressure gradients. A parameter commonly used to measure the pressure gradient in this context (**source?**) is really a measure of dimensionless acceleration;

$$K = \frac{\nu}{u_\infty^2} \frac{du_\infty}{dx} . \quad (4.330)$$

Because $u_\infty x$ is constant for sink flow, so is K . Given further that $u_\infty/u_\tau = \text{constant}$ and that $\lambda = x$, equation (4.330) can also be written

$$K = -\frac{\delta}{x} \frac{u_\tau}{u_\infty} \frac{\nu}{\delta u_\tau} . \quad (4.331)$$

Each of the three factors on the right decreases as the Reynolds number increases. The estimates already quoted ($u_\infty/u_\tau \geq 20$, $0 < \delta/x \leq -0.012$, $\frac{\delta u_\tau}{\nu} \geq 470$) then imply that fully turbulent flow will not be observed if K is greater than about 1.3×10^{-6} . Spalart obtains a plausible turbulent flow, in the weak sense that a logarithmic region is visible in the mean-velocity profile, for $K = 1.5 \times 10^{-6}$ but not for larger values of K .

Other authors (Kibens, Back) have studied this problem of relaminarization experimentally, and work up to 1979 has been reviewed by NARASIMHA and SREENIVASAN (1979). Attention was originally drawn to this phenomenon by Sergienko and Gretzov (19xx), who discovered that initially turbulent boundary layers in a converging-diverging plane nozzle could become laminar, or at least laminar-like, near the throat. This phenomenon is usually complicated by compressibility but the implication is that very large effects on heat transfer can occur near the throat.

The mechanism for inverse transition from turbulent to laminar flow seems to involve closer penetration of intermittency toward and eventually to the wall (Fiedler and Head). The discussion also tends to explain how the curve $D(P)$ can end in mid-air at the point $(D, P) = (1, 1)$. (This point is not yet defined.) A reasonable inference is that turbulent equilibrium flow does not exist for smaller

values of D or P , corresponding to negative Π . If it did, the entrainment would presumably be negative and the turbulence would expire. (More on entrainment. The problem is still a target of opportunity.)

4.11.2 Pure wake flow

The second limiting case, $\Pi = \infty$, corresponds to pure wake flow, with zero surface friction. For large Π , equation (4.300) becomes approximately

$$\kappa \frac{\delta^* u_\infty}{\delta u_\tau} = \Pi , \quad (4.332)$$

and the product of Π and u_τ is determined in the limit $\Pi \rightarrow \infty$ and $u_\tau \rightarrow 0$ by

$$\frac{\Pi u_\tau}{\kappa u_\infty} = \frac{\delta^*}{\delta} . \quad (4.333)$$

The general profile formula (4.250) therefore collapses to

$$\frac{u}{u_\infty} = \frac{\delta^*}{\delta} w\left(\frac{y}{\delta}\right) , \quad (4.334)$$

with the auxiliary condition $w(1) = \delta/\delta^* = 2$. Given that θ/δ and δ^*/δ are constant for the profile formula (4.334), the momentum-integral equation (4.231) with $\tau_w = 0$ can be written

$$-\left(2 + \frac{\delta^*}{\theta}\right) \frac{1}{u_\infty} \frac{du_\infty}{dx} = \frac{1}{\theta} \frac{d\theta}{dx} = \frac{1}{\delta^*} \frac{d\delta^*}{dx} = \frac{1}{\delta} \frac{d\delta}{dx} . \quad (4.335)$$

Integration gives immediately

$$\delta u_\infty^{2+\delta^*/\theta} = \text{constant} . \quad (4.336)$$

With the aid of equation (4.335) for $d\delta/dx$, the normal velocity component at the edge of the boundary layer can be calculated from

$$v_\infty = - \int_0^\delta \frac{\partial u}{\partial x} dy = -\delta^* \frac{du_\infty}{dx} \left[\int_0^1 w d\zeta + \left(2 + \frac{\delta^*}{\theta}\right) \int_0^1 \zeta \frac{dw}{d\zeta} d\zeta \right] . \quad (4.337)$$

The two integrals are known from equation (4.334);

$$\int_0^1 w \, d\zeta = \frac{\delta}{\delta^*} - 1, \quad \int_0^1 \zeta \frac{dw}{d\zeta} \, d\zeta = \frac{\delta}{\delta^*} - \int_0^1 w \, d\zeta = 1 . \quad (4.338)$$

Consequently, equation (4.337) becomes

$$v_\infty = -\delta^* \frac{du_\infty}{dx} \left[\left(\frac{\delta}{\delta^*} - 1 \right) + \left(2 + \frac{\delta^*}{\theta} \right) \right] . \quad (4.339)$$

Let this value of v_∞ be substituted in equation (4.289) for P . After some algebra, the result is

$$P = \frac{\delta^*}{\delta} \left(1 + \frac{\delta^*}{\theta} \right) \left(\frac{D}{1-D} \right) \quad (4.340)$$

for pure wake flow. The analysis so far does not specify laminar or turbulent flow or a particular form for the function $w(y/\delta)$.

Consider first laminar flow, for which, according to equation (4.292),

$$P = 2 \frac{\delta^*}{\delta} . \quad (4.341)$$

Solution for D in equation (4.340) gives

$$D = \frac{2}{3 + \delta^*/\theta} , \quad (4.342)$$

and equation (4.293) then gives

$$n = -\frac{1}{3 + 2\delta^*/\theta} , \quad \beta = -\frac{1}{1 + \delta^*/\theta} . \quad (4.343)$$

Use of the accurate laminar value $\delta^*/\theta = 4.02923$ (A.M.O. Smith) then gives the accurate values (**reverse order?**)

$$n = -0.09043, \quad \beta = -0.19884 . \quad (4.344)$$

However, if the value $\delta^*/\theta = 4$ for an antisymmetric profile such as $w = 2 \sin^2(\pi y/2\delta)$ had been taken as a reasonable estimate for continuously separating flow, these would have been replaced by

$$n = -\frac{1}{11} = -0.0909, \quad \beta = -\frac{1}{5} = -0.2000 . \quad (4.345)$$

4.11. MORPHOLOGY TURBULENT EQUILIBRIUM FLOW 323

For the laminar Falkner-Skan problem, therefore, the critical value $\beta = -0.1988$ could have been estimated quite accurately before the equations were solved. This conclusion is important because the value $\beta = -0.1988$ is a turning point. **(Define.)**

Now consider turbulent flow. For the pure wake flow of the turbulent equilibrium family, $P = 1 + \Pi$ is infinite in equation (4.340). Given that δ^*/δ and δ^*/θ are finite numbers, it follows that

$$D = 1 \tag{4.346}$$

for pure wake flow. This result is not expected, because $u_\tau \equiv 0$, and the limit of $u_\infty du_\tau / u_\tau du_\infty = 0/0$ is not defined. Nevertheless, the result is correct. The estimates $\delta^*/\delta = 1/2$ and $\delta^*/\theta = 4$ in equation (4.340) yield an asymptotic formula for large P (note sensitivity of δ^*/θ to Π),

$$P = 1 + \Pi = \frac{5}{2} \frac{D}{1 - D} \tag{4.347}$$

or

$$D = \frac{2 + 2\Pi}{7 + 2\Pi} = \frac{2P}{5 + 2P} . \tag{4.348}$$

(How good is this? See data for equilibrium flow. Better estimate?)

The velocity profile (4.334) and some algebra give, for the dimensionless normal velocity component in normalized form (check argument of w and plot both),

$$\left(2 + \frac{\delta^*}{\theta}\right) \frac{v/u}{d\delta/dx} = \left(2 + \frac{\delta^*}{\theta}\right) \frac{y}{\delta} - \left(1 + \frac{\delta^*}{\theta}\right) \frac{1}{w} \int_0^{y/\delta} w \, d\zeta , \tag{4.349}$$

and for the shearing stress

$$\left(2 + \frac{\delta^*}{\theta}\right) \frac{\tau/\rho u_\infty^2}{d\delta/dx} = \frac{y}{\delta} - \left(\frac{\delta^*}{\theta}\right)^2 \left[\left(1 + \frac{\delta^*}{\theta}\right) w \int_0^{y/\delta} w \, d\zeta - \frac{\delta^*}{\theta} \int_0^{y/\delta} w^2 \, d\zeta \right] . \tag{4.350}$$

It remains to dispose of x . I have not found a rigorous argument to show $d\delta/dx = \delta/x = \text{constant}$, although this condition is strongly

suggested by the fact that the viscosity ν is assumed to play no role, so that y/δ is the obvious independent variable. Equations (4.349) and (4.350) show that if $d\delta/dx = \text{constant}$, then v/u and $\tau/\rho u_\infty^2$ are functions only of y/δ , and this property is therefore at least plausible. The condition $\delta \sim x$ and equation (4.336) then imply

$$u_\infty \sim x^{-\frac{1}{2+\delta^*/\theta}} . \quad (4.351)$$

The estimate previously used; namely, $\delta^*/\theta = 4$, gives

$$u_\infty \sim x^{-0.167} . \quad (4.352)$$

The pure wake flow was also a hypothetical flow when it was first described by COLES (1957). Experiments are difficult but the difficulties are being overcome, as demonstrated in studies by STRATFORD (1959), by SPANGENBERG, ROWLAND, and MEASE (1967), and by DENGEL and FERNHOLZ (19xx).

4.11.3 The momentum-integral equation

A simple but tedious argument shows that a knowledge of the function $D(P)$ makes it possible to integrate the Karman momentum-integral equation,

$$u_\tau^2 = \frac{d}{dx} u_\infty^2 \theta + u_\infty \delta^* \frac{du_\infty}{dx} . \quad (4.353)$$

A count of variables (anticipating some remarks to follow) shows that there are five quantities, each depending on x ;

$$x; u_\infty(x), u_\tau(x), \delta^*(x), \theta(x), \delta(x) , \quad (4.354)$$

with the sixth variable P constant wherever it appears, to guarantee an equilibrium flow. Thus five independent equations are required before integration can be attempted. The quantity δ appears in the second of the required equations, the local friction law;

$$\frac{u_\infty}{u_\tau} = \frac{1}{\kappa} \ln \frac{\delta u_\tau}{\nu} + \text{constant} . \quad (4.355)$$

If the wall-wake formula is used, this becomes

$$\frac{u_\infty}{u_\tau} = \frac{1}{\kappa} \ln \frac{\delta u_\tau}{\nu} + c + \frac{2\Pi}{\kappa} \quad (4.356)$$

and thus introduces a sixth variable $\Pi(x)$. However, the argument can and will sometimes proceed without exhibiting the parameter Π explicitly, only P . For example,

$$\kappa \frac{\delta^* u_\infty}{\delta u_\tau} = C_1(P) = \text{constant} ; \quad (4.357)$$

$$\frac{\kappa^2}{2} \frac{(\delta^* - \theta)}{\delta} \frac{u_\infty^2}{u_\tau^2} = C_2(P) = \text{constant} . \quad (4.358)$$

The wall-wake formula (4.250) makes these more manageable;

$$\kappa \frac{\delta^* u_\infty}{\delta u_\tau} = \kappa \int_0^\infty \left(\frac{u_\infty - u}{u_\tau} \right) d \frac{y}{\delta} = 1 + \Pi = C_1(P) ; \quad (4.359)$$

$$\begin{aligned} \frac{\kappa^2}{2} \frac{(\delta^* - \theta) u_\infty^2}{\delta u_\tau^2} &= \frac{\kappa^2}{2} \int_0^\infty \left(\frac{u_\infty - u}{u_\tau} \right)^2 d \frac{y}{\delta} \\ &= 1 + \left[1 + \frac{Si(\pi)}{\pi} \right] \Pi + \frac{3}{4} \Pi^2 = C_2(P) , \end{aligned} \quad (4.360)$$

where

$$Si(x) = \int_0^x \frac{\sin u}{u} du = -x \int_0^1 \ln y \cos xy dy . \quad (4.361)$$

These formulas, incidentally, assume that the log law is valid in the sublayer, and therefore need a small correction.

The laws of physics and the accepted similarity laws are thus represented by the momentum-integral equation (4.353);

$$\tau_w = \rho u_\infty^2 \frac{d\theta}{dx} + (2\theta + \delta^*) \rho u_\infty \frac{du_\infty}{dx} \quad (4.362)$$

the local friction law (4.356);

$$\frac{u_\infty}{u_\tau} = \frac{1}{\kappa} \ln \frac{\delta u_\tau}{\nu} + c + \frac{2\Pi}{\kappa} \quad (4.363)$$

the formulas for displacement and momentum thickness (4.359) and (4.360); and the specification of equilibrium flow; i.e., flow with a defect law, according to Clauser, for which

$$\Pi = \text{constant} . \quad (4.364)$$

The notation $C_1(P)$ and $C_2(P)$ is intended to convey that a defect law is sufficient for the analysis, and the law of the wake is not required. Nevertheless, the notation Π will sometimes be retained for simplicity.

There are five equations for six dependent variables, $u_\infty(x)$, $u_\tau(x)$ or $\tau_w(x)$, $\delta^*(x)$, $\theta(x)$, and $\Pi(x)$. One additional independent equation is needed to determine the six variables and thus the flow field $u(x, y)$, $v(x, y)$, $\tau(x, y)$. Before the question of the last required equation is considered, the material so far on hand should be exploited. Let equations (4.359) and (4.360) be solved for δ^* and θ , respectively, and the indicated differentiation in equation (4.362) be carried out, noting that C_1 and C_2 are independent of x for equilibrium flow. The result is

$$\begin{aligned} \kappa^2 = \frac{\delta}{u_\infty} \frac{du_\infty}{dx} \left(2C_1 \kappa \frac{u_\infty}{u_\tau} \right) + \frac{\delta}{u_\tau} \frac{du_\tau}{dx} \left(C_1 \kappa \frac{u_\infty}{u_\tau} - 4C_2 \right) \\ + \frac{d\delta}{dx} \left(C_1 \kappa \frac{u_\infty}{u_\tau} - 2C_2 \right) . \quad (4.365) \end{aligned}$$

Now let equation (4.363) be solved for δ , differentiated, and the result substituted for $d\delta/dx$ in equation (4.365), which becomes (need assembly of derivatives)

$$\begin{aligned} \kappa^2 = \frac{\delta}{u_\infty} \frac{du_\infty}{dx} \left[C_1 \left(\kappa \frac{u_\infty}{u_\tau} \right)^2 + 2(C_1 - C_2) \kappa \frac{u_\infty}{u_\tau} \right] \\ - \frac{\delta}{u_\tau} \frac{du_\tau}{dx} \left[C_1 \left(\kappa \frac{u_\infty}{u_\tau} \right)^2 - 2C_2 \kappa \frac{u_\infty}{u_\tau} + 2C_2 \right] . \quad (4.366) \end{aligned}$$

4.11. MORPHOLOGY TURBULENT EQUILIBRIUM FLOW 327

Clearly it is time to simplify the notation by defining Karman's variable,

$$z = \kappa \frac{u_\infty}{u_\tau} . \quad (4.367)$$

This expression can also be differentiated to obtain

$$\frac{1}{z} \frac{dz}{dx} = \frac{1}{u_\infty} \frac{du_\infty}{dx} - \frac{1}{u_\tau} \frac{du_\tau}{dx} = (D - 1) \frac{1}{u_\tau} \frac{du_\tau}{dx} = \left(\frac{D - 1}{D} \right) \frac{1}{u_\infty} \frac{du_\infty}{dx} , \quad (4.368)$$

where D is the ratio of two derivatives, according to equation (4.288), and can depend on x . The derivatives on the right in equation (4.366) can now be eliminated in favor of D and dz/dx to obtain for equilibrium flow

$$\kappa^2 \frac{dx}{\delta} = \frac{dz}{z} \left[C_1 z^2 - 2C_2 z + 2 \left(\frac{D}{D - 1} \right) C_1 z - 2 \left(\frac{1}{D - 1} \right) C_2 \right] . \quad (4.369)$$

In the general case, little more can be done until the missing last equation is specified. Note that there is no obvious way to eliminate the factor δ on the left in the general case without re-introducing either u_τ or u_∞ . (**Say why pure wall, wake flow could be done; missing equation might be $u_\infty = \text{constant}$, $D = 0$, $D = \infty$, $u_\tau = \text{constant}$, $u_\infty/u_\tau = \text{constant}$, or $u_\tau = 0$; see above.**)

Clouser, second paper. Argument for $(\delta^/\tau_w) dp/dx$ is nonsense. It is based on eddy-viscosity attack, leading to a Blasius profile with non-zero velocity at the wall. One of the last figures is in fact the law of the wake, but Clouser weighted the outer departure from the log law equally with the inner departure. This is characteristic; authors do something useful and then run out of gas, thus leaving the next step for someone else.*

Stratford. The wall friction is not zero; the title is unfortunate. There is a good notion of what a good diffuser should look like.

Bradshaw. The exponent in $u_\infty \approx x^a$ cannot be more negative than -0.167 . Thus his value -0.255 must involve some funny business with the coordinate x , especially the apparent origin. These two flows have not been analyzed for $D(P)$.

East and Sawyer. The flows with $dp/dx < 0$ cannot be in equilibrium,

because the surface friction is not constant, but changing even more rapidly than for the flow with zero pressure gradient. The origin for x should be at the right, with $x < 0$. Where does $u_\infty x$ change sign?

Spalart. Each C_f and R_θ on a curve is a different flow. The issue is relaminarization. Launder had four separate tries at the pure sink flow. The stress distribution is completely incompatible with the assumption $\tau = \tau_w$ of the mixing-length theory. The theory gives the right answer for the wrong reasons. Note that figure 6 shows peak u^+ as 2.3, not 2.7.

4.11.4 Flow at constant pressure

However, there is one special case, first exploited by Karman in 1932 (Stockholm, Schiffs), in which the fifth equation is self-evident; namely (note also wall, wake flow, $\tau_w = \text{constant}$)

$$u_\infty = \text{constant} \quad \text{or} \quad D = 0 . \quad (4.370)$$

In this case, from equation (4.363),

$$\frac{\delta u_\tau}{\nu} = \text{constant} e^z , \quad (4.371)$$

where the constant is equal to $e^{-\kappa c - 2\Pi}$ for the wall-wake profile. At some arbitrary reference station, denoted by the subscript zero (do not assume $x = 0$ when $C_f = \infty$),

$$\frac{\delta_o u_{\tau_o}}{\nu} = \text{constant} e^{z_o} , \quad (4.372)$$

so that

$$\delta = \frac{\delta_o u_{\tau_o}}{\kappa u_\infty} z e^{z - z_o} . \quad (4.373)$$

When this expression is used for δ in equation (4.369), with $D = 0$, there is obtained

$$\left(\frac{\kappa^2 z_o e^{z_o}}{\delta_o} \right) dx = e^z (C_1 z^2 - 2C_2 z + 2C_2) dz . \quad (4.374)$$

4.11. MORPHOLOGY TURBULENT EQUILIBRIUM FLOW 329

This equation can be integrated in closed form between the limits z_o and z , with $x = x_o$ when $z = z_o$. It is also convenient to replace z_o and e^{z_o} by their physical equivalents; e.g., from equation (4.372). The result is (note that x_o is not the origin)

$$\kappa^3 \frac{u_\infty(x - x_o)}{\nu} = e^z [C_1 z^2 - 2(C_1 + C_2)z + 2(C_1 + 2C_2)] - e^{z_o} [C_1 z_o^2 - 2(C_1 + C_2)z_o + 2(C_1 + 2C_2)] . \quad (4.375)$$

This equation was derived by Karman, who chose for unknown reasons to keep only the dominant terms on the right for large z , and thus to write

$$R_x = \frac{u_\infty x}{\nu} = C z^2 e^z , \quad (4.376)$$

where C incorporates C_1 and κ^2 . Because

$$z = \kappa \frac{u_\infty}{u_\tau} = \kappa \left(\frac{2}{C_f} \right)^{1/2} , \quad (4.377)$$

where the local friction coefficient is defined as

$$C_f = \frac{2\tau_w}{\rho u_\infty^2} , \quad (4.378)$$

equation (4.376) is equivalent to

$$\left(\frac{2}{C_f} \right)^{1/2} = \frac{1}{\kappa} \ln(C_f R_x) + A , \quad (4.379)$$

where A is a constant. This equation was modified by Schoenherr (ref) to represent $C_F = (1/x) \int_0^x C_f dx$ rather than C_f , and was used to determine κ and A by a fit to overall drag data for towed submerged flat plates. I recommend against such use. The value obtained for κ is especially unreliable, in view of the severe and unnecessary approximation in equation (4.376). **(Read JAS paper again on point of arbitrary choice for δ and ν/u_τ at one station. Comment on need for x_o , but perhaps not for z_o . Note that origin for turbulent boundary layer cannot be defined experimentally.)**

I return now to the general case and make the seminal assumption

$$D = \frac{d \ln u_\infty}{d \ln u_\tau} = \text{constant} \quad (4.380)$$

for turbulent equilibrium flow. It follows that

$$\frac{u_\infty}{u_{\infty_o}} = \left(\frac{u_\tau}{u_{\tau_o}} \right)^D, \quad (4.381)$$

and therefore that (compare equation (4.368))

$$\frac{z}{z_o} = \left(\frac{u_\infty}{u_{\infty_o}} \right) \left(\frac{u_{\tau_o}}{u_\tau} \right) = \left(\frac{u_\tau}{u_{\tau_o}} \right)^{D-1} = \left(\frac{u_\infty}{u_{\infty_o}} \right)^{\frac{D-1}{D}}. \quad (4.382)$$

Consequently, δ in equation (4.369) can be eliminated using equation (4.374), and (u_τ/u_{τ_o}) can then be eliminated using equation (4.382). The final result is (note sink flow; $D = 1$ and $dz = 0$)

$$\begin{aligned} \kappa^2 z_o^{\frac{1}{1-D}} \frac{e^{z_o}}{\delta_o} dx = \\ z^{\frac{D}{1-D}} e^z dz \left[C_1 z^2 - 2C_2 z - 2 \left(\frac{D}{1-D} \right) C_1 z + 2 \left(\frac{1}{1-D} \right) C_2 \right]. \end{aligned} \quad (4.383)$$

It is possible that the form of equation (4.383) would suggest the hypothesis $D = \text{constant}$ even if attention had not been attracted to this hypothesis by manipulation of the continuity equation. Note that x now plays the role of dependent variable. (Need $D(P)$.)

Equation (16)⁹ can be integrated in closed form in terms of the function $E_i(z) = \int_{-\infty}^z (e^u/u) du$ if $D/(1-D)$ is an integer (or half integer? check); i.e., if D (plus or minus?) has one of the values 0, 1/2, 2/3, 3/4, 4/5, ... or ∞ , 2, 3/2, 4/3, 5/4, ... The value $D = 1$ is a dual special case corresponding either to pure wall flow or to pure wake flow. **(Comment on these as sub-cases. $D = 1$ is awkward, but $D = \infty$ goes all right. Give details about how to get $u_\infty(x)$, $\delta(x)$, $C_f(x)$ for equilibrium flow.)**

⁹Unclear reference

4.11. MORPHOLOGY TURBULENT EQUILIBRIUM FLOW 331

There are two limiting cases, namely $\Pi = 0$ and $\Pi = \infty$, that deserve special study. There are good reasons to associate the case $\Pi = 0$ with sink flow, the most important being the result (6)¹⁰ above, that $yu_\tau/\nu = \text{constant}$ defines a mean streamline. However, it has to be proved that $\delta u_\tau/\nu = \text{constant}$ for sink flow.

(There is a work sheet that concludes

$$(D - 1)\Pi = -\frac{5}{2}$$

in the limit. Try various plots?)

Falkner and Skan. The notation is not well chosen.

Hartree. introduced the modern notation.

Stewartson. found a second branch.

Cebeci and Keller. show profiles. There are two flows, say for a corner, one resembling a mixing layer (separated).

Look at limit to get mixing layer. This is a common node for several analyses.

Libby and Liu. Are there no flows for $-1 < \beta < -0.1988$?

4.11.5 Entrainment

All shear flows with free boundaries grow in thickness by a process called entrainment. If the flow is turbulent, the details of this process, in which irrotational external fluid acquires small-scale vorticity, are difficult, and to some extent controversial. From a phenomenological point of view, the Reynolds-averaged equations of motion contain the essential difficulty, which is the need to define a finite thickness for the layer. Laminar flow is free of this difficulty. The velocity in the shear layer approaches the free-stream value asymptotically to meet the boundary condition $f'(\infty) = 1$. Moreover, a characteristic local scale for the layer thickness is supplied by the similarity argument. For the Falkner-Skan flows, for example, this scale is the geometric

¹⁰Again, an unclear reference

mean of x and ν/u_∞ . By contrast, turbulent boundary-layer flow is bounded at a finite distance from the wall by an irregular interface having turbulent flow on one side and non-turbulent flow on the other. The associated finite thickness is thus connected with the concepts of interface and intermittency.

Even without these concepts, any profile formula that claims to describe the flow outside the sublayer and near the free stream must contain and in practice must define, however ambiguously, a thickness δ . The loosest definition dispenses with formulas by using the arbitrary condition that the mean velocity at $y = \delta$ is 99 percent, say, of the free-stream value. I believe that this definition should be a last resort, because of the heavy burden that it puts on the accuracy of the boundary-layer approximation and on the skill of the experimenter in measuring mean velocity to close resolution in a region of intermittent turbulence.

For an equilibrium flow with a velocity-defect law, the need to define a thickness δ can be finessed for some purposes, as first noted by SCHULTZ-GRUNOW (1940). In equation (x), neither δ nor the equilibrium constant A is well defined. The existence of a defect law can therefore be tested a priori by using yu_τ/δ^*u_∞ as independent variable. If the more specific wall-wake formula (x) is used instead to define δ^* , the parameter Π is well defined, and therefore so is δ (**compare with pipe or channel**).

Suppose therefore that δ can be usefully defined, and consider entrainment. In FIGURE 4.30, let s represent the component of velocity normal to the edge of the boundary layer at $y = \delta$, with s positive when the flow is into the layer. Evidently, for small angles,

$$\frac{s}{u_\infty} = \frac{d\delta}{dx} - \frac{v_\infty}{u_\infty} . \quad (4.384)$$

It has already been argued in equation (4.339) that

$$v_\infty = \frac{d}{dx}u_\infty \delta^* - \delta \frac{du_\infty}{dx} , \quad (4.385)$$

where v_∞ means $v(x, \delta)$. Consequently,

$$s = \frac{d}{dx}u_\infty(\delta - \delta^*) . \quad (4.386)$$

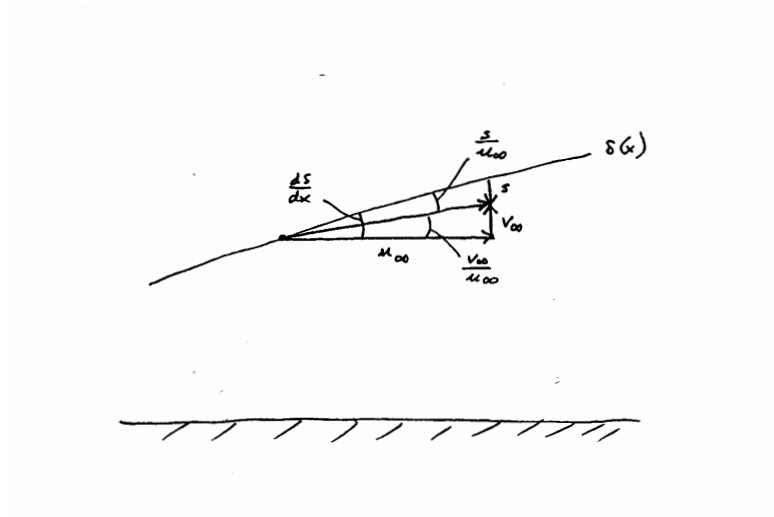


Figure 4.30: The definition of the entrainment velocity s with expanded vertical scale. Note that δ must be defined.

If the product $\delta^* u_\infty$ is replaced by its equivalent from equation (4.300), this result can be written

$$s = \frac{d}{dx} \left[\frac{\delta u_\tau}{\kappa} \left(\kappa \frac{u_\infty}{u_\tau} - 1 - \Pi \right) \right]. \quad (4.387)$$

The differentiation can now be carried out formally, with $\Pi = \text{constant}$ for equilibrium flow. It is convenient to choose the surviving derivative as $d\delta/dx$ by making use of the identity, $u_\tau du_\infty/dx = D u_\infty du_\tau/dx$ as well as the derivative of the local friction law (4.363). The final result for equilibrium flow is

$$\frac{s}{u_\infty} = \frac{d\delta}{dx} \left[\frac{z(1-D)}{z(1-D)+1} \right] \left(1 - \frac{\Pi u_\tau}{\kappa u_\infty} \right), \quad (4.388)$$

where $z = \kappa u_\infty / u_\tau$ as before. Note that the derivation has not used the momentum-integral equation (4.362). **(Need calculations and plots of s/u_∞ . What combination is independent of x ?)**

This formula has several useful implications. The last factor is deliberately written as $(1 - \Pi u_\tau / \kappa u_\infty)$ rather than as $(1 - \Pi / z)$ for the

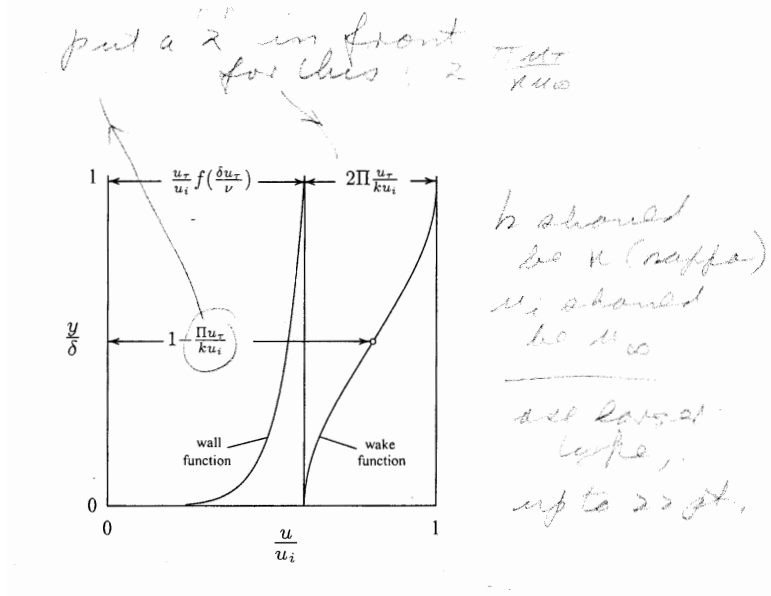


Figure 4.31: Decomposition of the wall-wake profile to show the characteristic velocity scale $\mathcal{L} = 1 - \Pi u_\tau / \kappa u_\infty$ that occurs in equation (4.388) for entrainment. [Note written corrections to add 2 to one coefficient and that k should be κ and u_i should be u_∞ . - K. Coles]

sake of the nice geometrical interpretation shown in FIGURE 4.31. The universal profile formula

$$\frac{u}{u_\tau} = f\left(\frac{yu_\tau}{\nu}\right) + \frac{\Pi}{\kappa} w\left(\frac{y}{\delta}\right) \tag{4.389}$$

can also be written

$$\frac{u}{u_\infty} = \frac{u_\tau}{u_\infty} f\left(\frac{yu_\tau}{\nu}\right) + \frac{\Pi u_\tau}{\kappa u_\infty} w\left(\frac{y}{\delta}\right) . \tag{4.390}$$

At the edge of the boundary layer, therefore, where $w(y/\delta) = w(1) = 2$,

$$1 = \frac{u_\tau}{u_\infty} f\left(\frac{\delta u_\tau}{\nu}\right) + \frac{2\Pi u_\tau}{\kappa u_\infty} . \tag{4.391}$$

Thus one factor in a reference velocity for entrainment is the free-stream velocity reduced by half of the strength of the wake component. The quantity $(1 - \Pi u_\tau / \kappa u_\infty)$ in equation (4.388) varies from 1 for pure wall flow at one extreme to 1/2 for pure wake flow at the other extreme as Π varies from 0 to ∞ . For intermediate equilibrium flows, it increases slowly with increasing x but always lies between 1/2 and 1. Vanishing entrainment for pure wall flow is enforced by the factor $(1 - D)$ in the numerator of equation (4.388). Because $d\delta/dx$ is negative for pure wall flow, the value $D = 1$ must be approached from above. For pure wake flow, the product $z(1 - D)$ remains finite. This property is most easily shown by putting $\delta^* = \delta/2$ in equation (4.386) and using the momentum-integral equation (4.335) to eliminate du_∞/dx . The result, which uses the profile equation (4.334) to estimate $\delta^*/\theta = 4$, is

$$\frac{s}{u_\infty} = \frac{1}{2} \frac{d\delta}{dx} \frac{(1 + \delta^*/\theta)}{(2 + \delta^*/\theta)} = \frac{5}{12} \frac{d\delta}{dx} . \quad (4.392)$$

When this result is compared with (4.388) with $\Pi u_\tau / \kappa u_\infty = 1/2$, it appears that in the limit $\Pi \rightarrow \infty$

$$z(1 - D) = P(1 - D) = 1 + \frac{\delta^*}{\theta} = 5 \quad (4.393)$$

Unfortunately, equation (4.393) is demonstrably not a useful approximation for $D(P)$ when $P \rightarrow \infty$ (see section *x*).

One hypothetical equilibrium flow that has not been observed but has a plausible structure is the flow with $u_\tau = \text{constant}$, or $D = \infty$. In the wall region, the flow is parallel to the wall. **(Discuss v , τ . Estimate Π . Give formula for s .)**

(Comment on Bradshaw's hypothesis, that $u_\infty \sim x^a$ for any equilibrium turbulent flow. He studied two flows claimed to be described by $a = -0.150$ and $a = -0.255$. Since neither flow was very close to separation, it is likely that the origin for x was not properly chosen. The same is true for the flows studied by East and Sawyer.)

(Comment on $P = \infty$ for pure wake flow, so that curve in coordinates $(\lambda v / P \delta u, y / P \delta)$ shrinks to the origin.)

(Note the incompatibility of linear growth and associated channel shape; boundary layers in a diffuser will eventually overlap.)

c is sensitive to roughness, mass transfer (these may be combined). The mixing length theory works better for mass transfer than anything else at the moment.

Continue with law of the wake and 1968 Stanford contest paper. Do separation profile as a limit. Arguments for the logarithmic profile are all quite porous. The mixing length is an exasperating relict of the early days, but it cannot be ignored for some problems (compressibility, mass transfer).

I keep looking over at the Falkner-Skan problem and trying to find ideas which will put the turbulent problem in the same condition.

Comment on s ; what is sought is a simple rule for s that will work for equilibrium and for non-equilibrium conditions. (Head and others; should argument be at some other value than δ ?). One guess might be $s \sim 2\Pi u_\tau / \kappa u_\infty$.

Note that D and P do not involve x explicitly. Moreover, $D = \text{constant}$ can be tested experimentally.

A possible device for interpolation in the curve $D(P)$ rests on the entrainment properties of equilibrium boundary layers. What is required is the component of the free-stream flow normal to the edge of the boundary layer at $y = \delta$. Since δ plays a central role, the analysis cannot be exact. It is always a delicate matter to define the part of the flow that lies within the boundary layer.

The sketch shows the relative position of the boundary-layer edge (comment on definition) and the local mean streamline. The velocity s normal to the edge is, for small angles,

$$s = u_\infty \left(\frac{d\delta}{dx} - \frac{v_\infty}{u_\infty} \right). \quad (4.394)$$

The entrainment velocity s is defined to be positive when there is flow into the boundary layer. Considerable effort has been spent, without result, in trying to put the last equation in a form showing explicitly the role of the equilibrium parameter Π . The velocity v_∞ at the edge

4.11. MORPHOLOGY TURBULENT EQUILIBRIUM FLOW 337

of the boundary layer has already been defined by equation (4.385);

$$v_\infty = \frac{d\delta^* u_\infty}{dx} - \delta \frac{du_\infty}{dx} . \quad (4.395)$$

Substitution for v_∞ in equation (4.394) gives

$$s = \frac{d}{dx} u_\infty (\delta - \delta^*) . \quad (4.396)$$

Use the identity $\delta u_\infty = z \delta u_\tau / k$, where $z = \kappa u_\infty / u_\tau$, and replace $\delta^* u_\infty$ by $(1 + \Pi) \delta u_\tau / \kappa$, from equation (4.300). Differentiation and elimination of $d\delta u_\tau / dx$ with the aid of equation (4.363) gives, for equilibrium flow,

$$\frac{s}{u_\infty} = \frac{s}{\kappa} \frac{dz}{dx} \left(1 - \frac{\Pi}{z} \right) \quad (4.397)$$

(Need several versions of derivative.)

$$\frac{s}{u_\infty} = \frac{d\delta}{dx} \left[\frac{\kappa \frac{u_\infty}{u_\tau} (1 - D)}{\kappa \frac{u_\infty}{u_\tau} (1 - D) + 1} \right] \left(1 - \frac{\Pi u_\tau}{\kappa u_\infty} \right) . \quad (4.398)$$

All of the factors on the right in this expression vary slowly with x in an equilibrium flow. The last factor, $(1 - \Pi u_\tau / \kappa u_\infty)$, has a useful geometric interpretation, shown in the sketch (Figure 4.31). It varies from unity for pure wall flow to 1/2 for pure wake flow. In short, the characteristic velocity for entrainment is the full velocity of the wall component at $y = \delta$, plus half of the velocity of the wake component. (Indicates wake component not dominant; cf. pure wall flow.) The quantity in square brackets in equation (4.398) is zero for pure wall flow, confirming that this flow has zero entrainment. For the other limit $\Pi = \infty$, it is necessary to invoke the asymptotic equation (4.347) for $D(P)$ and equation (A.5)¹¹ for the finite limit of Pu_τ to obtain (check this for completeness)

$$\frac{s}{u_\infty} = \frac{5}{12} \frac{d\delta}{dx} = \text{constant} \quad (4.399)$$

¹¹Probably an incorrect reference.

for pure wake flow, where δ^*/δ has been taken as $1/2$.

The entrainment formula (4.398) provides a useful interpolation device for the function $D(P)$. The quantity δ/u_∞ can be evaluated for the turbulent equilibrium flows listed in section x, as shown in figure y. (Check the x -dependence of the three factors in equation (4.398), separately and in combination, to try to find a constant.) A useful fit in the figure is provided by what?

Finally, it is a reasonable inference from equation (4.388) that there does not exist a turbulent equilibrium flow with $\delta = \text{constant}$, corresponding to the plane stagnation-point flow in the Falkner-Skan family. If such a flow did exist, it would have zero entrainment, and thus the entrainment could not vary monotonically with Π . This inference could be tested experimentally by constructing a flow with $\delta = \text{constant}$ and showing that it is not in equilibrium. (**Has this been done accidentally?**)

A related question in any attempt to construct a rigorous analogy between turbulent and laminar equilibrium flows is connected with the singular laminar case $\beta = 2$ or $\eta = \infty$ (see section x). This case separates laminar flows in which x and u_∞ have the same sign (e.g., Blasius flow) from flows in which x and u_∞ have opposite signs (e.g., sink flow). There is no obvious combination of variables in the turbulent problem, like $(u_\infty x)^{1/2}$ or $(u_\infty/x)^{1/2}$, to suggest that the same distinction needs to be made (*needs more thought*). At the same time, $d\delta/dx$ does change sign. (*Is s/u_∞ close to constant for equilibrium flow?*)

4.11.6 Experiments in equilibrium flow

- BAUER (1953) ASCE Sep. 281
- CLAUSER (1954) JAS **21**, 91
- STRATFORD (1959) JFM **5**, 17
- URAM and ROSENBERG (1959) Bull. APS.
- BRADSHAW (1967) JFM **29**, 625
- HERRING and NORBURY (1967) JFM **27**, 541

SPANGENBERG et al. (1967) FMIF, 110
 JONES and LAUNDER (1972)
 SHISHKOV et al. (1975) TVT **13**, 1302
 CHARNAY and BARIO (1976) Madrid
 EAST and SAWYER (1979) AGARD, Paper 6
 HASTINGS and MORETON (1982)
 SPALART (1986) JFM **172**, 307
 SPALART (1987)
 WHITE and TIEDERMAN (1990)
 DENGEL and FERNHOLZ

4.11.7 The function $D(P)$

A check on the internal consistency of various experimental realizations of turbulent equilibrium flows is useful. Let the momentum-integral equation (4.366) be rewritten, replacing $-u_\tau dx/du_\tau$ by λ and $-u_\infty dx/du_\infty$ by λ/D , to obtain

$$\kappa^2 \frac{\lambda}{\delta} = (C_z z^2 - 2C_2 z + 2C_2) - D(C_1 z^2 - 2C_2 z + 2C_1 z) . \quad (4.400)$$

A similar operation on the differential version of the local friction law (4.363), with Π constant, yields

$$\kappa^2 \frac{\lambda}{\delta} = \frac{\kappa^2}{d\delta/dx} [z(1 - D) + 1] . \quad (4.401)$$

These expressions can be equated and the result solved for $d\delta/dx$ (see footnote, p 502, my 1957 paper),

$$\frac{d\delta}{dx} = \frac{\kappa^2 [z(1 - D) + 1]}{(C_1 z^2 - 2C_2 z + 2C_2) - D(C_1 z^2 - 2C_2 z + 2C_1 z)} \quad (4.402)$$

or for D ,

$$D = \frac{(C_1 z^2 - 2C_2 z + 2C_2) - \frac{\kappa^2}{d\delta/dx} (z + 1)}{(C_1 z^2 - 2C_2 z + 2C_1 z) - \frac{\kappa^2}{d\delta/dx} z} . \quad (4.403)$$

(Look this whole business over to see if there is any other useful variable: du_∞/dx or du_τ/dx etc.)

Suppose that equations (4.402) and (4.403) are to be tested against experimental data for equilibrium flow. Thus $z = \kappa u_\infty/u_\tau$ and $\delta u_\tau/\nu$ are obtained from a fit to the mean-velocity profile; u_τ follows from z and the experimental value of u_∞ ; D is obtained from a plot of $\log u_\infty$ against $\log u_\tau$; and $d\delta/dx$ is obtained from δ of the first step. When this test is attempted, large discrepancies are found between $d\delta/dx$ as observed experimentally and $d\delta/dx$ as calculated from equation (4.402). The equation is ill-posed for D close to unity, because the denominator is then a small difference between two large numbers. The situation is better for equation (4.403), as may be seen by rewriting this equation for D near unity as

$$D = 1 - \frac{\frac{\kappa^2}{d\delta/dx} z}{(C_1 z^2 - 2C_2 z + 2C_1 z) - \frac{\kappa^2}{d\delta/dx} z} . \quad (4.404)$$

The point here is that the denominator for large Π is dominated by the two terms $C_1 z^2 - 2C_2 z$, and the influence of error in $d\delta/dx$, say because of three-dimensional effects, is small. **(Check again.)**

Chapter 5

THE SHEAR LAYER

The shear layer or mixing layer is a more delicate analytical problem than those treated so far. The main application of this flow is at the edge of a jet or flow over a cavity. See high-bypass jet engines. An important special case is that of different densities. This is a prototype problem for coherent structures.

Roshko and some other investigators prefer the term organized structure to the term coherent structure, because of the meaning of the word coherent in optics and other wave phenomena. My own position is that coherent has another meaning, as in coherent speech, that is quite appropriate.

5.1 Plane laminar shear layer

The flow shown in FIGURE X is a plane shear layer between two parallel streams having constant velocities u_1 and u_2 , where u_1 in a standard notation denotes the upper, higher-speed stream. The two streams are separated for $x < 0$ by a thin splitter plate or septum whose boundary layers are neglected in the analysis, although they can be a source of difficulty in practice. Especially when the velocity u_2 in the lower stream is small, the plane mixing layer is boundary-

layer-like in its upper portion and jet-like in its lower portion.

5.1.1 Equations of motion

The laminar boundary-layer approximation in rectangular coordinates is

$$\frac{\partial u}{\partial x} + \frac{\partial v}{\partial y} = 0 \quad (5.1)$$

$$\rho \left(\frac{\partial uu}{\partial x} + \frac{\partial uv}{\partial y} \right) = \mu \frac{\partial^2 u}{\partial y^2} . \quad (5.2)$$

The boundary conditions are that the pressure is constant everywhere and that the external streams are uniform;

$$u(x, \infty) = u_1 , \quad u(x, -\infty) = u_2 . \quad (5.3)$$

The global parameters for the shear layer are u_1 , u_2 , ρ , μ . These parameters provide two characteristic velocities, u_1 and u_2 , and corresponding lengths, ν/u_1 and ν/u_2 , but no dimensionless combination except the velocity ratio u_2/u_1 itself, so that the mixing layer forms a one-parameter family of flows.

Within the boundary-layer approximation, the flow in the shear layer is not fully determined by the global parameters just listed. The root of the problem is the lack of symmetry in the boundary conditions, and the resolution of the problem is in some degree still open.

The standard first step is to test for the existence of an integral invariant. Let the momentum equation (5.2) be integrated formally from $-\infty$ to ∞ in y (this means from $-y$ to y , with $y \rightarrow \infty$ as a final step). The form obtained is

$$\frac{d}{dx} \int_{-\infty}^{\infty} uu \, dy = -u_1 v_1 + u_2 v_2 \quad (5.4)$$

where

$$v_1 = v(x, \infty) , \quad v_2 = v(x, -\infty) . \quad (5.5)$$

The same operation on the continuity equation (5.1) yields

$$\frac{d}{dx} \int_{-\infty}^{\infty} u \, dy = -v_1 + v_2 . \quad (5.6)$$

To avoid the difficulty that the integrals diverge, consider the identity

$$\frac{d}{dx} \int_{-\infty}^{\infty} (u - u_1)(u - u_2) \, dy = \frac{d}{dx} \int_{-\infty}^{\infty} uu \, dy - (u_1 + u_2) \frac{d}{dx} \int_{-\infty}^{\infty} u \, dy . \quad (5.7)$$

Substitution of equations (5.4) and (5.6) in (5.7) yields

$$\frac{d}{dx} \int_{-\infty}^{\infty} (u - u_1)(u - u_2) \, dy = -u_1 v_2 + u_2 v_1 . \quad (5.8)$$

The dimensionless form of this integral will be considered in SECTION X.

A different but equivalent approach is to treat equations (5.4) and (5.6) as linear algebraic equations for v_1 and v_2 . Solution gives

$$v_1 = \frac{1}{(u_1 - u_2)} \frac{d}{dx} \int_{-\infty}^{\infty} u (u_2 - u) \, dy \quad (5.9)$$

and

$$v_2 = \frac{1}{(u_1 - u_2)} \frac{d}{dx} \int_{-\infty}^{\infty} u (u_1 - u) \, dy . \quad (5.10)$$

Substitution of these expressions in equation (5.4) leads back to equation (5.7).

5.1.2 Similarity

The appropriate affine transformation is

$$\begin{aligned}
 x &= a\hat{x} \\
 y &= b\hat{y} \\
 \psi &= c\hat{\psi} \\
 \rho &= d\hat{\rho} \\
 \mu &= e\hat{\mu} \\
 u_1 &= p\hat{u}_1 \\
 u_2 &= q\hat{u}_2 = p\hat{u}_2 \\
 u &= r\hat{u} = \frac{c}{b}\hat{u} \\
 v &= s\hat{v} = \frac{c}{a}\hat{v} .
 \end{aligned} \tag{5.11}$$

Some of the scaling factors in equation (5.4) are redundant, as indicated in the third column. First, introduction of a stream function defined by $\vec{u} = \text{grad } \psi \times \text{grad } z$ or equivalently by

$$u = \frac{\partial \psi}{\partial y} , \quad v = -\frac{\partial \psi}{\partial x} \tag{5.12}$$

leads to

$$r\hat{u} = \frac{c}{b} \frac{\partial \hat{\psi}}{\partial \hat{y}} , \quad s\hat{v} = -\frac{c}{a} \frac{\partial \hat{\psi}}{\partial \hat{x}} \tag{5.13}$$

and thus to the equalities $r = c/b$, $s = c/a$. Second, the boundary conditions (5.3) are transformed to

$$r\hat{u}(a\hat{x}, \infty) = p\hat{u}_1, \quad r\hat{u}(a\hat{x}, -\infty) = q\hat{u}_2 . \tag{5.14}$$

Because $a\hat{x}$ is read “any value of \hat{x} ,” the value of a is immaterial, so that $r = p = q$. These results are incorporated in the group (5.11). They yield one invariant of the mapping, representing the boundary conditions. I take u_1 as fundamental because it is by definition never zero, and rewrite the equivalence $r = c/b = p$ as

$$\frac{c}{bp} = 1 . \quad (5.15)$$

Transformation of the momentum equation (5.2) yields a second invariant,

$$\frac{bdc}{ae} = 1 . \quad (5.16)$$

After isolation of c and b , these invariants become

$$\frac{c^2d}{aep} = 1, \quad \frac{b^2dp}{ae} = 1 \quad (5.17)$$

and thus lead to the preliminary ansatz

$$A \frac{\psi}{(U\nu x)^{1/2}} = f \left[B \left(\frac{U}{\nu x} \right)^{1/2} y \right] = f(\xi) \quad (5.18)$$

where the quantity U is a generic global velocity whose essential property is that it transforms like u_1 or u_2 ; that is, $U = p\hat{U}$. The term generic is appropriate because any value of U on either side of equation (5.18) can be replaced by another value by a suitable choice of the normalizing constants A and B .

Substitution of the ansatz (5.18) in the momentum equation (5.2) leads to the Blasius differential equation

$$2ABf''' + ff'' = 0 \quad (5.19)$$

with the boundary conditions

$$f'(\infty) = \frac{A u_1}{B U} , \quad f'(-\infty) = \frac{A u_2}{B U} . \quad (5.20)$$

Note that only two boundary conditions have been established for a third-order ordinary differential equation. For all of the other

laminar shear flows considered in this monograph, a natural origin for the y -coordinate and a natural third boundary condition, usually in the form $\psi = 0$ on $y = 0$, or $f(0) = 0$, are provided either by an explicit symmetry condition or by an implicit symmetry condition associated, for example, with the presence of a plane wall bounding the flow on the high-speed side. For the shear layer, this condition is still appropriate in the upstream region where the two fluids are physically separated by the septum. Downstream from the trailing edge, the symmetry condition is replaced by the concept of the dividing streamline, defined as the locus where $\psi = 0$ or $f = 0$ for $x > 0$. The two fluids, although they are assumed to have identical physical properties, are still separated by a hypothetical surface that begins at the trailing edge. **(The problem of the shear layer for two incompressible and immiscible fluids having different densities and/or viscosities was treated by Keuligan (ref) and Lock (ref), both thinking of wind over water.)** The lack of symmetry makes it unlikely that the dividing streamline $\psi = 0$ coincides with $y = 0$ or $\xi = 0$, where ξ is the argument of f in equation (5.23). At the same time, similarity requires ξ to be constant on the dividing streamline. **(Why?)**

Successive differentiation of equation (5.18) shows that the correspondence between physical variables and dimensionless similarity variables is $\psi \sim f$, $u \sim f'$, $v \sim \xi f' - f$, $\tau \sim f''$, $\partial\tau/\partial y \sim f'''$. The Blasius equation (5.19) requires $f''' = 0$ when $f = 0$. Consequently, the dividing streamline coincides with a maximum in the shearing stress and with an inflection point in the velocity profile, as was first pointed out by **(ref)**. On practical grounds, it therefore seems preferable to move the origin for the dimensionless y -coordinate to the dividing streamline. That is, put

$$\eta = \xi + C . \quad (5.21)$$

The ansatz (5.18) should be revised to read

$$A \frac{\psi}{(U\nu x)^{1/2}} = f \left\{ B \left(\frac{U}{\nu x} \right)^{1/2} y + C \right\} = f(\eta) . \quad (5.22)$$

The differential equation is still (5.19), the first two boundary con-

ditions are still (5.20), and the third boundary condition is now

$$f(0) = 0 \quad (5.23)$$

on the dividing streamline, which for $x > 0$ is the parabola $B(U/\nu x)^{1/2}y = -C$, with $C > 0$. (Typical dependent variables for one value of u_2/u_1 are shown in figure x). The boundary condition (5.23) does not necessarily fix the position of the dividing streamline in physical space, because there may not be enough information to determine the constant C .

Point out somewhere the role of C in making a connection with Stewartson's limiting separating boundary layer and with the blow-off condition for the boundary layer with mass transfer.)

5.1.3 Normalization

The normalization used throughout this monograph for laminar plane flows requires putting

$$2AB = 1 \quad (5.24)$$

in equation (5.19) in order to obtain the standard Blasius operator $f''' + ff''$. One further condition is needed to determine A and B . The velocity parameter U stands in the way. Recall that the scaling parameter p in the affine group (5.11) can refer to u_1 or u_2 , which transform in the same way, or to any suitable combination, not necessarily linear, of u_1 and u_2 . Consider the case of a moving observer who starts a clock as he passes the station $x = 0$. The basic diffusion process provides an estimate $\delta^2 \sim \nu t$ for the layer thickness seen by the observer. A plausible choice for the velocity of the observer is the arithmetic mean of u_1 and u_2 , and his position is then $x \sim (u_1 + u_2)t$. He therefore sees a thickness

$$\delta \sim \left(\frac{\nu x}{u_1 + u_2} \right)^{1/2}. \quad (5.25)$$

If the constant of proportionality does not depend on u_2/u_1 , the rate of growth is decreased by a factor of $\sqrt{2}$, other things being

equal, as u_2 increases from zero to u_1 . (**Check the literature for calculations.**)

An independent condition on δ is implicit in the form of the dimensionless variable η in equation (5.22). The thickness δ represents an increment in y , and there is a corresponding increment in η which is not dependent on the value of C . It is enough to write the proportionality

$$\delta \sim \frac{1}{B} \left(\frac{\nu x}{U} \right)^{1/2} . \quad (5.26)$$

The last two equations are consistent if the equality holds,

$$U = u_1 + u_2 . \quad (5.27)$$

The boundary conditions (5.20) keep their parallel form. Since now $B = 1/2A$,

$$f'(\infty) = 2A^2 \left(\frac{u_1}{u_1 + u_2} \right) , \quad f'(-\infty) = 2A^2 \left(\frac{u_2}{u_1 + u_2} \right) . \quad (5.28)$$

Finally, for no better reason than that the values $f'(\infty) = 1$, $f'(-\infty) = 0$ seem well suited to the special case $u_2 = 0$, I take

$$2A^2 = 1 \quad (5.29)$$

so that $A = B = 2^{-1/2}$.

With this normalization, the ansatz (5.22) becomes

$$\frac{\psi}{[2(u_1 + u_2)\nu x]^{1/2}} = f \left[\left(\frac{u_1 + u_2}{2\nu x} \right)^{1/2} y + C \right] = f(\eta) . \quad (5.30)$$

The function f satisfies the Blasius equation

$$f''' + f f'' = 0 \quad (5.31)$$

with two boundary conditions

$$f'(\infty) = \frac{u_1}{u_1 + u_2} , \quad f'(-\infty) = \frac{u_2}{u_1 + u_2} . \quad (5.32)$$

The solutions of equation (5.31) form a single-parameter family, and the parameter, u_2/u_1 , say, appears explicitly only in the boundary conditions (5.32).

Integration of equation (5.31) can proceed formally without regard to the constant C or the global velocity U . To fix the ideas, and to avoid clutter, suppose that $A = B = 1$ in the ansatz (5.22). Then the function f satisfies the ordinary differential equation

$$2f''' + f f'' = 0 \quad (5.33)$$

with the boundary conditions

$$f(0) = 0, \quad f'(\infty) = \frac{u_1}{U}, \quad f'(-\infty) = \frac{u_2}{U}. \quad (5.34)$$

The solutions will form a one-parameter family in u_2/u_1 .

Integration, say by a shooting method, is complicated by the fact that both $f'(0)$ and $f''(0)$ must be properly chosen before the conditions at $\pm\infty$ can be satisfied (**what about U ?**). An ingenious procedure was proposed by Töpfer, who observed (in the context of the Blasius boundary-layer problem) that if $f(\eta)$ is a solution of equation (5.33), so is $g(\eta) = af(a\eta)$, where a is a constant. This property can be proved directly, but it can also be connected with the normalization procedure. Relabel the dependent variable f in equation (5.22) as g . Then g satisfies

$$2AB g''' + g g'' = 0 \quad (5.35)$$

with the boundary conditions

$$g(0) = 0, \quad g'(\infty) = \frac{A u_1}{B U}, \quad g'(-\infty) = \frac{A u_2}{B U}. \quad (5.36)$$

Equation (5.35) is the same as equation (5.33) if $AB = 1$. The boundary conditions become

$$g(0) = 0, \quad g'(\infty) = a^2 \frac{u_1}{U}, \quad g'(-\infty) = a^2 \frac{u_2}{U} \quad (5.37)$$

and the problem takes Töpfer's form. Thus choose a value of u_2/u_1 and a value of U , which depends somehow on u_1 and u_2 . Choose also

a value of $g'(0)$ and iterate $g''(0)$ until the condition $g'(-\infty)/g'(\infty) = u_2/u_1$ is satisfied. The parameter a then follows from the relation

$$a^2 = \frac{u_1}{U} \frac{1}{g'(\infty)} . \quad (5.38)$$

Since $f'(0) = a^2 g'(0)$ and $f''(0) = a^3 g''(0)$, the function $f(\eta)$ can be evaluated immediately by a final integration.

It remains to consider entrainment. The easiest way to determine v_1 and v_2 is through the definition $v = -\partial\psi/\partial x$ applied directly to the ansatz (5.30). The result is

$$v_1 = - \left[\frac{(u_1 + u_2)\nu}{2x} \right]^{1/2} \lim_{\eta \rightarrow \infty} \left[f - \left(\frac{u_1}{u_1 + u_2} \right) \eta \right] \quad (5.39)$$

$$v_2 = - \left[\frac{(u_1 + u_2)\nu}{2x} \right]^{1/2} \lim_{\eta \rightarrow -\infty} \left[f - \left(\frac{u_2}{u_1 + u_2} \right) \eta \right] . \quad (5.40)$$

Under certain common experimental conditions, the problem of evaluating the constant C solves itself. Suppose that $v_1 = 0$. This will be the case if there is a parallel wall above the shear layer, as shown in FIGURE X. A related configuration is the round jet, for which the core flow downstream from the exit can be expected to be uniform and at constant pressure. If the Reynolds number is large, the shear layer will be thin, and the effect of lateral curvature can be neglected, at least close to the exit. For such cases, equation (5.39) gives (**check again**)

$$C = \lim_{\eta \rightarrow \infty} (\eta - f) . \quad (5.41)$$

This result is noted in FIGURE X. Integration of the Blasius equation will lead to a value for C (**check**). The effect is very like the effect of the displacement thickness for a boundary layer, except for the direction of the deflection. (**Integrate in both directions from dividing streamline?**)

The conclusion (5.41) can also be argued from the continuity equation in a form that applies for both laminar and turbulent flow.

In FIGURE X, continuity requires for the contour $ABCD$, which is bounded in part by the wall $y = Y$ and in part by the dividing streamline $\eta = 0$ (**rethink this**),

$$\int_0^Y u_1 dy = \int_{(\eta=0)}^Y u dy \quad (5.42)$$

or

$$\int_0^Y (u_1 - u) dy = \int_{(\eta=0)}^0 u dy . \quad (5.43)$$

Thus the two shaded regions in the figure have equal areas. In similarity form, equation (5.43) is

$$\int_C^{(Y)} (1 - f') d\eta = \int_0^C f' d\eta = f(C) - f(0) \quad (5.44)$$

from which, if $f(0) = 0$,

$$\lim_{\eta \rightarrow \infty} (\eta - f) = C . \quad (5.45)$$

This conclusion does not depend on the parameter u_2/u_1 (**look at argument by Dimotakis; point out connection with displacement concept; upper wall may also be a parabola; note lines $x = \text{constant}$ are characteristics**).

The most challenging element of the analytical problem is the subtlety of the required third boundary condition (check refs to see who was clear about this first). As a practical matter, the laminar mixing layer is very unstable, and any experimental information is likely to be incidental to work on the instability (Sato). However, the problem needs to be considered here because it also comes up for turbulent flow, and should not be blamed on the presence of turbulence.

Read Lu Ting and other papers. The presence of a wall or of axial symmetry removes the difficulty. Note singularity at $x = 0$

because equations are parabolic and characteristics are $x = \text{constant}$. Note use of rectangular coordinates; mention Kaplun on optimal coordinates. The essence is the final additive constant in f . Note also the need for an additive constant in η to get the shear layer from Stewartson's solution at the origin. Represent flow by distributed sources and/or doublets? Must avoid pressure force on splitter plate. Is streamline displacement at infinity symmetric or antisymmetric or neither? Do control-surface argument.

The nonlinear equation (5.24) with the boundary conditions (5.16) and (5.17) has no known solution in closed form, and was first solved numerically by (refs.). The solution for f is fixed only within an additive constant in η , pending resolution of the third boundary condition.

5.2 Plane turbulent mixing layer

This flow is second only to the turbulent boundary layer in the volume of literature it has generated (**pipe flow?**). Much of the more recent work has aimed at the problem of chemistry, including the dominant role of coherent structure in turbulent mixing. The latter work also contributes substantially to the body of information on mean properties.

The turbulent mixing layer grows rapidly in the downstream direction. For a fixed ratio of the two constant external velocities, the growth is known to be very nearly linear and nearly independent of Reynolds number (see SECTION X). I will therefore not consider the laminar stresses, particularly since the problem of mixed similarity rules is beyond the state of my art. However, I can and will attempt to avoid some limitations of the usual boundary-layer approximation. The conical property suggests that cylindrical polar coordinates could be used, but experimenters move their probes in rectangular coordinates, and so will I. The equations of motion are

$$\rho \left(\frac{\partial uu}{\partial x} + \frac{\partial uv}{\partial y} \right) = -\frac{\partial p}{\partial x} + \frac{\partial}{\partial x}(-\rho \overline{u'u'}) + \frac{\partial}{\partial y}(-\rho \overline{u'v'}) \quad (5.46)$$

$$\rho \left(\frac{\partial uv}{\partial x} + \frac{\partial vv}{\partial y} \right) = -\frac{\partial p}{\partial y} + \frac{\partial}{\partial x}(-\rho \overline{u'v'}) + \frac{\partial}{\partial y}(-\rho \overline{v'v'}) . \quad (5.47)$$

No information can be obtained about the remaining Reynolds stress $-\rho \overline{w'w'}$, which is involved only indirectly in the dynamics of the mean flow. I am obliged to use boundary conditions of boundary-layer type in what amounts to a hybrid formulation,

$$u(x, \infty) = u_1 \quad , \quad u(x, -\infty) = u_2 \quad , \quad (5.48)$$

$$p(x, \infty) = p(x, -\infty) = p_\infty . \quad (5.49)$$

In addition, the Reynolds stresses are all assumed to vanish outside the shear layer. **(Is the pressure condition correct?)**

Let these equations and boundary conditions be subjected to

the affine transformation

$$\begin{aligned}
 x &= a\hat{x} \\
 y &= b\hat{y} \\
 \psi &= c\hat{\psi} \\
 \rho &= d\hat{\rho} \\
 \overline{u'u'} &= f(\widehat{u'u'}) \\
 \overline{u'v'} &= g(\widehat{u'v'}) \\
 \overline{v'v'} &= h(\widehat{v'v'}) \\
 p &= i\hat{p} \\
 p_\infty &= j\hat{p}_\infty = i\hat{p}_\infty \\
 u &= p\hat{u} = \frac{c}{b}\hat{u} \\
 v &= q\hat{v} = \frac{c}{a}\hat{v} \\
 u_1 &= r\hat{u}_1 \\
 u_2 &= s\hat{u}_2 = r\hat{u}_2 .
 \end{aligned} \tag{5.50}$$

The definitions $u = \partial\psi/\partial y$ and $\hat{u} = \partial\hat{\psi}/\partial\hat{y}$ require $p = c/b$. (**Mention v .**) Transformation of the boundary conditions on u leads, as in the laminar problem, to the relation $p = r = s$ and to an

invariant which I take as

$$\frac{c}{br} = 1 . \quad (5.51)$$

By inspection, the boundary condition (5.49) on p leads to the relation $i = j$. Invariance of the equations of motion implies

$$\frac{c^2}{abg} = 1 , \quad \frac{bi}{adg} = 1 , \quad \frac{fb}{ag} = 1 , \quad (5.52)$$

$$\frac{c^2}{a^2h} = 1 , \quad \frac{i}{dh} = 1 , \quad \frac{bg}{ah} = 1 . \quad (5.53)$$

Note from the second of equations (5.53) that $i/d = h$. From the second of equations (5.52) and the third of equations (5.53), it follows that $h = g$ and thus that

$$\frac{b}{a} = 1 . \quad (5.54)$$

Finally, from the third of equations (5.52), $f = g$. Thus equations (5.52) and (5.53), which are a necessary condition for similarity, imply that the layer grows linearly if the pressure perturbation and the three surviving Reynolds stresses all transform in the same way, and conversely.

Two invariants of the transformation are given by equations (5.51) and (5.54). But these and the first of equations (5.52) or (5.53) imply

$$\frac{g}{r^2} = 1 \quad (5.55)$$

and three similar equations, given $f = g = h = i/d$. These combinations require the pressure and the Reynolds stresses $-\rho\bar{u}_i\bar{u}_j$ to scale like ρu_1^2 . Since these stresses must vanish when $u_2 = u_1$, it is reasonable to adapt this conclusion to read that the Reynolds stresses must scale like $\rho(u_1 - u_2)^2$. (**Why not** $u_1^2 - u_2^2$?) In full, the ansatz

for the plane turbulent shear layer is **(introduce U)**

$$A \frac{\psi}{Ux} = f\left(B \frac{y}{x} + C\right) = f(\eta) \quad (5.56)$$

$$\overline{u'u'} = (u_1 - u_2)^2 F(\eta) \quad (5.57)$$

$$\overline{u'v'} = (u_1 - u_2)^2 G(\eta) \quad (5.58)$$

$$\overline{v'v'} = (u_1 - u_2)^2 H(\eta) \quad (5.59)$$

$$p - p_\infty = \rho(u_1 - u_2)^2 P(\eta) \quad (5.60)$$

where the constant C , as in the laminar case, supports the boundary condition $f(0) = 0$ by locating the dividing streamline $\psi = 0$ in the downstream flow as the straight line $y/x = -C/B$. The functions F and H are necessarily positive, and G is expected to be negative.

Substitution of the appropriate derivatives of equations (5.56)-(5.60) into the momentum equations (5.46) and (5.47) gives

$$-U^2 \frac{B^2}{A^2} \frac{f f''}{(u_1 - u_2)^2} = (\eta - C)P' + (\eta - C)F' - BG' \quad (5.61)$$

$$-U^2 \frac{B}{A^2} \frac{(\eta - C) f f''}{(u_1 - u_2)^2} = -BP' + (\eta - C)G' - BH' . \quad (5.62)$$

5.2.1 The boundary-layer approximation

A short digression is needed here to put into evidence the result that would be obtained if the boundary-layer approximation had been made in the beginning. The single momentum equation to be transformed is a truncated form of equation (5.46),

$$\rho \left(\frac{\partial uu}{\partial x} + \frac{\partial uv}{\partial y} \right) = \frac{\partial}{\partial y} (-\rho \overline{u'v'}) \quad (5.63)$$

with the boundary conditions (5.48). The invariants of the mapping are

$$\frac{c^2}{abg} = 1 , \quad \frac{c}{ar} = 1 . \quad (5.64)$$

If the Reynolds shearing stress transforms like $(u_1 - u_2)^2$, equation (5.55) again applies;

$$\frac{g}{r^2} = 1 . \quad (5.65)$$

When the first two relationships are used to isolate b and c , the main invariants are unchanged;

$$\frac{c}{br} = 1 , \quad \frac{b}{a} = 1 , \quad \frac{g}{r^2} = 1 . \quad (5.66)$$

Thus the appropriate ansatz is the subset (5.56) and (5.58). The implied similarity equation can be derived directly or by dropping terms multiplied by $(\eta - C)$ in equation (5.61). The same approximation in equation (5.62) gives $P' + H' = 0$ or

$$p + \overline{\rho v'v'} = p_\infty = \text{constant} . \quad (5.67)$$

The full equations yield a more complicated equation for the pressure. Multiply equation (5.61) by $(\eta - C)$ and equation (5.62) by B and subtract to obtain

$$[B^2 + (\eta - C)^2]P' = -(\eta - C)^2F' + 2B(\eta - C)G' - B^2H' . \quad (5.68)$$

With $(\eta - C) = By/x$, this becomes in physical variables

$$\left(1 + \frac{y^2}{x^2}\right) \frac{\partial(p - p_\infty)/\rho}{\partial y} = -\frac{\partial \overline{v'v'}}{\partial y} + 2\frac{y}{x} \frac{\partial \overline{u'v'}}{\partial y} - \frac{y^2}{x^2} \frac{\partial \overline{u'u'}}{\partial y} . \quad (5.69)$$

The three Reynolds stresses have similar shapes and comparable magnitudes (see section x). At least the second term on the right in equation (5.69) is not negligible since the coefficient $2y/x$ is typically about 0.2 in regions where the derivatives are appreciable. Note that equation (5.69) does not involve the constants A , B , and especially C in equation (5.56). **(Integrate by parts.)** Equation (5.69) will be tested experimentally and compared with the conventional boundary-layer approximation (5.67) in SECTION X. **(Note that $f = 0$ when $G' = 0$. Does $p(\infty) = p(-\infty)$?)**

To eliminate the pressure from the problem, multiply equation (5.61) by B and equation (5.62) by $(\eta - C)$ and add to obtain

(give boundary-layer approximation, comment on eddy viscosity)

$$\begin{aligned} & [B^2 - (\eta - C)^2] G' \\ = & \frac{U^2}{(u_1 - u_2)^2} \frac{B}{A^2} [B^2 + (\eta - C)^2] f f'' + B(\eta - C)(F' - H') \end{aligned} \quad (5.70)$$

This expression is useful for comparing values of G measured directly with those inferred from measurements of the other quantities; namely f , F , and H . The effect of making the boundary-layer approximation in equation (5.70) is less conspicuous than in the case of equation (5.68), because the difference $(F' - H')$ is much smaller than F' or H' alone. In physical variables, equation (5.70) becomes

$$\left(1 + \frac{y^2}{x^2}\right) \psi \frac{\partial u}{\partial y} = x \left[\frac{y}{x} \frac{\partial}{\partial y} (\overline{v'v'} - \overline{u'u'}) + \left(1 - \frac{y^2}{x^2}\right) \frac{\partial}{\partial y} (\overline{u'v'}) \right]. \quad (5.71)$$

Within the boundary-layer approximation, the dividing mean streamline $\psi = 0$ corresponds, as in the laminar case, to the condition $\partial\tau/\partial y = 0$, although not necessarily to an inflection point in the mean velocity profile. This condition should not be much in error for the full equations.

It remains to assign values to the scaling parameters A and B in the defining similarity equation (5.56), or better in its derivative (note that $\eta = 0$ is the dividing streamline).

$$\frac{A}{B} \frac{u}{U} = f' \left(B \frac{y}{x} + C \right) = f'(\eta). \quad (5.72)$$

As in the laminar problem, it is reasonable to take (**explain**)

$$\frac{A}{B} = 1 \quad (5.73)$$

and thereby to fix two of the boundary conditions as

$$f'(\infty) = \frac{u_1}{U}, \quad f'(-\infty) = \frac{u_2}{U}. \quad (5.74)$$

Again, the physical parameter u_2/u_1 of the problem appears only in the lower boundary condition. The normal component of velocity

outside the shear layer is the limit of $-\partial\psi/\partial x$, with ψ given by equation (5.56). The boundary conditions (5.9) and (5.10) lead to

$$v_1 = -\frac{u_1}{A} \lim_{\eta \rightarrow \infty} [f - (\eta - C)] , \quad (5.75)$$

$$v_2 = -\frac{u_1}{A} \lim_{\eta \rightarrow -\infty} \left[f - \frac{u_2}{u_1}(\eta - C) \right] . \quad (5.76)$$

If the condition $v_1 = 0$ is enforced by an upper wall or by axial symmetry with the faster stream near the axis, then again

$$C = \lim_{\eta \rightarrow \infty} (\eta - f) . \quad (5.77)$$

The present state of the art of normalization is based on a more empirical similarity approach suggested by FIGURE X. A thickness δ , commonly called the vorticity thickness, can be tentatively defined in terms of the maximum slope $\partial u/\partial y$, which no longer necessarily occurs on the dividing streamline. Within the boundary-layer approximation, the shearing stress in turbulent flow should have a maximum on the dividing streamline, because $Du/Dt = 0$ (**explain**). For a particular value of the parameter u_2/u_1 , the profile in FIGURE X can be represented in another similarity form, starting with

$$\frac{u - u_2}{u_1 - u_2} = g' \left(\frac{y^*}{\delta} \right) \quad (5.78)$$

where y^* is measured from the dividing streamline. The relationship between g' and f' follows from equations (5.53), (5.54), and (5.58);

$$\frac{u}{u_1} = f' \left(\frac{By^*}{x} \right) = \frac{u_2}{u_1} + \left(1 - \frac{u_2}{u_1} \right) g' \left(\frac{y}{\delta} \right) . \quad (5.79)$$

To preserve the benefits of the affine argument, it is necessary to have

$$B = \frac{x}{\delta} . \quad (5.80)$$

The notation σ for x/δ was introduced by Görtler (**ref**). This parameter σ , which is the same as my B , can be expected to depend on u_2/u_1 . For the most thoroughly studied case $u_2/u_1 = 0$, σ is

about 11, or δ/x is about 1/9. I prefer not to use Görtler's notation on the hard ground that a different definition of δ might prove more useful, and on the softer ground that the parameter σ seems to me to be defined upside down; the ratio δ/x has a greater graphic and mnemonic value. **(Is there an integral of $(u_1 - u)(u - u_2)$?)**

The boundary conditions for g' from equation (5.101)¹ are

$$g'(\infty) = 1, \quad g'(-\infty) = 0 . \quad (5.81)$$

Integration of (5.79) yields

$$f\left(\frac{y}{\delta}\right) = \frac{u_2 y}{u_1 \delta} + \left(1 - \frac{u_2}{u_1}\right)g\left(\frac{y}{\delta}\right) \quad (5.82)$$

with $g(0) = 0$ if $f(0) = 0$ (**where was the latter done?**).

The parameter u_2/u_1 has thus disappeared from the boundary conditions and appeared in the defining equation (5.82). An associated result, completely empirical at present, is based on the fact that the profile $g'(y/\delta)$ is a monotonic transition from one constant value to another. It is only a small step to the proposition that this profile is for practical purposes universal; i.e., it is the same function of y/δ for all values of u_2/u_1 . This proposition will be tested experimentally in section x. **(Look also at laminar case. Do entrained flow, both cases. Calculate $v(-\infty)$.)**

The dependence of B or δ/x or σ on u_2/u_1 was first studied by SABIN (1965), who worked with plane shear layers at quite low Reynolds numbers and who chose to plot x/δ against u_2/u_1 (**check**). It is now more common to see δ/x plotted against $(u_1 - u_2)/(u_1 + u_2)$. The reason is that the latter dependence is found to be very nearly linear;

$$\frac{\delta}{x} \sim \left(\frac{u_1 - u_2}{u_1 + u_2}\right) . \quad (5.83)$$

I suspect that this linear dependence is somehow implicit in the equations, especially equation (5.79), but I have not found a valid argument.

¹Possibly an incorrect reference.

5.2.2 Structure of the shear layer

Some guidance on normalization is provided by the device of the moving observer. For the case of a turbulent mixing layer, this device is both real and important, because it introduces the subject of coherent structure, and thus requires another digression.

At the level of eddy viscosity or mixing length, the turbulent mixing layer was thought to be a featureless wedge of turbulence, perhaps with a trivially irregular boundary. This view changed drastically with the work of BROWN and ROSHKO (1971, 1974) and WINANT and BROWAND (1974). It is now recognized that the turbulent mixing layer is inhabited by, or more properly is constructed from, large spanwise vortex structures that grow both by entrainment and by coalescence during the evolution of the flow. The structures originate in an inviscid Kelvin-Helmholtz instability that operates in both laminar and turbulent flow. In this coherent-structure model of turbulence, each structure is assumed to move as a unit, preserving its geometry and operational properties between coalescence events, while the ambient flow accommodates itself to the kinematic and dynamic needs of the structure. According to this model, the translational velocity of the structures in laboratory coordinates is well defined. It is often called convection velocity and occasionally phase velocity, although I will use the term celerity and the notation c .

When the averaging process introduced by REYNOLDS (1895) is stopped at second order, which is to say at the first revelation of the closure problem, all information about scale and phase of the turbulent motions is lost. Various methods are available to recover some of this information. If data are available at two points, for example, some phase information can be rescued by the technique of space-time correlation. The condition of optimum time delay then provides an imperfect measure of phase velocity or celerity. Without filtering, the results indicate that the celerity is not constant through the thickness of a given plane flow, but is biased in the direction of the mean-velocity profile. The bias can be reduced by retaining only the low-frequency or large-scale content of the signals, as demonstrated

for the boundary layer by FAVRE, GAVIGLIO, and DUMAS (Phys. Fluids **10**, Supplement, S138-S145, 1967). Early experimenters who used this technique were not in any doubt about the meaning of their work, as is evident from the fact that Favre and Kovasznay chose the French word *célérité* to describe their findings quantitatively, rather than the more conventional French word *vitesse*. (The technique of time-space correlation could in principle be applied to existing numerical solutions of the Navier-Stokes equations.) Much more accurate measures have been obtained by flow visualization, particularly for the mixing layer, where the large structures are two-dimensional in the mean.

FIGURE X is a sequence of frames from a motion picture of a mixing layer (Roshko, private communication; **what flow?**). FIGURE Y is a corresponding x - t diagram showing trajectories of the recognizable features marked by + symbols in the first frame. Coalescence events occur quickly, like punctuation marks in the text of turbulence. Similar figures have been published by DAMMS and KÜCHEMANN (RAE Tech Rep 72139, 1972), BROWN and ROSHKO (JFM **64**, 775, 1974), and ACTON (JFM **98**, 1, 1980). Each of these observers chose a particular local feature, not necessarily the same feature, in order to assign values to the variable $x(t)$ and hence to the celerity dx/dt , and each was successful in exposing the phenomenon of coalescence in the mixing layer.

These observations play a central role in normalization. FIGURE X (COLES 1981) is a cartoon of the instantaneous mean streamlines in the turbulent mixing layer, as seen by an observer moving with the celerity c . (**Look up Brown, thesis, Univ. Missouri, 1978.**) In the model, the vortices are stationary, the flow is inviscid, and the layer grows in time rather than in space. The essence of figure x is the topology, which consists of saddle points (stagnation points) alternating with stable foci (vortices). Fluid flowing toward each saddle point along the converging separatrices (instantaneous streamlines) must arrive at the saddle point with the same stagnation pressure. Suppose for the moment that Mach numbers are small but the streams have different densities. Far from the mixing layer, where the two streams have the same static pressure, Bernoulli's equation

requires

$$\frac{\rho_1}{2}(u_1 - c)^2 = \frac{\rho_2}{2}(u_2 - c)^2 . \quad (5.84)$$

When this equation is solved for c , the result is

$$c = \frac{(\rho_1)^{1/2}u_1 + (\rho_2)^{1/2}u_2}{(\rho_1)^{1/2} + (\rho_2)^{1/2}} . \quad (5.85)$$

Note that if the two densities are very different, the celerity approaches the velocity of the denser stream. Thus equation (5.85) contains more information about the mixing process than might have been anticipated. If the fluids are compressible, still with the same p outside the mixing layer and the same p_o at the saddle points, it follows from equation (1.82) of the introduction that equations (5.84) and (5.85) are unchanged, provided only that the flow along the separatrices is isentropic. If the velocity of one or both streams is supersonic relative to the large structures, shock waves and expansion waves may appear and may intersect the separatrices. The effect on equation (5.85) is at present an open question.

I first used the relation (5.85) in a survey paper (COLES 1985) that attempted to collect some important results that can be obtained using the concept of coherent structure and cannot be obtained without it. The same equation was derived independently by DIMOTAKIS (AIAA Paper 84-0368) and perhaps by others. There is persuasive evidence (WANG) that equation (5.85) predicts quite accurately the effect of density ratio on celerity for low-speed flow.

The calculation just made depends on the topological simplicity of the mixing layer. No comparable result has so far been obtained for any other turbulent shear flow, presumably because the large structures in other flows arise from more complex instabilities, are less dominant in the mixing process, and are almost certainly three-dimensional. Moreover, in any morphology of coherent structure, an important distinction arises between flows containing large-scale mean vorticity of only one sense and flows containing large-scale mean vorticity of both senses. The mixing layer is unique among the classical plane flows in that it is the only flow that is driven naturally toward a two-dimensional structure.

Now return to the problem of normalization. For the case of equal densities, the constant celerity of the large structures, and thus the proper velocity of the observer, is

$$U = c = \frac{u_1 + u_2}{2} . \quad (5.86)$$

It is a little ironic that this estimate is less of a guess than the same estimate (5.27) for laminar flow. It defines the global velocity U in the ansatz (5.56) and gives the position of an observer moving with the structures as

$$x \sim (u_1 + u_2) t . \quad (5.87)$$

For the laminar problem, another measure for the parameter t was obtained from the diffusive model $\delta \sim (\nu t)^{1/2}$, which does not apply when the flow is turbulent. DIMOTAKIS (1991) has proposed a different relation that involves δ and meets the need. The vorticity thickness δ , or more accurately the maximum-slope thickness, is defined by

$$\delta = \frac{u_1 - u_2}{(\partial u / \partial y)_{\max}} . \quad (5.88)$$

Since δ varies like x and like t , the reciprocal of the quantity $(\partial u / \partial y)_{\max}$ is a plausible time scale;

$$\delta \sim (u_1 - u_2) t . \quad (5.89)$$

Immediately, therefore,

$$\frac{\delta}{x} \sim \frac{(u_1 - u_2)}{(u_1 + u_2)} . \quad (5.90)$$

Equation (5.90) is a genuine scaling law only if the implied constant of proportionality is independent of the velocity ratio u_2/u_1 . The derivation here supposes and suggests that it is, although the argument, like many arguments in science, illustrates the principle that it helps to know the answer. Note that negative values for u_2/u_1 , which can occur for base or cavity flows, are permitted by the scaling law, with δ/x varying from zero to infinity as u_2/u_1 varies from +1 to -1. This question will be taken up in SECTION X. ABRAMOVICH (19xx) proposed equation (5.90) for the mixing layer, but stipulated

some further dependence on u_2/u_1 . SABIN (19xx) proposed equation (5.90) in a different form as a scaling law based on his own measurements at relatively low Reynolds numbers. ROSHKO in 19xx collected the experimental data available at that time and demonstrated an essentially linear relationship between the two sides of equation (5.90), with a constant of proportionality on the right of about xxx. There was considerable scatter in the data, especially for the case $u_2/u_1 = 0$.

The road to normalization is now open, as much as any road in turbulence is ever open. If the argument $B y/x$ of the function f in equation (5.56) is to be equivalent to y/δ , then it is necessary to have

$$B = \frac{x}{\delta} = b \left(\frac{u_1 + u_2}{u_1 - u_2} \right) \quad (5.91)$$

where b is independent of u_2/u_1 . Finally, as in the laminar case, I take

$$A = B \quad (5.92)$$

on esthetic rather than logical grounds. This normalization leads to the ansatz

$$\frac{2b\psi}{(u_1 - u_2)x} = f \left[b \left(\frac{u_1 + u_2}{u_1 - u_2} \right) \frac{y}{x} + C \right] \quad (5.93)$$

with the boundary conditions

$$f(0) = 0 \quad , \quad f'(\infty) = \frac{2u_1}{u_1 + u_2} \quad , \quad f'(-\infty) = \frac{2u_2}{u_1 + u_2} \quad . \quad (5.94)$$

The constant C is still unspecified.

From equation (5.94), with the boundary-layer result that f'' is a maximum on the dividing streamline $\eta = 0$ (**check**),

$$\left(\frac{\partial u}{\partial y} \right)_{\max} = \frac{b(u_1 + u_2)^2}{2x(u_1 - u_2)} f''(0) \quad (5.95)$$

and thus, with equations (5.88) and (5.91),

$$f''(0) = \frac{2}{b} \left(\frac{u_1 - u_2}{u_1 + u_2} \right) \quad . \quad (5.96)$$

This result will be tested experimentally in SECTION X.

FIGURE X shows the experimental evidence for equation (5.83) as presented by Roshko, with a number of later measurements. The scatter, especially for the case $u_2 = 0$, is unreasonable. Several reasons have been proposed for the scatter. One, due to BATT (1975) is that non-uniqueness is a relict of varying initial conditions, especially the laminar or turbulent state of the boundary layer at the trailing edge of the splitter plate or septum. This conjecture has inspired a number of detailed and difficult studies (**refs**). Another, which I favor as an equally plausible source of scatter, is three-dimensionality. An easy measure is the aspect ratio, or the ratio of shear-layer thickness to the distance between the side plates usually provided to control the entrainment process. The effect should not be present for the axisymmetric shear layer, but another more systematic effect of lateral curvature is likely to be present instead, along with any effect of initial conditions.

Collect profile data for plane flow, $u_2 = 0$. Plot $d\delta/dx$ (assign this to the mean x) against δ/w , where w is the spanwise width. Use \tanh for a fit to the central part of the profile. Do not use x/δ , because the origin of x depends on linear growth, which is not yet proved (thus argument is circular). For round jet, use $\delta/\pi D$, where D is orifice diameter (neglect effect of growing diameter of dividing surface).

For two-stream flows, comment on use of porous obstacle and two tailored nozzles, with a very delicate design condition. The direction of the dividing streamline may be seriously affected.

Note that the third boundary condition is still unspecified, as in the laminar problem.

Note also the singularity when $u_2 = -u_1$; the layer becomes infinitely thick. The origin for x is not unique. (Who did crossed flows?)

It might be more useful to work in terms of the variable (should

this be done during the transformation?)

$$\frac{u - u_2}{u_1 - u_2} = 1 + \frac{u_1}{u_1 - u_2} \left(\frac{B}{A} f' - 1 \right) . \quad (5.97)$$

The left-hand side is unity when $u = u_1$ and zero when $u = u_2$. Then

$$\frac{B}{A} f'(\infty) = 1, \quad \frac{B}{A} f'(-\infty) = \frac{u_2}{u_1} \quad (5.98)$$

suggesting $B = A$. (Look at ansatz and at momentum equations.) A different scheme is to put

$$F'(\eta) = \frac{u - u_2}{u_1 - u_2} = 1 + \frac{u_1}{u_1 - u_2} \left(\frac{B}{A} f' - 1 \right) . \quad (5.99)$$

Then

$$F(\eta) = \frac{u_1}{u_1 - u_2} \frac{B}{A} f(\eta) - \frac{u_2}{u_1 - u_2} + \text{constant} . \quad (5.100)$$

The third boundary condition reappears.

In the absence of an integral invariant, the thickness of the turbulent shear layer is usually defined by an ad hoc normalization. One easy definition is based on the maximum slope of the mean-velocity profile, as shown in figure *x*. The quantity δ so defined is called the vorticity thickness. Another definition seen in the literature uses more detail in the profile by measuring δ between points where specified fractions, say, 10 percent and 90 percent of the total velocity change are observed. I have no use for this definition.

For a particular value of the parameter u_2/u_1 , the profile in figure *x* can be represented by the equation (**fix this**)

$$\frac{u - u_2}{u_1 - u_2} = g' \left(\frac{y}{\delta} \right) \quad (5.101)$$

where y is now measured from the dividing streamline.

Chapter 6

THE ROUND WAKE

Chapter file created by B. Coles. There is no evidence that any part of this chapter was ever written, but it appears in the MS Table of Contents.

Chapter 7

THE PLANE WAKE

Chapter file created by B. Coles. There is no evidence that any part of this chapter was ever written, but it appears in the MS Table of Contents.

Chapter 8

THE ROUND JET

The classical laminar or turbulent round jet issues from a point source into a stagnant fluid. An extreme case is shown in the photograph.¹ An important reason for the popularity of the turbulent round jet as a subject for fundamental experimental study is economy. The geometry is simple, and a large part of the energy supplied to the fluid appears as turbulent motion before being dissipated in heat. An easily accessible and important variation on the basic problem of momentum transport is simultaneous transport of heat or mass.

A jet may be surrounded by a moving fluid, as in a rocket or jet engine. In such cases the problem can sometimes be linearized, giving a point of contact with the round wake. Jets are components of many practical devices such as torches and sprays. A jet may also be enclosed in a shroud or housing to produce a jet pump or ejector. Several jets may interact, or a non-circular jet may relax toward axial symmetry, or a jet may have a component normal to an ambient flow, as in thrust-control devices. Swirl is sometimes used to enhance mixing. Finally, a jet of one fluid into another is a nice problem in entrainment, mixing, and relaxation.

¹It is not clear what photograph was meant to be included here.

8.1 Laminar round jet into fluid at rest

8.1.1 Preview

The steady laminar flow associated with a point momentum source in a viscous incompressible fluid is one of the few known exact solutions of the Navier-Stokes equations. The reason that this solution came long ago to be known is not the usual one, which is that a particularly simple geometry has reduced the number of independent variables, as in pipe flow. The reason is dimensional in a different way, having to do with the number and nature of global parameters. A kindred case is the laminar sink flow in a wedge-shaped channel, treated earlier in SECTION X. These two flows have in common that the exact solution is known in closed form for all Reynolds numbers (if elliptic functions qualify as closed form). An important difference is that entrainment is an essential feature of the boundary-layer approximation for the round jet, but not for the channel flow. Hence the round jet is unique in providing an opportunity to practice the technique of matched asymptotic expansions to arbitrarily high order. As far as I know, this opportunity has never been exploited, and I will not attempt here to rise above the level of first-order boundary-layer theory in SECTIONS X, Y, and Z.

The organization of the next (**four**) sections is shown schematically in Figure 8.1. The box at the left, called “NS (Navier-Stokes) equations,” is the core element for the diagram. My first objective is to show that the two paths from “NS equations” to “BL (boundary-layer) solution” are precisely equivalent, as are the two paths from “NS equations” to “potential flow.” My second objective is to illustrate by example the use of the powerful technique of matched asymptotic expansions to construct a “composite expansion” that is not exact, but cannot for practical purposes be distinguished from the exact solution at the Reynolds number of the present exercise. These derivations lay a foundation for operations that build on boundary-layer theory in cases where no exact solution is known; e.g., the plane laminar jet, or any turbulent flow.

After some dimensional preliminaries, the exact solution is de-

PLACEHOLDER

Figure 8.1: Caption for Figure with label Fig15-7 (missing)

rived in SECTION 8.1.3. Most of the material there is not original, and can be found in ROSENHEAD, “Laminar Boundary Layers” (1963) or in BATCHELOR, “An Introduction to Fluid Dynamics” (1967). The original sources are papers by SLEZKIN (1934), LANDAU (1944), and SQUIRE (1951).

8.1.2 Dimensional argument

An appropriate coordinate system for the problem of the laminar round jet is the spherical polar system (r, θ, ϕ) shown at the left in FIGURE 8.2. For comparison and contrast, the corresponding plane jet from a line momentum source is also sketched in a cylindrical polar system, (R, θ, z) at the right. These coordinates are deliberately chosen so that one coordinate in the two-dimensional reduced system is dimensionless.

The global parameters for the point momentum source (round jet) or the line momentum source (plane jet) are the fluid properties ρ and μ (or ρ and $\nu = \mu/\rho$) and the specified momentum flux J , whose dimensions for the round jet are momentum per unit time and for the plane jet are momentum per unit time per unit length. This small descriptive difference has large consequences. In terms

PLACEHOLDER

Figure 8.2: Caption for Figure with label Fig15-6 (missing)

of mass, length, and time as fundamental units, the three global parameters have dimensions²

Point source	Line source	
$[J] = \frac{\mathbf{ML}}{\mathbf{T}^2}$,	$[J] = \frac{\mathbf{M}}{\mathbf{T}^2}$,	
$[\rho] = \frac{\mathbf{M}}{\mathbf{L}^3}$,	$[\rho] = \frac{\mathbf{M}}{\mathbf{L}^3}$,	(8.1)
$[\nu] = \frac{\mathbf{L}^2}{\mathbf{T}}$,	$[\nu] = \frac{\mathbf{L}^2}{\mathbf{T}}$.	

Rearrangement to isolate the characteristic scales \mathbf{M} , \mathbf{L} , and \mathbf{T} in each column yields quite different results for the two problems;

$\left[\frac{J}{\rho\nu^2} \right] = 0$.	$\left[\frac{\rho^4\nu^6}{J^3} \right] = \mathbf{M}$,	
	$\left[\frac{\rho\nu^2}{J} \right] = \mathbf{L}$,	(8.2)
	$\left[\frac{\rho^2\nu^3}{J^2} \right] = \mathbf{T}$.	

²In this section equations on the left refer to the point source (round jet) and on the right the line source (plane jet).

For the point source on the left, no characteristic scales can be defined. It is this fact that makes an exact solution possible. Such a solution can be expected to depend on one dimensionless parameter, $(J/\rho\nu^2)^{1/2}$, having the nature of a Reynolds number. For the line source on the right, the situation is quite otherwise. The characteristic scales are well defined, but there is no dimensionless parameter. Hence there can be only one solution. Note that this argument is not based on the equations of motion, but only on the physical parameters for each flow.

Let a suitable solution be anticipated in terms of a single stream function ψ , where

$$[\psi] = \frac{L^3}{T} \quad . \quad [\psi] = \frac{L^2}{T} \quad . \quad (8.3)$$

If L and T can be defined, these relations can be written in dimensionless form as equalities. To mark the profound change in content for the symbols, a different font is used;

$$\frac{\psi T}{L^3} = \text{fn} \left(\frac{r}{L} , \theta \right) \quad . \quad \frac{\psi T}{L^2} = \text{fn} \left(\frac{R}{L} , \theta \right) \quad . \quad (8.4)$$

When T is eliminated using $T = L^2/\nu$, these become

$$\frac{\psi}{\nu L} = \text{fn} \left(\frac{r}{L} , \theta \right) \quad . \quad \frac{\psi}{\nu} = \text{fn} \left(\frac{R}{L} , \theta \right) \quad . \quad (8.5)$$

In the left column, L can not be defined and therefore cannot appear. The only rational action is to replace L by r . In the right column, L can be defined as $\rho\nu^2/J$. Consequently, from one of equations (8.2).

$$\frac{\psi}{\nu r} = \text{fn} (1 , \theta) \quad . \quad \frac{\psi}{\nu} = \text{fn} \left(\frac{RJ}{\rho\nu^2} , \theta \right) \quad . \quad (8.6)$$

The result for the round jet on the left is much more than an accidental separation of variables. The result states that $\psi/\nu r$ depends only on θ , and must therefore be obtainable by solving an ordinary differential equation (with $J/\rho\nu^2$ as parameter). Such a conclusion normally requires a much more elaborate similarity argument based

on the transformation properties of the equations of motion. It may also require good judgment in choosing an appropriate system of coordinates.

No corresponding reduction appears for the line source on the right. This flow will be discussed in SECTION 9.1.2.

8.1.3 The exact solution

Take the velocity for the point momentum source to be $\vec{u} = (u, v, w)$ in spherical polar coordinates (r, θ, ϕ) . Consider steady axisymmetric flow without swirl; i.e., $\partial/\partial t = \partial/\partial\phi = w = 0$. The equations of motion (**reference**) are then

$$\frac{1}{r^2} \frac{\partial ur^2}{\partial r} + \frac{1}{r \sin \theta} \frac{\partial v \sin \theta}{\partial \theta} = 0, \quad (8.7)$$

$$u \frac{\partial u}{\partial r} + \frac{v}{r} \frac{\partial u}{\partial \theta} - \frac{v^2}{r} = -\frac{1}{\rho} \frac{\partial p}{\partial r} + \nu \left(\nabla^2 u - 2 \frac{u}{r^2} - \frac{2}{r^2 \sin \theta} \frac{\partial v \sin \theta}{\partial \theta} \right), \quad (8.8)$$

$$u \frac{\partial v}{\partial r} + \frac{v}{r} \frac{\partial v}{\partial \theta} + \frac{uv}{r} = -\frac{1}{\rho r} \frac{\partial p}{\partial \theta} + \nu \left(\nabla^2 v + \frac{2}{r^2} \frac{\partial u}{\partial \theta} - \frac{v}{r^2 \sin^2 \theta} \right), \quad (8.9)$$

where the Laplace operator is

$$\nabla^2 \alpha = \frac{1}{r^2} \frac{\partial}{\partial r} r^2 \frac{\partial \alpha}{\partial r} + \frac{1}{r^2 \sin \theta} \frac{\partial}{\partial \theta} \sin \theta \frac{\partial \alpha}{\partial \theta}. \quad (8.10)$$

It is convenient first to eliminate the pressure by working with the vorticity, $\vec{\Omega} = \text{curl } \vec{u} = (\xi, \eta, \zeta)$, which has only a ϕ -component;

$$\zeta = \frac{1}{r} \frac{\partial rv}{\partial r} - \frac{1}{r} \frac{\partial u}{\partial \theta}. \quad (8.11)$$

The velocity components are derivable from a stream function ψ using the definition $\vec{u} = \text{grad } \psi \times \text{grad } \phi$;

$$u = \frac{1}{r^2 \sin \theta} \frac{\partial \psi}{\partial \theta}, \quad v = -\frac{1}{r \sin \theta} \frac{\partial \psi}{\partial r}, \quad (8.12)$$

and consequently, from equation (8.11),

$$\zeta = -\frac{1}{r \sin \theta} \nabla^2 \psi + \frac{2}{r \sin \theta} (u \cos \theta - v \sin \theta). \quad (8.13)$$

The equation satisfied by ζ , from equations (8.8) and (8.9), is

$$u \frac{\partial \zeta}{\partial r} + \frac{v}{r} \frac{\partial \zeta}{\partial \theta} = \frac{\zeta}{r \sin \theta} (u \sin \theta + v \cos \theta) + \nu \left(\nabla^2 \zeta - \frac{\zeta}{r^2 \sin^2 \theta} \right) . \quad (8.14)$$

The first term on the right-hand side represents vortex stretching of a trivial kind. The meaning of this term emerges if it is noted that $r \sin \theta = R$, say, is the perpendicular distance from any point in the flow to the polar axis of symmetry. Moreover,

$$(u \sin \theta + v \cos \theta) = \vec{u} \cdot \nabla R = DR/D . \quad (8.15)$$

In the absence of diffusion due to viscosity, therefore, the vorticity obeys the equation (**need to display formula for grad?**)

$$\frac{1}{\zeta} \frac{D\zeta}{Dt} = \frac{1}{R} \frac{DR}{Dt} . \quad (8.16)$$

Hence ζ/R is constant following an element of the fluid; the strength of any (circular) vortex filament varies directly with the filament diameter. This observation is obviously not limited to the problem of the point momentum source, but is valid for any axially symmetric motion.

It has already been argued in equation (8.6) that the stream function must have the form $\psi = \nu r f(\theta)$. A convenient variant is

$$\psi = \nu r f(\cos \theta) = \nu r f(\xi) , \quad (8.17)$$

where $\xi = \cos \theta$. It follows from equations (8.12) and (8.11) that

$$u = -\frac{\nu}{r} f' , \quad (8.18)$$

$$v = -\frac{\nu}{r} \frac{f}{\sin \theta} , \quad (8.19)$$

$$\zeta = -\frac{\nu}{r^2} f'' \sin \theta , \quad (8.20)$$

where f' means $df/d \cos \theta = df/d\xi$. When these are substituted in equation (8.14), f satisfies

$$3f' f'' + f f''' + 4\xi f''' - (1 - \xi^2) f'''' = 0 . \quad (8.21)$$

This equation is fourth-order because the pressure is still a variable, although it has been formally suppressed by using the curl operator. Two successive integrals of equation (8.21) are

$$f' f' + f f'' - 2f' + 2\xi f'' - (1 - \xi^2) f''' = C_1 , \quad (8.22)$$

$$f f' - 2f - (1 - \xi^2) f'' = C_1 \xi + C_2 . \quad (8.23)$$

The boundary condition of axial symmetry is expressed by taking $f = 0$ on $\theta = 0$ and $\theta = \pi$, or $f(1) = f(-1) = 0$. At $\xi = 1$, equation (8.23) requires $C_1 + C_2 = 0$, and at $\xi = -1$ it requires $-C_1 + C_2 = 0$. Hence $C_1 = C_2 = 0$. A further integration gives

$$f^2 - 4\xi f - 2(1 - \xi^2) f' = C_3 = 0 , \quad (8.24)$$

where the same symmetry condition requires $C_3 = 0$. Finally, the substitution

$$h(\xi) = \frac{f(\xi)}{(1 - \xi^2)} \quad (8.25)$$

transforms equation (8.24) into

$$h' = \frac{h^2}{2} . \quad (8.26)$$

The final exact solution (retransformed) is therefore

$$f(\xi) = \frac{2(1 - \xi^2)}{1 - \xi + c} \quad (8.27)$$

or

$$f(\cos \theta) = \frac{2 \sin^2 \theta}{1 - \cos \theta + c} , \quad (8.28)$$

where $(1+c)/2$ is a constant of integration. The stream function, velocity components, and azimuthal vorticity are obtained from equa-

PLACEHOLDER

Figure 8.3: Caption for Figure with label Fig15-8 (missing)

tions (8.17)–(8.20) as

$$\psi = 2\nu r \frac{\sin^2 \theta}{1 - \cos \theta + c} , \quad (8.29)$$

$$u = \frac{2\nu}{r} \frac{[2c \cos \theta - (1 - \cos \theta)^2]}{(1 - \cos \theta + c)^2} , \quad (8.30)$$

$$v = -\frac{2\nu}{r} \frac{\sin \theta}{1 - \cos \theta + c} , \quad (8.31)$$

$$\zeta = \frac{4\nu}{r^2} c(c+2) \frac{\sin \theta}{(1 - \cos \theta + c)^3} . \quad (8.32)$$

Some typical streamline patterns are shown in FIGURE 8.3 [for?] values of the parameter c . The sense of the figure is borrowed from Batchelor, p. 208. The chief difference is that the stream function and other variables are here put in dimensionless form with the aid of a trick, which is the introduction of a length \mathbf{L} that is never defined. Lagerstrom used to call \mathbf{L} the length of the blackboard.

Thus write, in what might be called virtual variables,

$$\Psi = \frac{\psi}{4\nu\mathbf{L}} , \quad (8.33)$$

$$R = \frac{r}{\mathbf{L}} , \quad (8.34)$$

$$\Theta = \theta . \quad (8.35)$$

so that equation (8.29) becomes

$$\Psi = R \frac{\sin^2 \Theta}{2(1 - \cos \Theta + c)} . \quad (8.36)$$

(Define coordinates used in figure). Since ψ varies linearly with r at constant θ , one streamline suffices to define each flow, with other streamlines obtained by a zoom transformation. Also at constant θ , the velocities u and v vary inversely with r , according to equations (8.30) and (8.31). As the Reynolds number increases (the parameter c decreases toward zero) on the one hand, a strong narrow jet emerges along the polar axis. The remainder of the flow represents fluid motion induced by this jet. At values of c that are large compared with unity, on the other hand, c dominates the denominator of equation (8.27), giving a Stokes flow with streamlines that are symmetrical upstream and downstream.

There is no mass flux from the singularity at the origin. Consider an integral over a sphere of fixed radius r about the origin, with $dS = 2\pi r \sin \theta r d\theta$. The net flux for the sphere is

$$\iint \rho \vec{u} \cdot \vec{n} dS = 2\pi \rho r^2 \int_0^\pi u \sin \theta d\theta = 2\pi \rho \nu r \int_{-1}^1 f'(\xi) d\xi = 0 . \quad (8.37)$$

To compute the corresponding momentum flux, observe that the component of any vector $\vec{a} = (a_1, a_2, 0)$ along the polar axis (the

x -axis in FIGURE 8.2) is $(a_1 \cos \theta - a_2 \sin \theta) = a_x$ (say). Then

$$\begin{aligned}
 J &= \left[\iiint \rho \vec{F} \, dV \right]_x \\
 &= \left[\iint \rho \vec{u} (\vec{u} \cdot \vec{n}) \, dS \right]_x - \left[\iint (-p\mathbf{I} + \mu \text{def } \vec{u} \vec{n}) \, dS \right]_x \\
 &= \iint \rho (u \cos \theta - v \sin \theta) u \, dS + \iint p \cos \theta \, dS \\
 &\quad - \mu \iint \left[2 \frac{\partial u}{\partial r} \cos \theta - \left(\frac{1}{r} \frac{\partial u}{\partial \theta} + \frac{\partial v}{\partial r} - \frac{v}{r} \right) \sin \theta \right] dS .
 \end{aligned} \tag{8.38}$$

A brief digression is necessary to calculate the pressure p from the two non-zero components of the momentum equations (8.8) and (8.9) above. For the exact solution $\psi = \nu r f(\xi)$, these become

$$\begin{aligned}
 \frac{1}{\rho} \frac{\partial p}{\partial r} &= \frac{\nu^2}{r^3} \left[2\xi f'' - (1 - \xi^2) f''' + f' f' + f f'' + \frac{f^2}{(1 - \xi^2)} \right] \\
 &= \frac{\nu^2}{r^3} \left[2f' + \frac{f^2}{(1 - \xi^2)} \right]
 \end{aligned} \tag{8.39}$$

and

$$\frac{1}{\rho r} \frac{\partial p}{\partial \theta} = -\frac{\nu^2}{r^3} \left[f'' + \frac{f f'}{(1 - \xi^2)} + \frac{\xi f^2}{(1 - \xi^2)^2} \right], \tag{8.40}$$

after use of equation (8.22) with $C_1 = 0$ in equation (8.39). The first equation can be integrated to obtain

$$\frac{p}{\rho} = -\frac{\nu^2}{2r^2} \left[2f' + \frac{f^2}{(1 - \xi^2)} \right] + g(\xi) . \tag{8.41}$$

Differentiation then shows that the equation (8.40) is satisfied if $g(\xi) = \text{constant} = p_0/\rho$ (say). Given that ξ , $f(\xi)$, etc. are of order unity, the difference between p/ρ and p_0/ρ for large r is of order $(\nu/r)^2$, as are the squared velocities from equations (8.30) and (8.31). Another form of equation (8.41) that may be useful is

$$\frac{p}{\rho} + \frac{v^2}{2} - \frac{\nu u}{r} = \frac{p_0}{\rho} . \tag{8.42}$$

On the jet axis, where $f(1) = 0$ and $f'(1) = -4/c$ from equation (8.27), it follows from equation (8.41) that the static pressure

slightly exceeds the stagnation pressure p_0/ρ (why not Bernoulli equation far from jet?); **(is this so?)**

$$\frac{p}{\rho} = \frac{p_0}{\rho} + \frac{4\nu^2}{r^2 c} . \quad (8.43)$$

This expression already suggests that c should approach zero like ν^2 as the Reynolds number increases.

Use of equation (8.41) for p and equations (8.30) and (8.31) for u and v in equation (8.38) leads eventually to

$$J = 2\pi\rho\nu^2 \int_{-1}^1 \left[f' f' - \frac{f^2}{2(1-\xi^2)} - 3f' \right] \xi \, d\xi . \quad (8.44)$$

After substitution for $f(\xi)$ from equation (8.27) and evaluation of the integrals, there is obtained

$$\frac{J}{8\pi\rho\nu^2} = \frac{8}{3} \frac{(c+1)}{c(c+2)} + 2(c+1) - (c+1)^2 \ln \left(\frac{c+2}{c} \right) , \quad (8.45)$$

which shows precisely how the exact solution depends on the single parameter $J/\rho\nu^2$. Particularly useful for what follows is an expansion for small c ,

$$\begin{aligned} \frac{J}{8\pi\rho\nu^2} = \frac{4}{3c} + \ln c + \left(\frac{8}{3} - \ln 2 \right) + 2c \ln c + 2c \left(\frac{7}{12} - \ln 2 \right) + \\ + c^2 \ln c - c^2 \left(\frac{17}{24} + \ln 2 \right) + \dots , \end{aligned} \quad (8.46)$$

where \dots stands for the third and higher powers of c . There are no more logarithms. The series evidently converges for $0 < c < 2$. **(check)** The leading term represents the boundary-layer approximation (see below);

$$c = \frac{32}{3} \pi \frac{\rho\nu^2}{J} . \quad (8.47)$$

(Jet out of wall? Do θ_0 here?)

8.1.4 The boundary-layer approximation

Suppose now that the exact solution of the Navier-Stokes equations is not known. The round jet into fluid at rest can also be approached from the outset as a boundary-layer problem of classical type, and was approached in this way by SCHLICHTING (1933, **check**) before the exact solution was discovered. The essential assumption is that the jet is concentrated near the polar axis, as indicated in FIGURE 8.2. A suitable magnified boundary-layer variable in spherical polar coordinates is evidently

$$\bar{\theta} = \frac{\theta}{\epsilon} , \quad (8.48)$$

where the small quantity ϵ is specified to be dimensionless and independent of r and θ , with a magnitude chosen to make $\bar{\theta} = O(1)$ in the body of the jet. By assumption, $\epsilon \rightarrow 0$ as $\nu \rightarrow 0$ or $\text{Re} \rightarrow \infty$. The continuity equation (8.7) with $\sin \theta \sim \theta$ becomes

$$\frac{1}{r^2} \frac{\partial}{\partial r} u r^2 + \frac{1}{\epsilon r \bar{\theta}} \frac{\partial}{\partial \bar{\theta}} v \bar{\theta} = 0 . \quad (8.49)$$

The two terms must be of the same order, and the v -velocity must also be magnified by a factor $1/\epsilon$,

$$\bar{v} = \frac{v}{\epsilon} , \quad (8.50)$$

to give

$$\frac{1}{r^2} \frac{\partial}{\partial r} u r^2 + \frac{1}{r \bar{\theta}} \frac{\partial}{\partial \bar{\theta}} \bar{v} \bar{\theta} = 0 . \quad (8.51)$$

Now introduce a stream function in the usual way, putting

$$u = \frac{1}{r^2 \bar{\theta}} \frac{\partial \bar{\psi}}{\partial \bar{\theta}} , \quad \bar{v} = -\frac{1}{r \bar{\theta}} \frac{\partial \bar{\psi}}{\partial r} , \quad (8.52)$$

where the stream function ψ is magnified according to its own rule;

$$\bar{\psi} = \frac{\psi}{\epsilon^2} . \quad (8.53)$$

The azimuthal vorticity, defined by equation (8.11) becomes

$$\zeta = \frac{\epsilon}{r} \frac{\partial r \bar{v}}{\partial r} - \frac{1}{\epsilon r} \frac{\partial u}{\partial \bar{\theta}} \quad (8.54)$$

and leads to

$$\bar{\zeta} = \frac{\zeta}{\epsilon} . \quad (8.55)$$

After these preliminaries, the radial and azimuthal momentum equations (8.8) and (8.9) become, respectively (**check these carefully**),

$$u \frac{\partial u}{\partial r} + \frac{\bar{v}}{r} \frac{\partial u}{\partial \bar{\theta}} - \frac{\epsilon^2 \bar{v}^2}{r} = -\frac{1}{\rho} \frac{\partial p}{\partial r} + \frac{\nu}{\epsilon^2} \left(\frac{\epsilon^2}{r^2} \frac{\partial}{\partial r} r^2 \frac{\partial u}{\partial r} + \frac{1}{r^2 \bar{\theta}} \frac{\partial}{\partial \bar{\theta}} \bar{\theta} \frac{\partial u}{\partial \bar{\theta}} - 2 \frac{\epsilon^2 u}{r^2} - \frac{2\epsilon^2}{r^2 \bar{\theta}} \frac{\partial \bar{v} \bar{\theta}}{\partial \bar{\theta}} \right) , \quad (8.56)$$

$$\epsilon^2 \left(u \frac{\partial \bar{v}}{\partial r} + \frac{\bar{v}}{r} \frac{\partial \bar{v}}{\partial \bar{\theta}} + \frac{u \bar{v}}{r} \right) = -\frac{1}{\rho r} \frac{\partial p}{\partial \bar{\theta}} + \frac{\nu}{\epsilon^2} \left(\frac{\epsilon^4}{r^2} \frac{\partial}{\partial r} r^2 \frac{\partial \bar{v}}{\partial r} + \frac{\epsilon^2}{r^2 \bar{\theta}} \frac{\partial}{\partial \bar{\theta}} \bar{\theta} \frac{\partial \bar{v}}{\partial \bar{\theta}} + \frac{2\epsilon^2}{r^2} \frac{\partial u}{\partial \bar{\theta}} - \frac{\epsilon^2 \bar{v}}{r^2 \bar{\theta}^2} \right) . \quad (8.57)$$

The equations of motion are now ready for the boundary-layer approximation or inner limit. This is the limit $\epsilon \rightarrow 0$ with r and $\bar{\theta} = \theta/\epsilon$ fixed and $O(1)$, so that points in the body of the jet remain in the jet, even in the limit as the body of the jet becomes the polar axis.

Because at least one of the viscous terms in the first equation (8.56) must survive in the limit $\epsilon \rightarrow 0$, it is necessary that

$$\epsilon \sim \nu^{1/2} . \quad (8.58)$$

Each of the terms in the second equation (8.57), except possibly the pressure term, is at most $O(\epsilon^2)$, and this must therefore also be true of the pressure term. Hence $\partial p / \partial \bar{\theta} = O(\epsilon^2)$, or

$$\frac{\partial p}{\partial \theta} = O(\epsilon) = O(\nu^{1/2}) . \quad (8.59)$$

This estimate can be confirmed from equation (8.41) (**check**). To this order, the pressure is constant across the body of the jet, although the constant may depend on r . However, the ambient fluid has been stipulated to be at rest. Hence the centripetal-acceleration term and the pressure-gradient term can be dropped entirely. When physical variables are restored, the boundary-layer problem is defined by

$$u \frac{\partial u}{\partial r} + \frac{v}{r} \frac{\partial u}{\partial \theta} = \nu \left(\frac{1}{r^2 \theta} \frac{\partial}{\partial \theta} \theta \frac{\partial u}{\partial \theta} \right) \quad (8.60)$$

with

$$u = \frac{1}{r^2 \theta} \frac{\partial \psi}{\partial \theta}, \quad v = -\frac{1}{r \theta} \frac{\partial \psi}{\partial r}. \quad (8.61)$$

The pressure is no longer a dependent variable, but is determined as part of the boundary conditions. The order of the governing equations is reduced by one.

As is usual with boundary-layer problems, the validity of the argument just given can be tested *a posteriori* by using the boundary-layer solution in the full equations. (**Expand on this.**)

8.1.5 The boundary-layer Solution

The original dimensional argument for the form of the solution made no use of equations and is unchanged by the boundary-layer approximation leading to equation (8.60). It should be possible to argue this form using an affine transformation together with the associated invariants (a scheme which is equivalent to a dimensional argument), but I am not satisfied with the analysis at present. (**Do this**). The absence of characteristic scales again requires the ansatz

$$\psi = \nu r g(\theta) \quad (8.62)$$

where θ now means θ and not $\cos \theta$ as in the exact solution. The velocity components from equation (8.12) become

$$u = \frac{\nu}{r \theta} g', \quad v = -\frac{\nu}{r \theta} g, \quad (8.63)$$

with

$$\zeta = -\frac{1}{r} \frac{\partial u}{\partial \theta} = -\frac{\nu}{r} \left(\frac{g''}{\theta} - \frac{g'}{\theta^2} \right) . \quad (8.64)$$

Substitution for u and v in equation (8.60) yields

$$-\frac{g'g'}{\theta} + \frac{gg'}{\theta^2} - \frac{gg''}{\theta} - \frac{g'}{\theta^2} + \frac{g''}{\theta} - g''' = 0 . \quad (8.65)$$

This equation is third order (where equation (8.21) was fourth order) because the absence of the pressure in the boundary-layer approximation makes it unnecessary to take the curl. A first integration gives

$$-\frac{gg'}{\theta} + \frac{g'}{\theta} - g'' = C_1 = 0 . \quad (8.66)$$

To show that the constant C_1 is zero, note from the first of equations (8.63) that a power-series expansion for $g(\theta)$ must begin with a term in θ^2 . A second and non-trivial integration, with the same condition at $\theta = 0$, gives

$$-\frac{g^2}{2\theta} + \frac{2g}{\theta} - g' = C_2 = 0 \quad (8.67)$$

and finally

$$g = \frac{4\theta^2}{\theta^2 + 2c} , \quad (8.68)$$

where $2c$ is an undetermined constant of integration.

The boundary-layer approximation to the momentum integral (8.38) is **(connect this with momentum integral for plane jet)**

$$J = 2\pi\rho\epsilon^2 \int_0^\pi u^2 r^2 \bar{\theta} \, d\bar{\theta} . \quad (8.69)$$

Note that the axial or x -component of velocity, $u \cos \theta - v \sin \theta = u - \epsilon^2 \bar{v} \bar{\theta}$, is indistinguishable from the radial component for $\epsilon \rightarrow 0$. A similar statement holds for the radial and axial coordinates r and z . Consequently,

$$J = \epsilon^2 2\pi\rho\bar{v}^2 \int_0^\infty \frac{g'g'}{\theta} \, d\bar{\theta} . \quad (8.70)$$

Substitution from equation (8.68) for g and integration give a relation between J and c ,

$$\frac{J}{2\pi\rho\nu^2} = \frac{16}{3c} . \quad (8.71)$$

8.1.6 The inner limit

The operational diagram in FIGURE X ³ identifies the boundary-layer solution with the inner limit of the exact solution. With the preliminary approximation $\sin \theta \sim \theta$, $\cos \theta \sim 1 - \theta^2/2$ for small θ , the exact solution from equations (8.29)–(8.31) is reduced to

$$\psi = 4\nu r \frac{\theta^2}{(\theta^2 + 2c)} , \quad (8.72)$$

$$u = \frac{16\nu c}{r} \frac{1}{(\theta^2 + 2c)^2} , \quad (8.73)$$

$$v = -\frac{4\nu}{r} \frac{\theta}{(\theta^2 + 2c)} , \quad (8.74)$$

$$\zeta = \frac{4\nu}{r^2} c(c + 2) \frac{\theta}{(\theta^2/2 + c)^3} . \quad (8.75)$$

In the virtual variables defined by equations (8.33)–(8.35), the boundary-layer approximation for the stream function is

$$\Psi = R \frac{\Theta^2}{\Theta^2 + 2c} . \quad (8.76)$$

These streamlines are plotted in FIGURE 15.x for a value $c = 0.005$ (**check**).⁴ Again there is only one streamline, with others derived from this by a zoom transformation. The fictitious spherical stream surfaces at the left are generated by equation (8.76) when $\Theta \gg c$, so that $\Psi = R$, approximately. This behavior is an artifact of the spherical polar coordinate system and the fact that the boundary-layer

³It is not known what figure this is meant to refer to.

⁴Possibly refers to a missing Figure 8.4

solution has no meaning outside the boundary layer. The characteristics of the boundary-layer equations are the lines $r = \text{constant}$. There is no upstream diffusion of vorticity, and upstream here means directed inward toward the origin along a radius in FIGURE 15.x. SQUIRE (1955) encountered this behavior in his third paper, whose subject was conical laminar jets in spherical polar coordinates. He questioned the behavior, but did not resolve it.

Equations (8.xx) are identical with the boundary-layer solution given by equations (8.62), (8.63), and (8.68). Finally, equation (8.71) in the form

$$\frac{J}{2\pi\rho\nu^2} = \frac{16}{3c} \quad (8.77)$$

is seen to be the leading term in the expansion (8.46). In short, the inner limit of the exact solution coincides in all respects with the solution of the inner limit of the exact equations, as originally claimed for the operational diagram, FIGURE 8.1.

8.1.7 The outer limit

As a fluid element is entrained in the jet, it first undergoes a rapid acceleration. This is followed by a slow deceleration, as the element finds itself close to the jet axis, where $u \sim 1/r$. Each stream tube therefore first converges and then diverges. A convenient measure for the angle $\bar{\theta}$, say $\bar{\theta} = \bar{\theta}_0$, is provided by the point of closest approach to the axis (other nearly equivalent measures can be defined). In boundary-layer variables, as indicated in the sketch (**comment on outer flow**),

$$\bar{\psi} = \frac{4\nu r \bar{\theta}^2}{\bar{\theta}^2 + 2c} = \frac{4\nu z \bar{R}^2}{\bar{R}^2 + 2c z^2} . \quad (8.78)$$

Along a streamline, therefore,

$$\frac{d\bar{R}}{dz} = \frac{\bar{R}}{4c z^3} (2c z^2 - \bar{R}^2) . \quad (8.79)$$

The derivative vanishes when

$$\frac{\bar{R}_0^2}{z_0^2} = \theta_0^2 = 2c . \quad (8.80)$$

The parameter

$$\theta_0 = (2c)^{1/2} = \left(\frac{32}{3} \frac{2\pi\rho\nu^2}{J} \right)^{1/2} \quad (8.81)$$

suggests itself *a posteriori* as a suitable quantitative choice for the dimensionless parameter ϵ , with all of the correct properties, beginning with the property $\bar{\theta} = O(1)$. In fact, according to equation (8.48), where ϵ was first introduced, this choice amounts to putting $\bar{\theta}_0 = 1$. (*Is there an equivalent for other flows? Why stick to spherical polar coordinates? Note that the thickness of the laminar round jet varies like ν , not $\nu^{1/2}$: mention subcharacteristics. Figure out what this means for \bar{J} and $\bar{\nu}$.*)

(*Need to consider laminar round jet out of wall; see p. 19 of 1981 notes and paper by Squire.*)

Outside the jet; i.e., for $\theta \gg \theta_0$, the stream function and velocity components from equations (8.72)–(8.74) approach (**mention circle, Squire**)

$$\bar{\psi} = 4\bar{\nu}r \quad \text{or} \quad \psi = 4\nu r, \quad (8.82)$$

$$u = \frac{16\bar{\nu}c}{\bar{\theta}^4} \quad \text{or} \quad u = \frac{16\nu c}{\theta^4}, \quad (8.83)$$

$$\bar{v} = -\frac{4\bar{\nu}}{r\bar{\theta}} \quad \text{or} \quad v = -\frac{4\nu}{r\theta} = -\frac{4\nu}{R}. \quad (8.84)$$

It is worth noting that the streamwise velocity u approaches zero for large θ algebraically, like θ^{-4} , rather than exponentially; and also that a power series expansion for $u(\theta)$ converges only for $\theta < \theta_0$, and thus for $u(\theta)/u(0) > 1/4$ from equation (8.73). The reason is the existence of simple poles at $\theta = \pm i\theta_0$ in the complex θ -plane (**mention Weyl?**). (**Exact solution has same property?**)

The message of equation (8.74) is that rv outside the boundary layer is independent of r , and therefore that the action of the jet on the ambient fluid is essentially like that of a uniform line sink

along the positive z -axis. To calculate the associated potential flow, first use the representation for a sink of strength Q at the origin in spherical polar coordinates;

$$u = -\frac{Q}{4\pi\rho r^2} . \quad (8.85)$$

For a distribution of such sinks along the positive z -axis the velocity becomes

$$u = \int du = \int \cos(\theta' - \theta) du' = - \int \frac{\cos(\theta' - \theta)dQ}{4\pi\rho r'^2} \quad (8.86)$$

in the notation shown in the sketch. For a uniform sink, put (**explain why there should be a constant A**)

$$dQ = 4\pi\rho A dz' \quad (8.87)$$

where A is a constant to be determined from the boundary conditions. Note from the sketch that

$$\frac{z - z'}{r \sin \theta} = \cot \theta' , \quad dz' = \frac{r \sin \theta d\theta'}{\sin^2 \theta'} . \quad (8.88)$$

Finally, therefore,

$$u = -\frac{A}{r \sin \theta} \int_{\theta}^{\pi} \cos(\theta' - \theta) d\theta' = -\frac{A}{r} . \quad (8.89)$$

The outer stream function in spherical polar coordinates follows from the first of equations (8.12),

$$\psi = Ar \cos \theta + B(r) . \quad (8.90)$$

The boundary conditions are $\psi = 4\nu r$ at $\theta = 0$ and $\psi = 0$ at $\theta = \pi$. Consequently $A = 2\nu$ and $B(r) = 2\nu r$, and

$$\psi = 2\nu r(1 + \cos \theta) . \quad (8.91)$$

This expression is evidently the outer limit ($\epsilon \rightarrow 0$ or $c \rightarrow 0$ with r and θ fixed) of the exact solution (8.29). The streamlines described by equation (8.91) are confocal paraboloids of revolution,

as shown in the sketch.⁵ Write $\psi/2\nu = r + z$, take the square, and use $r^2 = R^2 + z^2$ to obtain

$$R^2 = \frac{\psi}{\nu} \left(\frac{\psi}{4\nu} - z \right) . \quad (8.92)$$

It is worth noting that the streamlines from the boundary-layer solution outside the boundary layer, $\psi = 4\nu r$, are concentric circles (see Squire). If the boundary-layer approximation had been made in cylindrical polar coordinates, there would have been obtained $\psi = 4\nu z = 4\nu r \cos \theta$. These streamlines are straight lines normal to the z -axis. Neither result is useful, because the boundary-layer approximation should not be relied on outside the boundary layer. The correct streamlines are the paraboloids (?) given by equation (8.91), $\psi = 2\nu r(1 + \cos \theta)$. (**Comment on the outer limit of the exact solution.**)

The rule for constructing the composite expansion (see Van Dyke 1975 and the sketch) is to add the inner and outer approximations and subtract the common part. The procedure is illustrated in the sketch. From equations (8.72) and (8.91),

$$\psi_c = 4\nu r \frac{\theta^2}{\theta^2 + \theta_0^2} + 2\nu r(1 + \cos \theta) - 4\nu r . \quad (8.93)$$

For $\theta \sim \theta_0$, the third term essentially cancels the second, and the first term dominates. For $\theta \gg \theta_0$, the third term essentially cancels the first, and the second term dominates. It is plausible that the expression (8.93) is a uniformly valid approximation to the exact solution of equation (8.29),

$$\psi_e = 2\nu r \frac{\sin^2 \theta}{1 - \cos \theta + c} . \quad (8.94)$$

That is, the quantity

$$\left| \frac{\psi_e - \psi_c}{2\nu r} \right| \quad (8.95)$$

should be a bounded function of θ for sufficiently small c (actually for all c).

⁵It is not known what sketch this refers to.

8.1.8 Miscellaneous remarks

CHIN (1981) recently showed that confocal paraboloidal coordinates are optimal for the Squire-Landau problem in the sense defined by KAPLUN (1954); the boundary-layer solution includes the outer solution, although the boundary-layer solution is not exact. In my review of Chin's paper for another journal, I objected (unsuccessfully) that it is not necessary to derive and solve the boundary-layer equations in the paraboloidal system, since Kaplun's substitution theorem is more efficient.

WYGNANSKI (1970) has extended the original exact Squire-Landau solution in equations (8.29)–(8.32) to the case of flow with swirl by resorting to numerical methods. The minimum in the axial velocity on the axis for large swirl, the increased entrainment, and the approach of the outer flow to a viscous core/potential vortex motion are clearly brought out.

SQUIRE in a second paper (1952) considered the exact problem when there is a conical wall at $\theta = \Theta$, particularly $\Theta = \pi/2$, with a slip boundary condition at the wall. The issue is mainly the evaluation of the constants c_1 , c_2 , c_3 in equations (8.22)–(8.24) when these are not all zero, as well as the complications that set in during the final integration step. SCHNEIDER (1981) claims to find an exact solution for this case with a no-slip condition, thus taking into account the displacement effect on the outer flow of the boundary layer on the wall. I have not studied this paper closely enough to understand in what sense the solution is exact. GINEVSKII (1966) carried out the outer-flow approximation for a turbulent jet with a wall at $\theta = \Theta$, in the manner used to obtain equation (8.91). The entrainment velocity was estimated by using the polynomial mean-velocity profile. The two-dimensional case is treated similarly. In no case was a no-slip condition applied at the wall.

A third paper by SQUIRE (1955) attempted to treat a conical jet lying along a surface $\theta = \theta^*$, with the radial jet ($\theta^* = \pi/2$) as an important special case. The analysis uses a boundary-layer approximation, and the streamlines outside the jet show the same pathological behavior shown by equations (8.72) for $\theta^2 \gg 2c$. The

outer flow and the composite expansion are not considered.

A few other references are cited in ROSENHEAD (1963), WYG-
NANSKI (1970), and SCHNEIDER (1981).

8.2 Laminar round jet into moving fluid

8.3 Transition

ANDRADE (1937)
DOMM et al (1955)
BECKER and MASSARO (1968)
SYMONS and LABUS (1971)
ZAUNER (1985)
TUCKER and ISLAM (1986)
PETERSEN et al (1988)
MEIBURG et al (1989)
LIEPMANN (1991)
BROZE and HUSSAIN (1994)
TONG and WARHAFT (1994)

References

- Batchelor, G. K. 1967 “An Introduction to Fluid Dynamics,” Cambridge, 205–211.
- Chin, W. C. 1981 *Optimal Coordinates for Squire’s Jet*. AIAA J. *19*, 123–124.
- Kaplun, S. 1954 *The Role of Coordinate Systems in Boundary-Layer Theory*. ZAMP *5*, 111–135.
- Landau, L. F. 1944 *A New Exact Solution of the Navier Stokes Equations*. Doklady Acad. Sci. **43**, 286–288.
- Rosenhead, L. (ed.) 1963 *Laminar Boundary Layers*, Oxford, 150–155.
- Schneider, W. 1981 *Flow Induced by Jets and Plumes*. J. Fluid Mech. **108**, 55–65.
- Slezkin, N. A. 1934 *On an Exact Solution of the Equations of Viscous Flow*. Scientific Papers, Moscow State University, No. 2 (I have not seen this paper).
- Squire, H. B. 1951 *The Round Laminar Jet*. Quart. J. Mech. Appl. Math. **4**, 321–329.
- Squire, H. B. 1952 *Some Viscous Fluid Flow Problems. I: Jet Emerging From a Hole in a Plane Wall*. Phil. Mag. (7) **43**, 942–945.
- Squire, H. B. 1955 *Radial Jets*. In *50 Jahre Grenzschichtforschung*, Vieweg, Braunschweig, 47–54.
- Van Dyke, M. 1975 “Perturbation Methods in Fluid Mechanics,” Parabolic Press.
- Wyganski, I. 1970 *Swirling Axisymmetrical Laminar Jet*. Phys. Fluids **13**, 2455–2460.

8.4 Turbulent round jet into fluid at rest

[This section was found in a separate file and appears to belong here, though in its found form it repeated the first two paragraphs of the start of this chapter]

For the round jet, cylindrical polar coordinates (r, θ, z) are appropriate because experimenters move their probes in a plane $z = \text{constant}$. The velocity components are (u, v, w) , and the jet motion is along the positive z -axis. The ambient fluid, which is here taken to be the same as the fluid in the jet, is nominally at rest, so that the pressure is nominally constant. If the mean motion is steady, axially symmetric, and free of swirl, the boundary-layer equations of motion are

$$\frac{1}{r} \frac{\partial ru}{\partial r} + \frac{\partial w}{\partial z} = 0 \quad , \quad (8.96)$$

$$u \frac{\partial w}{\partial r} + w \frac{\partial w}{\partial z} = \frac{1}{\rho r} \frac{\partial r\tau}{\partial r} \quad , \quad (8.97)$$

$$\tau = \mu \frac{\partial w}{\partial r} - \overline{\rho u'w'} \quad . \quad (8.98)$$

The first and second equations can be combined in the form

$$\frac{\partial rww}{\partial r} + \frac{\partial rww}{\partial z} = \frac{1}{\rho} \frac{\partial r\tau}{\partial r} \quad (8.99)$$

and this expression can be integrated over a plane $z = \text{constant}$, with boundary conditions $u = 0$ at $r = 0$ and $w = \tau = 0$ at $r = \infty$, to obtain the momentum integral

$$J = 2\pi\rho \int_0^\infty rww \, dr = \text{constant} \quad . \quad (8.100)$$

The parameters of the problem are J and ρ , with, from equation (8.100),

$$\left[\frac{J}{\rho} \right] = \frac{\mathbf{L}^4}{\mathbf{T}^2} = \mathbf{L}^2 \mathbf{U}^2 \quad . \quad (8.101)$$

There is nothing else to work with. The absence of a characteristic length means that the jet must grow conically. When a stream function is introduced such that

$$u = -\frac{1}{r} \frac{\partial \psi}{\partial z} \quad , \quad w = \frac{1}{r} \frac{\partial \psi}{\partial r} \quad (8.102)$$

it is seen that

$$[\psi] = \mathbf{L}^2 \mathbf{U} = \mathbf{L} \left[\frac{J}{\rho} \right]^{1/2} . \quad (8.103)$$

(Profile is f'/η , not f' . Can this be fixed?) The profile similarity assumption is therefore to use z and J/ρ to form the non-dimensionalizing combination; thus

$$A\psi = z \left(\frac{J}{\rho} \right)^{1/2} f \left(B \frac{r}{z} \right) \quad (8.104)$$

where A and B are disposable dimensionless constants. **(Why not use spherical polar coordinates?)**

The mean velocity components are

$$u = -\frac{1}{Ar} \left(\frac{J}{\rho} \right)^{1/2} (f - \eta f') \quad , \quad (8.105)$$

$$w = \frac{B}{Ar} \left(\frac{J}{\rho} \right)^{1/2} f' . \quad (8.106)$$

Papers with profiles can give both the growth rate and the centerline velocity decay. To begin with, use only data that include both sides of the profile (denoted by sym). Try 3 functions for fit near plane of symmetry. Look for constant in growth rate and distance required to achieve it after arbitrary initial condition. Apparent origins from $\delta(x)$ and $u_o/u_c(x)$ should be the same.

Papers with profiles:

VOORHEIS (1940)
 REICHARDT (1942) 9A (sym)
 ALBERTSON et al. (1948)

CORRSIN and UBEROI (1949)
HINZE and ZIJNEN (1949)
NOTTAGE (1951)
TAYLOR et al. (1951)
GAYLORD (1953) (sym)
CORRSIN and KISTLER (1954) 7N (sym)
LAURENCE (1956)
SUNAVALA et al. (1957)
HIDY (1962)
ROSLER (1962)
FARIS (1963)
KNYSTAUTAS (1964) 17A (sym)
LAWRENCE (1965)
DELLEUR et al. (1966) (sym)
SAMI (1967)
SAMI et al. (1967)
WHITE (1967)
KAMOTANI and WISKIND (1968) (sym)
WYGNANSKI and FIEDLER (1968)
CHUANG (1970)
CROW and CHAMPAGNE (1970)
EASTLAKE (1971) 17C
GOLDSCHMIDT et al. (1972) 17A
LABUS and SYMONS (1972) (sym)
WITZE (1974) 17G
ABBISS et al. (1975)
BRADBURY and KHADEM (1975)
HATTA and NOZAKI (1975) 17A
RODI (1975)
BARNETT and GIEL (1976)
EBRAHIMI and KLEINE (1977)
SHAUGHNESSY and MORTON (1977) (sym)
BORREGO and OLIVARI (1979) (sym)
MODARRESS et al. (1984)
CHUA and ANTONIA (1986)
OBOT and TRABOLD (1987)
SHLIEN (1987)

TAULBEE et al. (1987)
 KASAGI et al. (1988)
 KINDLER (1988)
 HUSSEIN and GEORGE (1989)
 DOWLING and DIMOTAKIS (1990)
 KUHLMAN and GROSS (1990)
 PANCHAPAKESAN and LUMLEY (1993)
 HUSSEIN et al. (1994)

Some other papers that give growth rate and/or velocity decay, but not profiles, are

KISER (1963)
 BECKER et al. (1965, 1967)
 SINGAMSETTI (1965)
 MONS and SFORZA (1971)
 SFORZA and MONS (1978)
 AHMED et al. (1988)
 DRUBKA et al. (1989)

Substitution of equations (8.105) and (8.106) in equation (8.97) leads to

$$\frac{ff''}{\eta} + \frac{f'f'}{\eta} - \frac{ff'}{\eta^2} = \frac{A^2}{B^3} \frac{z^2}{J} \frac{\partial r\tau}{\partial r} \quad (8.107)$$

where

$$\eta = B \frac{r}{z} . \quad (8.108)$$

In the course of this operation the term $w \partial w / \partial z$ in equation (8.97) was cancelled by another term. This property means that the left side of equation (8.107) must be a perfect differential; it is in fact $(ff'/\eta)'$. On the right, if the laminar stress is neglected, the dimensions of τ are

$$\left[\frac{\tau}{\rho} \right] = U^2 = \frac{1}{L^2} \left[\frac{J}{\rho} \right] . \quad (8.109)$$

The only length available is z , so that it is necessary to put (**need another constant?**)

$$\frac{\tau}{\rho} = \frac{J}{\rho z^2} g(\eta) . \quad (8.110)$$

It follows that

$$\frac{\partial r\tau}{\partial r} = \frac{J}{z^2}(\eta g)' \quad (8.111)$$

and therefore, from equation (8.107), that

$$\frac{f f'}{\eta} = \frac{A^2}{B^3}\eta g + c . \quad (8.112)$$

Since f'/η is bounded and f goes to zero as $\eta \rightarrow 0$ (see formula for w ; give B.C. separately), the constant c is zero. (**Something about eddy viscosity.**)

Various Reynolds stresses:

CORRSIN and UBEROI (1949)
 LITTLE and WILBUR (1951)
 ROSLER (1962)
 BRADSHAW et al. (1964)
 LAWRENCE (1965)
 BECKER et al. (1967)
 WYGNANSKI and FIEDLER (1968)
 CHUANG (1970)
 CROW and CHAMPAGNE (1970)
 GOLDSCHMIDT et al. (1972)
 ABBISS et al. (1975)
 RODI (1975)
 BARNETT and GIEL (1976)
 SHAUGHNESSY and MORTON (1977)
 CHEVRAY and TUTU (1978)
 CHUA and ANTONIA (1986)
 AHMED et al. (1988)
 KASAGI et al. (1988)
 HUSSEIN and GEORGE (1989)
 HUSSEIN et al. (1993)
 PANCHAPAKESAN and LUMLEY (1993)

Papers with intermittency data:

CORRSIN and KISTLER (1954) 7N

BECHER et al. (1965)
 WYGNANSKI and FIEDLER (1968)
 ANTONIA (1974)
 ANTONIA et al. (1975)
 SHAUGHNESSY and MORTON (1977)
 CHEVRAY and TUTU (1978)

The entrainment is given by

$$(ru)_{\infty} = -\frac{1}{A} \left(\frac{J}{\rho} \right)^{1/2} f(\infty) \quad (8.113)$$

provided that the product $\eta f'$ (i.e., $r^2 w$) goes to zero at infinity, a condition that is plausible but experimentally unprovable. The entrainment velocity is independent of z .

For flow out of a wall at $z = 0$, the outer flow responds to a uniform distributed sink on the positive z -axis, and the streamlines are radial. If there is no wall, the outer-flow streamlines are confocal parabolas, as in the laminar case. (**Do outer stream function and composite flow.**)

Scale: use r for $w/w_c = \frac{1}{2}$, or closest approach of mean streamlines. (**Comment on problem with hot wire rectifying, or seeding problem with LDV.**)

A comment can be made about dilution. If the flow comes from an orifice of diameter d with uniform velocity w_0 , as shown in the sketch, then

$$\frac{m_0}{\rho} = \frac{\pi}{4} w_0 d^2, \quad (8.114)$$

$$\frac{J}{\rho} = \frac{\pi}{4} w_0^2 d^2. \quad (8.115)$$

For turbulent flow, it follows from

$$\frac{m}{\rho} = 2\pi \int_0^{\infty} r w dr \quad (8.116)$$

and

$$w = \frac{1}{r} \frac{B}{A} \left(\frac{J}{\rho} \right)^{1/2} f'(\eta) \quad (8.117)$$

that

$$\frac{m}{\rho} = \frac{2\pi}{A} \left(\frac{J}{\rho} \right)^{1/2} f(\infty) z . \quad (8.118)$$

Now use equation (8.115) to eliminate J/ρ ; thus **(check this)**

$$\frac{m}{m_0} = \frac{f(\infty)}{A} (16\pi)^{1/2} \frac{z}{d} . \quad (8.119)$$

The condition that $m/m_0 \gg 1$, if $f(\infty)$ and A are $O(1)$ is, conservatively,

$$\frac{z}{d} \gg 1 . \quad (8.120)$$

Note that the spreading angle is not small, so that there is some uncertainty about the security of the boundary-layer approximation. However, the other turbulent stresses can be carried along. **(Say something about initial conditions.)**

(The round jet is a good flow for checking consistency of growth rate, because there are no side walls in the problem.) Newman. Column 3 is not quite correlation. Figure 2 has laminar profile, two guessed profiles, and one empirical profile. Thickness is not always defined consistently. On p. 3, there is reasonable agreement in $UL^{1/2}$. Comment on effect of wall for plane jet (and absence of wall). Check first on momentum balance.

Harsha. *Note large discrepancies in Reynolds stresses. Some of this may be real, and may depend on initial conditions. Such figures bound the accuracy that modelers can hope to get.*

Mention momentumless wake.

Put together derivation of turbulent energy equation.

Discuss scales, $\kappa - \epsilon$ models.

Notes on handout.

Round jet into moving fluid:

FORSTALL and SHAPIRO (1950)

TANI and KOBASHI (1951)

KOBASHI (1952)

PABST (1960)
BECKER et al. (1962, 1965)
ALPINIERI (1964)
CHIGIER and BEER (1964)
REICHARDT (1964, 1965)
CHAMPAGNE and WYGNANSKI (1970, 1971)
ROZENMAN and WEINSTEIN (1970)
RAZINSKY and BRIGHTON (1971)
DURAO and WHITELOW (1973)
MATSUMOTO et al. (1973)
HAMMERSLEY (1974)
ANTONIA and BILGER (1976)
OWEN (1976)
SMITH and HUGHES (1977)
DE WOLF and MUNNIKSMA (1980)
BINDER and KLAN (1983)
HUSAIN (1984)
SO and AHMED (1984)
KO and KWAN (1985)
KNUDSEN and WOOD (1986)
SUZUKI et al. (1987)
GORE and CROWE (1988)
KHODADI and VLACHOS (1989)
GLADNIK et al. (1990)
HENBEST and YACOUB (1991)
STRYKOWSKI and WILCOXON (1992)
HUANG and LIN (1994)

Round jet into different gas:

KEAGY et al. (1949)
WILSON and DANKWERTS (1964)
TOMBACH (1969)
TRENTACOSTE and SFORZA (1970)
LENZE (1976)
BIRCH et al. (1978)
CHEN et al. (1986)
BALLAL and CHEN (1987)

ZHU, SO, and OTUGEN (1988)
PANCHAPAKESAN and LUMLEY (1993)
SAUTET and STEPOWSKI (1995)
DJERIDANE et al. (1996)

Non-round jets:

Elliptic

TRENTACOSTE and SFORZA (1969)
HUSAIN (1984)
GUTMARK et al. (1985)
HUSAIN and HUSSAIN (1985)
HO and GUTMARK (1987)
QUINN (1989)
HUSAIN and HUSSAIN (1993)
BROWN et al. (1994)

Triangular

GUTMARK et al. (1985)
KOSHIGOE et al. (1989)
QUINN (1989, 1990)

Square

GRINSTEIN et al. (1995)

Chapter 9

THE PLANE JET

Consider a plane jet issuing into a stagnant fluid from a slit in a plane wall, as shown schematically in FIGURE 9.1. This configuration is often used in experimental work for the sake of its standard geometry. The most important quantity in any description of such a jet flow, whether laminar or turbulent, is J , the initial flux of momentum per unit span. As the flow develops in the downstream direction, this initial momentum is conserved as it is gradually transferred from the jet fluid to the ambient fluid by shearing stresses. The rate of momentum transfer will depend not only on the nature of these stresses, but also on the relative densities of the two fluids, if these are different, and on the effect of real rather than ideal initial and boundary conditions. In any case, the total rate of fluid flow in the jet will increase continuously in the downstream direction as external fluid is entrained. It is this entrainment process that dominates most practical problems.

For laminar flow, the solution of the boundary-layer problem is known in closed form, and the absence of a dimensionless parameter implies that all laminar plane jets are equivalent. So are all turbulent jets, for the same reason. However, for turbulent flow the growth rate is relatively rapid, and a boundary-layer approximation may not be appropriate.

A simple generalization of the classical flow is obtained if the wall is absent and the jet issues from a line momentum source into

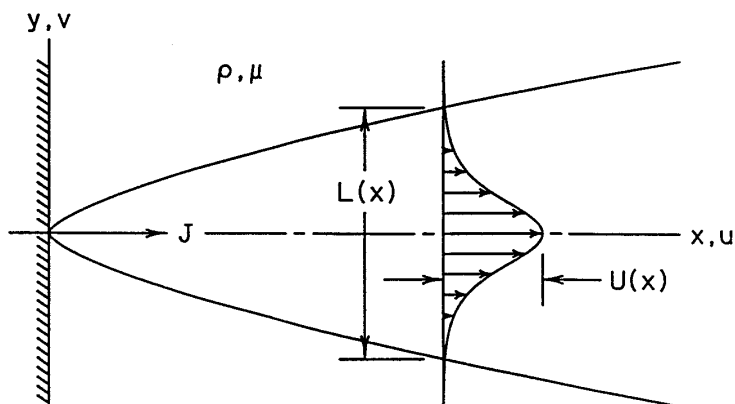


Figure 9.1: A schematic representation of the laminar plane jet out of a vertical wall. J is the rate of momentum flux per unit span.

a parallel moving stream. A small enough velocity difference, with or without a pressure gradient, may allow the jet problem to be linearized, thus providing a link with the problem of the plane wake. Even if the velocity difference is not small near the origin, it is likely to become small farther downstream, unless the pressure gradient is specially tailored to maintain a state of overall similarity.

In some practical applications, the jet may issue into a confined channel and act primarily as a jet pump or as a device for thrust augmentation. In other geometries, the objective may be to shield a region by means of a jet curtain, or to modify the flow around a lifting surface by means of a jet flap, or to exploit the Coanda effect, which is the tendency for jet entrainment to evacuate an unvented region on one side or the other to a point where the jet sheet must curve toward the unvented region in order to realize the required pressure gradient normal to the local flow direction.

Finally, multiple jets are known to interact strongly with each other under certain conditions. The flow immediately downstream of

a monoplane grid or cascade, for example, might be considered as an array of plane wakes or as an array of plane jets, depending on the solidity of the grid. In the latter case, large-scale instabilities may occur if entrainment by a jet tends to favor one unvented region over another, or if jets compete with each other in entraining fluid from the same unvented or partially vented region. FIGURE 9.2 shows a striking example of the second circumstance.

9.1 Laminar plane jet into fluid at rest

9.1.1 The equations of motion

The classical laminar plane jet in an incompressible fluid is an unexceptional flow in terms of similarity arguments. Appropriate velocity components are (u, v) in rectangular coordinates (x, y) . The motion is two-dimensional in the xy -plane and is symmetrical about the plane $y = 0$. The pressure and density are constant everywhere. The laminar boundary-layer equations are

$$\frac{\partial u}{\partial x} + \frac{\partial v}{\partial y} = 0 \quad , \quad (9.1)$$

$$\rho \left(u \frac{\partial u}{\partial x} + v \frac{\partial u}{\partial y} \right) = \mu \frac{\partial^2 u}{\partial y^2} \quad . \quad (9.2)$$

Boundary conditions that require the jet flow to be symmetric about the plane $y = 0$ and to vanish for large y are

$$\psi(x, 0) = 0 \quad \text{or} \quad v(x, 0) = 0 \quad , \quad (9.3)$$

$$u(x, \pm\infty) = 0 \quad , \quad (9.4)$$

where ψ is a stream function that links the velocities u and v through the relations

$$u = \frac{\partial \psi}{\partial y} \quad , \quad v = -\frac{\partial \psi}{\partial x} \quad , \quad (9.5)$$

and thus satisfies the continuity equation (9.1) identically.

Because pressure forces are neglected in the boundary-layer approximation, the momentum flux in the body of the jet must be



Figure 9.2: Visualization, using smoke filaments, of flow through a monoplane grid of cylindrical rods. The blockage is large enough to excite an entrainment instability (figure 3, plate 1, of Bradshaw 1965). Photograph courtesy of Cambridge University Press.

conserved during the mixing. If the continuity equation (9.1) is multiplied by ρu and added to the momentum equation (9.2), the result is

$$\rho \left(\frac{\partial uu}{\partial x} + \frac{\partial uv}{\partial y} \right) = \mu \frac{\partial^2 u}{\partial y^2} . \quad (9.6)$$

Formal integration with respect to y and use of the boundary conditions yields

$$\rho \frac{d}{dx} \int_{-\infty}^{\infty} uu \, dy = 0 \quad (9.7)$$

or

$$\rho \int_{-\infty}^{\infty} uu \, dy = \text{constant} = J . \quad (9.8)$$

The last expression is one form of the momentum-integral equation, which plays a role in every kind of boundary-layer problem. Equation (9.8) is derived from equation (9.2), but contains new information because it generates the conserved quantity J as an important dimensional parameter. Equation (9.8) also incorporates the boundary conditions at infinity, a point that will be developed later. Physically, the integral J represents the flux of momentum per unit time per unit span, or equally the reaction force of the jet at the origin per unit span. I have deliberately written the integrand as uu rather than u^2 because the two velocities have different physical meanings. One is momentum per unit mass, and the other is volume flux per unit area per unit time.

9.1.2 Dimensional properties

Intrinsic scales. If geometric details near the origin are ignored, the important physical parameters for the laminar plane jet are J , ρ , and μ . In terms of fundamental units **M** (mass), **L** (length), and **T** (time), denoted here and elsewhere by boldface symbols, these parameters have the dimensions

$$[J] = \frac{\mathbf{M}}{\mathbf{T}^2} , \quad [\rho] = \frac{\mathbf{M}}{\mathbf{L}^3} , \quad [\mu] = \frac{\mathbf{M}}{\mathbf{L}\mathbf{T}} , \quad (9.9)$$

where “[...] = ” means “the dimensions of ... are,” and where force is replaced for dimensional purposes by mass times acceleration. Let these statements now be interpreted as defining equations for intrinsic scales \mathbf{M} , \mathbf{L} , and \mathbf{T} . That is, write

$$\frac{\mathbf{M}}{\mathbf{T}^2} \equiv J \ , \quad \frac{\mathbf{M}}{\mathbf{L}^3} \equiv \rho \ , \quad \frac{\mathbf{M}}{\mathbf{L}\mathbf{T}} \equiv \mu \ . \quad (9.10)$$

These three definitions form an algebraic system that can be solved uniquely (in this particular instance) for the three quantities \mathbf{M} , \mathbf{L} , and \mathbf{T} ;

$$\mathbf{M} = \frac{\rho^4 \nu^6}{J^3} \ , \quad \mathbf{L} = \frac{\rho \nu^2}{J} \ , \quad \mathbf{T} = \frac{\rho^2 \nu^3}{J^2} \ , \quad (9.11)$$

where $\nu = \mu/\rho$, and for the derived quantity \mathbf{U} ;

$$\mathbf{U} = \frac{\mathbf{L}}{\mathbf{T}} = \frac{J}{\rho \nu} \ . \quad (9.12)$$

That the parameters μ and J should appear only in the kinematic combinations $\mu/\rho = \nu$ and J/ρ is implied by the form of equations (9.2) and (9.8), respectively. Note from equations (9.11) and (9.12) that the intrinsic length and velocity scales \mathbf{L} and \mathbf{U} have small magnitudes, in the sense that their product corresponds to unit Reynolds number;

$$\frac{\mathbf{U}\mathbf{L}}{\nu} = 1 \ . \quad (9.13)$$

Equations (9.11) define dimensional scales that can be used to make the problem dimensionless at the outset, without regard to the question of similarity. Such an exercise serves little purpose except to confirm, as one consequence of a dimensional inspection at the lowest possible level, that there is no dimensionless combination of J , ρ , and ν that can differ from one experiment to another. (**cf. an appeal to the Buckingham Π theorem. How is round jet different?**). In other words, there is only one laminar plane jet.

Local scales. Some standard variations on the theme of dimensions now follow. Ignore temporarily the intrinsic scales \mathbf{L} and \mathbf{U} just defined, and suppose instead that the flow has local length and

velocity scales $L(x)$ and $U(x)$, whose nature has to be determined. Similarity implies that the streamwise velocity should have the form

$$\frac{u}{U} = g\left(\frac{y}{L}\right) . \quad (9.14)$$

The form of the stream function follows on integration of the first of equations (9.5);

$$\frac{\psi}{UL} = \frac{1}{L} \int_0^y g \, dy = f\left(\frac{y}{L}\right) = f(\eta) . \quad (9.15)$$

Because $L(x)$ and $U(x)$ are designed to represent the local physical extent and the local velocity magnitude in the jet flow, the function f and its derivatives will be of order unity. Substitution in the momentum equation (9.2) gives eventually

$$f''' + \frac{L}{\nu} \frac{dUL}{dx} f f'' - \frac{L^2}{\nu} \frac{dU}{dx} f' f' = 0 , \quad (9.16)$$

where primes indicate differentiation with respect to $y/L = \eta$. If f is to depend only on η , the coefficients must be independent of x ;

$$\frac{L}{\nu} \frac{dUL}{dx} = \text{constant} , \quad \frac{L^2}{\nu} \frac{dU}{dx} = \text{constant} . \quad (9.17)$$

A brief trial shows that these equations are not sufficient to determine $U(x)$ and $L(x)$. The reason is that the boundary conditions have so far not been taken into account. The further relationship that is needed is contained in the momentum-integral equation (9.8), which incorporates the boundary conditions at infinity;

$$J = \rho U^2 L \int_{-\infty}^{\infty} f' f' \, d\eta . \quad (9.18)$$

Hence

$$U^2 L = \text{constant} . \quad (9.19)$$

It now follows easily, on integration of either of the two equations (9.17) with (9.19), that

$$U(x) \sim x^{-1/3} , \quad L(x) \sim x^{2/3} , \quad UL \sim x^{1/3} . \quad (9.20)$$

Note that the power-law dependence of U and L on x is derived rather than assumed.

A different scheme allows the exponents to be established correctly, without recourse to the governing momentum equation (9.2) except through its integral (9.8). The scheme uses the device of a moving observer in the style of H. W. Liepmann. An observer traveling with the fluid on the jet centerline moves at a variable speed $dx/dt = U(x)$. If a power law is appropriate, $U \sim x^n$. Integration gives

$$x \sim t^{1/(1-n)} . \quad (9.21)$$

A local diffusion approximation yields an estimate of the local jet thickness;

$$L(x) \sim (\nu t)^{1/2} \sim x^{(1-n)/2} . \quad (9.22)$$

The product U^2L being constant, according to equation (9.19), it follows that

$$U(x) \sim x^{(n-1)/4} \sim x^n . \quad (9.23)$$

Hence $n = -1/3$, and the local scales follow as before.

The three proportionalities (9.20) can be converted into equalities by incorporating the intrinsic scales of the problem. Thus put

$$U = \mathbf{U}\mathbf{L}^{1/3}x^{-1/3} = \left(\frac{J^2}{\rho^2\nu x} \right)^{1/3} , \quad (9.24)$$

$$L = \mathbf{L}^{1/3}x^{2/3} = \left(\frac{\rho\nu^2x^2}{J} \right)^{1/3} , \quad (9.25)$$

$$UL = \mathbf{U}\mathbf{L}^{2/3}x^{1/3} = \left(\frac{J\nu x}{\rho} \right)^{1/3} . \quad (9.26)$$

Equation (9.15) now becomes a complete dimensionless ansatz,

$$\left(\frac{\rho}{J\nu x} \right)^{1/3} \psi = f \left[\left(\frac{J}{\rho\nu^2x^2} \right)^{1/3} y \right] . \quad (9.27)$$

Affine transformation. The ansatz (9.27) is unique, although it can be derived by more than one method. I usually prefer

a different approach to similarity that has a stronger mathematical flavor, although it also depends implicitly on the physical premise that all of the terms in the momentum equation (9.2) must have the same dimension. Require this equation, together with its boundary conditions, to be invariant under an affine transformation (**see Bluman and Cole**). Let all of the variables and parameters of the problem, taken in a standard order x, y, ψ, ρ, μ followed by any special parameters—everything in sight—be rescaled according to the rules

$$\begin{aligned}
 x &= a\hat{x} \ , \\
 y &= b\hat{y} \ , \\
 \psi &= c\hat{\psi} \ , \\
 \rho &= d\hat{\rho} \ , \\
 \mu &= e\hat{\mu} \ , \\
 J &= j\hat{J} \ , \\
 u &= r\hat{u} = \frac{c}{b}\hat{u} \ , \\
 v &= s\hat{v} = \frac{c}{a}\hat{v} \ ,
 \end{aligned}
 \tag{9.28}$$

where a, b, c, \dots are positive constant numbers that stretch or shrink the scales used to measure the various quantities. The last two lines of this table are required if the equations to be transformed are taken initially in the form (9.1)–(9.2), in which u and v appear rather than ψ . Transformation of equations (9.5) then gives

$$r\hat{u} = \frac{c}{b} \frac{\partial \hat{\psi}}{\partial \hat{y}} \ , \quad s\hat{v} = -\frac{c}{a} \frac{\partial \hat{\psi}}{\partial \hat{x}} \ .
 \tag{9.29}$$

Invariance of the continuity equation thus requires $r = c/b$ and $s =$

c/a , so that u transforms like ψ/y and v like ψ/x .

The result of the transformation when applied to the momentum equation (9.2) is

$$\frac{c^2 d}{ab^2} \hat{\rho} \left(\hat{u} \frac{\partial \hat{u}}{\partial \hat{x}} + \hat{v} \frac{\partial \hat{u}}{\partial \hat{y}} \right) = \frac{ce}{b^3} \hat{\mu} \frac{\partial^2 \hat{u}}{\partial \hat{y}^2} . \quad (9.30)$$

The same procedure transforms the momentum integral (9.8) into

$$\frac{c^2 d}{b} \hat{\rho} \int_{-\infty}^{\infty} \hat{u} \hat{u} \, d\hat{y} = j \hat{J} . \quad (9.31)$$

No useful information is obtained by transforming the null boundary conditions (9.3)–(9.4). For example, the first of equations (9.3) becomes

$$c \hat{\psi}(a \hat{x}, 0) = 0 . \quad (9.32)$$

If the original boundary condition is read as “ ψ is zero for $y = 0$ and all x ,” then the transformed boundary condition is read as “ $\hat{\psi}$ is zero for $\hat{y} = 0$ and all \hat{x} ,” whatever the values of a and c might be.

If the problem defined by equations (9.30) and (9.31) is to be invariant under the affine transformation, it is necessary to put

$$\frac{bcd}{ae} = 1 , \quad \frac{c^2 d}{bj} = 1 . \quad (9.33)$$

Because the jet has a strongly preferred direction, it is most productive to work with ψ and y as dependent variable and primary independent variable, respectively (other strategies will work, but not as directly and efficiently). When equations (9.33) are solved to separate the corresponding scaling factors c and b , they become

$$\frac{c^3 d^2}{aej} = 1 , \quad \frac{b^3 dj}{a^2 e^2} = 1 . \quad (9.34)$$

These two conditions have magical properties. When a, b, c, \dots are replaced by the corresponding ratios from the table (9.28), the invariant combinations of the transformation appear in physical dress.

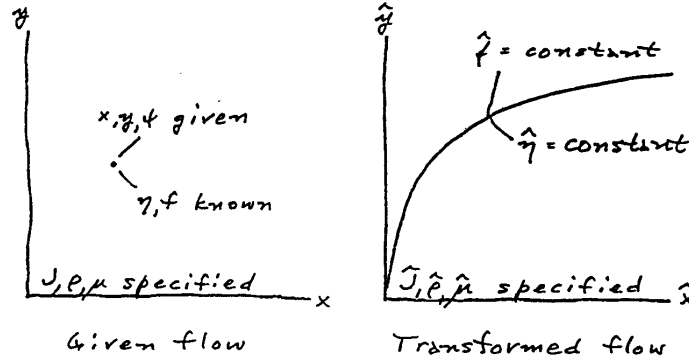


Figure 9.3: The final step of a similarity argument based on an affine transformation. For the example in the text, the curve on the right is $\hat{y} \sim \hat{x}^{2/3}$.

At corresponding points of the affine transformation,

$$f = \left(\frac{\rho}{J\nu x}\right)^{1/3} \psi = \left(\frac{\hat{\rho}}{\hat{J}\hat{\nu}\hat{x}}\right)^{1/3} \hat{\psi} = \hat{f}, \quad (9.35)$$

$$\eta = \left(\frac{J}{\rho\nu^2 x^2}\right)^{1/3} y = \left(\frac{\hat{J}}{\hat{\rho}\hat{\nu}^2 \hat{x}^2}\right)^{1/3} \hat{y} = \hat{\eta}. \quad (9.36)$$

This equivalence does not quite establish that the combination (9.35) must be a function only of the combination (9.36), although this conclusion is in fact correct, according to equation (9.27). This question was raised but not resolved in SECTION 1.3.5 of the introduction. The essence of the required argument is shown geometrically in FIGURE 9.3. The reasoning is symmetric, and could equally well proceed by interchanging the roles of the two flows (hence the term “symmetry analysis” sometimes used for the procedure). Suppose that the physical parameters J , ρ , and ν are known for the given flow at the left in FIGURE 9.3, and similarly that \hat{J} , $\hat{\rho}$, and $\hat{\nu}$ are known for the transformed flow at the right. Suppose also that ψ is known, analytically or experimentally, for one fixed point (x, y) in

the given flow. Then η and f are known at this point from equations (9.35) and (9.36). So also are $\widehat{\eta} = \eta$ and $\widehat{f} = f$. But the transformed point $(\widehat{x}, \widehat{y})$ is not a point but a curve, $\widehat{y}/\widehat{x}^{2/3} = \text{constant}$, which is defined through equation (9.36). Along this curve both $\widehat{\eta}$ and \widehat{f} are constant, and it follows that \widehat{f} depends only on $\widehat{\eta}$.

A final point is that the combinations (9.35) and (9.36) are guaranteed to be dimensionless by the terms of their construction. They are also guaranteed to be complete, since they incorporate all of the independent and dependent variables and all of the parameters that appear in the equations and the boundary conditions. If the frequent application in this monograph of the method of the affine transformation is viewed as a process of turning a crank, the crank is a handsome one. I should say that I developed the procedure just described about 1975, without realizing until later that I had reproduced a small portion of group theory (which was not a part of my early mathematical education). The system (9.28) evidently defines a group, since it contains the identity transformation ($a = b = \dots = 1$), the inverse transformation ($\widehat{x} = x/a = \alpha x, \dots$), and the product transformation ($x = a\widehat{x}$, $\widehat{x} = A\widehat{\widehat{x}}$, $x = aA\widehat{\widehat{x}} = \alpha\widehat{\widehat{x}}, \dots$). The two relations (9.34) are invariants of the group for the particular problem being considered here. A closely related system, called by its author a dilation group, is introduced early in the book on symmetry by CANTWELL (2002).

Similarity. Both of the similarity arguments just given have succeeded in reducing the number of independent variables from two to one. The ansatz for the stream function must have the form first discovered in equation (9.27),

$$A \left(\frac{\rho}{J\nu x} \right)^{1/3} \psi = f \left[B \left(\frac{J}{\rho\nu^2 x^2} \right)^{1/3} y \right] = f(\eta) , \quad (9.37)$$

where the new quantities A and B are positive numerical constants of order unity whose function is to support a final normalization of the variables f and η . The constant A adjusts the dimensionless volume flux (i.e., the stream function), and the constant B adjusts

the dimensionless thickness of the layer. Differentiation yields

$$u = \frac{\partial \psi}{\partial y} = \frac{B}{A} \left(\frac{J^2}{\rho^2 \nu x} \right)^{1/3} f' , \quad (9.38)$$

$$v = -\frac{\partial \psi}{\partial x} = \frac{1}{3A} \left(\frac{J\nu}{\rho x^2} \right)^{1/3} (2\eta f' - f) , \quad (9.39)$$

$$\tau = \mu \frac{\partial u}{\partial y} = \frac{B^2}{A} \frac{J}{x} f'' , \quad (9.40)$$

$$\frac{\partial \tau}{\partial y} = \frac{B^3}{Ax} \left(\frac{J^4}{\rho \nu^2 x^2} \right)^{1/3} f''' , \quad (9.41)$$

and so on, where the primes indicate differentiation with respect to η . Substitution of these expressions into equation (9.2) leads to the ordinary differential equation

$$3ABf''' + ff'' + f'f' = 0 . \quad (9.42)$$

The boundary conditions, from equations (9.3)–(9.4), are

$$f(0) = f'(\pm\infty) = f''(\pm\infty) = 0 . \quad (9.43)$$

These homogeneous relationships might seem to define an eigenvalue problem, but do not, because the constant-momentum condition (9.8) also has to be satisfied. Insertion of equation (9.38) for u in equation (9.8) yields the constraint

$$\int_{-\infty}^{\infty} f'f' d\eta = \frac{A^2}{B} . \quad (9.44)$$

9.1.3 The boundary-layer solution

Equation (9.42) can be solved in closed form. Three successive integrations, with the appropriate symmetry conditions, give

$$3ABf'' + ff' = \text{constant} = 0 ; \quad (9.45)$$

$$6ABf' + f^2 = \text{constant} = C^2 ; \quad (9.46)$$

$$f = C \tanh \left(\frac{C}{6AB} \eta \right) ; \quad (9.47)$$

where $C > 0$ is a constant of integration. The velocity profile is

$$f' = \frac{C^2}{6AB} \operatorname{sech}^2 \left(\frac{C}{6AB} \eta \right) . \quad (9.48)$$

Equation (9.42) was first derived by SCHLICHTING (1933), who did not notice that it could be integrated in closed form, and therefore resorted to numerical integration. The analytical integral (9.47) was supplied by BICKLEY (1937).

Compact variables. The boundary-layer solution emerges from equations (9.37) and (9.47) as

$$\frac{A}{C} \left(\frac{\rho}{J\nu x} \right)^{1/3} \psi = \tanh \left[\frac{C}{6A} \left(\frac{J}{\rho\nu^2 x^2} \right)^{1/3} y \right] = \tanh \left(\frac{C}{6AB} \eta \right) . \quad (9.49)$$

The streamline pattern contained in this equation is most instructive when it is expressed in what will shortly be defined as compact outer variables, with x and y made dimensionless in the same way. An intrinsic length scale is available for this purpose in the second of equations (9.11); namely, $\mathbf{L} = \rho\nu^2/J$. When J is eliminated in favor of \mathbf{L} in equation (9.49), this becomes

$$\frac{A}{C} \left(\frac{\mathbf{L}}{x} \right)^{1/3} \frac{\psi}{\nu} = \tanh \left[\frac{C}{6A} \left(\frac{y^3}{\mathbf{L}x^2} \right)^{1/3} \right] . \quad (9.50)$$

Compact dimensionless outer variables thus reveal themselves as

$$\Psi = \frac{\psi}{6\nu} , \quad X = \left(\frac{C}{6A} \right)^3 \frac{x}{\mathbf{L}} , \quad Y = \left(\frac{C}{6A} \right)^3 \frac{y}{\mathbf{L}} . \quad (9.51)$$

In these variables, equation (9.49) takes the simple form

$$\Psi = X^{1/3} \tanh \left(\frac{Y}{X^{2/3}} \right) , \quad (9.52)$$

which does not depend formally on the values chosen for the normalizing constants A , B , and C . However, these constants are not themselves independent. The integral in equation (9.44) applies for a general function $f(\eta)$. When the specific function of equation (9.47) is inserted, a specific value involving C is obtained for the integral;

$$\int_{-\infty}^{\infty} f' f' d\eta = \frac{2C^3}{9AB} = \frac{A^2}{B}, \quad (9.53)$$

from which

$$\left(\frac{C}{6A}\right)^3 = \frac{1}{48}. \quad (9.54)$$

Hence the proper dimensionless outer variables in equation (9.52) are

$$\Psi = \frac{\psi}{6\nu}, \quad X = \frac{x}{48\mathbf{L}}, \quad Y = \frac{y}{48\mathbf{L}}, \quad (9.55)$$

which are clearly independent of A , B , and C because \mathbf{L} depends only on ρ , ν , and J . The first of these equations could equally well be written as $\Psi = \psi/6\mathbf{UL}$.

Streamlines $\Psi(X, Y) = \text{constant}$ for the boundary-layer solution in compact outer variables are shown in FIGURE 9.4. Such a figure was first constructed, absent scales on the axes, by Bickley. Note that the ranges for X and Y in the figure extend to large numerical values, because the quantities \mathbf{U} and \mathbf{L} refer to a Reynolds number of unity. The local scales $U(x)$ and $L(x)$ are a different matter. These two scales are defined by equations (9.24) and (9.25) as

$$U = \left(\frac{J^2}{\rho^2\nu x}\right)^{1/3}, \quad L = \left(\frac{\rho\nu^2 x^2}{J}\right)^{1/3}. \quad (9.56)$$

Their product, which is one form of local Reynolds number, can be expressed in terms of X alone;

$$Re(x) = \frac{UL}{\nu} = \left(\frac{Jx}{\rho\nu^2}\right)^{1/3} = \left(\frac{x}{\mathbf{L}}\right)^{1/3} = (48X)^{1/3}. \quad (9.57)$$

FIGURE 9.4 therefore displays the flow in a laminar plane jet up to a local Reynolds number of about 36. There is only one jet, and only

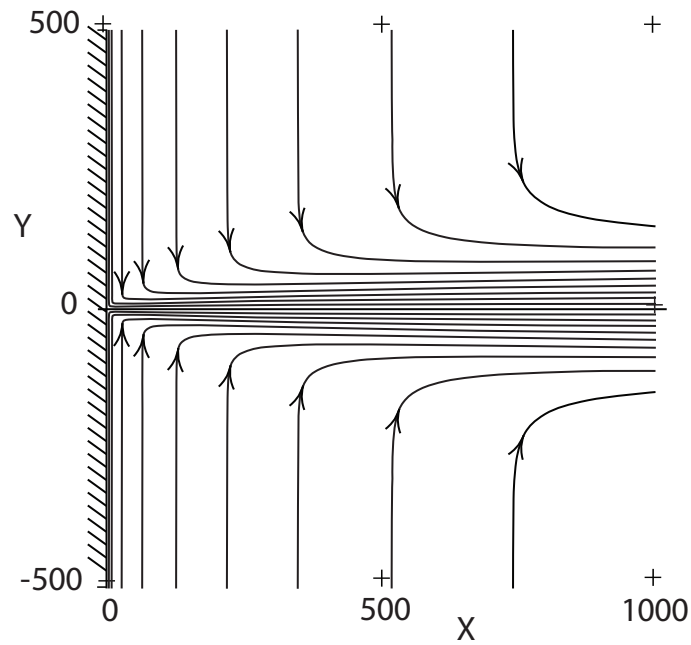


Figure 9.4: Streamlines $\Psi = \text{constant}$ of the boundary-layer approximation for the laminar plane jet according to equation (9.52). The range of Ψ is -9 (1) 9.

one figure. A change in displayed Reynolds number amounts to use of a larger or smaller mask for this figure. The local Reynolds number increases in the downstream direction like $x^{1/3}$, and the laminar plane jet can therefore be expected to become unstable at some point in its evolution.

The boundary-layer solution (9.52) is silent about the flow for $x < 0$ and is indifferent to the presence or absence of walls, whether along the y -axis or elsewhere. The reason is that the line $x = 0$ is a characteristic of the parabolic boundary-layer equations (9.1)–(9.2) and is the locus of a discontinuity in v . This property is entirely an artifact of the choice of coordinates, as explained by KAPLUN () in his beautiful paper on the role of coordinate systems in boundary-layer theory. It is possible that some early experimenters, beginning with ANDRADE (1939), may have been inspired to place a wall at $x = 0$ in order to guide the relatively slow induced flow in the proper direction in a drafty facility. A more cogent reason might be that the geometry is simple and easily reproduced. In any event, the streamline pattern in FIGURE 9.4 cannot be correct outside the body of the jet, because it represents a rotational flow. The derivative $\partial u/\partial y$ is zero, but the derivative $\partial v/\partial x$ is not. However, knowledge of the streamline pattern does allow a useful conclusion about the velocity history of fluid moving along a given streamline. It is clear from the streamline spacing in FIGURE 9.4 that this velocity starts at a low value, increases rapidly near the axis of symmetry, and then decreases slowly toward the right edge of the figure. The x -component of velocity has the same property and is easier to describe. The pressure being constant, the acceleration Du/Dt along a streamline from equation (9.2) is proportional to $\partial\tau/\partial y$, which in turn is proportional to f''' from equation (9.41). The maximum x -velocity therefore occurs when $f'''(\eta) = 0$, and the shearing stress τ is a maximum there. Differentiation of equation (9.48) shows that $f'''(\eta)$ vanishes when $\eta = \eta_m$, with

$$\cosh^2\left(\frac{C}{6AB}\eta_m\right) = \frac{3}{2}. \quad (9.58)$$

Substitution in equation (9.48) yields

$$f'(\eta_m) = \frac{2}{3} \frac{C^2}{6AB} = \frac{2}{3} f'(0) . \quad (9.59)$$

Within the boundary-layer approximation, therefore, the maximum streamwise velocity on a streamline occurs at the inflection point of the profile and is two thirds of the velocity in the plane of symmetry at the same value of x .

Mathematically speaking, the jet described here entrains the whole universe (more accurately, half of it). It may be useful to think of a fluid element upstream from its velocity maximum as not yet entrained, because it is still acquiring momentum from fluid closer to the axis of the jet, whereas a fluid element downstream from its maximum is losing momentum to fresh fluid being entrained in its vicinity and is effectively part of the body of the jet. The sharp change in direction of the streamlines in FIGURE 9.4, incidentally, serves notice that static pressure variations, although small at this order, may be relatively greater in a jet than in a more unidirectional flow such as a boundary layer.

9.1.4 Normalization

So far, I have deliberately left the normalizing constants A and B and the constant of integration C in the boundary-layer solution (9.46) unspecified, for the sake of generality. Most but not all authors have followed Bickley in putting $f'(0) = 1$, $f(\infty) = 1$, and $\int_{-\infty}^{\infty} f' f' d\eta = 4/3$. According to equations (9.48), (9.47), and (9.44), this amounts to putting $A = (2/9)^{1/3}$, $B = (1/48)^{1/3}$, and $C = 1$. However, I prefer a slightly different normalization that aims primarily at consistency among the various flows treated in this monograph. The present analysis has provided one relation between A and C in equation (9.54);

$$\frac{C}{A} = \left(\frac{9}{2}\right)^{1/3} , \quad (9.60)$$

which is consistent with Bickley's selection. Another condition is suggested by the form of the differential equation (9.42). In favor of the

condition $3AB = 1$ is the fact that the reduced operator $f''' + ff''$ is common to all of the plane laminar boundary-layer problems considered here, with a numerical coefficient for the term f''' that varies from one flow to another. The quantities f''' and ff'' represent, respectively, viscous diffusion and transport (of vorticity). They are commensurate in the physics, and I propose that they should also be commensurate in the mathematics; i.e., not weighted differently for different flows. Consequently, I take as a second condition

$$3AB = 1 . \quad (9.61)$$

The constant C . Equation (9.61) allows several properties derived above for the boundary-layer solution to be expressed in terms of the undefined constant of integration C alone. In particular,

$$f'(0) = \frac{C^2}{2} ; \quad (9.62)$$

$$\int_0^\infty f'(\eta) d\eta = f(\infty) = C . \quad (9.63)$$

Now let the functions $f(\eta)$ and $f'(\eta)$ be plotted against η , as in FIGURES 9.5 and 9.6.

The numerical magnitudes needed to plot these curves have been suppressed in each case. As one possible scale, consider the maximum-slope thickness indicated in FIGURE 9.5. The tangent line is defined by $f = f'(0)\eta$. This line can be terminated when $f = f(\infty) = C$ and $\eta = \eta_s$, say. Then

$$f(\eta_s) = C = f'(0) \eta_s = \frac{C^2}{2} \eta_s . \quad (9.64)$$

If the characteristic scale η_s is arbitrarily put equal to unity, then

$$C = 2 . \quad (9.65)$$

Next, define an integral scale η_i (reminiscent of the displacement thickness for a boundary layer) as shown in the right half of FIGURE 9.6, with

$$\int_0^\infty f' d\eta = C = f'(0) \eta_i = \frac{C^2}{2} \eta_i . \quad (9.66)$$

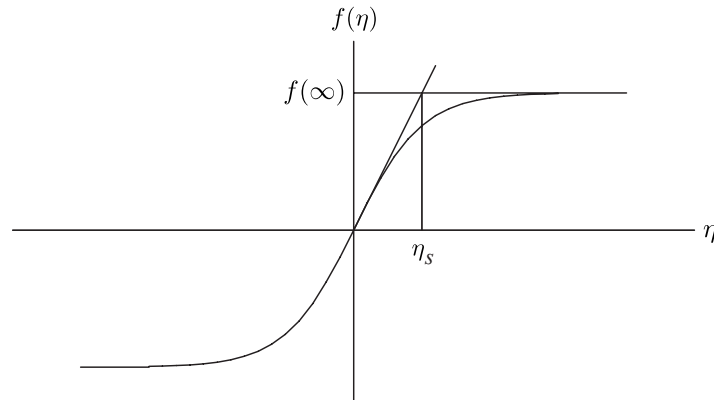


Figure 9.5: Graphical definition of the maximum-slope thickness η_s for the laminar plane jet.

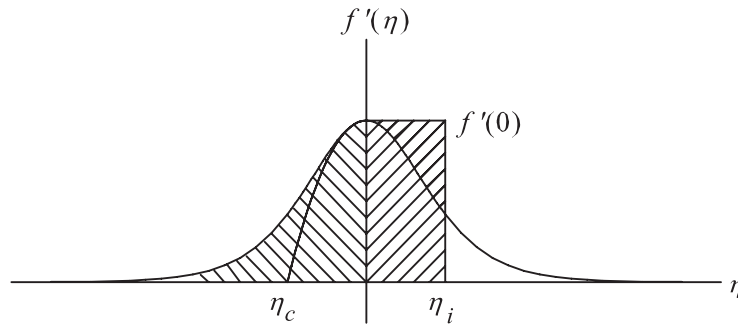


Figure 9.6: Graphical definition of the half-integral scale η_i for the laminar plane jet, on the right, and the half-width η_c for the osculating parabola, on the left.

If η_i is put equal to unity, then again $C = 2$. The areas of the two cross-hatched regions are equal.

Finally, define a curvature scale η_C (reminiscent of the Taylor microscale in turbulence) as the intersection at $f' = 0$, $\eta = \eta_C$ of the osculating parabola in the left half of FIGURE 9.6. The parabola is defined by the first two terms of a power series,

$$f'(\eta) = f'(0) + f'''(0) \frac{\eta^2}{2} . \quad (9.67)$$

Put $f'(0) = C^2/2$ and $f'''(0) = -[f'(0)]^2$, the latter from equation (9.42). Thus

$$f'(0) = \frac{C^2}{2} = [f'(0)]^2 \frac{\eta_C^2}{2} = \frac{C^4}{8} \eta_C^2 . \quad (9.68)$$

If η_C is put equal to unity, then once more $C = 2$. Note that these three arguments are related, in the sense that they all involve $f'(0)$.

These results are persuasive, even without the observation that there is no obvious reason why the argument of f should not be taken, strictly for simplicity, as η rather than $C\eta/2$ with $C \neq 2$. In this connection, I should mention a condition sometimes used to define a scale for turbulent shear flows. This is to use the point where the velocity is half of some suitable characteristic velocity, say the velocity on the centerline of the present jet (*cf.* the treatment of the wake function in the turbulent boundary layer). If this point has the value $\eta = 1$, then the constant C is the root of the transcendental equation $\cosh(C/2) = \sqrt{2}$. Other authors may prefer a different normalization from the ones proposed here.

After some reflection, I believe that the weight of the evidence just described is on the side of taking the integral scale as fundamental. The three equations (9.60), (9.61), and (9.65) then imply

$$A = \left(\frac{16}{9}\right)^{1/3} , \quad B = \left(\frac{1}{48}\right)^{1/3} , \quad C = 2 . \quad (9.69)$$

The effect of this normalization is to set the boundary-layer problem

and its solution for the laminar plane jet in the form

$$\left(\frac{16\rho}{9J\nu x}\right)^{1/3} \psi = f \left[\left(\frac{J}{48\rho\nu^2 x^2}\right)^{1/3} y \right] = f(\eta) , \quad (9.70)$$

$$f''' + f f'' + f' f' = 0 , \quad (9.71)$$

$$f(\eta) = 2 \tanh \eta , \quad (9.72)$$

$$f'(\eta) = 2 \operatorname{sech}^2 \eta , \quad (9.73)$$

$$f'(0) = 2 , \quad (9.74)$$

$$f''(\eta) = 4 \frac{\sinh \eta}{\cosh^3 \eta} = f(\eta) f'(\eta) , \quad (9.75)$$

$$\frac{1}{2} \int_{-\infty}^{\infty} f' d\eta = f(\infty) = 2 , \quad (9.76)$$

$$\int_{-\infty}^{\infty} f' f' d\eta = \frac{16}{3} , \quad (9.77)$$

where the equation for f'' takes account of equation (9.45). The normalized functions $f(\eta)$ and $f'(\eta)$ for the boundary-layer solution are displayed as solid curves in FIGURE 9.7. The connection with the physical variables ψ, u, v, τ is given by properly normalized versions of equations (9.37)–(9.40);

$$f(\eta) = \left(\frac{16\rho}{9J\nu x}\right)^{1/3} \psi = 2 \tanh \eta , \quad (9.78)$$

$$f'(\eta) = \left(\frac{256\rho^2\nu x}{3J^2}\right)^{1/3} u = \frac{2}{\cosh^2 \eta} , \quad (9.79)$$

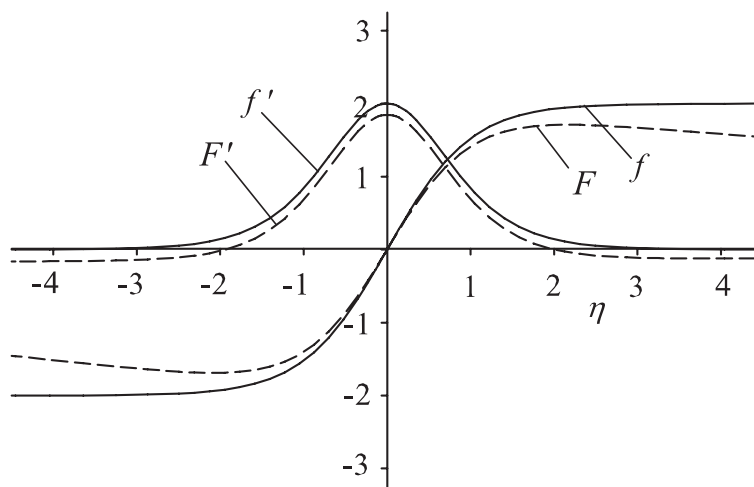


Figure 9.7: The solid lines show the boundary-layer solution $f(\eta)$ and $f'(\eta)$ for the laminar plane jet according to equations (9.72) and (9.73). The dashed lines show the two-term composite solution according to equations (9.113)--(9.116) with $X = 1000$.

$$2\eta f'(\eta) - f(\eta) = \left(\frac{48 \rho x^2}{J\nu} \right)^{1/3} v = \frac{4\eta - \sinh 2\eta}{\cosh^2 \eta} , \quad (9.80)$$

$$f''(\eta) = 16 \frac{x}{J} \tau = -4 \frac{\sinh \eta}{\cosh^3 \eta} . \quad (9.81)$$

Reynolds number. As part of the dimensional argument of SECTION 9.1.2, local velocity and length scales U and L were defined from the ostensible data of the problem in equations (9.24) and (9.25). The normalization just described allows a more physical definition of Reynolds number. Define a half-thickness for the jet boundary layer, call it δ , and require $y = \delta$ when $\eta_i = 1$ (*cf.* figure 9.6). Then, from equations (9.2) and (9.56),

$$\delta = \left(\frac{48 \nu^2 x^2}{J} \right)^{1/3} = (48)^{1/3} L . \quad (9.82)$$

(An experimenter might elect to take the value of δ two times larger in order to include more of the jet layer.) Take the appropriate velocity for forming a Reynolds number as u_C , the velocity on the jet centerline. Then, from equations (9.79) and (9.56),

$$u_C = 2 \left(\frac{3}{256} \frac{J^2}{\rho^2 \nu x} \right)^{1/3} = \left(\frac{3}{32} \right)^{1/3} U . \quad (9.83)$$

At the right edge of figure 9.4, therefore,

$$Re = \frac{\delta u_C}{\nu} = 10(216)^{1/3} = 60 , \quad (9.84)$$

a number that is better fitted to experimental usage than the Reynolds number defined earlier by equation (9.57).

9.1.5 Entrainment

A realistic description of the entrainment process for the laminar plane jet requires a part of perturbation theory called the method of matched asymptotic expansions. Perturbation theory is a large subject, capable of supporting arduous full-year graduate courses

and challenging monographs, among which those by VAN DYKE (1975), KEVORKIAN and COLE (1981), and NAYFEH () are well known. In a typical boundary-layer problem, outer and inner expansions can be constructed by considering alternately successive terms in physical or outer variables (x, y) and in boundary-layer or inner variables $(x, y/\epsilon)$, where ϵ is a small parameter. The analysis often begins with the first term in the outer expansion. Terms in the two expansions are made consistent by a matching process that contains the art of the method. The expansions are seldom carried beyond second order and may be asymptotic or even divergent. They may also involve the appearance of logarithms and undetermined constants.

In the present problem, the first term of the outer expansion for the jet flow represents fluid at rest, and is a null term. In particular, the pressure is constant, and the jet flow is therefore properly referred to in a first approximation as a plane jet into stagnant fluid, or sometimes as a submerged jet. The first term of the inner expansion is the boundary-layer solution (9.49). After the boundary-layer problem is solved, with boundary conditions appropriate for an outer fluid at rest, the outer fluid is found to be not at rest, but flowing toward the jet to provide the fluid being entrained and pumped away. The difference at this order is referred to as the displacement effect. The matching process models this pumping action as a distributed sink flow, and the second term of the outer expansion is a potential flow that is matched accordingly. The rule for matching in the elementary theory is “the inner limit of the outer limit is equal to the outer limit of the inner limit.” Applied to the present case, the rule yields the matching condition,

$$\psi_o(x, 0) = \psi_i(x, \infty) , \quad (9.85)$$

where the subscripts o and i indicate that the function ψ is expressed in outer variables (x, y) or in inner variables $(x, y/\epsilon)$. An index indicating the order of the matching approximation is omitted for simplicity.

The laminar plane jet is well suited for practicing this technique, because the potential outer flow can be readily obtained by

conformal mapping. The ansatz for the first-order inner stream function in the general form $f(\eta)$, with the constants A , B restored, is equation (9.37),

$$\psi_i(x, y) = \frac{1}{A} \left(\frac{J\nu x}{\rho} \right)^{1/3} f \left[B \left(\frac{J}{\rho\nu^2 x^2} \right)^{1/3} y \right]. \quad (9.86)$$

Outside the body of the jet, with $f(\infty)$ replaced by C , this implies

$$\psi_i(x, \infty) = \frac{C}{A} \left(\frac{J\nu x}{\rho} \right)^{1/3}. \quad (9.87)$$

The outer streamlines of the boundary-layer approximation are therefore normal to the plane of the jet, as already indicated in FIGURE 9.4, with

$$v_i(x, \infty) = -\frac{C}{3A} \left(\frac{J\nu}{\rho x^2} \right)^{1/3} \quad (9.88)$$

for the upper half of the flow. In outer variables, this equation (9.88) represents the jet in the limit $\nu \rightarrow 0$ as a distributed plane sink whose strength decreases with increasing x . The matching process takes this sink flow as a boundary condition for a potential external flow that will depend also on the wall geometry. Because the jet is infinitely thin in the limit $\nu \rightarrow 0$, the matching condition is applied in the plane of symmetry.

Outer flow. The form (9.88) is by itself a sufficient basis for construction of the entrained flow. However, because the desired flow is plane and irrotational, and because more general wall geometries may be wanted, it is convenient to proceed by conformal mapping.

It is common experimental practice to place a wall along the y -axis, as in FIGURE 9.1. In order to emphasize the effect of walls on the composite flow, I will take the walls to be at a symmetric but unspecified angle σ measured from the x -axis, as shown in the physical plane at the right in FIGURE 9.8. The desired potential flow in the upper half of the z -plane can be found by mapping of a uniform flow in the ζ -plane at the left. The other half of the physical flow is obtained by reflection in the x -axis, which is a branch cut

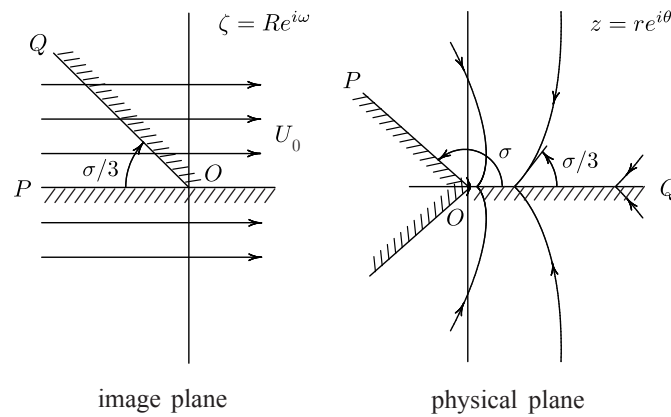


Figure 9.8: Conformal mapping of the outer flow for the upper half of a plane jet. The flow is symmetrical about the x -axis, which is a branch cut. There are upstream walls in the physical plane at an angle $\pm\sigma$ to the x -axis (see equation (9.96)). Note the preservation of angles.

in the complex z -plane. The boundary conditions for the outer flow, identified by the subscript o , are obtained from equation (9.87), and the matching condition is obtained from equation (9.85);

$$\psi_o = 0 \quad \text{for} \quad \theta = \sigma ; \quad (9.89)$$

$$\psi_o = \frac{C}{A} \left(\frac{J\nu x}{\rho} \right)^{1/3} \quad \text{for} \quad \theta = 0 . \quad (9.90)$$

The appearance of the factor $x^{1/3}$ suggests that the mapping should be of the form

$$\zeta = L_0^{2/3} z^{1/3} e^{i\alpha} , \quad (9.91)$$

where α represents a possible rotation and L_0 is a constant length that is introduced for dimensional reasons, since ζ and z both have the dimensions of length. With

$$\zeta = R e^{i\omega} , \quad z = r e^{i\theta} , \quad (9.92)$$

it follows from equation (9.91) that

$$\omega = \frac{\theta}{3} + \alpha . \quad (9.93)$$

The mapping of the line OP in FIGURE 9.8 requires $\theta = \sigma$ when $\omega = \pi$, so that

$$\alpha = \pi - \frac{\sigma}{3} . \quad (9.94)$$

The position of the line OQ is then given by the equivalence

$$\omega = \alpha \quad (9.95)$$

when $\theta = 0$, thus fixing this line in the image plane. Equation (9.91) becomes

$$\zeta = -L_0^{2/3} r^{1/3} e^{i(\theta-\sigma)/3} . \quad (9.96)$$

The uniform flow in the ζ -plane is defined by the complex potential

$$F(\zeta) = \phi + i\psi = U_0 \zeta , \quad (9.97)$$

where U_0 is a suitable constant velocity. After the mapping,

$$F(z) = \phi_o + i\psi_o = U_0 \zeta(z) = -U_0 L_0^{2/3} z^{1/3} e^{-i\sigma/3} . \quad (9.98)$$

Consequently,

$$\psi_o(x, y) = U_0 L_0^{2/3} r^{1/3} \sin [(\sigma - \theta)/3] . \quad (9.99)$$

The form of this equation shows, incidentally, that the outer flow could have been obtained by separation of variables in the equation satisfied by the stream function in cylindrical polar coordinates. When $\theta = 0$, r can be replaced by x , and therefore in the plane of symmetry

$$\psi_o(x, 0) = U_0 L_0^{2/3} x^{1/3} \sin(\sigma/3) . \quad (9.100)$$

Comparison of this result with equation (9.90) fixes the matching condition;

$$\sin(\sigma/3) U_0 L_0^{2/3} = \frac{C}{A} \left(\frac{J\nu}{\rho} \right)^{1/3} = \frac{C}{A} \mathbf{UL}^{2/3} , \quad (9.101)$$

where \mathbf{U} and \mathbf{L} are the intrinsic scales defined earlier by equations (9.12) and (9.11). The final form of the second term in the outer expansion in the upper half plane is therefore

$$\psi_o(x, y) = \frac{C}{A} \left(\frac{J\nu r}{\rho} \right)^{1/3} \frac{\sin [(\sigma - \theta)/3]}{\sin(\sigma/3)} . \quad (9.102)$$

In the compact outer coordinates (X, Y) defined by equations (9.51), this equation becomes

$$\Psi_0 = R^{1/3} \frac{\sin [(\sigma - \Theta)/3]}{\sin(\sigma/3)} \quad (9.103)$$

where $R^2 = X^2 + Y^2$ and $\Theta = \tan^{-1}(Y/X)$. Streamlines defined by equation (9.103) are plotted in FIGURE 9.9 for the case of a vertical wall; i.e., for $\sigma = \pi/2$. The associated pressure can be calculated once the velocity components for the irrotational outer flow are known. These components are most easily obtained in rectangular coordinates by taking the derivative $dF/dz = u_o - iv_o$ of equation (9.98);

$$u_o = -\frac{C}{3A} \left(\frac{J\nu}{\rho r^2} \right)^{1/3} \frac{\cos [(\sigma + 2\theta)/3]}{\sin(\sigma/3)} , \quad (9.104)$$

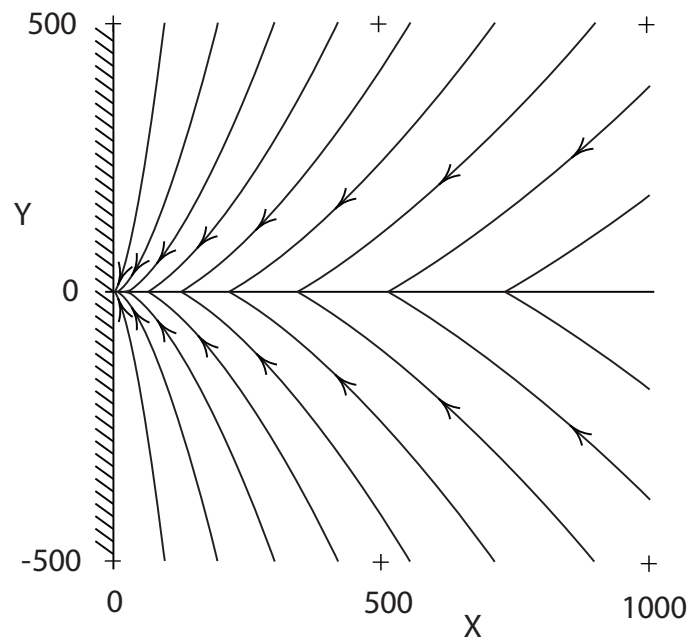


Figure 9.9: Streamlines $\Psi_o = \text{constant}$ in the outer potential flow of a laminar plane jet out of a wall along the y axis, according to equation (9.103). The range of Ψ is -9 (1) 9 .

$$v_o = -\frac{C}{3A} \left(\frac{J\nu}{\rho r^2} \right)^{1/3} \frac{\sin [(\sigma + 2\theta)/3]}{\sin(\sigma/3)}. \quad (9.105)$$

The pressure follows from the Bernoulli integral as

$$\frac{p_0 - p}{\rho} = \frac{(u_o^2 + v_o^2)}{2} = \frac{1}{18 \sin^2(\sigma/3)} \frac{C^2}{A^2} \left(\frac{J\nu}{\rho r^2} \right)^{2/3} \quad (9.106)$$

and is constant on circles centered on the origin, whatever the value of σ .

9.1.6 The composite expansion

The final step in this development is the construction of a composite expansion according to the rule “add the inner and outer expansions and subtract the common part.” The terms in the expansion are the first-order boundary-layer flow (equation (9.52)) and the second-order outer flow (equation (9.103)). The common part, according to equation (9.85), is $X^{1/3}$. Thus in compact variables (C for composite),

$$\Psi_C = H(X)X^{1/3} \left[\tanh \left(\frac{Y}{X^{2/3}} \right)^{-1} \right] + R^{1/3} \frac{\sin[(\sigma - \Theta)/3]}{\sin(\sigma/3)} \quad (9.107)$$

where $H(X)$ is a step function equal to unity (zero) when X is positive (negative) to express the fact that the boundary-layer solution in rectangular coordinates has no meaning when x is negative.

Equation (9.107) generates FIGURE 9.10 for the case of a laminar plane jet out of a vertical wall ($\sigma = \pi/2$) and generates FIGURE 9.11 for a laminar plane jet out of a thin horizontal channel ($\sigma = \pi$). In both cases the computing algorithm determines Ψ_C on a rectangular grid (X, Y) in the upper or lower half plane and then calls a contour-plotting routine.

The prime property of this analysis is an appropriate cancellation for small ν . In the body of the jet, where $\eta = O(1)$ but $\theta \ll 1$ and $r \approx x$, the outer flow drops out, and the boundary-layer solution remains. Outside the jet, where $\eta \gg 1$ but $\theta = O(1)$, the terms in the first square brackets in equation (9.107) cancel, and the potential entrained flow remains.

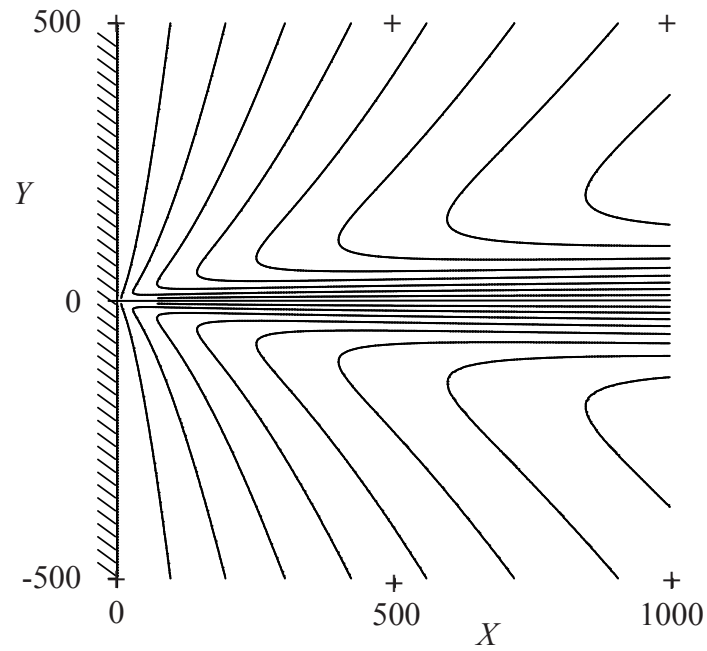


Figure 9.10: Composite streamlines $\Psi_c = \text{constant}$ for a laminar plane jet with a wall along the y axis, according to equation (9.107) with $\sigma = \pi/2$. The range of Ψ is -8 (1) 8 .

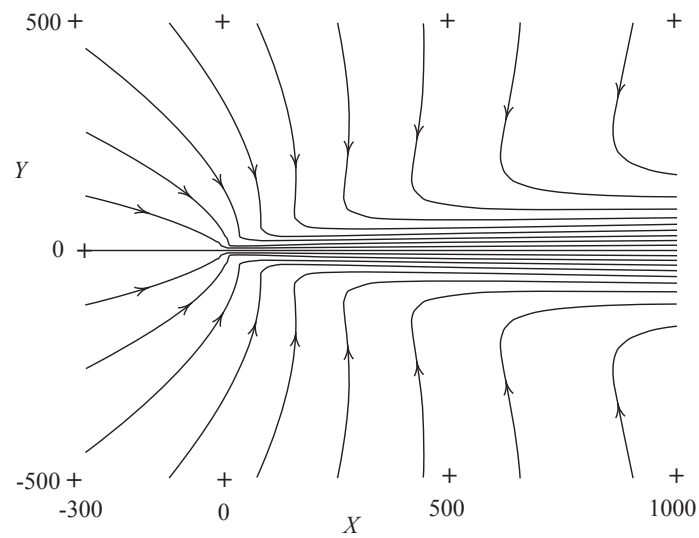


Figure 9.11: Composite streamlines $\Psi_c = \text{constant}$ for a laminar plane jet with a wall along the negative x axis according to equation (9.107) with $\sigma = \pi$. The range of Ψ is $-9 (1) 9$.

A figure similar to FIGURE 9.10, but without scales on the axes, was first published by REICHARDT (1942) in a remarkable display of insight. The formal machinery of matched asymptotic expansions did not yet exist, and Reichardt's method was simply to connect the inner and outer streamlines manually near their intersection. A similar method of manual fairing was used by KRAEMER (1971) for the case of laminar (and turbulent) plane jets without a wall, as in FIGURE 9.11. Kraemer apparently did not develop the appropriate composite expansion, although he did treat the corresponding laminar round jet rigorously by using the boundary-layer solution, the entrained-flow solution, and the exact solution, all of which are known in closed form (see SECTION 8.X).

In the composite flow, the pressure in the viscous region is no longer constant, and the u -component of velocity outside the viscous region is no longer zero. In fact, this velocity is directed upstream, with a magnitude that depends on Reynolds number and on the position of the wall. In effect, the jet creates its own head wind. This statement can be made quantitative in physical variables, working from the composite equivalent of equation (9.70), namely

$$\left(\frac{16}{9} \frac{\rho}{J\nu x}\right)^{1/3} \psi_C = f(\eta) - 2 + \frac{2 \sin[(\sigma - \theta)/3]}{(\cos \theta)^{1/3} \sin(\sigma/3)} = F(\eta) . \quad (9.108)$$

If this relation is differentiated with respect to y , with x positive and fixed, the result after some algebra is

$$\left(\frac{256}{3} \frac{\rho^2 \nu x}{J^2}\right)^{1/3} u_C = f'(\eta) - \frac{2}{3} \frac{\cos[(\sigma + 2\theta)/3](\cos \theta)^{2/3}}{\sin(\sigma/3)X^{1/3}} = F'(\eta) . \quad (9.109)$$

For the special case $\sigma = \pi/2$ and $X = 1000$ (at the right edge of FIGURE 9.10), the functions $F(\eta)$ and $F'(\eta)$ have been added to FIGURE 9.7 as dashed lines.

On the jet centerline, where $\eta = 0$ and $\theta = 0$, equation (9.109) reduces to (cc for composite centerline)

$$\left(\frac{256}{3} \frac{\rho^2 \nu x}{J^2}\right)^{1/3} u_{cc} = 2 \left[1 - \frac{\cot(\sigma/3)}{3X^{1/3}} \right] . \quad (9.110)$$

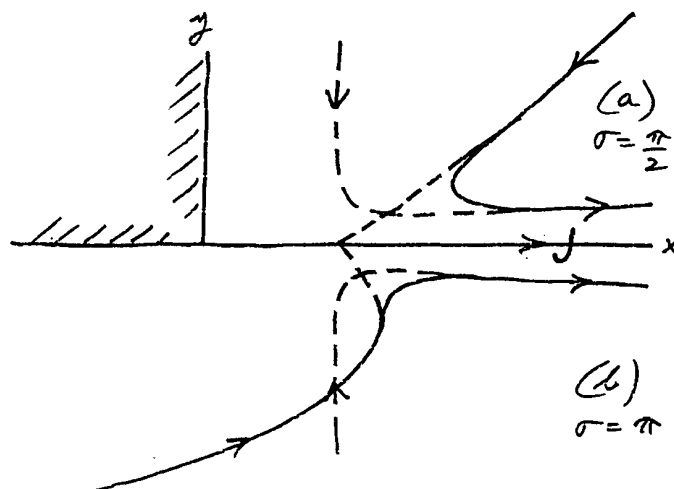


Figure 9.12: Exploratory view of streamlines near the stagnation point that appears at $X = 0.1925$ in the composite expansion of a plane laminar jet out of a vertical wall. The streamlines are not equally spaced in Ψ . This curious result is not real; it is an artifact created by use of the boundary approximation at low Reynolds number.

For $X = 1000$, the decrease in u_{cc} is 6 percent for $\sigma = \pi/2$ and 2 percent for $\sigma = \pi$. Note the unplanned result that the right side of this equation vanishes at one location on the jet centerline, where the composite flow has a stagnation point. When $\sigma = \pi/2$, this point is at $X = [\cot(\sigma/3)/3]^3 = 0.1925$, a value that is vanishingly small compared to the extent of the original figure 9.10. An exploratory plot of some streamlines near this point is shown in FIGURE 9.12. The curious flow field here is of course not physical. It is an artifact created by use of the boundary-layer approximation at Reynolds numbers much less than unity in a region of rising pressure.

The value in the plane of symmetry, from equation (9.104), is

$$u_o(x, 0) = -\frac{\cot(\sigma/3)}{3} \frac{C}{A} \left(\frac{J\nu}{\rho x^2} \right)^{1/3}. \quad (9.111)$$

The net velocity u_c (c for centerline) in the plane of symmetry of the composite flow is the sum of this value and the value from the boundary-layer approximation, equation (9.38) with $f'(0) = C^2/6AB$. In appropriate dimensionless variables, the sum is (**why is $u_c/\mathbf{U} \ll 1$?**)

$$\frac{u_c(x)}{\mathbf{U}} = \frac{1}{8X^{1/3}} \left(1 - \frac{\cot(\sigma/3)}{3X^{1/3}} \right). \quad (9.112)$$

At a Reynolds number corresponding to conditions at the right edge of the flow patterns in FIGURES 9.10 and 9.11 ($X = 1000$, $Re = 36$), the effect of the outer flow is to reduce the velocity on the jet centerline by about six percent when there is a wall along the y -axis, and by about two percent when there is a wall along the negative x -axis. In either case, the effect is larger closer to the origin. However, the boundary-layer approximation must eventually fail at low enough Reynolds numbers, as demonstrated by the fact that equation (9.112) has the fluid at rest in the plane of symmetry at $X = 0.19$ when $\sigma = \pi/2$ (**need a close-up of streamlines**).

To prepare for a discussion of the same effect for the turbulent plane jet in SECTION 9.3, some further details can be worked out for the case of a wall along the y -axis; i.e., for $\sigma = \pi/2$. From the composite expansion (9.107) with the function $f(\eta)$ restored, the similarity form of the variables ψ , u , v , τ in rectangular coordinates, normalized according to equations (9.69), is (c for composite)

$$S_c(\eta, X) = \left(\frac{16\rho}{9J\nu x} \right)^{1/3} \psi_c = f(\eta) - 2 - 4 \frac{\sin[(\theta - \pi/2)/3]}{(\cos\theta)^{1/3}}, \quad (9.113)$$

$$U_c(\eta, X) = \left(\frac{256\rho^2\nu x}{3J^2} \right)^{1/3} u_c = f'(\eta) - \frac{4}{3} \frac{(\cos\theta)^{2/3}}{X^{1/3}} \cos[(2\theta + \pi/2)/3], \quad (9.114)$$

$$V_c(\eta, X) = \left(\frac{48 \rho x^2}{J \nu} \right)^{1/3} v_c = 2\eta f'(\eta) - f(\eta) + 2 - 4 (\cos \theta)^{2/3} \sin \left[(2\theta + \pi/2)/3 \right] , \quad (9.115)$$

$$T_c(\eta, X) = 16 \frac{x}{J} \tau_c = f''(\eta) + \frac{8}{9} \frac{(\cos \theta)^{5/3}}{X^{2/3}} \sin \left[(5\theta + \pi/2)/3 \right] . \quad (9.116)$$

The quantities η and θ are related by

$$\eta = X^{1/3} \tan \theta . \quad (9.117)$$

The normalized boundary-layer functions $f(\eta)$, $f'(\eta)$, $2\eta f'(\eta) - f(\eta)$, $f''(\eta)$ are given by equations (9.78)–(9.81). When equations (9.113)–(9.117) are evaluated for $X = 1000$, the result is as shown by the dashed lines in FIGURE 9.7. The jet creates its own head wind, whose magnitude varies like $1/Re$ in x but is nearly constant in y . The shearing stress is almost unchanged. A slight discontinuity in T on the branch cut at $\eta = 0$ in equation (9.116) is not detectable at this Reynolds number. However, the stream function and the v -velocity show a strong effect of the altered outer conditions.

One final comment about FIGURE 9.12 is useful if this figure is taken literally as a representation of unsymmetrical jet flow directed to the right from the corner of a rectangular block. Recall equation (9.106) for the static pressure in the outer flow. According to this equation, the pressure is higher just below the jet in the figure than just above it. The pressure difference must be balanced by curvature of the jet, concave upward. This behavior was mentioned by KRAEMER (1971) in connection with turbulent flow, and is another manifestation of the Coanda effect. Steering of the jet and even forced attachment might be possible through deflection of one or both walls. More generally, for either laminar or turbulent flow, it may be important for close questions of experimental uniqueness and repeatability that the pattern of entrained streamlines can be affected by obstacles near the jet. Such obstacles might include room boundaries, instrumentation packages, or the corpus of the experimenter.

9.1.7 Experimental evidence

The effect of entrainment just described should be experimentally detectable. There are two main experimental aspects. The first is that the centerline velocity is less than the value from the similarity solution by an amount that varies with local Reynolds number, so that a correction is required before the theoretical similarity exponent can be tested. The second is that the upstream velocity near the outer edge of the jet will not be properly measured by instruments such as the impact tube, the hot-wire anemometer, or the unbiased laser-Doppler velocimeter, and may even be rectified. (**What did Andrade do?**) These aspects have greater weight if the flow is turbulent, and will be discussed again in SECTION X.

There is no question that the composite expansion (9.107) describes the flow in and near a laminar plane jet more accurately than the boundary layer approximation (9.49) alone. However, there are serious non-uniformities in the composite solution at the present order. The most serious of these appears when a momentum balance is attempted for the composite flow. If there is a wall at $\theta = \pi$, or at $\theta = \pm\pi/2$, or at some other angle, the no-slip condition should be imposed at this wall. The pressure deficit on the wall varies like $r^{-4/3}$, according to equation (9.106), and is not integrable at the origin. Viewed in coordinates (s, n) attached to the wall, the free stream for the resulting boundary layer moves with continuously increasing velocity from negative infinity in s toward an origin at $s = 0$. Specifically, $u_\infty \sim (-s)^{-2/3} \sim (-s)^m$, say. This program for free-stream velocity falls formally into the class of similar Falkner-Skan boundary layers (see SECTION 4.3.1 and particularly FIGURE 4.3). However, there is no similar Falkner-Skan flow with $m = -2/3$ and with the free stream flowing toward the origin. (**Did Wygnanski make this point?**) The method of matched asymptotic expansions thus leads to difficulties near the origin of the same kind that are encountered in the Blasius problem (see **Van Dyke, Schneider, Capell, Rubin and Falco**).

Various instruments respond in various ways to the composite flow field. Among the techniques commonly used today, single-

channel laser-Doppler velocimetry with frequency bias, and also the emerging technique called particle-image velocimetry, can be trusted when used with care to produce the dashed line labelled U in FIGURE 9.7.¹ Without frequency bias, the velocity will be rectified. A single hot-wire anemometer normal to the xy -plane will respond essentially to the magnitude $q = (u^2 + v^2)^{1/2}$ of the velocity. The dimensionless version of this magnitude can be obtained from relations already given as

$$Q_c(\eta, X) = \frac{A}{B} \left(\frac{\rho^2 \nu x}{J^2} \right)^{1/3} (u_c^2 + v_c^2)^{1/2} = \left(U_c^2 + \frac{V_c^2}{9X^{2/3}} \right)^{1/2}. \quad (9.118)$$

However, the hot wire is a very difficult instrument at the low velocities in the outer flow because it is sensitive to temperature, even at low overheat. My own experience makes me reluctant to rely on this instrument at velocities below about 1 m/sec in air. A pitot tube with square-cut entrance will respond well enough to Q up to a relative angle $\phi = \tan^{-1}(v/u)$ of at most about ten degrees. This point is marked in the figure. The remainder of the jet profile is accessible only with a probe that has been calibrated at high angles of attack. The correct response is

$$\tan \phi = \frac{v_c}{u_c} = \frac{1}{3X^{1/3}} \frac{V_c}{U_c}, \quad (9.119)$$

and the measurement, like that based on equation (9.118), must be supported by some other measurement or assumption to obtain U and V separately.

In summary, the main qualitative conclusion here is that the jet flow is affected by the presence and position of shielding walls. Although the effect should be easily detectable experimentally, I am not aware that any experimenter has studied it quantitatively for either the laminar or the turbulent case (**check again**). The effect should be understood because it enters explicitly into any check on conservation of momentum or any check on the exponent in the decay law for centerline velocity.

¹An earlier version of Figure 9.7 had the label U_c in place of F' .

There must be a corresponding dependence of the boundary-layer solution at second order. The analysis has been extended to higher order by Capell (1972), who worked in the ζ -plane of FIGURE 9.8 and took the stream function and vorticity as dependent variables. The momentum-integral condition needs study. It is noteworthy that the laminar round jet, for which the exact solution of the Navier-Stokes equations is available in simple closed form for resolution of fine details of higher-order matching, has apparently not been analyzed at higher order.

The first experiments on the laminar plane jet were carried out by Andrade (1939). The orifice was rectangular, without side walls. Flow visualization with dye showed the spanwise dimension decreasing in the flow direction as if affected by surface tension, although the flow is dyed water into clear water. The decrease in width is presumably a consequence of inward spanwise momentum of entrained fluid near the ends of the jet; it will be discussed again for the turbulent case. The velocity profile was measured and showed an effective origin far upstream of the orifice plane. The main finding, however, was instability at low Reynolds numbers (What Re , how low?). Comment on Reynolds number based on orifice conditions. The stability properties of such a jet were calculated by (who) and others and were studied experimentally by Sato and Sakao (1964). It is very difficult and probably not worth while to document the laminar plane jet experimentally in more detail, and the flow is essentially an exercise in matched asymptotic expansions.

For experimental work, see

ANDRADE (1939)
SATO (1960)
CHANAUD and POWELL (1964)
SATO and SAKAO (1964)

9.2 Laminar plane jet into moving fluid

9.2.1 Similarity

The similarity analysis is a variation on the Falkner-Skan problem with $f'(0) \neq 0$, $f''(0) = 0$. See

STEWARTSON (1954, 7)
 KENNEDY (1964, 7)
 STEIGER and CHEN (1965, 7)
 WYGNANSKI (1967)
 WYGNANSKI and FIEDLER (1968)
 WILKS and HUNT (1981)

The subject is the plane jet or wake in a pressure gradient, and the main reference is Wygnanski and Fiedler. The reason for dwelling on the jet in a pressure gradient is that pressure gradients are common in ejectors. If the behavior of an equilibrium flow; i.e., a flow with similarity, can be established, there is some hope of using this information to cope with flows not in equilibrium. A precedent is available for the boundary layer in Thwaites' method. Consider first laminar flow, with the momentum equation in the form

$$\rho \left(u \frac{\partial u}{\partial x} + v \frac{\partial u}{\partial y} \right) = -\frac{dp}{dx} + \mu \frac{\partial^2 u}{\partial y^2} . \quad (9.120)$$

At infinity the derivatives $\partial u / \partial y$ and $\partial^2 u / \partial y^2$ go to zero, and u goes to u_∞ . Thus

$$\rho u_\infty \frac{du_\infty}{dx} = -\frac{dp}{dx} . \quad (9.121)$$

This expression can be viewed as a boundary-layer approximation to the Bernoulli equation. It allows the momentum equation to be written as

$$\rho(\psi_y \psi_{xy} - \psi_x \psi_{yy}) = \rho u_\infty \frac{du_\infty}{dx} + \mu \psi_{yyy} . \quad (9.122)$$

There are several problems to be treated, as shown in the sketch. ²

²This sketch is missing or was never created.

The stream function will be taken in the form

$$\psi = u_\infty y + UL F\left(\frac{y}{L}\right) \quad (9.123)$$

where the notation F rather than f is used to indicate that this function does not include the background flow, which is described separately by the first term $u_\infty y$. This notation is different from the normal usage, at least for the boundary layer. The notation used here implies

$$u = u_\infty + U F'\left(\frac{y}{L}\right) \quad (9.124)$$

and the natural boundary condition at infinity is $F'(\infty) = 0$. The normal usage is

$$\begin{aligned} \psi &= UL f\left(\frac{y}{L}\right) \\ u &= U f'\left(\frac{y}{L}\right) \end{aligned} \quad (9.125)$$

so that the boundary condition is $f'(\infty) = u_\infty/U$.

Substitutions of equation (9.123) in equation (9.122) leads to the relation

$$\begin{aligned} F''' + \left(\frac{L}{\nu} \frac{dUL}{dx}\right) FF'' - \left(\frac{L^2}{\nu} \frac{dU}{dx}\right) F'F' + \left(\frac{L^2}{\nu} \frac{du_\infty}{dx}\right) \eta F'' \\ - \left(\frac{L^2}{\nu U} \frac{du_\infty U}{dx}\right) F' = 0 . \end{aligned} \quad (9.126)$$

Old Problem 1: There are no real characteristics for the pressure. No discontinuities can occur.

New Problem 1: The energy equation has $u\partial\tau/\partial y = \partial(\tau u)/\partial y - \tau\partial u/\partial y$. The last term is dissipation, which at low speed does not provide enough heat to change the density. The fluid can be treated as incompressible. The term $\partial(\tau u)/\partial y$ is what is left of a divergence, and accounts for internal work done by one part of the fluid on the other. This process has no net contribution over the layer. I need a physical meaning, and I need to know if anything can be done with turbulent flow.

The various coefficients in equation (9.126) must be constant for a flow with similarity. Inspection shows that only three combinations are independent;

$$\begin{aligned}\frac{L^2}{\nu} \frac{dU}{dx} &= \text{constant} \\ \frac{L^2}{\nu} \frac{du_\infty}{dx} &= \text{constant} \\ \frac{UL}{\nu} \frac{dL}{dx} &= \text{constant}\end{aligned}\tag{9.127}$$

inasmuch as the first two of these imply

$$\frac{u_\infty}{U} = c = \text{constant} .\tag{9.128}$$

Now add the first of equations (9.127) to twice the third equation to obtain

$$\frac{1}{\nu} \frac{dUL^2}{dx} = \text{constant} .\tag{9.129}$$

Integration gives

$$\frac{UL^2}{x} = \text{constant}\tag{9.130}$$

except for the special case when the constant in equation (9.129) is zero, in which case

$$UL^2 = \text{constant} .\tag{9.131}$$

According to the first and last of equations (9.127), the general case (9.129) implies

$$u_\infty \approx U \approx x^n, \quad L \approx x^{\frac{1-n}{2}} .\tag{9.132}$$

The special case (9.131) implies

$$u_\infty \approx U \approx e^{\alpha x}, \quad L \approx -\alpha x/2 .\tag{9.133}$$

(This needs to be redone with the affine transformation.)

To put equation (x)³ in the similarity form required by the present problem, replace u by $u_\infty + U F'(y/L)$, replace u_∞ by cU , and

³This reference is uncertain

note that $\int_0^\infty F' d\eta = F(\infty)$ if $F(0) = 0$; i.e. if $y = 0$ is a streamline. Then

$$c \left(\frac{LU}{\nu} \frac{dL}{dx} + 3 \frac{L^2}{\nu} \frac{dU}{dx} \right) F(\infty) + \left(\frac{LU}{\nu} \frac{dL}{dx} + 2 \frac{L^2}{\nu} \frac{dU}{dx} \right) \int_0^\infty F' F' d\eta + F''(0) = 0 \quad (9.134)$$

The jet and wake in a pressure gradient have a precedent in the Falkner-Skan boundary layer. Next year the boundary layer will probably be done first. The strategy is to develop some system, partly empirical in the case of laminar flow and completely empirical in the case of turbulent flow, that defines and connects input (boundary and initial conditions) and output (evolution of the flow). Parameters are needed to measure input and output. Equilibrium flows can help to define useful parameters that can then be applied for non-equilibrium cases. The classic precedent is the Thwaites method for boundary layers. Free flows like jets and wakes also have to function in a pressure gradient.

Wynanski and Fiedler have an incompatible notation and a different set of parameters. This should be fixed.

Note that the power law and exponential law follow without considering the momentum integral. The special case and the general case both lead to a continuum of solutions (parameters n , a), although the special case starts as a single point. Not everything is a power law. The exponential case is usually treated as a curiosity. **(Does the affine transformation work? What is the invariant?)** In the Falkner-Skan problem, the special case corresponds to $n = \infty$, but computers have no trouble.

The general case defined by equation (9.132) will be discussed first. The characteristic scales U and L vary like powers of x , and the coefficients in equations (9.126) and (9.134) can be reduced to

$$\frac{2}{1+n} \frac{\nu x}{UL^2} F''' + FF'' - \frac{2n}{1+n} F'F' + c\eta F'' - \frac{4cn}{1+n} F' = 0 \quad (9.135)$$

$$c(5n+1)F(\infty) + (3n+1) \int_0^{\infty} F'F' d\eta + \frac{2\nu x}{UL^2} F''(0) = 0 \quad (9.136)$$

The variables here are not ideal, and it is desirable to put the equations in a form closer to the form of the Falkner-Skan problem. As Wygnanski and Fiedler attack the wake-jet problem, the variables are

$$\begin{aligned} \psi &= u_{\infty}y + UL F\left(\frac{y}{L}\right) \\ u &= u_{\infty} + U F' \end{aligned} \quad (9.137)$$

with boundary conditions $F(0) = 0$, $F'(0) = 1$, $F'(\infty) = 0$. Suppose instead that the free stream is included in the function denoted by F . Thus put (**better to use g or h here?**)

$$\psi = UL f\left(\frac{y}{L}\right) \quad (9.138)$$

$$u = U f' \quad (9.139)$$

The altered boundary conditions follow from a comparison;

$$\begin{aligned} \frac{\psi}{UL} &= f = c\eta + F \\ \frac{u}{U} &= f' = c + F' \end{aligned} \quad (9.140)$$

They are $f(0) = 0$, $f'(0) = 1 + c$, $f'(\infty) = c$. Note that this operation has not changed the definition of U or L. When the dependent variable in equations (9.135) and (9.136) is changed from F to f, the result is (**check equation (9.142)**)

$$\frac{2}{1+n} \frac{\nu x}{UL^2} f''' + f f'' - \frac{2n}{1+n} (f' f' - c^2) = 0 \quad (9.141)$$

$$c(5n+1) \int_0^{\infty} (f' - c) d\eta + (3n+1) \int_0^{\infty} (f' - c)^2 d\eta + \frac{2\nu x}{UL^2} f''(0) = 0 \quad (9.142)$$

The last expression uses the fact that $(f' - c)$ approaches zero as η approaches infinity; in fact, from equation (x) ⁴

$$c \frac{\delta^*}{L} = - \int_0^{\infty} (f' - c) d\eta \quad (9.143)$$

and from equation (y),

$$c^2 \frac{\theta}{L} = - \int_0^{\infty} (f' - c)^2 d\eta - c \int_0^{\infty} (f' - c) d\eta . \quad (9.144)$$

There are still some awkward constants in these equations. To begin their removal, replace $f(\eta)$ temporarily by $g(c\eta)$. Restore the notation f , now with argument $c\eta$. If the prime notation is retained for derivatives with respect to $c\eta$, equation (9.141) becomes

$$\frac{2}{1+n} \frac{\nu x c}{UL^2} f''' + f f'' - \frac{2n}{1+n} (f' f' - 1) = 0 \quad (9.145)$$

and equation (9.142) becomes

$$(5n+1) \int_0^{\infty} (f' - 1) d\eta + (3n+1) \int_0^{\infty} (f' - 1)^2 d\eta + \frac{2\nu x}{UL^2} f''(0) = 0 . \quad (9.146)$$

The boundary conditions become $f(0) = 0$, $f'(0) = 1 + 1/c$, $f'(\infty) = 1$. Suppose that the first coefficient in (9.145) is set equal to unity. Then the two equations

$$\begin{aligned} U &= \frac{u_{\infty}}{c} \\ UL^2 &= \frac{2\nu x c}{1+n} \end{aligned} \quad (9.147)$$

define U and L . In particular,

$$L = c \left(\frac{2\nu x}{(1+n)u_{\infty}} \right)^{1/2} . \quad (9.148)$$

⁴It is not known which equation is meant here or in next reference.

With these changes, the final forms for equations (9.138) and (9.141) are

$$\psi = \left(\frac{2\nu x u_\infty}{1+n} \right)^{1/2} f \left[y \left(\frac{(1+n)u_\infty}{2\nu x} \right)^{1/2} \right] \quad (9.149)$$

$$f''' + f f'' - \frac{2n}{1+n} (f' f' - 1) = 0 \quad (9.150)$$

with boundary conditions $f(0) = 0$, $f'(0) = 1 + 1/c$, $f'(\infty) = 1$.

Equation (9.150) is the Falkner-Skan equation, in which the parameter is usually taken as β , defined by

$$\beta = \frac{2n}{1+n} \quad (9.151)$$

From here on, the fact that the flow is a jet or a wake is manifested by the boundary conditions associated with symmetric flow,

$$f'(0) \neq 0, \quad f''(0) = 0 \quad (9.152)$$

Thus equation (9.142) becomes

$$c(5n+1) \int_0^\infty (f' - c) d\eta + (3n+1) \int_0^\infty (f' - c)^2 d\eta = 0. \quad (9.153)$$

(Need to do special case with exponential.)

Consider a constant-area ejector, as shown in the sketch.⁵

The flow will be turbulent, but we are practicing with laminar flow. Profiles are needed to handle the bubble, and these come from the Wygnanski and Fiedler paper.

If $F''(0)$, which is $\partial u / \partial y$ at the wall, is zero, the flow has symmetry. If it is not zero, the flow is a boundary layer. Both can be done together.

(Need Bibliography on Falkner-Skan Flows)

⁵This sketch is missing or was never created.

The wedge interpretation of the Falkner-Skan flows is not very useful if $\beta \geq 2$. When $\beta = -0.1988$ (about 20°) the flow is continuously separating. This is a clue to the expansion that is permitted without separation.

How did Wagnanski and Fiedler connect c and m in general?

When $n = 1/3$, $c = 0$, and $u_\infty = 0$, the similarity argument collapses. This problem is connected with the fact that this layer grows like $\nu^{2/3}$, whereas all other cases grow like $\nu^{1/2}$. Something has to be done; see "sub-characteristics". When $c = \infty$, $n = -1/5$, $m = 3/5$. This is the linearized case with pressure gradient. Mixing layer is $n = 0$, $m = 1/2$, $c = -1$, when the two sides of jet separate from each other. There are two flows with $c = -1$; one is the mixing layer and the other is the separating boundary layer with $f''(0) = 0$. (Find out what the "trivial solution" is.)

I have given up for the present on jet ejectors, because I cannot find any analytical formulation that I consider to be above the line.

9.3 Turbulent plane jet into fluid at rest

9.3.1 Dimensional preamble

There is ample experimental evidence that free turbulent shear flows are insensitive to Reynolds number; i.e., to the viscosity of the fluid. It is a very bold step to replace the phrase "insensitive to" by the phrase "independent of". Nevertheless, this step is the key to an organization of empirical data through an analysis that can proceed for some distance without using the equations of motion. When the viscosity μ is deleted from the list of global parameters for the plane jet, leaving only the momentum flux J and the density ρ , there is a profound effect on the global dimensional argument in equations (9.9)–(9.13), which now yields only

$$\mathbf{U}^2 \mathbf{L} = \frac{J}{\rho} . \quad (9.154)$$

At this point the quantity J is not yet defined precisely, but its dimensions at least are expected to be the same as in the laminar problem.

Take as a generic description of the flow the statement

$$\psi = \psi(x, y) . \quad (9.155)$$

When this description is put in dimensionless form using hypothetical local scales $U(x)$, $L(x)$, it becomes

$$\frac{\psi}{UL} = F\left(\frac{x}{L}, \frac{y}{L}\right) . \quad (9.156)$$

For the laminar problem, the scales U and L were found in SECTION 9.1.2 to be $(J^2/\rho^2\nu x)^{1/3}$ and $(\rho\nu^2 x^2/J)^{1/3}$, respectively. But for the turbulent problem there is no U or L , only $\mathbf{U}^2\mathbf{L}$. The empirical rule then is “use x for L and improvise.” In the present instance, this means “use x for L and use $(\mathbf{U}^2\mathbf{L}/x)^{1/2}$ for U .” Thus write

$$\frac{\psi}{UL} = \frac{\psi}{(\mathbf{U}^2\mathbf{L}x)^{1/2}} = \left(\frac{\rho}{Jx}\right)^{1/2} \psi = \Phi\left(\frac{x}{x}, \frac{y}{x}\right) = \phi\left(\frac{y}{x}\right) . \quad (9.157)$$

It is inherent in the empirical rule just quoted, and it is a frequent conclusion in this monograph, that a flow without an intrinsic global length scale must be conical (or wedgical). Other examples besides the plane jet are the round jet (laminar or turbulent) and the turbulent mixing layer. (**How about laminar mixing layer?**)

A more important consequence of the passage to turbulence is that a similarity law has to be invented for the turbulent stresses. If $\overline{u'v'}$ is taken as an example, the obvious generic form is

$$-\frac{\overline{u'v'}}{U^2} = G\left(\frac{x}{L}, \frac{y}{L}\right) . \quad (9.158)$$

But there is no U or L , only $\mathbf{U}^2\mathbf{L}$. Hence it is necessary to write, in view of equation (9.154),

$$-\frac{\overline{u'v'}}{U^2} = -\frac{\overline{u'v'}x}{\mathbf{U}^2\mathbf{L}} = -\frac{\rho\overline{u'v'}x}{J} = g\left(\frac{y}{x}\right) \quad (9.159)$$

and so on.

9.3.2 The affine transformation

As in the laminar problem, a more polished argument can be based on the transformation properties of the equations of motion, despite the fact that these equations are not complete. It is almost mandatory to choose a rectangular coordinate system, because experimenters almost always move their probes in a rectangular way. The Reynolds equations, without approximation except that the viscous stress terms are omitted as negligible (see SECTION X for an estimate), are

$$\rho \left(u \frac{\partial u}{\partial x} + v \frac{\partial u}{\partial y} \right) = -\frac{\partial p}{\partial x} + \frac{\partial}{\partial x}(-\rho \overline{u'u'}) + \frac{\partial}{\partial y}(-\rho \overline{u'v'}) , \quad (9.160)$$

$$\rho \left(u \frac{\partial v}{\partial x} + v \frac{\partial v}{\partial y} \right) = -\frac{\partial p}{\partial y} + \frac{\partial}{\partial x}(-\rho \overline{u'v'}) + \frac{\partial}{\partial y}(-\rho \overline{v'v'}) . \quad (9.161)$$

Symmetry is imposed on the flow by the boundary condition

$$\psi(x, 0) = 0 \quad \text{or} \quad v(x, 0) = 0 . \quad (9.162)$$

A standard boundary-layer approximation that assumes $v \ll u$ and $\partial/\partial x \ll \partial/\partial y$ would discard equation (9.161) together with the terms in p and $\overline{u'u'}$ in equation (9.160), and this approximation is commonly made in the literature. However, the experimental evidence to be cited shortly shows first, that the turbulent plane jet far enough from the orifice grows rapidly and linearly, showing little qualitative or quantitative difference between flows at different Reynolds numbers; second, that the three Reynolds stresses and the static pressure variation have comparable magnitudes; and third, that x -derivatives, although generally smaller than y -derivatives, are by no means negligible. I will therefore retain all of the terms displayed in (9.160) and (9.161). Lacking initial guidance, I have no option except to write boundary conditions outside the jet in hybrid form, as if the jet were thin and the boundary-layer approximation were still being made with respect to a stagnant outer fluid, as in the laminar case. Thus I write (**think about boundary-layer approximation**)

$$u(x, \pm\infty) = 0 , \quad (9.163)$$

$$p(x, \pm\infty) = p_\infty = \text{constant} . \quad (9.164)$$

Under these conditions there is an integral invariant, easily derived from (9.160) but more complex than in the laminar case (**explain why** p_∞);

$$J = \int_{-\infty}^{\infty} (\rho uu + \overline{\rho u' u'} + p - p_\infty) dy = \text{constant} . \quad (9.165)$$

No corresponding integral emerges from (9.161) because of the anti-symmetry of each of its terms.

Now consider the affine transformation

$$x = a\hat{x}$$

$$y = b\hat{y}$$

$$\psi = c\hat{\psi}$$

$$\rho = d\hat{\rho}$$

$$\overline{u' u'} = f \overline{\hat{u}' \hat{u}'} \quad (9.166)$$

$$\overline{u' v'} = g \overline{\hat{u}' \hat{v}'}$$

$$\overline{v' v'} = h \overline{\hat{v}' \hat{v}'}$$

$$p - p_\infty = i (\hat{p} - \hat{p}_\infty)$$

$$J = j \hat{J}$$

where p , p_∞ , u , and v are not listed separately for reasons argued earlier in connection with equation (9.29) of the laminar problem (**check**). The velocity components are derived from a stream func-

tion in the usual way,

$$u = \frac{\partial\psi}{\partial y} , \quad v = -\frac{\partial\psi}{\partial x} . \quad (9.167)$$

Let the scaling combinations that appear during the transformation be arrayed schematically like the terms in equations (9.160), (9.161), and (9.165), with the combinations in the last column normalized to unity;

$$\frac{c^2}{abg} = 1 , \quad \frac{bi}{adg} = 1 , \quad \frac{bf}{ag} = 1 , \quad 1 = 1 \quad (9.168)$$

$$\frac{c^2}{a^2h} = 1 , \quad \left(\frac{i}{dh} \right) = 1 , \quad \frac{bg}{ah} = 1 , \quad 1 = 1 \quad (9.169)$$

$$\frac{j}{bi} = 1 , \quad \frac{c^2d}{b^2i} = 1 , \quad \left(\frac{df}{i} \right) = 1 , \quad 1 = 1 . \quad (9.170)$$

Each of these combinations must be separately equal to unity if the equations are to be invariant under the transformation. Inspection of the two combinations in parentheses shows that $f = h = i/d$. But now $bf/ag = bh/ag = 1$, from the third of equations (9.168), and also $bg/ah = 1$, from the third of equations (9.169). It follows that $a = b$ and $g = h = f = i/d$. There remain two independent combinations containing c and j , respectively. These can be written

$$\frac{c^2}{b^2g} = 1, \quad \frac{j}{adg} = 1 . \quad (9.171)$$

The first relation implies that the Reynolds stresses and the static-pressure variation transform like ρu^2 , and the second implies that they transform like $J/\rho x$, as in equation (9.159). Finally, when c (or ψ) and g (or $\overline{u'v'}$) are isolated, the invariants of the affine transformation are defined by

$$\frac{c^2d}{aj} = 1, \quad \frac{adg}{j} = 1, \quad \frac{b}{a} = 1 . \quad (9.172)$$

The first and last of these equations reproduce the dependence expressed by equation (9.157). When numerical constants A and B are

inserted for purposes of later normalization, the proper ansatz for the stream function is seen to be

$$A\left(\frac{\rho}{Jx}\right)^{1/2}\psi = f\left(B\frac{y}{x}\right) = f(\eta) . \quad (9.173)$$

One consequence of this ansatz can be exploited at once. Differentiation gives

$$u = \frac{\partial\psi}{\partial y} = \frac{B}{A}\left(\frac{J}{\rho x}\right)^{1/2} f'(\eta) . \quad (9.174)$$

Denote the velocity on the plane of symmetry by u_c (c for centerline), with

$$u_c = \frac{B}{A}\left(\frac{J}{\rho x}\right)^{1/2} f'(0) . \quad (9.175)$$

Now the middle equation of the row (9.172), or alternatively equation (9.159), implies that the Reynolds stresses are proportional to J/x ; i.e., are properly made dimensionless with J/x . According to equation (9.175), the product ρu_c^2 has the same property. Hence it is convenient to complete the ansatz (9.173) by putting

$$p - p_\infty = \rho u_c^2 P(\eta) \quad (9.176)$$

$$\overline{u'u'} = u_c^2 F(\eta) \quad (9.177)$$

$$\overline{u'v'} = u_c^2 G(\eta) \quad (9.178)$$

$$\overline{v'v'} = u_c^2 H(\eta) . \quad (9.179)$$

The functions P , F , and H are even in η , and the function G is odd. These four equations again state that the three Reynolds stresses and the pressure variation must scale in the same way. More precisely, it follows from equations (9.168)–(9.170) that if $f = g = h = i/d$, then $a = b$, and conversely. Put into words, the meaning here is that if the turbulent plane jet grows linearly, the turbulent stresses and the pressure variation are proportional to each other at corresponding points, and conversely. **(Show that viscous stress terms are negligible. Is there a constant tensor eddy viscosity?)**

Substitution of these relationships in the momentum equations (9.160) and (9.161), with the observation from equation (9.175) that $u_c^2 x$ is constant and therefore that $du_c/dx = -u_c/2x$, leads to

$$\frac{(ff'' + f'f')}{2C^2} = -(\eta P)' - (\eta F)' + BG' \quad (9.180)$$

$$\frac{\eta}{B} \frac{(ff'' + f'f')}{2C^2} = BP' - (\eta G)' + BH' \quad (9.181)$$

where C is a convenient notation for a recurring combination,

$$C = u_c \frac{A}{B} \left(\frac{\rho x}{J} \right)^{1/2} = f'(0) . \quad (9.182)$$

Similarly, substitution in the integral invariant (9.165) leads to

$$\int_{-\infty}^{\infty} [f'f' + C^2(F + P)] d\eta = \frac{A^2}{B} , \quad (9.183)$$

a relationship that can also be obtained from equation (9.180) by taking the definite integral (**check this**).

The laws of mechanics are exhausted by equations (9.180) and (9.181), which provide only two equations for five dependent variables f , F , G , H , P , and give no information whatever about a sixth variable, the dimensionless version of the Reynolds normal stress $-\overline{\rho w'w'}$. The laws of mechanics are therefore of limited value for describing the dynamics of the plane jet, except for testing the accuracy of experimental data. Two such tests are primary. One emphasizes the dominant terms in f and G in equation (9.180) to test the relationship between turbulent shearing stress and mean velocity field, with or without a boundary-layer approximation. The other, at higher order, emphasizes the dominant terms in P and H in equation (9.181) to test the presumed proportionality between the static pressure and the various Reynolds stresses. (**Say where this is done.**)

Equations (9.180) and (9.181) can be integrated once to obtain

$$\frac{ff'}{2C^2} = BG - \eta P - \eta F , \quad (9.184)$$

$$\frac{f^2}{2} - \eta f f' = \eta G - BP - BH . \quad (9.185)$$

When P is eliminated and the result solved for G , the Reynolds shearing stress is found to be related to the mean-velocity field and the Reynolds normal stresses by

$$\left(1 - \frac{\eta^2}{B^2}\right)G = \left(1 + \frac{\eta^2}{B^2}\right)\frac{ff'}{2BC^2} - \frac{\eta}{B}\frac{f^2}{4B^2C^2} + \frac{\eta}{B}(F - H) . \quad (9.186)$$

This observation can be expressed in physical variables, with the aid of equations (9.173)–(9.179), as

$$\left(1 - \frac{y^2}{x^2}\right)\overline{u'v'} = \left(1 + \frac{y^2}{x^2}\right)\frac{\psi u}{2x} - \frac{y}{x}\frac{\psi^2}{4x^2} + \frac{y}{x}(\overline{u'u'} - \overline{v'v'}) . \quad (9.187)$$

Because the jet thickness increases rapidly with x , $\eta/B = y/x$ is not a negligible quantity within the jet. (**Discuss terms in y/x and y^2/x^2 . Power series?**)

The mean static pressure within the jet is part of the integral invariant (9.165). The pressure can also be related to the Reynolds stresses by a different use of (9.180) and (9.181). Multiply the first equation by η/B and subtract the second equation to obtain

$$\left(1 + \frac{\eta^2}{B^2}\right)P' + \frac{\eta}{B}\frac{P}{B} = -\frac{\eta}{B}\left(\frac{\eta}{B}F\right)' + \left(\frac{\eta}{B}G\right)' + \frac{\eta}{B}G' - H' . \quad (9.188)$$

Division by the coefficient of P' puts this equation in a standard form, $dW/dz + R(z)W = S(z)$, whose integral is known. After some integration by parts to convert differentiation of experimental data for F , G , and H into integration, the derivation leads eventually to

$$\begin{aligned} \left(1 + \frac{\eta^2}{B^2}\right)P &= -\frac{\eta^2}{B^2}F + 2\frac{\eta}{B}G - H \\ &+ \left(1 + \frac{\eta^2}{B^2}\right)^{1/2} \int_{-\infty}^{\eta/B} \frac{\left[\frac{\eta}{B}F - \left(1 - \frac{\eta^2}{B^2}\right)G - \frac{\eta}{B}H\right]}{\left(1 + \frac{\eta^2}{B^2}\right)^{3/2}} d\frac{\eta}{B} . \end{aligned} \quad (9.189)$$

In physical variables, this is

$$\begin{aligned} \left(1 + \frac{y^2}{x^2}\right) \frac{(p - p_\infty)}{\rho} &= -\frac{y^2}{x^2} \overline{u'u'} + 2\frac{y}{x} \overline{u'v'} - \overline{v'v'} \\ + \left(1 + \frac{y^2}{x^2}\right)^{1/2} \int_{-\infty}^{y/x} &\frac{\left[\frac{y}{x} (\overline{u'u'} - \overline{v'v'}) - \left(1 - \frac{y^2}{x^2}\right) \overline{u'v'}\right]}{\left(1 + \frac{y^2}{x^2}\right)^{3/2}} d\frac{y}{x} . \end{aligned} \quad (9.190)$$

9.3.3 Normalization

It is common practice for experimenters to normalize the variable η by putting $\eta = 1$ at the half-velocity point; i.e., by putting $By/x = \eta = 1$ when $u/u_c = 1/2$. The effect is to define the parameter B . This condition is much the same one used to develop the law of the wake in SECTION X. It amounts to inventing the law of the jet.

A more rational scheme is to define an integral scale (maximum-slope thickness) by requiring the shaded area in FIGURE X to be unity;

$$\int_0^\infty f'(\eta) d\eta = f(\infty) = f'(0) \tilde{\eta} = 1 \quad (9.191)$$

just as in the laminar case (see equation (9.74)). For the body of the jet to lie essentially in the interval $-1 < \eta < +1$, it is sufficient to take $\tilde{\eta} = 1/2$ or

$$f(\infty) = 1 , \quad f'(0) = 2 . \quad (9.192)$$

This argument provides one further boundary condition on the mean-velocity profile $f'(\eta)$, in company with the null conditions $f(0) = 0$, $f'(\pm\infty) = 0$.

With the two normalizing conditions (9.192), the three equations of the problem become

$$ff' = 8[BG - \eta(F + P)] , \quad (9.193)$$

$$f^2 - 2\eta ff' = 16B [\eta G - B(H + P)] , \quad (9.194)$$

$$\int_{-\infty}^{\infty} [f' f' + 4(F + P)] d\eta = \frac{A^2}{B} . \quad (9.195)$$

9.3.4 Entrainment and composite flow

It is not necessary to have a complete set of equations to calculate formally the entrained flow for the plane turbulent jet, although certain difficulties appear. The chief of these is the matching condition. The absence of a small parameter means that there is no inner limit process to collapse the body of the jet onto the x -axis and allow the plane jet to be represented as a distributed sink. At the same time, the entrainment process is still active, although it is modified by the different growth law for the turbulent case. Moreover, the turbulence and the turbulent transport are confined to a finite region by an irregular and unsteady but sharply defined interface. It might be supposed that the matching process should be applied not on $y = 0$ but along a line at some finite angle, say a line through the locus where the intermittency factor is equal to $1/2$. Voids and/or discontinuities will surely occur. Different authors might choose different options, and I wish them well. For myself, I see only one way at present to keep some kind of system and order in this and other turbulent problems, and that is to ignore the difficulty of the finite angle occupied by the jet at all Reynolds numbers and to apply the matching condition in the plane of symmetry as in the laminar case.

As y or y/x or η goes to infinity, the stream function (9.173) for the turbulent plane jet goes to

$$\psi_i(x, \infty) = \frac{1}{A} \left(\frac{Jx}{\rho} \right)^{1/2} f(\infty) . \quad (9.196)$$

The potential flow with

$$\psi_o(x, 0) = \frac{1}{A} \left(\frac{Jx}{\rho} \right)^{1/2} f(\infty) \quad (9.197)$$

can again be obtained by conformal mapping, with the aid of FIGURE 9.9;

$$\zeta = L_0^{1/2} z^{1/2} e^{i\alpha} . \quad (9.198)$$

With $\zeta = Re^{i\omega}$ and $z = re^{i\theta}$,

$$\omega = \frac{\theta}{2} + \alpha . \quad (9.199)$$

The same two cases are of interest as for laminar flow. If there is a wall at $y = 0$, $x < 0$, with $\theta = \pi$ when $\omega = \pi$ on OA , it follows that $\alpha = \pi/2$. On OB , $\theta = 0$, and therefore $\omega = \pi/2$. The stream function for uniform flow in the ζ -plane,

$$F(\zeta) = \phi + i\psi = U_0\zeta \quad (9.200)$$

implies in the z -plane

$$\psi_o(x, y) = U_0 L_0^{1/2} r^{1/2} \sin\left(\frac{\theta + \pi}{2}\right) . \quad (9.201)$$

Hence matching in the plane of symmetry, $\theta = 0$ or $\eta = \infty$, gives

$$\frac{1}{A} \left(\frac{Jx}{\rho}\right)^{1/2} f(\infty) = U_0 L_0^{1/2} x^{1/2} = (\mathbf{U}^2 \mathbf{L}x)^{1/2} \quad (9.202)$$

so that

$$\psi_o(x, y) = \frac{1}{A} \left(\frac{Jr}{\rho}\right)^{1/2} f(\infty) \sin\left(\frac{\theta + \pi}{2}\right) . \quad (9.203)$$

The streamlines for the outer or entrained flow are confocal parabolas opening to the left. The composite expansion in the upper half-plane (c for composite) is

$$\psi_c(x, y) = \frac{1}{A} \left(\frac{Jr}{\rho}\right)^{1/2} f(\infty) \left[(\cos\theta)^{1/2} \frac{f(\eta)}{f(\infty)} - 1 + \sin\left(\frac{\theta + \pi}{2}\right) \right] . \quad (9.204)$$

If there is a wall at $x = 0$ or $\theta = \pi/2$, with $\omega = \pi$ on OA , it follows from equation (9.199) that $\alpha = 3\pi/4$, and therefore that $\omega = 3\pi/4$ when $\theta = 0$ on OB . The mapping is as shown in FIGURE ⁶, with the streamlines of the entrained flow making an angle of 45°

⁶Figure with draft number 17-13 either missing or not completed

at the x axis. These streamlines are again confocal parabolas, but differently oriented (**check**). The stream function is

$$\psi_o(x, y) = U_0 L_0^{1/2} r^{1/2} \sin\left(\frac{\theta + 3\pi/2}{2}\right). \quad (9.205)$$

Matching gives

$$\frac{1}{A} \left(\frac{Jx}{\rho}\right)^{1/2} f(\infty) = \frac{U_0 L_0^{1/2} x^{1/2}}{(2)^{1/2}} \quad (9.206)$$

and thus the outer flow is

$$\psi_o(x, y) = \frac{(2)^{1/2}}{A} \left(\frac{Jr}{\rho}\right)^{1/2} f(\infty) \sin\left(\frac{\theta + 3\pi/2}{2}\right). \quad (9.207)$$

The composite expansion is

$$\psi_c(x, y) = \frac{1}{A} \left(\frac{Jx}{\rho}\right)^{1/2} f(\infty) \left[\frac{\frac{f(\eta)}{f(\infty)} - 1 + \sin\left(\frac{\theta + 3\pi/2}{2}\right)}{(\cos\theta)^{1/2}} \right]. \quad (9.208)$$

(For the first case (no wall) there should be a brief reference to the subject of optimal coordinates, parabolic cylinder coordinates, and Kaplun's mapping theorem. This case and the round turbulent jet are the only suitable cases.) (**Need composite-flow figures.**)

9.3.5 The boundary-layer approximation

To avoid being overwhelmed by algebraic detail, I propose sometimes to work within the boundary-layer approximation, which discards F , H , P , together with the second momentum equation (9.181) and all of its consequences. On integrating equation (9.180), the remaining Reynolds stress, the shearing stress G , is found to be related to the mean velocity by

$$G = \frac{ff'}{2BC^2} \quad (9.209)$$

or, in physical variables (**sign?**)

$$\overline{u'v'} = \frac{\psi u}{2x} . \quad (9.210)$$

This equation is free of undetermined constants. It does not at all resemble the equation $\overline{u'v'} = -(\mu_t/\rho)\partial u/\partial y$ of the usual eddy-viscosity model or the equation $\overline{u'v'} = -\ell^2(\partial u/\partial y)^2$ of the usual mixing-length model (**discuss**). The result (9.209) can also be obtained from equation 9.186) by discarding terms in η/B and $(\eta/B)^2$. (**Study these approximations.**)

The boundary-layer approximation to (9.189), after terms of order η/B and $(\eta/B)^2$ are discarded, is

$$P + H = -\frac{1}{B} \int_{-\infty}^{\eta} G \, d\eta . \quad (9.211)$$

But G is expressed in terms of f by (9.209), so that also

$$P + H = -\frac{1}{4BC^2} [f^2(\eta) - f^2(\infty)] . \quad (9.212)$$

The physical version of equation (9.211) is (what about (9.212)?)

$$p - p_\infty + \rho \overline{v'v'} = - \int_{-\infty}^{y/x} \rho \overline{u'v'} \, d\frac{y}{x} . \quad (9.213)$$

(**Insert a section on use of eddy viscosity; this gives tanh profile which can be used for fitting. Need to work on integral J. Cite Liepmann for parabolic and hyperbolic models.**)

The boundary-layer approximation has, instead of (9.184) and (9.183),

$$ff' = 8BG , \quad (9.214)$$

$$\int_{-\infty}^{\infty} f' f' \, d\eta = \frac{A^2}{B} . \quad (9.215)$$

The two constants A and B have to be evaluated experimentally. They are connected by (9.14) and by two factors of (9.219), namely

$$\int_{-\infty}^{\infty} u dy = \frac{2}{A} \left(\frac{Jx}{\rho} \right)^{1/2} \quad (9.216)$$

and

$$\int_{-\infty}^{\infty} u dy = \frac{u_c x}{B} . \quad (9.217)$$

(Are these redundant with (9.14)?) (What to do with (9.56) in (9.195)?) The result is

$$\int_{-\infty}^{\infty} \left[f' f' - \frac{f f'}{2\eta} + \frac{4BG}{\eta} \right] d\eta = \frac{A^2}{B} \quad (9.218)$$

which seems a step backward.)

9.3.6 Experimental evidence

The necessary information about turbulent plane jets that must be obtained experimentally includes the two normalizing constants A and B and the functions f , F , G , H , P . Even if the similarity analysis is taken to be rigorously correct, the extraction of this information is a major undertaking. There is the upstream component of velocity in the outer flow to be accounted for. There are problems with various instruments, such as their response to intermittent turbulence and their rectification of signals in the case of stationary hot wires or unbiased LDV probes. Single hot wires are as sensitive to v as to u , especially near the outer edges of the jet flow. My experience has been that hot wires are very difficult instruments at low speeds, say below 50 cm/sec in air. Jet flows in the laboratory are always three-dimensional to some extent, whether the edges are free or are constrained by side walls. Some experimenters report only half profiles, without verifying symmetry. Transition is difficult to detect from the mean-velocity signature alone. Measurable effects of compressibility may be encountered. Finally, there is one extra degree of

freedom in fitting the data to the formulas. This is the origin for the x -coordinate. The functions to be fitted have to be determined as part of the fit.

Papers with mean velocity profiles in turbulent plane jets are listed. Many of these have Reynolds stresses also. The slot aspect ratios vary widely. An important early issue is the effect of side walls and aspect ratio.

BICKNELL (1934)
FORTHMANN (1934, 19A)
REICHARDT (1942, 9A)
HANNUM and GRIFFITH (1955)
MILLER AND COMINGS (1957) 40/1, walls
HESKESTAD (1962) 132/1, walls
OLSON (1962)
KNYSTAUTAS (1964) 98, 127, 192/1, walls
HETSRONI et al (1965)
GOLDSCHMIDT and ESKINAZI (1966) 16/1, walls
SRIDHAR and TU (1966, 19A)
TAILLAND et al (1967)
BETTOLI (1968)
OSEBERG and KLINE (1971)
GOLDSCHMIDT et al (1972)
JENKINS and GOLDSCHMIDT (1973) 24/1, walls
NEWBERT (1973)
DAVIES et al (1974) 6/1, ?
HATTA and NOZAKI (1975) 20, 40, 80/1, walls
KOTSOVINOS (1975, 25A)
PERSEN and SKUAG (1975)
GUTMARK and WYGNANSKI (1976) 38/1, walls
HUSSAIN and CLARK (1977) 44/1, ?
CERULLO (1979)
PERSEN (1981) 20, 200/1, free
CHAMBERS and GOLDSCHMIDT (1982) 48/1, walls
BROWNE et al (1983) 20/1, walls
ELBANNA et al (1983, 17F)

GILBERT (1983)
 GOLDSCHMIDT et al (1983)
 LEMIEUX and OOSTHUIZEN (1985) 58/1, walls
 OTUGEN (1986) 56/1, ?
 THOMPSON (1986)
 BALLAL and CHEN (1987)
 THOMAS and PRAKASH (1991)

A few papers report the static pressure;

BARAT (1954)
 MILLER AND COMINGS (1957)
 KNYSTAUTAS (1964)
 NEWBERT (1973)
 HUSSAIN and CLARK (1977)

Other papers with emphasis on low jet aspect ratio are (see SECTION X and Y ⁷). (The note (xover) means major and minor axes are interchanged.)

van der HEGGE ZIJNEN (1958) 20, 25/1, free 17C
 SFORZA et al (1966) 15E (xover)
 McCABE (1967) 17C
 TRENTACOSTE and SFORZA (1967) 1, 80/1, free 15E, 17C (xover)
 FOSS and JONES (1968) 6/1, walls 17C
 EASTLAKE (1971) 17C (xover)
 GRAY and SHEARER (1971) 17C
 EASTLAKE (1972)
 BOURQUE (1973)
 BASHIR and UBEROI (1975) 20, 40, 140/1, walls
 HOLDEMAN and FOSS (1975) 17C
 SFEIR (1976) 10, 20, 30/1, ? 17C (xover)
 MARSTERS (1979) 15E, 17C
 SFORZA and STASI (1979) 10/1, free 15E, 17C (xover)
 MARSTERS and FOTHERINGHAM (1980) 3, 12/1, free 17C (xover)
 KROTHAPALLI et al (1981) 6, 17/1, ? 17C (xover)

⁷Draft refers to unwritten section of Chapter 8 and this Section (The turbulent plane jet into fluid at rest).

HSIA et al (1983) 17C (xover)
 QUINN et al (1983) 17C
 HUSAIN (1984) 15E (xover)
 POLLARD and IWANIW (1985) 17C
 GILBERT (1986) 17C
 TSUCHIYA et al (1986) 1, 5/1, free 17C (xover)
 GRANDMAISON et al (1987) 10/1, ?
 SARIPALLI (1987)
 POLLARD and SCHWAB (1988) 10/1, free 17C
 QUINN and MILITZER (1988) 17C
 HUSSAIN and HUSAIN (1989) 15E (xover)
 KOSHIGOE et al (1989) 15E (xover)
 MORRISON and SWAN (1989)
 QUINN (1989) 15E (xover)
 HITCHMAN et al (1990) 60/1, free, walls
 QUINN (1990) 15E, 17C (xover)
 QUINN (1991, 1992) 15E, 17C (xover)
 AUSTIN and HO (1992) 15E (xover)

The centerline velocity is

$$u_c = \frac{2B}{A} \left(\frac{J}{\rho x} \right)^{1/2} \quad (9.219)$$

with $f(\infty) = 1$ and $f'(0) = 2$.

Equation (9.14) in physical form is

$$\int_{-\infty}^{\infty} uu \, dy = \frac{J}{\rho} . \quad (9.220)$$

Hence to use (9.78) and (9.79), it is necessary to evaluate the two integrals and to have an effective origin for the streamwise coordinate x . The profiles are assumed to be given as $u(y)$ for fixed x . It may be necessary to correct the tails of the profile for the effect of the v -component, especially if a hot wire is used. As a first try, fit each profile to an assumed curve. A convenient curve is the laminar profile

$$u = u_c \operatorname{sech}^2 [K(y' - y_o)] \quad (9.221)$$

which amounts to assuming a constant eddy viscosity. The fit gives u_c , K , and y_o , the latter in case of experimental unsymmetry. The role of u_c should be checked. If the function is a bad fit near the plane of symmetry, should the experimental value of u_c be used? In the fit, use only data with $u/u_c > 0.4$, to avoid tails. Get also a value for b , the breadth at the half-velocity point $u/u_c = 0.5$.

Check that u_c^2/b is constant, which should be the case if x is large enough. Plot $1/u_c^2$ and b against x and look for a common origin for x . Finally, evaluate the integral in (9.79) and determine B for each station. By now η is known and all the Reynolds stresses can be plotted. Plot B against B/x to see effect of aspect ratio, or use some other method.

Get a preliminary estimate of J/ρ from the integral, with and without the boundary-layer approximation, and check variation with x . Get a value for A and check overall consistency. What can be done about the use of x/D as streamwise variable?

In my own mind I draw a line below equation (15) ⁸.

This line marks a limit defined by the laws of mechanics and a plausible conjecture about the transformation properties of the Reynolds stresses. There are more variables than equations. Of course, a purist would point out that the laws of physics are really represented by the Navier-Stokes equations, which are assumed to govern this and every other flow. The power of large computers allows these equations to be solved, presently only at low Reynolds numbers. The average solution must satisfy equation (15). However, there is no real prospect that mechanisms can be extracted from such data. This line of attack is cumbersome and expensive and is on no more than an equal footing with imaginative experiments. The practitioner of CFD has the equivalent of a blowdown wind tunnel with very short duration but with a vast number of probes.

In any event, I think of everything above the line as relatively permanent and useful. Everything below the line has a short life expectancy.

⁸This reference is unknown

From the analytical point of view, equation (15) is the end of the road until and unless another functional relationship between f (velocity) and g (stress) is introduced. From the experimental point of view, however, equation (15) is a very useful relationship. It allows the force g to be easily inferred from measurements of the acceleration $f f'$. Such an inference, common in this and other shear-flow problems, allows the Reynolds stress τ to be calculated from the measured mean-velocity profile (cite early examples). Since τ can also be measured directly, as $-\rho \overline{u'v'}$, it can be treated as a real quantity. Given good experimental technique, any discrepancies can be examined, for example, in terms of possible three-dimensionality of the mean flow or in terms of weakness in the boundary-layer approximation for flows like the turbulent plane jet which do not grow slowly. Of course, the concept of similarity is not essential to this argument, which is also implicit in the original momentum equation (x).

Comments on handout of 22 Oct.

Andrade. Check out apparent origin. Comment on convergence in plan view as effect of distributed sink felt at edges.

Capell. Read paper carefully to find out what is meant by “logarithmic terms associated with the occurrence of eigensolutions.”

Kraemer. Check on comment that mass and momentum flux are not normal.

Sato. Study for evolution of profile, apparent origin, relevance of fluctuation data for stability theory.

As far as a second relationship between f and g is concerned, two are part of the tradition of the field. First, define an eddy viscosity by

$$\tau = \mu_t \frac{\partial u}{\partial y} \quad (9.222)$$

from which

$$g = \frac{B^2 C}{A} \left(\frac{\mu_t^2}{J \rho x} \right)^{1/2} f'' . \quad (9.223)$$

Thus the function f is again a hyperbolic tangent. However, for similarity to be preserved, two conditions have to be included in the

definition of μ_t ;

(1) μ_t varies like $x^{1/2}$ or like UL ;

(2) μ_t is of order $(J\rho x)^{1/2}$.

Ignorance about turbulent flow has thus been moved from the stress τ to the viscosity μ_t , or the kinematic eddy viscosity $\epsilon_t = \mu_t/\rho$. The hope is that μ_t will follow simpler rules and generate simpler descriptions of the flow. (What are consequences? Note that $\rho U(x)L(x)/\mu_t$ is constant; about 50? same for other flows? Need an argument for order of μ_t/μ . Compare round jet. Can μ_t be treated as a scalar, not a tensor? Note that μ_t is not real in the same sense as τ .)

Second, define a mixing length by

$$\tau = \rho l^2 \left. \frac{\partial u}{\partial y} \right| \left. \frac{\partial u}{\partial y} \right| \quad (9.224)$$

from which (what is solution? Keep an eye out in literature)

$$g = \frac{B^4 C}{A^2} \frac{l^2}{x^2} f'' |f''| \quad (9.225)$$

where now

(1) l varies like x or like L (2) l is of order x (not reasonable).

As an optional problem, propose the simple central [sic] plane ejector. The sketch shows the problem: Note that the jet entrains the whole universe. At least, consider the pressure rise in the potential flow and its effect on the jet. Since the jet will normally be turbulent, it fills the duct at about $x = 6d$. A more realistic picture of the streamlines is There will be a pressure rise across the separation bubble to drive the flow upstream. If the inlet flow is restricted by a valve, the flow may eventually oscillate (Curtet) because of competition between the two sides for entrainment. The oscillation should not occur for the axisymmetric central ejector because of venting around the jet.

(Analysis of jet data: check momentum flux first. Look for evidence of effect of aspect ratio on centerline velocity or growth rate;

latter will give less trouble with apparent origin. Note that intermittency is a more sensitive test of similarity than velocity, but fluctuation level changes rapidly in case of jet. Hot wires become more difficult downstream.)

Comments on handout of 24 October in two large sections.

Reichardt. Four flows; apparently effort to form data collection. No hot-wire data, but similarity under control, including plane wake. Fig. 7 is entrained flow for plane turbulent jet out of wall.

Bradbury. Jet in co-flowing stream. Growth is not linear; mostly behaves like wake. Static pressure. Energy balance. Measured and calculated stress profile. Intermittency. Fluctuations in outer flow OK.

Heskestad. Stress calculated; note disagreement. General indication of hot-wire errors.

Gutmark and Wagnanski. Note small aspect ratio. Note definition of δ ; δ/x is about 0.4. Note rms stresses are about 30 percent. Error in figure 28?

Bashir and Uberoi. Momentum dominates buoyancy.

Katsovinos. Took Ae 204. Does not believe in linear growth.

Goldschmidt and Eskinazi. Scalar contaminant. What about Schmidt number?

Miller and Comings. Figure 5 shows poor technique; Figure 6 shows correction for v at large y . Figure 8 shows large changes in static pressure.

Katsovinos. Problems with conservation of momentum.

Lippisch. Figure 22 shows entrained flow.

Miller and Comings. Figure 4 shows static pressure. Note constant curvature of jet trajectory. Discuss back flow.

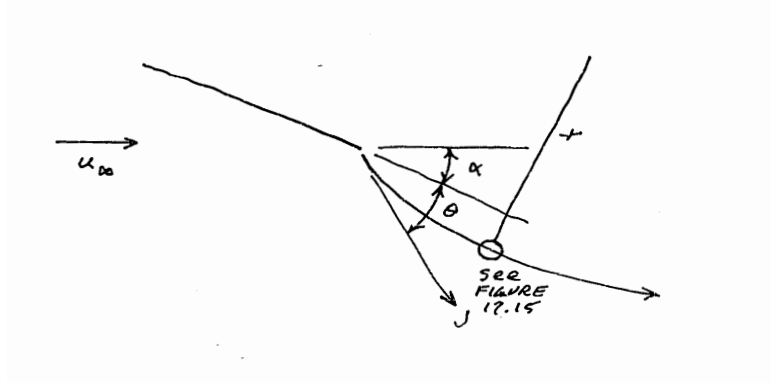


Figure 9.13: Elements of the linearized jet flap.

9.4 Turbulent plane jet into moving fluid

9.5 The jet ejector

9.6 The Coanda effect

9.7 Multiple jets

9.8 The jet flap

9.8.1 Potential flow

The main properties of the pure jet flap were established experimentally and analytically during a few years centered around 1957. Most of this work was done in England, where the linearized potential theory was worked out in an elegant paper by SPENCE (1956) (**mention Dimmock, Davidson, Stratford**). The two-dimensional jet-flap configuration is shown in FIGURE 9.13.⁹ A thin jet issues from the trailing edge of an airfoil at an angle θ with the chord direction.

⁹Figure 17.15 referred to in sketch is Figure 9.14

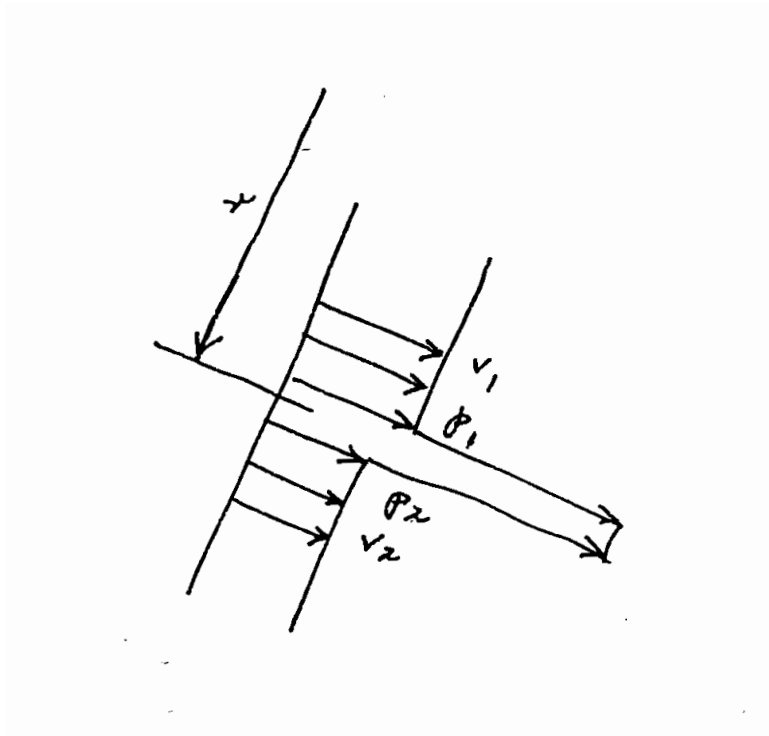


Figure 9.14: Detail of the flow near the jet.

The airfoil itself has an angle of attack α .

Spence. The jet sheet acts in all important respects like an impermeable but flexible extension of the airfoil chord. The position of the jet sheet is not known initially, and has to be found as part of the solution. In Spence's analysis, liberties are also taken with other properties of the sheet, the most important being that mixing is neglected. The jet sheet is taken to be arbitrarily thin, with zero mass flux and finite momentum flux J per unit span.

A model of flow conditions near the jet sheet is shown in FIGURE 9.14. A local radial momentum balance for inviscid flow gives

$$\frac{dp}{dr} = \frac{\rho v^2}{r} \quad (9.226)$$

where v is the velocity in the θ -direction. If the thickness of the jet is small compared to the radius of curvature, an integral across the jet provides what amounts to a jump condition,

$$p_2 - p_1 = \int_1^2 \frac{\rho v^2}{r} dr = \frac{1}{R} \int_1^2 \rho v^2 dr = \frac{J}{r} \quad (9.227)$$

where J is momentum flux per unit span. Since the free-stream flow on the two sides of the jet has the same stagnation pressure, the Bernoulli integral applies,

$$p_1 + \frac{\rho v_1^2}{2} = p_2 + \frac{\rho v_2^2}{2} \quad (9.228)$$

and it follows that

$$\frac{J}{\rho r} = (v_1 - v_2) \frac{(v_1 + v_2)}{2} . \quad (9.229)$$

Note that $p_2 > p_1$ and $v_2 < v_1$. Let the circulation Γ be defined as positive in the clockwise direction, so that $(v_1 - v_2)ds = d\Gamma$, where s is arc length along the jet sheet to the right. For convenience, put $U = (v_1 + v_2)/2$ to obtain (**something wrong with sign?**)

$$\frac{d\Gamma}{ds} = \frac{J}{\rho r U} . \quad (9.230)$$

The jet velocity is assumed to be much larger than the other velocities in the flow field, and the jet fluid has a much larger stagnation pressure. If changes in pressure of order $\rho u_\infty^2/2$ are ignored, the jet momentum J is conserved along the jet sheet. In particular, the jet sheet must become parallel to the free-stream direction at downstream infinity, to ensure finite vertical momentum for the flow field. A balance in the stream direction then requires the full jet momentum, not only the streamwise component at the trailing edge, to be recovered as thrust (**this conclusion was initially controversial; explain**).

A convenient dimensionless form for J is the jet momentum coefficient

$$C_j = \frac{2J}{\rho u_\infty^2} . \quad (9.231)$$

(A more recent notation is C_{μ} .) Equation (9.230) becomes

$$\frac{d\Gamma}{ds} = \frac{C_j u_\infty^2}{2rU} . \quad (9.232)$$

The problem is to determine the position and strength of the jet sheet, together with the distribution of circulation over the airfoil, such that the local velocities are parallel to these two elements of the system. The linearized version of this problem was solved by Spence. The idealized geometry is shown in FIGURE 9.13. There is a leading-edge suction force which ordinarily enforces the condition of zero drag for the airfoil without the jet (**more on this; see Spence**).

In the linearized theory, the airfoil and jet sheet are replaced by a distribution of circulation along the x axis, and the boundary condition is applied there, although it is calculated for the real geometry of the sketch. The linearized boundary condition of tangential flow along the airfoil is

$$\frac{v(x)}{u_\infty} = \frac{dy}{dx} = -\alpha \quad (0 < x < c) \quad (9.233)$$

where α is the angle of attack. The corresponding condition along the jet sheet is

$$\frac{v(x)}{u_\infty} = \frac{dy}{dx} = y'(x) \quad (c < x < \infty) . \quad (9.234)$$

The induced velocity v is defined generally by

$$dv(x) = \frac{d\Gamma(\xi)}{2\pi(\xi - x)} . \quad (9.235)$$

On the airfoil, put (**fix sign**)

$$\frac{1}{u_\infty} \frac{d\Gamma}{dx} = -f(x) . \quad (9.236)$$

On the jet sheet, replace ds in equation (9.232) by dx , U by u_∞ , and $1/r$ by $d^2y/dx^2 = y''$ to obtain

$$\frac{1}{u_\infty} \frac{d\Gamma}{dx} = \frac{C_j}{2} y''(x) . \quad (9.237)$$

In integral form, from equations (9.233)–(9.237),

$$-\frac{1}{2\pi} \int_0^c \frac{f(\xi)d\xi}{\xi-x} + \frac{C_j}{4\pi} \int_c^\infty \frac{y''(\xi)d\xi}{\xi-x} = \begin{cases} -\alpha & (0 < x < c) \\ y'(x) & (c < x < \infty) \end{cases} . \quad (9.238)$$

These are two simultaneous integro-differential equations for $f(x)$ and $y'(x)$, with the additional conditions

$$\begin{aligned} y'(c+) &= -(\alpha + \theta) , \\ y'(\infty) &= 0 . \end{aligned} \quad (9.239)$$

The first of these is equivalent to the usual Kutta condition at the trailing edge (**check**).

The solution depends on three parameters; the angle of attack α , and the direction θ and strength C_j of the jet. The distribution $f(x)$ has the usual square-root singularity at $x = 0$ and a logarithmic singularity at $x = c$. Spence's solution includes contributions from these singularities and from a regular part evaluated as a Fourier series. For the α -dependence, the coefficients are B_n ; for the θ -dependence, the coefficients are A_n . A partial tabulation of these coefficients, which depend on C_j but not on θ or α , is given by Spence.

Among the conclusions:

The lift coefficient to first order is

$$C_L = 4\pi A_o\theta + 2\pi(1 + 2B_o)\alpha . \quad (9.240)$$

For any value of C_j , no matter how small, and for $\theta \neq 0$, the center of pressure moves to mid-chord (**check**). In this sense there is no limiting flow corresponding to the airfoil without jet flap, because the Kutta condition is not correct in the limit (**check**).

In a second paper, SPENCE (1958) showed that for an airfoil with $\alpha = 0$, the lift is

$$C_L = 2(\pi C_j)^{1/2}\theta . \quad (9.241)$$

Analytical papers on jet flap;

KORBACHER (1960)

WYGNANSKI (1966)
 HEROLD (1973)
 HALSEY (1974)

9.8.2 Experiment

Experimental papers on jet flap;

SCHUBAUER (1933)
 DIMMOCK (1957)
 FOLEY and REID (1959)
 TSONGAS (1962)
 QUANBECK (1963)
 HACKETT and LYMAN (1973)
 BEVILAQUA et al (1984)

(Read Siestrunk, Korbacher again.)

(Read Foley, Tsongas, Quanbeck.)

(Study Bevilaqua et al. and references therein.)

(See paper by Maskell and Gates on validity of $L = \rho u_\infty \Gamma$.)

(supplement)

The jet flap has an upper limit when separation occurs at the leading edge or elsewhere.

The jet flap was discovered more or less accidentally by two Germans in 1938 (try to get a copy; see also Schubauer). Instead of gap, blow from the knee of the flap.

Difficulties: part of the wing volume is needed for ducting; single-engine-out failure; aft shift of center of pressure; ground effect; separation at leading edge.

In radius of curvature, dy/dx is not necessarily small; it may be ∞ if the jet is straight down.

Should cy'' replace y'' to get a dimensionless variable?

Should have included in handout Spence's curves of $\partial C_L/\partial\theta$ and $\partial C_L/\partial\alpha$. Do these reduce to free airfoil with $\partial C_L/\partial\alpha = 2\pi$ when $C_j = 0$?

Look up actual current applications of jet flaps in general terms; advantages and disadvantages.

One last point about Spence's paper. The derivative $\partial C_L/\partial\alpha$ is finite at $C_j = 0$, and is probably 2π . If so, the correct Kutta condition is probably built into the method used to handle the singularity at the jet origin. (Check this.)

Foley: the inviscid argument for the induced-drag correction in the open-jet tunnel is quite plausible, as worked out in the sketch.

This requires assigning a high lift without the jet. Such a condition cannot be realized experimentally. The data look good; 94 percent of the jet momentum is recovered as thrust. At any rate, if the measured drag (negative) is corrected by adding $0.94 C_L^2$, a straight line with very little scatter is obtained. The remaining 6 percent may be caused by entrainment into the jet. Note also surveys showing wake thickness. Dotted line is direction of reaction force with jet on and tunnel off; the direction of the jet is not accurately known. The thrust recovery can be strongly affected by separation on the forward part of the airfoil; see Bevilaqua. In the wake survey, check $p + \overline{\rho v'v'} = \text{constant}$. Is C_j a ratio of dynamic pressures? What about ratios less than one?

9.9 The radial jet

9.9.1 Dimensional preamble

For the purposes of this section, a radial jet is a flat jet with its maximum velocity lying in a plane normal to an axis of symmetry, as shown at the right in FIGURE X.¹⁰ The radial free jet is not technically important, and the laminar case has never been studied experimentally. The technically important flow is the radial wall jet, especially the turbulent wall jet discussed at length in SEC-

¹⁰This reference is to an unknown figure.

TION 10.4.1. My primary purpose here is to put in evidence an elegant transformation between the boundary-layer approximations for plane and radial flows. The transformation, originally discovered by Mangler (1948), is rigorous for strictly laminar flow and can also be demonstrated formally for strictly turbulent flow. It is of uncertain value for flows such as the turbulent wall jet in which both laminar and turbulent transport mechanisms are active simultaneously, such as the turbulent radial wall jet.

Begin with the usual similarity argument. In cylindrical coordinates (r, θ, z) , with velocity components $(\check{u}, \check{v}, \check{w})$, the boundary-layer approximation for flat radial flow, laminar or turbulent, is

$$\frac{1}{r} \frac{\partial r \check{u}}{\partial r} + \frac{\partial \check{w}}{\partial z} = 0 \quad , \quad (9.242)$$

$$\rho \left(\check{u} \frac{\partial \check{u}}{\partial r} + \check{w} \frac{\partial \check{u}}{\partial z} \right) = \frac{\partial \check{\tau}}{\partial z} \quad , \quad (9.243)$$

where the breve is a mnemonic symbol used with the parameters and dependent variables of the radial flow. In particular,

$$\check{\tau} = \mu \frac{\partial \check{u}}{\partial z} - \rho \overline{\check{u}' \check{w}'} \quad . \quad (9.244)$$

The stream function for the radial flow follows from the condition that the flow lies in planes $\theta = \text{constant}$; thus

$$\vec{\check{u}} = \begin{pmatrix} \check{u} \\ \check{v} \\ \check{w} \end{pmatrix} = -\text{grad } \check{\psi} \times \text{grad } \theta \quad . \quad (9.245)$$

This definition includes a change of sign to accommodate the Mangler transformation (**could use order** (r, z, θ) ; **think again**). Calculation gives

$$\vec{\check{u}} = - \begin{vmatrix} \vec{i}_r & \vec{i}_\theta & \vec{i}_z \\ \frac{\partial \check{\psi}}{\partial r} & \frac{1}{r} \frac{\partial \check{\psi}}{\partial \theta} & \frac{\partial \check{\psi}}{\partial z} \\ 0 & \frac{1}{r} & 0 \end{vmatrix} = \begin{pmatrix} \frac{1}{r} \frac{\partial \check{\psi}}{\partial z} \\ 0 \\ -\frac{1}{r} \frac{\partial \check{\psi}}{\partial r} \end{pmatrix} \quad , \quad (9.246)$$

or

$$r\check{u} = \frac{\partial\check{\psi}}{\partial z} , \quad r\check{w} = -\frac{\partial\check{\psi}}{\partial r} . \quad (9.247)$$

It will be important that the stream function has different dimensions in the plane and radial flows.

The integral invariant of the radial problem is obtained in the usual way. Multiply equation (9.242) by $\rho\check{u}r$ and equation (9.243) by r and add. The result is

$$\rho \left(\frac{\partial r\check{u}\check{u}}{\partial r} + \frac{\partial r\check{u}\check{w}}{\partial z} \right) = r \frac{\partial\check{\tau}}{\partial z} . \quad (9.248)$$

Integrate from $-\infty$ to ∞ in z and use the boundary conditions

$$\check{u}(r, \pm\infty) = 0, \quad \check{\tau}(r, \pm\infty) = 0 \quad (9.249)$$

to obtain

$$\rho \frac{d}{dr} \int_{-\infty}^{\infty} r\check{u}\check{u}dz = 0 , \quad (9.250)$$

or

$$\rho r \int_{-\infty}^{\infty} \check{u}\check{u}dz = \text{constant} = \check{J} . \quad (9.251)$$

Strictly speaking, the integration should be carried out with respect to both z and θ on a cylindrical surface $r = \text{constant}$. However, I prefer to suppress the resulting factor 2π in the special context of the Mangler transformation. Thus \check{J} in equation (9.251) for the radial jet is radial momentum flux per radian.

9.9.2 Laminar similarity

Assume that global scales \mathbf{M} , \mathbf{L} , \mathbf{T} can be formed from the three parameters of the problem, \check{J} , ρ , and μ , which have dimensions

$$[\check{J}] = \frac{\mathbf{ML}}{\mathbf{T}^2} , \quad [\rho] = \frac{\mathbf{M}}{\mathbf{L}^3} , \quad [\mu] = \frac{\mathbf{M}}{\mathbf{LT}} . \quad (9.252)$$

Elimination of \mathbf{M} gives

$$\left[\frac{\check{J}}{\rho} \right] = \frac{\mathbf{L}^4}{\mathbf{T}^2} , \quad \left[\frac{\mu}{\rho} \right] = \frac{\mathbf{L}^2}{\mathbf{T}} . \quad (9.253)$$

Evidently the assumption is wrong. The dimensional parameters of the radial flow do not define global scales \mathbf{M} , \mathbf{L} , \mathbf{T} separately, as they did in the plane problem. Instead, the parameters collapse to a single dimensionless quantity,

$$\frac{\check{J}}{\rho\nu^2} = \text{constant} , \quad (9.254)$$

which has the nature of the square of a Reynolds number. Recall from SECTION 9.1.3 that there is only one laminar plane jet. However, laminar radial jets form a single-parameter family, with $\check{J}/\rho\nu^2$ as parameter. In the analysis that follows, it will be seen that this parameter automatically incorporates itself in the variables of the similarity solution. (**Exact solution of N-S equations? See Squire.**) Because there does not exist a global length scale \mathbf{L} , the laminar radial jet is constrained to grow linearly with r . Because there does exist a global scale for the combination $\mathbf{L}^2/\mathbf{T} = \mathbf{UL} = \nu$, the global Reynolds number is again unity;

$$\frac{\mathbf{UL}}{\nu} = 1 . \quad (9.255)$$

Now search for a laminar similarity solution of the boundary-layer equations by the method of local scales $\check{U}(r)$ and $\check{L}(r)$. The solution is wanted in the form $\check{u}/\check{U} = g(z/\check{L})$, which does not assume linear growth. The appropriate ansatz, according to the first of equations (9.247), is

$$\frac{\check{\psi}}{r\check{U}\check{L}} = \check{f}\left(\frac{z}{\check{L}}\right) = \check{f}(\check{\eta}) . \quad (9.256)$$

Substitution of this ansatz in the momentum equation (9.243) and in the integral invariant (9.251) yields the equations

$$\check{f}''' + \frac{\check{L}}{\nu r} \frac{dr\check{U}\check{L}}{dr} \check{f}\check{f}'' - \frac{\check{L}^2}{\nu} \frac{d\check{U}}{dr} \check{f}'\check{f}' = 0 , \quad (9.257)$$

$$\rho r \check{U}^2 \check{L} \int_{-\infty}^{\infty} \check{f}' \check{f}' d\check{\eta} = \check{J} . \quad (9.258)$$

Consequently, three necessary conditions for similarity are

$$\frac{\check{L}}{\nu r} \frac{dr \check{U} \check{L}}{dr} = \text{constant} , \quad \frac{\check{L}^2}{\nu} \frac{d\check{U}}{dr} = \text{constant} , \quad r \check{U}^2 \check{L} = \text{constant} . \quad (9.259)$$

One of these equations is redundant, because any two imply the third. They are satisfied by $\check{L} \sim r$, $\check{U} \sim 1/r$, from which $\check{U} \check{L} = \text{constant} = \nu$, say. The ansatz (9.256) becomes

$$\check{A} \frac{\check{\psi}}{\nu r} = \check{f} \left(\check{B} \frac{z}{r} \right) = \check{f}(\check{\eta}) , \quad (9.260)$$

where \check{A} and \check{B} are constants provided for later normalization. In similarity variables, the momentum equation (9.243) takes the form

$$\check{A} \check{B} \check{f}''' + \check{f} \check{f}'' + \check{f}' \check{f}' = 0 , \quad (9.261)$$

with boundary conditions

$$\check{f}(0) = 0, \quad \check{f}'(\pm\infty) = 0, \quad \check{f}''(\pm\infty) = 0 , \quad (9.262)$$

and the integral invariant (9.251) takes the form

$$\int_{-\infty}^{\infty} \check{f}' \check{f}' d\check{\eta} = \frac{\check{A}^2}{\check{B}} \frac{\check{J}}{\rho \nu^2} , \quad (9.263)$$

in which the single parameter $\check{J}/\rho \nu^2$ appears explicitly.

Now turn to the second and more complete argument for similarity, based on the idea of an affine transformation. Consider the

group

$$\begin{aligned}
 r &= a\widehat{r} \\
 z &= b\widehat{z} \\
 \check{\psi} &= c\widehat{\psi} \\
 \rho &= d\widehat{\rho} \\
 \mu &= e\widehat{\mu} \\
 \check{J} &= j\widehat{J} \\
 \check{u} &= \frac{c}{ab}\widehat{u} \\
 \check{w} &= \frac{c}{a^2}\widehat{w} ,
 \end{aligned} \tag{9.264}$$

where the last two lines reflect the relations between velocity and stream function in equations (9.247). The invariants of the affine transformation, from equation (9.243) with $\check{\tau}$ replaced by $\mu\partial\check{u}/\partial z$, and from equation (9.251), are

$$\frac{bcd}{a^2e} = 1, \quad \frac{c^2d}{abj} = 1 . \tag{9.265}$$

Solved for b and c , these become

$$\frac{b^3dj}{a^3e^2} = 1, \quad \frac{c^3d^2}{a^3ej} = 1 . \tag{9.266}$$

The complete similarity ansatz for the laminar radial jet is therefore

$$\check{A}\left(\frac{\rho\nu^2}{\check{J}}\right)^{1/3} \frac{\check{\psi}}{\nu r} = \check{f}\left[\check{B}\left(\frac{\check{J}}{\rho\nu^2}\right)^{1/3} \frac{z}{r}\right] = \check{f}(\check{\eta}) . \tag{9.267}$$

This form, like equation (9.260), verifies the conclusion drawn earlier about linear growth. It also shows explicitly how the single parameter $\check{J}/\rho\nu^2$ enters into the independent and dependent similarity variables by changing the constants \check{A} and \check{B} in the earlier ansatz (9.260) without changing their product. With this modified ansatz, the equation and boundary conditions satisfied by \check{f} are again equations (9.261) and (9.262). The factor $\check{J}/\rho\nu^2$ disappears from the right-hand side of equation (9.263), which becomes

$$\int_{-\infty}^{\infty} \check{f}' \check{f}' d\check{\eta} = \frac{\check{A}^2}{\check{B}} . \quad (9.268)$$

An analysis parallel to the one in SECTION 9.1.3 for the laminar plane jet can be carried out for the laminar radial jet. Equation (9.261) has the integral

$$\check{f} = \check{C} \tanh \left(\frac{\check{C}\check{\eta}}{2\check{A}\check{B}} \right) , \quad (9.269)$$

where $\check{C} = \check{f}(\infty)$ is a constant of integration. Substitution for \check{f} in equation (9.267) leads to

$$\frac{2\check{A}}{\check{C}} \left(\frac{\rho\nu^2}{\check{J}} \right)^{1/3} \frac{\check{\psi}}{2\nu r} = \tanh \left[\frac{\check{C}}{2\check{A}} \left(\frac{\check{J}}{\rho\nu^2} \right)^{1/3} \frac{z}{r} \right] . \quad (9.270)$$

Canonical dimensionless variables again suggest themselves;

$$\check{\Psi} = \frac{\check{\psi}}{2\nu\lambda} , \quad (9.271)$$

$$R = \frac{\check{C}}{2\check{A}} \left(\frac{\check{J}}{\rho\nu^2} \right)^{1/3} \frac{r}{\lambda} , \quad (9.272)$$

$$Z = \frac{\check{C}}{2\check{A}} \left(\frac{\check{J}}{\rho\nu^2} \right)^{1/3} \frac{z}{\lambda} . \quad (9.273)$$

Consequently,

$$\frac{\check{\Psi}}{R} = \tanh \left[\frac{\check{C}}{2\check{A}} \left(\frac{\check{J}}{\rho\nu^2} \right)^{1/3} \frac{Z}{R} \right]. \quad (9.274)$$

Two comments are needed here. First, I have introduced an arbitrary length λ in equations (9.271)–(9.273) for dimensional reasons. The geometrical effect is a zoom transformation. The physical effect is null, because λ cancels out everywhere. Second, I have looked at the possibility of incorporating the factor $(\check{C}/2\check{A})(\check{J}/\rho\nu^2)^{1/3}$ in equation (9.274) into the variable Z , so that the argument of \tanh becomes simply Z/R . There is then only one flow pattern, and only one jet. However, this pattern is very unphysical. The region occupied by the jet is a sector with a total included angle of more than two radians. I consider that a much more sensible choice is to make the boundary layer approximation apparent by using the same scale for z and r , so that an increase in the value of the parameter $\check{J}/\rho\nu^2$ (the Reynolds number) is accompanied by a visible thinning of the jet.

As in the plane case, the ratio \check{C}/\check{A} in these equations is not negotiable. When the particular function \check{f} from equation (9.269) is used to evaluate the integral in the constraint equation (9.268), the result is

$$\int_{-\infty}^{\infty} \check{f}' \check{f}' d\eta = \frac{2}{3} \frac{\check{C}^3}{\check{A}\check{B}}. \quad (9.275)$$

Comparison of this expression with the general form (9.268) shows that the ratio \check{C}/\check{A} has the numerical value

$$\frac{\check{C}}{\check{A}} = \left(\frac{3}{2} \right)^{1/3}. \quad (9.276)$$

The canonical space variables (9.272) and (9.273) can therefore be rewritten as

$$R = \left(\frac{3}{16} \frac{\check{J}}{\rho\nu^2} \right)^{1/3} \frac{r}{\lambda}, \quad (9.277)$$

$$Z = \left(\frac{3}{16} \frac{\check{J}}{\rho\nu^2} \right)^{1/3} \frac{z}{\lambda} , \quad (9.278)$$

for use in

$$\check{\Psi} = \check{\Psi}_i = R \tanh \left[\left(\frac{3}{16} \frac{\check{J}}{\rho\nu^2} \right)^{1/3} \frac{Z}{R} \right] . \quad (9.279)$$

The subscript i identifies the stream function as part of an inner or boundary-layer solution.

Single streamlines from equation (9.279) are shown in FIGURE X ¹¹ for several values of the parameter $\check{J}/\rho\nu^2$, and a full streamline pattern is shown in FIGURE Y ¹² for the particular value

$$\frac{\check{J}}{\rho\nu^2} = 10^3 . \quad (9.280)$$

The boundary-layer streamlines in the latter figure are related by a zoom transformation. SQUIRE (1955) was the first to point out the property of linear growth. He also noted that streamlines close to the plane of symmetry are straight and parallel to this plane, since Ψ_i is proportional to Z for small Z/R .

9.9.3 The Mangler transformation

The laminar radial jet can also be investigated with the aid of a transformation between plane and radial flows that has nothing to do with the affine transformation just discussed. The boundary-layer approximation for the plane case is conveniently identified by using an overbar for the parameters and dependent variables of the plane geometry;

$$\frac{\partial \bar{u}}{\partial x} + \frac{\partial \bar{v}}{\partial y} = 0 , \quad (9.281)$$

$$\rho \left(\bar{u} \frac{\partial \bar{u}}{\partial x} + \bar{v} \frac{\partial \bar{u}}{\partial y} \right) = \frac{\partial \bar{\tau}}{\partial y} , \quad (9.282)$$

¹¹Unknown reference.

¹²Unknown reference.

where

$$\bar{\tau} = \mu \frac{\partial \bar{u}}{\partial y} - \rho \bar{u}' \bar{v}' . \quad (9.283)$$

The stream function for the plane flow is the usual one;

$$\bar{u} = \frac{\partial \bar{\psi}}{\partial y}, \quad \bar{v} = -\frac{\partial \bar{\psi}}{\partial x} . \quad (9.284)$$

I leave it as an exercise to show that the plane continuity and momentum equations (9.281) and (9.282) are transformed into the radial equations (9.242) and (9.243) of SECTION 9.9.1, and conversely, by the transformation

$$\begin{aligned} \bar{\psi} &= \frac{\check{\psi}}{\lambda} & \check{\psi} &= \lambda \bar{\psi} \\ \bar{u} &= \check{u} & \check{u} &= \bar{u} \\ \bar{v} &= \frac{r}{\lambda} \frac{dr}{dx} \left(\check{w} + \frac{z}{r} \check{u} \right) & \check{w} &= \frac{\lambda}{r} \left(\frac{dx}{dr} \bar{v} - \frac{y}{r} \bar{u} \right) \\ x &= x(r) & r &= r(x) \\ y &= \frac{r}{\lambda} z & z &= \frac{\lambda}{r} y \\ \bar{\tau} &= \frac{r}{\lambda} \frac{dr}{dx} \check{\tau} & \check{\tau} &= \frac{\lambda}{r} \frac{dx}{dr} \bar{\tau} . \end{aligned} \quad (9.285)$$

As in the preceding SECTION 9.9.2, the notation recognizes that $\bar{\psi}$ and $\check{\psi}$ have different dimensions by introducing at the outset an arbitrary constant length λ that must drop out in the final description of either flow. Lagerstrom used to refer to such lengths as “the length of the blackboard.” For simplicity, the density ρ and viscosity μ are taken to be the same for the two flows, which are both stipulated to be real; i.e., observable in a laboratory. The boundary conditions must also satisfy the transformation.

For laminar flow, my transformation (9.285) is a special case of the MANGLER transformation (1948), which was originally developed for laminar boundary layers on bodies of revolution in a compressible fluid. My transformation is more general in one respect, because it does not specify a laminar or turbulent mechanism for the shearing stress τ . Mangler does not say how he discovered his transformation, and he is not required to say, of course, as long as the transformation can be verified directly. I was able to derive equations (9.285) independently by using the same methods that are described in my paper of 1964 on the problem of transforming a turbulent boundary layer in a compressible fluid into an equivalent turbulent boundary layer in a fluid of constant density. That effort failed, I now believe, because viscous and turbulent transport, when they are both present, can never be transformed by the same rule. The present effort will eventually encounter the same problem in the case of the turbulent radial wall jet, discussed in SECTION 10.4.1. **(can this be fixed?)**

For laminar flow, the condition on the shearing stress is $\check{\tau} = \mu \partial \check{u} / \partial z$, $\bar{\tau} = \mu \partial \bar{u} / \partial y$, with $\partial \bar{u} / \partial y = (\lambda/r) \partial \check{u} / \partial z$. Hence $\bar{\tau} / \check{\tau} = \lambda/r$. At the same time, $\bar{\tau} / \check{\tau} = (r/\lambda) dr/dx$, from the last of equations (9.285). Consequently,

$$r^2 \frac{dr}{dx} = \lambda^2 \quad \text{and} \quad x = \frac{r^3}{3\lambda^2} . \quad (9.286)$$

Given the Mangler transformation, the position is that everything that is known analytically or experimentally about the plane case, laminar or turbulent, can be immediately adduced for the corresponding radial case, and conversely. It is easy to verify this position for laminar flow, using the relations (9.285) as modified by equa-

tion (9.286). The modified relations are

$$\begin{aligned}\bar{\psi} &= \frac{\check{\psi}}{\lambda} \\ \bar{u} &= \check{u} \\ \bar{v} &= \frac{\lambda}{r} \left(\check{w} + \frac{z}{r} \check{u} \right) \\ x &= \frac{r^3}{3\lambda^2} \\ y &= \frac{r}{\lambda} z .\end{aligned}\tag{9.287}$$

Suppose therefore that nothing is known about the radial jet flow except for the limited material in the dimensional preamble, SECTION 9.9.1 above, and turn instead to the transformation (9.287). First, transform the integral invariant \bar{J} , which is defined for the plane jet by equation (9.251);

$$\bar{J} = \rho \int_{-\infty}^{\infty} \bar{u}\bar{u}dy = \frac{1}{\lambda} \rho r \int_{-\infty}^{\infty} \check{u}\check{u}dz = \frac{\check{J}}{\lambda} .\tag{9.288}$$

Using this result, assume that $\check{f} = \bar{f}$ and $\check{\eta} = \bar{\eta}$, and transform the ansatz (9.37) for the plane or barred flow,

$$\bar{A} \left(\frac{\rho}{\bar{J}\nu x} \right)^{1/3} \bar{\psi} = \bar{f} \left[\bar{B} \left(\frac{\bar{J}}{\rho\nu^2 x^2} \right)^{1/3} y \right] = \bar{f}(\bar{\eta}) ,\tag{9.289}$$

into

$$\bar{A} \left(\frac{3\rho\nu^2}{\check{J}} \right)^{1/3} \frac{\check{\psi}}{\nu r} = \check{f} \left[\bar{B} \left(\frac{9\check{J}}{\rho\nu^2} \right)^{1/3} \frac{z}{r} \right] = \check{f}(\check{\eta}) .\tag{9.290}$$

The last equation coincides with equation (9.267) provided that

$$\begin{aligned}\check{A} &= 3^{1/3} \bar{A} \\ \check{B} &= 3^{2/3} \bar{B}\end{aligned}\tag{9.291}$$

$$\check{C} = \bar{C}$$

where $\check{C} = \check{f}(\infty) = \bar{f}(\infty) = \bar{C}$. Hence the differential equation (9.261) and the constraint (9.268) are recovered. Proceed to the solution (9.47),

$$\bar{f} = \bar{C} \tanh\left(\frac{\bar{C}}{6\bar{A}\bar{B}} \bar{\eta}\right),\tag{9.292}$$

which turns into equation (9.269),

$$\check{f} = \check{C} \tanh\left(\frac{\check{C}}{2\check{A}\check{B}} \check{\eta}\right).\tag{9.293}$$

The normalizing condition (9.54),

$$\left(\frac{\bar{C}}{6\bar{A}}\right)^3 = \frac{1}{48},\tag{9.294}$$

becomes

$$\left(\frac{\check{C}}{2\check{A}}\right)^3 = \frac{3}{16},\tag{9.295}$$

as it should. Finally, the canonical variables (9.55) for the plane case,

$$\bar{\Psi} = \frac{\bar{\psi}}{6\nu}, \quad X = \frac{\bar{J}x}{48\rho\nu^2}, \quad Y = \frac{\bar{J}y}{48\rho\nu^2},\tag{9.296}$$

turn into

$$\bar{\Psi} = \frac{\check{\Psi}}{3}, \quad X = \left(\frac{R}{3}\right)^3, \quad Y = \left(\frac{3}{16} \frac{\check{J}}{\rho\nu^2}\right)^{1/3} \frac{R}{3} \frac{Z}{3},\tag{9.297}$$

where $\check{\Psi}$, R , and Z are the combinations defined in equations (9.271), (9.277), and (9.278), respectively. Substitution in equation (9.52),

$$\bar{\Psi} = X^{1/3} \tanh \left(\frac{Y}{X^{2/3}} \right), \quad (9.298)$$

yields

$$\frac{\check{\Psi}}{3} = \frac{R}{3} \tanh \left[\left(\frac{3}{16} \frac{\check{J}}{\rho \nu^2} \right)^{1/3} \frac{Z}{3} / \frac{R}{3} \right] \quad (9.299)$$

which is the same as equation (9.279) except that $\check{\Psi}$, R , Z are all multiplied by a factor $1/3$, *vice* $1/\lambda$. This factor cancels identically.

Two other relationships that have not so far been stated will be needed in the next section. These are the velocity components, which are defined for the plane case by equations (9.38) and (9.39);

$$\bar{u} = \frac{\bar{B}}{\bar{A}} \left(\frac{\bar{J}^2}{\rho^2 \nu x} \right)^{1/3} \bar{f}', \quad (9.300)$$

$$\bar{v} = \frac{1}{3\bar{A}} \left(\frac{\bar{J}\nu}{\rho x^2} \right)^{1/3} (\bar{f} - 2\bar{\eta}\bar{f}'). \quad (9.301)$$

Transformed, these become

$$\check{u} = \frac{\check{B}}{\check{A}} \frac{\nu}{r} \left(\frac{\check{J}}{\rho \nu^2} \right)^{2/3} \check{f}', \quad (9.302)$$

$$\check{v} = \frac{1}{\check{A}} \frac{\nu}{r} \left(\frac{\check{J}}{\rho \nu^2} \right)^{1/3} (\check{f} - \check{\eta}\check{f}'). \quad (9.303)$$

These relations can also be obtained, by differentiation of equation (9.267).

(What is the maximum velocity on a stream tube?)

9.9.4 Entrainment and composite flow

The method of conformal mapping is not available to determine the outer potential flow representing entrainment into the laminar radial jet. Neither is the Mangler transformation, which applies only to the inner or boundary-layer solution. It is therefore necessary to calculate directly the flow due to an equivalent sink distribution. Equation (9.303) gives the axial component of velocity $w_i(r, z)$ within the body of the jet. A suitable matching condition for construction of a composite flow is therefore

$$\check{w}_i(r, \infty) = -\frac{\check{C}\nu}{\check{A}r} \left(\frac{\check{J}}{\rho\nu^2} \right)^{1/3} = \check{w}_o(r, 0) , \quad (9.304)$$

where again $\check{C} = \check{f}(\infty)$.

To calculate the outer flow, use the geometry and notation shown in FIGURE X. The volume flux dQ per unit time from a small element of surface at $(\rho, \theta, 0)$ can be expressed in two ways;

$$dQ = 2\check{w}_i(\rho, \infty)\rho d\rho d\theta = 4\pi s^2 dq , \quad (9.305)$$

where $4\pi s^2$ is the area of a sphere of radius s surrounding the source element, and dq is the increment of outward velocity through the spherical surface. The geometry of the sketches also provides the relations

$$\sigma^2 = r^2 + \rho^2 - 2r\rho \cos \theta = s^2 - z^2 \quad (9.306)$$

and

$$\frac{d\check{w}_o}{dq} = \frac{z}{s} . \quad (9.307)$$

These equations are sufficient to determine $w_o(r, z)$ as a definite integral. After some manipulation, there is obtained (**check: should not vanish at $z = 0$.**)

$$\check{w}_o(r, z) = -\frac{\check{C}\nu}{\check{A}\pi} \left(\frac{\check{J}}{\rho\nu^2} \right)^{1/3} \frac{z}{r^2} \int_0^\pi \int_0^\infty \frac{dx d\theta}{\left(1 + \frac{z^2}{r^2} + x^2 - 2x \cos \theta \right)^{3/2}} , \quad (9.308)$$

where x stands for ρ/r .

With some effort, the integral can be evaluated in closed form. A different and more amiable procedure was suggested by one of my students. The desired flow is axially symmetric and irrotational, with

$$\text{curl } \vec{u} = -\text{curl} (\text{grad } \check{\psi}_o \times \text{grad } \theta) = 0 \quad (9.309)$$

The outer stream function in cylindrical polar coordinates satisfies the equation

$$r \frac{\partial}{\partial r} \frac{1}{r} \frac{\partial \check{\psi}_o}{\partial r} + \frac{\partial^2 \check{\psi}_o}{\partial z^2} = 0 \quad (9.310)$$

and the axial velocity $\check{w}_o = -(1/r)\partial\psi_o/\partial r$ satisfies the Laplace equation,

$$\frac{1}{r} \frac{\partial}{\partial r} r \frac{\partial \check{w}_o}{\partial r} + \frac{\partial^2 \check{w}_o}{\partial z^2} = 0 . \quad (9.311)$$

Now note that equation (9.308) is of the form

$$\check{w}_o(x, z) = \frac{1}{r} g\left(\frac{z}{r}\right) = \frac{1}{r} g(n) . \quad (9.312)$$

Substitution in equation (9.311) for \check{w}_o yields

$$(1 + n^2) g'' + 3 n g' + g = 0 . \quad (9.313)$$

The integral of this equation that is regular at $n = \infty$ is

$$g = \frac{\text{constant}}{(1 + n^2)^{1/2}} . \quad (9.314)$$

When this quantity is put in equation (9.312) and the result is compared with the matching condition (9.304), there is obtained

$$\check{w}_o(r, z) = -\frac{\check{C}\nu}{\check{A}} \left(\frac{\check{J}}{\rho\nu^2} \right)^{1/3} \frac{1}{(r^2 + z^2)^{1/2}} . \quad (9.315)$$

One more integration gives the outer stream function,

$$\check{\psi}_o(r, z) = \frac{\check{C}\nu}{\check{A}} \left(\frac{\check{J}}{\rho\nu^2} \right)^{1/3} \left[(r^2 + z^2)^{1/2} - z \right] . \quad (9.316)$$

This expression for the outer flow can be put in canonical form, for combination with the boundary-layer expression (9.279);

$$\Psi_o = R \left[\left(1 + \frac{Z^2}{R^2} \right)^{1/2} - \frac{Z}{R} \right]. \quad (9.317)$$

The composite expansion adds the inner representation (9.270) and the outer representation (9.316) and subtracts the common part;

$$\begin{aligned} \check{\psi}_c = \frac{\check{C}\nu r}{\check{A}} \left(\frac{\check{J}}{\rho\nu^2} \right)^{1/3} \left\{ \tanh \left[\frac{\check{C}}{2\check{A}} \left(\frac{\check{J}}{\rho\nu^2} \right)^{1/3} \frac{z}{r} \right] \right. \\ \left. + \left[\left(1 - \frac{z^2}{r^2} \right)^{1/2} - \frac{z}{r} \right] - 1 \right\}. \quad (9.318) \end{aligned}$$

In canonical variables, this is

$$\begin{aligned} \check{\psi}_c = R \left\{ \tanh \left[\frac{3}{16} \left(\frac{\check{J}}{\rho\nu^2} \right)^{1/3} \frac{Z}{R} \right] \right. \\ \left. + \left[\left(1 - \frac{Z^2}{R^2} \right)^{1/2} - \frac{Z}{R} \right] - 1 \right\}. \quad (9.319) \end{aligned}$$

The composite streamlines from equation (9.319) are shown in FIGURE X for $J/\rho\nu^2 = 10^3$.

(What is the angle of the outer streamlines at the plane of symmetry? See Squire for exact solution.)

9.9.5 Turbulent similarity

The relationship $x(r)$ or $r(x)$ is different if the two flows being compared are laminar or if they are turbulent. This property prevents thinking of turbulent plane and radial wall jets in SECTION X below as being related in the same way as the corresponding free jets, because of the mixed transport mechanisms in the presence of a wall. However, it does not prevent use of the free jet as a rough model for the wall jet in either geometry.

Some assumption is required to define the Mangler transformation for the case of turbulent flow. If $\check{\tau}$ scales or transforms like $\rho\check{u}_c^2$, where \check{u}_c is the mean velocity in the plane of symmetry, then in the notation of equation (9.178) for the plane jet

$$\check{\tau} = -\overline{\rho\check{u}'\check{w}'} = -\rho\check{u}_c^2\check{G}(\check{\eta}) . \quad (9.320)$$

Transformation gives

$$\bar{\tau} = -\overline{\rho\bar{u}'\bar{v}'} = -\rho\bar{u}_c^2\bar{G}(\bar{\eta}) . \quad (9.321)$$

If the dimensionless Reynolds stresses and hence the two functions \check{G} and \bar{G} are the same at corresponding points, then $\tau = \bar{\tau}$. From the last of equations (9.285), $d\bar{x}/dr = r/\lambda$, and therefore, since $\check{u}_c = \bar{u}_c$,

$$\bar{x} = \frac{r^2}{2\lambda} . \quad (9.322)$$

An immediate consequence is that at corresponding points

$$\frac{z}{r} = \frac{1}{2} \frac{y}{x} , \quad (9.323)$$

so that the turbulent radial jet should grow at half the rate of the turbulent plane jet. This conclusion can be tested experimentally (**do so**). (**Who else had this? See Tritton.**)

Alternatively, if the two jets grow at the same rate, with $z/r = y/x$ at corresponding points, then

$$x = \frac{r^2}{\lambda} \quad (9.324)$$

and $\check{\tau} = 2\bar{\tau}$. If the two flows grow at the same rate, the Reynolds shearing stress, and presumably also the Reynolds normal stresses for the turbulent radial jet, when made dimensionless with $\rho\check{u}_c^2$, should be twice as large as those for the turbulent plane jet.

Neither of the hypotheses just stated is supported by experimental data. However, there is another way to state the problem. The last two lines of the transform table (9.285) both contain the

arbitrary length λ . If this length is eliminated, the ratio of shearing stress to growth rate for the radial and plane flows appears as

$$\frac{\check{\tau}}{z/r} = \left(\frac{x}{r} \frac{dr}{dx} \right) \frac{\bar{\tau}}{y/x} . \quad (9.325)$$

The power laws for $r(x)$ in equations (9.322) and (9.324) both have $x \sim r^2$, so that the quantity in parentheses in the last equation is equal to 1/2;

$$\frac{\check{\tau}}{z/r} = \frac{1}{2} \frac{\bar{\tau}}{y/x} . \quad (9.326)$$

This hypothesis can be checked directly, using the data of Heskestad who studied both flows using similar instrumentation.

The latter flows probably are not close to a state of similarity, primarily because the initial conditions remain important. The difficulty is that the development process cannot be accounted for, because the radial coordinate cannot be displaced to an apparent origin as in the plane case. In either the free flow or the wall flow, there is also a practical consideration that radial velocities decrease very rapidly and are difficult to measure accurately at large distances from the axis of symmetry. (One relevant property of the transformation to be considered here is, from equations (9.285)

$$\frac{\bar{\tau}}{\bar{u}\bar{v}} = \frac{\check{\tau}}{\check{u}\check{v} + \frac{z}{r} \check{u}\check{u}} . \quad (9.327)$$

Does this apply for Reynolds stresses or only for mean flow?)

(Do turbulent case without boundary-layer approximation, do approximation, verify transformation, do entrainment).

One issue is the transformation; why does it not work? If $\tau = \bar{\tau}$, then the radial free jet should grow at half the rate of the plane jet. If the growth rates are the same, the Reynolds stresses should be twice as large for the radial case. The Reynolds equations are believable, and the transformation is flawless. Something is not under control. **(Turn one knob at a time.)**

Heskestad studied both flows, so instrument errors should be consistent. The growth rates are the same; the Reynolds stresses are

about 25% higher for the radial jet. However, the radial jet is not at equilibrium (**see the intermittency data**). The stresses are not the same when made dimensionless with the local mean velocity on the plane of symmetry, nor do they differ by a factor of two. Note also the large size of the generator and the proximity of the laboratory floor, which interferes with axial symmetry.

The property of linear growth for the radial jet can be argued immediately. From equation (9.286) and the fifth of equations (9.285),

$$\frac{z}{r} = \frac{1}{3} \frac{r}{\lambda} \frac{y}{x} . \quad (9.328)$$

When local layer thicknesses $\bar{\delta}$ and $\check{\delta}$ are defined, say by specifying a particular value of $\bar{\eta} = \check{\eta}$, this becomes

$$\frac{\check{\delta}}{r} = \frac{1}{3} \frac{r}{\lambda} \frac{\bar{\delta}}{x} . \quad (9.329)$$

For the case of the laminar plane jet, I showed in SECTION 9.1.2 that $\bar{\delta} \sim x^{2/3}$, so that $\bar{\delta}/x \sim x^{-1/3} \sim 1/r$. Consequently,

$$\frac{\check{\delta}}{r} = \text{constant} . \quad (9.330)$$

This property of linear growth is explicit in the similarity ansatz (9.267). It was also deduced by a related argument by SQUIRE (1955).

Chapter 10

THE WALL JET

A plane jet flowing parallel to an adjacent wall—a wall jet—is a configuration often encountered in ejector design, in film-cooling applications, and in boundary-layer control. The radial wall jet is a variation that is important in problems of heat and mass transfer, as in heating by a torch or drying by an impinging jet. The situations of interest are almost always turbulent. The latter flows are sensitive to residual effects of transition, and the approach to experimental similarity is awkward because a simple displacement of the origin is not compatible with the radial geometry.

In CHAPTER 4, the model for the turbulent boundary layer is a continuously evolving turbulent wake, modified in a definite way by the insertion of a wall along the plane of symmetry. The no-slip condition reduces the velocity to zero at the wall and strongly affects the flow near the original plane of symmetry. In particular, the presence of the wall radically changes the normal or v' fluctuations, which are now reduced to zero at $y = 0$. The no-slip condition also changes the other two fluctuations u' and w' in a more complicated way, as discussed in various places in this monograph. As far as I am aware, the corresponding model has never been considered seriously for the wall jet. This model might be expected to lead to something called the law of the jet and to further development of the concept of equilibrium flow, and it will be addressed in SECTION 10.3.2.

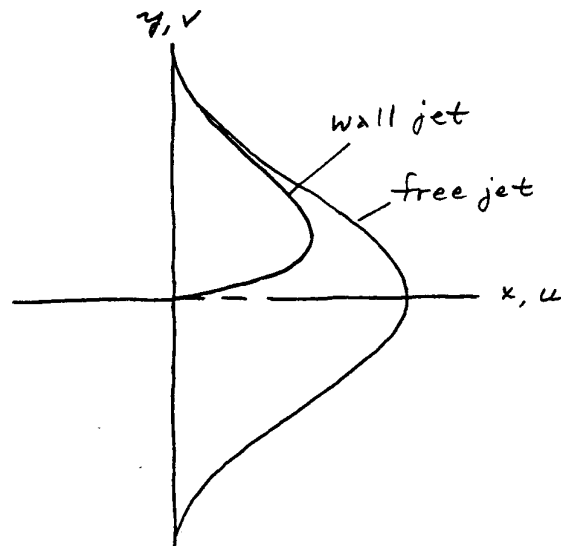


Figure 10.1: Schematic connection between the laminar plane free jet and wall jet.

The laminar wall jet can be visualized as a laminar plane jet with a thin plate inserted on the plane of symmetry, as shown in FIGURE 10.1. The main mathematical consequence of the loss of symmetry for the wall-jet flow is a qualitative change in the similarity argument, which now leads to an eigenvalue problem. It is therefore more important than usual to practice technique with the problem of laminar flow. Part of this technique is an application in SECTION 10.1.6 of the Mangler transformation, which relates a plane flow and a radial flow in the manner shown earlier for the free jet. Many of the other operations carried out in this chapter have already been encountered in CHAPTER 9 on the free jet, where they are described in somewhat greater detail and supported by more extensive arguments.

10.1 Laminar plane wall jet into fluid at rest

10.1.1 The eigenvalue problem

Priority in solving the problem of the laminar plane wall jet with similarity is generally assigned to GLAUERT (1956), although an essentially complete account was published earlier by TETERVIN (1948). The problem is more subtle than the problem of the plane free jet, and the subtleties were fully appreciated by Glauert. The momentum equation in the boundary-layer approximation is the same as for the free jet;

$$\rho \left(\frac{\partial uu}{\partial x} + \frac{\partial uv}{\partial y} \right) = \mu \frac{\partial^2 u}{\partial y^2} = \frac{\partial \tau}{\partial y} . \quad (10.1)$$

The boundary conditions are suitably chosen from

$$\psi = u = v = 0 \text{ at } y = 0, \quad u = \tau = 0 \text{ at } y = \infty . \quad (10.2)$$

The momentum-integral equation is easily written down by inspection of equation (10.1);

$$\rho \frac{d}{dx} \int_0^{\infty} u u \, dy = \frac{dJ}{dx} = -\tau_w , \quad (10.3)$$

where $\tau_w = \mu(\partial u/\partial y)_w$ and J is the momentum integral previously defined for the plane free jet by equation (9.8). The fact that J is no longer a constant, as it was for the free jet, prevents the introduction at the outset of intrinsic scales for mass, length, and time. The friction at the wall continuously removes momentum from the wall jet, beginning at the origin of the flow at $x = 0$, at a rate that is slow but significant. It will be found for the case of laminar flow that similarity requires the terms in equation (10.3) to behave like $x^{-5/4}$ near the origin (see equations (10.60) and (10.61) below). Thus the singularity in τ_w at $x = 0$ is not integrable. Moreover, since the integral in equation (10.3) behaves like $x^{-1/4}$ near $x = 0$, the initial momentum flux J in the similarity formulation is infinite. I emphasize these points because some experimenters have assumed that the

momentum flux J measured at the jet exit or elsewhere in a laminar laboratory flow has some important role to play in similarity formulations of their data. Similar problems with turbulent flow are taken up in SECTION 10.3.1.

One primitive but popular version of dimensional analysis is to assume a power-law behavior and to determine the exponents for two local scales $U(x) \sim x^p$ and $L(x) \sim x^q$ by substitution of a suitable ansatz in the momentum equation (10.1) and its integral (10.3). This approach is demonstrated for several different flows by BIRKHOFF and ZARANTONELLO (1957), for example. These authors did not anticipate the problem of the wall jet, but did comment on an eigenvalue problem for a different flow, the momentumless wake. The new feature in the case of the momentumless wake is that the global constant defined by the momentum integral, the drag, vanishes identically. The new feature in the case of the wall jet is that the two equations (10.1) and (10.3) have essentially the same dimensional structure. In either case, only one condition can be found for the two exponents p and q unless the problem is attacked at a deeper level.

Glauert. To arrive at a dimensionless ansatz, Glauert assumed power-law behavior. He took the free jet as a model and a point of departure. The analysis that follows is faithful in spirit to Glauert's presentation, but the notation and certain details have been changed to suit the style of this monograph. I have also chosen to begin with plane flow rather than radial flow. Glauert postulated the existence of a local velocity scale U and a corresponding local length scale ν/U , and assumed a solution of the form

$$\frac{\psi/\nu}{(Ux/\nu)^a} = f \left[\frac{(Uy/\nu)}{(Ux/\nu)^b} \right] = f(\eta) , \quad (10.4)$$

where

$$u = \frac{\partial \psi}{\partial y} , \quad v = -\frac{\partial \psi}{\partial x} , \quad (10.5)$$

as usual. Substitution in equation (10.1) yields

$$(a-b)f'f' - af f'' = (Ux/\nu)^{1-a-b} f''' , \quad (10.6)$$

where primes indicate differentiation with respect to η . If f is required to depend only on η and not separately on x , this equation

supplies one relation between the exponents a and b ;

$$a + b = 1 \quad , \quad (10.7)$$

together with an ordinary differential equation for f ,

$$f''' + (1 - b)ff'' - (1 - 2b)f'f' = 0 \quad , \quad (10.8)$$

whose boundary conditions, from equations (10.2), are

$$f(0) = f'(0) = f'(\infty) = 0 \quad . \quad (10.9)$$

Glauert's first major contribution was to establish that there exists at least one non-trivial similarity solution of equation (10.8), satisfying the null boundary conditions (10.9), provided that the exponent b has the eigenvalue $3/4$. The analysis begins with an integration whose purpose is to examine the shearing stress f'' and to deal with the absence of symmetry. Replace ff'' by $(ff')' - f'f'$ and integrate equation (10.8) formally from some arbitrary positive value of η to $\eta = \infty$ to obtain

$$f'' + (1 - b)ff' + (2 - 3b)g = 0 \quad , \quad (10.10)$$

where

$$g(\eta) = \int_{\eta}^{\infty} f'f' d\eta \quad . \quad (10.11)$$

The range of integration is evidently chosen to exploit the fact that f' and f'' vanish at infinity for both the free jet and the wall jet. In particular,

$$f''(0) = (3b - 2)g(0) \quad , \quad (10.12)$$

where

$$g(0) = \int_0^{\infty} f'f' d\eta \quad . \quad (10.13)$$

A brief digression disposes of the symmetric problem (the free jet). The boundary conditions in the plane of symmetry are then $f(0) = 0$ and $f''(0) = 0$, corresponding to $\psi(x, 0) = 0$ and $\tau(x, 0) =$

0, with $f'(0) \sim u_c(x)$ left unspecified. Since $g(0)$ is a positive constant, it follows from equation (10.12) that the boundary condition $f''(0) = 0$ can be satisfied only if $b = 2/3$, $a = 1/3$, in agreement with the result obtained more directly in SECTION 9.1.2 above.

Now return to the unsymmetric problem, the wall jet. The boundary conditions at the wall are $f(0) = 0$ and $f'(0) = 0$, corresponding to $\psi(x, 0) = 0$ and $u(x, 0) = 0$, with $f''(0) \sim \tau_w(x)$ left unspecified. Nothing can be learned from equation (10.12), and something more is required. Glauert eliminated f'' by multiplying equation (10.10) by f' and integrating through the thickness of the wall jet. After some integration by parts and use of the identity $g' = -f'f'$ and the boundary condition $g(\infty) = 0$, the result is

$$(3 - 4b) \int_0^{\infty} f'g \, d\eta = 0 . \quad (10.14)$$

The integral in equation (10.14) is a positive constant, provided that the velocity f' is non-negative everywhere, and the equation can therefore be satisfied only for the exponents

$$b = \frac{3}{4} , \quad a = \frac{1}{4} . \quad (10.15)$$

This value for b requires, from equation (10.12),

$$f''(0) = \frac{1}{4} g(0) . \quad (10.16)$$

It reduces the differential equation (10.8) to

$$4f''' + ff'' + 2f'f' = 0 \quad (10.17)$$

and also provides the necessary invariant, which can have different forms;

$$\begin{aligned} \int_0^{\infty} f'g \, d\eta &= \int_0^{\infty} f' \int_{\eta}^{\infty} f'f' \, d\eta \, d\eta = - \int_0^{\infty} fg' \, d\eta = \\ &= \int_0^{\infty} ff'f' \, d\eta = \text{constant} . \end{aligned} \quad (10.18)$$

Of these, the two dominant forms in physical variables are the second and the fourth;

$$\rho \int_0^{\infty} u \int_y^{\infty} uu \, dy \, dy = \rho \int_0^{\infty} \psi uu \, dy = F = \text{constant} . \quad (10.19)$$

Like Glauert, I have some difficulty in assigning a physical meaning to the quantity F . His best effort produced the phrase “flux of exterior momentum flux.”

Having established the structure of his problem, Glauert repeated his derivation from the beginning in physical variables for readers who do not object to a strong element of *deus ex machina*. Note, as did Glauert, that this second derivation does not require the assumption of similarity or of power-law behavior. First, write an incomplete integral corresponding to equation (10.3) in the form

$$\frac{\partial}{\partial x} \rho \int_y^{\infty} uu \, dy - \rho uv + \tau = 0 . \quad (10.20)$$

Denote the integral by W , say;

$$W = \rho \int_y^{\infty} uu \, dy , \quad (10.21)$$

and observe that good things happen if the equation

$$\frac{\partial W}{\partial x} - \rho uv + \tau = 0 \quad (10.22)$$

is multiplied by the streamwise velocity u and if it is noticed that $-\rho uv = \partial W / \partial y$ from equation (10.21). Thus

$$u \frac{\partial W}{\partial x} + v \frac{\partial W}{\partial y} + \tau u = 0 . \quad (10.23)$$

Add to this the continuity equation multiplied by W to obtain

$$\frac{\partial uW}{\partial x} + \frac{\partial vW}{\partial y} + \tau u = 0 . \quad (10.24)$$

Finally, integrate over the thickness of the layer and use the boundary conditions $v(0) = 0$, $W(\infty) = 0$. The result is

$$\frac{d}{dx} \int_0^{\infty} uW \, dy + \int_0^{\infty} \tau u \, dy = 0 . \quad (10.25)$$

A last crucial step can be carried out provided that the flow is laminar, with $\tau = \mu \partial u / \partial y$. Then the second term in equation (10.25) drops out;

$$\int_0^{\infty} \tau u \, dy = \mu \int_0^{\infty} \frac{\partial u^2 / 2}{\partial y} \, dy = 0 , \quad (10.26)$$

since u is zero at both limits. For laminar flow, this procedure has reproduced the conserved quantity (10.19);

$$\int_0^{\infty} uW \, dy = \rho \int_0^{\infty} u \int_y^{\infty} uu \, dy \, dy = F = \text{constant} . \quad (10.27)$$

For turbulent flow, neither equation (10.26) nor equation (10.27) is valid.

(Interpret this process in terms of work done on fluid? Minimize the integral of τu ? W is the momentum flux outboard of a particular point in the flow. Equation (10.23), written as

$$\frac{DW}{Dt} + \tau u = 0 , \quad (10.28)$$

suggests that the rate of change of this quantity following a streamline is given by the rate that work is done by the shearing stress (this needs work). Look at the difference between F and the conserved quantity J for the free jet. Interpret as divergence. Look at energy. Comment on vorticity as variable, with no symmetry and zero integral. See the Rayleigh problem in the introduction.)

Intrinsic scales. Given the existence of the integral invariant F , it is now a simple matter to work out intrinsic scales for the laminar wall jet. The dimensional statements

$$[F] = \frac{\mathbf{ML}^2}{\mathbf{T}^3} , \quad [\rho] = \frac{\mathbf{M}}{\mathbf{L}^3} , \quad [\mu] = \frac{\mathbf{M}}{\mathbf{LT}} \quad (10.29)$$

imply, in their alternative role as definitions,

$$\mathbf{M} = \frac{\rho^4 \nu^9}{F^3} \ , \quad \mathbf{L} = \frac{\rho \nu^3}{F} \ , \quad \mathbf{T} = \frac{\rho^2 \nu^5}{F^2} \ , \quad (10.30)$$

with

$$\mathbf{U} = \frac{\mathbf{L}}{\mathbf{T}} = \frac{F}{\rho \nu^2} \quad (10.31)$$

and, as for the free jet,

$$\frac{\mathbf{U}\mathbf{L}}{\nu} = 1 \ . \quad (10.32)$$

The relation (10.31) provides *a posteriori* justification for Glauert's original ansatz (10.4), because \mathbf{U} is now precisely defined. In fact, substitution for \mathbf{U} yields immediately

$$\left(\frac{\rho}{F\nu x}\right)^{1/4} \psi = f \left[\left(\frac{F}{\rho \nu^3 x^3}\right)^{1/4} y \right] \ . \quad (10.33)$$

Another brief calculation shows that this expression is equivalent to

$$\frac{\psi}{\mathbf{U}\mathbf{L}^{3/4}x^{1/4}} = f\left(\frac{y}{\mathbf{L}^{1/4}x^{3/4}}\right) \ . \quad (10.34)$$

Tetervin. Tetervin's earlier approach to the same problem was handicapped by a dreadful notation and by failure to introduce a stream function until the last possible moment. What follows is a radical paraphrase of his argument. In effect, he assumed similarity in terms of local scales for velocity U and layer thickness L ;

$$\frac{\psi}{UL} = f\left(\frac{y}{L}\right) = f(\eta) \ , \quad (10.35)$$

where $U(x)$ and $L(x)$ have to be determined. Substitution in the momentum equation (10.1) gives, just as in the case of the laminar free jet (see SECTION 9.1.2),

$$f''' + \frac{L}{\nu} \frac{dUL}{dx} f f'' - \frac{L^2}{\nu} \frac{dU}{dx} f' f' = 0 \ . \quad (10.36)$$

Substitution in the momentum-integral equation (10.3) gives

$$\frac{L}{\nu U} \frac{dU^2 L}{dx} \int_0^\infty f' f' d\eta = -f''(0) . \quad (10.37)$$

Tetervin eventually normalized the integral to unity;

$$\int_0^\infty f' f' d\eta = g(0) = 1 , \quad (10.38)$$

so that

$$\frac{L}{\nu U} \frac{dU^2 L}{dx} = -f''(0) . \quad (10.39)$$

Only two of the three constant coefficients involving U and L in equations (10.36) and (10.39) are independent, and these two are not sufficient to determine $U(x)$ and $L(x)$ explicitly. Neither is the device of the moving observer useful for resolving the question of exponents. Tetervin, like Glauert, found another way.

When ν is eliminated between equations (10.36) and (10.39), and the variables depending on x and on η are separated, the result is

$$\frac{L dU/dx}{U dL/dx} = \frac{-f''' + f''(0) f f''}{2f''' - f''(0)(f f'' - f' f')} = -k , \quad (10.40)$$

where k must be a positive constant because x and η are arbitrary and $dU/dx < 0$, $dL/dx > 0$. This expression strongly suggests that power laws are appropriate for $U(x)$ and $L(x)$, and guarantees in any case that

$$UL^k = \text{constant} . \quad (10.41)$$

Tetervin noted in passing that the boundary condition $f''(0) = 0$ in equation (10.40) implies $k = 1/2$ and thus $U^2 L = \text{constant}$, so that the case of the plane free jet is accounted for. The present interest is in the case of lost symmetry with its eigenvalue k . This eigenvalue appears along with $f''(0)$ in the differential equation obtained from the second part of equation (10.40);

$$f''' + \left(\frac{1-k}{2k-1} \right) f''(0) f f'' + \left(\frac{k}{2k-1} \right) f''(0) f' f' = 0 . \quad (10.42)$$

At this point, Tetervin's argument becomes opaque. The essence of his procedure, suitably revised to leave open the question of normalization, is to multiply equation (10.42) by f and integrate over the thickness of the wall jet. After the usual integration by parts and use of the boundary conditions, the result is

$$\left(\frac{3k-2}{2k-1}\right) f''(0) \int_0^{\infty} f f' f' d\eta = 0 . \quad (10.43)$$

Both the integral and the factor $f''(0)$ are necessarily positive, so that the desired invariant emerges from this equation together with the eigenvalue

$$k = \frac{2}{3} . \quad (10.44)$$

Equation (10.42) becomes

$$\frac{f'''}{f''(0)} + f f'' + 2 f' f' = 0 . \quad (10.45)$$

Equation (10.41) becomes

$$U^3 L^2 = \text{constant} , \quad (10.46)$$

and it follows from this result and equation (10.39) that

$$U \sim x^{-1/2} , \quad L \sim x^{3/4} . \quad (10.47)$$

Tetervin integrated equation (10.45) numerically for the particular initial conditions $f(0) = f'(0) = 0$ and $f''(0) = 1/4$. His conversion of a two-point boundary-value problem to an initial-value problem was successful, although he may not have been aware of the reason, which involves a property first pointed out for the Blasius equation by TÖPFER (1912). The argument is easily extended by inspection to equation (10.45), which also has no pressure-gradient term. If $f(\eta)$ is a solution, so is $\phi(\eta) = \alpha f(\alpha\eta)$, where α is any constant. It follows that $f''(0)$ can be chosen arbitrarily, with $\phi(\infty)$ adjusted later to any desired value by a proper choice of α (see SECTION X).

10.1.2 Similarity

The affine transformation. Discovery of the integral invariant F allows the problem of the laminar plane wall jet to be treated by the method of the affine transformation. Let a stream function ψ be introduced in the usual way to satisfy the continuity equation. Rewrite equation (10.1) as

$$\rho \left(\frac{\partial \psi}{\partial y} \frac{\partial^2 \psi}{\partial x \partial y} - \frac{\partial \psi}{\partial x} \frac{\partial^2 \psi}{\partial y^2} \right) = \mu \frac{\partial^3 \psi}{\partial y^3} \quad (10.48)$$

and apply the affine transformation

$$\begin{aligned} x &= a\hat{x} , \\ y &= b\hat{y} , \\ \psi &= c\hat{\psi} , \\ \rho &= d\hat{\rho} , \\ \mu &= e\hat{\mu} , \\ F &= f\hat{F} . \end{aligned} \quad (10.49)$$

This is the same group as equations (9.28) for the plane free jet, except that F replaces J . The result is

$$\frac{c^2 d}{ab^2} \hat{\rho} \left(\frac{\partial \hat{\psi}}{\partial \hat{y}} \frac{\partial^2 \hat{\psi}}{\partial \hat{x} \partial \hat{y}} - \frac{\partial \hat{\psi}}{\partial \hat{x}} \frac{\partial^2 \hat{\psi}}{\partial \hat{y}^2} \right) = \frac{ce}{b^3} \hat{\mu} \frac{\partial^3 \hat{\psi}}{\partial \hat{y}^3} . \quad (10.50)$$

Invariance of equation (10.48) thus requires

$$\frac{bcd}{ae} = 1 , \quad (10.51)$$

just as in the case of the plane free jet. Transformation of equation (10.19),

$$\rho \int_0^\infty \psi \frac{\partial \psi}{\partial y} \frac{\partial \psi}{\partial y} dy = F , \quad (10.52)$$

yields

$$\frac{c^3 d}{b} \hat{\rho} \int_0^{\infty} \hat{\psi} \frac{\partial \hat{\psi}}{\partial \hat{y}} \frac{\partial \hat{\psi}}{\partial \hat{y}} d\hat{y} = f \hat{F} \ , \quad (10.53)$$

and requires for invariance

$$\frac{c^3 d}{b f} = 1 \ . \quad (10.54)$$

As usual, I take the primary variables to be ψ and y . When equations (10.51) and (10.54) are revised to isolate for c and b , the result is

$$\frac{c^4 d^2}{a e f} = 1 \ , \quad \frac{b^4 d^2 f}{a^3 e^3} = 1 \ . \quad (10.55)$$

Hence the proper ansatz, including constants A and B for later normalization, is again equation (10.33),

$$A \left(\frac{\rho}{F \nu x} \right)^{1/4} \psi = f \left[B \left(\frac{F}{\rho \nu^3 x^3} \right)^{1/4} y \right] = f(\eta) \ . \quad (10.56)$$

Substitution of this ansatz in the momentum equation (10.48) yields

$$4ABf''' + ff'' + 2f'f' = 0 \ , \quad (10.57)$$

with boundary conditions

$$f(0) = f'(0) = 0, \quad f'(\infty) = 0 \ , \quad (10.58)$$

corresponding to $\psi = u = 0$ at $y = 0$ and $u = 0$ at $y = \infty$. If $AB = 1$, equation (10.57) is identical with my version of Glauert's result, equation (10.17). Substitution of equation (10.56) in equation (10.52) for F gives

$$\int_0^{\infty} f f' f' d\eta = \frac{A^3}{B} \ . \quad (10.59)$$

The singular behavior of the flow at the origin, mentioned earlier, is demonstrated by the relations

$$J = \rho \int_0^{\infty} uu \, dy = \frac{B}{A^2} \left(\frac{F^3 \rho}{\nu x} \right)^{1/4} \int_0^{\infty} f' f' d\eta \quad (10.60)$$

and

$$\frac{\tau_w}{\rho} = \frac{B^2}{A} \left(\frac{F^3}{\rho^3 \nu x^5} \right)^{1/4} f''(0) . \quad (10.61)$$

10.1.3 The boundary-layer solution

Glauert's second major contribution was to obtain the eigenfunction $f(\eta)$ in closed form. First, multiply equation (10.57) by f and integrate to obtain

$$4AB \left(ff'' - \frac{f'f'}{2} \right) + ff f' = 0 , \quad (10.62)$$

where the constant of integration vanishes by virtue of the first two boundary conditions (10.58). Multiply this result by $f^{-3/2}$ and integrate again, to obtain

$$4AB \frac{f'}{f^{1/2}} + \frac{2}{3} \left(f^{3/2} - C^{3/2} \right) = 0 , \quad (10.63)$$

where $C > 0$ is a constant of integration. The boundary condition (10.58) at infinity requires

$$C = f(\infty) . \quad (10.64)$$

Finally, integrate equation (10.63) with the aid of the change of variable

$$f = Ch^2 = CH \quad (10.65)$$

and the method of partial fractions. An intermediate result is

$$\frac{C}{4AB} d\eta = \frac{dh}{(1-h)} + \frac{2dh}{(1+h+h^2)} + \frac{hdh}{(1+h+h^2)} . \quad (10.66)$$

The final result in terms of h , after use of the boundary condition $f(0) = h(0) = 0$ to evaluate the constant of integration, can be written

$$\frac{C}{2AB} \eta = \ln \frac{(1-h^3)}{(1-h)^3} + 2\sqrt{3} \tan^{-1} \left(\frac{\sqrt{3}h}{2+h} \right) . \quad (10.67)$$

Equations (10.65) and (10.67) are a parametric system for $f(\eta)$, with h as parametric variable. Note that h depends not directly on η but on $C\eta/2AB$.

Pause here to look at experimental data for the laminar profile; see

BAJURA and SZEWCZYK (1970)
 BAJURA and CATALANO (1975)
 TSUJI et al. (1977)
 TSUJI and MORIKAWA (1977)
 HORNE and KARAMCHETI (1979)
 SCIBILIA and DUROX (1980)
 PAIGE (1988)
 ZHOU et al. (1992)

It remains to consider the streamlines of the boundary-layer flow in compact outer variables (x, y) having equal scales. A unique representation of the flow can again be found, without regard for the values of the three constants A, B , and C . Rewrite equation (10.56) in terms of H as

$$\frac{A}{C} \left(\frac{\rho}{F\nu x} \right)^{1/4} \psi = \frac{f(\eta)}{C} = H \left(\frac{C}{2AB} \eta \right) = H \left[\frac{C}{2A} \left(\frac{F}{\rho\nu^3 x^3} \right)^{1/4} y \right]. \quad (10.68)$$

In the combinations containing ψ and y , use the second of equations (10.30) to eliminate the quantity F in favor of $\mathbf{L} = \rho\nu^3/F$. Thus write

$$\frac{A}{C} \left(\frac{\mathbf{L}}{x} \right)^{1/4} \frac{\psi}{\nu} = H \left[\frac{C}{2A} \left(\frac{y^4}{\mathbf{L}x^3} \right)^{1/4} \right]. \quad (10.69)$$

Compact outer variables define themselves immediately as

$$\Psi = \frac{\psi}{2\nu}, \quad X = \left(\frac{C}{2A} \right)^4 \frac{x}{\mathbf{L}}, \quad Y = \left(\frac{C}{2A} \right)^4 \frac{y}{\mathbf{L}}, \quad (10.70)$$

and equation (10.68) takes the form

$$\Psi = X^{1/4} H \left(\frac{Y}{X^{3/4}} \right). \quad (10.71)$$

Note that $H = h^2 = f(\eta)/C$, but that the argument of H is the quantity $C\eta/2AB$ on the left in equation (10.67). The example of the free jet suggests that a useful relation involving the constants A and C should emerge when the integral invariant (10.59) is evaluated for Glauert's closed-form solution. Use equation (10.65) and its derivative, together with equation (10.63), to replace the variable f by h . The result is

$$\int_0^{\infty} f f' f'' d\eta = \frac{C^4}{3AB} \int_0^1 h^4(1-h^3) dh = \frac{C^4}{40AB} = \frac{A^3}{B}, \quad (10.72)$$

from which

$$\left(\frac{C}{2A}\right)^4 = \frac{5}{2}. \quad (10.73)$$

The variables in equation (10.71) can therefore be written

$$\Psi = \frac{\psi}{2\nu}, \quad X = \frac{5x}{2\mathbf{L}}, \quad Y = \frac{5y}{2\mathbf{L}}. \quad (10.74)$$

Streamlines for the boundary-layer approximation (10.71) are shown in FIGURE 10.2¹ for the case of a laminar wall jet flowing from the origin along a plane wall that extends to infinity in the positive x -direction. Rather than calculate Ψ on a large rectangular array (X, Y) and find level curves on which Ψ is constant, it is simpler here to define each streamline separately. The algorithm is: fix Ψ , vary X . Calculate $H = \Psi/X^{1/4} = h^2$. Calculate h . Calculate $C\eta/2AB = Y/X^{3/4}$ from equation (10.67). Calculate Y .

A local Reynolds number can be expressed in compact outer variables by beginning with dimensionless versions of equations (10.47);

$$U(x) = \mathbf{U}\mathbf{L}^{1/2}x^{-1/2}, \quad L(x) = \mathbf{L}^{1/4}x^{3/4}. \quad (10.75)$$

Use of equations (10.30) and (10.31) leads to

$$U = \left(\frac{F^2}{\rho^2\nu^2x^2}\right)^{1/4}, \quad L = \left(\frac{\rho\nu^3x^3}{F}\right)^{1/4}, \quad (10.76)$$

¹A longer handwritten version of the caption for this figure in the 1996 ms. reads "Streamlines $\Psi = \psi/2\nu = \text{constant}$ of the boundary-layer approximation for the laminar plane wall jet according to equation (10.71). The range of Ψ is 0(1)10 (check).

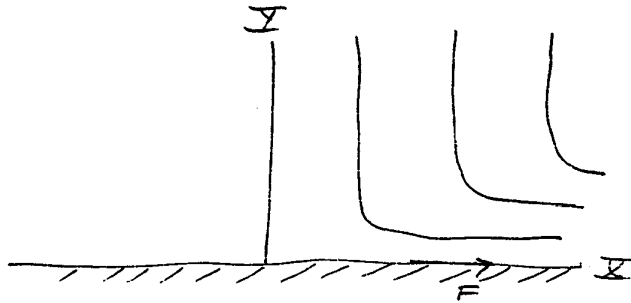


Figure 10.2: Streamlines of the boundary-layer model for the laminar plane wall jet according to equation (10.71). The range of.....

and thus to

$$Re(x) = \frac{UL}{\nu} = \left(\frac{Fx}{\rho\nu^3}\right)^{1/4} = \left(\frac{x}{L}\right)^{1/4} = \left(\frac{2}{5}X\right)^{1/4} . \quad (10.77)$$

10.1.4 Normalization

The three constants A , B , and C for the plane wall jet can be assigned sensible values by operations that run in parallel with similar operations for the plane free jet in SECTION 9.1.4. The condition

$$4AB = 1 \quad (10.78)$$

establishes the standard operator $f''' + ff''$ in equation (10.57). A second and mandatory condition, just derived, is

$$\frac{C}{A} = (40)^{1/4} . \quad (10.79)$$

(See end of Part A of this chapter. This is too messy. No tidy normalization seems to be in view. Sort through this material to find

something simple, elegant, and redundant. Consider equation (10.67) for h near 1 and for h large and negative. Note that for $h = 1$ the angle is 30 degrees. Should square root be \pm ? Need to match to plane jet at infinity. Try osculating parabola.)

The third condition determining the constants A, B, C requires definition of a length or velocity scale. The simplest choice, suggested by the example of the free jet (see SECTION 9.1.4), is to set the argument of h ; i.e., the left-hand side of equation (10.67), equal to η itself, so that $C/2AB = 1$ or $C = 1/2$.

The maximum velocity $U = u_m$ (m for maximum) is easily worked out;

$$Re = \frac{UL}{\nu} = \frac{1}{\nu} \int_0^{\infty} u dy = \frac{\psi(x, \infty)}{\nu} = \frac{1}{A} \left(\frac{Fx}{\rho\nu^3} \right)^{1/4} f(\infty) = 2X^{1/4} . \quad (10.80)$$

This Reynolds number is small compared with the corresponding value $Re = 12 X^{1/3}$ for the plane free jet. In FIGURE 10.2, which extends **(ten)** times farther than FIGURE 9.4, the Reynolds number at the right boundary is **(six)** times smaller. Comparison of equation (10.80) with equation (9.57) for the free jet suggests that the two measures just cited are associated with the exponent and the coefficient, respectively.

The maximum streamwise velocity η_m occurs when $\partial u/\partial y \sim f'' = 0$. With this condition, equations (10.62) and (10.63) can be restated in terms of h and h' and solved algebraically to produce **(see Tetervin)**

$$f(\eta_m) = \left(\frac{1}{4} \right)^{2/3} C ; \quad (10.81)$$

$$f'(\eta_m) = \left(\frac{1}{4} \right)^{1/3} \frac{C^2}{8AB} . \quad (10.82)$$

Thus if $f'(\eta_m) = 1$, then $C^2/4AB$ or $C = (32)^{1/6}$. Conversely, if $C = 1/2$, then $f'(\eta_m) = (2)^{1/3}/16$.

Several other choices suggest themselves, chief among them the integral scale L for the profile. Define this integral scale in terms of

the maximum velocity u_m (m for maximum) by

$$u_m L = \int_0^{\infty} u dy = \psi(x, \infty) . \quad (10.83)$$

After use of the ansatz (10.56) and the second of conditions (10.82), this turns into

$$\tilde{\eta} = B \left(\frac{F}{\rho \nu^3 x^3} \right)^{1/4} L = \int_0^{\infty} \frac{f'(\eta)}{f'(\eta_m)} d\eta = (4)^{1/3} \frac{8AB}{C} . \quad (10.84)$$

Hence if $\tilde{\eta} = 1$, $C/4AB = 2(4)^{1/3}$.

A similar calculation, with h replacing f , leads from the definition (10.13) to

$$g(0) = \int_0^{\infty} f' f' d\eta = \frac{1}{18} \frac{C^3}{AB} . \quad (10.85)$$

Finally, integration of the primary differential equation (10.57) between the limits zero and infinity leads to

$$f''(0) = \frac{g(0)}{4AB} = \frac{1}{72} \frac{C^3}{A^2 B^2} . \quad (10.86)$$

Either of these relationships, as well as

$$f(\infty) = \int_0^{\infty} f' d\eta = C , \quad (10.87)$$

could provide a third condition if its right-hand side is arbitrarily set equal to unity, say. The results, respectively, are $C^3 = 9/2$ if $g(0) = 1$, $C^3 = 9/2$ if $f''(0) = 1$, and $C = 1$ if $f(\infty) = 1$, where $4AB$ is read as unity.

The inflection point in the profile at $\eta = \eta_i$, say, is found by putting $f''' = 0$. This point also marks the maximum velocity along a streamline, since $Du/Dt = \nu \partial^2 u / \partial y^2 = 0$ for laminar flow. Then

equation (10.57) becomes $ff'' + 2f'f' = 0$, and other derivatives at the inflection point can be calculated from this truncated form together with equations (10.62) and (10.63). The results are

$$f(\eta_i) = \left(\frac{5}{8}\right)^{2/3} C ; \quad (10.88)$$

$$f'(\eta_i) = \frac{1}{16} \left(\frac{5}{8}\right)^{1/3} \frac{C^2}{AB} ; \quad (10.89)$$

$$f''(\eta_i) = -\frac{1}{128} \frac{C^3}{A^2B^2} . \quad (10.90)$$

Hence if $f'(\eta_i) = 1$, then $C^2/4AB = 8/5^{1/3}$.

The vorticity thickness η_ζ is defined graphically in FIGURE X and is defined algebraically by

$$\eta_\zeta = -\frac{f'(\eta_m)}{f''(\eta_i)} = 16 \left(\frac{1}{4}\right)^{1/3} \frac{AB}{C} , \quad (10.91)$$

where $f'(\eta_m)$ is given by equation (10.82). Hence if $\eta_\zeta = 1$, $C/4AB = (4)^{2/3}$.

The normalizations used by Glauert and Tetervin can be inferred by using my notation in the ansatz (10.56) and the relations that follow. Glauert put $C = 1$ and also $4AB = 1$, according to his equation (4.1). It follows that $A = (1/40)^{1/4}$, $B = (5/32)^{1/4}$; and these are the numbers that appear in Glauert's equations (4.9) for the plane case. Tetervin's final normalization can be deduced from his equation (20), in which his $G(\xi)$ is the same as my $f(\eta)$. He put $4AB = 4/3$ and $f''(0) = 1/4$, and these together with equation (10.86) above imply $C = f(\infty) = (2)^{1/3} = 1.259921$. His numerical result for large η , namely $f(14.95) = 1.259916$, is evidence that his integration was carried out with remarkable accuracy.

(Give normalized f , f' , etc.)

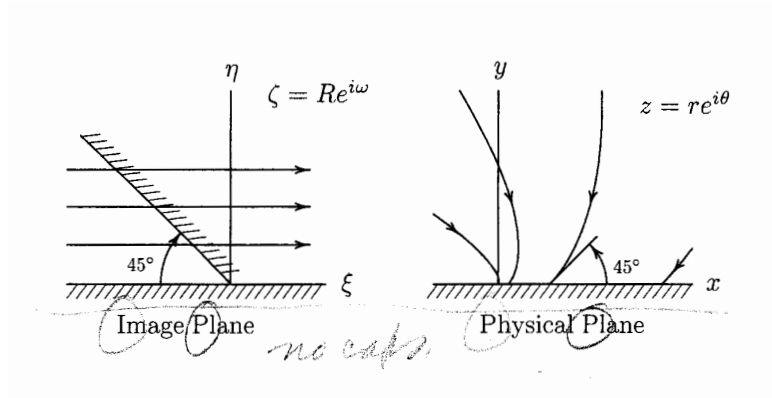


Figure 10.3: Mapping of the outer entrained flow for the laminar plane wall jet.

10.1.5 Entrainment and composite flow

The outer or entrained flow associated with the boundary-layer solution in FIGURE 10.2 can again be obtained by the method of conformal mapping, as indicated in FIGURE 10.3. The complex potential for uniform flow in the ζ -plane is

$$F(\zeta) = \phi + i\psi = U_0\zeta . \quad (10.92)$$

The mapping can be assumed to be of the form

$$\zeta = L_0^{3/4} z^{1/4} e^{i\alpha} , \quad (10.93)$$

where $\zeta = Re^{i\omega}$ and $z = re^{i\theta}$, with U_0 , L_0 , and α to be determined. Angles are related by

$$\omega = \frac{\theta}{4} + \alpha . \quad (10.94)$$

Consequently, if $\theta = \pi$ when $\omega = \pi$ on OA ,

$$\alpha = \frac{3\pi}{4} . \quad (10.95)$$

Since now $\theta = 0$ when $\omega = 3\pi/4$ on OB , streamlines of the outer flow will intersect the x -axis at an angle of 45 degrees. The complex

potential in the z -plane becomes

$$F(z) = \phi_o + i\psi_o = U_0\zeta(z) = U_0L_0^{3/4} r^{1/4} e^{i\left(\frac{\theta+3\pi}{4}\right)}, \quad (10.96)$$

and the outer stream function is

$$\psi_o(r, \theta) = U_0L_0^{3/4} r^{1/4} \sin\left(\frac{\theta + 3\pi}{4}\right). \quad (10.97)$$

At the wall, where $\theta = 0$ and $r = x$,

$$\psi_o(x, 0) = \frac{1}{\sqrt{2}} U_0L_0^{3/4} x^{1/4}. \quad (10.98)$$

This outer flow on the positive x -axis in the physical plane is to be matched to the inner stream function at infinity, from equation (10.56) with $f(\infty) = C$;

$$\psi_i(x, \infty) = \frac{C}{A} \left(\frac{F\nu x}{\rho}\right)^{1/4}. \quad (10.99)$$

Matching therefore requires

$$\frac{1}{\sqrt{2}} U_0L_0^{3/4} = \frac{C}{A} \left(\frac{F\nu}{\rho}\right)^{1/4} = \frac{C}{A} \mathbf{UL}^{3/4}, \quad (10.100)$$

where the last equality makes use of equations (10.30). Finally, therefore,

$$\psi_o(r, \theta) = \sqrt{2} \frac{C}{A} \left(\frac{F\nu r}{\rho}\right)^{1/4} \sin\left(\frac{\theta + 3\pi}{4}\right). \quad (10.101)$$

(Work out pressure here.)

The composite stream function ψ_c is the sum of the inner component (10.56) and the outer component (10.101) with the common part (10.99) subtracted,

$$\psi_c = \frac{C}{A} \left(\frac{F\nu r}{\rho}\right)^{1/4} \left\{ \left(\frac{x}{r}\right)^{1/4} \left[\frac{f(\eta)}{C} - 1\right] + \sqrt{2} \sin\left(\frac{\theta + 3\pi}{4}\right) \right\}. \quad (10.102)$$

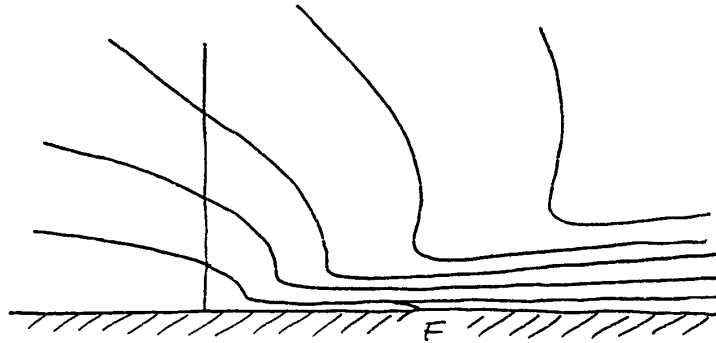


Figure 10.4: Streamlines $\Psi = \text{constant}$ of the composite model for the laminar plane wall jet into a stagnant fluid according to equation (10.103).

In terms of the reduced similarity variables X and Y defined by equations (10.70), with $R = (X^2 + Y^2)^{1/2}$ and $\tan \Theta = Y/X$, this is

$$\Psi_c = R^{1/4} \left\{ I(\Theta) \left[H \left(\frac{Y}{X^{3/4}} \right) - 1 \right] + \sqrt{2} \sin \left(\frac{\Theta + 3\pi}{4} \right) \right\}, \quad (10.103)$$

where

$$\begin{aligned} I(\Theta) &= (\cos \Theta)^{1/4} && \text{for } x > 0, \\ &= 0 && \text{for } x < 0. \end{aligned} \quad (10.104)$$

Streamlines for the composite flow are shown in FIGURE 10.4. The calculation here requires an iteration for $h(\eta)$ and a contour subroutine. The figure can be viewed as a conceptual model for flow near the nozzle of a plane wall ejector with small induced flow (see SECTION X).

(Want S , U , V , T ; see free jet. Plot corrected profile, etc.)

10.1.6 The laminar radial wall jet**10.1.7 Stability and transition****10.2 Laminar plane wall jet into moving fluid****10.2.1 Similarity****10.3 Turbulent plane wall jet into fluid at rest****10.3.1 Similarity**

A preliminary step is to determine if the turbulent plane wall jet is also an eigenvalue problem. Physically, it can never be established whether or not there is a finite initial momentum flux J , because turbulent flow cannot be observed at sufficiently low Reynolds numbers. The argument below refers only to the boundary-layer approximation, with the momentum equation written as

$$u \frac{\partial u}{\partial x} + v \frac{\partial u}{\partial y} = \frac{1}{\rho} \frac{\partial \tau}{\partial y} . \quad (10.105)$$

The boundary conditions are $u = 0$ and $\psi = 0$ at $y = 0$ and $u = 0$ and $\tau = 0$ at $y = \infty$. (**Use the best and highest version of the invariant.**)

With the laminar problem of SECTION 10.1.1 in mind as both a model and a special case, multiply equation (10.105) by the product ψu , where ψ is the usual stream function, and add to the result the two identities

$$\psi u \frac{\partial u}{\partial x} + \psi u \frac{\partial v}{\partial y} = 0 \quad (10.106)$$

and

$$uu \frac{\partial \psi}{\partial x} + uv \frac{\partial \psi}{\partial y} = -uuv + uvu = 0 \quad (10.107)$$

to obtain

$$\frac{\partial \psi uu}{\partial x} + \frac{\partial \psi uv}{\partial y} = \frac{\psi}{\rho} \frac{\partial \tau}{\partial y} . \quad (10.108)$$

Integration, with $\psi = 0$ at the wall and $\tau = 0$ at infinity, gives

$$\int_0^{\infty} \frac{\partial \psi uu}{\partial x} dy = \frac{1}{\rho} \int_0^{\infty} \psi \frac{\partial \tau}{\partial y} dy = -\frac{1}{\rho} \int_0^{\infty} \tau \frac{\partial \psi}{\partial y} dy . \quad (10.109)$$

Consequently,

$$\frac{d}{dx} \int_0^{\infty} \psi uu dy = -\frac{1}{\rho} \int_0^{\infty} \tau u dy . \quad (10.110)$$

If the flow is laminar, $\tau = \mu \partial u / \partial y$, and

$$\int_0^{\infty} \tau u dy = \mu \int_0^{\infty} \frac{\partial u^2 / 2}{\partial y} dy = 0 \quad (10.111)$$

because u^2 vanishes at both limits. Thus

$$\int_0^{\infty} \psi uu dy = F = \text{constant} . \quad (10.112)$$

If the flow is turbulent, the integral (10.111) does not necessarily vanish. The velocity is presumably always positive, and the stress τ changes sign, being positive near the wall and negative farther out, so there is the possibility. **Calculate τ from $\int Du/Dt dy$ and see what happens.**

Forthmann did not look at wall law because he did not know the wall friction. He also introduced the half-velocity scheme for defining δ .

Schwartz and Cosart separated the profile into two parts at the point of maximum velocity. The wall jet should be treated by the same methods that are successful for the boundary layer.

The growth rate for a wall jet is about 3/4 of the growth rate for a free jet. This is because the vertical fluctuations are inhibited and the effect is felt in all of the Reynolds stresses and in entrainment. Comment on cases where τ and du/dy do not go to zero at the same point. This is a blow to the idea of eddy viscosity.

Need a handout on methods for measuring surface friction.

10.3.2 The law of the jet

Measured mean-velocity profiles in plane wall jets can be found in

FORTHMANN (1934)
BAKKE (1957)
SIGALLA (1958)
SCHWARZ and COSART (1961)
PATEL (1962)
RAJARATNAM (1965)
SRIDHAR and TU (1966)
TAILLAND and MATHIEU (1967)
GUITTON (1968)
KOHAN (1968)
HUBBARTT and NEALE (1972)
SPETTEL et al. (1972)
KIND and SUTHANTHIRAN (1973)
HO and HSIAO (1983)
SCHNEIDER (1987)
ABRAHAMSSON et al. (1991)
KATZ et al. (1992)
WYGNANSKI et al. (1992)

Measured Reynolds-stress profiles can be found in

FORTHMANN (1934)
TAILLAND and MATHIEU (1967)
GUITTON (1968)
SPETTEL et al. (1972)
SCHNEIDER (1987)
ABRAHAMSSON et al. (1991)
WYGNANSKI et al. (1992)

10.3.3 Entrainment and composite flow

10.3.4 Coanda effects

10.4 The turbulent radial wall jet

10.4.1 Similarity

The mean-velocity profile in turbulent radial wall jets is reported in

POREH (1959)
POREH and CERMAK (1959)
SCHRODER (1961)
TSUEI (1962)
LUDWIEG (1964)
CHAO and SANDBORN (1966)
DONALDSON (1966)
JOHNSON (1967) 19D
POREH et al. (1967)
HRYCAK (1970)
SCHOLTZ and TRASS (1970)
DONALDSON et al. (1971)
GOVINDAN and RAJU (1974)
ERA and SAIMA (1976)
BOLDMAN and BRINICH (1977)
LEISTER (1977)
MITACHI and ISHIGURO (1977)
TANAKA and TANAKA (1977, 1978)
TANI and KOMATSU (1977)
ARAUJO et al. (1981)
DESHPANDE and VAISHNAV (1982)
KATAOKA et al. (1983)
CODAZZI et al. (1983)

Tanaka. Figure 13 is useful.

Tanaka. Combined jet far downstream behaves like a single jet. In-

cludes single jet for reference.

Bradshaw. Clumping.

Knystautas. Study this again.

Hegge Zijnen (two papers). Note no side plates. Figure 6 implies turbulent Prandtl number.

Foss and Jones. Effect of low aspect ratio with side walls. Mechanism? Mean velocity profile is insensitive.

Curtet. Not ejector; secondary stream is controlled. Figure V.4 has fitting constant. Figure V.7 shows positive and negative flow ratios. Figure VII.1 shows separation bubble.

It is probably time to invent the law of the jet. The sketch² shows the decomposition of the profile. The corresponding formula is

$$\frac{u}{u_\tau} = f\left(\frac{yu\tau}{\nu}\right) - \frac{uc}{u_\tau} j\left(\frac{y}{\delta}\right) \quad (10.113)$$

where a tentative form for $j(y/\delta)$ is $\sin^2(\pi y/2\delta)$. The defect form is obtained by subtracting the local friction law

$$0 = f\left(\frac{\delta u\tau}{\nu}\right) - \frac{uc}{u_\tau} \quad (10.114)$$

to obtain

$$\frac{u}{u_\tau} = \frac{1}{\kappa} \frac{y}{\delta} + \frac{uc}{u_\tau} \cos^2\left(\frac{\pi y}{2\delta}\right). \quad (10.115)$$

In wall-law variables, equation (1)³ has the form shown in the sketch. If the defect law is equivalent to equilibrium, then u_c/u_τ must be constant, and so must $\delta u_\tau/\nu$. Each equilibrium flow has an invariant profile, which changes with (??) The data do not seem to have this property, perhaps because none of the flows are fully developed.

The boundary-layer problem has been wrapped up for 30 years. The wall jet has a number of properties in common, but is still being treated by 19th-century methods.

²No such sketch has been found.

³Unclear reference.

Tanaka and Tanaka also studied the free jet and wall jet. They divide the profile at the maximum velocity. Note that r is measured from the outside of the pipe, not from the axis of symmetry. The estimates of C_f from the momentum equation and the fit to the wall law do not agree.

The stability paper seems to show a vena contracta, but this may be the cylindrical geometry. The paper allows the observed vortex pairs to be treated along with the eigenfunctions. This is a good paper on stability.

Describe profile formula for wall jet. Invent the law of the jet to supply rigor and detail. (Need sketch). Since the jet function is not known, the process is iterative. (Need sketch in wall-law coordinates.) If u_c/u_τ is constant, so is $\delta u_\tau/\nu$, and there is only one profile for a given flow. Different profiles may apply for different Reynolds numbers.

The colliding round jets (Witze and Dwyer) form a radial jet that grows at an abnormally large rate.

Several authors have compared the flow near the wall in a wall jet to the log law, with considerable variations on both sides of the Prandtl law.

Irwin's data have low scatter.

These wall-jet data should reinforce a conviction that the law of the wall, which was originally recovered from pipe data, is really universal. The law of the wall is the largest handle striking out of the problem of shear flow near a wall. It should be central in any global study.

It remains to consider the usual momentum-integral equation. The development is at first completely general. Rewrite equation (xxx), with the aid of the continuity equation $\partial u/\partial x + \partial v/\partial y = 0$, as

$$\rho \left(\frac{\partial uu}{\partial x} + \frac{\partial uv}{\partial y} \right) = \rho u_\infty \frac{du_\infty}{dx} + \frac{\partial \tau}{\partial y} \quad (10.116)$$

and integrate from $y = 0$ to some fixed value of y , with the boundary condition $v = 0$ at $y = 0$ (either because of symmetry or because of

the presence of a wall). The result can be written

$$\rho \int_0^y \frac{\partial uu}{\partial x} dy + \rho uv = \rho \frac{du_\infty}{dx} \int_0^y u_\infty dy + \tau - \tau_w \quad (10.117)$$

where τ_w is the value of τ at $y = 0$; this value may be zero.

The continuity equation also yields an integral,

$$\int_0^y \frac{\partial u}{\partial x} dy + v = 0 \quad (10.118)$$

so that equation (10.117) can be written

$$\rho \int_0^y \frac{\partial uu}{\partial x} dy - \rho u \int_0^y \frac{\partial u}{\partial x} dy - \rho \frac{du_\infty}{dx} \int_0^y u_\infty dy - \tau + \tau_w = 0 \quad (10.119)$$

To eliminate the divergent integrals when the upper limit goes to infinity, add to this the identity

$$-\rho \int_0^y \frac{\partial uu_\infty}{\partial x} dy + \rho u_\infty \int_0^y \frac{\partial u}{\partial x} dy + \rho \frac{du_\infty}{dx} \int_0^y u dy = 0 \quad (10.120)$$

to obtain

$$\begin{aligned} \rho \frac{\partial}{\partial x} \int_0^y (uu - uu_\infty) dy + \rho(u_\infty - u) \frac{\partial}{\partial x} \int_0^y u dy + \\ + \rho \frac{du_\infty}{dx} \int_0^y (u - u_\infty) dy - \tau + \tau_w = 0 \quad (10.121) \end{aligned}$$

Finally, let the upper limit go to infinity and change the signs;

$$\rho \frac{d}{dx} \int_0^\infty u(u_\infty - u) dy + \rho \frac{du_\infty}{dx} \int_0^\infty (u_\infty - u) dy - \tau_w = 0 \quad (10.122)$$

Equation (10.122) is the momentum-integral equation of Karman. It is customary to define a displacement thickness δ^* or δ_1 by

$$u_\infty \delta^* = \int_0^\infty (u_\infty - u) dy \quad (10.123)$$

and a momentum thickness θ or δ_2 by

$$u_\infty^2 \theta = \int_0^\infty u(u_\infty - u) dy . \quad (10.124)$$

(Use a sketch to define these graphically, particularly concept of displacement.) Equation (10.122) can then be succinctly written

$$\tau_w = \frac{\rho d}{dx} u_\infty^2 \theta + \rho u_\infty \delta^* \frac{du_\infty}{dx} . \quad (10.125)$$

If $u_\infty = \text{constant}$, this becomes

$$\tau_w = \rho u_\infty^2 \frac{d\theta}{dx} . \quad (10.126)$$

This expression is often used to determine the surface friction τ_w (as is 10.125) in the more general case). If a turbulent boundary layer is visualized as a wake, with a wall continuously removing momentum, this equation exposes the process of local momentum removal.

The invariant J for the radial jet should probably include a factor 2π to represent integration over the azimuthal angle.

Practice source-sink method for plane laminar jet, where outer flow is known (obtained by conformal mapping). (Will separation of variables work? Variables are separated in known answer.)

Handout on boundary layer. Ideas are rare, one every few years or occasionally much longer. Millikan looked at the departure h from the log law, but had no good data except for pipe and possible channel in 1938. Millikan's paper was absolutely ignored. Are there any citations before my thesis? Ludwig and Tillmann were interested in the failure of the momentum-integral equation to give the correct friction in flows going to separation. Ludwig invented the heated element as an

alternative. They stumbled on the result that the log law is independent of pressure gradient as well as Reynolds number. (Put $\partial w/\partial z$ in derivation.) Clauser also has a plot of h but did not comment on the shape or meaning.

10.5 Turbulent plane wall jet into moving fluid

10.5.1 Similarity

10.5.2 Relaxation

10.5.3 Effectiveness

10.5.4 Boundary-layer control

10.6 Three-dimensional wall jets

10.6.1 Single jets

10.6.2 Film cooling through holes

Chapter 11

THE PLANE PLUME

11.1 Generalities

Plumes are an important subject in civil and environmental engineering, because of the frequent need to dispose of waste heat and/or combustion products. In a uniform ambient fluid at rest, similarity solutions exist for round and plane plumes for both laminar and turbulent flow. The new property of such flows is that momentum is continuously added to the fluid, so that the velocity on the centerline increases, or at least does not decrease, with increasing distance from the source. If the initial momentum flux is not negligible, the flow may behave like a jet for a time, and then like a plume, as the acquired momentum begins to dominate the motion. The problem of a plume in a stably stratified ambient fluid is also important. Finally, the plume in a crossflow is an even more difficult problem than the jet in a crossflow, a problem already discussed in section x.

11.1.1 Dimensional preamble

Plumes are usually treated within the Boussinesq approximation, which assumes that variations in density can be ignored everywhere except in the energy equation and in the driving buoyancy term in the momentum equation. In the engineering literature, the approx-

imation is often stated as if it were self-evident. In what follows, a more rigorous argument will be attempted.

Recall the result of taking the limit $M \rightarrow 0$ in the equations of motion for a perfect gas in SECTION 1.2.3. The equations of continuity, momentum, energy, and state have the form

$$\frac{D\rho}{Dt} + \rho \operatorname{div} \vec{u} = 0 \quad (11.1)$$

$$\rho \frac{D\vec{u}}{Dt} = -\operatorname{grad} p + \rho \vec{F} + \operatorname{div} \underline{\tau} \quad (11.2)$$

$$\rho c_p \frac{DT}{Dt} = -\operatorname{div} \vec{q} + \rho Q \quad (11.3)$$

$$\rho T = \text{constant} \quad (11.4)$$

where the last two equations assume a calorically and thermally perfect fluid ($h = c_p T$ and $p = \rho R T$, respectively, with c_p and R constant). To these are added Newton's hypothesis for viscous stress and Fourier's hypothesis for heat flow,

$$\underline{\tau} = \mu (\underline{\operatorname{grad}} \vec{u} + \underline{\operatorname{grad}} \vec{u}^*) = \mu \underline{\operatorname{def}} \vec{u} \quad (11.5)$$

$$\vec{q} = -k \operatorname{grad} T \quad (11.6)$$

where the two constants μ and k are assumed to depend only on the state of the fluid.

The steady laminar plane plume is defined in FIGURE 11.1. The flow is driven by a line heat source at the origin, with E the energy input per unit time per unit length. The fluid is characterized by the temperature and density in the uniform ambient region, and by four secondary state variables, the viscosity, the heat conductivity, the specific heat at constant pressure, and the volume coefficient of expansion. The coordinates are labelled for consistency with other flows already considered, with x increasing upward. The acceleration of gravity g is directed downward, in the negative x -direction.

There are altogether eight parameters, listed below in the form of dimensional statements. For the present, the argument will proceed

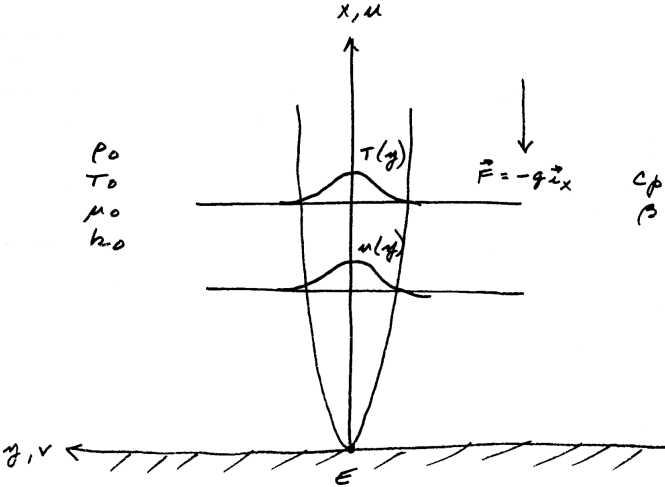


Figure 11.1: Steady laminar plane plume. (Caption provided by B. Coles)

without benefit of equations. (**Change sub 0 to sub α ?**)

$$\begin{aligned}
 [E] &= \frac{\mathbf{ML}}{\mathbf{T}^3} \\
 [\rho_0] &= \frac{\mathbf{M}}{\mathbf{L}^3} \\
 [\mu_0] &= \frac{\mathbf{M}}{\mathbf{LT}} \\
 [T_0] &= \Theta \\
 [k_0] &= \frac{\mathbf{ML}}{\mathbf{T}^3\Theta} \\
 [g] &= \frac{\mathbf{L}}{\mathbf{T}^2} \\
 [c_p] &= \frac{\mathbf{L}^2}{\mathbf{T}^2\Theta} \\
 [\beta] &= \frac{1}{\Theta} .
 \end{aligned} \tag{11.7}$$

Let the first four statements be interpreted as defining equations for \mathbf{M} , \mathbf{L} , \mathbf{T} , Θ and solved, to obtain

$$\mathbf{M} = \left(\frac{\rho_0^5 \nu_0^9}{E^3} \right)^{1/2}, \quad \mathbf{L} = \left(\frac{\rho_0 \nu_0^3}{E} \right)^{1/2}, \quad \mathbf{T} = \frac{\rho_0 \nu_0^2}{E}, \quad \Theta = T_0 . \tag{11.8}$$

In passing, define

$$\mathbf{U} = \frac{\mathbf{L}}{\mathbf{T}} = \left(\frac{E}{\rho_0 \nu_0} \right)^{1/2} . \tag{11.9}$$

and note that, as usual,

$$\frac{\mathbf{UL}}{\nu_0} = 1 . \tag{11.10}$$

The relationships (11.8) can now be inserted in the last four of equations (11.7) to obtain four dimensionless groups,

$$P_1 = \frac{k_0 T_0}{E}, \quad P_2 = \frac{\rho_0^3 \nu_0^5 g^2}{E^3}, \quad P_3 = \frac{\rho_0 \nu_0 c_p T_0}{E}, \quad P_4 = \beta T_0 \quad (11.11)$$

in which the four physical parameters k_0 , g , c_p , and β are isolated. Within limits, a different group of four statements might have been selected initially, with the same result, since the four groups (11.11) can be multiplied or divided arbitrarily by one another. This operation is evidently an ad hoc illustration of Buckingham's Π theorem (**ref**), which states that p dimensional parameters and $q < p$ dimensional units imply $p - q$ dimensionless groups. One of these, obtained by dividing the third group in (11.11) by the first, is familiar;

$$\Pi_3 = \frac{P_3}{P_1} = \frac{\rho_0 \nu_0 c_p}{k_0} = \frac{\nu_0}{\kappa_0} = Pr \quad (11.12)$$

Another, a global Froude number, follows on rearrangement of P_2 ;

$$\Pi_2 = P_2^{-1/2} = \frac{1}{g} \left(\frac{E^3}{\rho_0^3 \nu_0^5} \right)^{1/2} = \frac{1}{g} \left(\frac{E}{\rho_0 \nu_0} \right) \left(\frac{E}{\rho_0 \nu_0^3} \right)^{1/2} = \frac{\mathbf{U}^2}{\mathbf{gL}} = Fr^2 \quad (11.13)$$

A third amounts to a global Rayleigh number,

$$\begin{aligned} \Pi_1 &= \frac{P_2^{1/2} P_3 P_4}{P_1} = g \left(\frac{\rho_0^3 \nu_0^5}{E^3} \right)^{1/2} \frac{\nu_0}{\kappa_0} \beta T_0 \\ &= g \left(\frac{\rho_0^3 \nu_0^9}{E^3} \right)^{1/2} \frac{\beta T_0}{\kappa_0} = \frac{g \beta T_0 \mathbf{L}^3}{\kappa_0 \nu_0} = Ra \quad (11.14) \end{aligned}$$

The ratio Π_1/Π_3 also has a name (see Eckert for comment),

$$\frac{Ra}{Pr} = \frac{g \beta T_0 \mathbf{L}^3}{\nu_0^2} = Gr \quad (11.15)$$

Finally, a fourth parameter is P_4 itself,

$$\Pi_4 = P_4 = \beta T_0 \quad (11.16)$$

Note from equation (x) of section x that $\Pi_4 = 1$ for a perfect gas. For water at 20 °C, $\Pi_4 = xxx$. (**Do the moving observer argument.**)

The similarity argument for the equations of motion is essentially independent of the dimensional argument just completed, which did not use equations except to establish the relevance of the eight quantities in equations (11.7). The two most common sources of buoyancy forces are heating (**why is cooling not allowed?**) as in the sketch, or programmed density differences, as for flow of fresh or hot water into salt or cold water. The first case will be considered here and the second, which is a jet-plume relaxation, in section x. (**Should also do thermal.**)

The equations of motion for the laminar plane plume, with the boundary-layer and Boussinesq approximations, are

$$\frac{\partial u}{\partial x} + \frac{\partial v}{\partial y} = 0 \quad , \quad (11.17)$$

$$\rho_0 \left(\frac{\partial uu}{\partial x} + \frac{\partial uv}{\partial y} \right) = \beta \rho_0 (T - T_0) g + \mu_0 \frac{\partial^2 u}{\partial y^2} \quad , \quad (11.18)$$

$$\rho_0 c_p \left(\frac{\partial u(T - T_0)}{\partial x} + \frac{\partial v(T - T_0)}{\partial y} \right) = k_0 \frac{\partial^2 (T - T_0)}{\partial y^2} \quad . \quad (11.19)$$

Suitable boundary conditions for $u(x, y)$ and $T(x, y)$ are

$$u(x, \pm\infty) = 0 \quad (11.20)$$

$$T(x, \pm\infty) = 0 \quad (11.21)$$

and the symmetry condition

$$\psi(x, 0) = v(x, 0) = 0 \quad (11.22)$$

with null conditions on higher derivatives as needed.

Two integrals can be found immediately by integrating (11.18) and (11.19) from $-\infty$ to ∞ in y ;

$$\rho \frac{d}{dx} \int_{-\infty}^{\infty} uu \, dy = \beta \rho g \int_{-\infty}^{\infty} (T - T_0) \, dy \quad (11.23)$$

$$\rho c_p \frac{d}{dx} \int_{-\infty}^{\infty} u(T - T_0) \, dy = 0 \quad (11.24)$$

from which, in the second case,

$$\rho c_p \int_{-\infty}^{\infty} u(T - T_0) dy = E = \text{constant} . \quad (11.25)$$

Equation (11.23) describes the budget for the changing momentum, which increases with increasing x if $T > T_0$. The integral in equation (11.24), when expressed in terms of $(\rho - \rho_0)$, is often referred to as “buoyancy flux”, for reasons that are not apparent to me; it is obviously an energy flux. The constant E has the units of energy per unit time per unit length passing any station $x = \text{constant}$ and is here identified with the power per unit length at the heat source at the origin.

The momentum equation (11.18) and energy equation (11.19), together with the integral conservation law (11.25),

$$\rho_0 c_p \int_{-\infty}^{\infty} u(T - T_0) dy = E , \quad (11.26)$$

are the substance of the similarity formulation. The affine transformation operates on a large number of quantities; there are eight parameters (11.7) and five variables x, y, u, v, T . (**Recall the rule “transform everything in sight.” Note that T transforms like**

T_0 . Discuss ψ , boundary conditions.) Put

$$\begin{aligned}x &= a\hat{x} \\y &= b\hat{y} \\ \psi &= c\hat{\psi} \\ \mu_0 &= d\hat{\mu}_0 \\ \rho_0 &= e\hat{\rho}_0 \\ \kappa_0 &= f\hat{\kappa}_0 \\ c_p &= p\hat{c}_p \\ \beta &= q\hat{\beta} \\ T &= r\hat{T} \\ T_0 &= r\hat{T}_0 \\ E &= s\hat{E} \\ g &= t\hat{g}\end{aligned}\tag{11.27}$$

Four alphabetic invariants are obtained, constituting a complicated but faithful image of the equations of the problem (**where is T**

replaced by $T - T_0$);

$$\frac{bce}{ad} = 1 \quad , \quad (11.28)$$

$$\frac{b^3 eqrt}{cd} = 1 \quad , \quad (11.29)$$

$$\frac{bcep}{af} = 1 \quad , \quad (11.30)$$

$$\frac{cepr}{s} = 1 \quad . \quad (11.31)$$

If equation (11.30) is divided by equation (11.28), the result is

$$\frac{dp}{f} = 1 \quad (11.32)$$

which requires invariance for one of the dimensionless parameters;

$$\frac{c_p \mu_0}{k_0} = \frac{\nu_0}{\kappa_0} = Pr = \widehat{Pr} \quad . \quad (11.33)$$

The remaining three equations, say (11.28), (11.29), and (11.31), can be solved for b, c, r to establish dimensionless forms for $y, \psi, (T - T_0)$;

$$\frac{b^5 e^2 qst}{a^2 d^3 p} = 1 \quad , \quad (11.34)$$

$$\frac{c^5 e^3 p}{a^3 d^2 qst} = 1 \quad , \quad (11.35)$$

$$\frac{r^5 a^3 d^2 e^2 p^4 qt}{s^4} = 1 \quad . \quad (11.36)$$

Hence choose an ansatz of the form

$$A \left(\frac{c_p \rho_0}{\beta g E \nu_0^2 x^3} \right)^{1/5} \psi = f \left[B \left(\frac{\beta g E}{\rho_0 c_p \nu_0^3 x^2} \right)^{1/5} y \right] = f(\eta) \quad , \quad (11.37)$$

$$D \left(\frac{\beta g c_p^4 \rho_0^4 \nu_0^2 x^3}{E^4} \right)^{1/5} (T - T_0) = \theta(\eta) \quad (11.38)$$

with boundary conditions

$$f(0) = f'(\pm\infty) = f''(\pm\infty) = \theta(\pm\infty) = \theta'(\pm\infty) = 0 . \quad (11.39)$$

(Note from the form of η that δ varies like $\nu^{3/5}$ and like $x^{2/5}$. What about u_c and Fr ?)

Substitution in (11.34)-(11.36)¹ yields

$$\frac{5}{3} AB f''' + f f'' - \frac{1}{3} f' f' - \frac{5}{3} \frac{A^2}{B^2 D} \theta = 0 , \quad (11.40)$$

$$\frac{5}{3} \frac{AB}{Pr} \theta'' + f \theta' + f' \theta = 0 , \quad (11.41)$$

$$\int_{-\infty}^{\infty} f' \theta \, d\eta = AD \quad (11.42)$$

with one parameter, the Prandtl number. (**Check the other integral** (11.23).)

Equation (11.41) can be integrated once to obtain

$$\frac{5}{3} \frac{AB}{Pr} \theta' + f \theta = 0 . \quad (11.43)$$

The velocities u and v are (note $\beta g E / c_p \rho_0$ recurs)

$$u = \frac{B}{A} \left(\frac{\beta^2 g^2 E^2 x}{c_p^2 \rho_0^2 \nu_0} \right)^{1/5} f'(\eta) \quad (11.44)$$

and

$$v = \frac{1}{A} \left(\frac{\beta g \nu_0^2 E}{c_p \rho_0 x^2} \right)^{1/5} \left(\frac{2}{5} \eta f' - \frac{3}{5} f \right) . \quad (11.45)$$

¹Original ms is unclear about these equation numbers.

Provided that $\eta f' \rightarrow 0$ as $\eta \rightarrow \infty$, the entrainment velocity at the edge of the plume is

$$v(x, \infty) = -\frac{3}{5} \frac{1}{A} \left(\frac{\beta g \nu_0^2 E}{c_p \rho_0 x^2} \right)^{1/5} f(\infty) . \quad (11.46)$$

The notation will eventually put $f(\infty) = C$. A constant local Froude number can be formed from the centerline velocity, which varies like $x^{1/5}$, and the plume thickness, which varies like $x^{2/5}$. A maximum-slope thickness for the plume can be defined in the same way as for the plane jet in SECTION X, namely

$$\Delta = 2 \frac{f(\infty)}{f'(0)} . \quad (11.47)$$

A second relationship is obtained by putting $\eta = \Delta/2$ when $y = \delta/2$, in the argument of f in equation (11.37);

$$\Delta = B \left(\frac{\beta g E}{\rho_0 c_p \nu_0^3 x^2} \right)^{1/5} \delta . \quad (11.48)$$

Elimination of δ gives

$$\delta = \frac{2}{B} \frac{f(\infty)}{f'(0)} \left(\frac{c_p \rho_0 \nu_0^3 x^2}{\beta g E} \right)^{1/5} . \quad (11.49)$$

Finally, from equation (11.44) at $y = 0$,

$$u_c = \frac{B}{A} \left(\frac{\beta^2 g^2 E^2 x}{c_p \rho_0^2 \nu_0} \right)^{1/5} f'(0) . \quad (11.50)$$

It follows that **(must be small)**

$$Fr^2 = \frac{u_c^2}{g\delta} = \frac{B^3 [f'(0)]^3}{2A^2 f(\infty)} \left(\frac{\beta E}{c_p \rho_0 \nu_0} \right) \quad (11.51)$$

which is constant **(of what order?)** and formally independent of T_0 , k_0 , and g . The dimensionless combination in parentheses can be recognized as the ratio of the fourth to the third of the dimensionless groups (11.11). (*How does $T - T_0$ vary with x ? Who solved the problem first? Proceed to entrained flow, with and without wall. If source is cold and there is a wall, is the outcome a wall plume? Do thermal. Discuss Grashof number, Richardson number. See Schmidt and Beckmann.*)

11.1.2 The plane turbulent plume

In the turbulent case, the boundary-layer approximation for the equations of motion for a plane plume, with the usual stream function ($u = \partial\psi/\partial y$, $v = -\partial\psi/\partial x$) is

$$\rho_0(\psi_y\psi_{xy} - \psi_x\psi_{yy}) = \rho_0\beta g(T - T_0) + \frac{\partial\tau}{\partial y} , \quad (11.52)$$

$$\rho_0c_p[\psi_y(T - T_0)_x - \psi_x(T - T_0)_y] = \frac{\partial q}{\partial y} . \quad (11.53)$$

The integral conservation law is again (**mention buoyancy flux**)

$$\rho_0c_p \int_{-\infty}^{\infty} u(T - T_0)dy = E . \quad (11.54)$$

In these equations,

$$\tau = -\rho_0\overline{u'v'} , \quad (11.55)$$

$$q = -\rho_0\overline{T'v'} . \quad (11.56)$$

The second of these is usually defined without the factor c_p .

To implement an affine transformation, list the variables and

parameters in a table, together with their dimensions;

$$\begin{aligned}
 x &= a\hat{x} & \mathbf{L} \\
 y &= b\hat{y} & \mathbf{L} \\
 \psi &= c\hat{\psi} & \mathbf{L}^2/\mathbf{T} \\
 \rho_0 &= d\hat{\rho}_0 & \mathbf{M}/\mathbf{L}^3 \\
 c_p &= p\hat{c}_p & \mathbf{L}^2/\mathbf{T}^2\Theta \\
 \beta &= q\hat{\beta} & \mathbf{1}/\Theta \\
 T &= r\hat{T} & \Theta \\
 T_0 &= r\hat{T}_0 & \Theta \\
 E &= s\hat{E} & \mathbf{ML}/\mathbf{T}^3 \\
 g &= t\hat{g} & \mathbf{L}/\mathbf{T}^2 \\
 \tau &= m\hat{\tau} & \mathbf{M}/\mathbf{LT}^2 \\
 q &= n\hat{q} & \mathbf{M}/\mathbf{T}^3 .
 \end{aligned} \tag{11.57}$$

From the six parameters ρ_0 , c_p , β , T_0 , E , and g , characteristic scales appear as

$$\mathbf{M} = \left(\frac{E^6}{g^9 \rho_0} \right)^{1/5}, \quad \mathbf{L} = \left(\frac{E^2}{g^3 \rho_0^2} \right)^{1/5}, \quad \mathbf{T} = \left(\frac{E}{g^4 \rho_0} \right)^{1/5}, \quad \Theta = T_0 \tag{11.58}$$

together with two dimensionless groups,

$$\beta T_0, \quad \frac{c_p^5 \rho_0^2 T_0^5}{g^2 E^2} . \tag{11.59}$$

The second of these is also a group for the laminar problem (**therefore basic?**).

Affine transformation of equations (11.52) - (11.54) yields the following alphabetical relations:

$$\frac{c^2 d}{abm} = 1 \quad , \quad (11.60)$$

$$\frac{bdqrt}{m} = 1 \quad , \quad (11.61)$$

$$\frac{cdr}{an} = 1 \quad , \quad (11.62)$$

$$\frac{cdpr}{s} = 1 \quad . \quad (11.63)$$

Equations (11.62) and (11.63) can first be combined in the form (**why?**)

$$\frac{anp}{s} = 1 \quad (11.64)$$

and (11.62) discarded. An equivalent condition to (11.62) is that q transforms like $\rho \psi_x (T - T_0)$. If it is also assumed that τ transforms like $\rho \psi_y^2$, the relation implied is

$$\frac{mb^2}{c^2 d} = 1 \quad . \quad (11.65)$$

When this is compared with (11.60), it appears that

$$\frac{a}{b} = 1 \quad . \quad (11.66)$$

(**Question by Hall: is this above the line or below the line? Answer: below the line.**) Hence the combination y/x is invariant under the transformation, and is evidently the proper independent variable. When b is replaced by a throughout, three relations remain, in addition to (11.64);

$$\frac{c^2 d}{a^2 m} = 1, \quad \frac{adqrt}{m} = 1, \quad \frac{cdpr}{s} = 1 \quad . \quad (11.67)$$

These can be solved for c , m and r . The result is

$$\frac{c^3 dp}{a^3 qst} = 1, \quad \frac{r^3 a^3 d^2 p^2 qt}{s^2} = 1, \quad \frac{m^3 p^2}{d^2 q^2 s^2 t^2} = 1 . \quad (11.68)$$

The proper similarity variables, with constants for future use, are therefore

$$A \frac{\psi}{x} \left(\frac{\rho_0 c_p}{\beta g E} \right)^{1/3} = f \left(B \frac{y}{x} \right) = f(\eta) , \quad (11.69)$$

$$C (T - T_0) x \left(\frac{\rho_0^2 \beta g c_p^2}{E^2} \right)^{1/3} = \theta(\eta) , \quad (11.70)$$

$$\tau \left(\frac{c_p^2}{\rho_0 \beta^2 g^2 E^2} \right)^{1/3} = g(\eta) , \quad (11.71)$$

$$q \frac{c_p x}{E} = h(\eta) . \quad (11.72)$$

When these are substituted in equations (11.52) - (11.54), the result is

$$f f'' + \frac{A^2}{B^2 C} \theta + \frac{A^2}{B} g' = 0 , \quad (11.73)$$

$$f' \theta + f \theta' + A C h' = 0 , \quad (11.74)$$

$$\int_{-\infty}^{\infty} f' \theta d\eta = A C . \quad (11.75)$$

Note from equation (11.74) that there is a relation between f , θ and h independent of position in the dimensionless flow;

$$f \theta + A C h = \text{constant} = 0 \quad (11.76)$$

since f and h are zero on the plane of symmetry. In physical variables, this is

$$\psi(T - T_0) - x \overline{T'v'} = 0 . \quad (11.77)$$

The mean-velocity components in the turbulent plane plume are

$$u = \frac{B}{A} \left(\frac{\beta g E}{c_p \rho_0} \right)^{1/3} f' , \quad (11.78)$$

$$v = \frac{1}{A} \left(\frac{\beta g E}{c_p \rho_0} \right)^{1/3} (\eta f' - f) . \quad (11.79)$$

Hence the velocity in the plane of symmetry, u_c , is constant. The entrainment velocity is

$$v(x, \infty) = -\frac{1}{A} \left(\frac{\beta g E}{c_p \rho_0} \right)^{1/3} f(\infty) \quad (11.80)$$

and is also constant. In the plane of symmetry the temperature ($T_c - T_0$) and the turbulent heat transfer vary like $1/x$, while the Reynolds shearing stress is constant. **(Why not $\tau \sim u_c^2$, $T - T_0 \sim T_c - T_0$? Should do without boundary-layer approximation.)**

Note from (11.78) that u_c is independent of x ;

$$u_c = \frac{B}{A} \left(\frac{\beta g E}{C_p \rho_0} \right)^{1/3} f'(0) \quad (11.81)$$

and from (11.70) that

$$T_c - T_0 = \frac{1}{Cx} \left(\frac{E^2}{\rho_0^2 \beta g c_p^2} \right)^{1/3} \theta(0) \quad (11.82)$$

so that the Reynolds shearing stress (11.71) and the Reynolds heat transfer (11.72) can be written

$$\tau = \frac{A^2}{B^2 [f'(0)]^2} \rho_0 u_c^2 g(\eta) \quad (11.83)$$

and

$$q = \frac{AC}{B f'(0) \theta(0)} \rho_0 u_c (T_c - T_0) h(\eta) . \quad (11.84)$$

(Why not do this in the beginning?) *From handout:*

Laminar plume: nice work. No evidence of instability. Velocity in plane of symmetry is increasing with x . Thickness goes like $\nu^{2/3}$.

Sparrow. If (similarity) theory and experiment do not agree, I choose to believe the theory and look for sources of experimental error. This

policy might be useful for the turbulent problem, where there is no theory.

Sparrow. Note turbulent case; independent variable is y/x , and uses up 0.6: this flow is not a boundary layer. The entrained flow for the round turbulent plume uses Legendre polynomials.

Kotsovinos. Good on relaxation from jet to plume, given some initial momentum. K's plume not very wide; tank is small. See also picture of jet.

Anwar. Does not comment on development into pair of counter-rotating vortices.

Chapter 12

FLOW CONTROL

Flow through a plane gauze, or screen, is accompanied by a pressure drop and, if the flow is not normal to the screen, by a flow deflection toward the normal, much like the refraction of light when moving from an optically less dense into an optically more dense medium.

Screens are usually woven wire, but may be cloth or may be perforated plates or have other geometries. There are two effects to be considered. One is attenuation of turbulence existing upstream and the other is generation of new turbulence to be studied for its own sake or for its effect on other phenomena, such as transition, surface friction, or heat transfer. That is, make a non-uniform flow uniform or vice versa. I propose not to become involved with turbulence for its own sake, as this subject is very difficult and is covered in monographs by Hinze, Batchelor, Townsend, Monin and Yaglom, and elsewhere. (*Comment on curious identity of sizes of woven-wire screens available from different manufacturers, as if they bought from each other.*)

(*Look up the reasons why each author was interested in screens to show wide applicability. Note that early wind tunnels had no contractions; see paper by Prandtl. Mention Wright brothers, van der Hegge Zijnen.*)

The earliest competent study of the behavior of screens is by

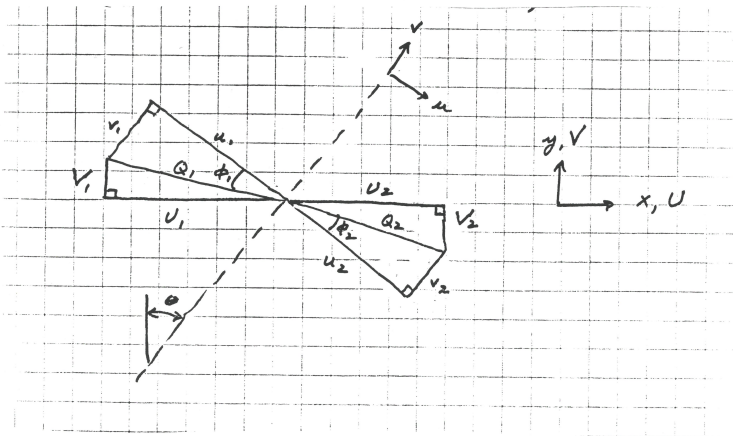


Figure 12.1: Flow through a screen. (Figure and caption added by K. Coles.)

TAYLOR and BATCHELOR (1949).

Assume that the resistance of the screen depends only on the component of velocity normal to its plane. If $p_2 - p_1$ is the pressure drop, the loss coefficient for flow normal to the screen ($\theta = 0$) will be defined as **(consider including solidity; what happens? Note that overall velocity decreases if there is a deflection; compare to shock wave.) (Put solidity s in denominator.)** (Need FIGURE X.) ¹

$$C_n = \frac{p_1 - p_2}{\frac{1}{2}\rho Q_1^2} \quad (12.1)$$

where Q , u , v are velocities in screen coordinates; u is the component normal to the screen and is necessarily conserved; i.e., $u_2 = u_1$. The component parallel to the screen is not conserved, being reduced by the drag of the screen elements. Here a second loss coefficient can be defined as

$$C_t = \frac{F}{\frac{1}{2}\rho u_1 v_1} \quad (12.2)$$

¹A sketch found in ms that may be the one cited is included here as Figure 12.1.

where T ² is the force per unit area in the plane of the screen and the subscript t refers to the tangential component. (**Notation is a problem. Can the Taylor and Batchelor argument be put in vector form?**) Note that both coefficients are designed to be of order unity, although they can also be expected to depend on solidity as well as on Reynolds number, Mach number, and geometrical details. The relationships

$$\begin{aligned} u_1 &= Q_1 \cos \phi_1 \\ u_2 &= Q_2 \cos \phi_2 \\ v_1 &= Q_1 \sin \phi_1 \\ v_2 &= Q_2 \sin \phi_2 \end{aligned} \tag{12.3}$$

and the tangential momentum equation

$$T = \rho u_1 (v_1 - v_2) \tag{12.4}$$

allow equation (12.2) to be put in the form

$$C_t = 2 \left(1 - \frac{\cos \phi_1 \sin \phi_2}{\sin \phi_1 \cos \phi_2} \right). \tag{12.5}$$

This coefficient C_t is called F_θ/θ by Taylor and Batchelor. The analogy with optics can be made explicit by writing

$$n = \frac{\sin \phi_1}{\sin \phi_2} \tag{12.6}$$

in which case, to first order in θ (**give also exact expression**),

$$C_t = 2 \left(\frac{n-1}{n} \right) \tag{12.7}$$

(Cite experiments on ϕ_2 vs ϕ_1 , especially Schubauer, Spangenberg, and Klebanoff. Mention experimental setup. Mention fit $F_\theta/\theta = 2 - 2.2/(1 + k_\theta)^{\frac{1}{2}}$ and T & B's figure 5. See JAS.)

² T may be same as F in 12.2, i.e., a transcription error from ms.

The proper geometric parameters for analyzing screen performance are the solidity s and the index of refraction n . For a square wire-mesh screen, the solidity is defined by the sketch;

$$s = \frac{\text{blocked area}}{\text{total area}} = \frac{2dD - d^2}{D^2} = 2\frac{d}{D} - \frac{d^2}{D^2} \quad (12.8)$$

The resistance coefficient C_n can be expected to increase with increasing solidity, as in sketch *A*.

There is a weak Reynolds-number effect, as indicated in sketch *B*, which can be expected to look like the drag coefficient of a cylinder. Finally, there is a Mach number effect, as shown in sketch *C* (*if density changes are appreciable, take them into account*).

(Combine to reproduce figure 5 of Taylor and Batchelor. Can solidity effect in A be estimated by adding up cylinders? See Wieghardt.)

(Structural strength is a factor; work out some details. Different companies sell the same screens. Better to put screen in low-velocity region, for sake of lower loads and lower losses. Keep Re based on stream velocity and wire diameter below shedding frequency.)

(In handout, note better scheme used by Dryden and Schubauer for determining angle; Simmons and Cowdrey were clumsy.)

To determine the effect of the screen on a small disturbance in the oncoming flow, linearize the problem. Suppose that the upstream flow is two-dimensional, with a perturbation that depends only on y ; say **(now U , not Q ; comment)**

$$U_1 = U_0 + u_1 \cos \kappa y . \quad (12.9)$$

This flow is assumed to be normal to the screen, and u_1 is now the amplitude of the perturbation. If viscosity is neglected, except perhaps in the close vicinity of the screen, the vorticity is constant on streamlines;

$$\frac{D\zeta}{Dy} = 0 . \quad (12.10)$$

In the two-dimensional flow, define a stream function ψ , with

$$\zeta = -\nabla^2 \psi . \quad (12.11)$$

To first order, therefore, $\partial \nabla^2 \psi / \partial x = 0$, and

$$\nabla^2 \psi = f(y) . \quad (12.12)$$

Note that this analysis is essentially for a two-dimensional screen; in three dimensions the vortex-stretching terms would appear and also there would be no stream function. But see pp. 11–12 of Taylor and Batchelor for a counter-argument. Far upstream,

$$\zeta = -\frac{\partial U_1}{\partial y} = \kappa u_1 \sin \kappa y \quad (12.13)$$

and in general, for the perturbation,

$$\nabla^2 \psi_1 = -\kappa u_1 \sin \kappa y . \quad (12.14)$$

The solution, easily obtained by separation of variables, is of the form

$$\psi(x, y) = C e^{\pm \kappa x} \frac{\sin \kappa y}{\cos \kappa y} . \quad (12.15)$$

To this must be added the particular solution. For an anti-symmetric flow, with $\psi(x, 0) = 0$ and with the upstream boundary condition (12.9),

$$\psi_1 = \left(\frac{u_1}{\kappa} + A e^{\kappa x} \right) \sin \kappa y . \quad (12.16)$$

A similar argument for the downstream region gives

$$\psi_2 = \left(\frac{u_2}{\kappa} + B e^{-\kappa x} \right) \sin \kappa y \quad (12.17)$$

where

$$U_2 = U_0 + u_2 \cos \kappa y . \quad (12.18)$$

Three conditions are needed to determine A , B , and u_2/u_1 . First, the component $u = \partial \psi / \partial y$ must be continuous. At the screen $x = 0$, therefore,

$$u_1 + \kappa A = u_2 + \kappa B = u_s, \text{ say.} \quad (12.19)$$

The meaning of the quantity u_s (for screen) is indicated in the sketch. Where the stream velocity is higher, more resistance will

be encountered, and the stream will diverge and reach the screen at an angle (**how does linearization prevent appearance of $\sin 2 \kappa y$, etc.?**). The amplitude u_1 will decrease to u_3 ; see below. Since $n = \sin \phi_1 / \sin \phi_2 = v_1 / v_2$, the v -components across the screen are related by

$$v_2 = -\frac{\partial \psi_2}{\partial x} = \frac{v_1}{n} = -\frac{1}{n} \frac{\partial \psi_1}{\partial x} \quad (12.20)$$

from which

$$A + nB = 0 \quad (12.21)$$

The final condition is obtained from Bernoulli's equation. To first order, with $U_1 = U_2 = U$, the total pressures differ by the loss at the screen;

$$\begin{aligned} p_1 + \frac{\rho}{2}(U^2 + 2U u_1 \cos \kappa y) - p_2 - \frac{\rho}{2}(U^2 + 2U u_2 \cos \kappa y) &= \\ = C_n \frac{\rho}{2}(U^2 + 2U u_s \cos \kappa y) \quad . \end{aligned} \quad (12.22)$$

This becomes, after cancelling terms of order unity,

$$u_1 - u_2 = C_n u_s \quad (12.23)$$

When A , B , and u_s are eliminated from equations (12.19), (12.21), and (12.23), the result is a formula for attenuation;

$$\frac{u_2}{u_1} = \frac{1 + n - C_n}{1 + n + nC_n} \quad (12.24)$$

(Note that this result is independent of κ and that the numerator may vanish. There is no practical upper limit on C_n . If $n = 3/2$, then $C_n = 5/2$ removes the upstream perturbation completely. Note that v -perturbations are attenuated by a factor $1/n$. This might be neater in a vector notation.)

The velocity u_s can be expressed in two ways:

$$\frac{u_s}{u_1} = \frac{1 + n}{1 + n + nC_n} \quad (12.25)$$

$$\frac{u_s}{u_2} = \frac{1 + n}{1 + n - C_n} \quad (12.26)$$

from which it is obvious that

$$u_1 > u_s > u_2 . \quad (12.27)$$

In all of this, the screen is assumed to have no structure, so that the effect on the turbulence spectrum is not treated. For a screen with high resistance, there is a high price in power required. The method has been used in diffusers (**comment on effect on boundary layer or on separated region**) and is worth the cost if a good downstream flow is essential. The same kind of analysis can be used for turning vanes. Compare S-duct in Lockheed 1011, Boeing 727.

Reprise of Taylor and Batchelor; see 20 April, 22 April.

- Glauert et al., R & M 1469, 1932*
Flachsbart, IV Lief., 112, 1932
 Ower and Warden, R & M 1559, 1934
 Collar, R & M 1867, 1939
Eckert and Pfluger, Lufo. 18, 142, 1941
 Czarnecki, WR L-342, 1942
 Simmons et al., ARC, 1943
Taylor, ARC R & M 2236, 1944
Simmons and Cowdrey, R & M 2276, 1945
Adler, NACA, 1946
Dryden and Schubauer, JAS 14, 221, 1947
 Kovasznay, Cambr. Phil. 44, 58, 1948
 Dryden and Schubauer, appendix, 1949
Hoerner, AFTR, 1950
Schubauer et al., TN2001, 1950
 Baines and Peterson, ASME 73, 467, 1951
 Weighardt, AQ 4, 186, 1953
 MacDougall, thesis, 1953
Annand, JRAS 57, 141, 1953
 Grootenhuis, PIME 168, 837, 1954
 Gedeon and Grele, RM, 1954
Dannenberg et al., TN 3094, 1954
 Tong, Stanford, 1956
 Tong and London, ASME 79, 1558, 1957
 Davis, thesis, 1957

Cornell, ASME 80, 791, 1958
Morgan, JRAS 63, 474, 1959
Morgan, JRAS 64, 359, 1960
London et al., ASME 82, 199, 1960
Siegel et al., TN D2924, 1965
Morgan, Austr. A347, 1966
Pinker and Herbert, JMES 9, 11, 1967
Blockley, thesis, 1968
Luxenberg and Wiskind, CWRV, 1969
Reynolds, JMES 11, 290, 1969
Rose, JFM 44, 767, 1970
Valensi and Rebont, AGARD, 27, 1970
Castro, JFM 46, 599, 1971
Carrothers and Baines, ASME 97, 116, 1975
Bernardi et al., ASME 98, 762, 1976
Graham, JFM 73, 565, 1976
Richards and Norton, JFM 73, 165, 1976
Murota, WES, 105, 1976
Durbin and Muramoto, NASA, 1985

Shaped Screens

Taylor, ZAMM 15, 91, 1935.
Okaya and Hasegawa, JJP 14, 1, 1941.
Stevens, ARC, 1942.
Taylor and Davies, R & M 2237, 1944.
Squire and Hogg, RAE, 1944.
Taylor and Batchelor, QJMAM 2, 1, 1949
Townsend, QJMAM 4, 308, 1951.
Bonnerville and Harper, thesis, 1951.
Lockard, thesis, 1951.
Owen and Zienkiewicz, JFM 2, 521, 1957.
Elder, JFM 5, 355, 1959.
Brighton, thesis, 1960.
Mc Carthy, JFM 19, 1964.
Livesey and Turner, IJMES 6, 371, 1964.
Davis, Austr 191, 1964.
Livesey and Turner, JFM 20, 201, 1964.

Vickery, NPL 1143, 1965.
 Rose, JFM 25, 97, 1966.
 Cockrell and Lee, JRAS 70, 724, 1966.
 Livesey, JRAS 70, 1966.
Kotansky, AIAA 4, 1490, 1966.
 Uberoi and Wallace, PF 10, 1216, 1967.
 Lau and Baines, JFM 33, 721, 1968.
 Mobbs, JFM 33, 227, 1968.
Reynolds, JMES 11, 290, 1969.
 Turner, JFM 36, 367, 1969.
 Cockrell and Lee, AGARD, 13, 1970.
Maull, AGARD, 16, 1970.
 Hannemann, thesis, 1970.
 Durgin, MIT, 1970.
 Champagne et al., JFM 41, 81, 1970.
 Kachhara, thesis, 1973.
 Sajben et al., AIAA, 1973.
 Koo and James, JFM 60, 513, 1973.
 Livesey and Laws, AIAA 11, 184, 1973.
Livesey and Laws, JFM 59, 737, 1973.
 Livesey and Laws, CES 29, 306, 1974.
Laws and Livesey, ARFM 10, 247, 1978.
 Tan-atichat, thesis, 1980.
 Scheiman, NASA, 1981.

A gauze, or screen, or grid, is a high-drag device that is normally used to redistribute the flow in a channel. Other uses include prevention of separation in diffusers, generation of turbulence, and reduction of turbulence, depending on the properties of the screen. (See Taylor and Batchelor for turbulence reduction.)

The basic problem considered by ELDER (**ref**) is modification of flow in a straight channel by a single shaped screen located in the vicinity of $x = 0$.

The coordinates are (x, y) , and the corresponding velocities are (U, V) . The flow is uniform but rotational far upstream and far downstream, and the effect of the screen is to introduce a discontinuity in vorticity at $x = 0$. The screen has no structure and is treated

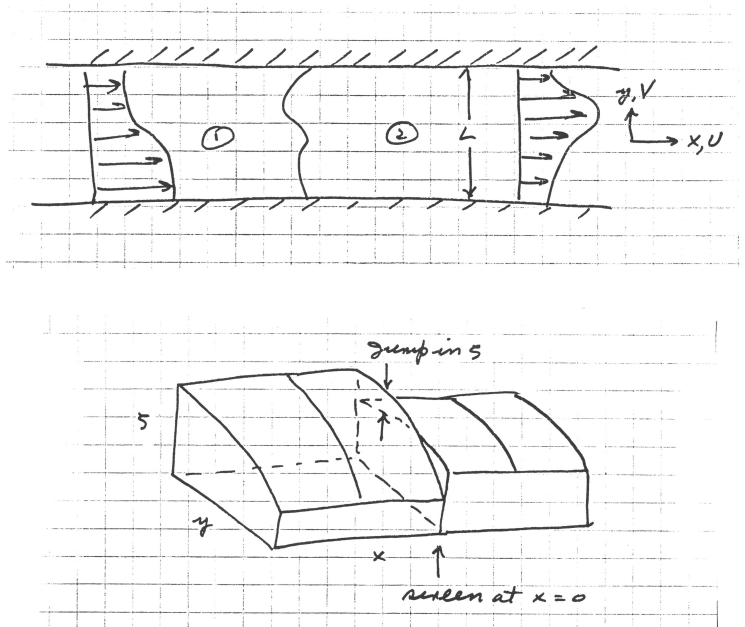


Figure 12.2: Flow in a channel modified by a single shaped screen. (Figure and caption added by K. Coles.)

like an actuator sheet.

Suppose that the flow is rotational but steady, incompressible, inviscid, and two-dimensional. Start with the flow in the sketch.³ A subscript 1 or 2 denotes upstream conditions or downstream conditions, respectively. Denote by a superscript 0 the one-dimensional flow that coincides with the initial or final state far from the screen; typical variables are ψ^0 , $U^0 = \partial\psi^0/\partial y$, $\zeta^0 = -\partial U^0/\partial y$.

In the two-dimensional flow, the continuity equation is satisfied if

$$\vec{U} = \nabla\psi \times \nabla z \quad (12.28)$$

³Two sketches found in ms that appear related to this discussion, the first of which may be the one cited, are included here as Figure 12.2.

where ψ is a stream function. Taking the curl yields

$$\zeta = -\nabla^2\psi . \quad (12.29)$$

The conditions already stated also imply

$$\frac{D\zeta^0}{Dt} = \vec{U}^0 \cdot \text{grad } \zeta^0 . \quad (12.30)$$

For the flow in the sketch,

$$\frac{D\zeta^0}{Dt} = U^0 \frac{d\zeta^0}{dx} = (\zeta_2^0 - \zeta_1^0)\delta(x) . \quad (12.31)$$

However, the velocity cannot be continuous, because $\partial U^0/\partial y$ is different for the upstream and downstream regions. It is necessary to add another flow near the screen. If the basic flow carries the vorticity, the proper composition is

$$\nabla^2\psi = \nabla^2\psi^0 + \nabla^2\psi' \quad (12.32)$$

where the perturbation ψ' is irrotational;

$$\nabla^2\psi^0 = -\zeta_0 , \quad (12.33)$$

$$\nabla^2\psi' = 0 . \quad (12.34)$$

The assumptions are:

1. The jump in vorticity is carried by the basic flow ψ^0 .
2. The condition that U is constant through the screen is carried by the combined flow.
3. A jump in V , to implement the jump in ζ , is carried by the perturbation flow. In particular, both ψ^0 and ψ' are discontinuous at the screen, but the sum is continuous.

The solution of the equation $\nabla^2\psi' = 0$ in rectangular coordinates is easily obtained by separation of variables. The solution can be written in dimensionless form for the upstream region

$$\frac{\psi'_1}{LU} = \sum \frac{1}{m\pi} P_m e^{m\pi x/L} \sin m\pi \frac{y}{L} \quad (x < 0) \quad (12.35)$$

and for the downstream region,

$$\frac{\psi'_2}{L\bar{U}} = \sum \frac{1}{m\pi} Q_m e^{-m\pi x/L} \sin m\pi \frac{y}{L} \quad (x > 0) \quad (12.36)$$

where L is the channel width and \bar{U} is the mean velocity over the cross section,

$$\bar{U} = \frac{1}{L} \int U \, dy . \quad (12.37)$$

It follows from the geometry that this velocity is the same far from the screen in both directions.

The flow represented by ψ' vanishes at $x = \pm\infty$. The form automatically satisfies the requirement that the flow follow the two walls, since $\psi' = 0$ at $y = 0$ and at $y = L$. Note that there is no net flow, so that the condition $\bar{U}_1 = \bar{U}_2$ must be satisfied by the primary flow.

The velocity components associated with ψ'_1 are

$$\frac{U'_1}{\bar{U}} = \sum P_m e^{m\pi x/L} \cos m\pi \frac{y}{L} , \quad (12.38)$$

$$\frac{V'_1}{\bar{U}} = - \sum P_m e^{m\pi x/L} \sin m\pi \frac{y}{L} , \quad (12.39)$$

and for ψ'_2 are

$$\frac{U'_2}{\bar{U}} = \sum Q_m e^{m\pi x/L} \cos m\pi \frac{y}{L} , \quad (12.40)$$

$$\frac{V'_2}{\bar{U}} = \sum Q_m e^{-m\pi x/L} \sin m\pi \frac{y}{L} . \quad (12.41)$$

The screen properties are referred to screen coordinates, as shown in the sketch;

The velocity normal to the screen is

$$u_1 = U_1 \cos \theta - V_1 \sin \theta , \quad (12.42)$$

$$u_2 = U_2 \cos \theta - V_2 \sin \theta . \quad (12.43)$$

Since $u_1 = u_2$, it follows that

$$(U_1 - U_2) = (V_1 - V_2) \tan \theta . \quad (12.44)$$

The velocity parallel to the screen is

$$v_1 = U_1 \sin \theta + V_1 \cos \theta , \quad (12.45)$$

$$v_2 = U_2 \sin \theta + V_2 \cos \theta , \quad (12.46)$$

from which

$$v_1 - v_2 = (U_1 - U_2) \sin \theta + (V_1 - V_2) \cos \theta \quad (12.47)$$

or, in view of equation (12.44),

$$v_1 - v_2 = \frac{V_1 - V_2}{\cos \theta} . \quad (12.48)$$

Elder notices that the combination (his BUT)

$$G = \left(\frac{v_1 - v_2}{v_1} \right) U_1 \frac{\sin \theta}{\cos \theta} \quad (12.49)$$

can be developed by using equation (12.45) to eliminate $\sin \theta$;

$$\begin{aligned} G &= \frac{(v_1 - v_2)}{v_1} \frac{(v_1 - V_1 \cos \theta)}{\cos \theta} \\ &= \frac{(v_1 - v_2)}{\cos \theta} - \frac{(v_1 - v_2)}{v_1} V_1 \\ &= \frac{(V_1 - V_2)}{\cos^2 \theta} - \frac{(v_1 - v_2)}{v_1} V_1 \end{aligned} \quad (12.50)$$

where the last step requires equation (12.48). When terms in V_1 and V_2 are collected and the identity $1/\cos^2 \theta = 1 + \tan^2 \theta$ is used, this becomes

$$G = V_1 \left[1 - \frac{(v_1 - v_2)}{v_1} + \tan^2 \theta \right] - V_2 (1 + \tan^2 \theta) \quad (12.51)$$

or finally, if $\tan^2 \theta$ is neglected on the right-hand side, U_1 is replaced by \bar{U} , and the original form (12.49) is restored,

$$\frac{(v_1 - v_2)}{v_1} \bar{U} \tan \theta = \left[1 - \frac{(v_1 - v_2)}{v_1} \right] V_1 - V_2 . \quad (12.52)$$

In terms of the index of refraction, with the approximation $\sin \phi = \tan \phi$ and the condition $u_1 = u_2$,

$$\tan \phi_1 = \frac{v_1}{u_1} = \sin \phi_1, \quad \tan \phi_2 = \frac{v_2}{u_1} = \sin \phi_2 \quad (12.53)$$

and therefore $v_1 = nv_2$. Equation (12.52) becomes

$$\left(\frac{n-1}{n}\right)\bar{U} \tan \theta = \frac{V_1}{n} - V_2. \quad (12.54)$$

This expression defines the jump in V at the screen when the screen properties n and θ are specified. The approximations include neglecting $\tan^2 \theta$ compared to unity, replacing $\tan \phi$ by $\sin \phi$, and replacing U_1 by \bar{U} .

When the right-hand side of equation (12.54) is rewritten using equations (12.39) and (12.41) with $x = 0$, the result is

$$\left(\frac{n-1}{n}\right) \tan \theta = \sum \left(-\frac{P_m}{n} - Q_m\right) \sin m\pi \frac{y}{L}. \quad (12.55)$$

This relation provides the coefficients in a Fourier series for $\tan \theta$ if the coefficients P_m and Q_m are known. (**Define n for a honeycomb.**)

It remains to express the jump in pressure in the same way. The momentum equation can be written

$$-\frac{1}{\rho} \nabla p = \nabla \frac{\vec{u} \cdot \vec{u}}{2} + (\text{curl } \vec{u}) \times \vec{u}. \quad (12.56)$$

The y -component of this equation is

$$-\frac{1}{\rho} \frac{\partial p}{\partial y} = \frac{\partial}{\partial y} \left(\frac{U^2 + V^2}{2}\right) + \zeta U. \quad (12.57)$$

Far upstream and downstream of the screen (**close to screen?**)

$$-\frac{1}{\rho} \frac{\partial p_1}{\partial y} = \frac{\partial}{\partial y} \frac{U_1^2}{2} + \zeta_1 U_1 \quad (12.58)$$

$$-\frac{1}{\rho} \frac{\partial p_2}{\partial y} = \frac{\partial}{\partial y} \frac{U_2^2}{2} + \zeta_2 U_2 \quad (12.59)$$

and therefore

$$\frac{1}{\rho} \frac{\partial}{\partial y} (p_1 - p_2) = \frac{\partial}{\partial y} \frac{(U_2^2 - U_1^2)}{2} + \zeta_2 U_2 - \zeta_1 U_1 . \quad (12.60)$$

This condition should be applied at the screen, and the approximation is made that streamline displacements are small. If the second term is discarded, on the ground that $U_1 = U_2 = \bar{U}$ approximately, then

$$\frac{1}{\rho} \frac{\partial}{\partial y} (p_1 - p_2) = \zeta_2 U_2 - \zeta_1 U_1 . \quad (12.61)$$

By definition,

$$p_1 - p_2 = \frac{1}{2} \rho u^2 C_n \quad (12.62)$$

where $u = u_1 = u_2$. Moreover, from (12.42), $u = U \cos \theta$ approximately. Substitution gives

$$\frac{1}{2} \frac{\partial}{\partial y} U^2 \cos^2 \theta C_n = \bar{U} \left(-\frac{dU_2^0}{dy} + \frac{dU_1^0}{dy} \right) \quad (12.63)$$

where it is also assumed on the right that $U_1 = U_2 = U$. One integration gives

$$\frac{1}{2} U^2 \cos^2 \theta C_n = \bar{U} (U_1^0 - U_2^0) + C \quad (12.64)$$

where C is a constant of integration. Put

$$U = \bar{U}(1 + \epsilon) \quad (12.65)$$

to obtain

$$\frac{1}{2} \bar{U} (1 + \epsilon) \cos^2 \theta C_n = \bar{U} (U_1^0 - U_2^0) + \frac{C}{\bar{U}} (1 - \epsilon) . \quad (12.66)$$

A second integration from $y = 0$ to $y = L$, with $\cos^2 \theta$ treated as constant, and with

$$\int_0^L \epsilon dy = 0 \quad (12.67)$$

by virtue of equation (?)⁴, gives

$$C = \frac{\bar{U}^2}{2} C_n . \quad (12.68)$$

Equation (12.64) can therefore be written, to leading order, and with $\cos^2 \theta$ taken as unity,

$$(U - \bar{U}) \frac{C_n}{2} = U_1^0 - U_2^0 . \quad (12.69)$$

The stage is now set for the solution of equations (?)⁵ and (12.69) above. Continuity of the streamwise velocity at the screen requires (Elder's Eq. 2.5)

$$U_1^0 + \bar{U} \sum P_m \cos m\pi \frac{y}{L} = U_2^0 + \bar{U} \sum P_m \cos m\pi \frac{y}{L} . \quad (12.70)$$

The difference in the V -component across the screen is

$$V_1' - V_2' = -\bar{U} \sum (P_m + Q_m) \sin m\pi \frac{y}{L} . \quad (12.71)$$

(There is some missing algebra here.) After some algebra, there is obtained

$$\left(\frac{U_2^0}{\bar{U}} - 1 \right) \frac{(n+1 + n \frac{C_n}{2})}{n \frac{C_n}{2}} - \left(\frac{U_1^0}{\bar{U}} - 1 \right) \frac{(n+1 - \frac{C_n}{2})}{n \frac{C_n}{2}} \quad (12.72)$$

$$= - \sum \alpha_m \cos m\pi \frac{y}{L} = 0 \quad (12.73)$$

where

$$\alpha_m = \frac{P_m}{n} + Q_m . \quad (12.74)$$

Equation (12.73) has to be compared to equation 12.55, which can be written

$$\left(\frac{n-1}{n} \right) \bar{U} \tan \theta = - \sum \alpha_m \sin m\pi \frac{y}{L} . \quad (12.75)$$

⁴Equation number not recorded

⁵Equation number not recorded

Equations (12.73) and (12.75) define two functions expressed as Fourier series. The series have the same coefficients, but one is in terms of $\sin n\pi y/L$ and the other is in terms of $\cos n\pi y/L$. There is a theorem due to Hardy that applies to this situation. Given

$$g(\theta) = \sum h_m \sin m\theta \quad (12.76)$$

$$g^*(\theta) = \sum h_m \cos m\theta \quad (12.77)$$

valid in the interval $0 < \theta < \pi$, it follows that

$$g^* = H(g), \quad g = H^*(g^*) \quad (12.78)$$

where

$$H(g) = \frac{1}{2\pi} \int_0^\pi [g(\theta + t) - g(\theta - t)] \cot \frac{t}{2} dt . \quad (12.79)$$

(Look up the theorem and describe the symmetry. Did this theorem drive Elder's analysis, or was it discovered in time to save the analysis? Ask him?) The theorem connects the screen angle to the velocities upstream and downstream. The analysis should reduce for $\theta = 0$ and $m = 1$ to the Taylor-Batchelor formula.

(There is an error in Elder's application of his analysis; see Livesey and Laws and others.)

Appendices

Appendix A

NOTE: This section appears to have been part of the chapter on the boundary layer (Chapter 4) but was pulled out as a separate file and labeled “Appendix A.” It has no title of its own. The file name is “highre.tex,” presumably for “high Reynolds number.” –B. Coles

In 1962, I undertook an extensive survey of experimental data in low-speed turbulent boundary layers at constant pressure, in an attempt to identify a fully developed (standard, normal, ideal, equilibrium, asymptotic) state and determine its properties. My objective at that time was to establish a point of departure for a study of compressibility. My survey appeared as Appendix A of a RAND report (COLES 1962), but was never published outside of the subliterature. Because the work is not readily accessible, I will summarize here my methods and conclusions. I set out to test a large number of mean-velocity profiles for their consistency with the momentum-integral equation and the momentum-defect law, which is to say the departure of the outer part of the profile from the logarithmic law of the wall. The next four figures are copied from Appendix A to show the test method. Given a profile and a value for ν , I first determined a value for u_τ in equation (xxx)¹ that would put one point belonging to the hypothetical log region on the straight line defined by the particular constants of the time, $\kappa = 0.41$ and $c = 5.0$, as shown in FIGURE A.1. I then drew a parallel straight line through the point of maximum departure of the profile from the log line. Great precision was not needed for this oper-

¹Given as equation (A-1) on p. 54 of COLES 1962 Rand Report, available at <http://www.rand.org/content/dam/rand/pubs/reports/2006/R403.pdf>

PLACEHOLDER

Figure A.1: Caption for Figure with label 7.40 (figure on p. 54 of COLES 1962).

ation, and there was no formal curve-fitting. (Both the non-linear regression scheme of Levenberg and Marquardt (SECTION X) and the corner modification proposed by Sandham (SECTION Y) were still in the future.) The vertical distance between the two lines, labeled $\Delta u/u_\tau$, is a measure of the strength of the wake component of the profile. I found that this quantity, although it represents only about ten percent of u_∞ for flow at constant pressure, was distinguished by an almost exquisite sensitivity to the history and environment of each particular flow. This property in turn made possible not only a close classification of boundary-layer flows at constant pressure, but a refinement and rationalization of the similarity laws for the profile.

The upper part of FIGURE A.2 shows $\Delta u/u_\tau$ as a function of the local Reynolds number R_θ for flows that I classified as normal. The lower part of the figure compares two estimates of the surface friction τ_w for the same data; first, the momentum-integral result $\rho u_\infty^2 d\theta/dx$, where θ is the momentum thickness, and second, the result from the graphical procedure for u_τ in the form ρu_τ^2 . The agreement is generally within ten percent, and usually better. I take this agreement as strong evidence in favor of identifying u_τ with $(\tau_w/\rho)^{1/2}$.

By way of contrast, FIGURE A.3 shows the corresponding

PLACEHOLDER

Figure A.2: Caption for Figure with label 7.41 (figures 10 and 11 on p. 56 of COLES 1962).

PLACEHOLDER

Figure A.3: Caption for Figure with label 7.43 (figures 12 and 13 on p. 58 of COLES 1962).

quantities for flows that I classified as abnormal. I noted as a significant point of technique that the normal data were obtained for the most part in closed wind tunnels, either on plates having blunt leading edges or some equally effective tripping means, or on tunnel walls having a long approach length. Some of the anomalous data were obtained in open-jet tunnels using models not equipped with adequate side plates. In view of the generally poor momentum balance in FIGURE A.3, I blamed the anomalies in these flows for the most part on three-dimensionality of the mean flow.

One major finding of the study, which perhaps should have been anticipated, was that $\Delta(u/u_\tau)$ decreases, and hence that the traditional defect law fails, as the Reynolds number R_θ decreases below a value of about 5000. In fact, the wake component in FIGURE A.2 disappears entirely and rather abruptly by the time R_θ has decreased to a value near 500. This behavior was present in all of the data, I therefore do not view it normal or not. The behavior might be viewed as a residual effect of transition, because I would not expect such a high degree of commonality in such a diverse population of data. A better hypothesis is that the flows are fully turbulent and in equilibrium, in the special sense that two characteristic scales δ and ν/u_τ are emerging and separating from each other as discrete parameters for turbulent flow near a wall. It is possible, although difficult to prove experimentally, that the constants in the log law are also evolving. If so, I doubt that the graphical classification scheme of FIGURE A.1 is seriously compromised.

In the RAND report I also looked at the strength of the wake component in the presence of high stream turbulence and in the flow downstream from very strong tripping devices. These effects will not be discussed here. (**Elsewhere?**) I turn instead to my second major finding, which was that the quantity $\Delta u/u_\tau$ seemed to decrease substantially at Reynolds numbers larger than the upper limit in FIGURES A.2–A.3. This second finding, if correct, signals a serious and perhaps fatal defect in the defect law.

In 1962, almost the only reliable data in low-speed boundary-layer flow at high Reynolds numbers were the careful and extensive measurements by SMITH and WALKER (1958), which offered them-

selves by default as definitive for Reynolds numbers R_θ from 15000 to 50000. I found no evidence that these measurements might be affected by pressure gradient, stream turbulence, or three-dimensionality. My conclusion at the time was that these data could only be questioned on some other ground. Failing this, the defect law is not valid at the high level of precision attempted in my survey.

Fortunately, there is other ground. Because the freestream velocities in the experiments by Smith and Walker reached 110 meters per second, I propose here to make one more test of these and certain other data, a test based on the premise that the apparent problem with the defect law may be solved by considering the effect of compressibility. I cannot recall why I did not test this hypothesis in my 1962 report, except that suitable descriptions of mean-velocity profiles, including my own failed description of 1962, were not part of the machinery of the time. In particular, in 1962 the proposal by VAN DRIEST (1951) was still a decade or more away from being generally accepted as the best available means for organizing the effects of compressibility. This proposal will be examined to what follows.

Standard methods exist for data processing in studies of turbulent boundary layers in compressible fluids. The fluid is invariably assumed to be a perfect gas, with equation of state

$$p = \rho RT \quad . \quad (\text{A.1})$$

The two specific heats c_p and c_v are taken as constants, as are their combinations $R = c_p - c_v$ and $\gamma = c_p/c_v$. The instrument of choice is the impact or total-pressure tube. Almost without exception, each measurement of velocity begins with the local Mach number M , which is inferred from the ratio of impact pressure to static pressure. If the flow is supersonic, the operational equation (LIEPMANN and ROSHKO 1957) is

$$\frac{p'_0}{p} = \frac{\left(\frac{\gamma+1}{2} M^2\right)^{\frac{\gamma}{\gamma-1}}}{\left(\frac{2\gamma}{\gamma+1} M^2 - \frac{\gamma-1}{\gamma+1}\right)^{\frac{1}{\gamma-1}}} \quad , \quad (\text{A.2})$$

where the prime denotes probe impact pressure behind a normal shock wave, and p is the static pressure at the probe entrance in the absence of the probe. The latter pressure is usually measured at an adjacent wall or is computed by assuming isentropic expansion to a Mach number M_∞ in the free stream. In either case the static pressure is taken as constant through the boundary layer. If the flow is subsonic and thus free of shock waves, equation (A.2) is replaced by

$$\frac{p_0}{p} = \left(1 + \frac{\gamma - 1}{2} M^2\right)^{\frac{\gamma}{\gamma - 1}} . \quad (\text{A.3})$$

Finally, if the Mach number is much less than unity, the last equation reduces to Bernoulli's integral,

$$p_0 = p + \frac{1}{2} \rho u^2 . \quad (\text{A.4})$$

The last two equations are the ones plotted in FIGURE 1.1 of the introduction. I will assume in what follows that accuracy in measurement of p and p'_0 and hence of the local Mach number M have been accurately measured. I will also ignore for the moment any corrections for effects of turbulence or mean-flow gradients on the probe readings.

The state equation (A.1) and the condition $p = p_w = p_\infty$ reduce the number of independent thermodynamic variables from three to one. One thermodynamic quantity must therefore be measured or assumed. The usual choice is the local stagnation temperature T_0 or the local static temperature T . The definition of T_0 for a perfect gas with $M = u/a = u/(\gamma RT)^{1/2}$ is

$$T_0 = T + \frac{u^2}{2c_p} = T \left[1 + \left(\frac{\gamma - 1}{2}\right) M^2\right] . \quad (\text{A.5})$$

If the flow is laminar, there exist under certain conditions an energy integral, which is to say a relation between temperature and velocity, or more accurately between enthalpy and kinetic energy, that satisfies the equations of motion and is valid independent of

position in the flow. Suppose that the wall temperature T_w is constant and the Prandtl number

$$Pr = \frac{c_p \mu}{k} \quad (\text{A.6})$$

is equal to unity. With the further restriction that there is no heat transfer, a primitive energy integral, first found by BUSEMANN (1931), is

$$T_0 = T + \frac{u^2}{2c_p} = \text{constant} = T_{0\infty} = T_w . \quad (\text{A.7})$$

There is no restriction on pressure gradient. A different integral obtains if there is heat transfer, still with $T_w = \text{constant}$ and $Pr = 1$, but now with the restriction of constant pressure. For these conditions a generalization of Busemann's energy integral was found by CROCCO (1932), and independently by BUSEMANN (1935) (**check**);

$$T + bu + \frac{u^2}{2c_p} = \text{constant} = T_w , \quad (\text{A.8})$$

where the parameter b will be shown shortly to be a measure of heat transfer at the wall.

The relations just given are often summarily adopted as a model for turbulent flow. FERNHOLZ and FINLEY (1980) recommend a relationship between temperature and velocity originally proposed by WALZ (1966) (**check**),

$$\frac{T}{T_\infty} = A + B \frac{u}{u_\infty} + C \frac{u^2}{u_\infty^2} . \quad (\text{A.9})$$

This expression is formally identical with the Crocco-Busemann integral (A.8) but has no physical basis in turbulent flow except that it is capable of satisfying the two boundary conditions

$$T = T_w \text{ at } u = 0 , \quad T = T_\infty \text{ at } u = u_\infty . \quad (\text{A.10})$$

It follows that

$$A = \frac{T_w}{T_\infty} , \quad B + C = 1 - \frac{T_w}{T_\infty} . \quad (\text{A.11})$$

The derivative of equation (A.9) at the wall is

$$\frac{1}{T_\infty} \left(\frac{\partial T}{\partial y} \right)_w = \frac{B}{u_\infty} \left(\frac{\partial u}{\partial y} \right)_w . \quad (\text{A.12})$$

Hence $B = 0$ corresponds to adiabatic flow at constant wall temperature. The discussion hereafter will be limited to this special case of zero heat transfer. (**A reference?**)

The energy integral (A.9) with $B = 0$ becomes

$$\frac{T}{T_\infty} = \frac{T_w}{T_\infty} + \left(1 - \frac{T_w}{T_\infty} \right) \frac{u^2}{u_\infty^2} . \quad (\text{A.13})$$

In most experiments in compressible fluids, as already pointed out, the measured quantity is the Mach number, and it is necessary to prepare equation (A.13) for this situation. For a perfect gas, the temperature, velocity, and Mach number are related by the definition of M ;

$$\rho u^2 = \gamma p M^2 \quad (\text{A.14})$$

Whether or not the pressure p depends only on x , the ratio p/ρ is always equal to RT . Hence a suitable normalized form of equation (A.14) is

$$\frac{u^2}{u_\infty^2} = \frac{T}{T_\infty} \frac{M^2}{M_\infty^2} . \quad (\text{A.15})$$

When this equation is used to eliminate the velocity in equation (A.13), the result is

$$\frac{T_w}{T} = 1 - \left(1 - \frac{T_w}{T_\infty} \right) \frac{M^2}{M_\infty^2} . \quad (\text{A.16})$$

For the sake of symmetry, the energy integral (A.13) can be rewritten as

$$\frac{T}{T_w} = 1 + \left(\frac{T_\infty}{T_w} - 1 \right) \frac{u^2}{u_\infty^2} . \quad (\text{A.17})$$

Within this formulation, the Mach number determines the temperature, and the temperature determines the velocity (and the density). In dimensional form, the argument assumes a knowledge of T_w and one of the three parameters T_{0_∞} , T_∞ , u_∞ , together with use of the rigorous definitions (A.5) and (A.14).

To recapitulate, the preceding discussion refers to impact-probe measurements of the Mach-number profile in adiabatic boundary layers. Nothing in the discussion requires that the flow be specified as laminar or turbulent. If the flow is laminar and adiabatic and the Prandtl number is unity, the relationships are rigorous within the boundary-layer approximation ($\partial p/\partial y = 0$) and the usual considerations of experimental accuracy. Moreover, the wall temperature is equal to the free-stream stagnation temperature, according to equation (A.7). It is a difficulty, readily overcome by numerical means if the flow is laminar, that the Prandtl number for common gases is nearly constant but usually at a value near 0.7 rather than unity. This difficulty is usually expressed by introduction of a recovery factor r , defined as

$$r = \frac{T_r - T_\infty}{T_{0_\infty} - T_\infty} , \quad (\text{A.18})$$

where T_r , the recovery temperature, is the wall temperature T_w when there is no heat transfer. In practice, the recovery factor is close to unity, although it is different for laminar and turbulent flows.

(Paragraph on high thermal price, case $T_w \rightarrow T_{0_\infty}$ if $Pr > 1$, etc.)

Experimenters may sometimes have direct access to the velocity in high-speed flow through laser Doppler velocimetry or particle-image velocimetry or the like; all these techniques face formidable difficulties in supersonic flow. In such cases, the temperature can be estimated from equation (A.17) in order to determine the density, which is required for any test of momentum balance.

(Section on experimental T or T_0 profile.)

There is not much evidence that the energy ansatz (A.9) is a real improvement over other possible forms, such as the form $T_0 = T_{0_\infty}$, commonly used, or the form $T_0 = T_w$, both of which have no less claim to validity than the form (A.9). To see the effect of errors in T_0 , suppose first that p , M , and T_0 are known exactly. Hence so is T , from $T_0/T = 1 + (\gamma - 1)M^2/2$. So is u , from $u/(\gamma RT)^{1/2} = M$. So is ρ , from $\rho u^2 = \gamma p M^2$. If M is known but T_0 is estimated rather than measured, with a local relative error of ϵ in T_0 , then the local relative

errors in T , u , ρ , and ρu are ϵ , $\epsilon/2$, $-\epsilon$, and $-\epsilon/2$, respectively.

Van Driest. The most widely accepted scheme for comparing data for $M \neq 0$ with data for $M = 0$ is the scheme now called Van Driest II. It has been endorsed by Fernholz and Finley in their massive survey of data for $M \neq 0$, and by numerous other authors (**Name some.**). These authors sometimes refer to the scheme as a transformation, but I prefer to reserve this term for a relationship based on the equations of motion, and to use the term “mapping” for a relationship based on variables only. The compressibility mapping proposed by VAN DRIEST (1951) begins with the mixing-length expression

$$\tau = \tau_w = \rho \ell^2 \left(\frac{du}{dy} \right)^2, \quad (\text{A.19})$$

together with Prandtl’s hypothesis

$$\ell = \kappa y, \quad (\text{A.20})$$

and arrives at the ansatz

$$\rho^{1/2} \frac{du}{dy} = \frac{\tau_w^{1/2}}{\kappa y}. \quad (\text{A.21})$$

The appearance of the combination $(\rho^{1/2} du)$ suggests that the physical velocity u can be replaced by an effective velocity u^* , say, defined by $du^* \sim \rho^{1/2} du$, or by its definite integral,

$$u^* = \int_0^u \left(\frac{\rho}{\rho^*} \right)^{1/2} du, \quad (\text{A.22})$$

where ρ^* is a constant reference density included for dimensional reasons. It is apparent that the Van Driest mapping (A.22) has the effect of rotating the profile in the counter-clockwise direction in the usual semi-logarithmic coordinates, since ρ is small where u is small, near the wall, and ρ is large where u is large, near the free stream. This is the property that makes the scheme an attractive device in any attempt to restore the defect law to respectability, as noted at the beginning of this section.

An alternative expression for the mixing length is Karman's similarity hypothesis,

$$l = x \frac{du/dy}{d^2u/dy^2} . \quad (\text{A.23})$$

This form was proposed simultaneously and independently by Wilson (1950), and both Wilson and Van Driest developed their hypothesis into formulas for skin friction as a function of Mach number and Reynolds number (**check**). These two authors were not alone; several other authors, working independently, used the same or similar methods and approximations to complete their analyses. The situation in 1953 was surveyed by COLES (1953) and by CHAPMAN and KESTER (1953), and the various proposals to that time were collected by Chapman and Kester in a celebrated figure that is reproduced here as FIGURE 4.xx.² There were few competent measurements in 1951, and it should not be surprising that the various predictions filled a plot of C_f against M almost uniformly densely.

Chapman and Kester used the designations Van Driest I and II and for the Prandtl and Karman forms, although they misplaced the second one in their figure. A later survey by SPALDING and CHI (1964) used the same designations, but reversed taking Karman as I and Van Driest as II. In fact, Van Driest and Wilson were fully informed very early about their respective contributions, according to the proceedings of a Navy conference in 1951. Van Driest in 1956 described both models, Prandtl first and Karman second, without attributing either. The confusion was made permanent by Spalding and Chi, and made permanent by FERNHOLZ and FINLEY (1978?) (**Check all this.**) It is only necessary to know that Van Driest's first and only analysis was based on the Prandtl model and is now universally referred to as Van Driest II. Details follow.

The definition (A.22) is readily integrated in closed form for the energy integral (??)³ for adiabatic flow, putting T_∞/T for ρ/ρ_∞ .

²Unclear reference.

³Unclear equation reference.

The result is the Van Driest mapping for velocity;

$$m \left(\frac{\rho^*}{\rho_w} \right)^{1/2} \frac{u^*}{u_\infty} = \sin^{-1} \left(m \frac{u}{u_\infty} \right), \quad (\text{A.24})$$

where m , defined by **(check)**

$$m^2 = \frac{T_w - T_\infty}{T_w} = \frac{r \left(\frac{\gamma - 1}{2} \right) M_\infty^2}{1 + r \left(\frac{\gamma - 1}{2} \right) M_\infty^2}, \quad (\text{A.25})$$

lies between 0 and 1 and in any case requires $T_w > T_\infty$. Given the specified energy integral, the dimensionless mean-velocity profile u/u_∞ can be replaced at each value of y by

$$\frac{u^*}{u_\infty^*} = \frac{\sin^{-1} \left(m \frac{u}{u_\infty} \right)}{\sin^{-1}(m)}, \quad (\text{A.26})$$

without regard to the definition of ρ^* . Incidentally, the \sin^{-1} operator is the unique signature of the Van Driest mapping for any energy law that has T quadratic in u .

The mapping defined by equation (A.26) is not based on any observable process or mechanism. Whether or not the accepted similarity laws remain valid for the mean velocity profile after the Van Driest mapping is a question to be settled experimentally. Before the evidence can be tested, the friction velocity u_τ and some other constants have to be redefined in a plausible way for the case of variable density.

For this purpose, integrate the mixing-length equation (A.21) formally, with $du = (\rho^*/\rho)^{1/2} du^*$, to obtain the modified law of the wall,

$$u^* = \frac{1}{\kappa} \left(\frac{\tau_w}{\rho^*} \right)^{1/2} \ln \left(\frac{y}{y^*} \right) + \text{constant}, \quad (\text{A.27})$$

where y^* is a constant reference length also included for dimensional reasons. Equation (A.27) is typical of mixing-length formulas in that

it is at best an unclear description of a fragment of the mean-velocity profile. The choices for ρ^* and y^* and the value of the constant in equation (A.27) are customarily resolved by an extension of the mapping to the wall, taking care to be consistent with the earlier treatment of an incompressible fluid in SECTION X. First, write the functional dependence in the profile formula (A.27) in dimensionless form as

$$\left(\frac{\rho^*}{\tau_w}\right)^{1/2} u^* = f\left(\frac{y}{y^*}\right) . \quad (\text{A.28})$$

Near the wall, this becomes approximately

$$\left(\frac{\rho^*}{\tau_w}\right)^{1/2} u^* = \frac{y}{y^*} . \quad (\text{A.29})$$

As u and y approach zero, the definition (A.22) and its integral (A.24) both lead to

$$u^* = \left(\frac{\rho_w}{\rho^*}\right)^{1/2} u . \quad (\text{A.30})$$

Finally, the requirement of Newtonian friction at the wall implies, to the same approximation,

$$\tau_w = \mu_w \frac{u}{y} . \quad (\text{A.31})$$

When u^* is eliminated between equations (A.29) and (A.30), and u/y is eliminated between this result and equation (A.31), the constant of integration y^* emerges in terms of well-defined quantities,

$$y^* = \nu_w \left(\frac{\rho_w}{\tau_w}\right)^{1/2} . \quad (\text{A.32})$$

At the same time, a generalized friction velocity u_τ emerges as

$$u_\tau = \left(\frac{\tau_w}{\rho_w}\right)^{1/2} , \quad (\text{A.33})$$

and equation (A.27) becomes

$$\left(\frac{\rho^*}{\rho_w}\right)^{1/2} \frac{u^*}{u_\tau} = \frac{1}{\kappa} \ln \left(\frac{y u_\tau}{\nu_w}\right) + \text{constant} . \quad (\text{A.34})$$

This form and equation (A.24) strongly suggest, although they do not require, defining ρ^* by

$$\rho^* = \rho_w , \quad (\text{A.35})$$

whereupon

$$u^* = u \quad (\text{A.36})$$

very near the wall.

As usual, this reasoning for $y \rightarrow 0$ is not part of the mixing-length argument, which applies only for fully turbulent flow outside the sublayer. Given the choices (A.33) and (A.35), then in a usual notation equation (A.27) becomes

$$u^+ = \frac{1}{\kappa} \ln y^+ + c , \quad (\text{A.37})$$

where now

$$u^+ = \frac{u^*}{u_\tau} , \quad y^+ = \frac{y u_\tau}{\nu_w} , \quad \rho_w u_\tau^2 = \tau_w , \quad (\text{A.38})$$

and

$$m \frac{u^*}{u_\infty} = \sin^{-1} \left(m \frac{u}{u_\infty} \right) . \quad (\text{A.39})$$

The fragile derivation just given, with Prandtl's equation (A.20) for ℓ , is commonly referred to as Van Driest II. The choice for ρ^* , u_τ , and y^* is important because it controls the dependence of the generalized κ and c on M_∞ and γ . What is wanted is the particular choice that minimizes this dependence. There is substantial evidence, for example, in papers by FENTER and STALMACH (1957), ROTTA (1960), MOORE and HARKNESS (1964), MAISE and MCDONALD (1968), MICHEL, QUEMART, and ELENA (1969), DANBERG (1971), SQUIRE (1971), and FERNHOLZ (1976) that use of wall quantities as in equations (A.37)–(A.39) is very nearly optimum from this point of view, at least for adiabatic flow at constant pressure at Mach numbers up to perhaps 5.

Most of these authors have also gone beyond the mixing-length argument to consider a more general fit to a defect law or to a

combined wall-wake formulation of the mean profile, in the manner adopted by COLES (1968) for low-speed flow; i.e., a fit to

$$u^+ = \frac{1}{\kappa} \ln y^+ + c + 2 \frac{\Pi}{\kappa} \sin^2 \eta \quad , \quad (\text{A.40})$$

where

$$\eta = \frac{\pi}{2} \frac{y}{\delta} \quad . \quad (\text{A.41})$$

The present method for determining the strength of the wake component is the third in an evolving series. In 1962 the fit of the mean-velocity profile used only one point. In 1968 I tried to involve a fit of the entire profile to equation (A.40) but had to finesse the problem of a misfit near $y = \delta$ by omitting data for y/δ greater than some threshold value noted in the tabulation in the “Young person’s guide.” In this monograph, I have made room for the omitted data by using the Sandham scheme (SECTION 4.9.3) for rounding the profile near $y = \delta$. In addition, the constants κ and c now have new values based on Zagarola’s pipe measurements (SECTION 2.5.7). The constants κ and c are here given their new incompressible values, $\kappa = 0.435$ and $c = 6.10$. The parameters u_τ , δ , and n (need equation) are then determined by a three-parameter least-squares fit of the experimental data to equation (A.40), after eliminating Π temporarily with the aid of the constraint imposed by the local friction law,

$$u_\infty^+ = \frac{1}{\kappa} \ln \delta^+ + c + 2 \frac{\Pi}{\kappa} \quad . \quad (\text{A.42})$$

The quality of Van Driest scaling, when universal constant values are assumed for κ and c , can be tested in different ways. One test is to compare values inferred for the local friction coefficient (**does this make sense?**)

$$C_f = 2 \frac{\rho_w}{\rho_\infty} \left(\frac{u_\tau}{u_\infty} \right)^2 \quad , \quad (\text{A.43})$$

with values obtained by other means. A second test is to compare values obtained for the profile parameter Π with corresponding values for low-speed flow. This second comparison will be made first and

will lead to the conclusion is that there is very little effect of compressibility on the shape of the mean-velocity profile in Van Driest II coordinates, at least for Mach numbers up to about 3.

Such tests are not new. The first paper to compare various mappings of C_f was the extensive survey by SPALDING and CHI (1964). Tests were also carried out by JACKSON et al (1965), PETERSEN (19xx), MILES and KIM (19xx), DANBERG (1971), HOPKINS and INOUE (1971), and WINTER and GAUDET (1973). These efforts are not necessarily redundant, since they differed in their choice of data, viscosity law, and handling of temperature. The consensus is that the Van Driest scheme is at least as good as any other when taken as a high-level technical application.

Full profile fits and reports of wake strength have been carried out by (Winter, Gaudet, others). Among the most satisfactory studies to my mind is one by D. Collins at JPL, for which I was consultant and eventually co-author (COLLINS, COLES, and HICKS 1978). The invariance of the defect law under Van Driest mapping was strongly supported by these data for Mach numbers up to 2.2.

FERNHOLZ and FINLEY (1977) in their massive catalog of boundary-layer measurements involving compressibility, did not include the operation of curve fitting for the mean velocity profile. In a second volume (1980), they provided numerous plots in Van Driest coordinates, but still without a fitting operation. The survey has a large clerical component limited mainly to major issues such as effects of flow history and the validity of empirical energy integrals. I have relied very heavily on this survey in the new analysis that follows. (**Say how to get data.**)

I have used this scheme before in connection with work by D. Collins at JPL, in which I participated as consultant and co-author. The objective was to document a set of flows for LDV measurements of $\overline{u'v'}$ in supersonic flow, a quantity that was then under a cloud, and perhaps still is. The next few paragraphs are borrowed from that report.

Values for viscosity are obtained from the Sutherland viscosity

law,

$$\frac{\mu}{\mu_r} = \left(\frac{T_r + S}{T + S} \right) \left(\frac{T}{T_r} \right)^{3/2}, \quad (\text{A.44})$$

where $T_r = 291.75$ K, $S = 110$ K, and $\mu_r = 1.827 \times 10^{-4}$ gm/cm-sec.

Integral thicknesses for the boundary layer are computed from

$$\delta^* = \int_0^\delta \left(1 - \frac{\rho u}{\rho_\infty u_\infty} \right) dy, \quad (\text{A.45})$$

and

$$\theta = \int_0^\delta \frac{\rho u}{\rho_\infty u_\infty} \left(1 - \frac{u}{u_\infty} \right) dy. \quad (\text{A.46})$$

The boundary-layer form parameter H is defined as

$$H = \frac{\delta^*}{\theta}. \quad (\text{A.47})$$

For two-dimensional mean flow, the surface friction can be obtained from von Kármán's momentum-integral equation, (**What is cap P?**)

$$C_f = 2 \frac{d\theta}{dx} - 2(2 + H - M_\infty^2) \frac{\theta}{\gamma M_\infty^2} \frac{1}{P} \frac{dP}{dx}. \quad (\text{A.48})$$

The accuracy of equation (A.48) is expected to be low, primarily because of difficulty in differentiating experimental data for $\theta(x)$ and $u_\infty(x)$ (see Table A3 of the Appendix).⁴ For the JPL measurements, the second term in equation (A.48) is at most 3 percent of the first term, and is uncertain by a comparable amount. Hence this term has been discarded. Values for $C_f = 2 d\theta/dx$ are listed in Table 3, which compares values obtained for C_f by this and several other methods.

Note that these measurements at JPL were the last hurrah of the 20-inch tunnel before it was dismantled and moved to Langley in 1980. Hence there was ample time to do the work well. Note also that the boundary layer experiments reported in my thesis at Caltech were almost the first tests conducted in this tunnel in 1951, 29 years earlier.

⁴Table A3 or Table 3 mentioned later have not been found.